AD-A110 862 GEORGIA INST OF TECH ATLANTA ENGINEERING EXPERIMENT --ETC F/G 17/7
MARINE AIR TRAFFIC CONTROL AND LANDING SYSTEM (MATCALS INVESTIG--ETC(U)
SEP 81 E R GRAF, C L PHILLIPS, S A STARKS N00039-80-C-0032
UNCLASSIFIED GIT/EES-1-A-2550-VOL-1 NL

1 of 5
AD
A110862

LEVEL III

(1)

ELECTRICAL

ENGINEERING EXPERIMENT STATION
AUBURN UNIVERSITY
AUBURN, ALABAMA

81 11 26 069

TECHNICAL REPORT
CONTRACT 1-A-2550
(SUBCONTRACTED FROM N-00039-80-C-0032)
MARINE AIR TRAFFIC CONTROL
AND LANDING SYSTEM
(MATCALS INVESTIGATION)
VOLUME I

E. R. Graf, C. L. Phillips, and S. A. Starks
CO-PROJECT LEADERS

September, 1981

Prepared for

The Engineering Experiment Station
Georgia Institute of Technology
Atlanta, Georgia

Prepared by

The Electrical Engineering Department
Auburn University
Auburn University, Alabama

FOREWORD

This technical report is submitted to the Georgia Institute of Technology to comply with the report requirements of contract 1-A-2550, which is a subcontract under United States Navy contract N-00039-80-C-0032. This report is published in two volumes, and each volume consists of two parts.

REPORT CONTENTS

PART ONE

REPORT SUMMARY

Prepared for

Georgia Institute of Technology
ATLANTA, GEORGIA

Under

Contract 1-A-2550

by

Electrical Engineering Department
Auburn University
Auburn, Alabama

Prepared by: Charles L. Phillips

REPORT SUMMARY

Auburn University, under contracts N66314-73-C-0565, N66314-74-C-1352, N66314-74-C-1634, N00228-75-C-2080, N00228-76-C-2069, and N00228-78-C-2233 with the United States Navy, and has investigated various aspects of the Marine Air Traffic Control and Landing System (MATCALS). This report contains the results of the continuation of these investigations under contract 1-A-2550 with the Georgia Institute of Technology. The report is organized into three main sections, namely Part Two, Part Three, and Part Four. Part Two presents a method of estimating the centroid location of a target utilizing a scan return amplitude versus angle information. Part Three contains the results of an investigation into replacing the α-β filter in the MATCAL digital controller with an observer, in order to reduce the effects of radar noise. Part Four presents the results of an investigation into replacing the same α-β filter with a tri-state adaptive filter, in order to reduce the effects of radar noise.

Centroid Estimation

Essential to the performance of any tracking radar is an effective target centroid estimator. The purpose of the work reported in Part Two is to examine the accuracy of several target centroid estimators in a comparative fashion, and to introduce a non-thresholding algorithm developed as part of this research. This analysis was conducted using a software simulation of a landing system radar tracking a passive target. The algorithm developed in Part Two is a method of estimating the centroid location of a target utilizing scan return amplitude versus angle information. The method is compared to three thresholding estimators and a first moment estimator in a computer-simulated automatic landing system.

It was found that the method introduced was the most robust and accurate of the estimators in noise, due to its unique scan rejection capability. In periods of high signal-to-noise ratio the method had less error than the thresholding methods, and was similar in ability to the first moment estimator. Further, the pulse transmissions required to obtain a desired level of performance is much reduced from the thresholding methods employed in this simulation.

Observer Design

Presently a problem exists in the closed-loop control of the MATCALS system due to the noise generated in AN/TPN 22 radar. An α-β filter in the flight dynamic and control module is employed to reduce the noise effects while estimating the position and the velocity of the aircraft. An observer may also be used to estimate the status of the aircraft. Part Three of this report presents the results of an investigation of the replacement of the α-β filter with an observer.

The F4J aircraft lateral control system is employed as an example in this investigation. Several different controllers are utilized to determine which yield the best radar-noise response and which yield the best wind response.

The proposed MATCALS system contain an α-β filter in the controller. Alternative controllers are constructed by replacing the α-β filter with an observer.

In general the observer control systems exhibit significantly less radar-noise response than do the α-β systems, but exhibit somewhat more wind response. These studies indicate that the observer controllers improve the MATCALS system's operation when compared to the α-β controllers, and that the observer systems should be considered further.

Tri-State Adpative Filters

A tri-state adaptive tracking filter was designed for use in the F4J aircraft lateral control system in an automatic landing configuration. The system presently uses an α-β tracking filter to estimate the aircraft's lateral position and velocity. The tri-state adaptive filter is designed to replace the α-β filter.

Three digital tracking filters, each based upon a different aircraft dynamic model, were combined to form the tri-state adaptive tracking filter. The selection of the appropriate filter output was determined by the variance of the filters' smoothed position estimates. The tri-state adaptive filter was implemented in the simulation of the F4J lateral control system. The results given in Part Four suggest that the performance of the F4J lateral control system may be improved through the use of a tri-state adaptive tracking filter. Since the F4J longitudinal control system is structurally identical to the lateral control system, the tri-state adpative filter may, in a similar manner, provide an improvement in the performance of the longitudinal control system.

The overall performance of the tri-state adaptive tracking filter may be enhanced by selecting the parameters of each of the three component filters in such a manner as to achieve a more complementary filter response. Another modification which might improve the performance of the tri-state adaptive filter is the adjustment of the variance thresholds of the alpha and alpha-beta filters. As was shown by the results of the F4J lateral control system simulation, the frequency response of the tri-state adaptive filter may be altered by the selection of the appropriate variance thresholds.

PART TWO

REPORT SUMMARY

Prepared for

Georgia Institute of Technology
ATLANTA, GEORGIA

Under

Contract 1-A-2550

by

Electrical Engineering Department
Auburn University
Auburn, Alabama

Prepared by: R. J. Machuzak and E. R. Graf

ACKNOWLEDGEMENTS

The authors would like to acknowledge the efforts of James F. Byrd, who assisted in debugging the MATCALS computer program and Michael Riggs, who created the basic plotting programs used in this work.

SIMULATION DEVELOPMENT

The fundamental MATCALS simulation was developed by E. W. Smith, D. G. Burks and J. C. Brand.

A CENTROID ALGORITHM BASED UPON RETURN AMPLITUDE-

VERSUS-ANGLE SIGNATURE

R. J. Machuzak, E. R. Graf, C. L. Phillips and S. A. Starks

ABSTRACT

A method of estimating the centroid location of a target utilizing scan return amplitude versus angle information is introduced. The method is compared to three thresholding estimators and a first moment estimator in a computer-simulated automatic landing system.

It was found that the method introduced was the most robust and accurate of the estimators in noise, due to its unique scan rejection capability. In periods of high signal-to-noise ratio the method had less error than the thresholding methods, and was similar in ability to the first moment estimator. Further, the pulse transmissions required to obtain a desired level of performance is much reduced from the thresholding methods employed in this simulation.

TABLE OF CONTENTS

LIST OF TABLES

LIST OF FIGURES

FIGURES FOR BASELINE FLIGHTS
ALL SCANS USED

FIGURES FOR BASELINE FLIGHTS WITH NOISE
ALL SCANS USED

FIGURES FOR BASELINE FLIGHTS WITH TURBULENCE
ALL SCANS USED

FIGURES FOR FLIGHTS WITH TURBULENCE AND NOISE
ALL SCANS USED

FIGURES FOR BASELINE FLIGHTS WITH NOISE
SCANS WITH A SNR 13 dB OR GREATER USED

FIGURES FOR FLIGHTS WITH TURBULENCE AND NOISE
SCANS WITH A SNR 13 dB OR GREATER

FIGURES FOR BASELINE FLIGHTS WITH NOISE
SCAN SNR AT OR BELOW 10 dB

FIGURES FOR FLIGHTS WITH TURBULENCE AND NOISE
SCAN SNR AT OR BELOW 10 dB

FIGURES FOR BASELINE FLIGHTS
ALL SCANS USED

FIGURES FOR FLIGHTS WITH TURBULENCE AND NOISE
ALL SCANS USED

FIGURES FOR BASELINE FLIGHTS WITH NOISE
SCANS WITH A SNR 13 dB OR GREATER USED

FIGURES FOR FLIGHTS WITH TURBULENCE AND NOISE
SCANS WITH A SNR 13 dB OR GREATER USED

FIGURES FOR BASELINE FLIGHTS WITH NOISE
SCAN SNR AT OR BELOW 10 dB

FIGURES FOR FLIGHTS WITH TURBULENCE AND NOISE
SCAN SNR AT OR BELOW 10 dB

FIGURES FOR BASELINE FLIGHTS
ALL SCANS USED

FIGURES FOR BASELINE FLIGHTS WITH NOISE
ALL SCANS USED

FIGURES FOR BASELINE FLIGHTS WITH TURBULENCE
ALL SCANS USED

FIGURES FOR FLIGHTS WITH TURBULENCE AND NOISE
ALL SCANS USED

FIGURES FOR BASELINE FLIGHTS WITH NOISE
SCANS WITH A SNR 13 dB OR GREATER USED

FIGURES FOR FLIGHTS WITH TURBULENCE AND NOISE
SCANS WITH A SNR 13 dB OR GREATER USED

FIGURES FOR BASELINE FLIGHTS WITH NOISE
SCAN SNR AT OR BELOW 10 dB

FIGURES FOR FLIGHTS WITH TURBULENCE AND NOISE
SCAN SNR AT OR BELOW 10 dB

FIGURES FOR BASELINE FLIGHTS
ALL SCANS USED

FIGURES FOR BASELINE FLIGHTS WITH NOISE
ALL SCANS USED

FIGURES FOR BASELINE FLIGHTS WITH TURBULENCE
ALL SCANS USED

FIGURES FOR FLIGHTS WITH TURBULENCE AND NOISE
ALL SCANS USED

FIGURES FOR BASELINE FLIGHTS WITH NOISE
SCANS WITH A SNR 13 dB OR GREATER USED

FIGURES FOR FLIGHTS WITH TURBULENCE AND NOISE
SCANS WITH A SNR 13 dB OR GREATER USED

FIGURES FOR BASELINE FLIGHTS WITH NOISE
SCAN SNR AT OR BELOW 10 dB

FIGURES FOR FLIGHTS WITH TURBULENCE AND NOISE
SCAN SNR AT OR BELOW 10 dB

I. INTRODUCTION

Essential to the performance of any tracking radar is an effective target centroid estimator. The purpose of this work is to examine the accuracy of several target centroid estimators in a comparative fashion, and to introduce a non-thresholding algorithm developed as part of this research. This analysis was conducted using a software simulation of a landing system radar tracking a passive target. Gaiccari and Nucci [1], Shradar [2], Mueke [3], and Gilbert [4], provide an excellant discussion of air traffic control radars. The results of this work are most applicable to sequential-lobing tracking radars.

II. OVERVIEW OF THE SIMULATION

The computer simulation used in this work describes a large jet fighter aircraft in a normal ground controlled approach (GCA) with the radar antenna located 500 meters from the runway touchdown point, as shown in Figure 2-1. The simulation initiates the flight with the target 3.72 nmi downrange from the runway touchdown point, or 4.0 nmi downrange from the radar antenna. The target model is allowed to approach the runway at a constant 148.6 mph on a 3.5 degree glideslope, which is a typical approach for the jet fighter being modelled [5]. The radar is a phased-array 3-D pencil beam radar utilizing a null-to-null cross-type scan, which scans the target as it moves. Since the tracking mode of an operating radar attempts to find the target within a small area of space designated by the search mode, this simulation varies the location of the target in the scanning window by use of a uniform random number generator before the start of each scan. The scanning window is always wide enough to fully scan the target.

The simulation executes a single scan on the moving target and then increments time to allow the modelled radar to perform its other search and track duties, and to move the target down the glidepath. The simulation aborts when the target is within 90 meters of the runway touchdown point.

The target model used is an ensemble of three anisotropic scattering complexes representing the left wing, right wing, and fuselage,

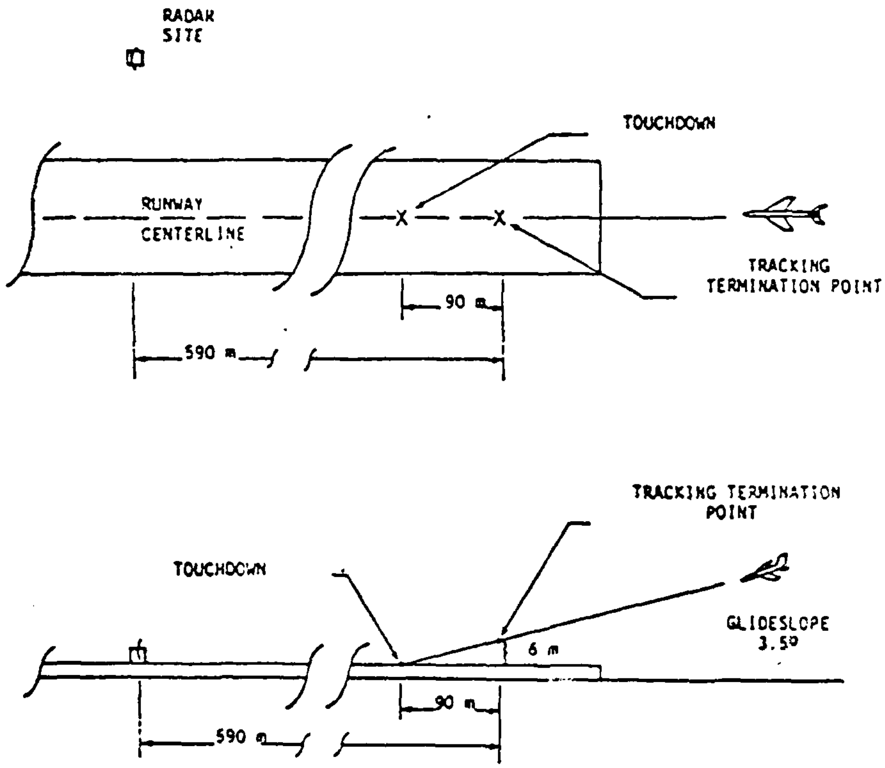

Figure 2-1. Siting of the precision approach radar and final approach glideslope used in the computer simulation.

slightly modified from the model of Loomis and Graf [6]. The location of the scattering complexes in the target coordinate system is shown in Figure 2-2(a), and the arrangement of the scattering points in a scattering complex are shown in Figure 2-2(b). The equations describing the scattering complexes is given in Table 2-1. In this work, the angles ϕ and θ are not the typical spherical phi and theta, but rather relative angles measured from the nose axis of the target coordinate system. Phi describes the angle in azimuth, and theta describes the angle in elevation. Figures 2-3, 2-4, and 2-5 are plots of the radar cross section (RCS) in azimuth of the fuselage, right wing, and left wing, respectively. The composite cross sections of the target model in azimuth, Figure 2-6, and in elevation, Figure 2-7, are not used by the simulation, and are presented here for completeness. The radar cross sections in polar form of the fuselage, right wing, and left wing, are shown in Figures 2-8, 2-9, and 2-10, respectively. The built-in shadowing effect of the fuselage on the wings is especially evident in Figures 2-9 and 2-10. The composite cross sections in azimuth, Figure 2-11, and elevation, Figure 2-12, are again shown for completeness. All figures are for a wavelength of 3.3 cm.

The individual returns from each of the scattering complexes are weighted by the antenna pattern before being summed on a power basis. This process is repeated for every simulated transmission of a pulse from the radar. Although only one pulse is transmitted at each beam pointing location, time is incremented as though three pulses are transmitted. When the simulation noise option is enabled, random gaussian noise is

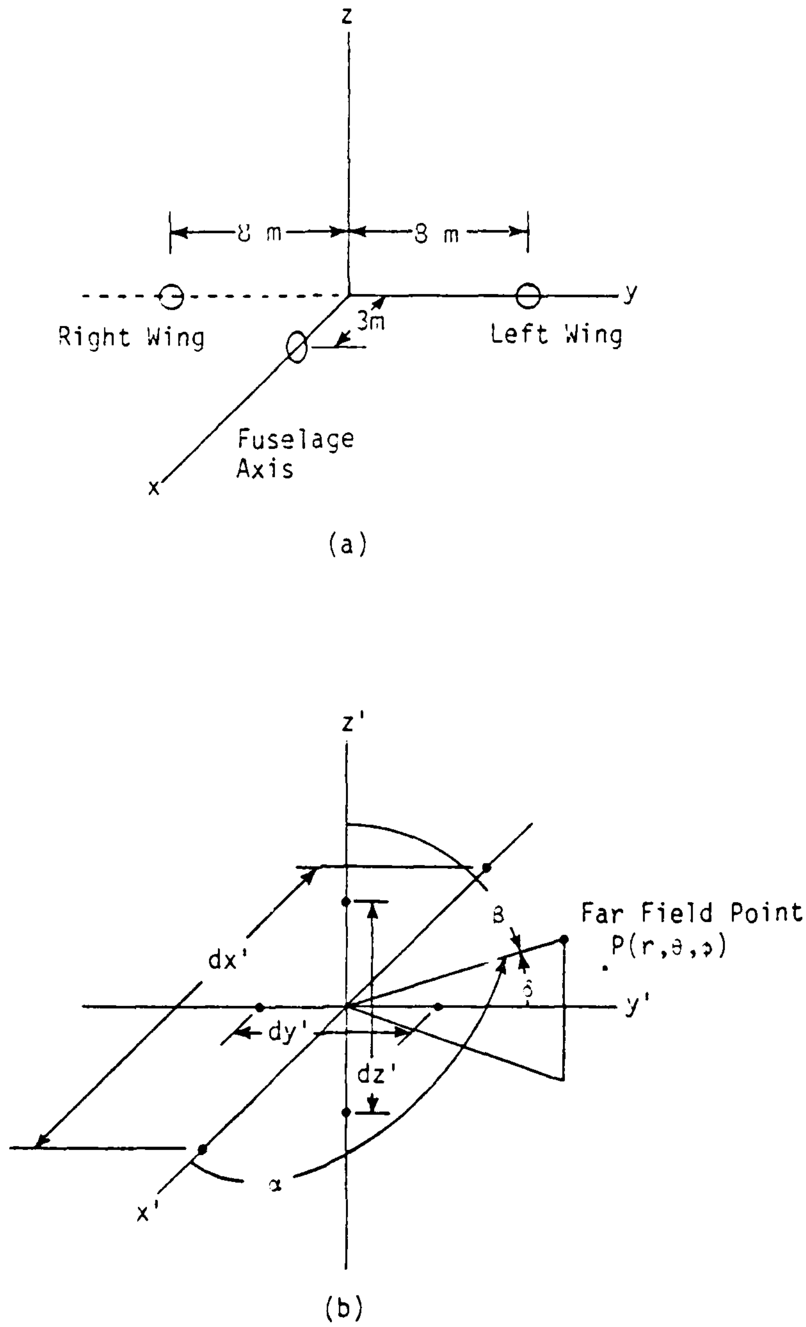

Figure 2-2. (a) Physical orientation of the ensemble scatterers.
(b) Arrangement of the two-element scatterer complexes for the coordinate systems of the fuselage and wing scattering points.

Table 2-1. Radar cross section equations for the target model scattering complexes

<u>RCS equation for all points</u>:

$$\sigma(\theta,\phi) = A(\theta,\phi)\left|A_x(\alpha) + A_y(\beta) + A_z(\delta)\right| \quad (m^2)$$

where:

$$A_x(\alpha) = \cos\left(\frac{kd_x}{2}\cos\alpha\right)$$

$$A_y(\delta) = \cos\left(\frac{kd_y}{2}\cos\delta\right)$$

$$A_z(\beta) = \cos\left(\frac{kd_z}{2}\cos\beta\right)$$

α, δ, β are assumed the same for each scatterer and are defined in Figure 2-2.

Fuselage (FUS)	*RH Wing (RW)*	*LH Wing (LW)*
d_x = 10m	d_x = 6m	d_x = 6m
d_y = 2m	d_y = 4m	d_y = 4m
d_z = 2 m	d_z = 2m	d_z = 2m

<u>Amplitude Envelopes</u>

$$A_{FUS}(\theta,\phi) = \begin{cases} (10(\theta-\pi/2)^2 + 1)\left(\frac{75}{(\pi/2)^2}\phi^2 + 8\right) & -\frac{\pi}{2} \le \phi \le \frac{\pi}{2} \\ (10(\theta-\pi/2)^2 + 1)\left(\frac{75}{(\pi/2)^2}(\pi-\phi)^2 + 8\right) & \frac{\pi}{2} < \phi < \frac{3\pi}{2} \end{cases}$$

$$A_{RW}(\theta,\phi) = (100(\theta-\pi/2)^2 + 1)(1 - \sin(\phi))$$

$$A_{LW}(\theta,\phi) = (100(\theta-\pi/2)^2 + 1)(1 + \sin(\phi))$$

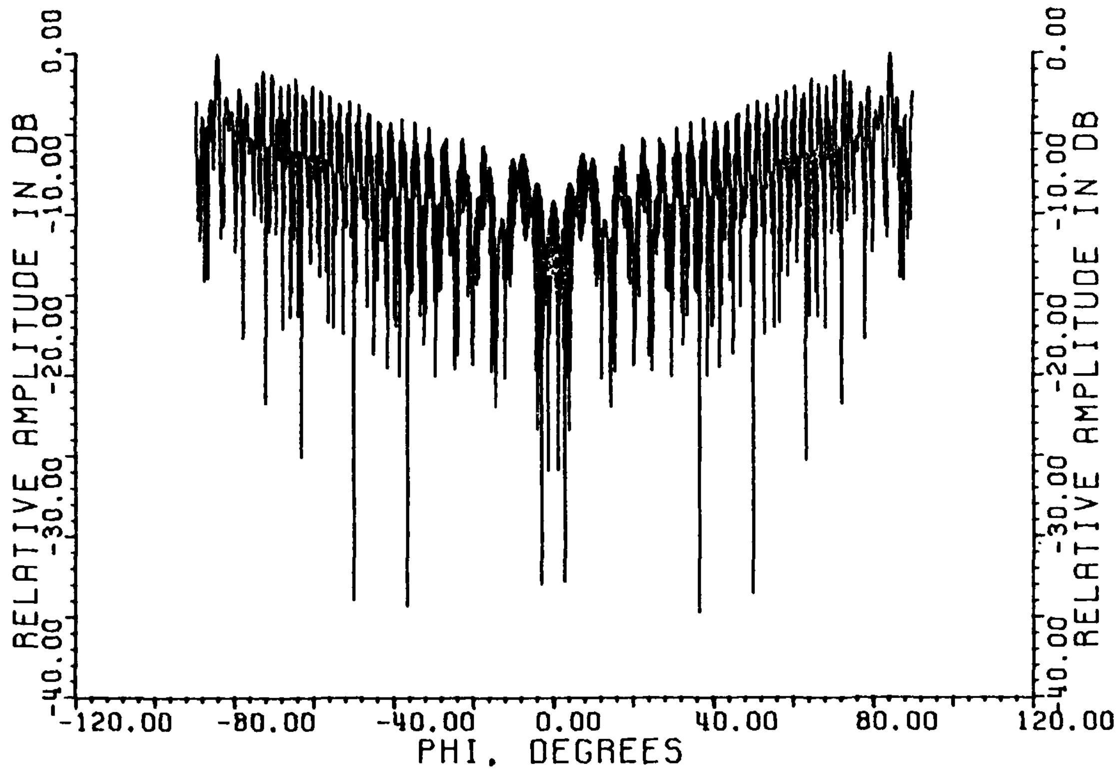

Figure 2-3. Radar cross section of fuselage scattering complex in azimuth, with the azimuth angle measured from the nose axis of the coordinate system.

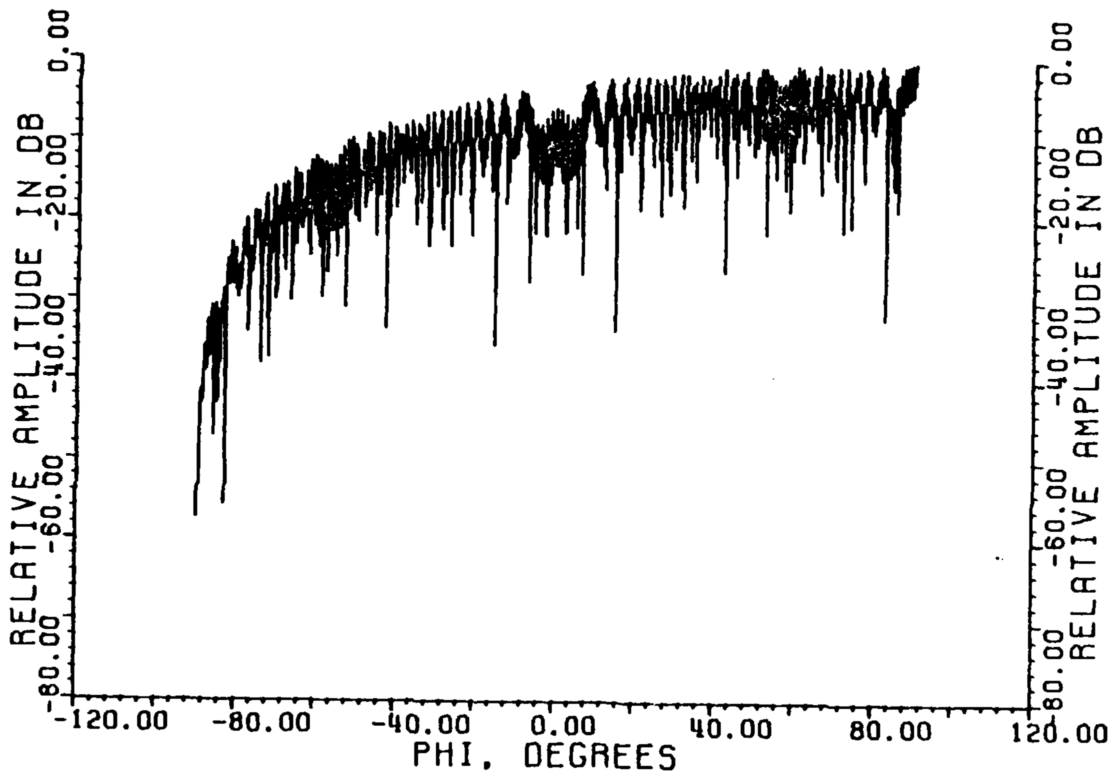

Figure 2-4. Radar cross section of right wing scattering complex in azimuth, with the azimuth angle measured from the nose axis of the coordinate system.

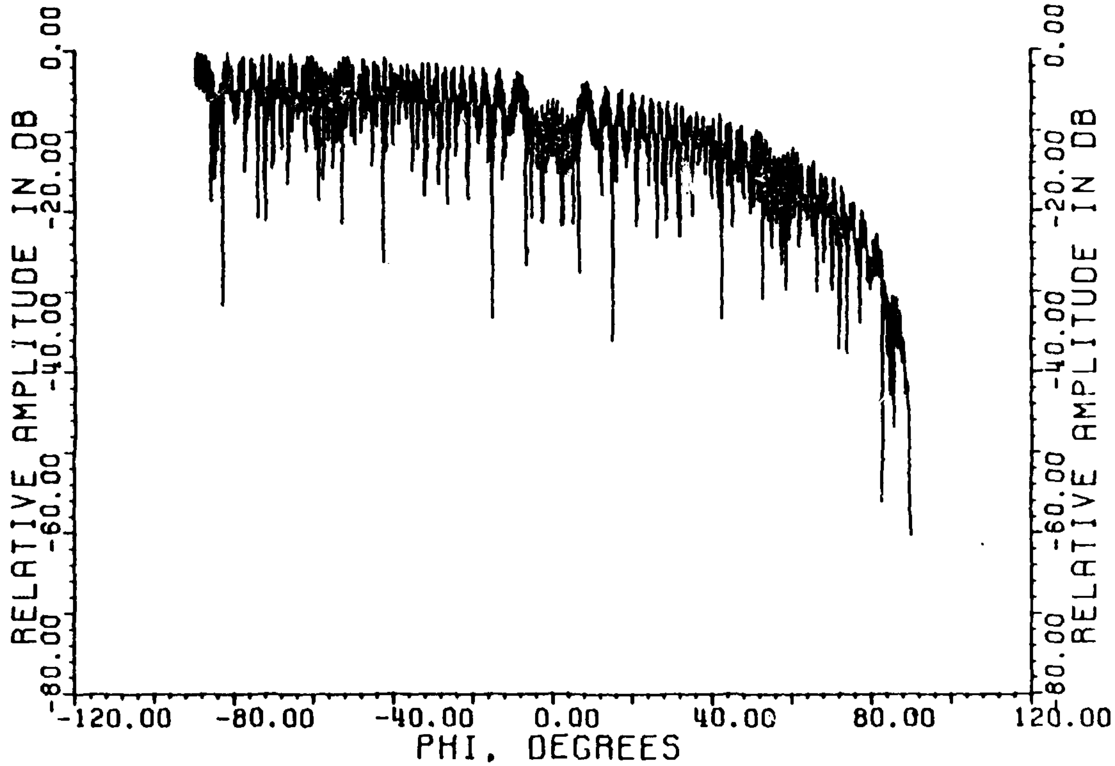

Figure 2-5. Radar cross section of left wing scattering complex in azimuth, with the azimuth angle measured from the nose axis of the coordinate system.

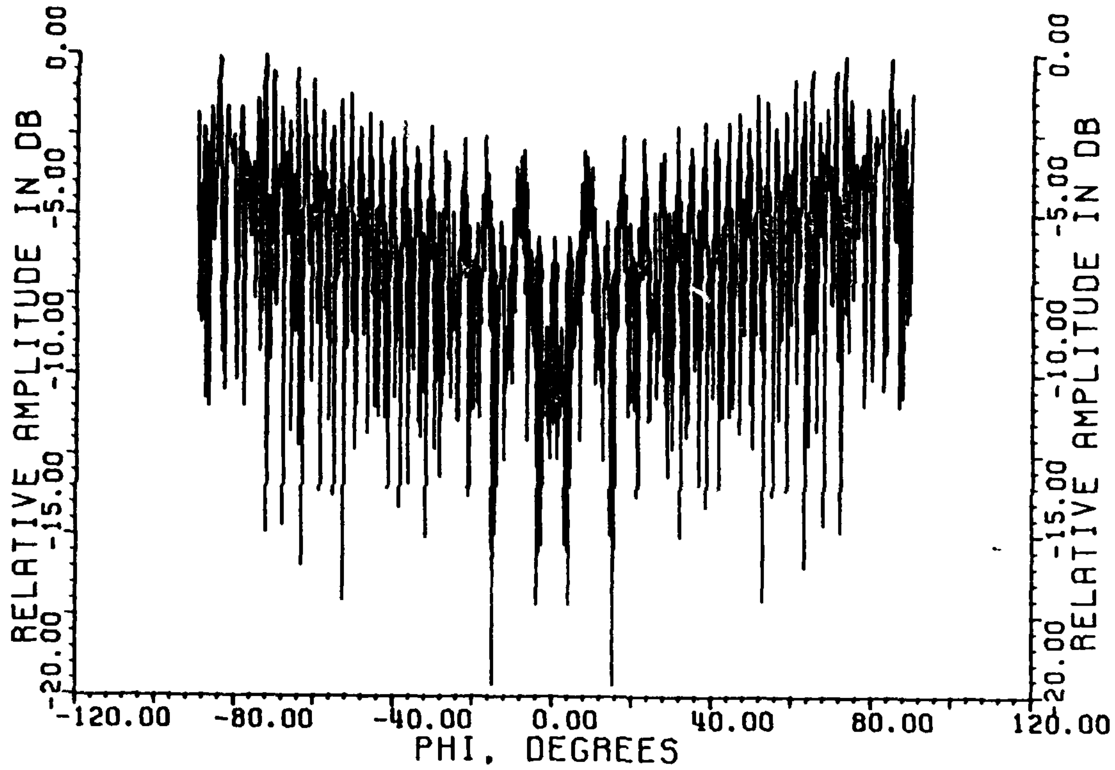

Figure 2-6. Composite cross section in azimuth, with the azimuth angle measured from the nose axis of the coordinate system.

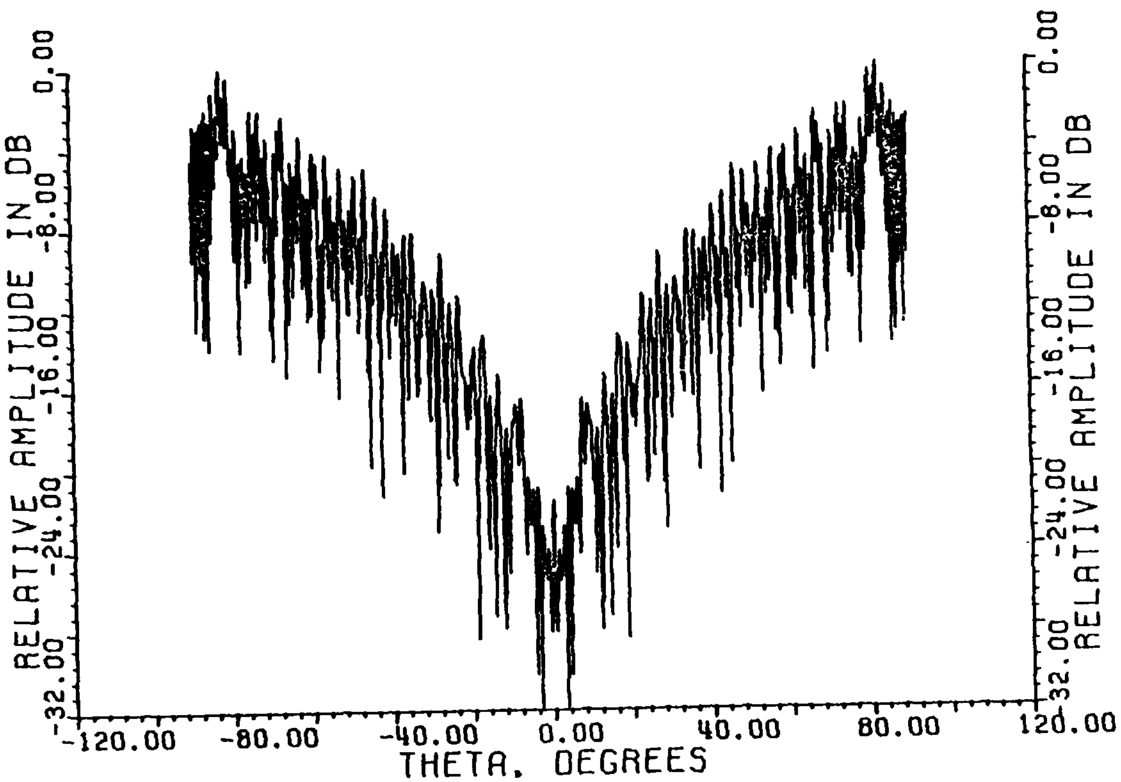

Figure 2-7. Composite cross section in elevation, with the elevation angle measured from the nose axis of the coordinate system.

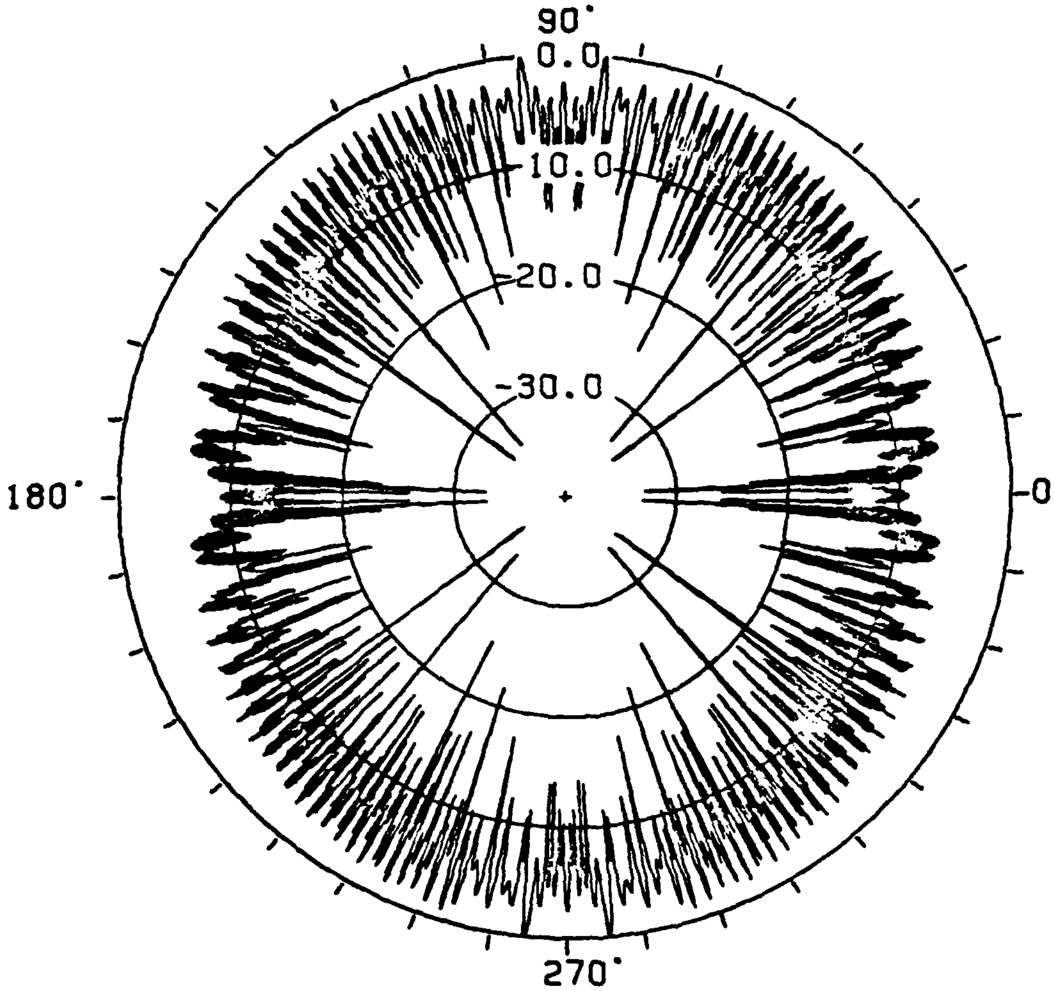

Figure 2-8. Radar cross section of fuselage scattering complex in azimuth, with the azimuth angle measured from the nose axis of the coordinate system. Amplitudes are in dB down from maximum.

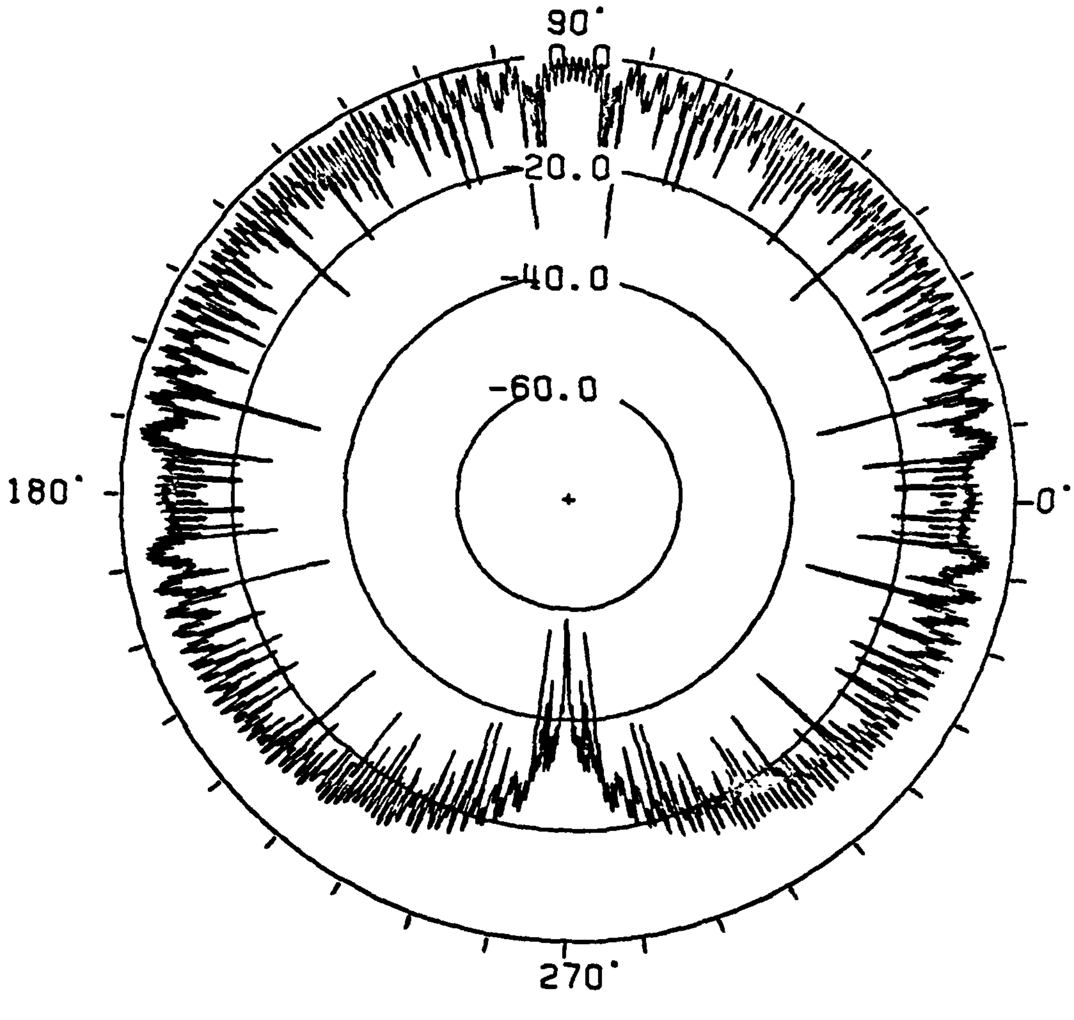

Figure 2-9. Radar cross section of right wing scattering complex in azimuth, with the azimuth angle measured from the nose axis of the coordinate system. Amplitudes are in dB down from maximum.

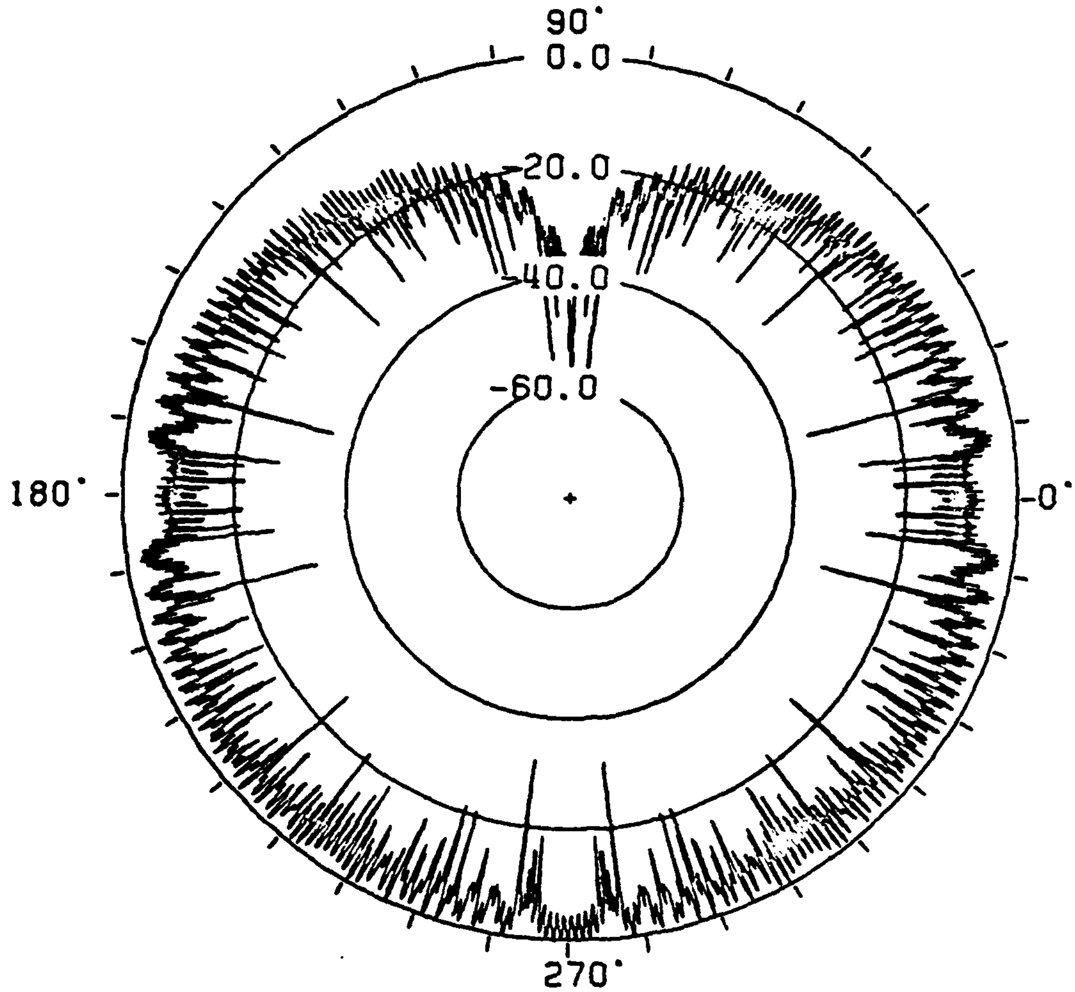

Figure 2-10. Radar cross section of left wing scattering complex in azimuth, with the azimuth angle measured from the nose axis of the coordinate. Amplitudes are in dB down from maximum.

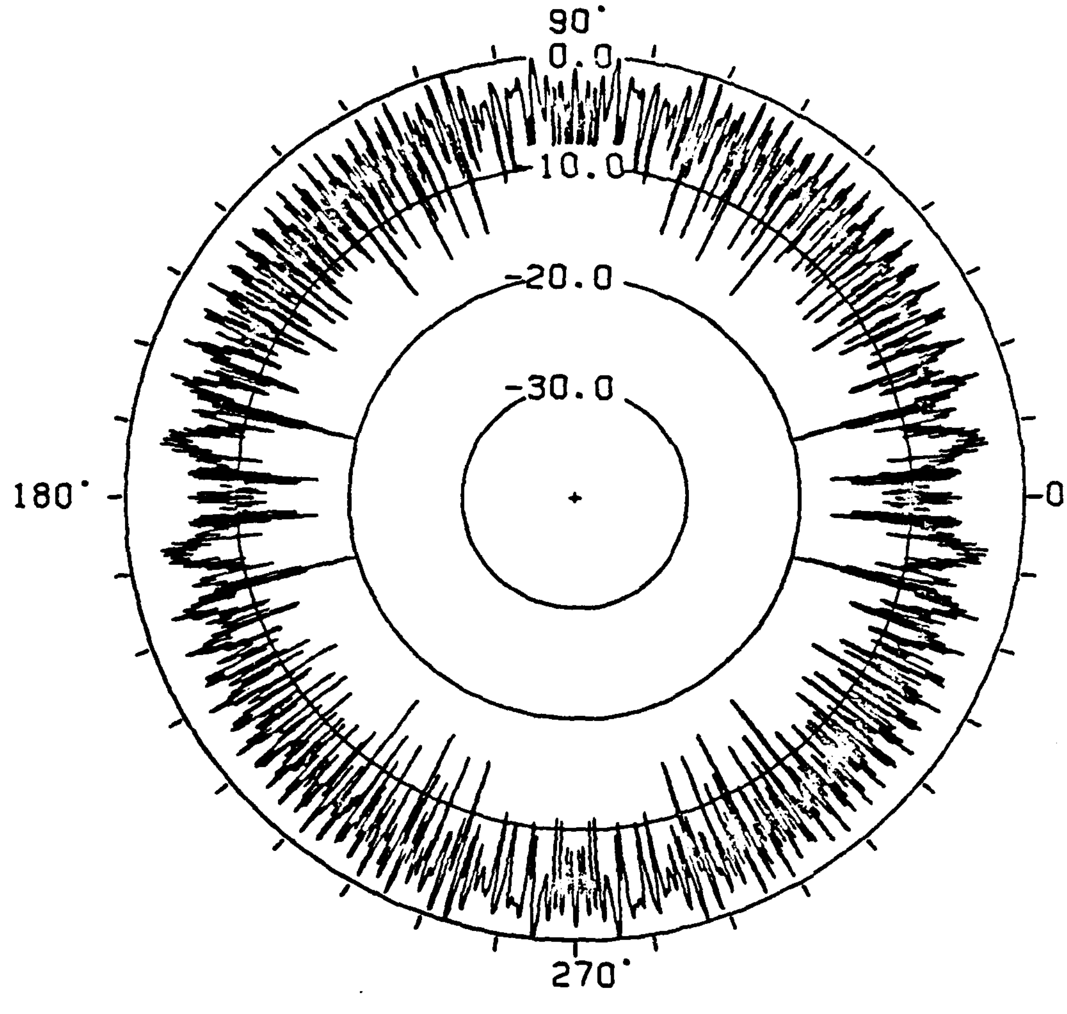

Figure 2-11. Composite cross section in azimuth, with the azimuth angle measured from the nose axis of the coordinate system. Amplitudes are in dB down from maximum.

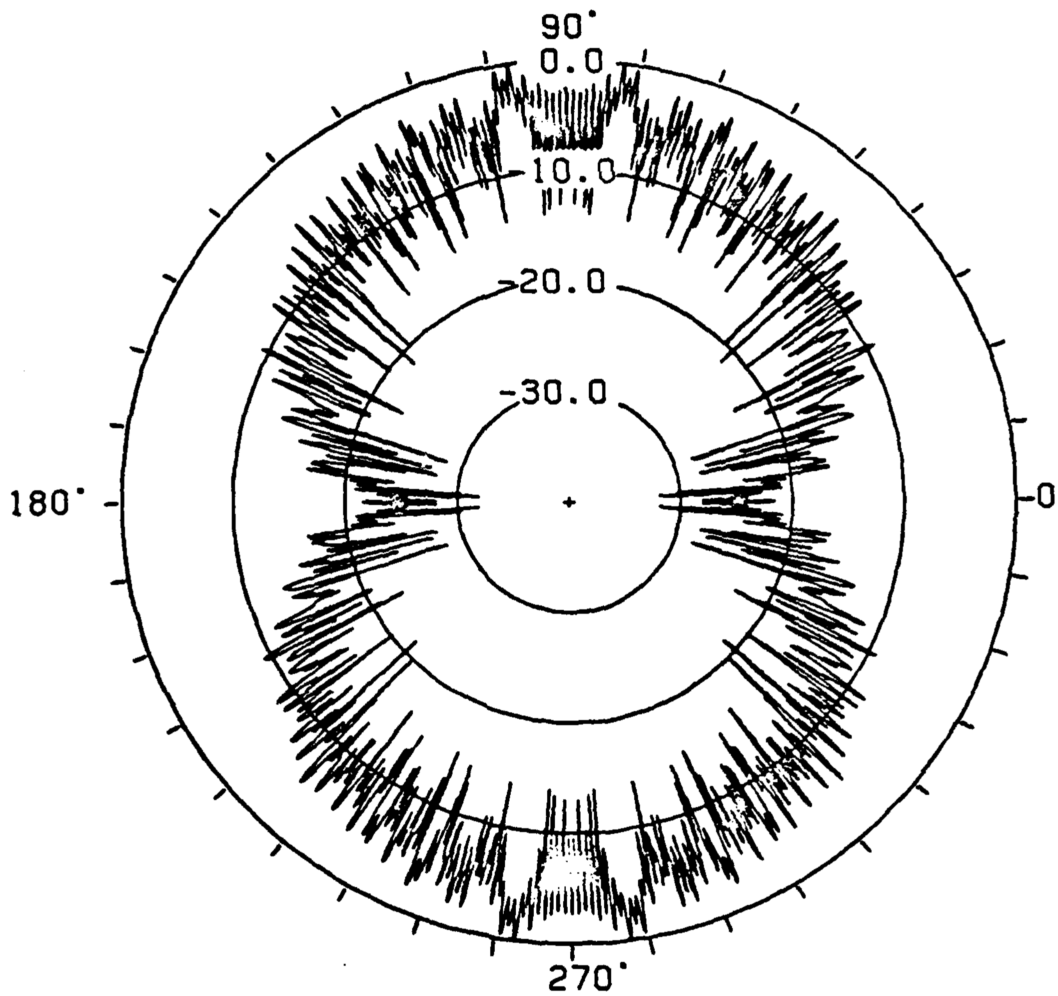

Figure 2-12. Composite cross section in elevation, with the elevation angle measured from the nose axis of the coordinate system. Amplitudes are in dB down from maximum.

added to the resultant return on a power basis. The magnitude of the noise power is such that the variance of the noise is 15 dB down from a relative maximum scan (without noise) at far range.

To simulate turbulence, the target coordinate system is allowed roll, pitch, and yaw, with the origin of the target coordinate system locked on the 3.5 degree glideslope. To simulate calm air, the target model maintains a "wings level" attitude for the duration of the flight.

The target returns are calculated with the simplified form of the radar equation [7], and are output to the centroid estimators. The basic system parameters are listed in Table 2-2.

Table 2-2. Parameters for landing system simulation.

Frequency	9.1 GHz
Pulse repetition frequency	6 KHz
Target initial elevation	56.6 mrad
Target model initial range from touchdown	6890 meters
Target model speed	148.6 mph
Turbulence rates	10 deg/s roll
	5 deg/s pitch
	5 deg/s yaw
Signal-to-noise ratio at a far range	15 dB
Antenna beamwidth (null-to-null)	
Azimuth	1.83°
Elevation	1.77°
Simulation duration	103 scans

III. SIGNAL PROCESSING

The computer simulation just described creates a sequence of scan returns from the target. In order to neglect the effects of multipath, this work will address itself solely to that data generated by the scan in azimuth. The target centroid is calculated from the returns as follows. A threshold determined from the scan returns is applied to the scan. Moving in from the edges of the scan, the first occurrence of two consecutive return voltages exceeding the threshold is located. The outermost of those return voltages are tagged as the edge-points of the target. Since the angle to the returns are known, the centroid of the target is judged to be midway between the edge-points.

Three methods of setting the threshold are used in this work. Two are the mean, and median, post-determined thresholds. That is, the target is scanned and the returns are recorded. The mean of the scan returns is calculated, and a threshold is set at that level. Likewise, the median scan return is found and a threshold is set at that level.

A third method is a pre-determined thresholding method. The antenna beam is placed in the center of the scanning window to measure the anticipated maximum return from that scan. The threshold is set 12 dB down from that return level, which was empirically determined as optimal with regard to certain system model parameters. When two consecutive returns are above the 12 dB threshold, the edge is marked and the scanning translates to the other side to determine the other edge-point. The requirement that the target be fully scanned no longer exists for this method, so that fewer pulses are needed to locate the target with little or no increase in estimating error.

A fourth method used is a non-thresholding technique called the radar centroid (RADARCG), similar to that used by Gordon and Casowitz [8]. This estimator weights each antenna pointing angle in the scanning window by the return from that angle, and divides the sum of the weighted angles by the sum of the weights (returns). The result is the angle to the center of gravity of the body of the return. Since it requires that the window be fully scanned, all available pulses are used.

The above methods form the basis for comparison with the centroid algorithm based upon return amplitude-versus-angle signature introduced next.

IV. THE TARGET CENTROID ESTIMATING ALGORITHM

Introduction

Since all target centroid estimators are based on scan returns, it is instructive to examine the flight scan-return history of a target. Figure 4-1 is the scan return history of the model in still air without noise added, which shall now be referred to as a baseline flight. This plot was made with the target in the center of the scanning window. The first and last beam pointing locations have negligible return amplitudes since a null-to-null cross track is employed; the first null in the antenna pattern is placed on the target at those beam locations. As is to be expected, the maximum return occurs in the center of the scan. It is readily seen that the scan returns over the flight are modulated, specifically by the scintillation of the target model radar cross section. In particular, note scan number 90. At this scan, the antenna is clearly in a null of the target RCS. We can also pick out scans 78, and with greater difficulty, scan 58, as being in nulls of the target model cross section. It is in these scans, with poor target returns, that we would expect the target location error of the estimators to increase.

A flight with noise is shown in Figure 4-2. The two large bodies of return between scans 58 and 90 are still clearly seen, but the effect of noise is pronounced on the rest of the flight. Beam pointing locations 1 and 49 are no longer at zero amplitude, but vary with noise. It is clearly seen from observation of scans 90, 78, and 58 that an accurate

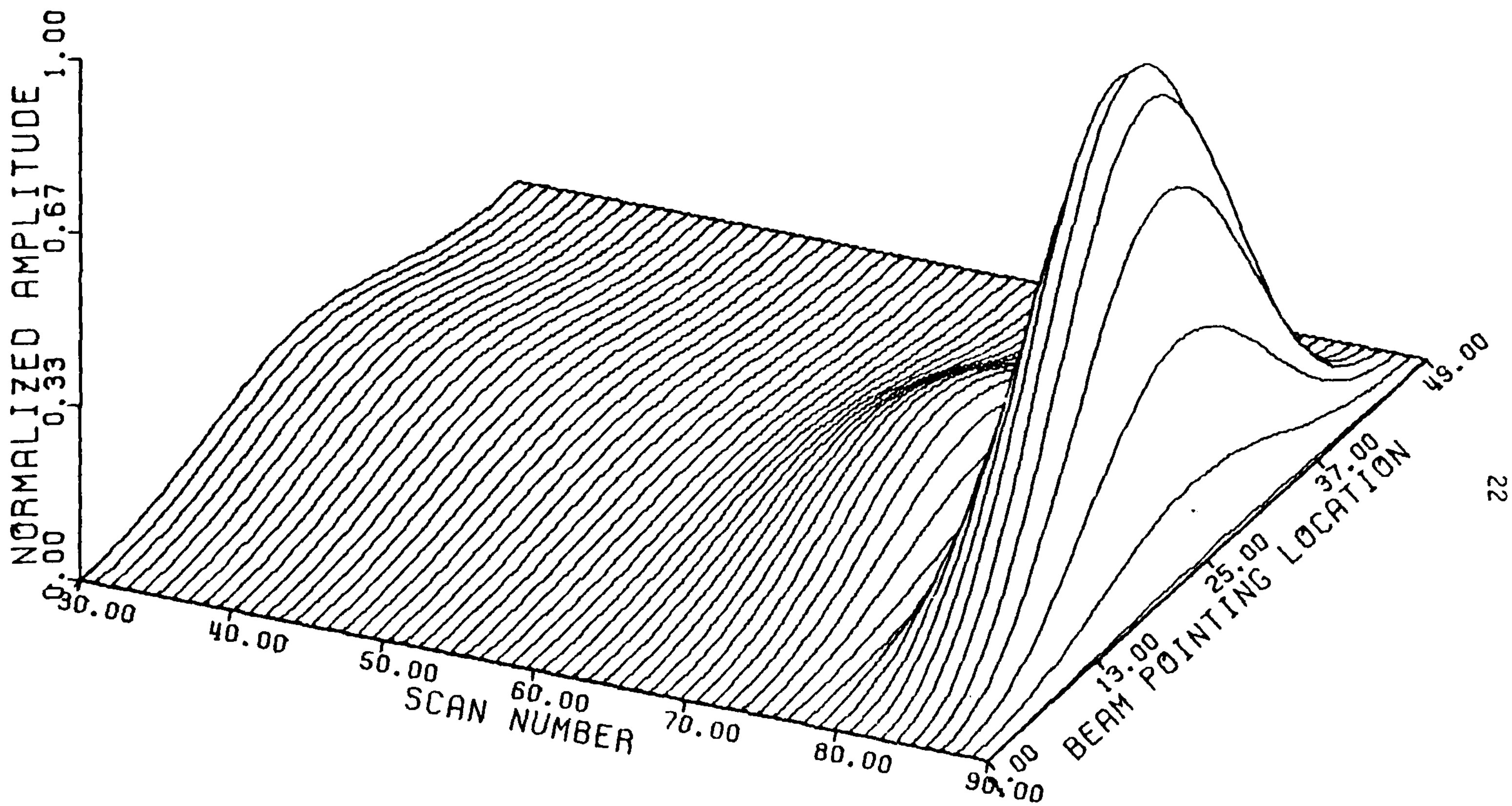

Figure 4-1. Target return history for a baseline flight with 49 beam pointing locations in the scanning window, with the target in the center of the cross track, azimuth scan. Shown is a portion of the flight from the 30th to the 90th scan, inclusive.

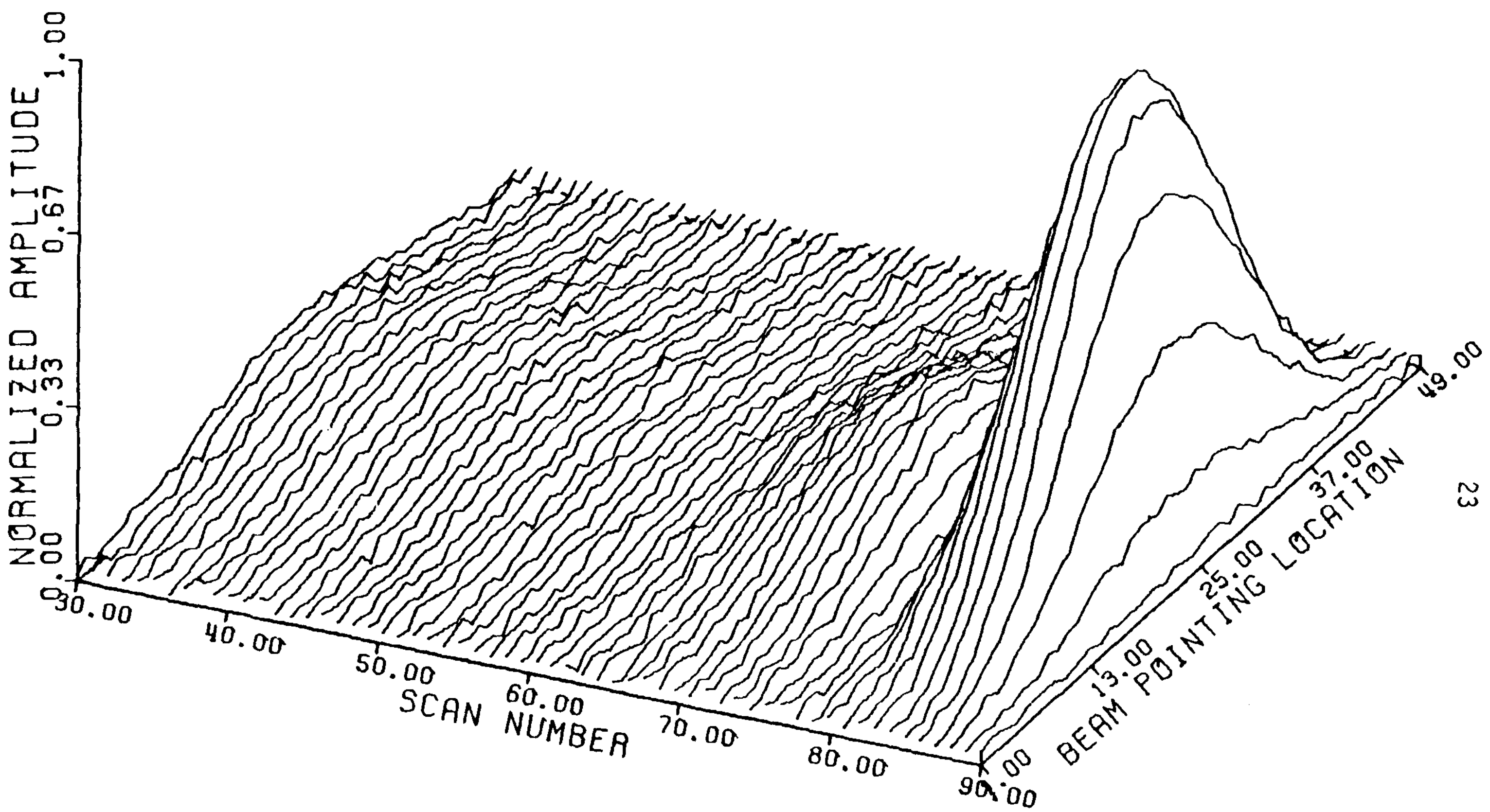

Figure 4-2. Target return history for a baseline flight with noise added, 49 beam pointing locations in the scanning window, target in the center of the cross track, azimuth scan. Shown is a portion of the flight from the 30th to the 90th scan, inclusive.

determination of the presence of a target at those scans would be very difficult and prone to error, whereas the detection of the target with a good signal return, even in the presence of noise, is less prone to error.

Figure 4-3 is of a baseline flight with turbulence. The many nulls in this plot are the result of the modulation of the target model radar cross section on the target returns as the model rotates on its axis in simulation of turbulent wind conditions. Again, beam locations 1 and 49 exhibit negligible returns as the null in the antenna pattern is on the target.

Addition of noise to the flight with turbulence is shown in Figure 4-4. The many returns that were of low signal level are now filled in with noise. Only those scans whose signal level rises above the noise are suitable for target detection.

It is in this light that the work to develop a new centroid algorithm was conducted. The goal was to produce an algorithm which would be able to determine which scans are suitable for target detection and location - and to discard all others.

Before proceeding, a determination of the expected scan signal-to-noise ratios in a typical flight is in order. Three baseline flights with noise were made with the target at the initial point 3.72 nmi from touchdown to the release point. Figure 4-5 is the flight with a granularity of 9 beam pointing locations in the scanning window, Figure 4-6 has a granularity of 29, and Figure 4-7 has a granularity of 49 beam pointing locations. It is seen that the SNR amplitude over the flights have the same envelope for all granularities. That is, all are around 14

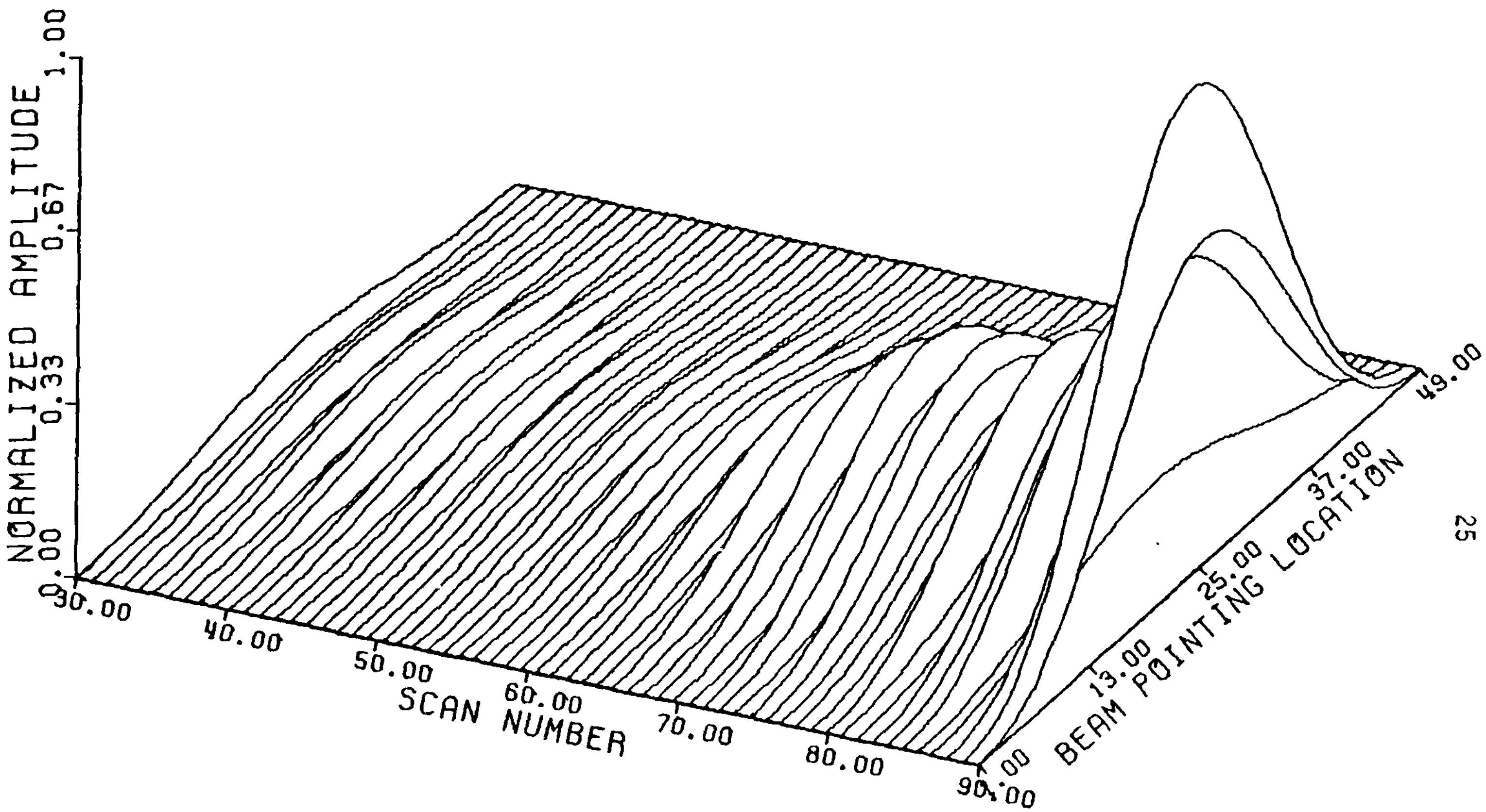

Figure 4-3. Target return history for a baseline flight with turbulence added, 49 beam pointing locations in the scanning window, target in the center of the cross track, azimuth scan. Shown is a portion of the flight from the 30th to the 90th scan, inclusive.

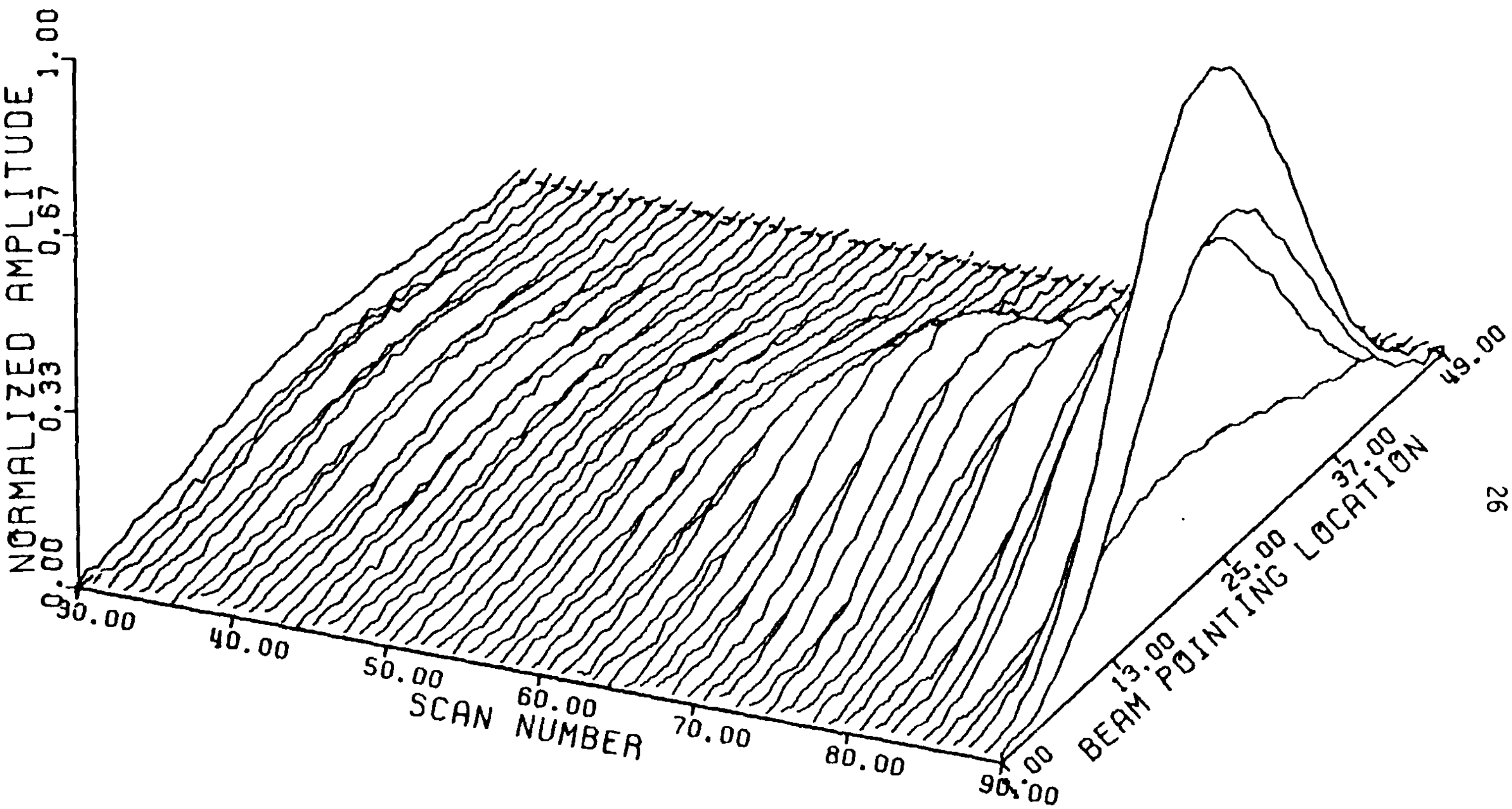

Figure 4-4. Target return history for a baseline flight with noise and turbulence added, 49 beam pointing locations in the scanning window, target in the center of the cross track, azimuth scan. Shown is a portion of the flight from the 30th to the 90th scan, inclusive.

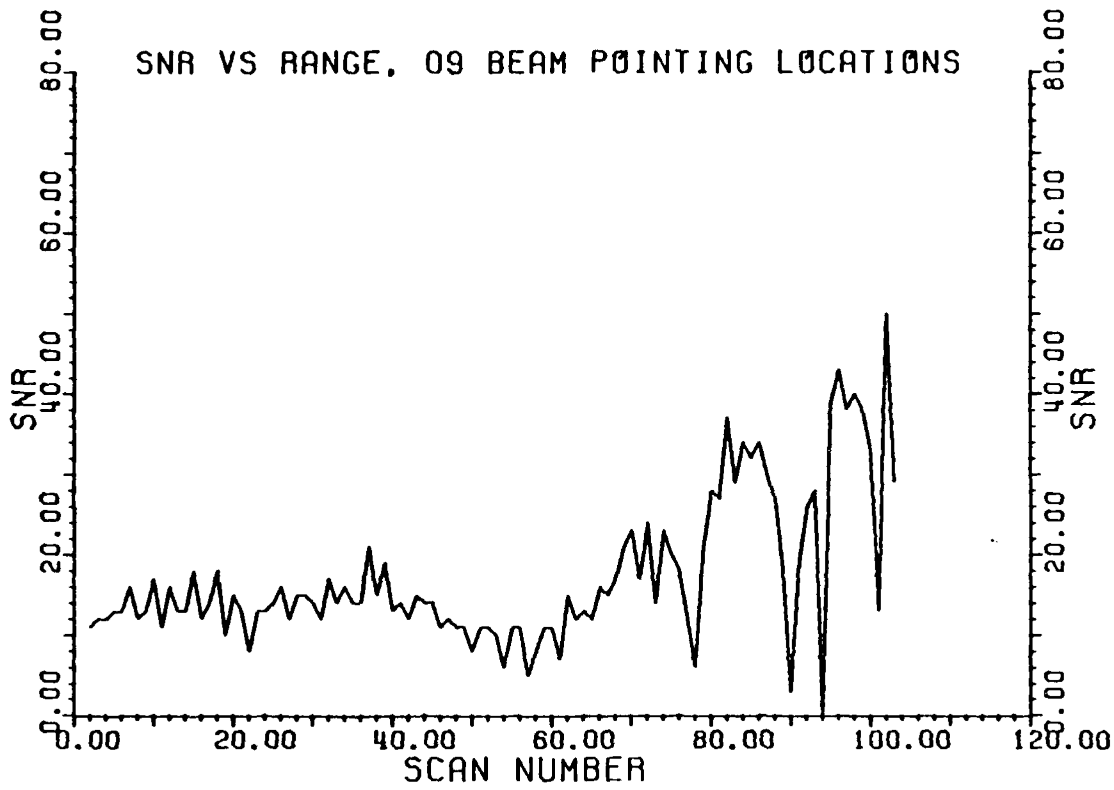

Figure 4-5. SNR versus range for a flight with noise and a scanning window containing 9 beam pointing locations, plotted as a function of scan number.

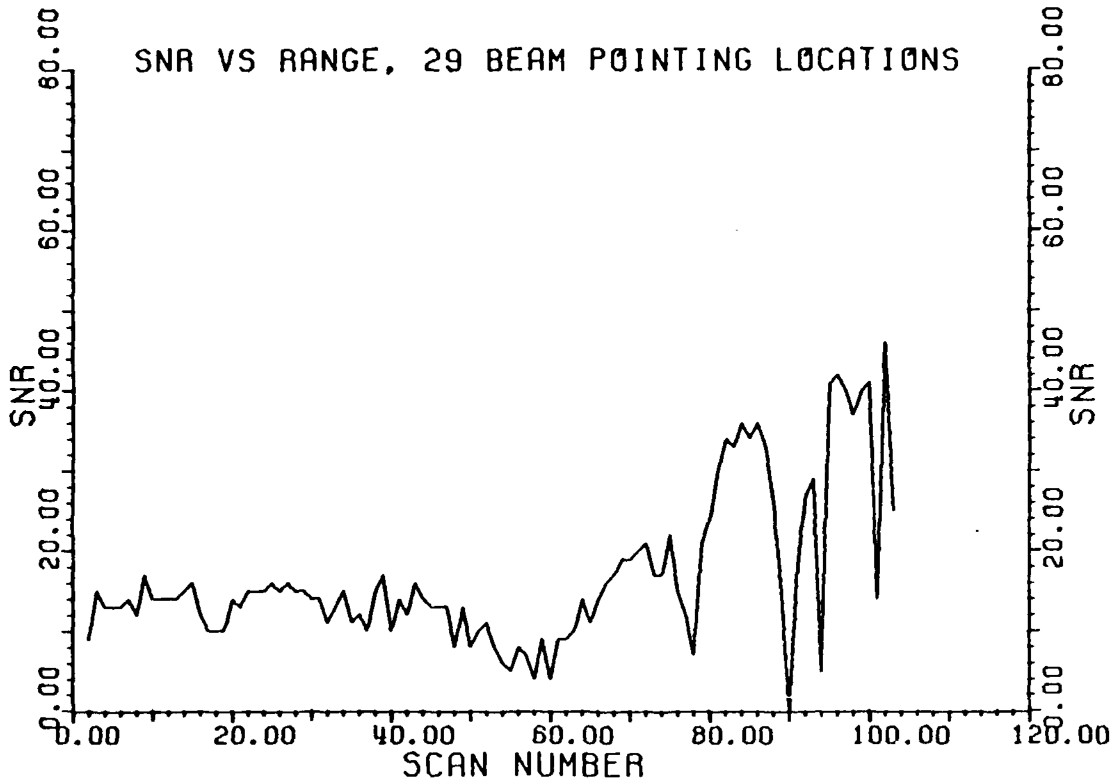

Figure 4-6. SNR versus range for a flight with noise and a scanning window containing 29 beam pointing locations, plotted as a function of scan number.

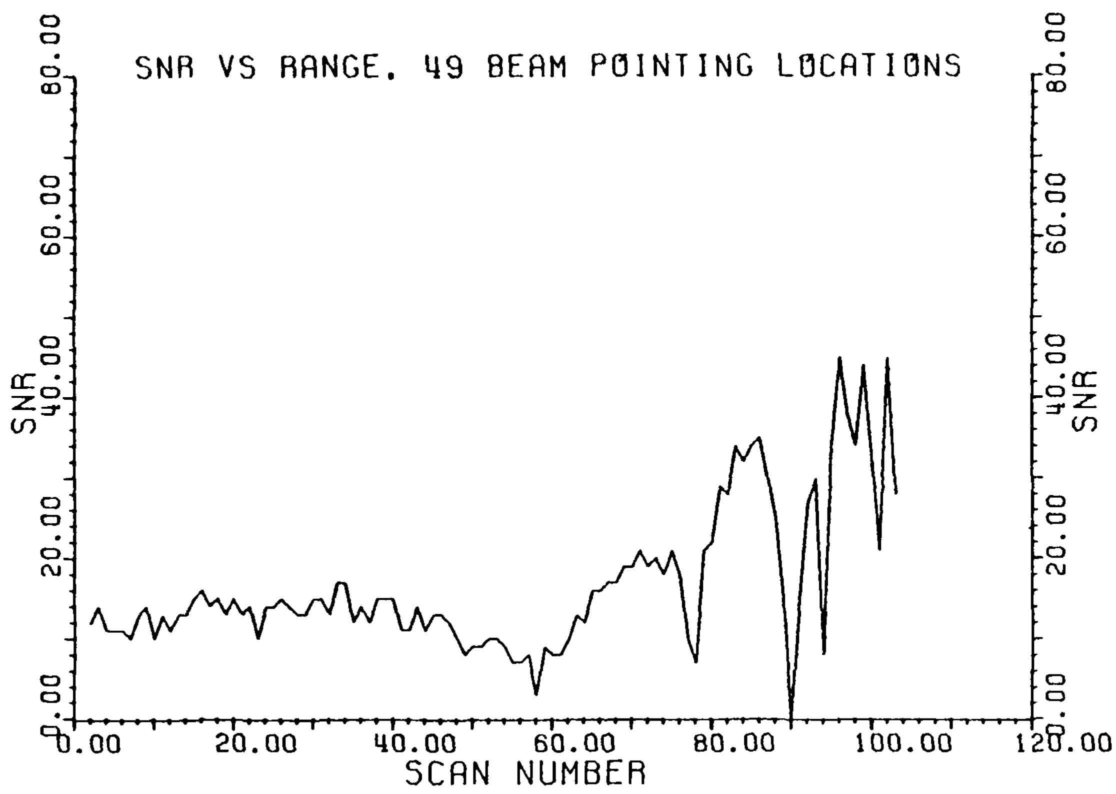

Figure 4-7. SNR versus range for a flight with noise and a scanning window containing 49 beam pointing locations, plotted as a function of scan number.

dB until the vicinity of the fiftieth scan where the SNR drops a bit, due to a relative null in the RCS of the target. From there the SNRs generally increase significantly as the target draws nearer to the release point. Note that in all three plots there are nulls at scan numbers 58, 78, and 90, which verify the observations made earlier on Figures 4-1 and 4-2. There are also nulls at scans 94, 101, and 103 on the plots. The fact that the nulls appears on all three plots, that is, independent of granularity, at those scans is due to a peculiarity of this simulation. In order to reduce computer execution time, the target is not scanned 10 times a second as in the actual system, but rather the entire flight is broken into equal time units of such a length as to provide a large number of scans for a statistical analysis while keeping the execution time down. This was done by scanning the target, moving it down the glidepath, scanning it again, etc., until the release point was reached, yielding a large dead time between scans. In order to provide an equal number of statistical data points for all flights regardless of granularity (and therefore independent of the number of pulses transmitted), the dead time between scans is variable. It is the greatest when the granularity is 9, and the least when there are 49 pulses to be transmitted. Each scan begins at the same range from touchdown. Therefore, range and scan number are related, and will be used synonymously in this work. So the fact that nulls occur at scans 58, 78, 90, 94, 101, and 103, regardless of granularity, is because the target is at the same point in space at the beginning of the scan. The target position at the end of the scan will vary according to the number of pulses that need to be transmitted in the scanning window.

Returning to Figures 4-5, 4-6, and 4-7, it is seen that all the target centroid estimators must work with scan signal-to-noise ratios of around 14 dB for at least half of the flight.

Figures 4-8, 4-9, and 4-10 are of a typical flight with noise and turbulence for granularities of 9, 29, and 49 beam pointing locations, respectively. All plots show a general degradation in the SNR due to the fluctuating target model RCS in turbulence. Half the flight is now down to between 10 and 12 dB, a loss in signal strength of half from the flights without turbulence.

The Scan Return Amplitude-Versus-Angle Signature Algorithm

It is observed in Figure 4-1, which graphically depicts the scan history of a baseline flight, that all scan envelopes have a high degree of symmetry. That is, as the antenna beam illuminates the target first with the pattern null, then increasing the illumination as the main lobe moves onto the target, reaching the maximum when the beam is centered on the target, then diminishing as the target is placed in the pattern null, the overall scan envelope takes on a bell shape due to the modulation of the antenna beam. Since the return envelopes are of this shape, each side of the bell shape has a unique point, the point of maximum slope. Returning to Figure 4-2 it is observed that the maximum slope of a scan with a low SNR (such as scans 58, 78, and 90) is relatively small, and those scans with large SNR's have a relatively large maximum slope. This, then, is the chosen criteria:

Find the point of maximum slope;

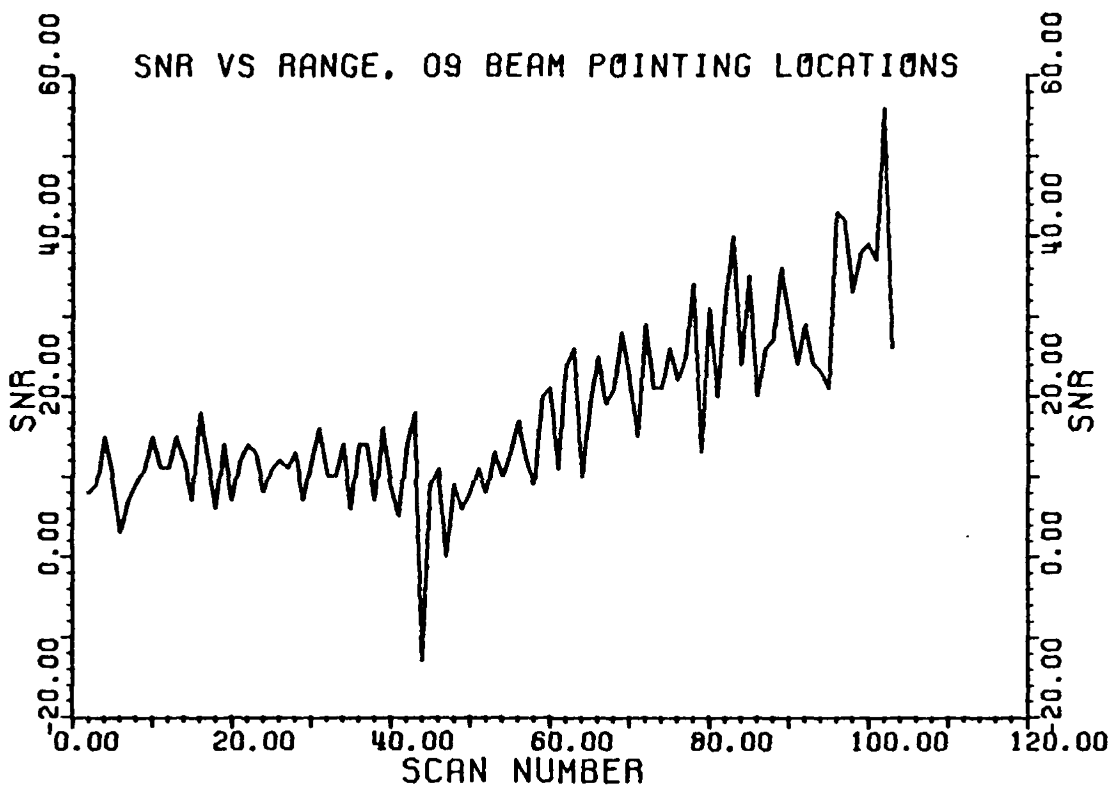

Figure 4-8. SNR versus range for a flight with noise and turbulence and a scanning window containing 9 beam pointing locations, plotted as a function of scan number.

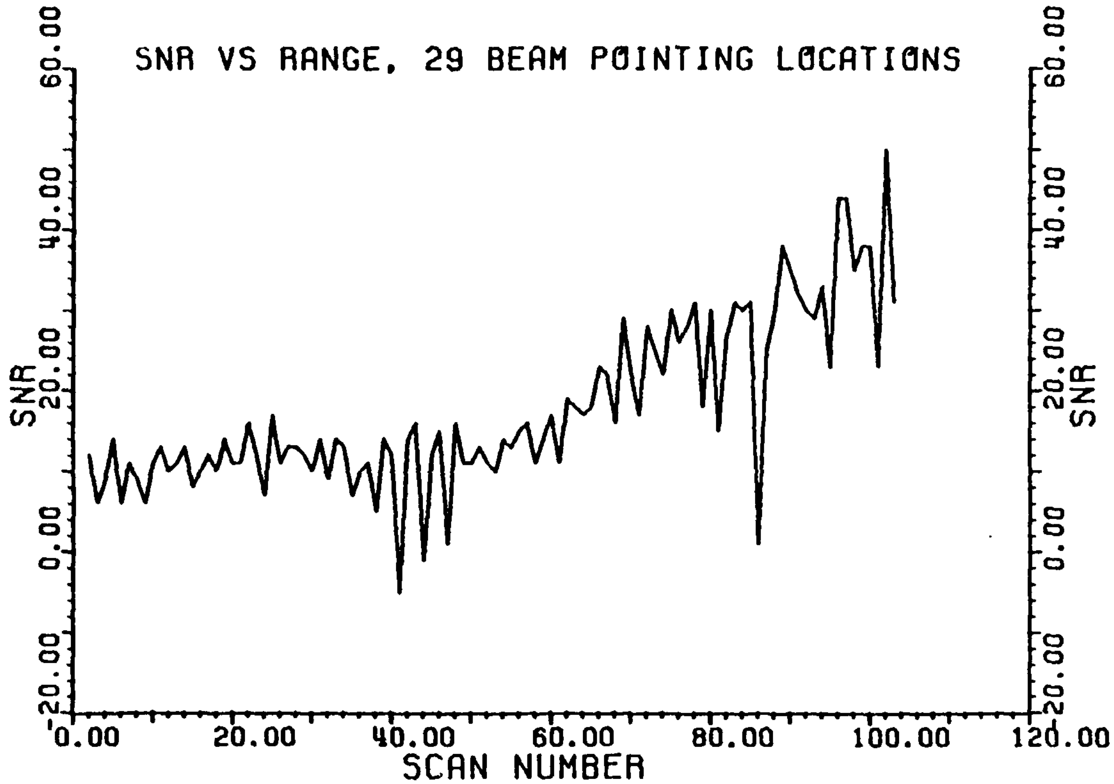

Figure 4-9. SNR versus range for a flight with noise and turbulence and a scanning window containing 29 beam pointing locations, plotted as a function of scan number.

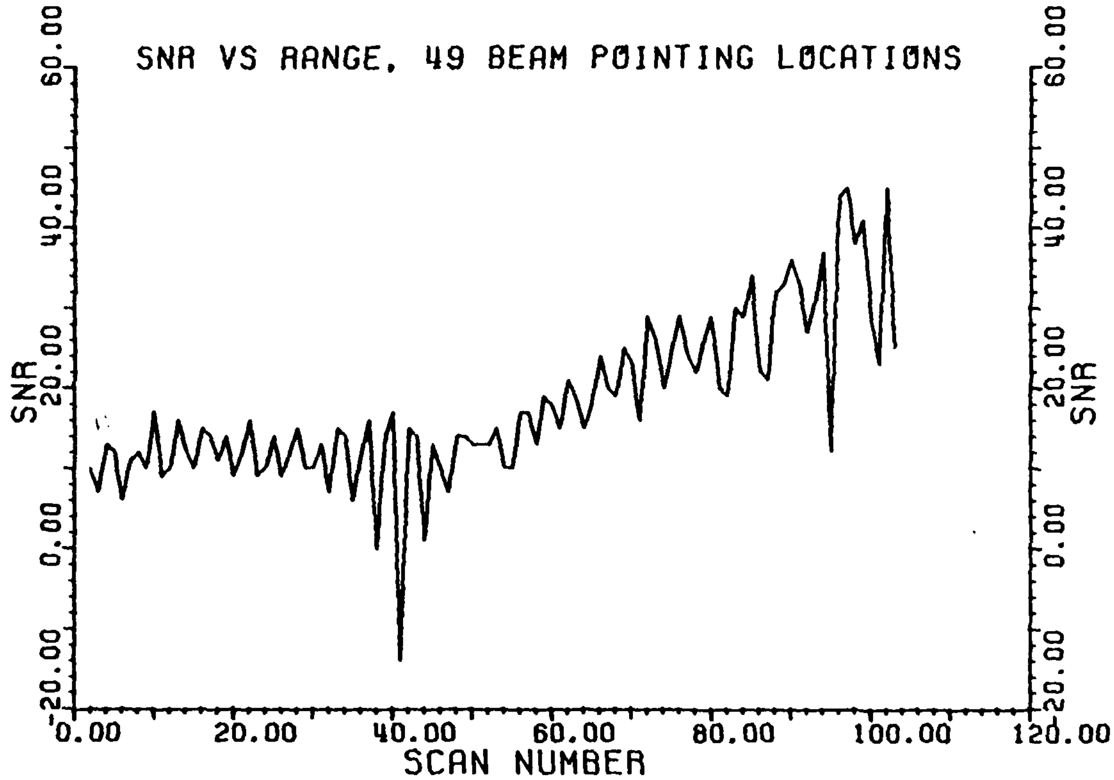

Figure 4-10. SNR versus range for a flight with noise and turbulence and a scanning window containing 49 beam pointing locations, plotted as a function of scan number.

Compare the slope at that point to a minimum acceptable value based on the characteristics of the receiver;

Accept or reject the scan;

Determine target location if the scan was accepted.

The method used to find the point of maximum slope is based on the scan shape. Referring to Figure 4-11, let us assume that we are using a cross track with a granularity of 7 beam pointing locations. The relative amplitudes of the expected returns are marked by the lettered X's on the drawing. Moving from left to right, the first three returns have a positive second derivative, since the slope $\overline{BC}$ is greater than slope $\overline{AB}$. Points B, C, and D have a negative second derivative, since slope $\overline{CD}$ is less than slope $\overline{BC}$. Since the point of maximum slope is where the second derivative is zero, that is, where the second derivative changes sign, the maximum slope must have occurred between points B and C. Having found the maximum slope, we check to ensure that its magnitude is greater than the minimum acceptable slope. If it is, the target edge is marked as being midway between points B and C, and scanning translates to the other side of the scan. The process is then repeated for returns G, F, E, and D. When the two target edges are found, the centroid is placed midway between the edge points. Since the target is located by calculating second derivatives, this method shall be referred to in this work as the second derivative method or SDRV.

A method used to integrate the scan returns with the second derivative method is as follows. The first half of the scan is broken into four equal parts, or windows, as shown in Figure 4-12. For the remainder of this work, scanning window is an area identified by the search mode

TARGET CENTROID LOCATION

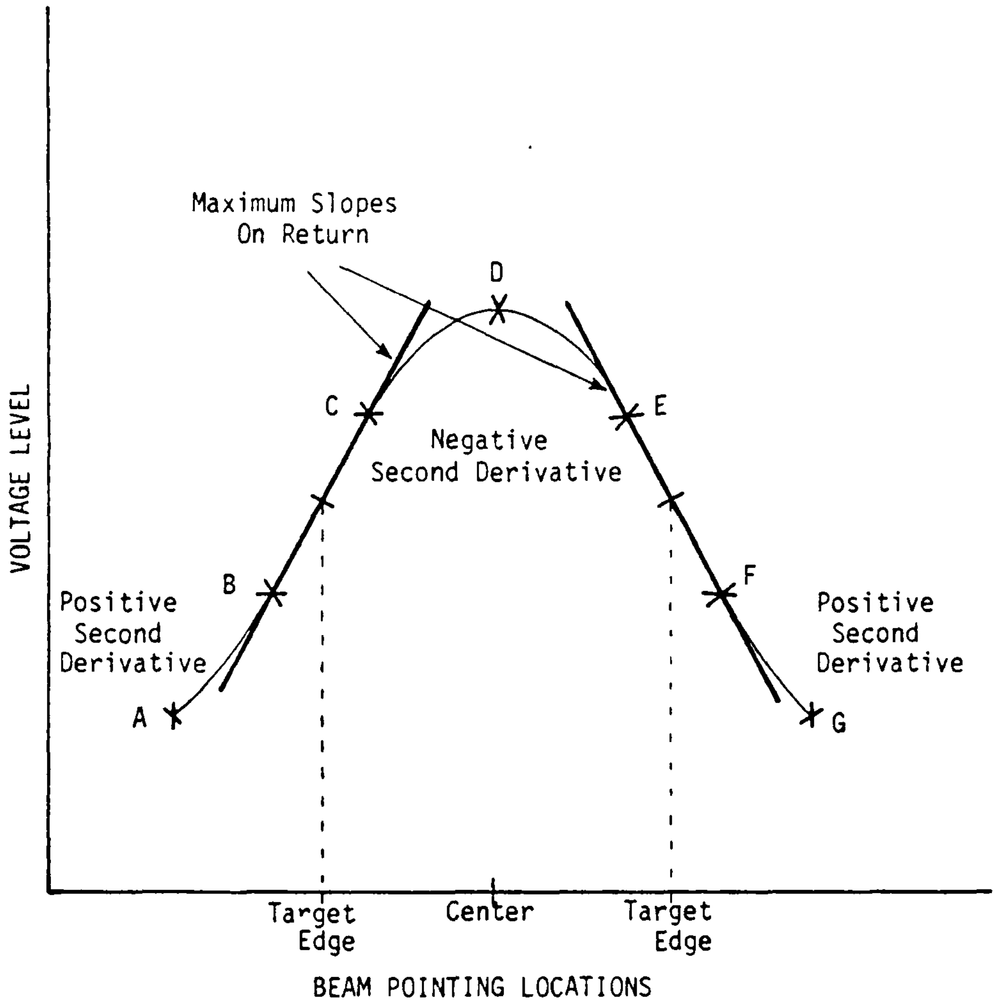

Figure 4-11. Illustration of the method employed to determine the target centroid location based on the shape of the scan envelope. The signal returns are marked by X.

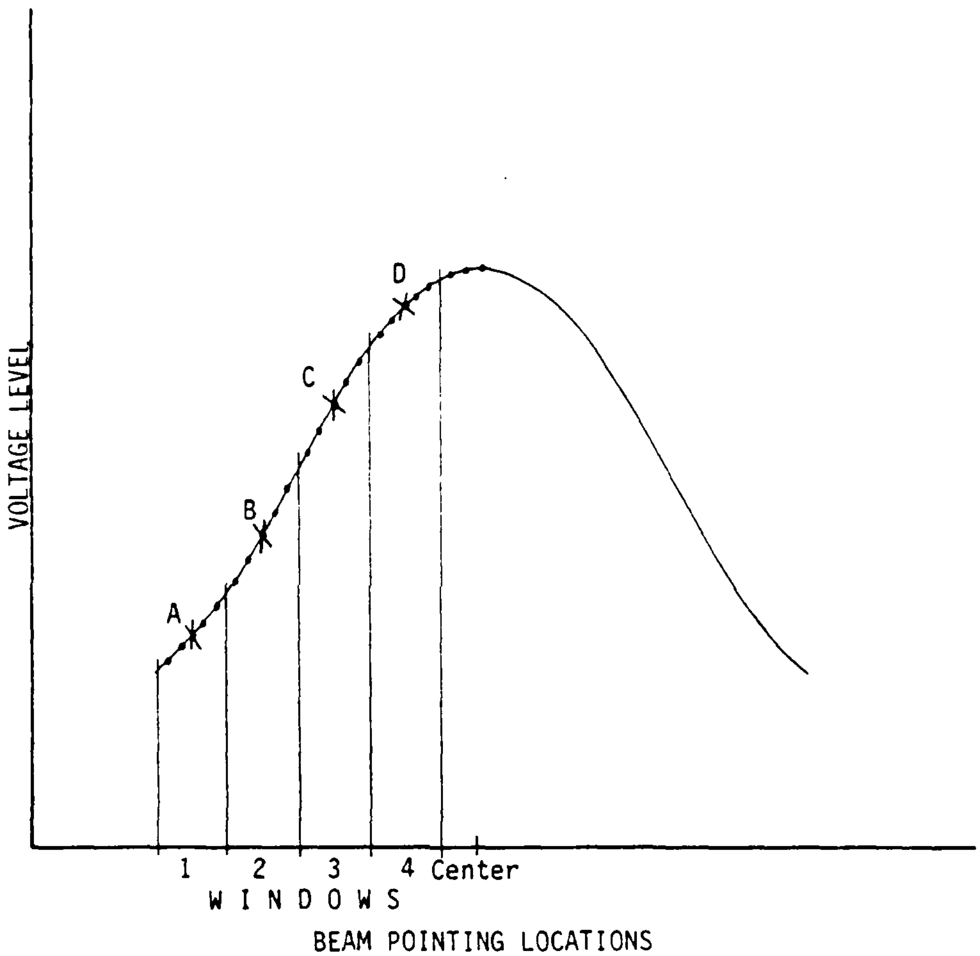

Figure 4-12. Illustration of the pulse integration technique employed with the second derivative algorithm.

of the radar which contains a target. A section of the scanning window segmented by SDRV shall be referred to as a window in this work. The number of pulses in each window is determined by the granularity and is easily calculated. The returns from the beam pointing positions inside the windows are averaged together, and the location of the averaged return is placed in the center of the window. That is, the average of the five returns in window 1 is placed in the center of the window (in this case, it has the same angular location as the third return) as shown by the average return labelled A. The amplitude of A is not necessarily equal to the center return in the window. When the four average returns A, B, C, and D, are calculated, the determination of a target edge proceeds as has been previously described in Figure 4-11. Since the noise is gaussian with zero mean, the effect of noise will decrease as more returns are placed in the window and averaged together. In the event that the averaged returns A, B, C, and D, do not satisfy the criterion, the windows are shifted one beam location to the right, and A, B, C, and D, recalculated. This process is continued until a target edge is found, whereby the scanning then translates to the other side of the target. Otherwise the scanning continues until the fourth window has shifted to within two window widths of the right side of the scanning window, in which case the scan is rejected and further pulse transmissions are aborted. In the event that a target edge was found, scanning will proceed from right to left until the last beam location in the fourth window reaches the position calculated as the first target edge. If this occurs, the scan is rejected and further transmissions aborted, but the area of the last two windows in the first target edge was rescanned, both using more pulses and being doubly sure that no target was present. No centroid location decision is determined from a rejected scan.

In this simulation, the minimum acceptable rise of the maximum slope in the scan is related to the amount of noise introduced into the flight by 1.5 times the standard deviation of the noise. This value was chosen after making many runs of the simulation and observing the effect of the minimum slope on both the number of rejected scans and on the accuracy of the estimator. The accuracy of an accepted scan is affected since, with scans of poor SNR, there may be more than one set of returns for which the criteria are satisfied, due to the effect of noise.

A third and final criterion is implemented in the algorithm. With no or little signal present, it is possible for return B to be below both returns A and C, because the probability of obtaining a negative value at any time from a zero mean gaussian process is one half. If B is a negative quantity, subtracting B from C is a large number, sometimes greater than the minimum slope criterion. To this end, return B is first compared to a voltage reference. If it is below the reference, the windows are shifted and B recalculated. The voltage reference is initially set to zero at the beginning of the flight, and is then modified as follows. Each time a set of returns is rejected, a beam pointing location drops out of window 1 in Figure 4-12 as the windows shift to the right. The return from that beam location is averaged into the existing value of the voltage reference. That is, the return is added to a register which contains the sum of all past returns dropped out of the first window. A second register is incremented by one to record the number of returns in the sum. The average is recalculated for every shift of the windows, for the duration of the flight. A voltage reference such as just described can be set at a constant level according to Ward [9] for a practical radar receiver.

In summary, the second derivative algorithm uses three criteria. In the order the criteria are implemented, they are

1) (Averaged) return B must be greater than a specified voltage reference,
2) (Averaged) returns A, B, and C must have a positive second derivative and (averaged) returns B, C, and D must have a negative second derivative, and
3) the maximum slope $\overline{BC}$ must be greater than the minimum acceptable slope.

If the scan returns satisfy the criteria, a target edge is assigned to be midway between B and C, and scanning translates to find the second target edge.

The first responsibility of the algorithm is to reject scans for which an estimate of the target position is subject to severe error. Figure 4-13 is a plot which illustrates this capability. A flight with noise was flown with a granularity of 9 beam locations in the scanning window, and with the antenna on the runway centerline. The antenna was then moved to 25 meters from the runway centerline and the target reflown. The antenna position was moved again by 25 meters, and so on, ending with the antenna located 250 meters from the runway centerline for a total of 11 flights. In all flights, and for all data in the remainder of this

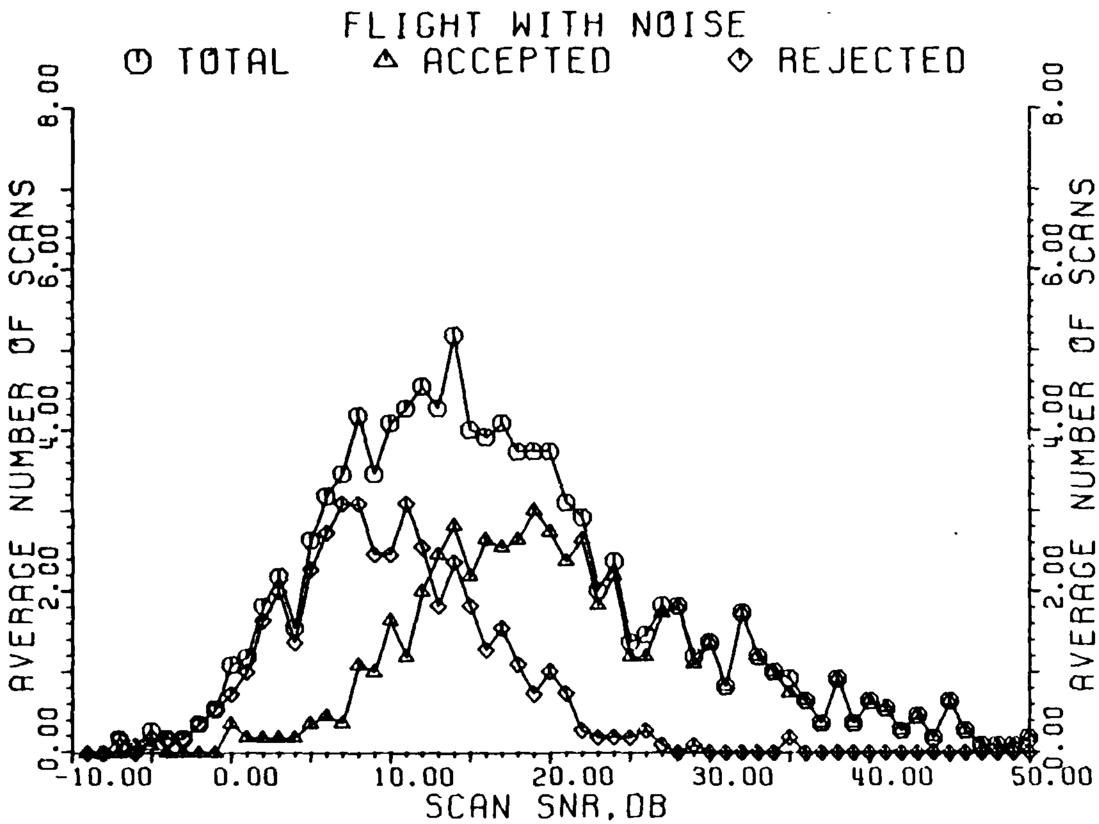

Figure 4-13. Rejection/acceptance performance of the second derivative algorithm for a granularity of 9 beam pointing locations, averaged over 11 flights with noise. Location of the target in the scanning window is randomly varied.

work, the target location in each scanning window was varied randomly. Figure 4-13 is the result of those 11 flights. It clearly shows that the average number of rejected scans closely follows the total number of scans for low scan SNRs, and decreases as the SNR increases. There the number of accepted scans increases and matches the total number of scans. The crossover point is between 12 and 15 dB.

Flights with noise and turbulence were flown as before and results plotted in Figure 4-14. There is a higher average number of scans with both low and high SNRs due to the effects of turbulence. These plots are truncated; no scan SNR less than -9 dB or greater than 50 dB were taken into account. Figure 4-14 is flatter than Figure 4-13, and the crossover point between the number of accepted and rejected scans is still about 12-15 dB.

The cumulative number of accepted and rejected scans for the flight with noise is shown in Figure 4-15. The rejected scans closely follow the total number of scans until around 10 dB, when it begins to level off and the number of accepted scans increases. On the average, 59 scans are accepted and about 44 scans rejected out of a total of 103 scans, which verify our observations of Figure 4-5 that about half the scans were in low SNR.

Figure 4-16 depicts an average flight with noise and turbulence. Here there are fewer than sixty scans accepted with 100 scans evaluated (three of the scans were below -9 dB or greater than 50 dB, and do not appear in the plot). It is again evident that there are more poor scans with turbulence than without turbulence, as was observed in Figure 4-8.

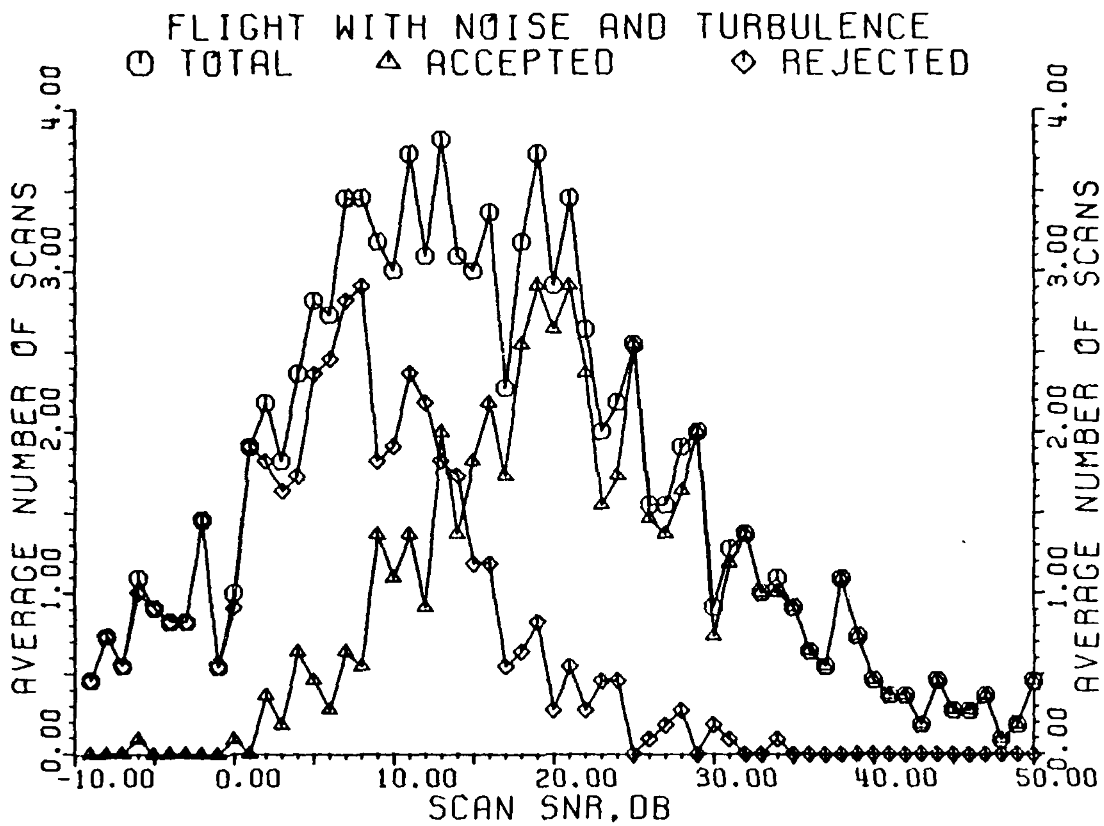

Figure 4-14. Rejection/acceptance performance of the second derivative algorithm for a granularity of 9 beam pointing locations, averaged over 11 flights with noise and turbulence. Location of the target in the scanning window is randomly varied.

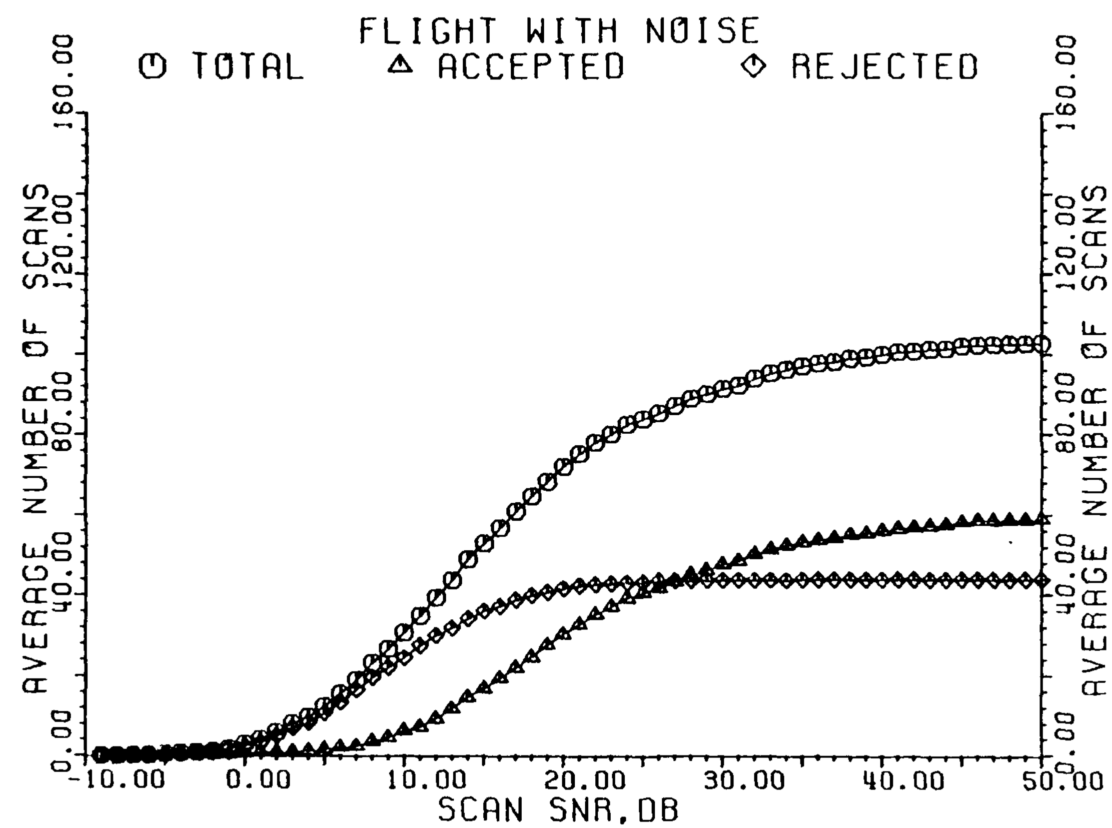

Figure 4-15. Cumulative number of accepted, rejected, and total scans for a flight with noise, granularity of 9 beam pointing locations.

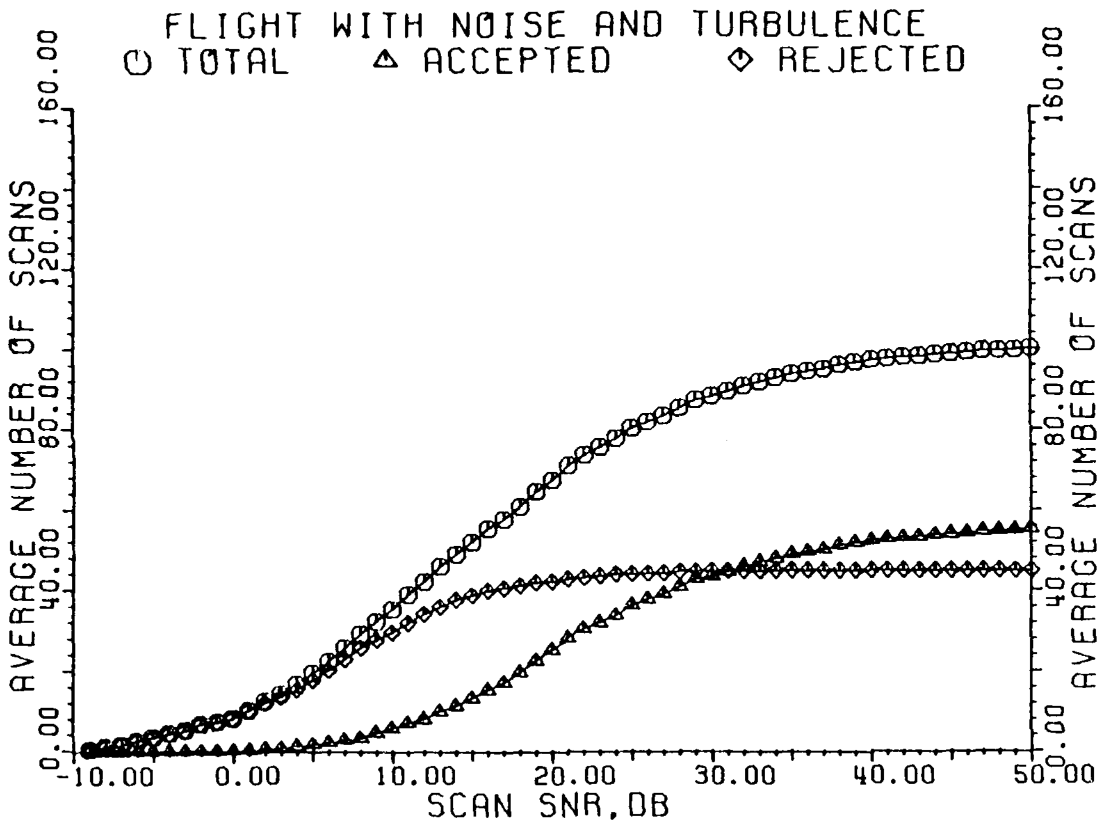

Figure 4-16. Cumulative number of accepted, rejected, and total scans for a flight with noise and turbulence, granularity of 9 beam pointing locations.

For a granularity of 9 beam pointing locations in a scanning window where the location of the target is varied randomly, there is only one beam location in each window. For a granularity of 29 beam pointing locations, there are two beam locations in each window and integration can occur.

Figure 4-17 was generated in a similar manner as was Figure 4-13, but with 29 beam locations. The effect of pulse integration, even for only two pulses, is already apparent by noticing that the crossover point is moved further down, to 8 or 9 dB. Also, the average number of rejected and accepted scans follow the total number of scans exactly below 2 dB and above 17 dB, respectively. The flight with noise and turbulence, Figure 4-18, has more scans at low SNR's as does the flight with noise only, but the crossover remains at 8-9 dB. The advantage of the integration is clearly seen in the cumulative number of scans accepted and rejected, Figures 4-19 and 4-20. By comparing these figures with Figures 4-16 and 4-17 the increase in the number of accepted scans, and decrease in the number of rejected scans, is readily apparent. But reference to Figures 4-6 and 4-9 shows no real increase in the number of scans with a high SNR. Therefore, the increase in the number of accepted scans was due solely to the integration process.

A granularity of 49 beam locations places 4 beam pointing positions in each window, permitting 4 returns to be averaged. Figure 4-21, an average of flights with noise, shows the crossover point moved back to 6 dB. Virtually every scan above 12 dB is accepted, which was the crossover point for the single return integration of Figure 4-13. Also note that the crossover region becomes narrower. In Figure 4-13, a gap

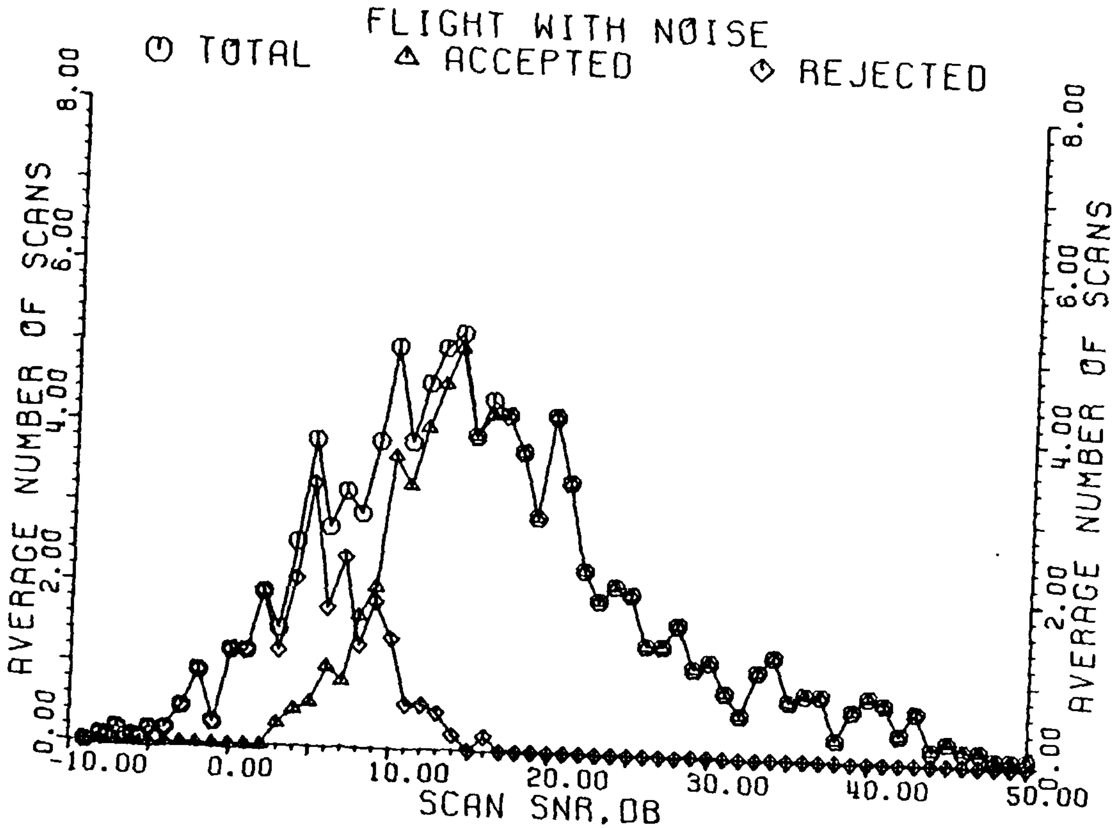

Figure 4-17. Rejection/acceptance performance of the second derivative algorithm for a granularity of 29 beam pointing locations, averaged over 11 flights with noise. Location of the target in the scanning window is randomly varied.

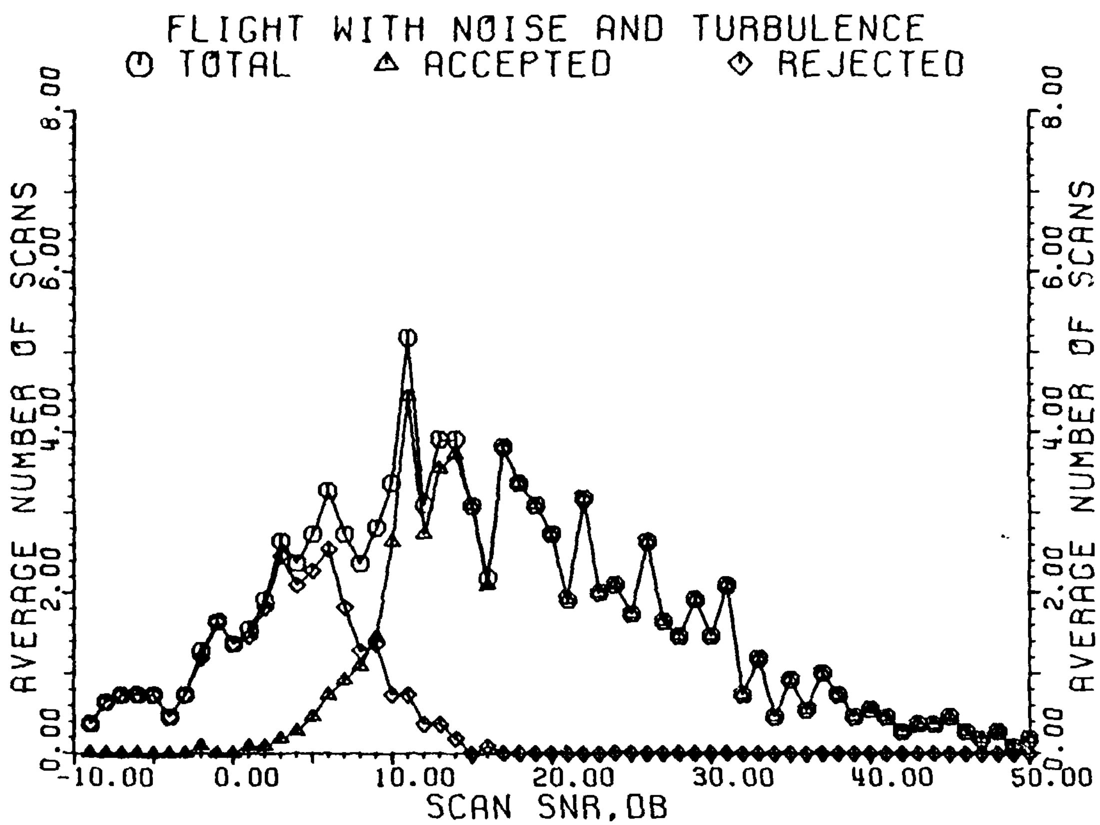

Figure 4-18. Rejection/acceptance performance of the second derivative algorithm for a granularity of 29 beam pointing locations, averaged over 11 flights with noise and turbulence. Location of the target in the scanning window is randomly varied.

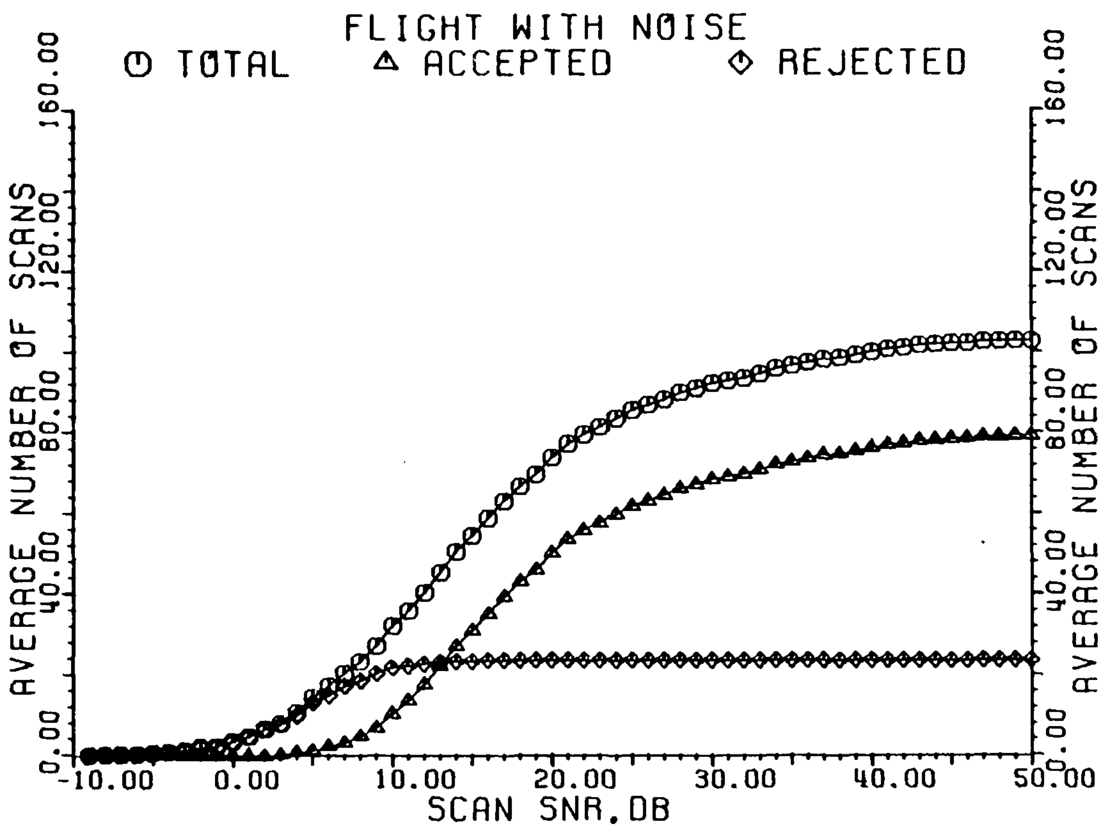

Figure 4-19. Cumulative number of accepted, rejected, and total scans for a flight with noise, granularity of 29 beam pointing locations.

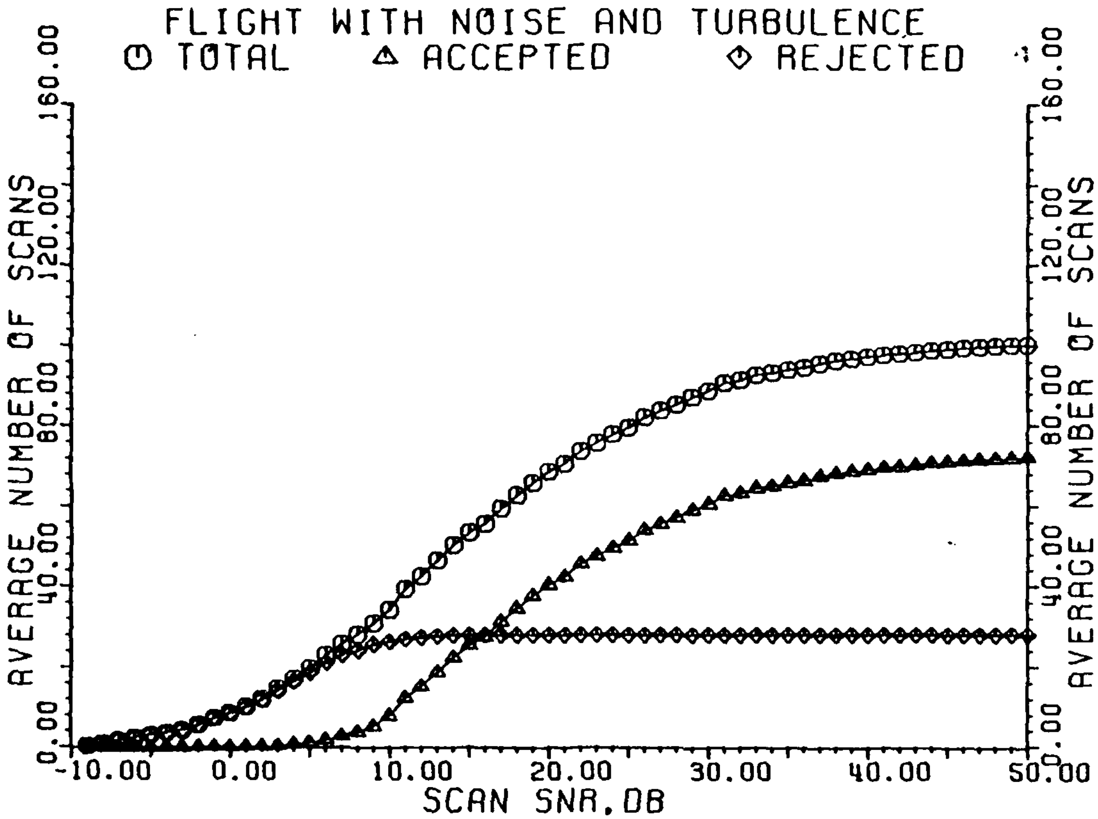

Figure 4-20. Cumulative number of accepted, rejected, and total scans for a flight with noise and turbulence, granularity of 29 beam pointing locations.

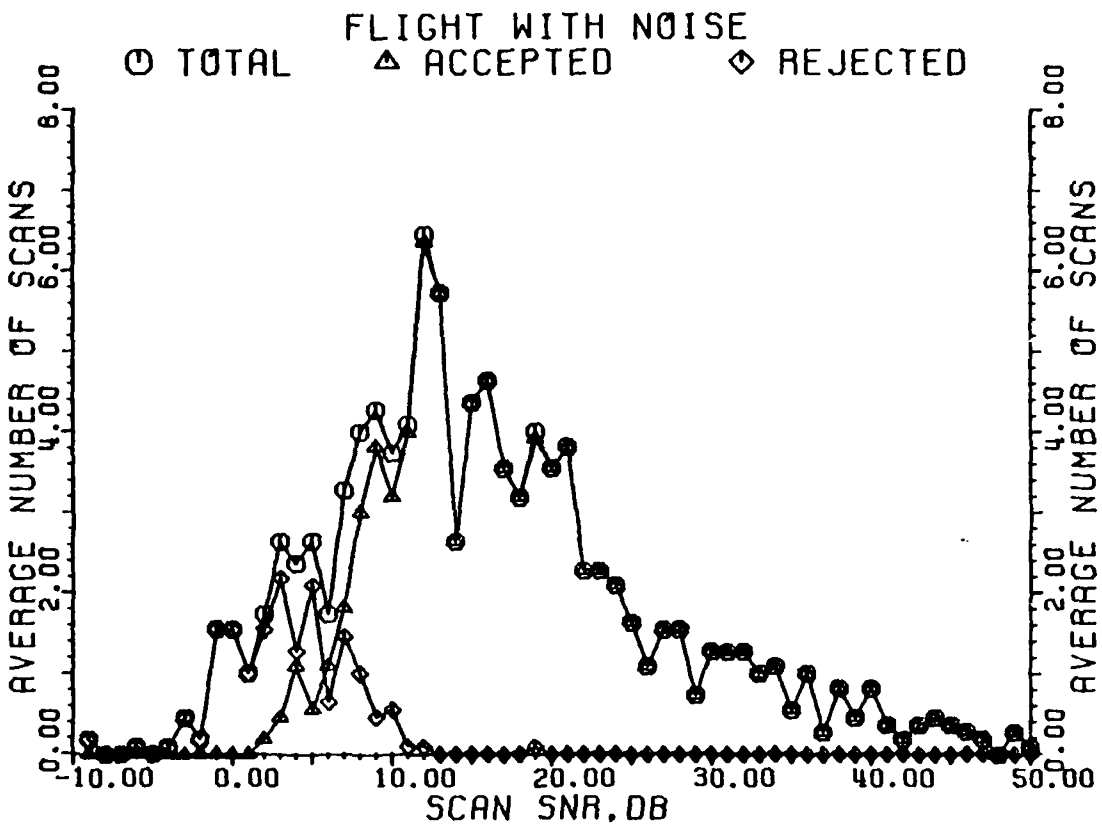

Figure 4-21. Rejection/acceptance performance of the second derivative algorithm for a granularity of 49 beam pointing locations, averaged over 11 flights with noise. Location of the target in the scanning window is randomly varied.

of 27 dB occurs between the points where all scans are either accepted or rejected, centered at 13 dB. In Figure 4-17, with two returns averaged in a window, this gap is reduced to 12 dB, centered at 8 dB. With four returns integrated in each window, the gap is down to 11 dB centered on 6-7 dB. In Figure 4-22, the average of flights with turbulence, the same observations can be made. The crossover is lower than the other granularities, now at 6 dB, and virtually all scans above 12 dB are accepted. As is to be expected, the average cumulative number of accepted scans for flights with noise, Figure 4-23, has increased, again due to the integration of pulses in windows. The number of rejected scans also is reduced. For flights with noise and turbulence, Figure 4-24, the same is true. The number of accepted scans has increased by over 20 on the average, and the number of rejected scans dropped by a like amount in comparison to the implementation of the second derivative algorithm without pulse integration.

The algorithm having been introduced and its rejection ability verified, the comparison of the centroid estimation accuracy of the second derivative method to the other estimators may now proceed.

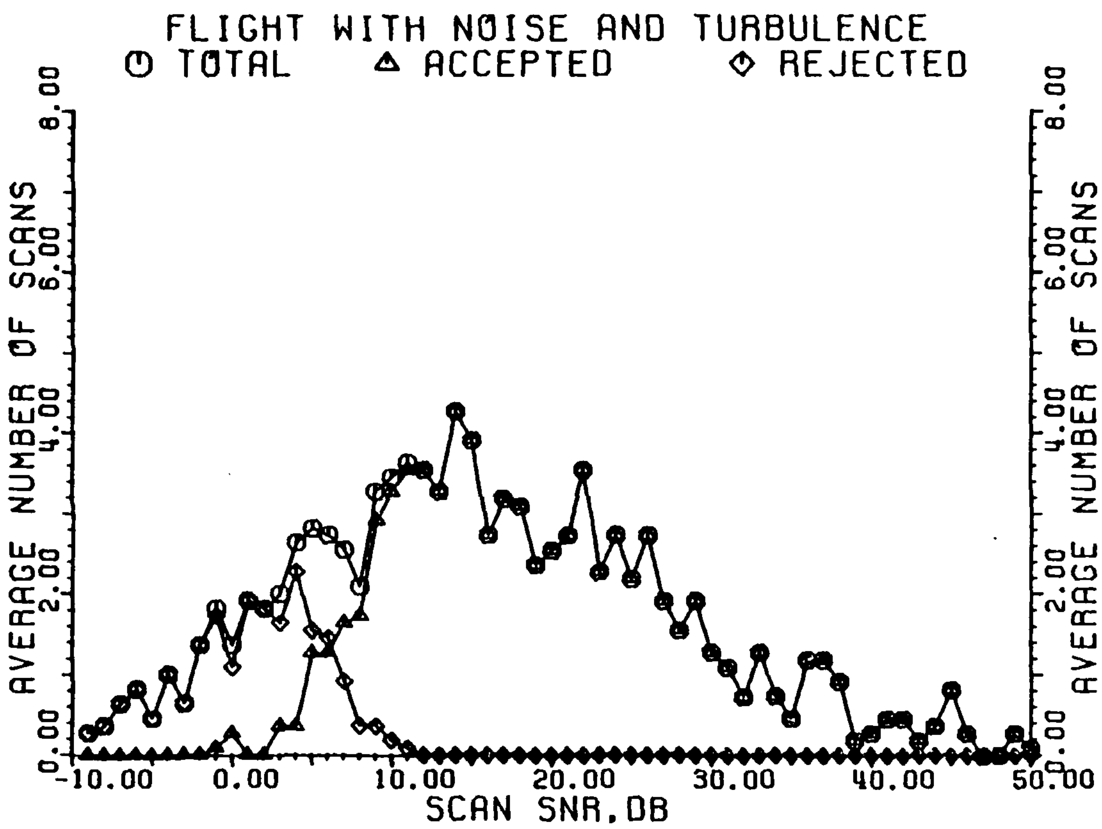

Figure 4-22. Rejection/acceptance performance of the second derivative algorithm for a granularity of 49 beam pointing locations, averaged over 11 flights with noise and turbulence. Location of the target in the scanning window is randomly varied.

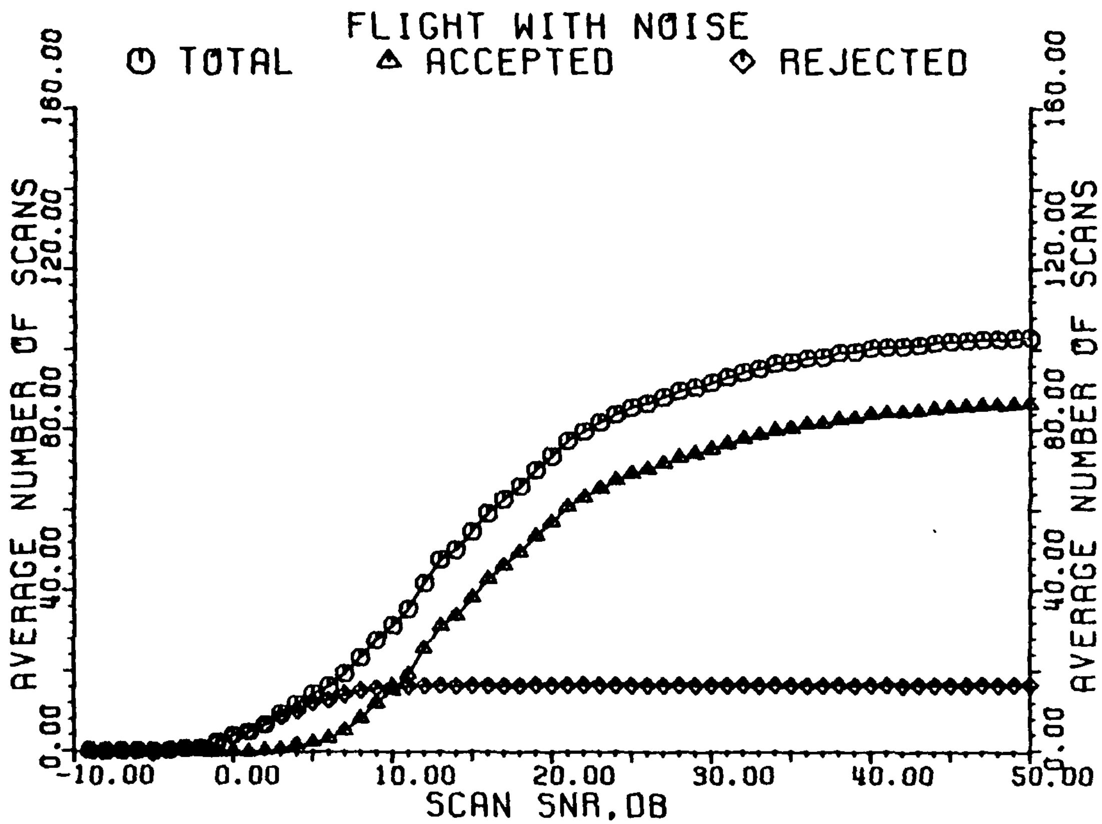

Figure 4-23. Cumulative number of accepted, rejected, and total scans for a flight with noise, granularity of 49 beam pointing locations.

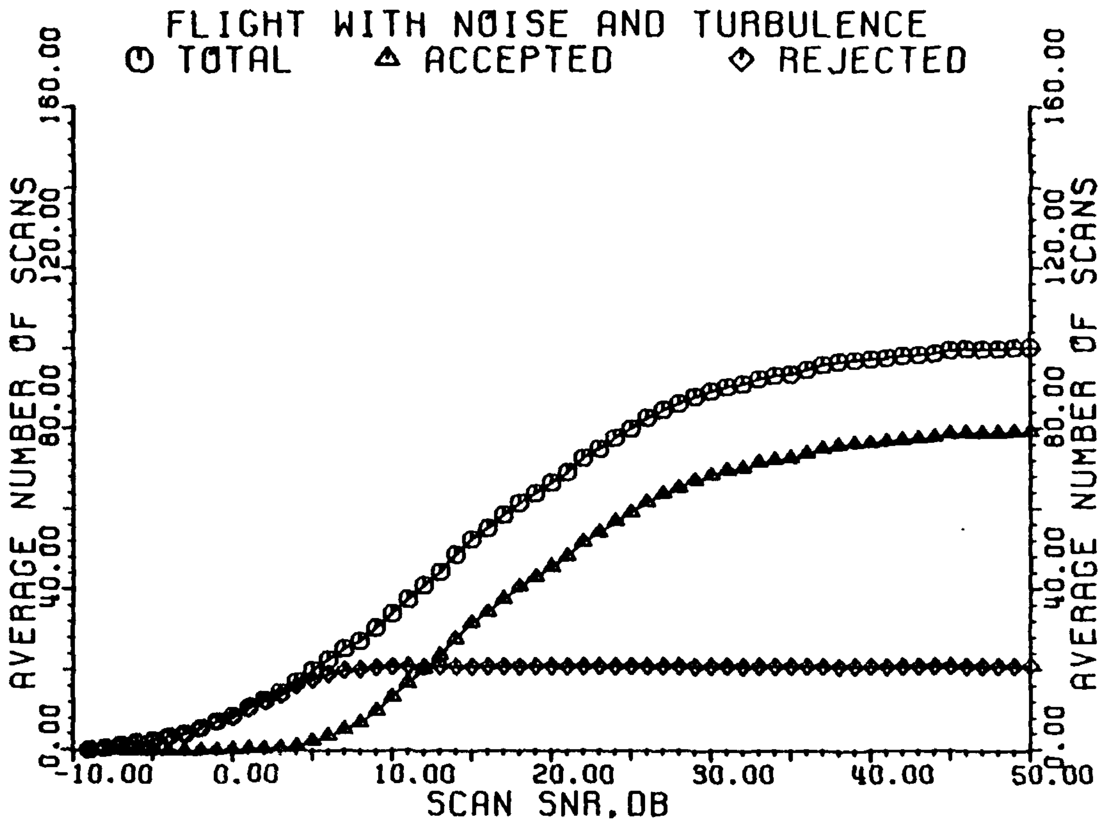

Figure 4-24. Cumulative number of accepted, rejected, and total scans for a flight with noise and turbulence, granularity of 49 beam pointing locations.

V. COMPARISON OF THE TECHNIQUES

Each of the five centroid estimators operate on the same returns in a different fashion. It would be appropriate to examine the action of each on scans of different signal-to-noise ratios by way of introduction to a statistical analysis of the estimating error.

A plot of the scan returns for a scan with a SNR of 21 dB is shown in Figure 5-1 with the antenna located 125 m from the runway centerline. The mean algorithm set the highest threshold, followed by the 12 dB and median thresholds, all set low on the curve. The average returns inside the windows of SDRV cause the windows to closely follow the shape of the curve. The set of windows shown by the triangles which calculated the first edge, shown by the small left-most arrow, are well up on the body of the return where the least error should occur. The second target edge calculated by SDRV occurred when the windows shifted to the positions and amplitudes shown by the diamonds. The actual target location was calculated during the transmission from the 22nd beam location, and is denoted by the large arrow. The target location calculated by the radar center of gravity (RADARCG) method is shown by the large X. In this scan, the mean, median, and RADARCG methods used all 41 pulses, 12 dB used 28, and SDRV used 38. The error for this scan for all five estimators is shown on the plot.

The second derivative method used one fourth more of the scan than did the 12 dB estimator to be sure that it was on an actual target

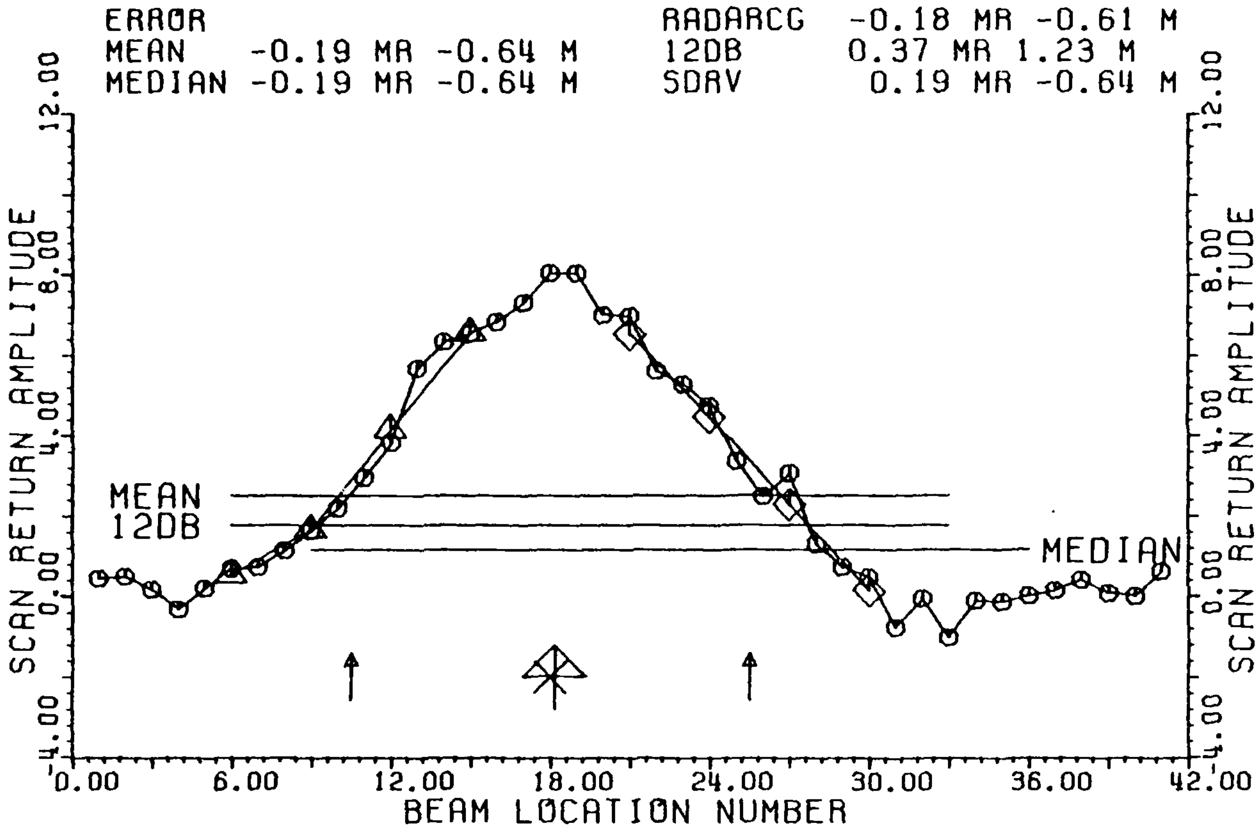

Figure 5-1. Target returns in the scanning window for a granularity of 41 beam pointing locations. The distance from target to antenna is 3343 M, scan SNR=21.0 dB. The location of the centroid calculated by RADARCG is shown by the symbol X. The triangles and diamonds are the SDRV window averaged returns when the target edges (small arrows) were found. The large arrow is the actual location of the target. The error for the scan is shown.

return. Since the thresholds are all set relatively low on the scan, it would be easy for the thresholds to be prematurely tripped by noise. Comparison of Figures 5-2 with 5-3 show this to be the case. Both the median and 12 dB estimators were satisfied by the noise outliers on the left part of the scan in Figure 5-2. These were rejected by SDRV which shifted the windows until it moved onto the main body of the return. Due to the uniformity of the noise in Figure 5-3, the 12 dB estimator properly set the edges for the most accurate estimate of the target location. SDRV did move well onto the return, but misjudged the location of the target by 0.6 mrad to the left. The mean and median estimators made the same estimate as SDRV, and the radar center of gravity estimator positioned the target as shown by the X due to the noise of the right part of the scan.

A scan of low SNR is shown in Figure 5-4. Note the signal return magnitudes on this plot in comparison to Figures 5-1, 5-2, and 5-3. The thresholding methods all set the thresholds low on the scan, in the noise, and came out well due to the uniformity in the noise. Although a main body of return appears obvious in this plot, it is of such low amplitude that it was dismissed as noise by SDRV and the scan rejected.

The comparison of the techniques is in two basic parts. In the first part, the output of the estimators is plotted as a function of antenna offset for three different scanning granularities. In the second part, the output of the estimators is plotted as a function of granularity for a given antenna offset. Both parts are composed of the results of a baseline flight, flight with noise, flight with turbulence, and flight with noise and turbulence, for each data point, in that order.

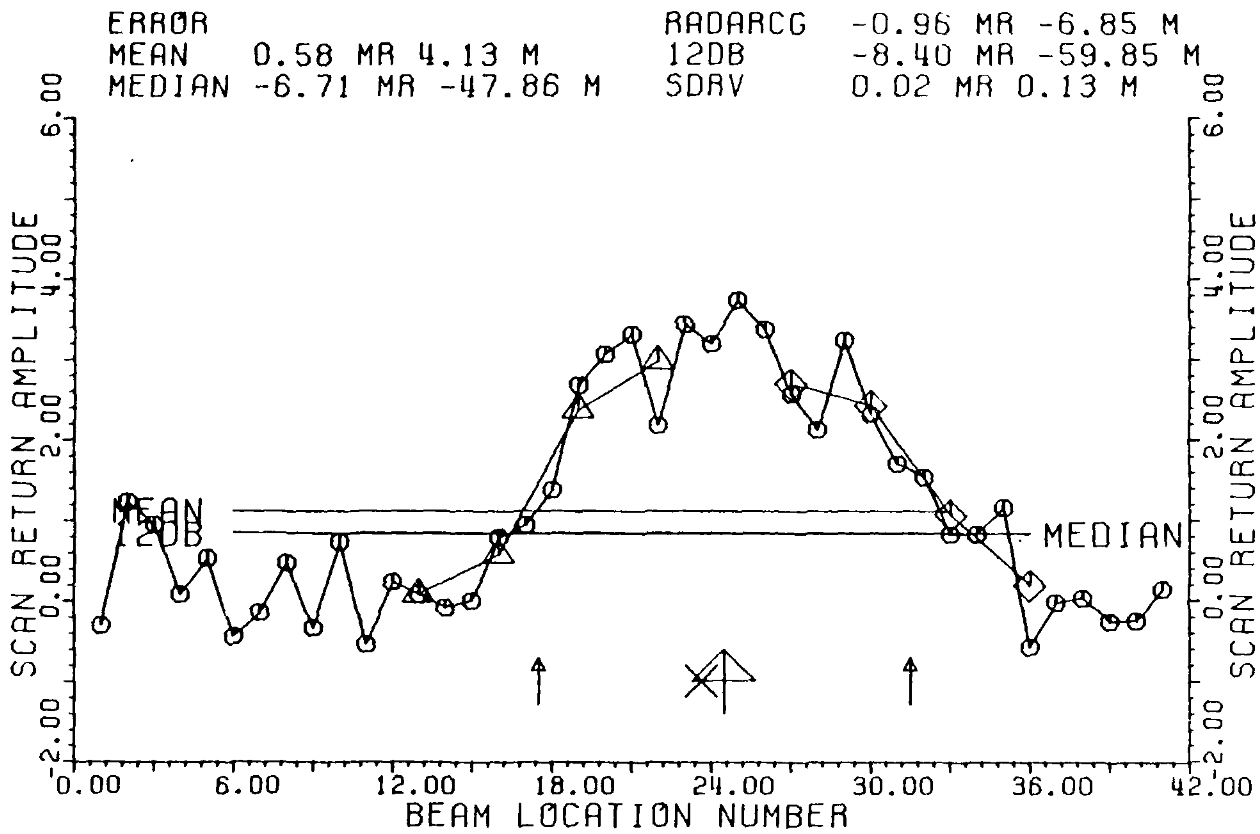

Figure 5-2. Target returns in the scanning window for a granularity of 41 beam pointing locations. The distance from target to antenna is 7128 M, scan SNR=12.0 dB. The location of the centroid calculated by RADARCG is shown by the symbol X. The triangles and diamonds are the SDRV window averaged returns when the target edges (small arrows) were found. The large arrow is the actual location of the target. The error for the scan is shown.

AD-A110 862   GEORGIA INST OF TECH ATLANTA ENGINEERING EXPERIMENT --ETC F/G 17/7
MARINE AIR TRAFFIC CONTROL AND LANDING SYSTEM (MATCALS INVESTIG--ETC(U)
SEP 81 E R GRAF, C L PHILLIPS, S A STARKS   N00039-80-C-0032
UNCLASSIFIED GIT/EES-1-A-2550-VOL-1   NL

2 of 5
AD A110862

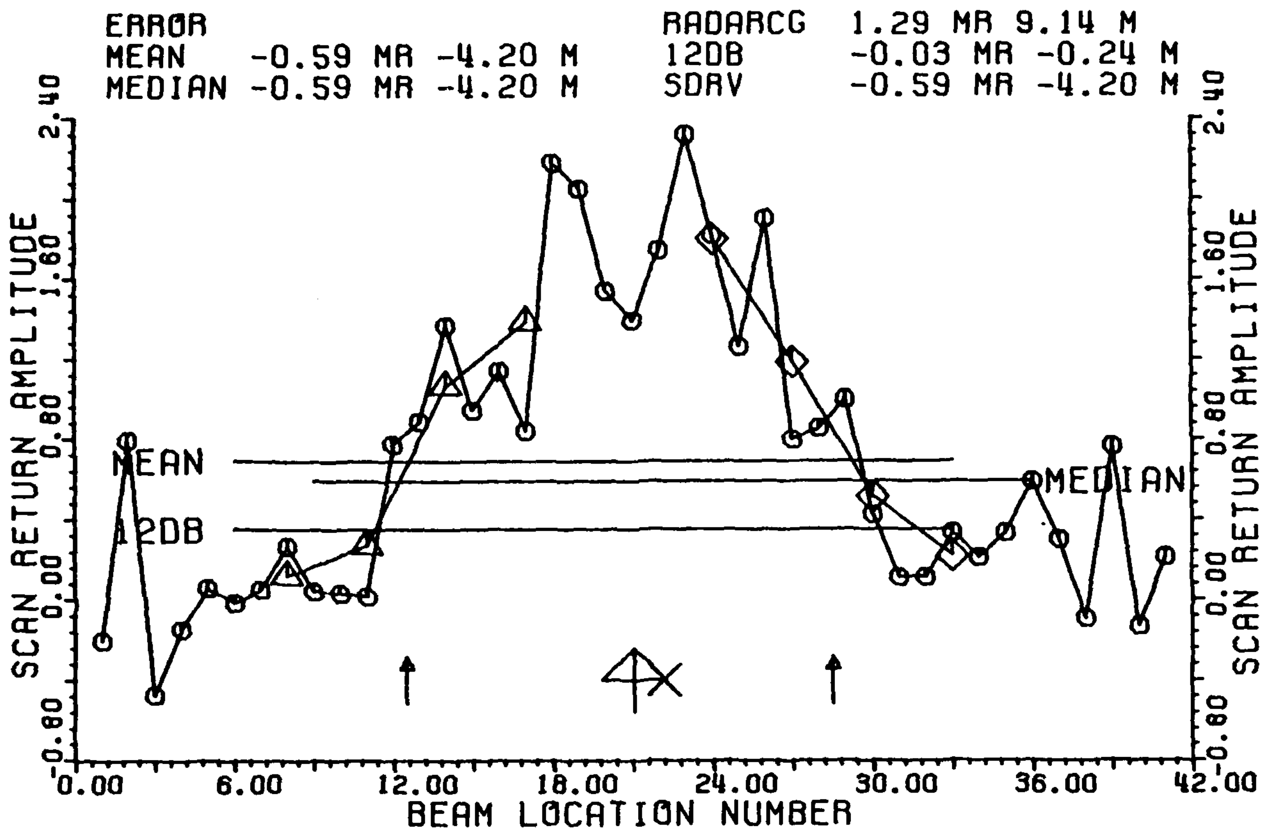

Figure 5-3. Target returns in the scanning window for a granularity of 41 beam pointing locations. The distance from target to antenna is 7062 M, scan SNR=12.4 dB. The location of the centroid calculated by RADARCG is shown by the symbol X. The triangles and diamonds are the SDRV window averaged returns when the target edges (small arrows) were found. The large arrow is the actual location of the target. The error for the scan is shown.

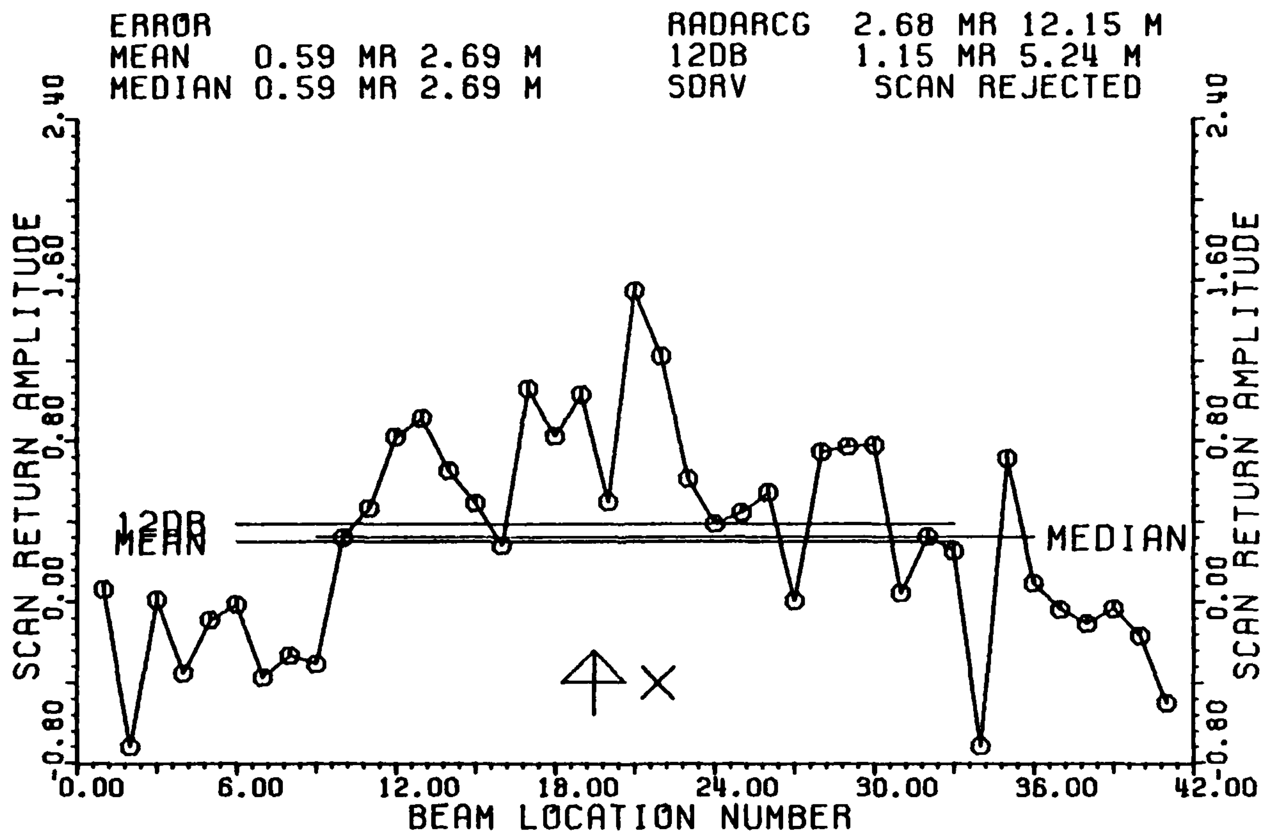

Figure 5-4. Target returns in the scanning window for a granularity of 41 beam pointing locations. The distance from target to antenna is 4538 M, scan SNR=5.3 dB. The location of the centroid calculated by RADARCG is shown by the symbol X. No target edges were found by the SDRV algorithm. The large arrow is the actual location of the target. The error for the scan is shown.

The output of the estimators requires eight plots for each set of flights, one plot each for the mean error, mean square error, standard deviation of the error, and the variance of the error, in milliradians and meters. Each data point on each plot is the result of 103 scans (one flight) on the target. The equations used are:

$$X = (\text{Estimated value} - \text{Actual value})$$

$$\text{Mean Error} = \frac{1}{N} \Sigma X$$

$$\text{Mean Square Error} = \frac{1}{N} \Sigma X^2$$

$$\text{Standard Deviation} = \sqrt{\frac{1}{N-1} \left(\Sigma X^2 - \frac{1}{N} (\Sigma X)^2\right)}$$

$$\text{Variance} = \frac{1}{N-1} \left(\Sigma X^2 - \frac{1}{N} (\Sigma X)^2\right)$$

where N = Number of samples

The data input to the estimators in the baseline flights and flights with noise are somewhat correlated. After the estimators used the scan returns of the baseline flight, zero mean random gaussian noise was added to each scan return, and the estimators were called again. That data is plotted as the flight with noise. In the same way, the data input to the estimators for the flights with turbulence and noise were made from the scan returns of the flights with turbulence.

In the next thirty two plots, all scans were used in the error analysis irregardless of the scan SNR. A scanning granularity of 9 beam pointing locations was employed. The plots of the baseline flights versus antenna location, Figures 5-5 through 5-12, all show the RADARCG estimator to have the least error, with the SDRV estimator almost as

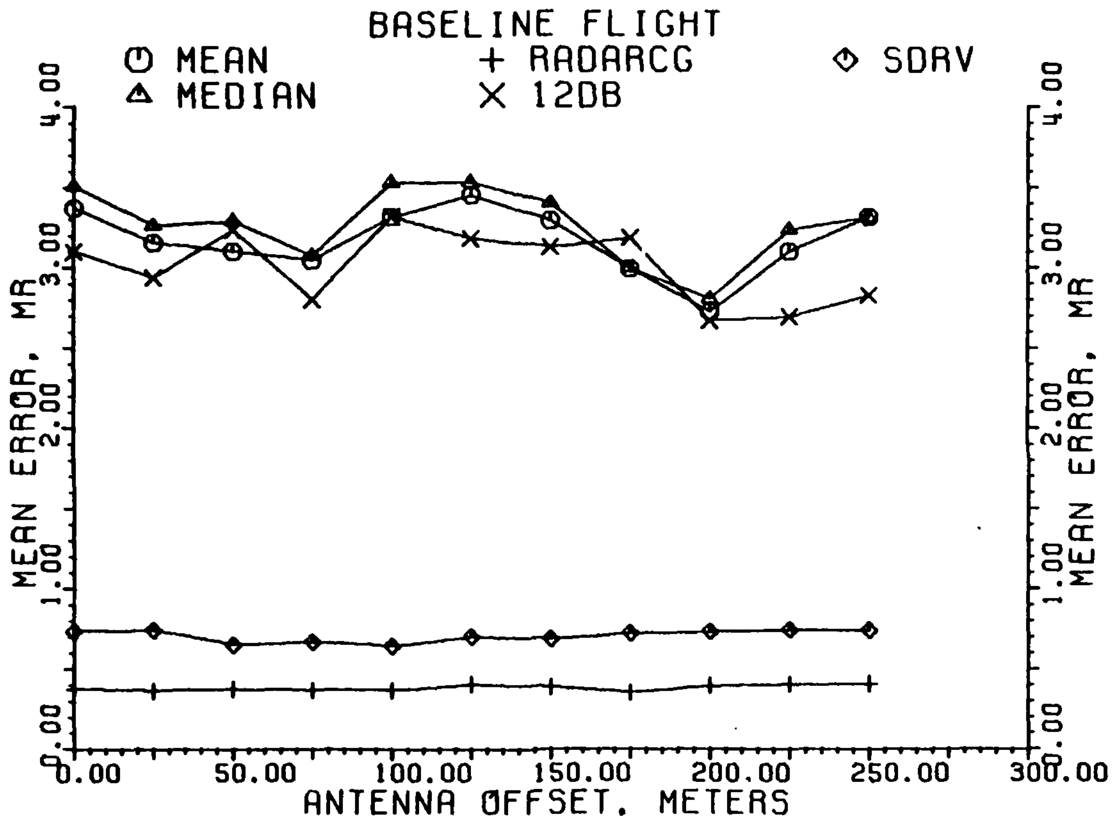

Figure 5-5. Mean error of estimators in milliradians for a granularity of 9 beam pointing locations. Each data point is the result of one flight, all scans used.

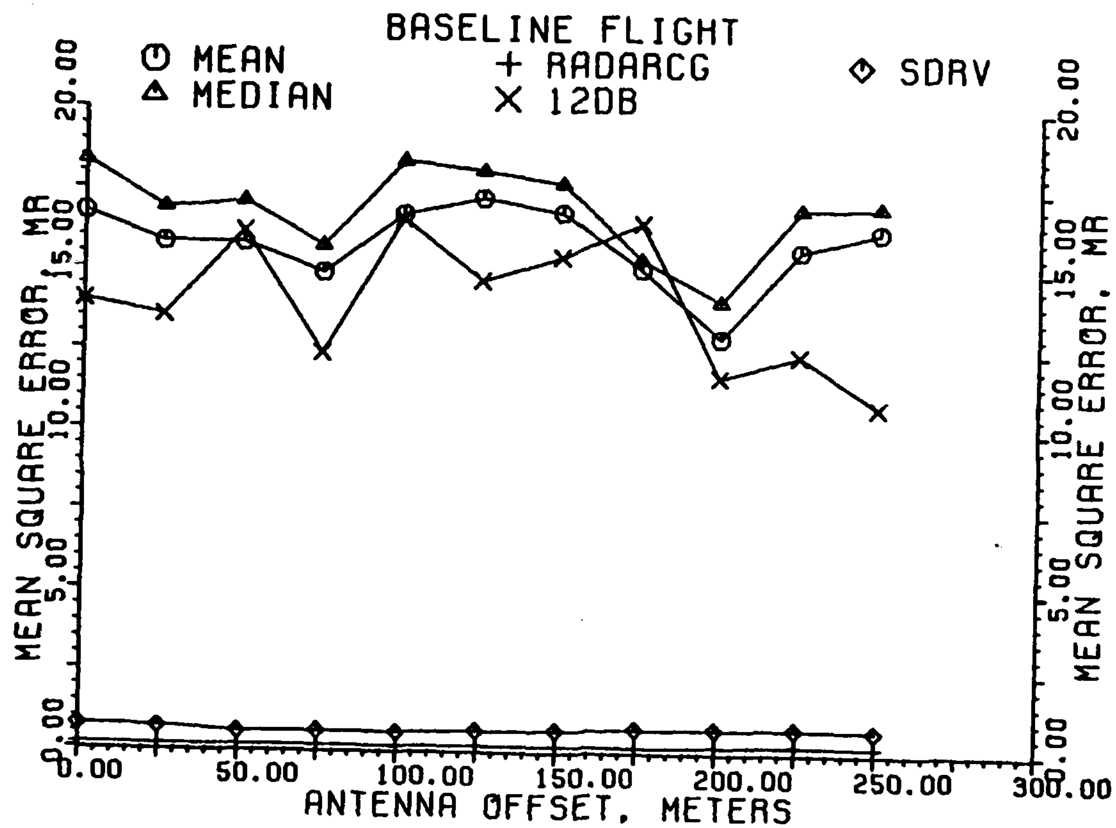

Figure 5-6. Mean square error of estimators in milliradians for a granularity of 9 beam pointing locations. Each data point is the result of one flight, all scans used.

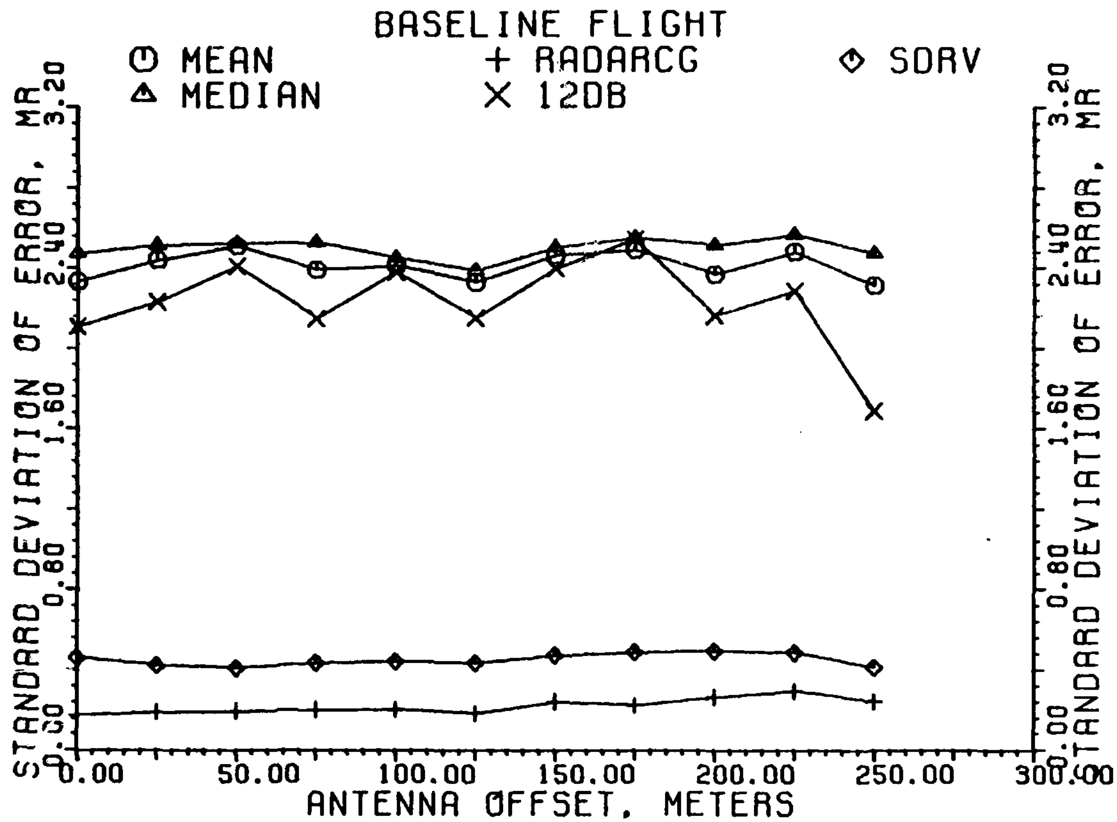

Figure 5-7. Standard deviation of error of estimators in milliradians for a granularity of 9 beam pointing locations. Each data point is the result of one flight, all scans used.

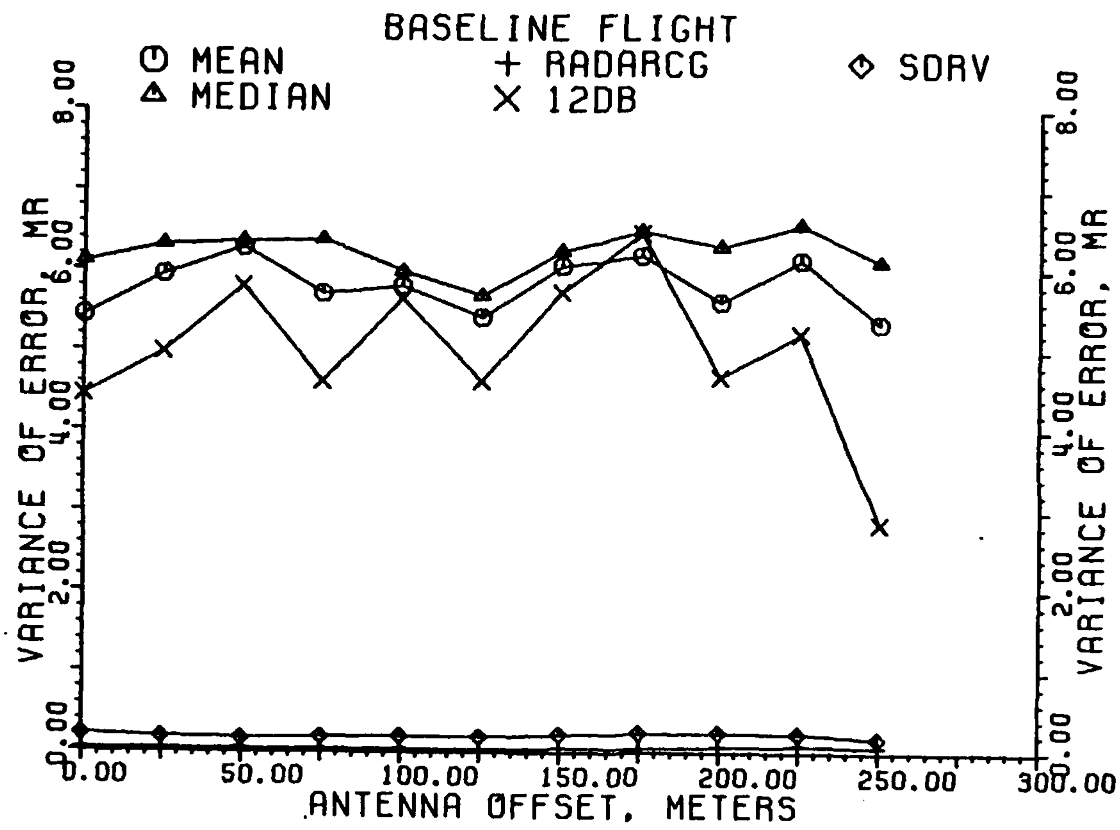

Figure 5-8. Variance of error of estimators in milliradians for a granularity of 9 beam pointing locations. Each data point is the result of one flight, all scans used.

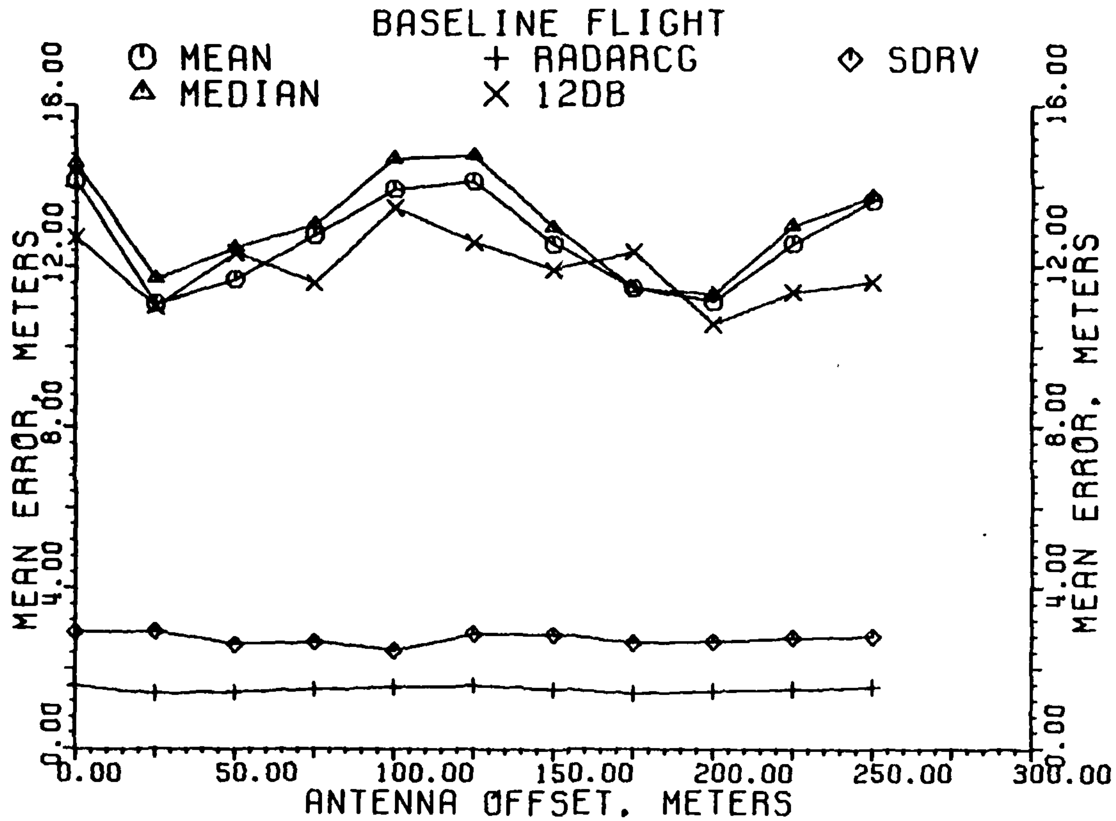

Figure 5-9. Mean error of estimators in meters for a granularity of 9 beam pointing locations. *Each data point is the result of one flight, all scans used.*

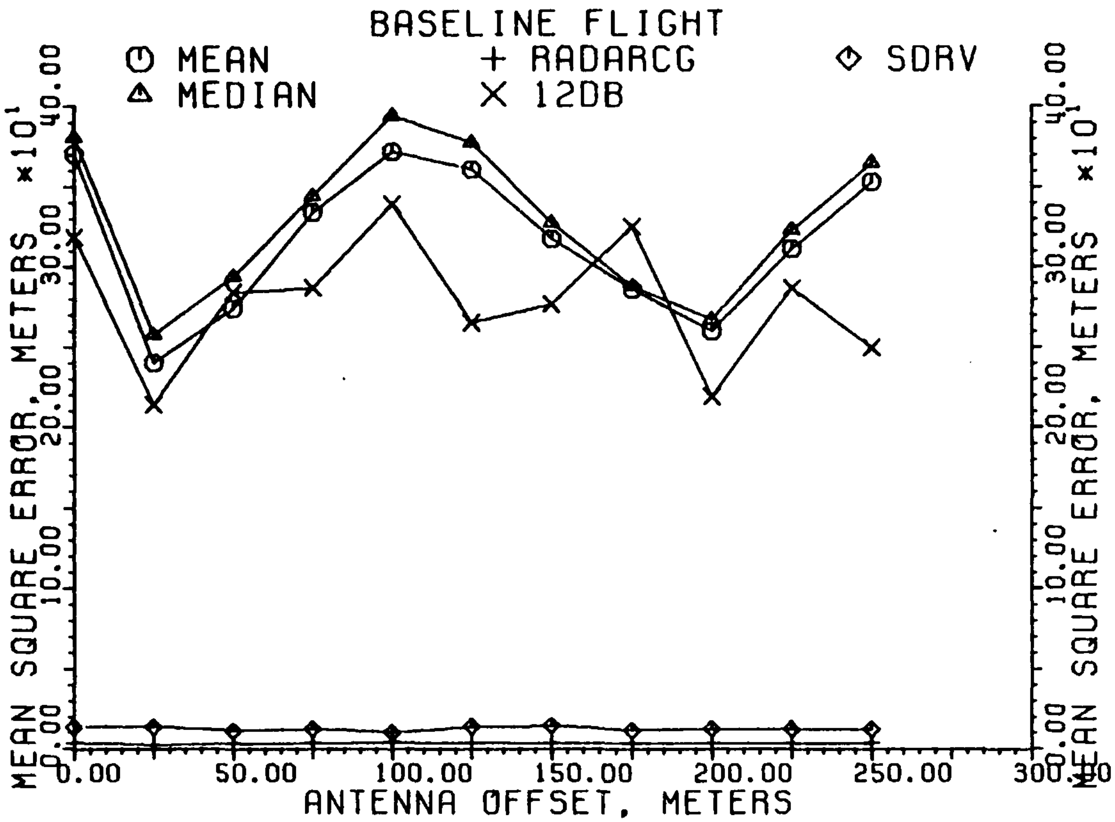

Figure 5-10. Mean square error of estimators in meters for a granularity of 9 beam pointing locations. Each data point is the result of one flight, all scans used.

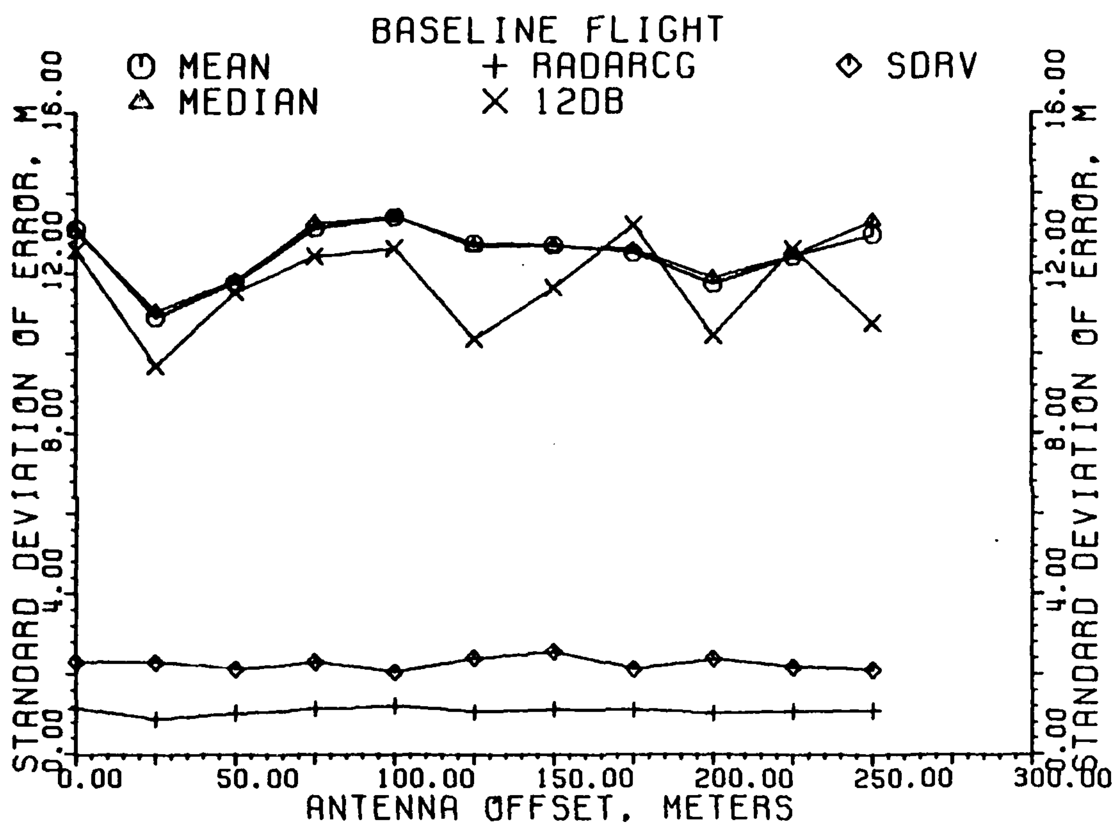

Figure 5-11. Standard deviation of error of estimators in meters for a granularity of 9 beam pointing locations. Each data point is the result of one flight, all scans used.

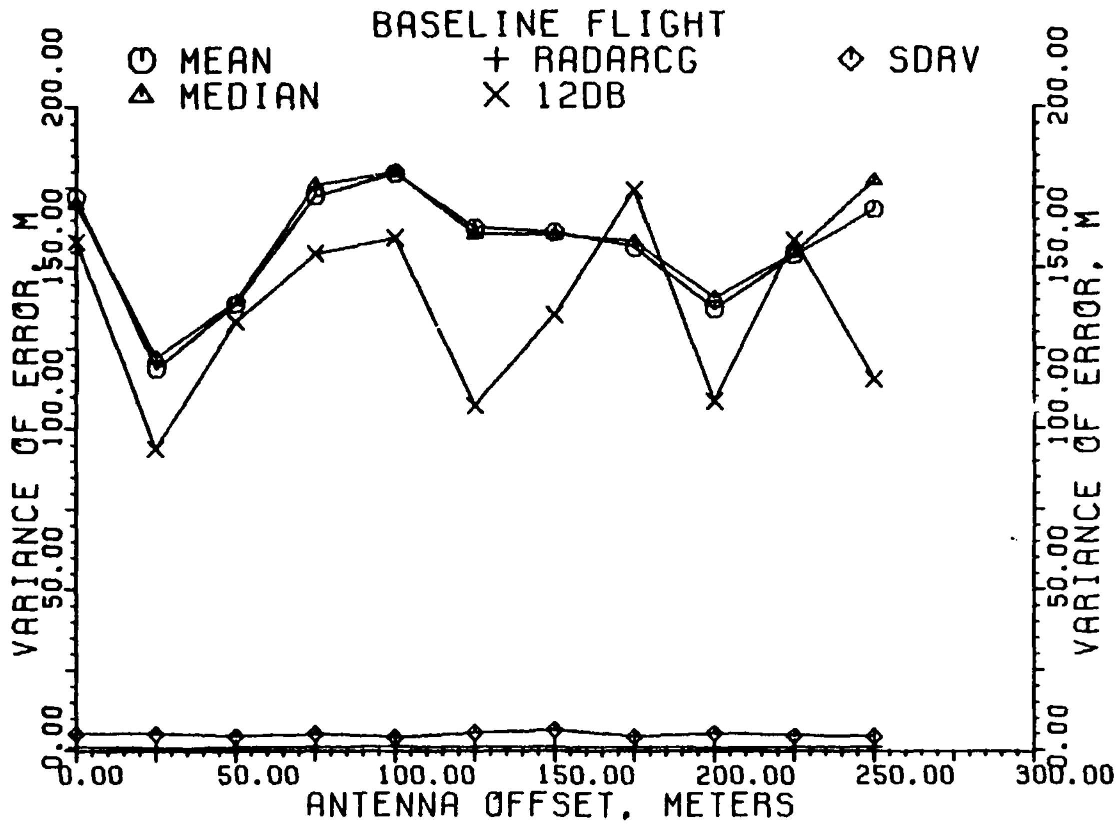

Figure 5-12. Variance of error of estimators in meters for a granularity of 9 beam pointing locations. Each data point is the result of one flight, all scans used.

accurate. The three thresholding methods are very nearly equal, but comparison of the plots will show that the 12 dB estimator has the least error, then the mean estimator, and finally the median estimator. Under these no-noise, non-turbulent conditions, there does not appear to be any appreciable error introduced by siting the antenna 250 meters from the runway centerline as compared to being on the runway itself.

The flights with noise, Figures 5-13 through 5-20, begin to show the relative merits of the estimators. Here the second derivative algorithm clearly has the least error in noise alone, less than 1.5 mrad or around 4 meters on the average according to Figures 5-13 and 5-17. It is also the most stable, as shown by Figures 5-15, 5-16, 5-19, and 5-20. Whereas RADARCG was excellent without noise, the figures indicate that it is significantly degraded in noise. The thresholding estimators are still very close to each other, with the same approximate order of error as in the baseline flights. While all estimators were degraded with the introduction of noise, there is still no apparent effect due to antenna offset.

The flights with turbulence only, Figures 5-21 through 5-28, show little error difference in comparison to the corresponding plots of the baseline flights, Figures 5-5 through 5-12. This illustrates that for a low order granularity, the effect of turbulence on the estimators is small.

The flights with noise and turbulence, Figures 5-29 through 5-36, again show the second derivative method to be the most accurate and most robust estimator for a scan with nine beam locations in noise and turbulence. The thresholding methods still appear to be about equal in

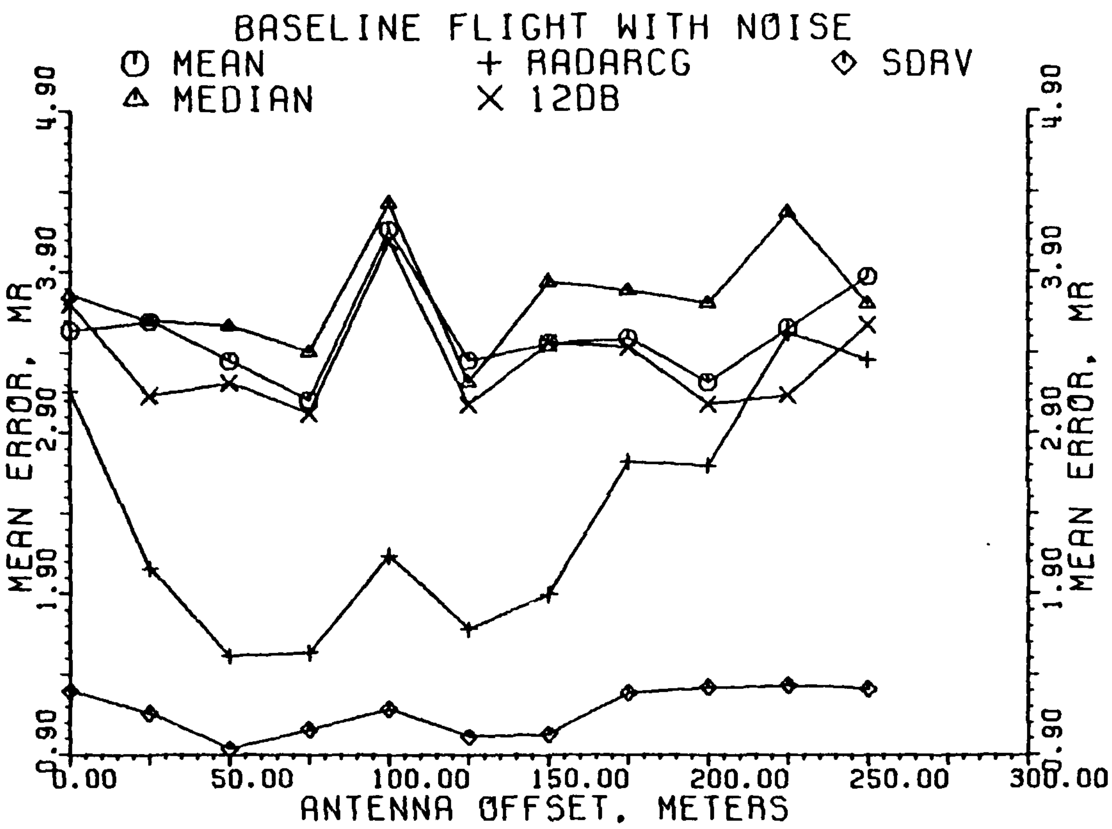

Figure 5-13. Mean error of estimators in milliradians for a granularity of 9 beam pointing locations. Each data point is the result of one flight, all scans used.

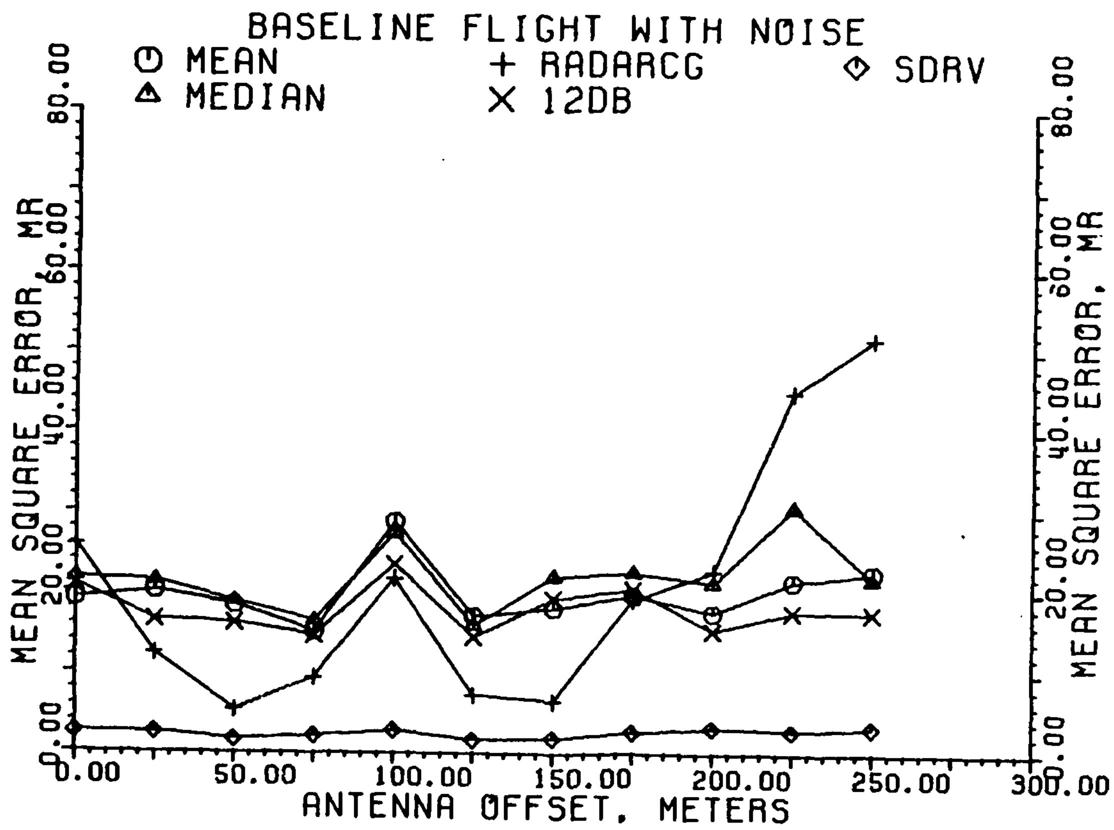

Figure 5-14. Mean square error of estimators in milliradians for a granularity of 9 beam pointing locations. Each data point is the result of one flight, all scans used.

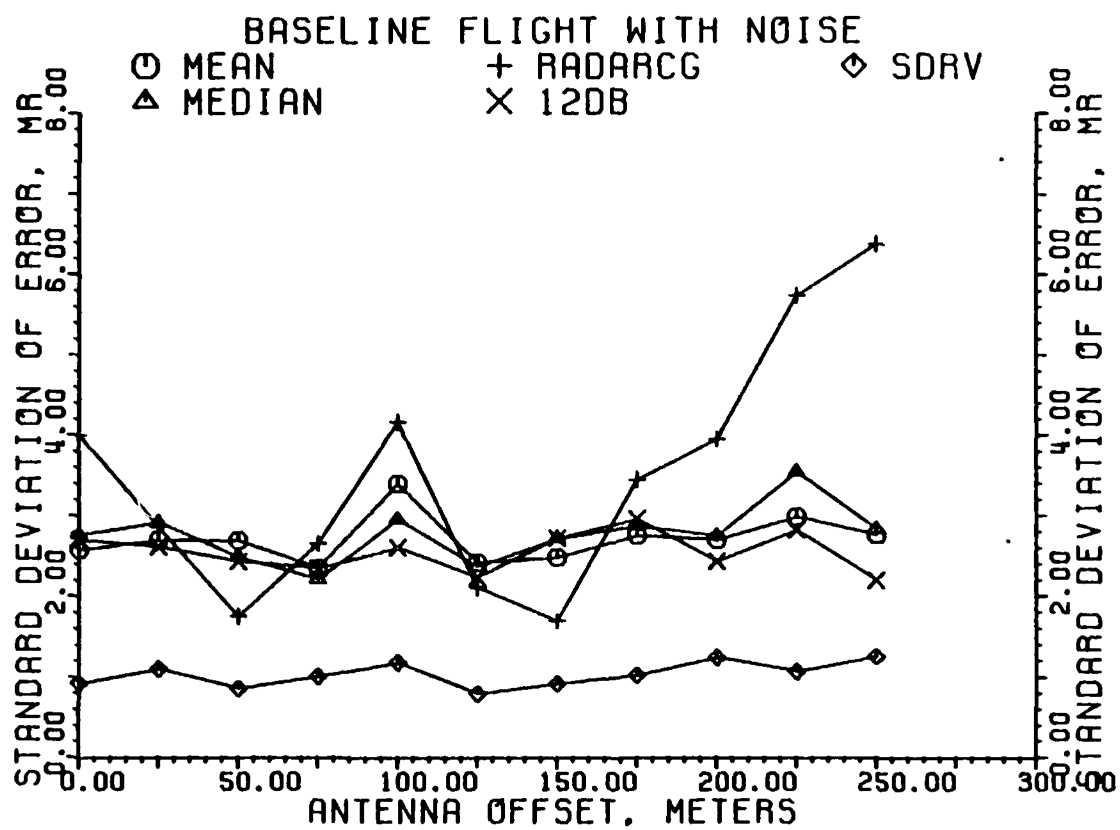

Figure 5-15. Standard deviation of error of estimators in milliradians for a granularity of 9 beam pointing locations. Each data point is the result of one flight, all scans used.

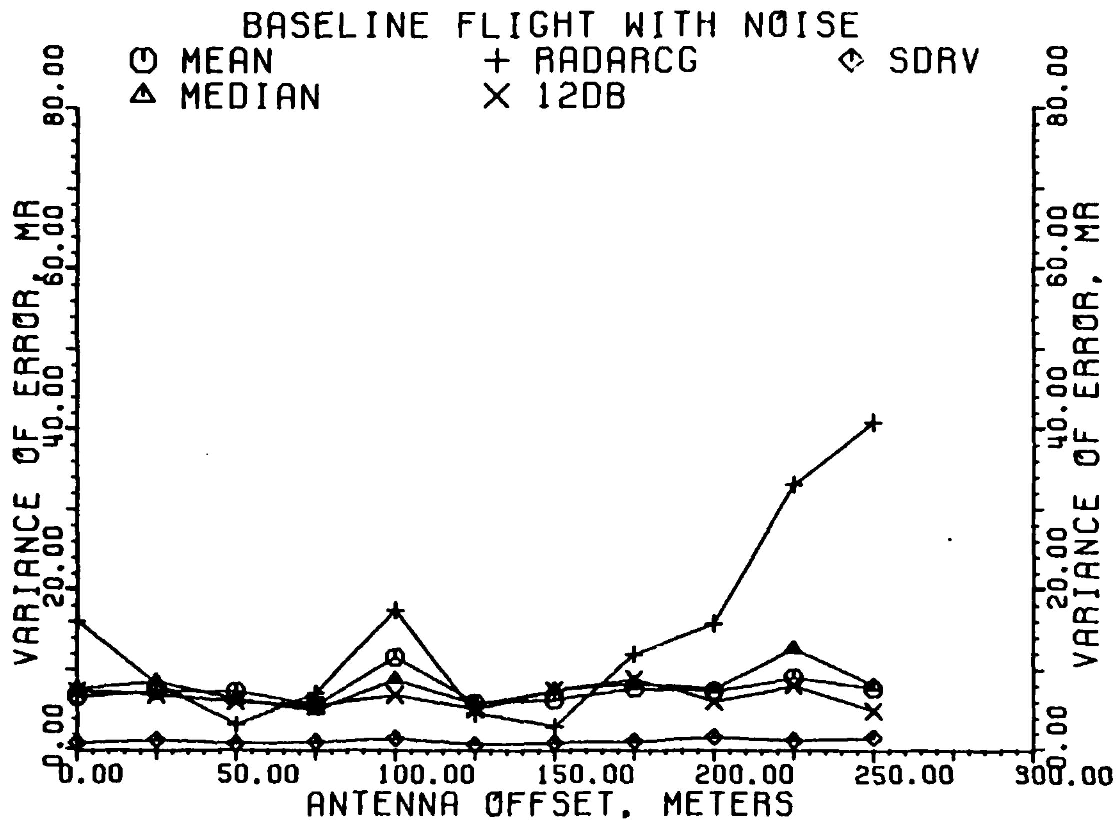

Figure 5-16. Variance of error of estimators in milliradians for a granularity of 9 beam pointing locations. Each data point is the result of one flight, all scans used.

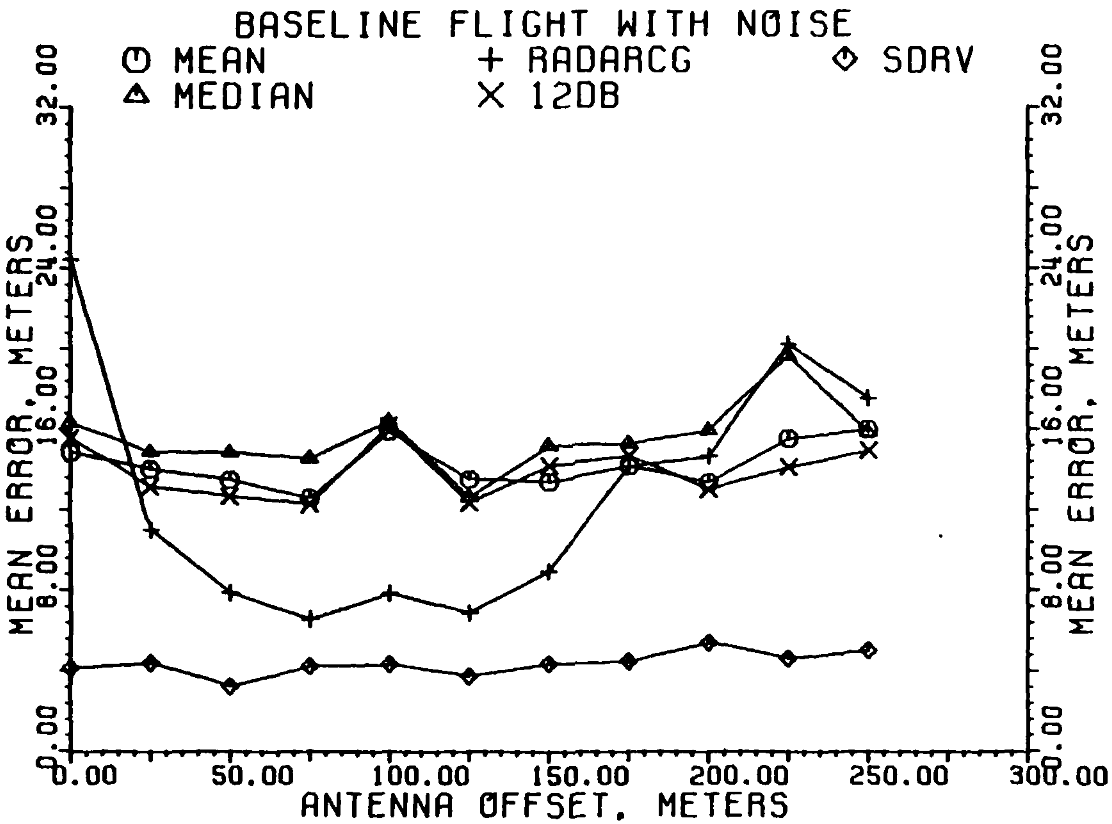

Figure 5-17. Mean error of estimators in meters for a granularity of 9 beam pointing locations. Each data point is the result of one flight, all scans used.

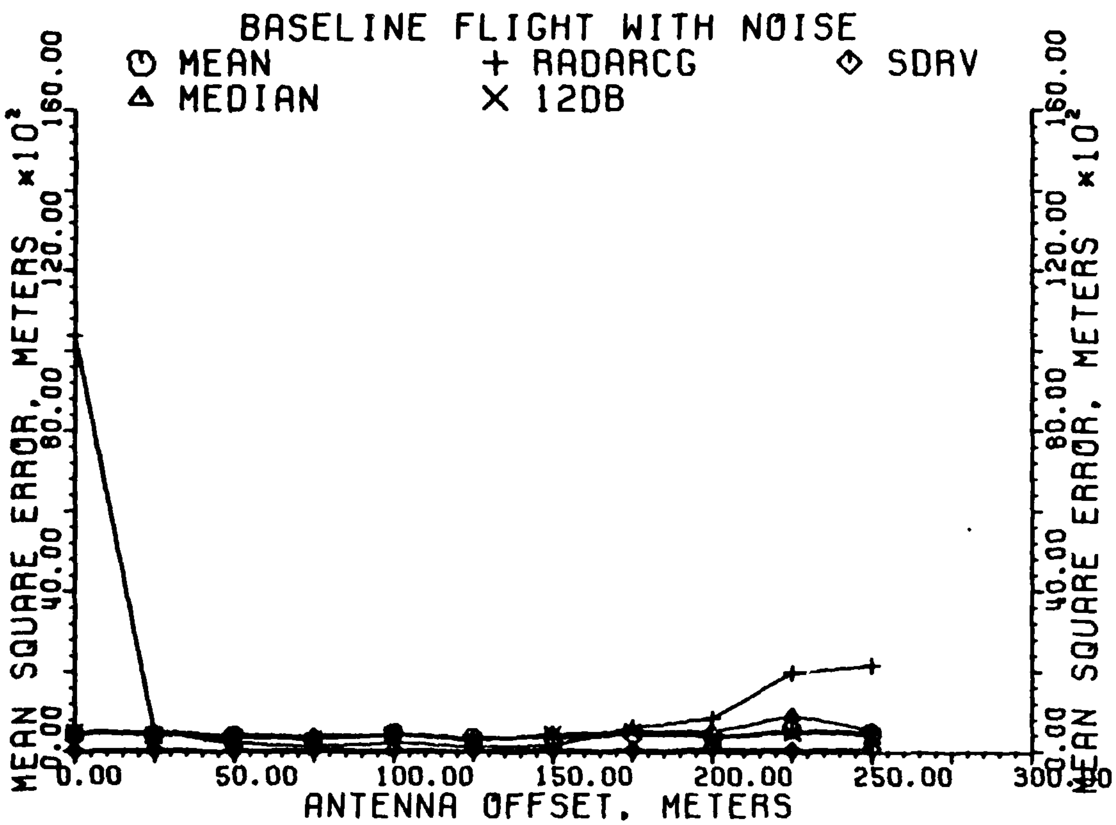

Figure 5-18. Mean square error of estimators in meters for a granularity of 9 beam pointing locations. Each data point is the result of one flight, all scans used.

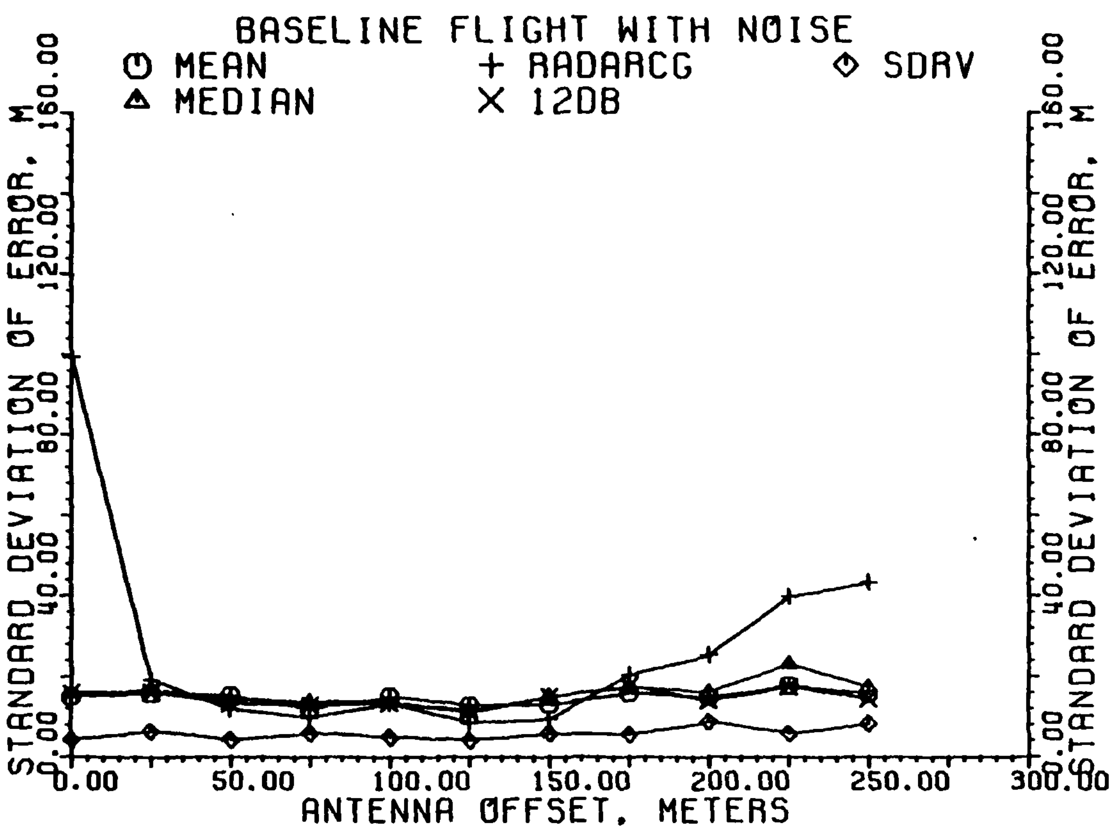

Figure 5-19. Standard deviation of error of estimators in meters for a granularity of 9 beam pointing locations. Each data point is the result of one flight, all scans used.

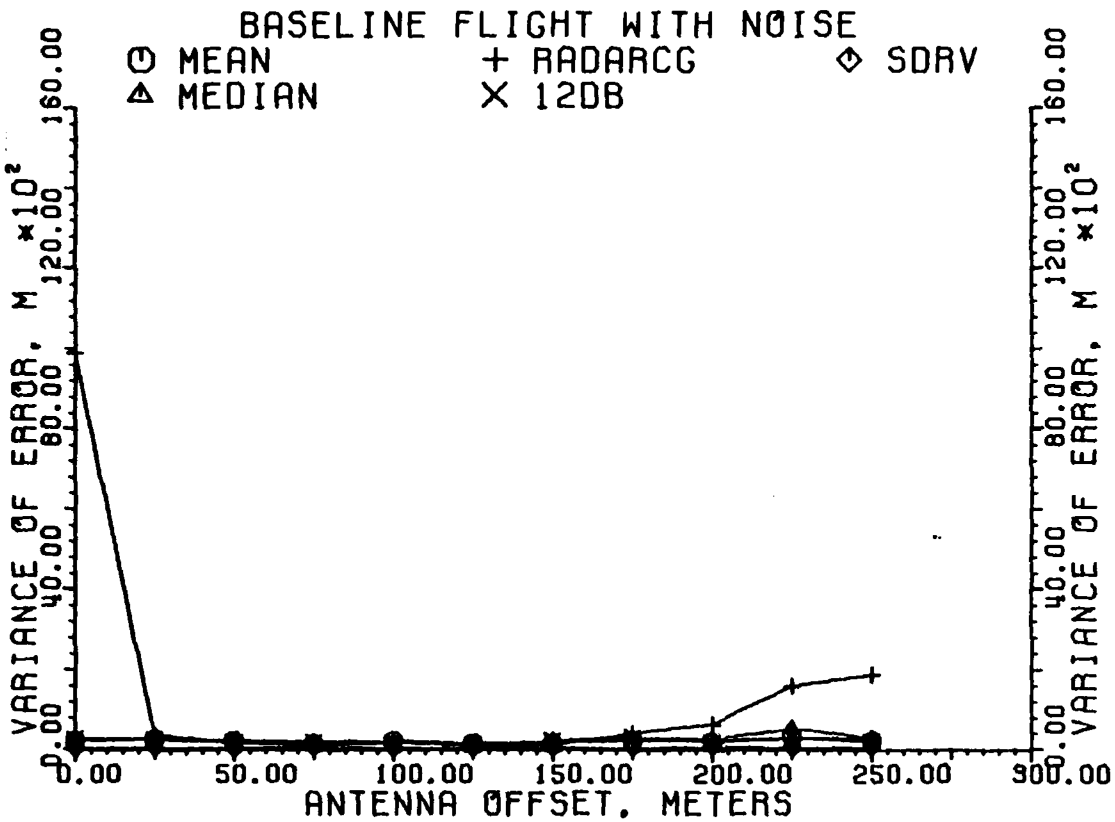

Figure 5-20. Variance of error of estimators in meters for a granularity of 9 beam pointing locations. Each data point is the result of one flight, all scans used.

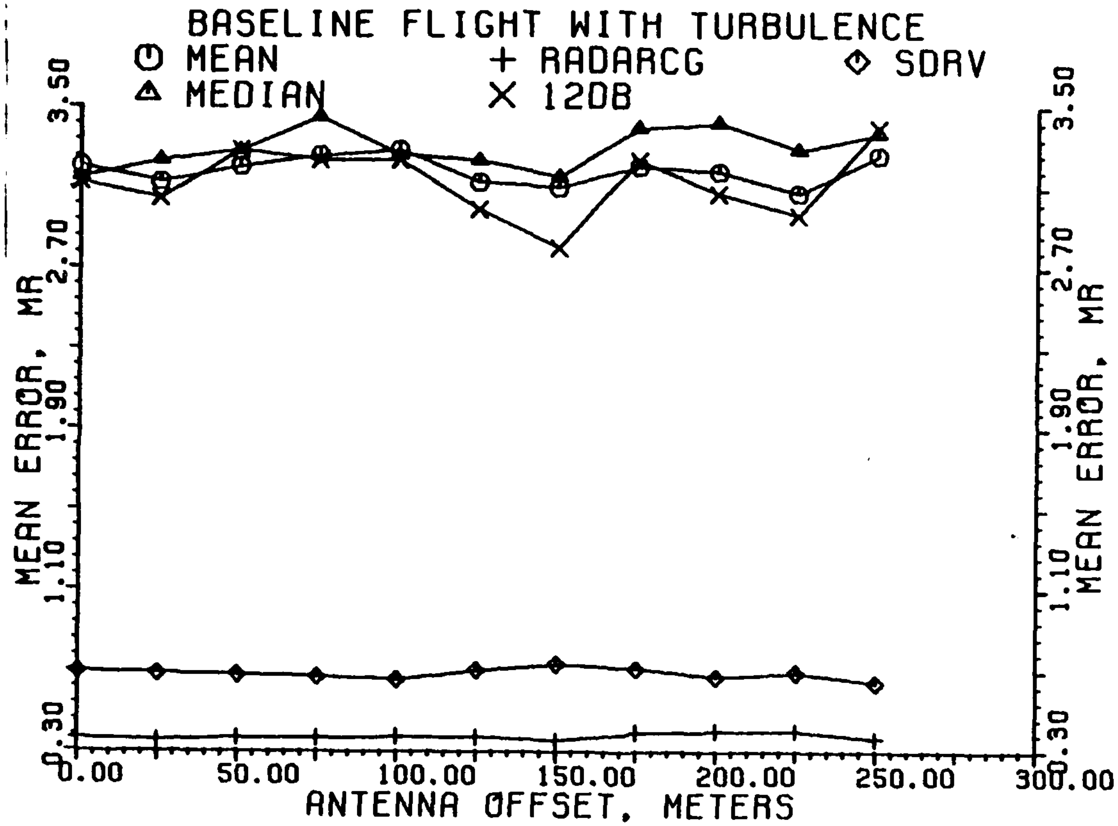

Figure 5-21. Mean error of estimators in milliradians for a granularity of 9 beam pointing locations. Each data point is the result of one flight, all scans used.

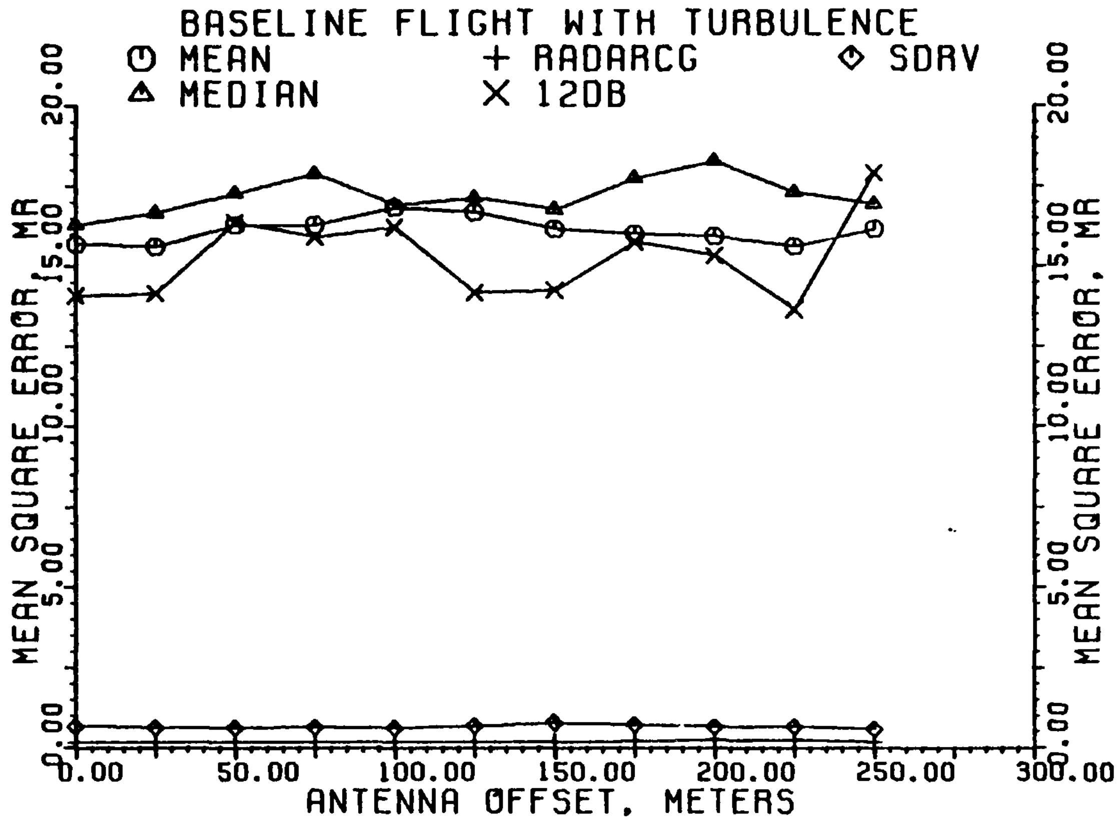

Figure 5-22. Mean square error of estimators in milliradians for a granularity of 9 beam pointing locations. Each data point is the result of one flight, all scans used.

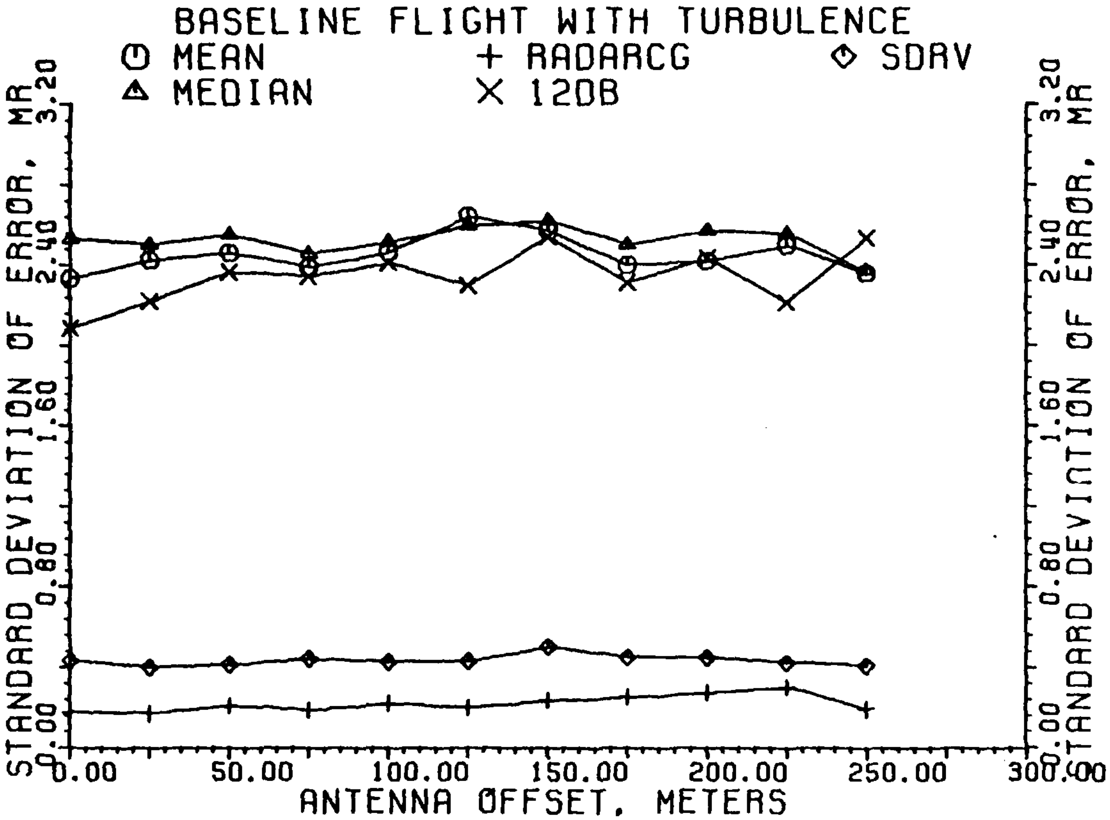

Figure 5-23. Standard deviation of error of estimators in milliradians for a granularity of 9 beam pointing locations. Each data point is the result of one flight, all scans used.

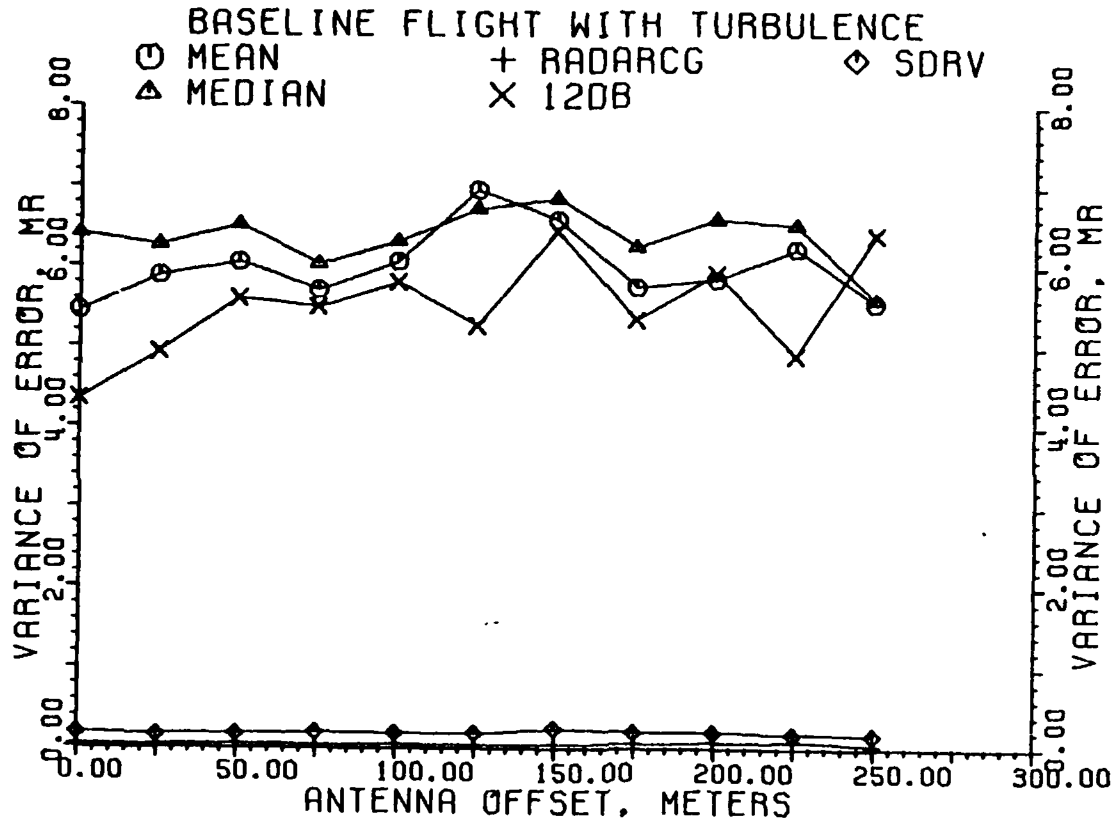

Figure 5-24. Variance of error of estimators in milliradians for a granularity of 9 beam pointing locations. Each data point is the result of one flight, all scans used.

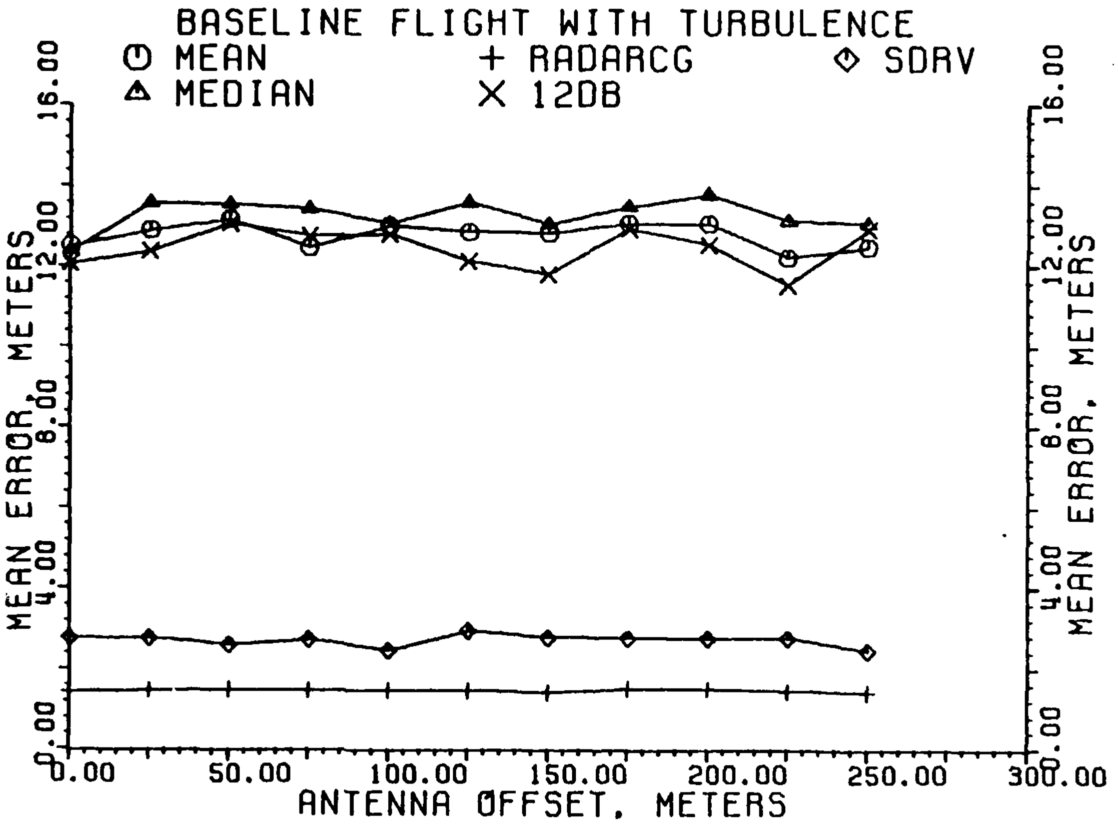

Figure 5-25. Mean error of estimators in meters for a granularity of 9 beam pointing locations. Each data point is the result of one flight, all scans used.

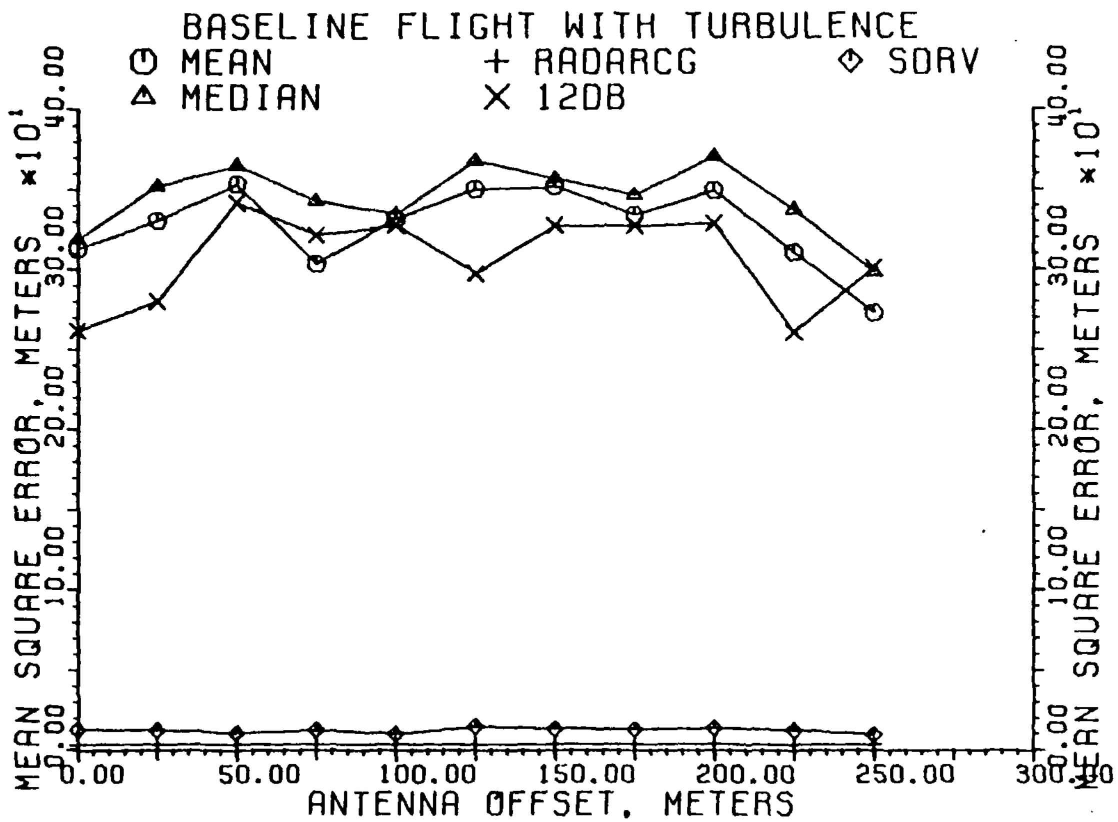

Figure 5-26. Mean square error of estimators in meters for a granularity of 9 beam pointing locations. Each data point is the result of one flight, all scans used.

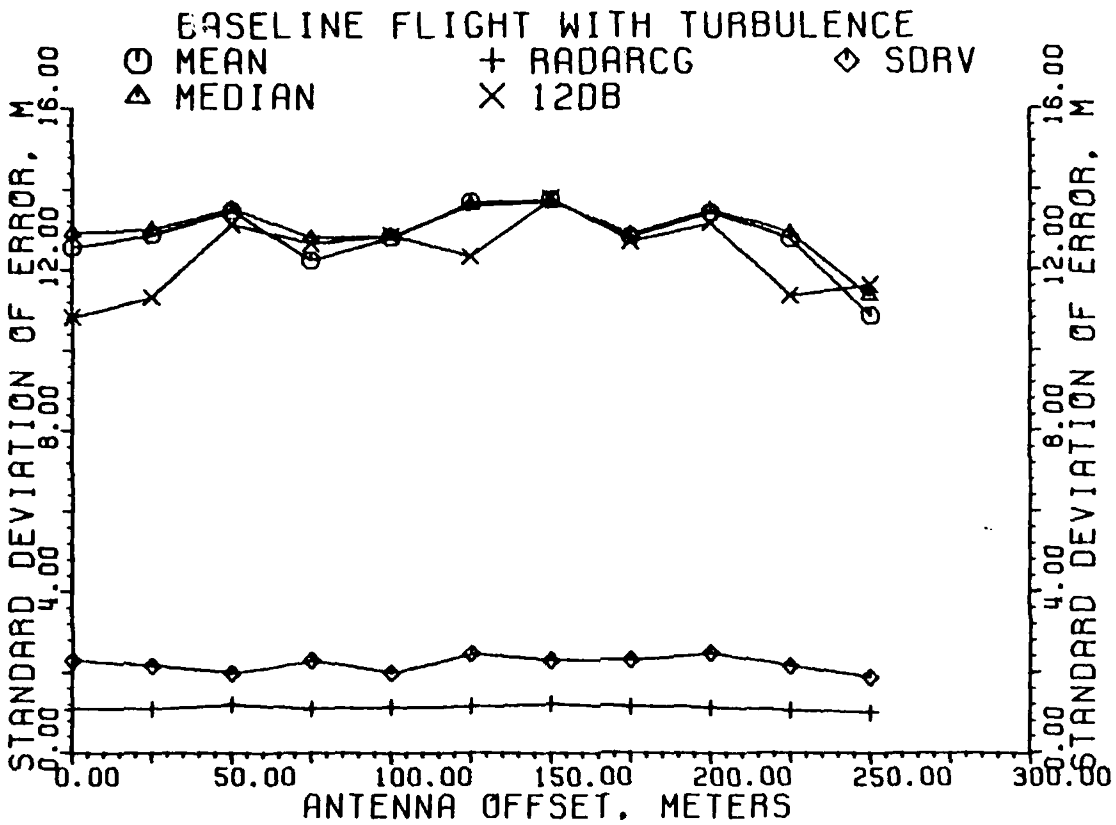

Figure 5-27. Standard deviation of error of estimators in meters for a granularity of 9 beam pointing locations. Each data point is the result of one flight, all scans used.

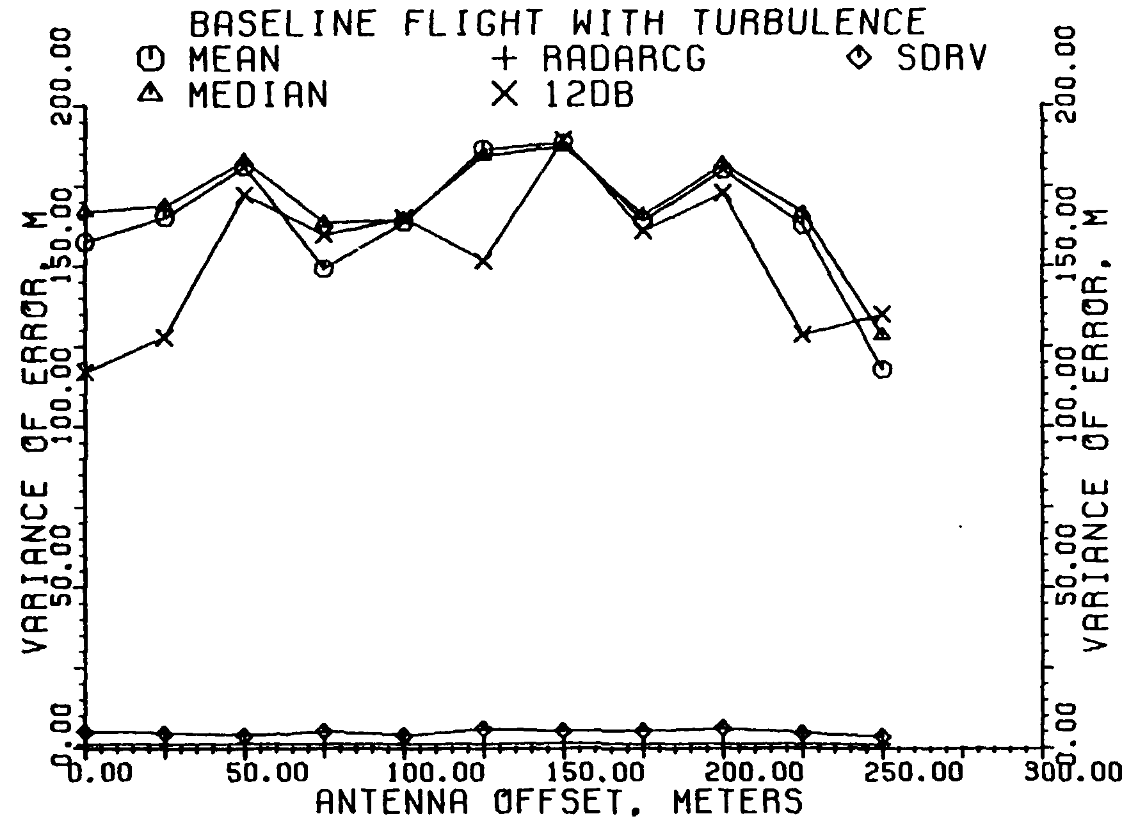

Figure 5-28. Variance of error of estimators in meters for a granularity of 9 beam pointing locations. Each data point is the result of one flight, all scans used.

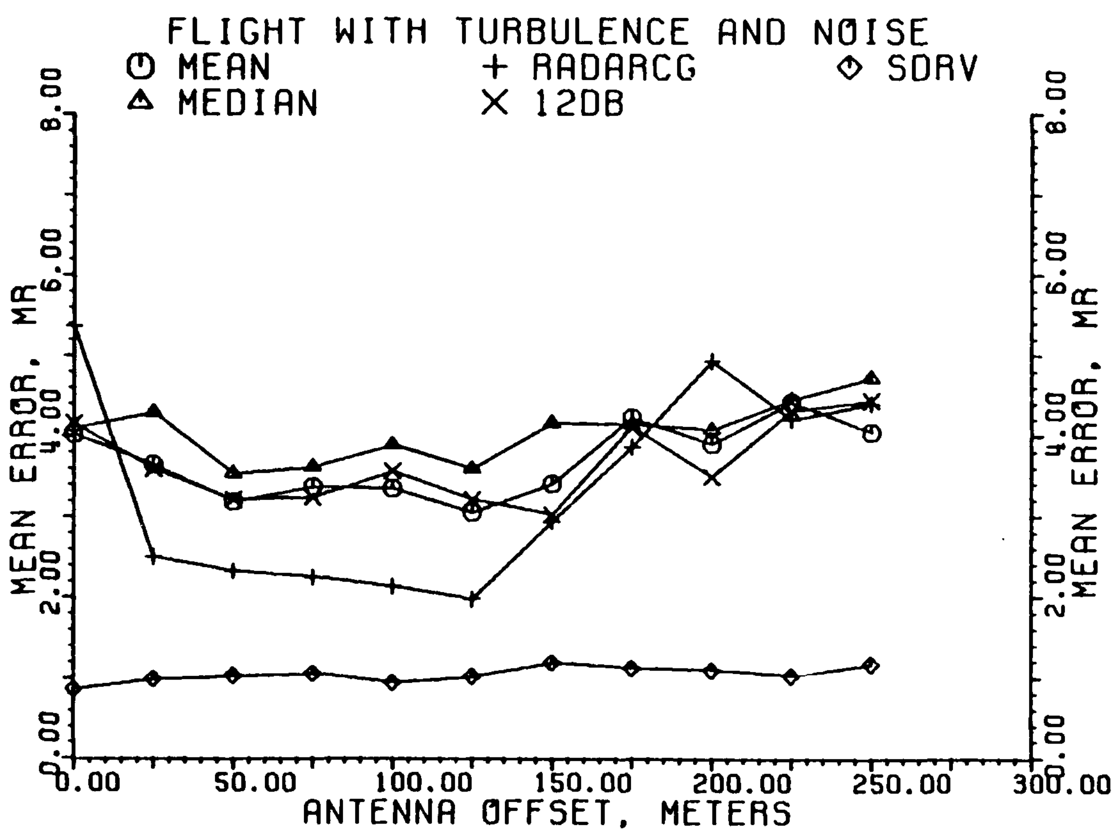

Figure 5-29. Mean error of estimators in milliradians for a granularity of 9 beam pointing locations. Each data point is the result of one flight, all scans used.

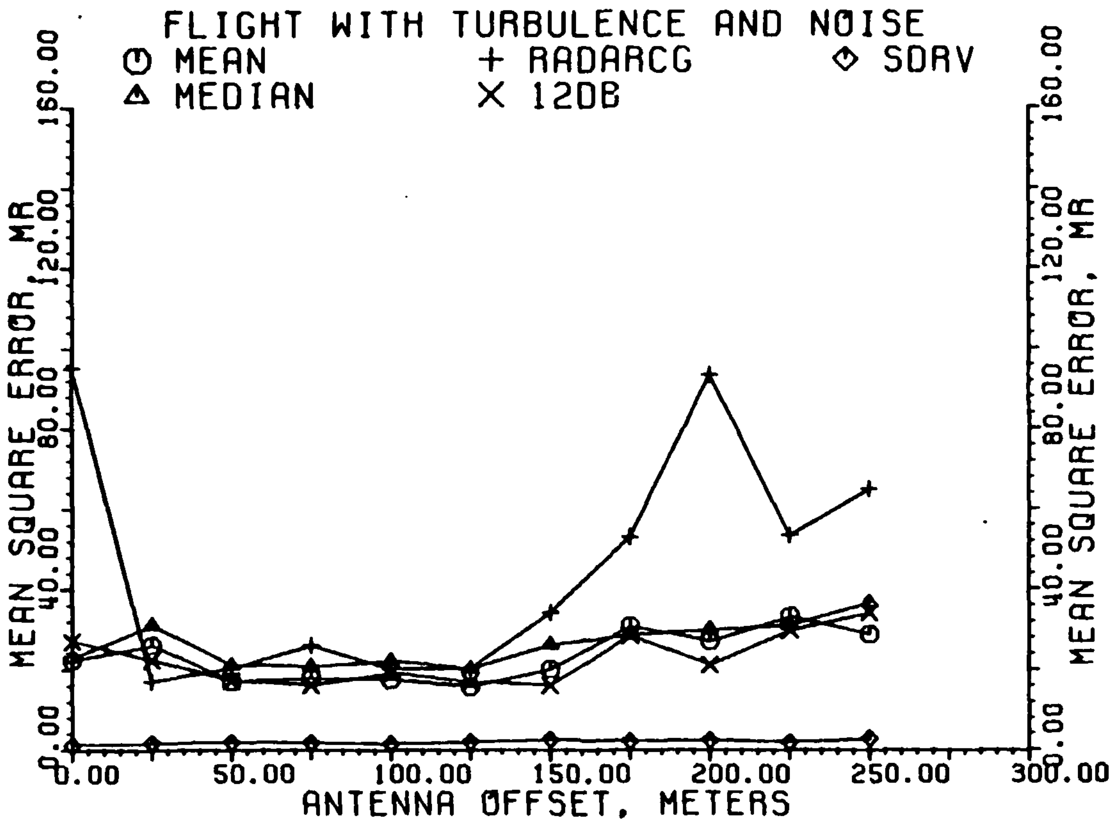

Figure 5-30. Mean square error of estimators in milliradians for a granularity of 9 beam pointing locations. Each data point is the result of one flight, all scans used.

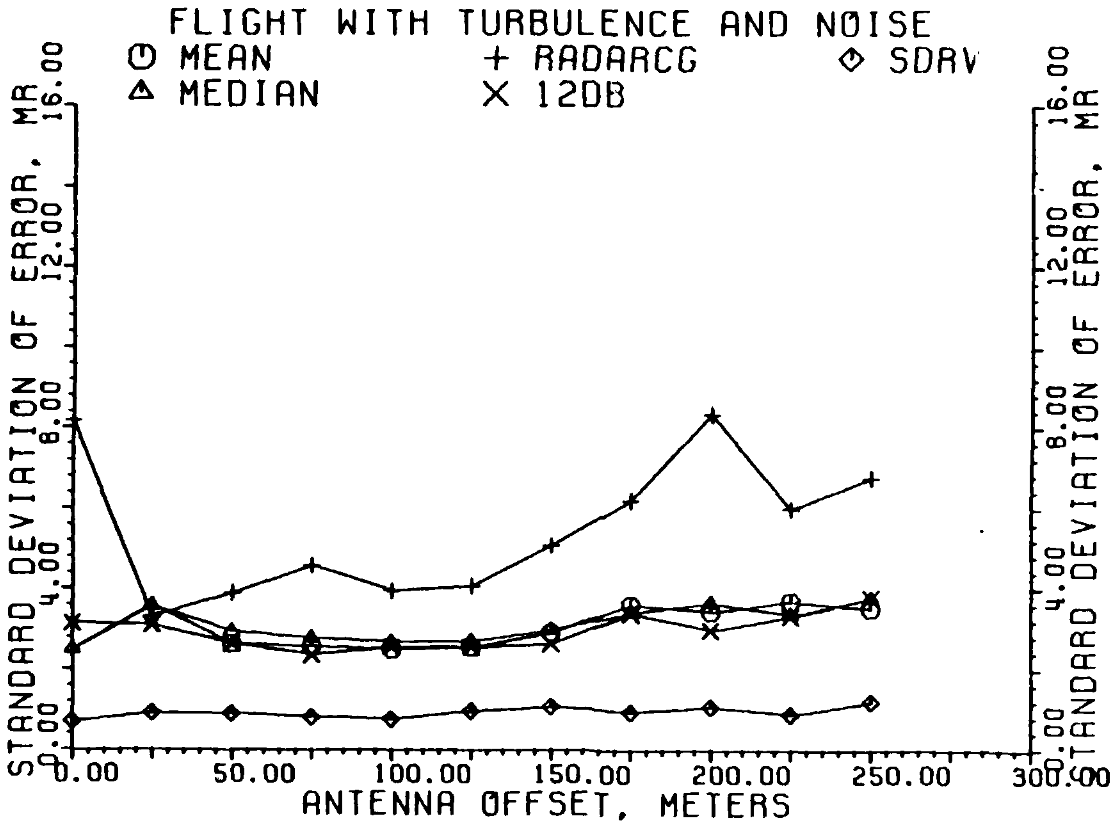

Figure 5-31. Standard deviation of error of estimators in milliradians for a granularity of 9 beam pointing locations. Each data point is the result of one flight, all scans used.

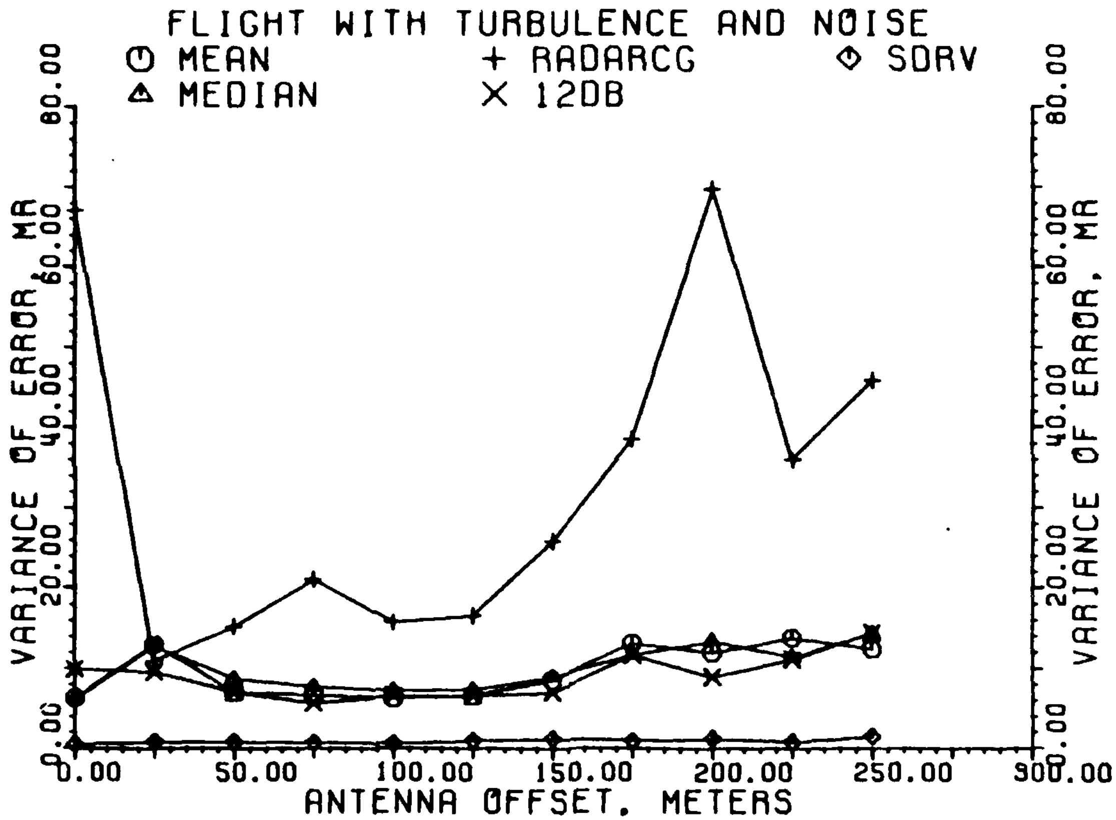

Figure 5-32. Variance of error of estimators in milliradians for a granularity of 9 beam pointing locations. Each data point is the result of one flight, all scans used.

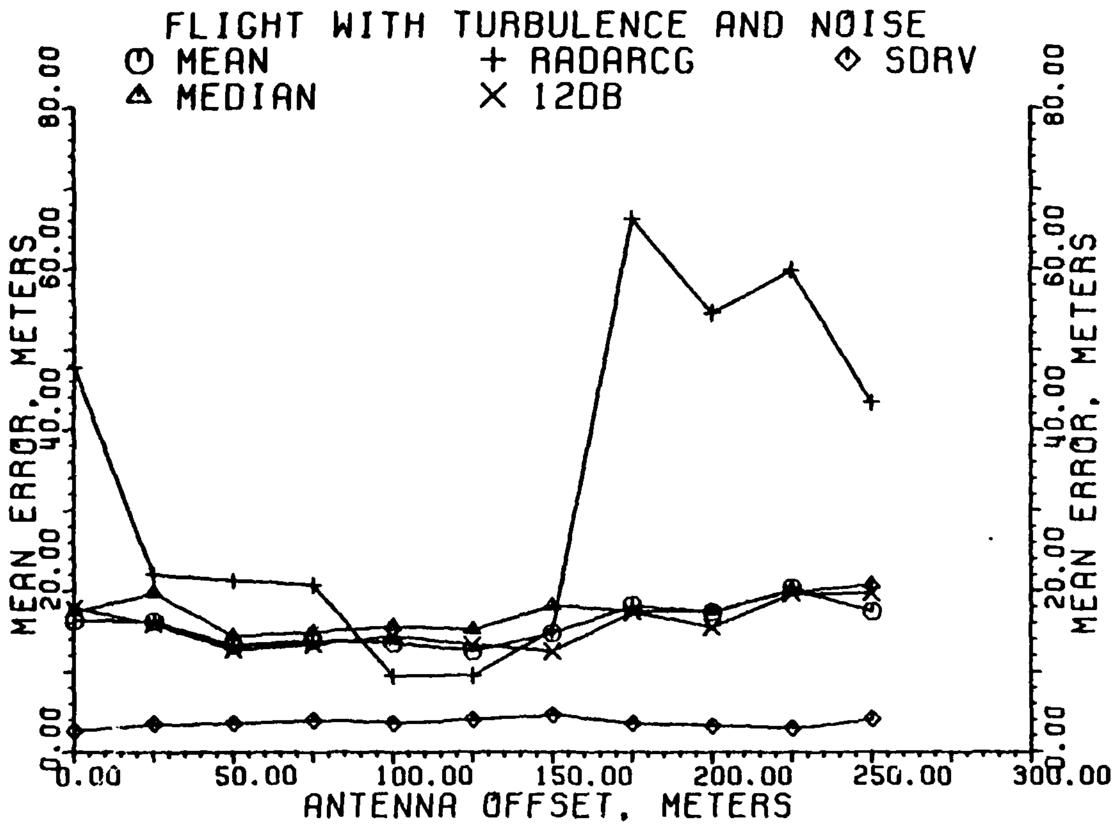

Figure 5-33. Mean error of estimators in meters for a granularity of 9 beam pointing locations. Each data point is the result of one flight, all scans used.

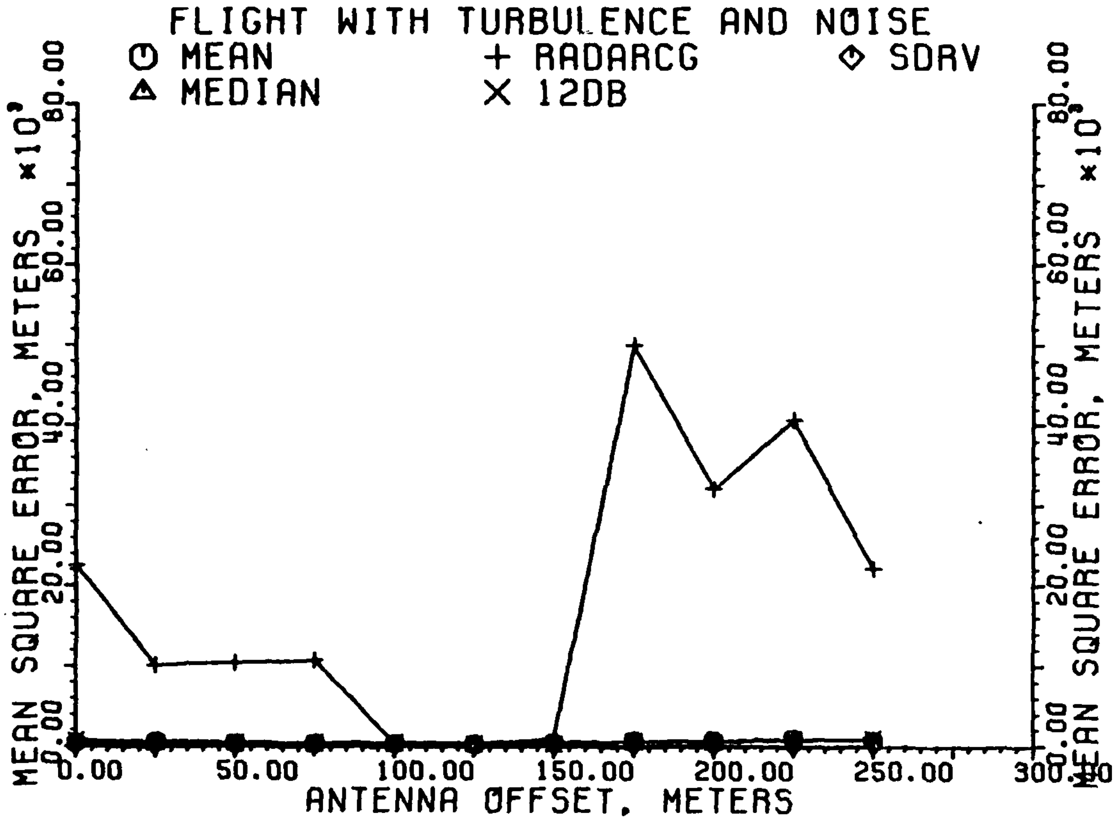

Figure 5-34. Mean square error of estimators in meters for a granularity of 9 beam pointing locations. Each data point is the result of one flight, all scans used.

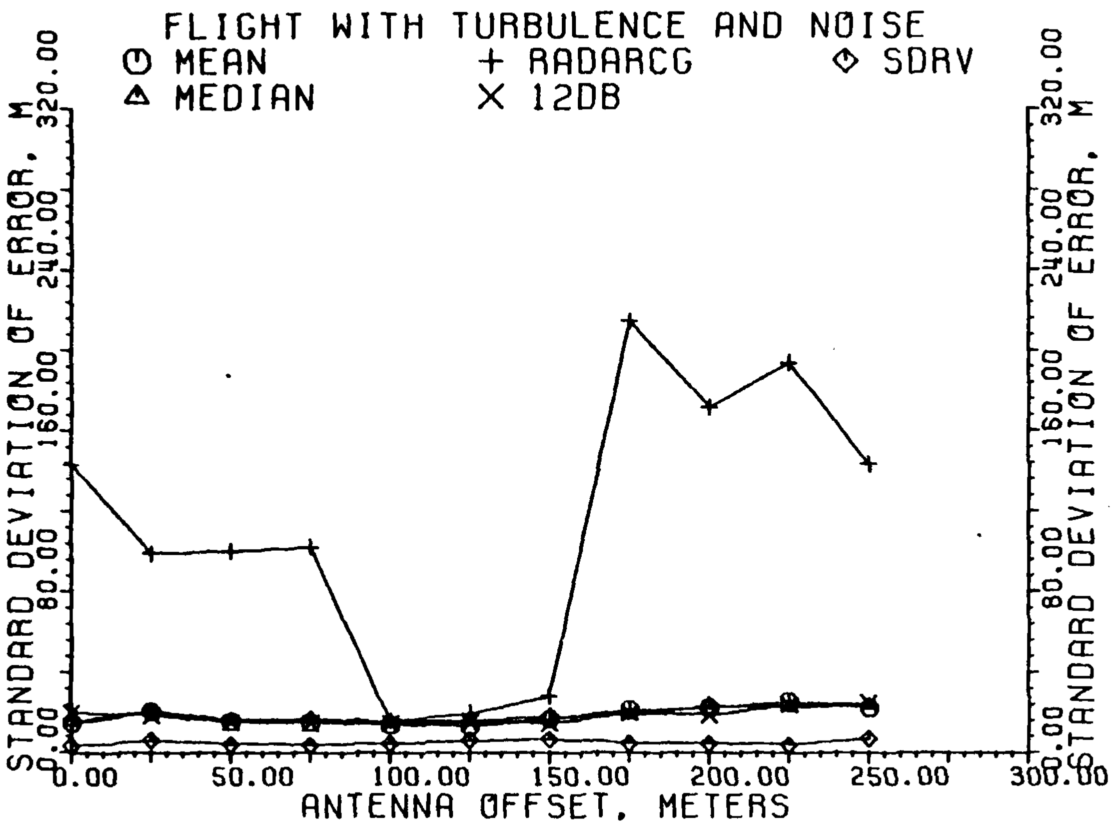

Figure 5-35. Standard deviation of error of estimators in meters for a granularity of 9 beam pointing locations. Each data point is the result of one flight, all scans used.

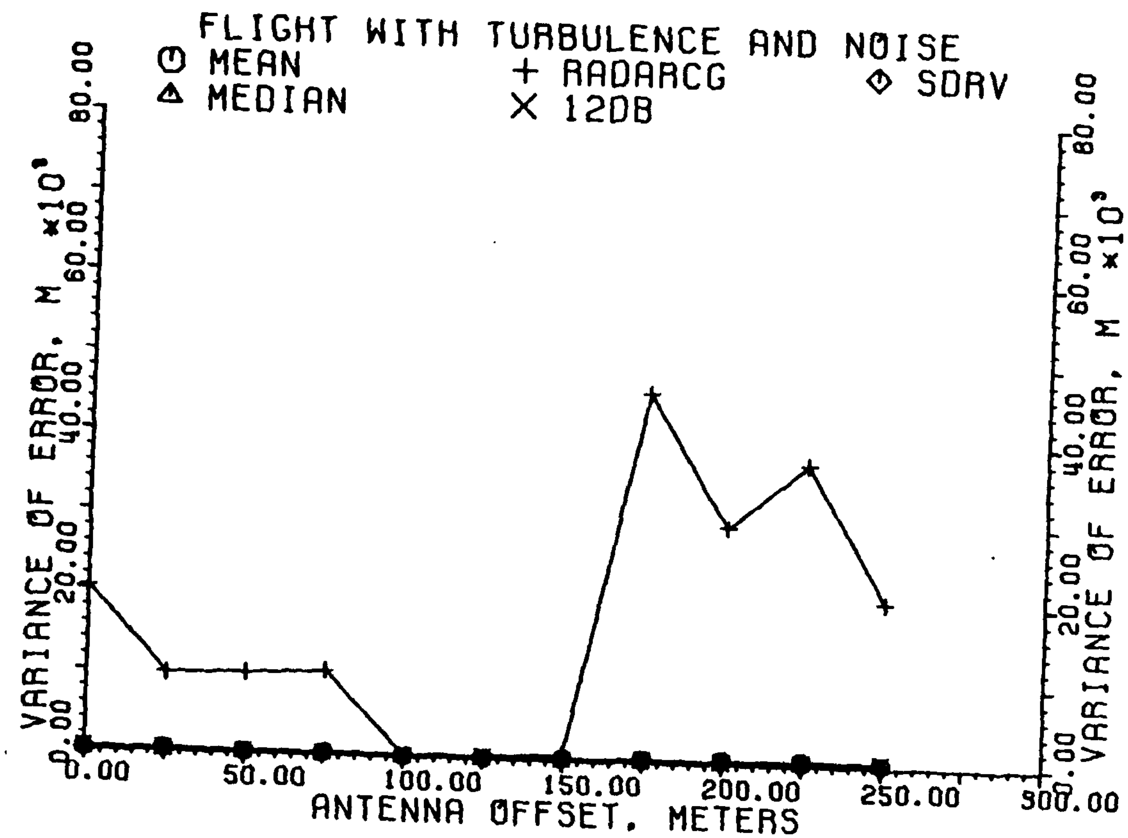

Figure 5-36. Variance of error of estimators in meters for a granularity of 9 beam pointing locations. Each data point is the result of one flight, all scans used.

quality, with a slight preference to 12 dB. RADARCG has now deteriorated to the least accurate and least robust estimator, due to the low data rate which does not allow the algorithm to properly decouple the noise.

While the above graphs included all scans, it would be worthwile to examine the performance of the estimators with signal-to-noise ratios of 13 dB or greater. Only those scans were selected from the data and plotted in the next series of figures.

The flights with noise, all scans above 13 dB, Figures 5-37 through 5-44, indicate that SDRV and RADARCG are both approximately equal in performance. SDRV is slightly favored since it appears to be more robust at the various antenna offsets. The thresholding estimators are of equal quality.

With turbulence, Figures 5-45 through 5-52, the same is true. While it would appear that SDRV is slightly less accurate than RADARCG by viewing the plots with the error in milliradians, Figures 5-45 through 5-48, SDRV was more accurate in the actual meter error from the target, Figures 5-48 through 5-52. This error occurred when the target was at close range, when a large error in milliradians is a small error in meters. The thresholding techniques are comparable to each other and are not as accurate as SDRV or RADARCG.

Scans which had signal-to-noise ratios of 10 dB or less reflect the ability of the estimators to find the target in noise. The flights with noise, Figures 5-53 through 5-60, show the second derivative method to be the most accurate with the least deviation or variance in noise. RADARCG has the greatest error of the estimators. The thresholding methods are, again, of similar quality.

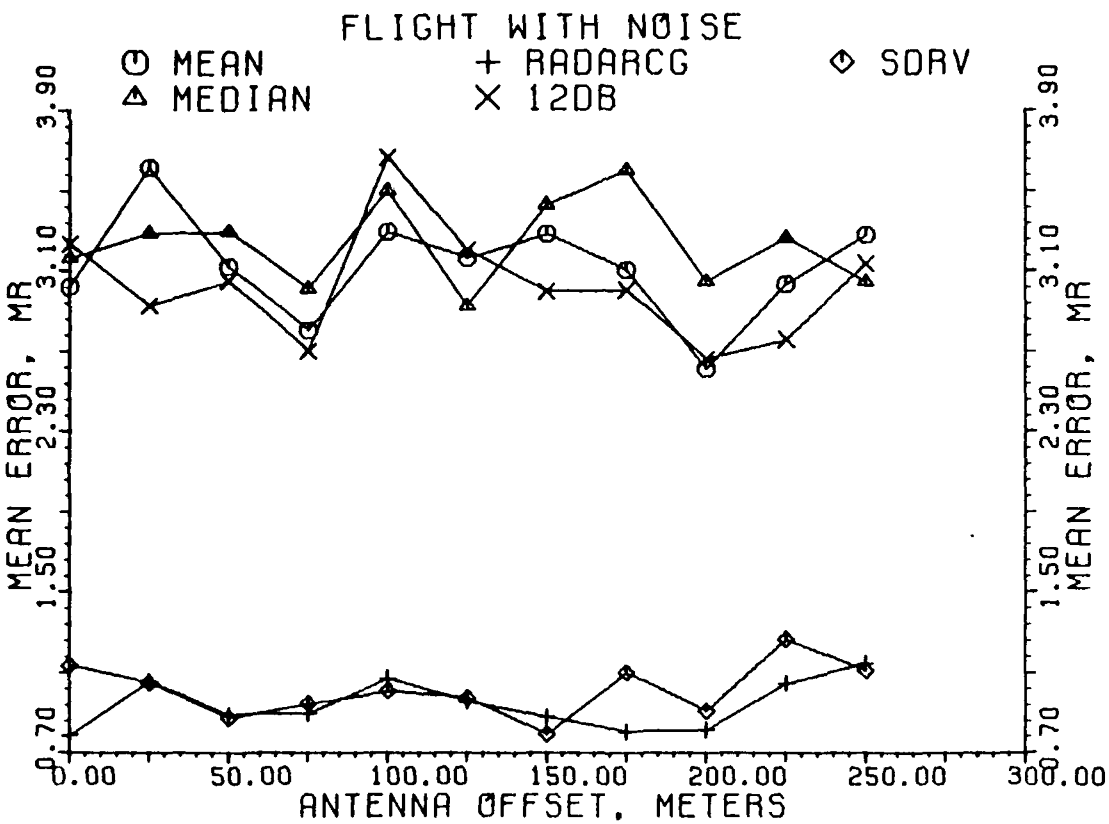

Figure 5-37. Mean error of estimators in milliradians for a granularity of 9 beam pointing locations. Each data point is the result of one flight, all scans with a SNR 13 dB or greater used.

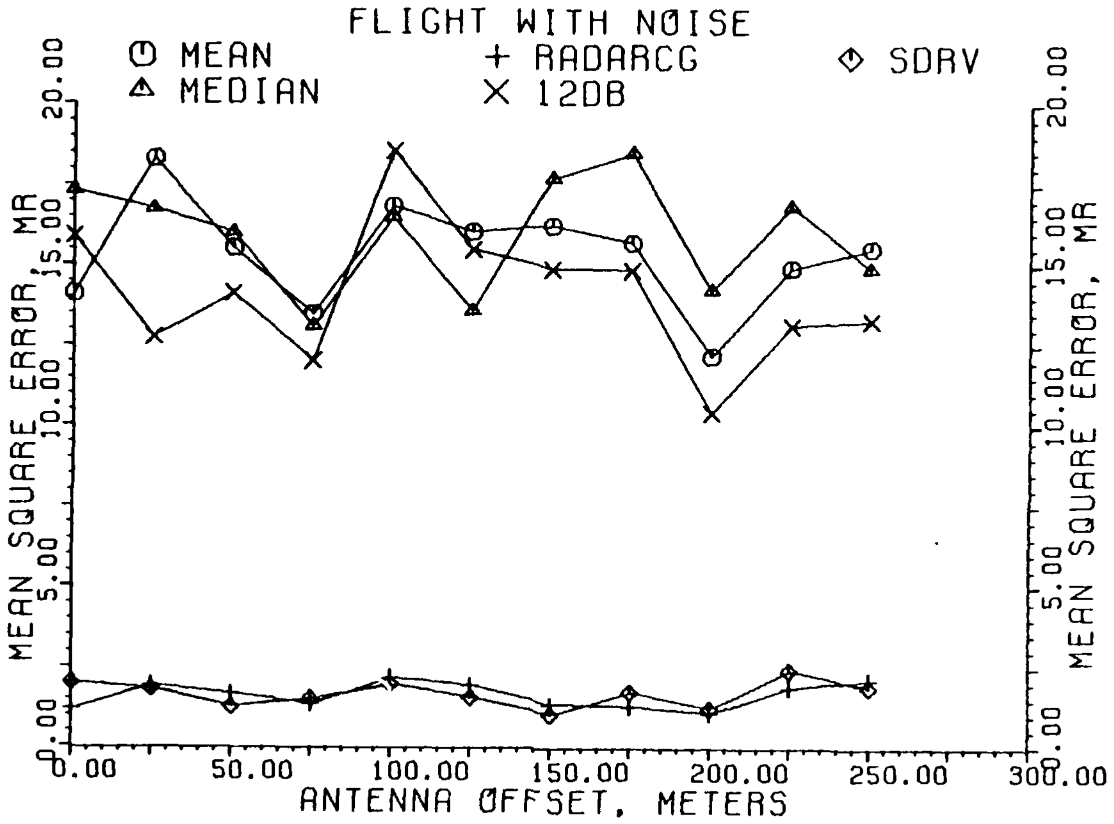

Figure 5-38. Mean square error of estimators in milliradians for a granularity of 9 beam pointing locations. Each data point is the result of one flight, all scans with a SNR 13 dB or greater used.

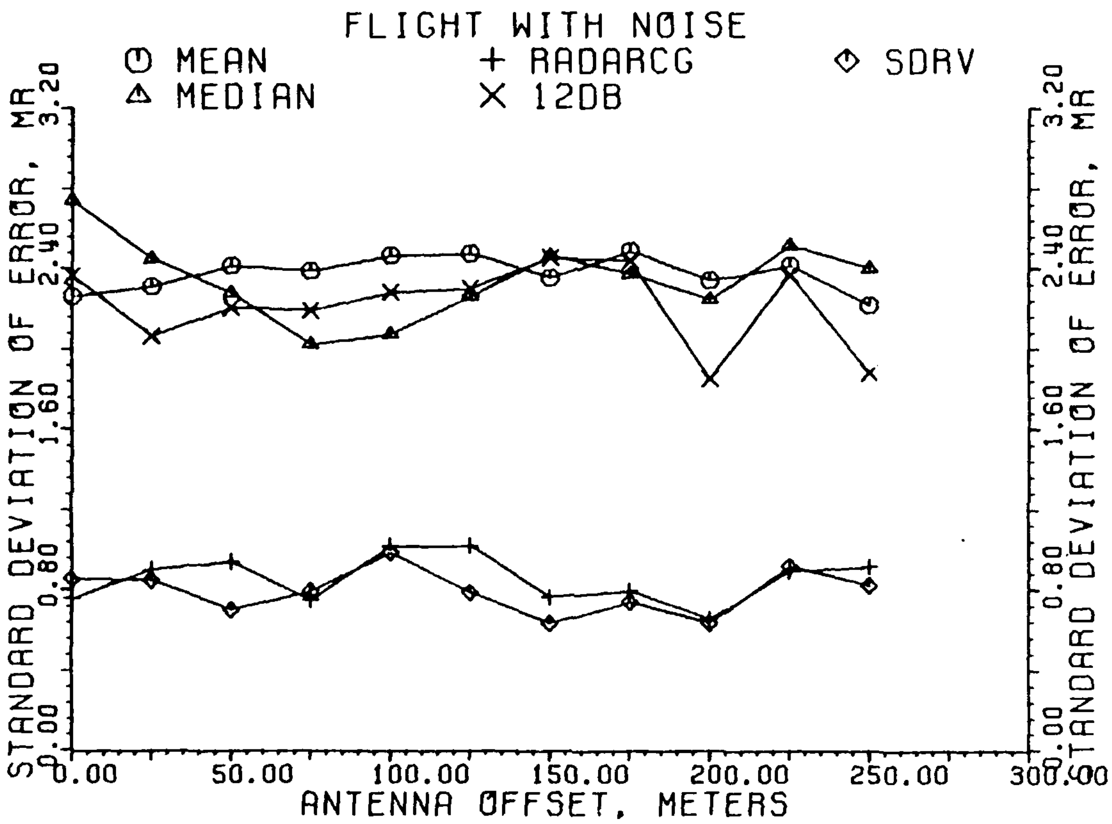

Figure 5-39. Standard deviation of error of estimators in milliradians for a granularity of 9 beam pointing locations. Each data point is the result of one flight, all scans with a SNR 13 dB or greater used.

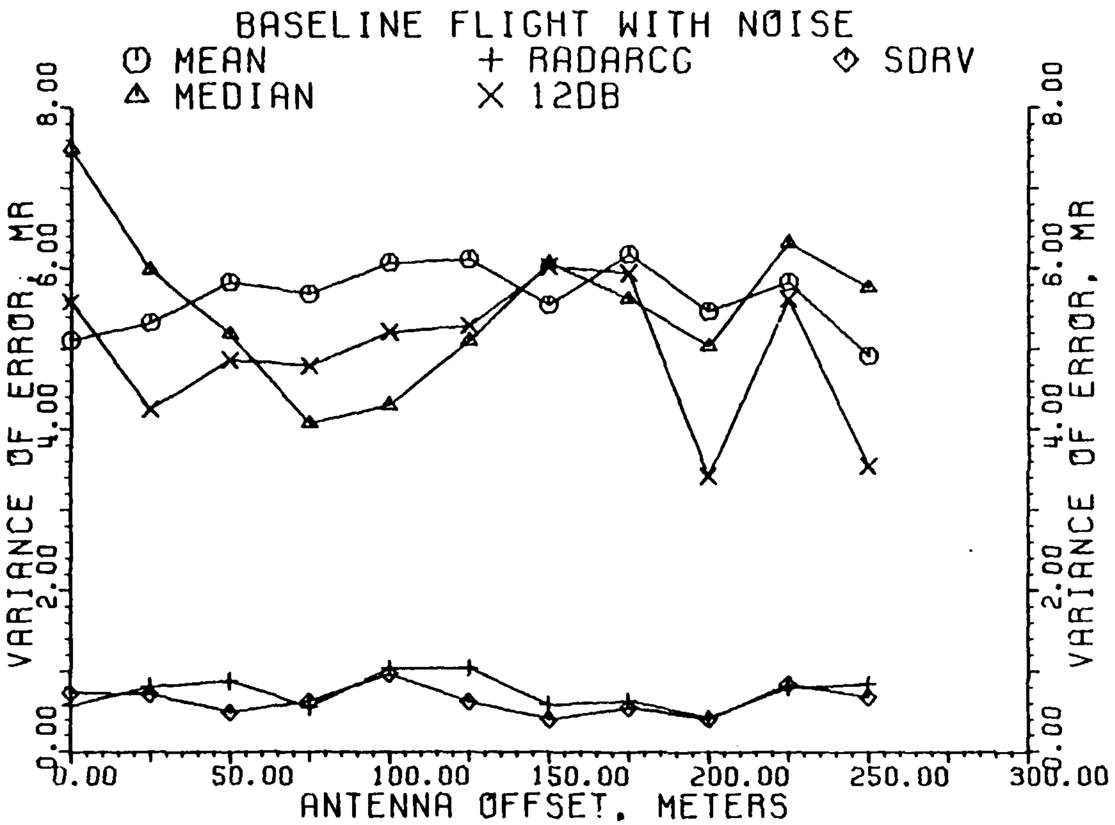

Figure 5-40. Variance of error of estimators in milliradians for a granularity of 9 beam poincing locations. Each data point is the result of one flight, all scans with a SNR 13 dB or greater used.

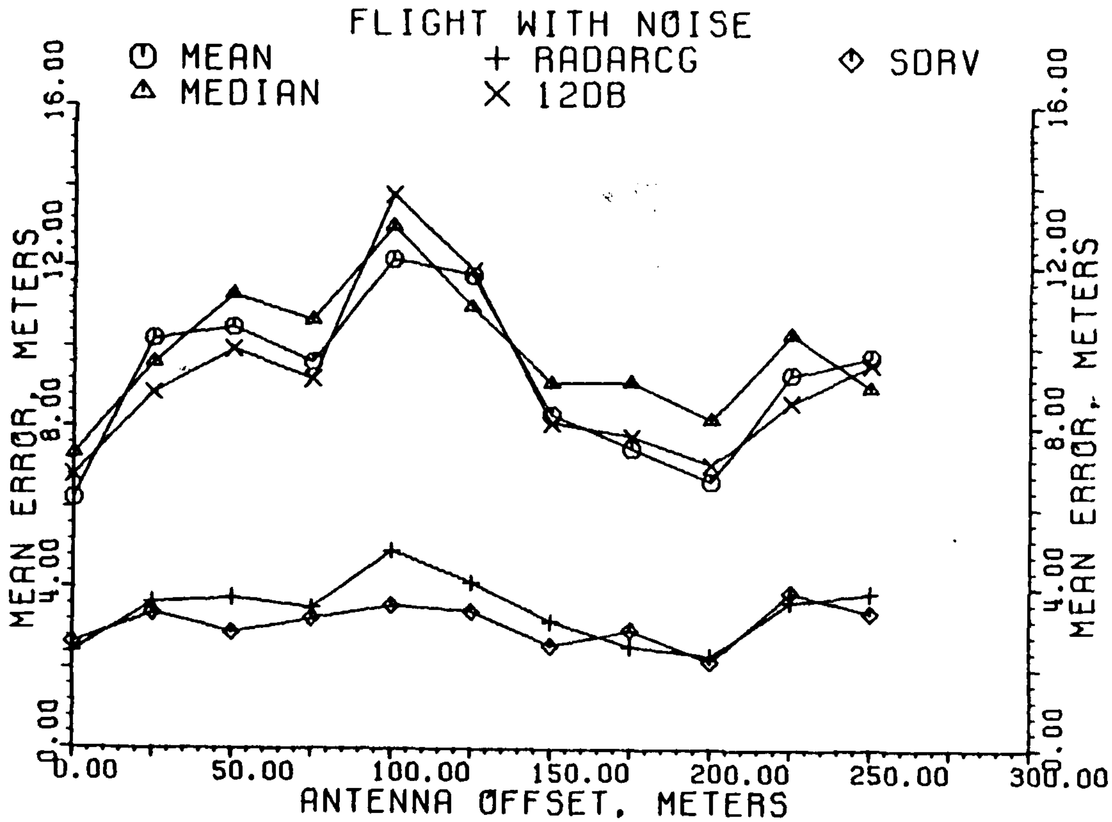

Figure 5-41. Mean error of estimators in meters for a granularity of 9 beam pointing locations. Each data point is the result of one flight, all scans with a SNR 13 dB or greater used.

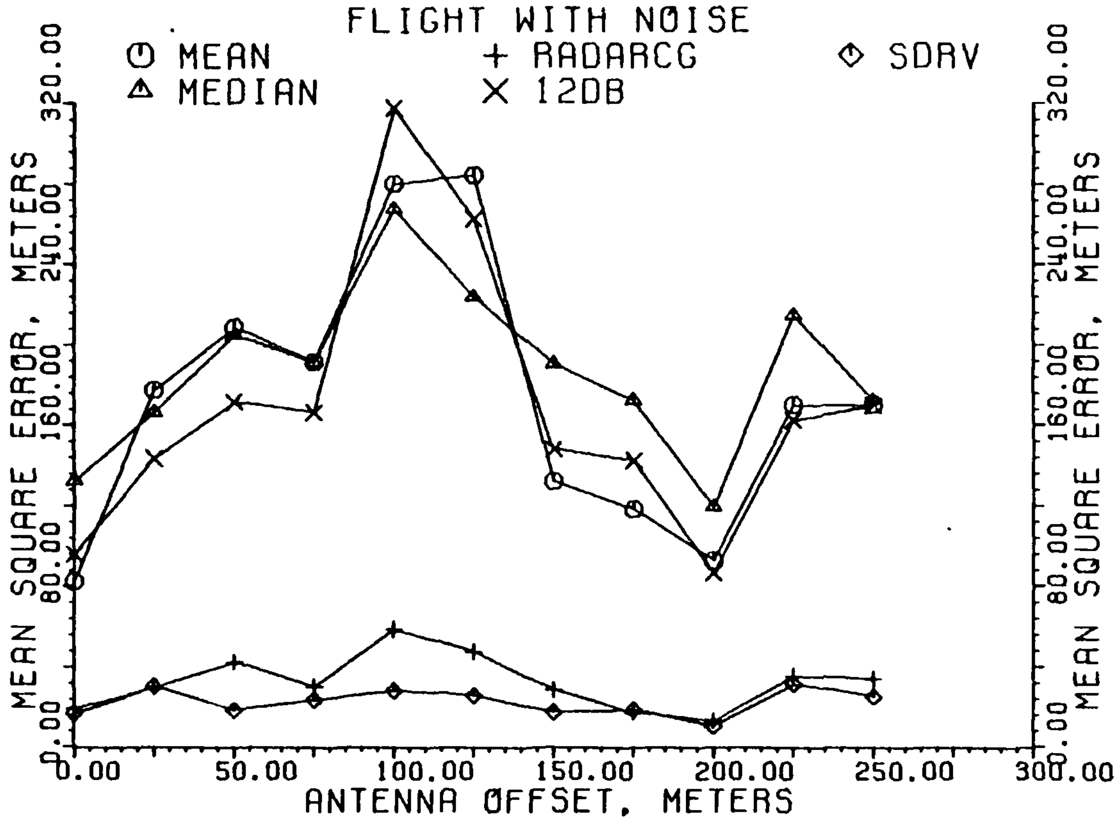

Figure 5-42. Mean square error of estimators in meters for a granularity of 9 beam pointing locations. Each data point is the result of one flight, all scans with a SNR 13 dB or greater used.

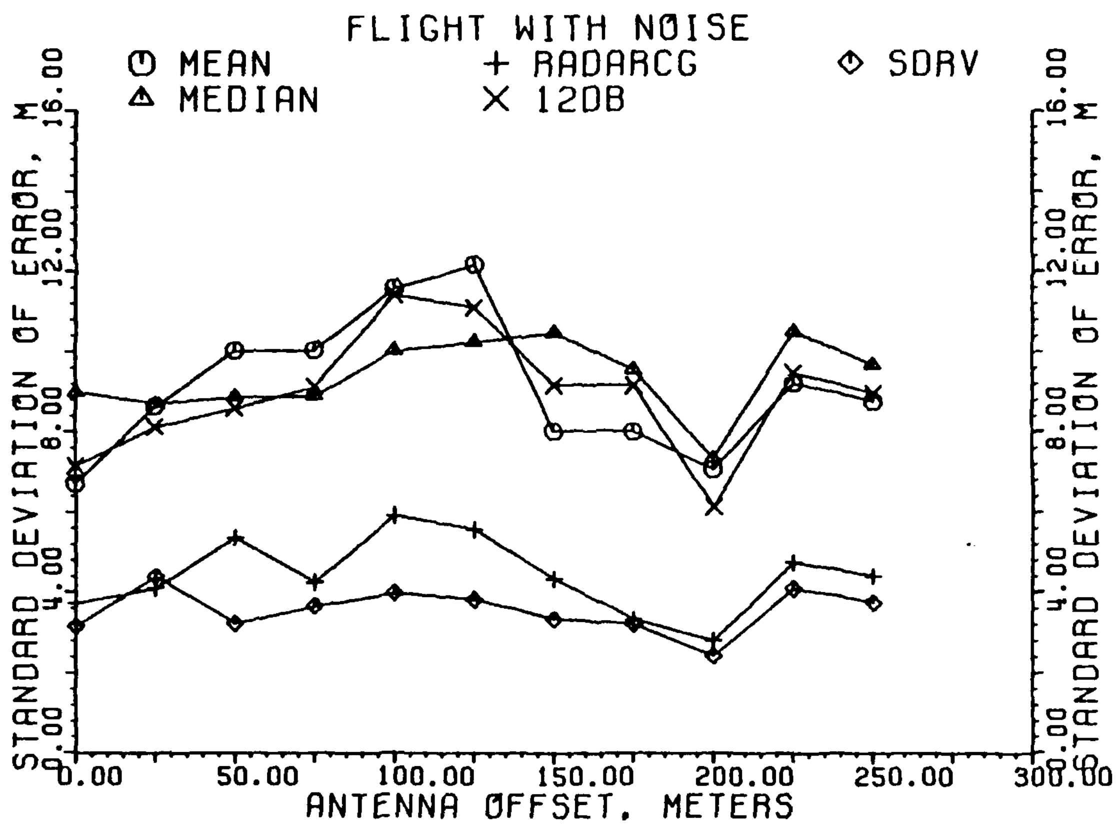

Figure 5-43. Standard deviation of error of estimators in meters for a granularity of 9 beam pointing locations. Each data point is the result of one flight, all scans with a SNR 13 dB or greater used.

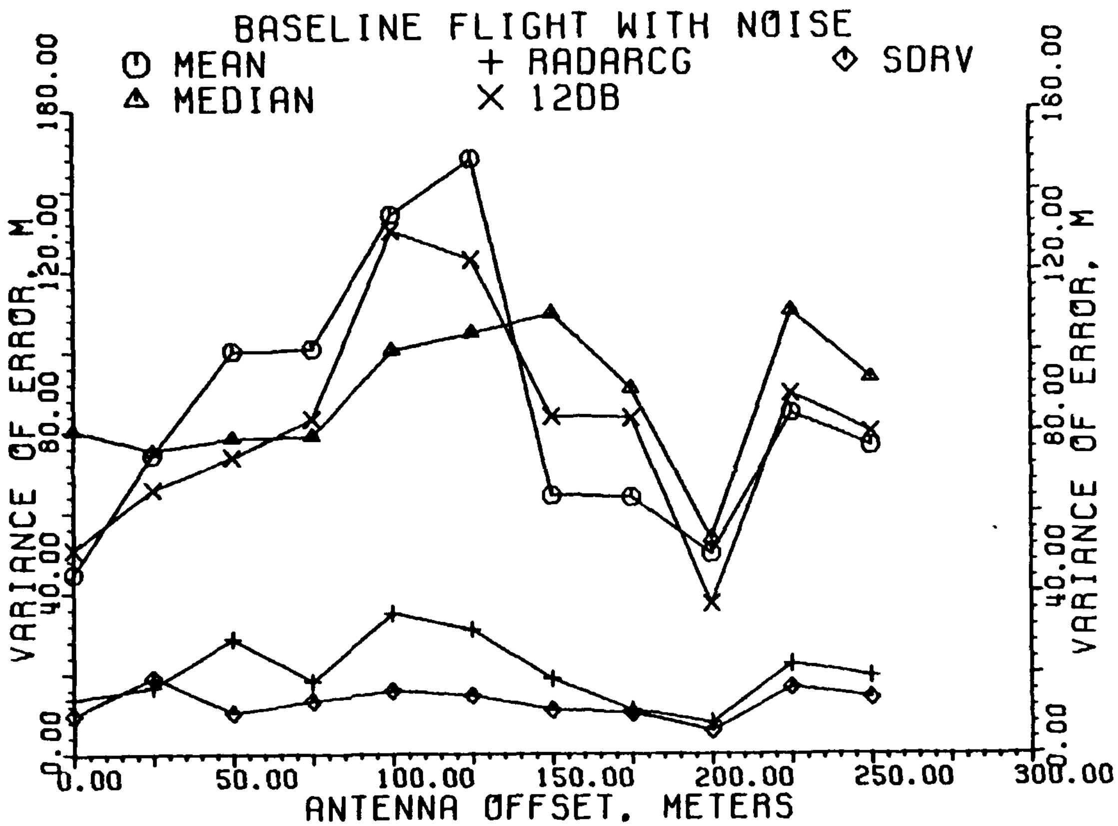

Figure 5-44. Variance of error of estimators in meters for a granularity of 9 beam pointing locations. Each data point is the result of one flight, all scans with a SNR 13 dB or greater used.

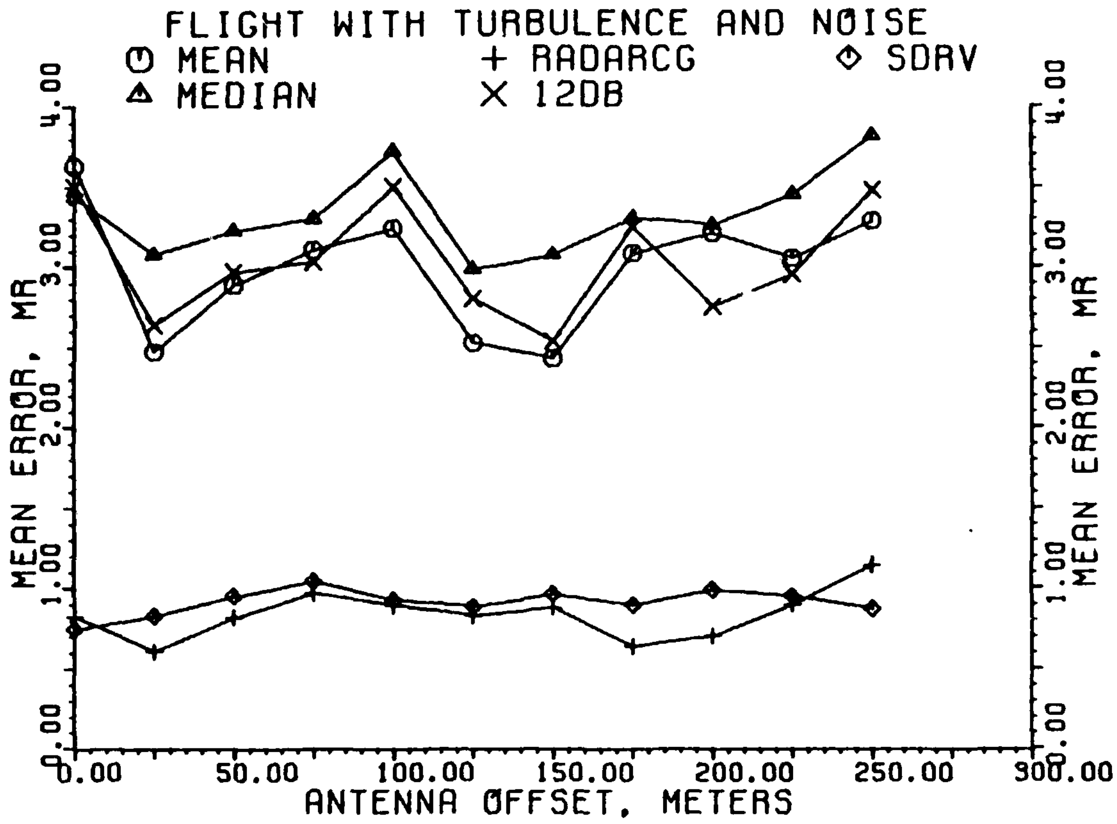

Figure 5-45. Mean error of estimators in milliradians for a granularity of 9 beam pointing locations. Each data point is the result of one flight, all scans with a SNR 13 dB or greater used.

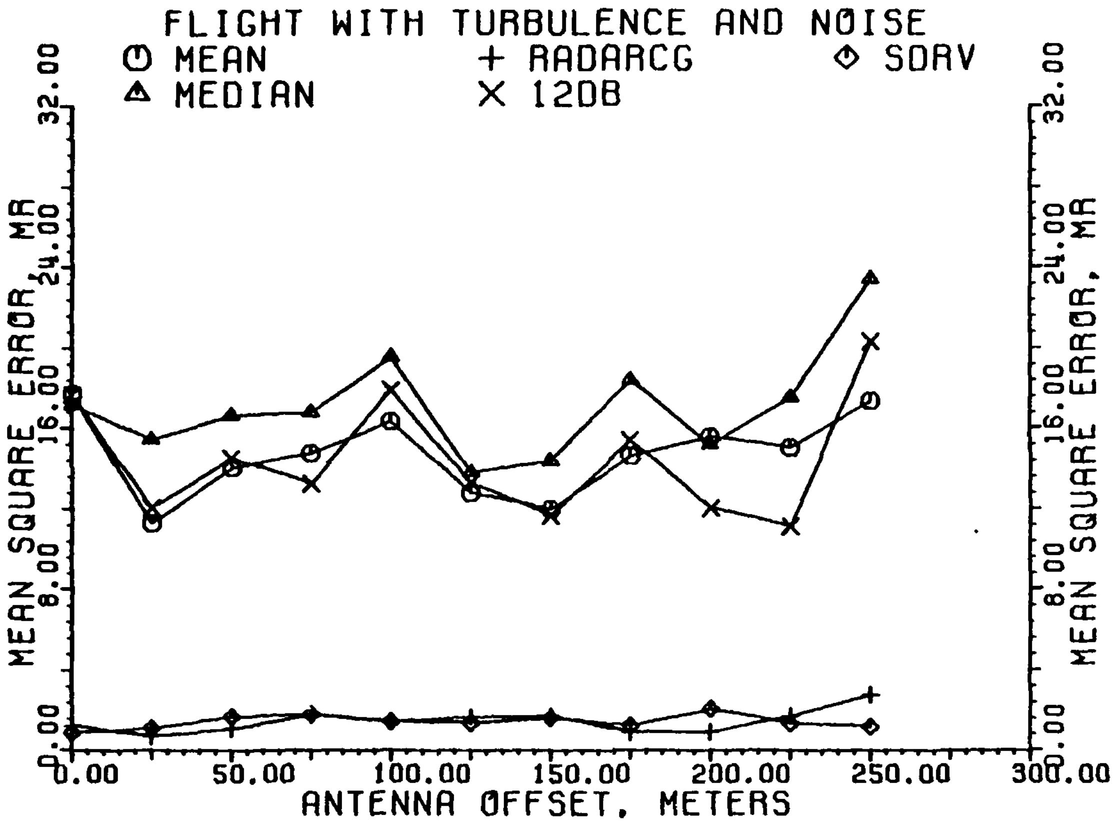

Figure 5-46. Mean square error of estimators in milliradians for a granularity of 9 beam pointing locations. Each data point is the result of one flight, all scans with a SNR 13 dB or greater used.

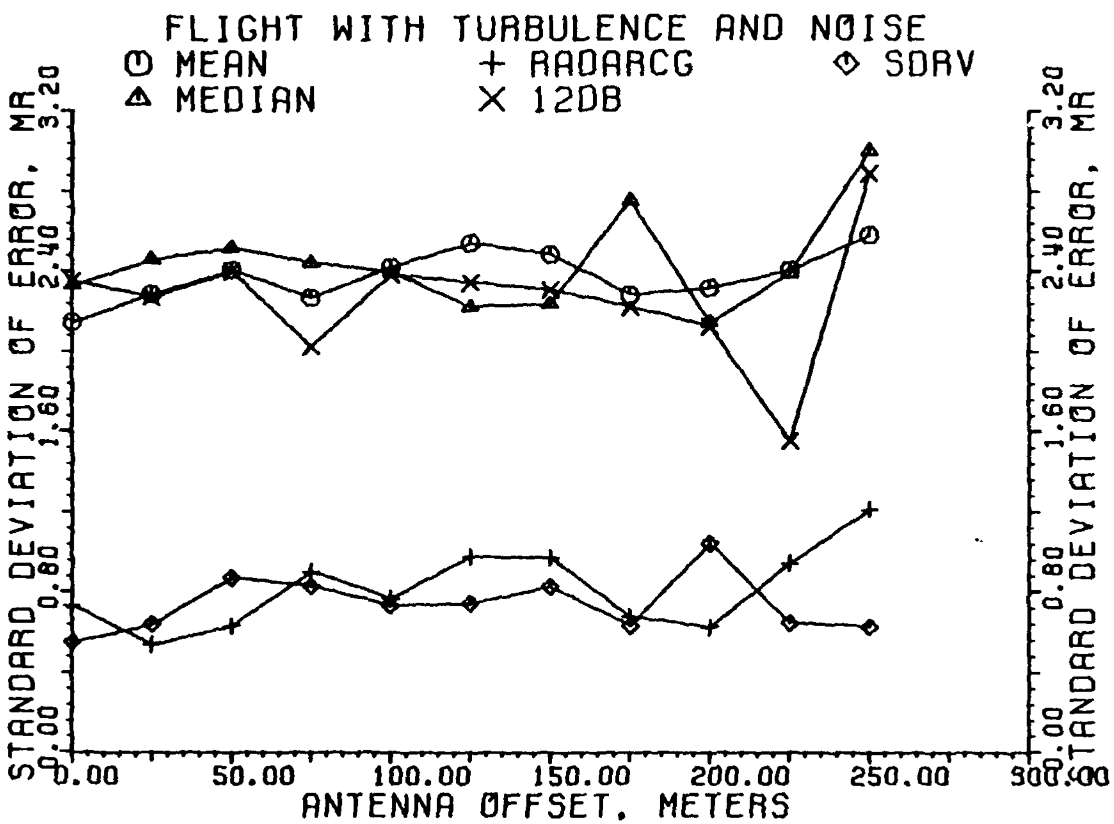

Figure 5-47. Standard deviation of error of estimators in milliradians for a granularity of 9 beam pointing locations. Each data point is the result of one flight, all scans with a SNR 13 dB or greater used.

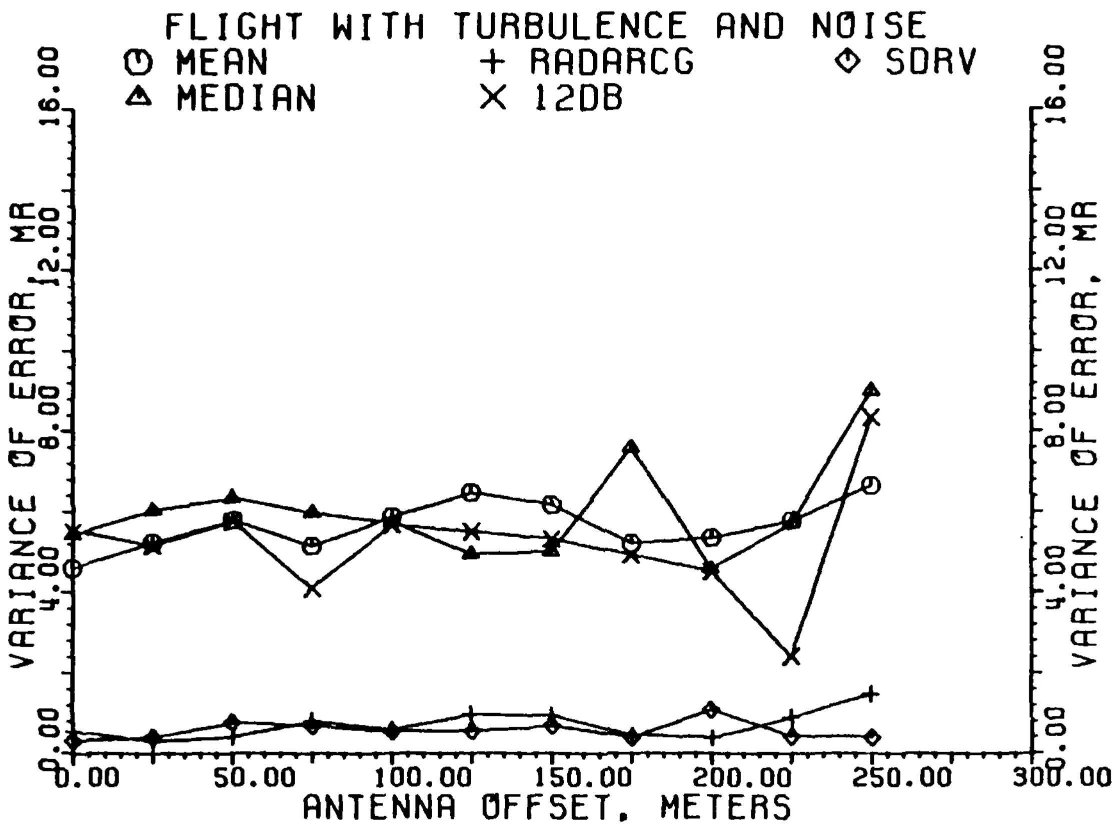

Figure 5-48. Variance of error of estimators in milliradians for a granularity of 9 beam pointing locations. Each data point is the result of one flight, all scans with a SNR 13 dB or greater used.

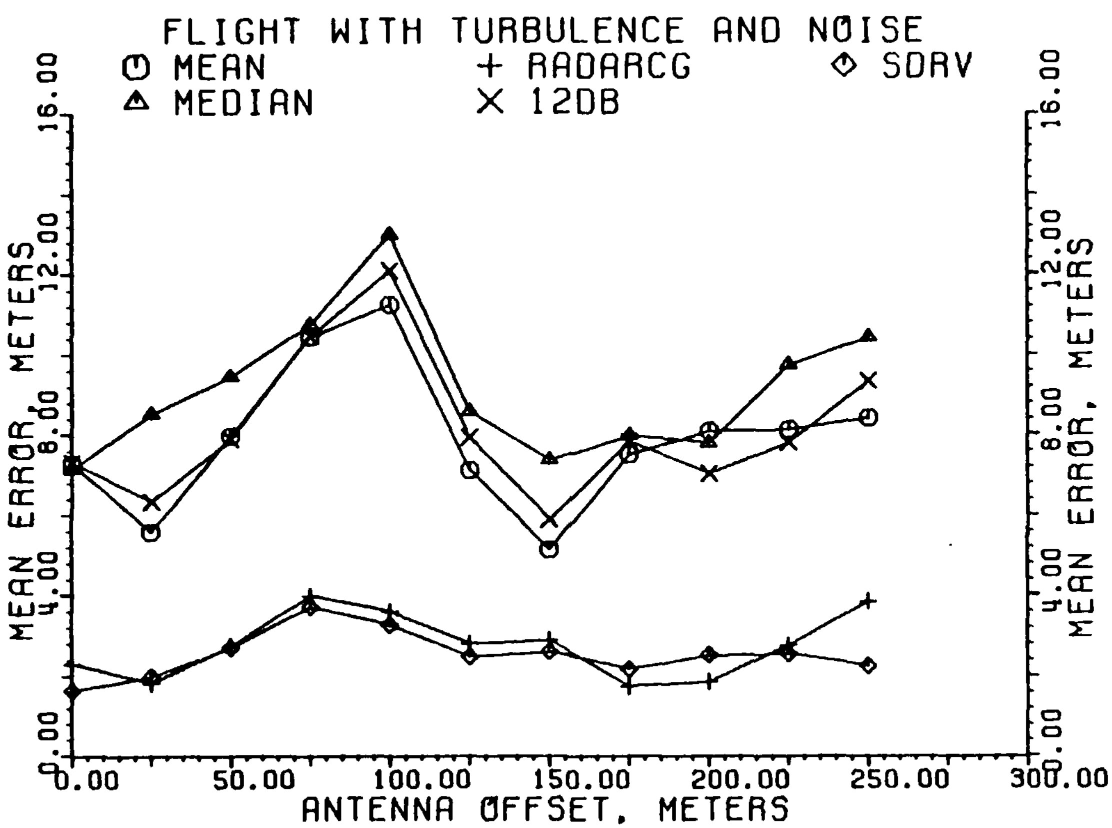

Figure 5-49. Mean error of estimators in meters for a granularity of 9 beam pointing locations. Each data point is the result of one flight, all scans with a SNR 13 dB or greater used.

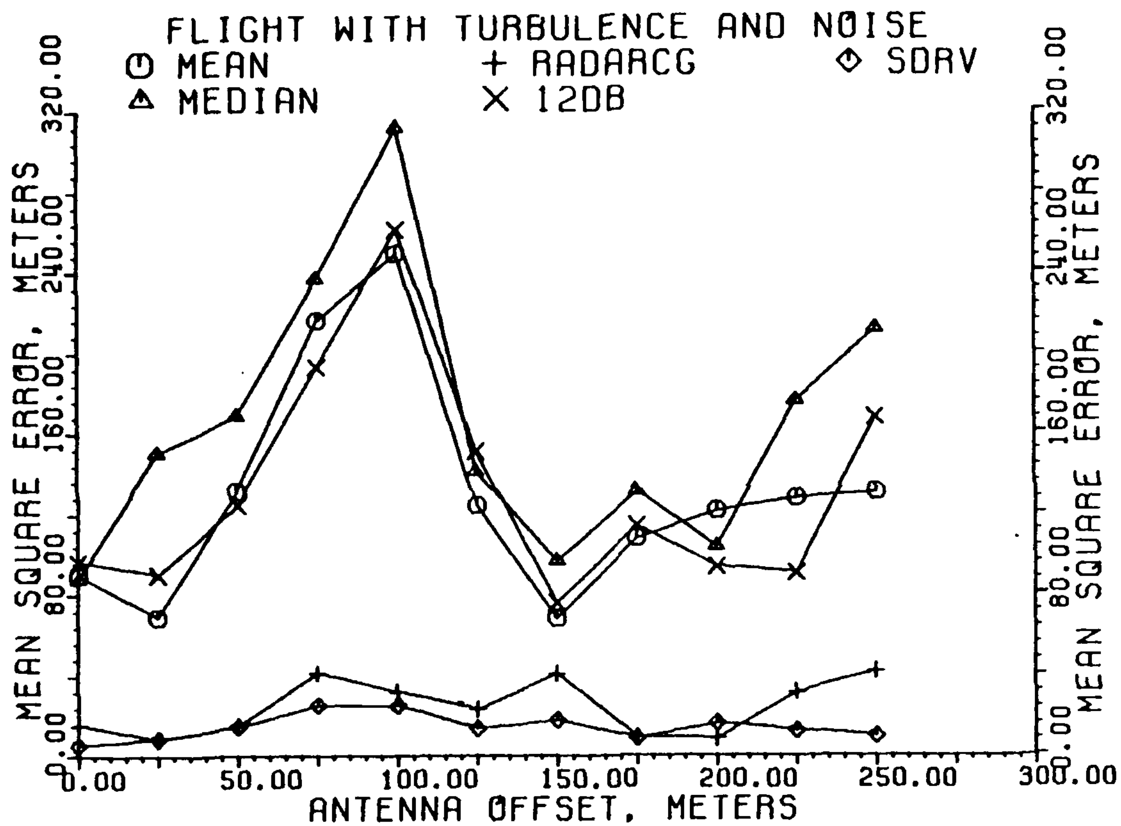

Figure 5-50. Mean square error of estimators in meters for a granularity of 9 beam pointing locations. Each data point is the result of one flight, all scans with a SNR 13 dB or greater used.

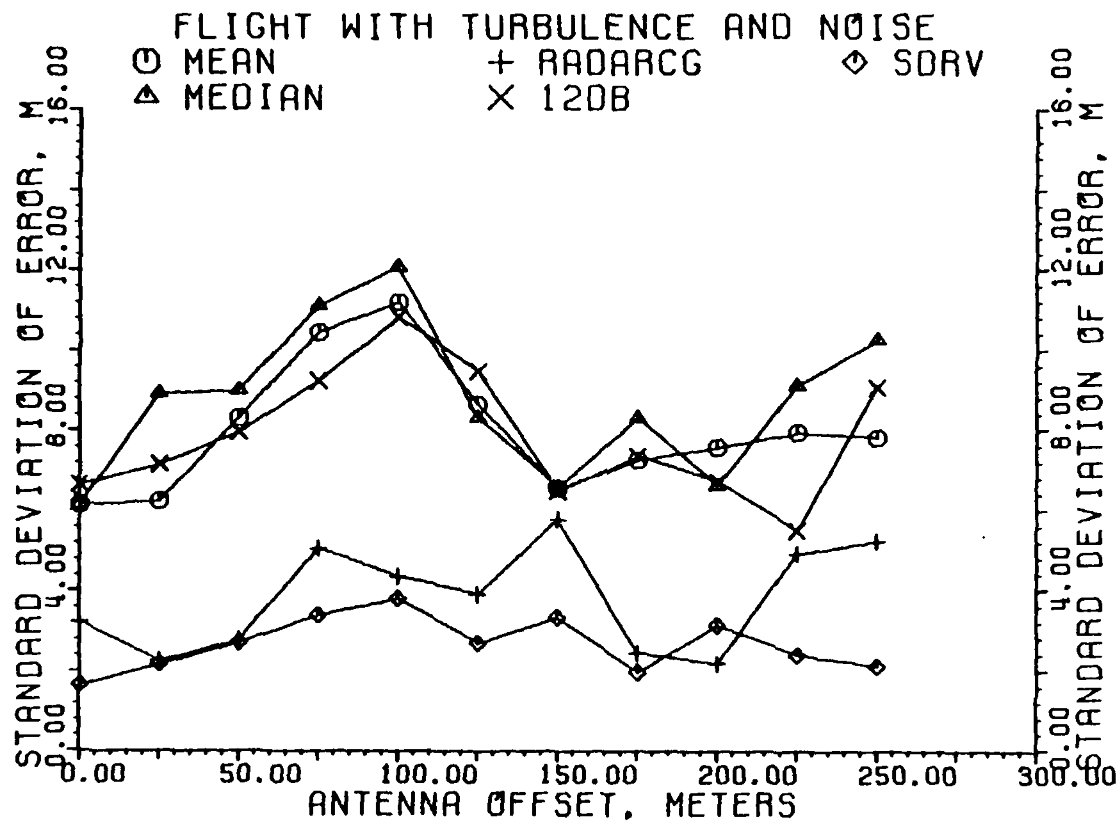

Figure 5-51. Standard deviation of error of estimators in meters for a granularity of 9 beam pointing locations. Each data point is the result of one flight, all scans with a SNR 13 dB or greater used.

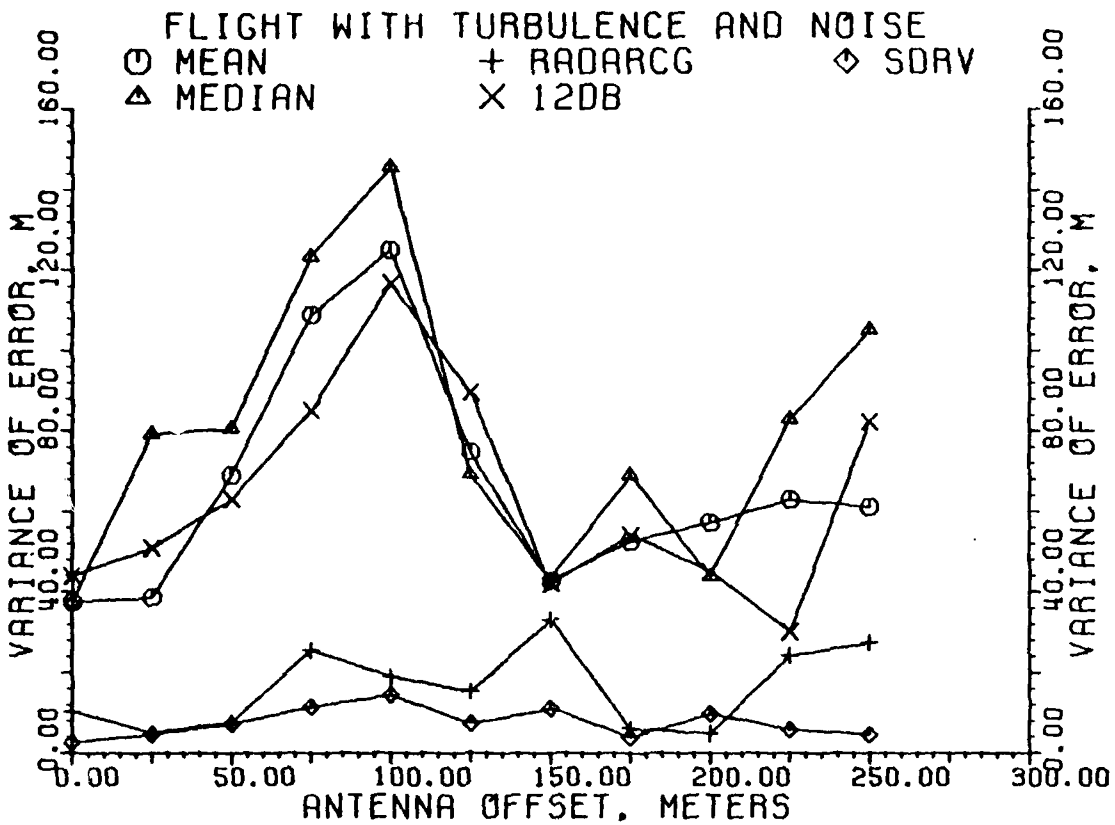

Figure 5-52. Variance of error of estimators in meters for a granularity of 9 beam pointing locations. Each data point is the result of one flight, all scans with a SNR 13 dB or greater used.

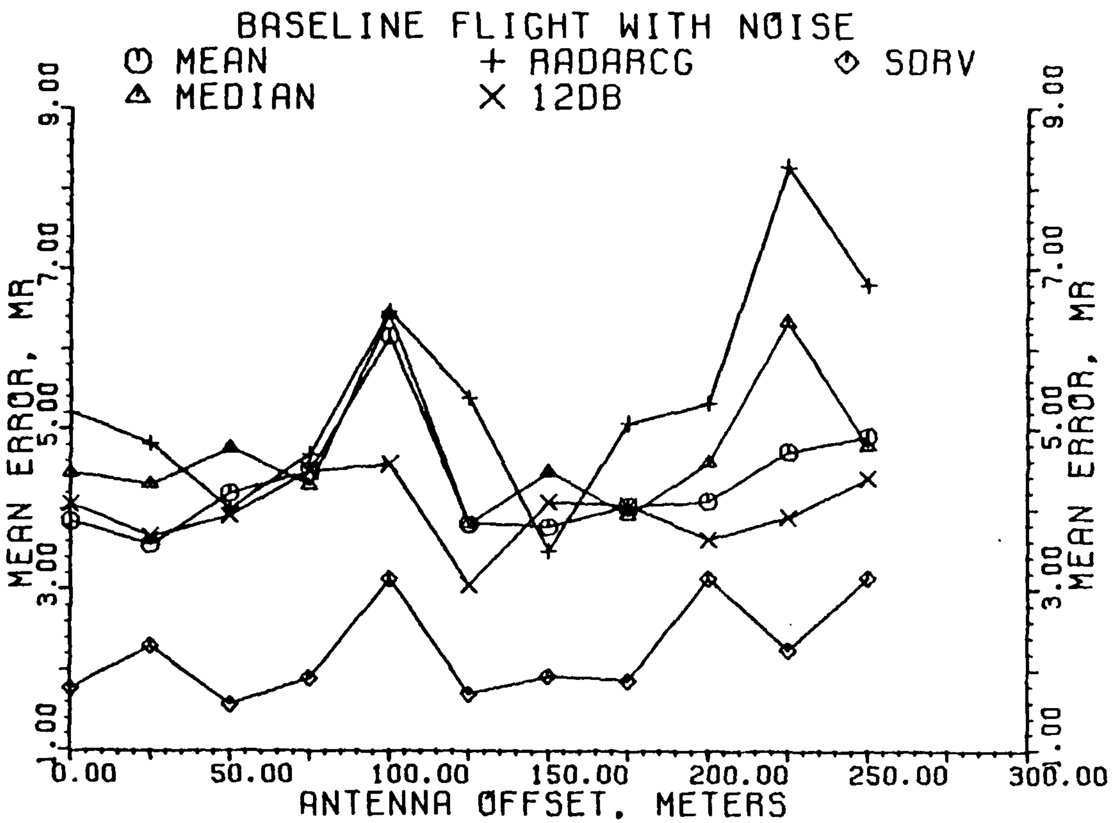

Figure 5-53. *Mean error* of estimators in milliradians for a granularity of 9 beam pointing locations. Each data point is the result of one *flight*, all scans *with a* SNR *at or* below 10 dB used.

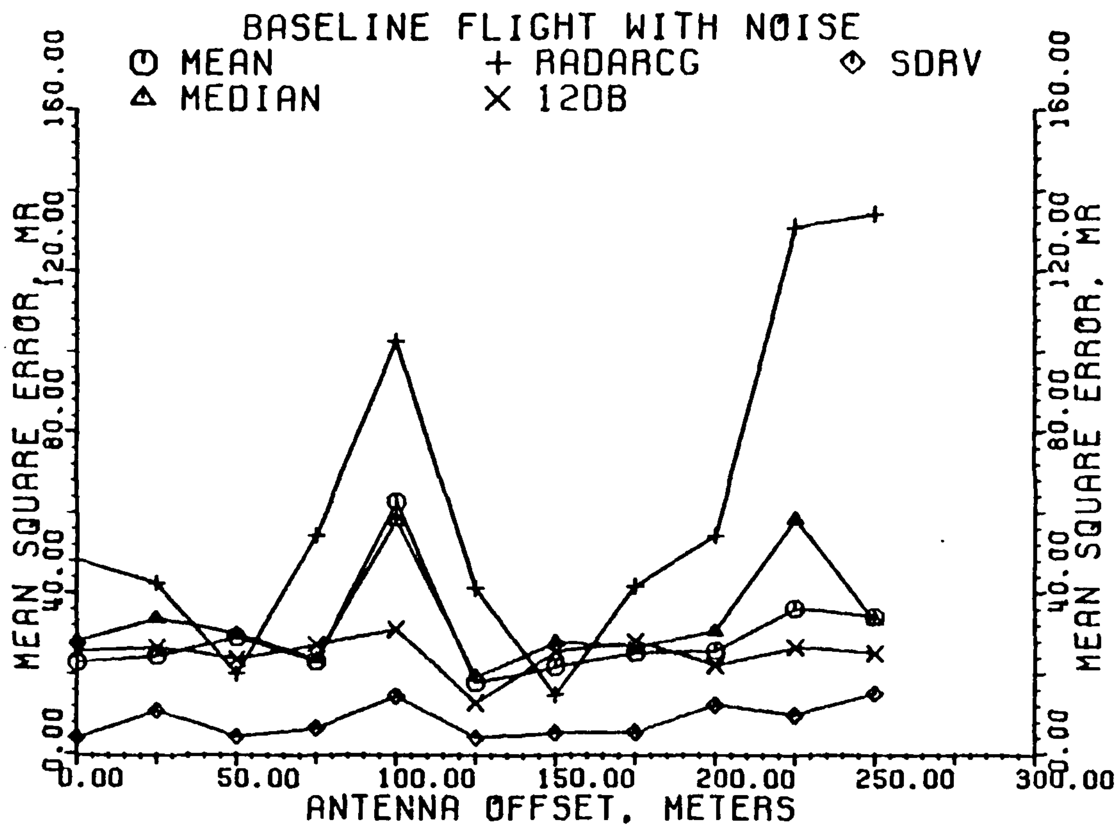

Figure 5-54. Mean square error of estimators in milliradians for a granularity of 9 beam pointing locations. Each data point is the result of one flight, all scans with a SNR at or below 10 dB used.

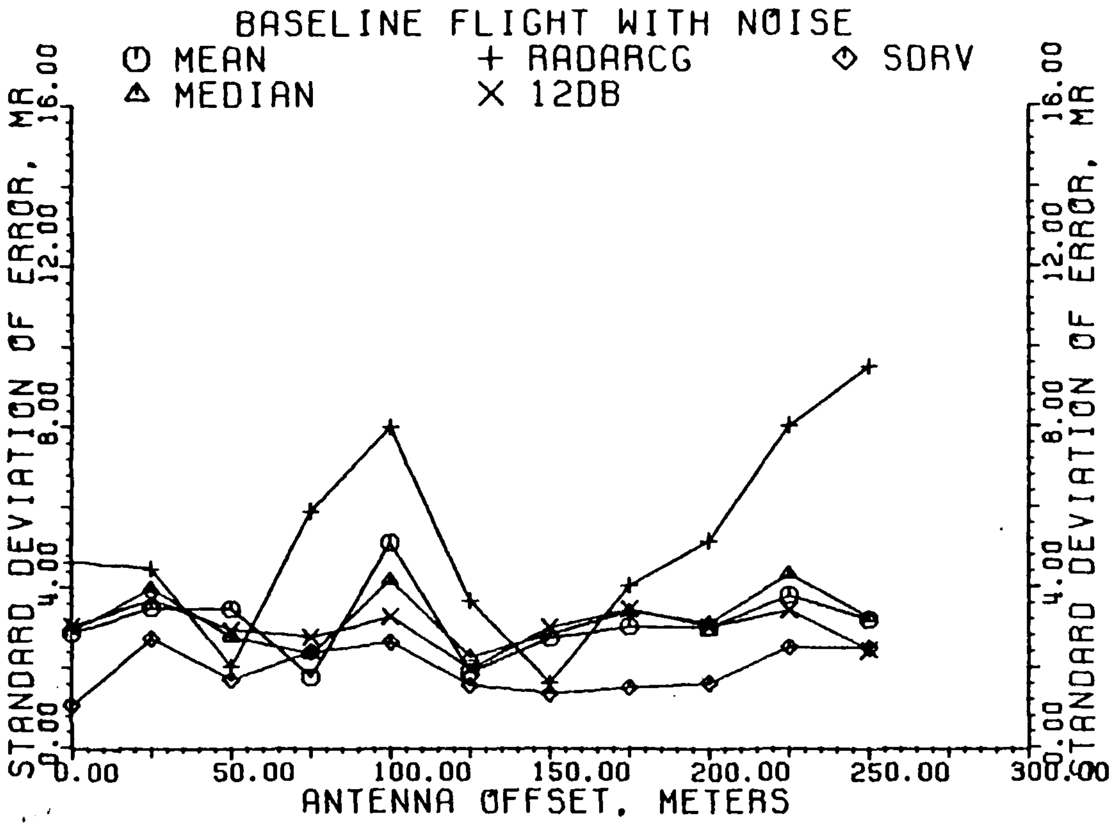

Figure 5-55. Standard deviation of error of estimators in milliradians for a granularity of 9 beam pointing locations. Each data point is the result of one flight, all scans with a SNR at or below 10 dB used.

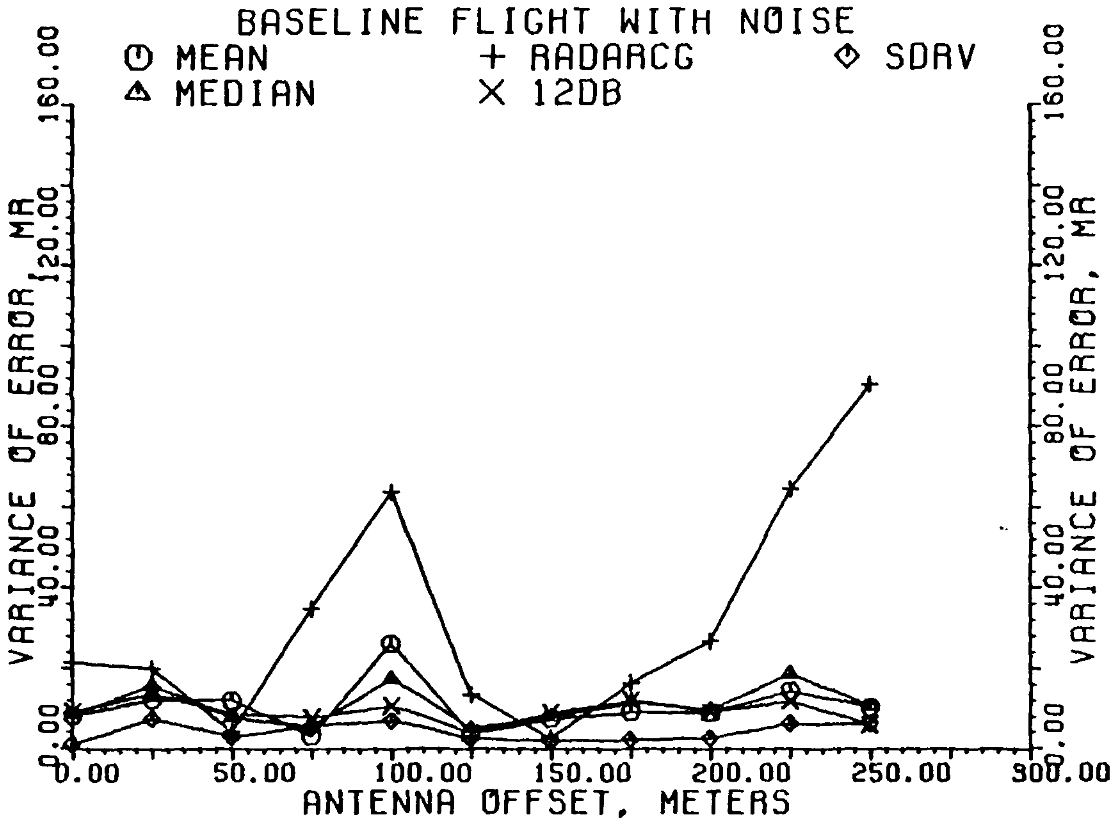

Figure 5-56. Variance of error of estimators in milliradians for a granularity of 9 beam pointing locations. Each data point is the result of one flight, all scans with a SNR at or below 10 dB used.

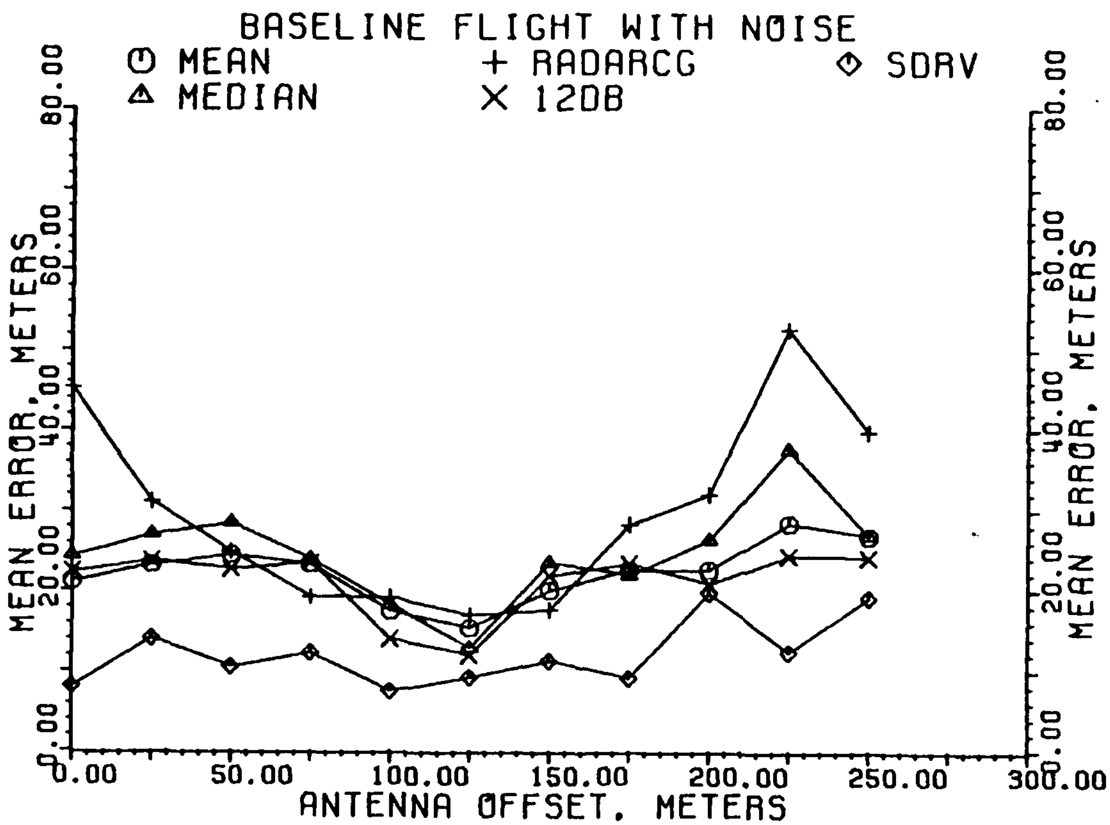

Figure 5-57. Mean error of estimators in meters for a granularity of 9 beam pointing locations. Each data point is the result of one flight, all scans with a SNR at or below 10 dB used.

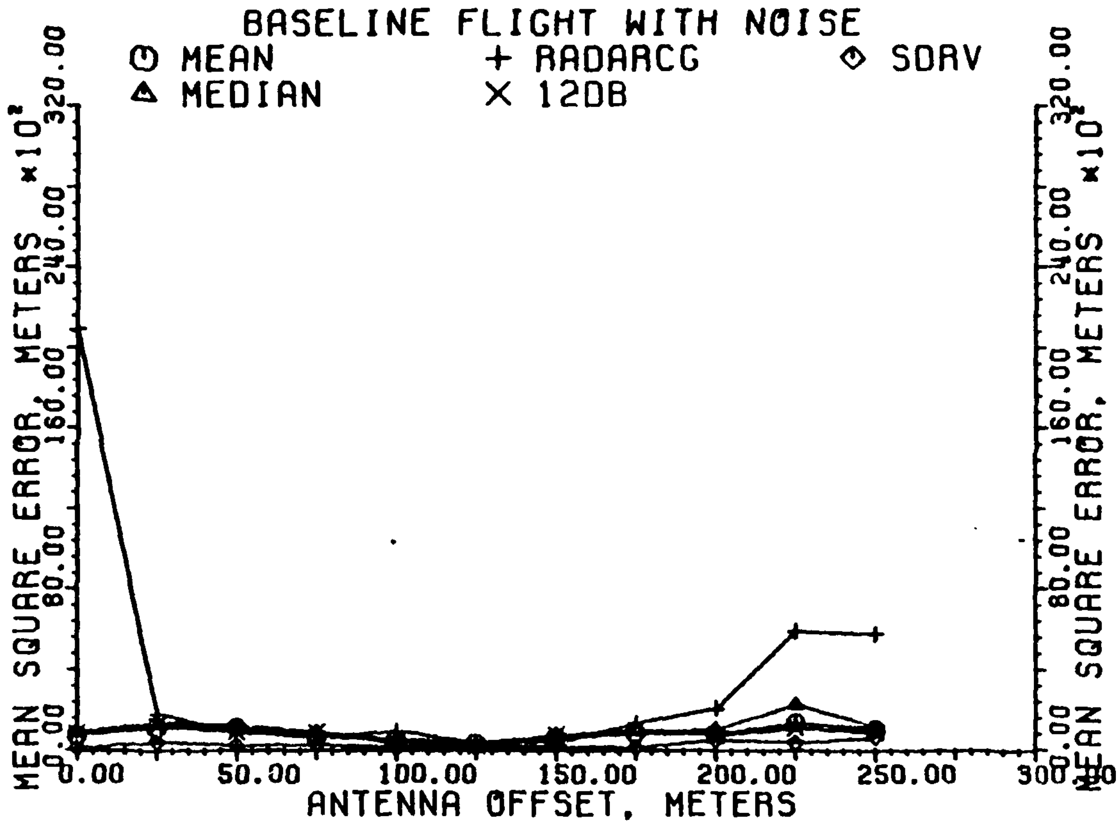

Figure 5-58. Mean square error of estimators in meters for a granularity of 9 beam pointing locations. Each data point is the result of one flight, all scans with a SNR at or below 10 dB used.

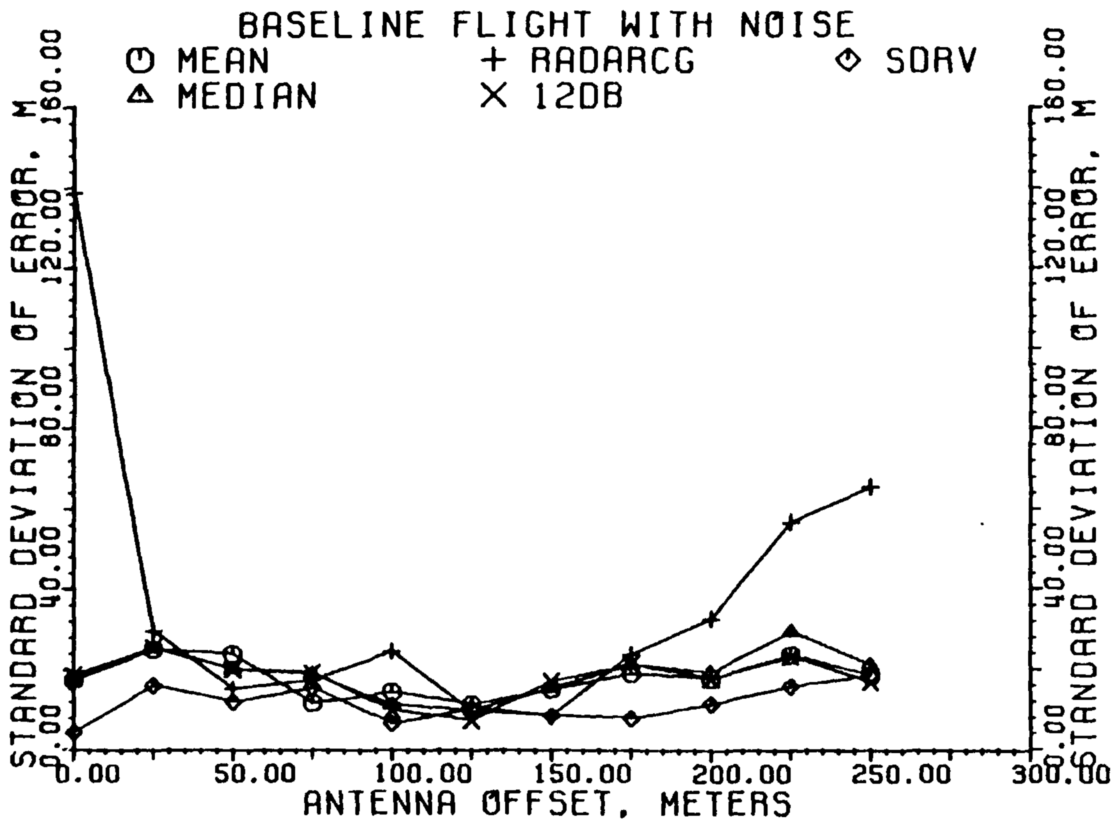

Figure 5-59. Standard deviation of error of estimators in meters for a granularity of 9 beam pointing locations. Each data point is the result of one flight, all scans with a SNR at or below 10 dB used.

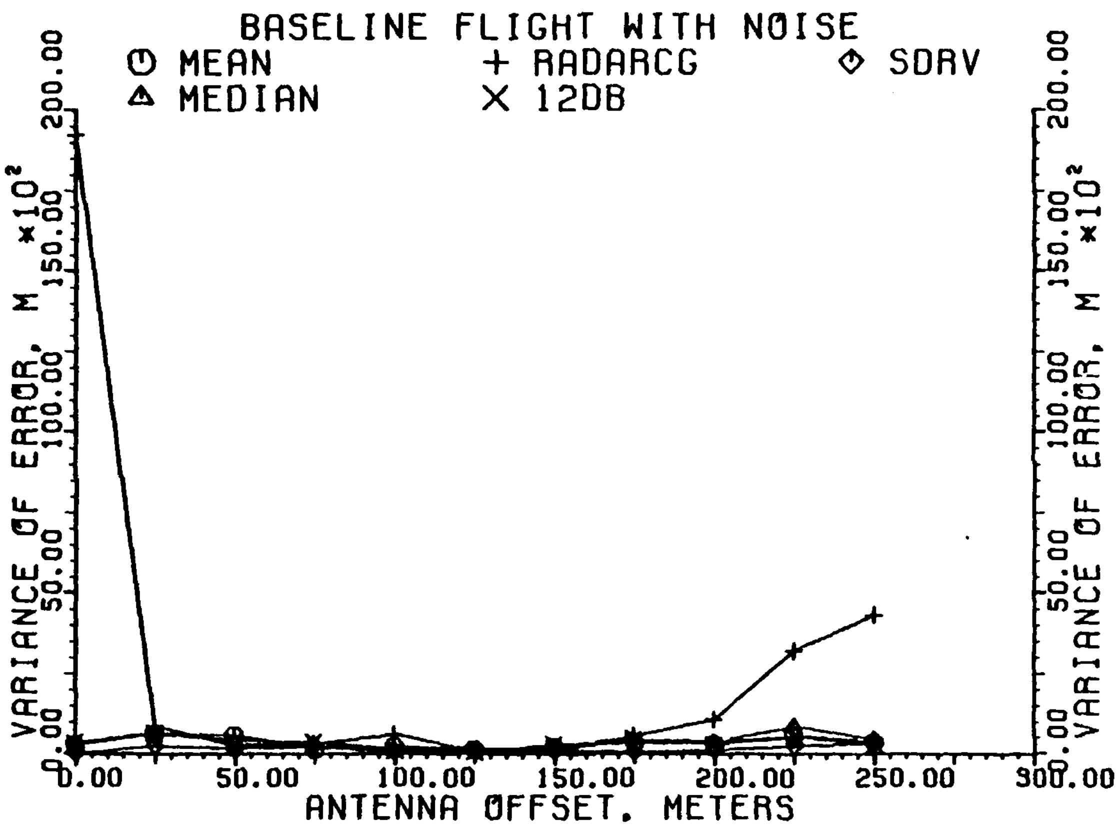

Figure 5-60. Variance of error of estimators in meters for a granularity of 9 beam pointing locations. Each data point is the result of one flight, all scans with a SNR at or below 10 dB used.

The flights with turbulence and noise, Figures 5-61 through 5-68, reflect the same observations made earlier. It is interesting to note that with turbulence and noise, Figure 5-61, the second derivative estimator is as accurate as the thresholding methods were with an infinite SNR and no turbulence, Figure 5-5. This clearly shows the increased ability of SDRV to track targets over the thresholding methods.

A granularity of 9 beam pointing locations forced the second derivative method to have only one beam location in each window. No pulse integration was possible. With 29 beam locations in the scanning window, each window contains two beam locations, and some noise rejection action will occur due to the averaging of the returns in each window.

The results of a baseline flight versus antenna offset for a scanning window with 29 beam locations are shown in Figures 5-69 through 5-76. The second derivative method has the least error, followed closely by RADARCG, followed by the thresholding estimators. Of the thresholding methods, the 12 dB method has the least deviation and variance, shown in Figures 5-71, 5-72, 5-75, and 5-76, and thus distinguishes itself from the mean and median methods. Comparison of these plots with the baseline flight plot of 9 beam pointing locations, specifically comparing Figures 5-69 and 5-73 with Figures 5-5 and 5-9, shows that whereas the thresholding methods and RADARCG have no real change in their estimating ability due to the increased amount of data, the error of the SDRV algorithm was cut by approximately two-thirds.

The flights with noise, Figures 5-77 through 5-84, show the SDRV method to be the most accurate as well as the most robust estimator. RADARCG improved significantly with the increased rate, and the thresholding algorithms are still comparable, with the 12 dB estimator leading.

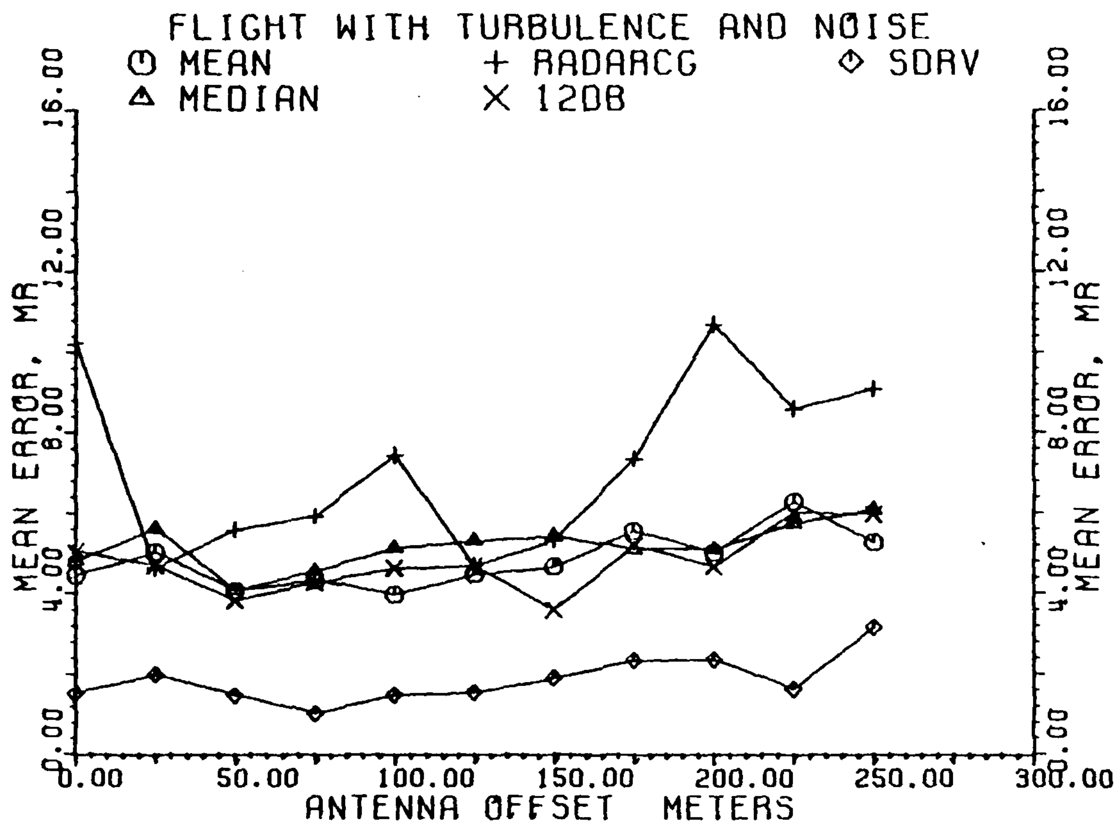

Figure 5-61. Mean error of estimators in milliradians for a granularity of 9 beam pointing locations. Each data point is the result of one flight, all scans with a SNR at or below 10 dB used.

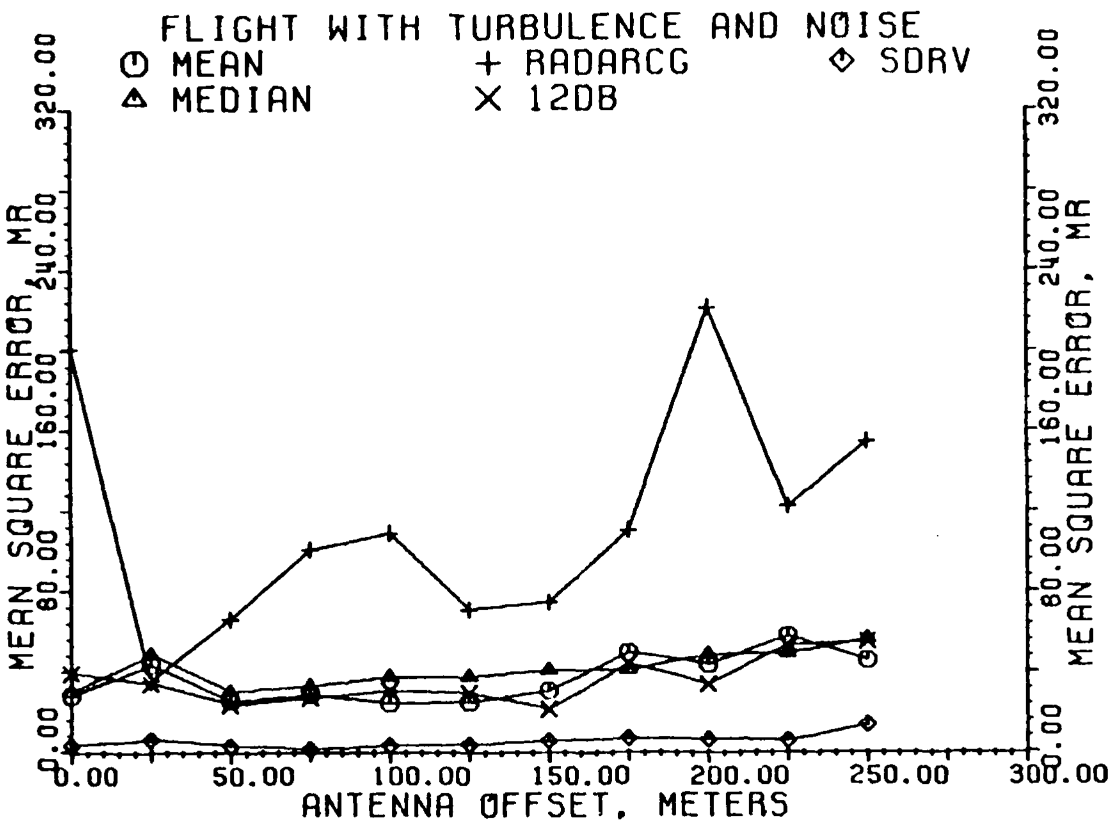

Figure 5-62. Mean square error of estimators in milliradians for a granularity of 9 beam pointing locations. Each data point is the result of one flight, all scans with a SNR at or below 10 dB used.

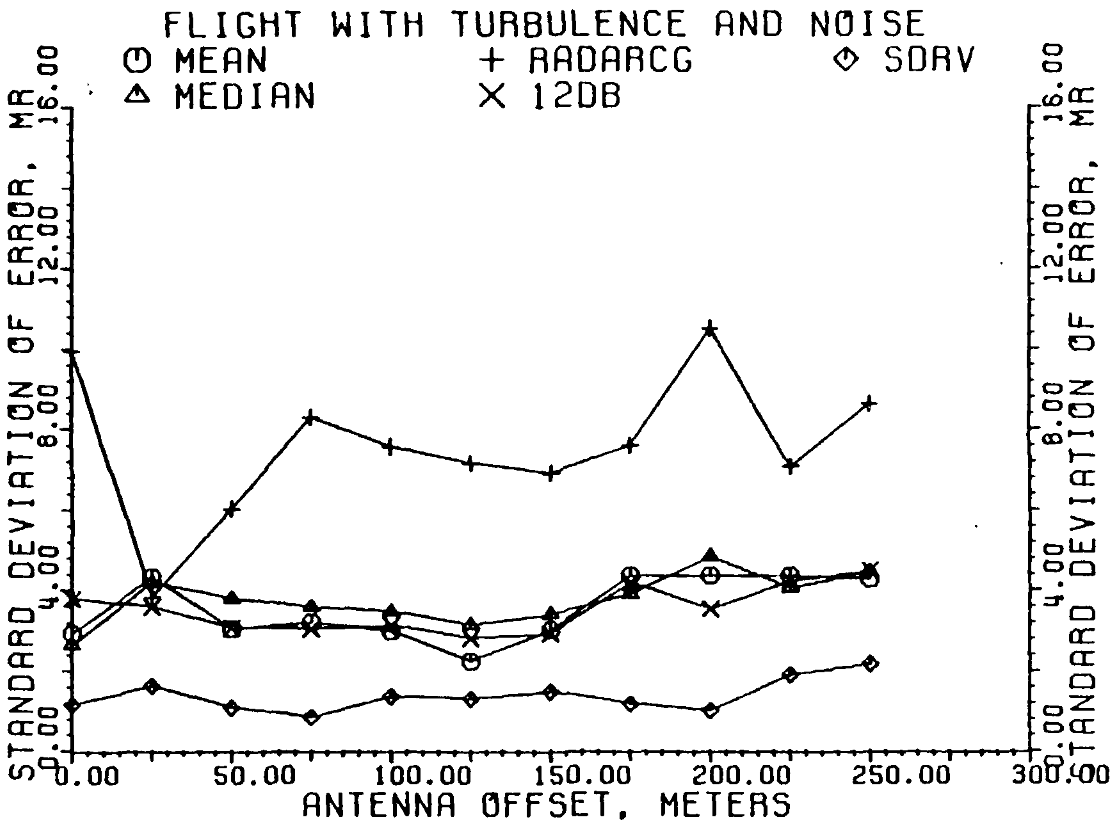

Figure 5-63. Standard deviation of error of estimators in milliradians for a granularity of 9 beam pointing locations. Each data point is the result of one flight, all scans with a SNR at or below 10 dB used.

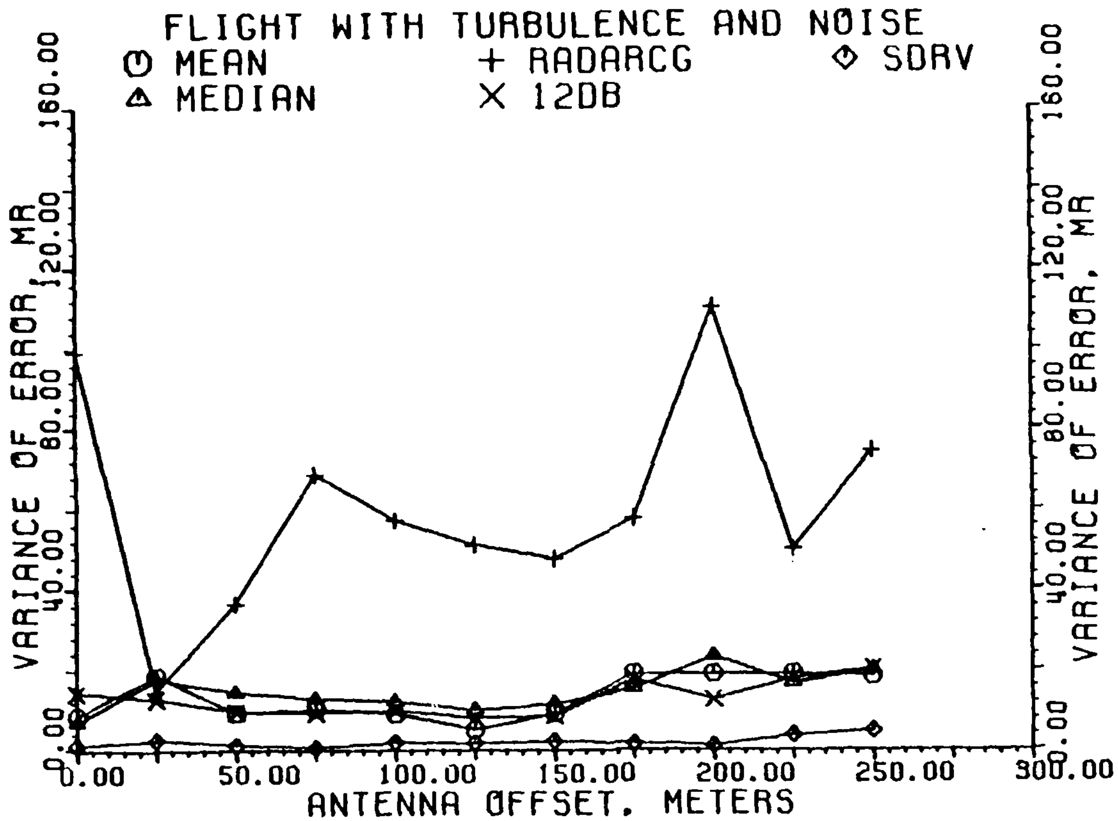

Figure 5-64. Variance of error of estimators in milliradians for a granularity of 9 beam pointing locations. Each data point is the result of one flight, all scans with a SNR at or below 10 dB used.

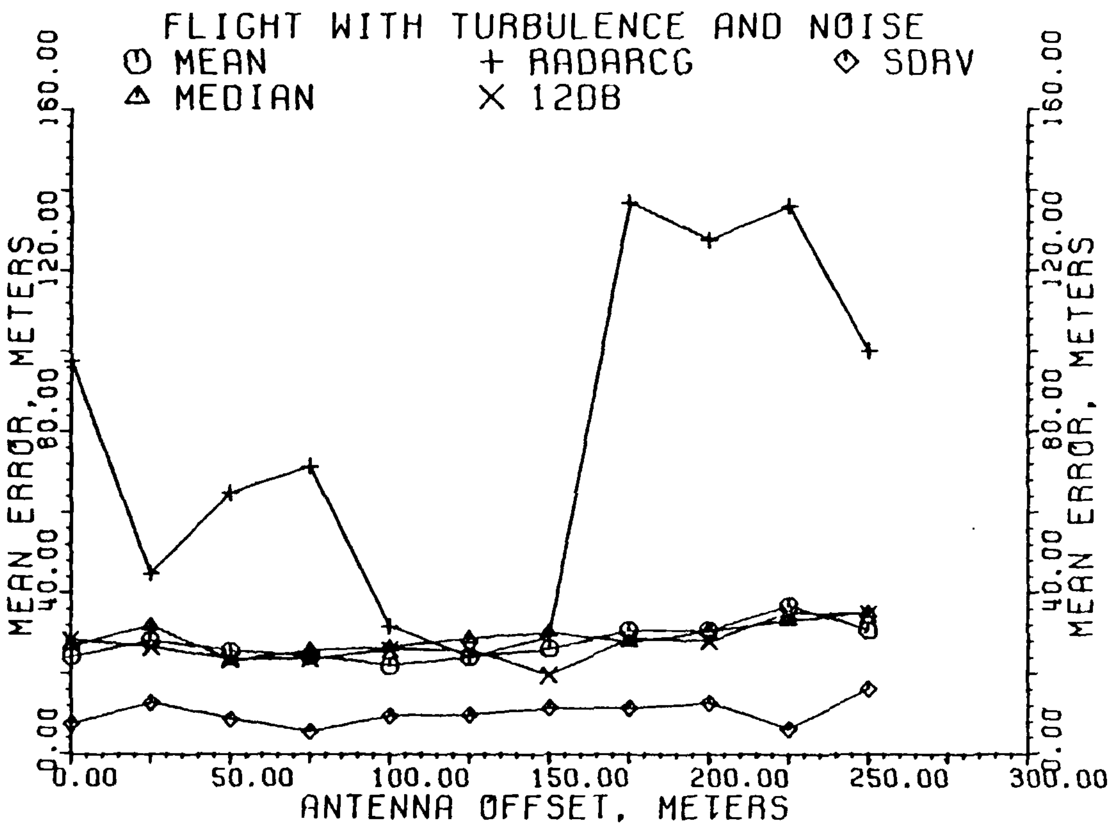

Figure 5-65. Mean error of estimators in meters for a granularity of 9 beam pointing locations. Each data point is the result of one flight, all scans with a SNR at or below 10 dB used.

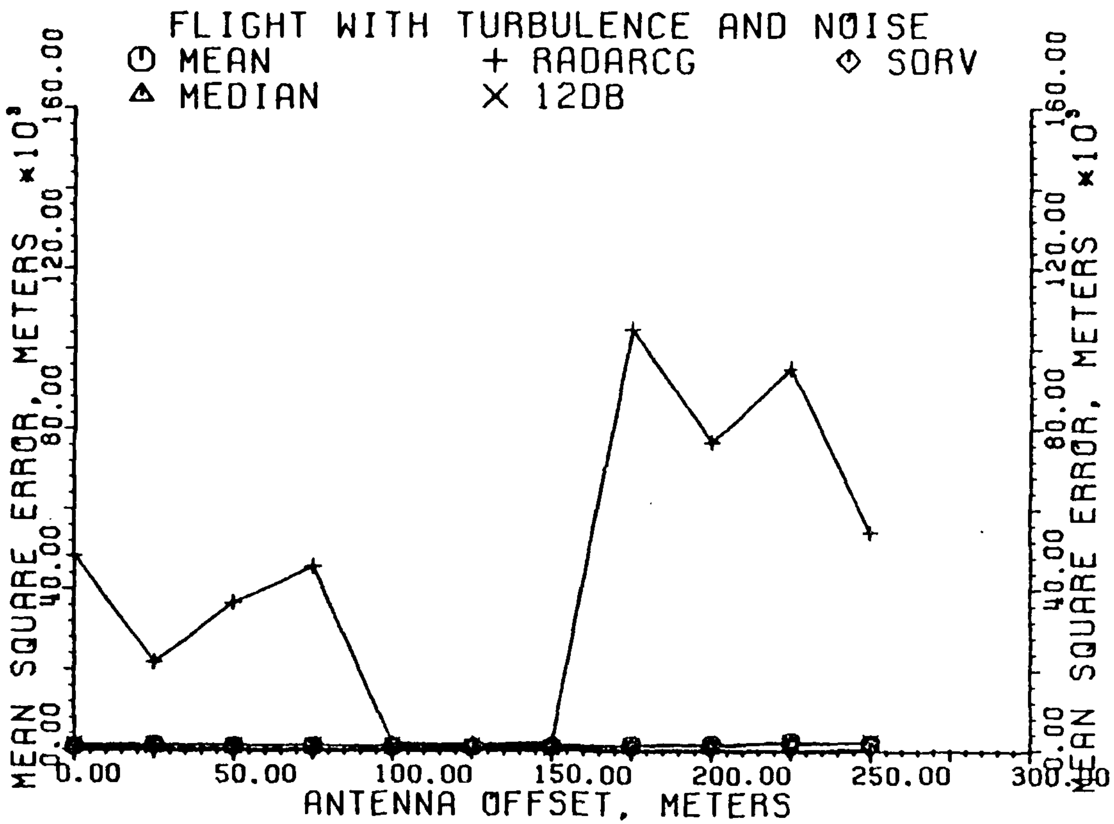

Figure 5-66. Mean square error of estimators in meters for a granularity of 9 beam pointing locations. Each data point is the result of one flight, all scans with a SNR at or below 10 dB used.

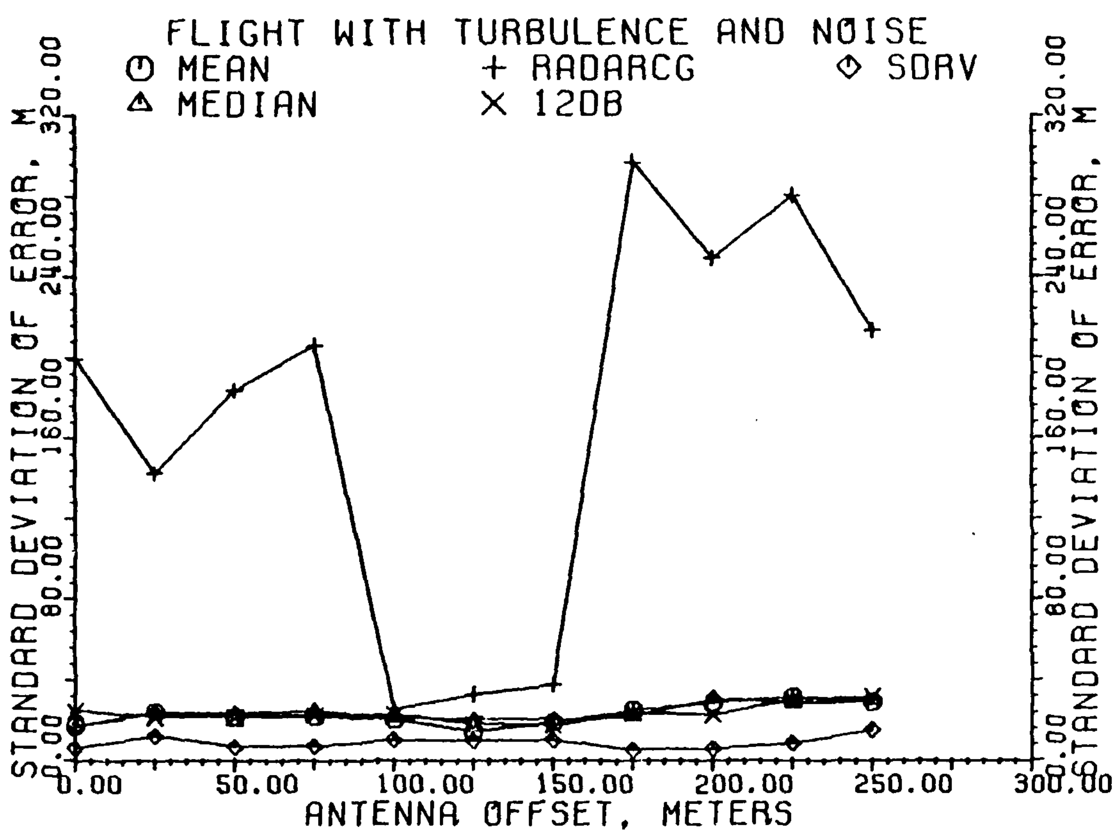

Figure 5-67. Standard deviation of error of estimators in meters for a granularity of 9 beam pointing locations. Each data point is the result of one flight, all scans with a SNR at or below 10 dB used.

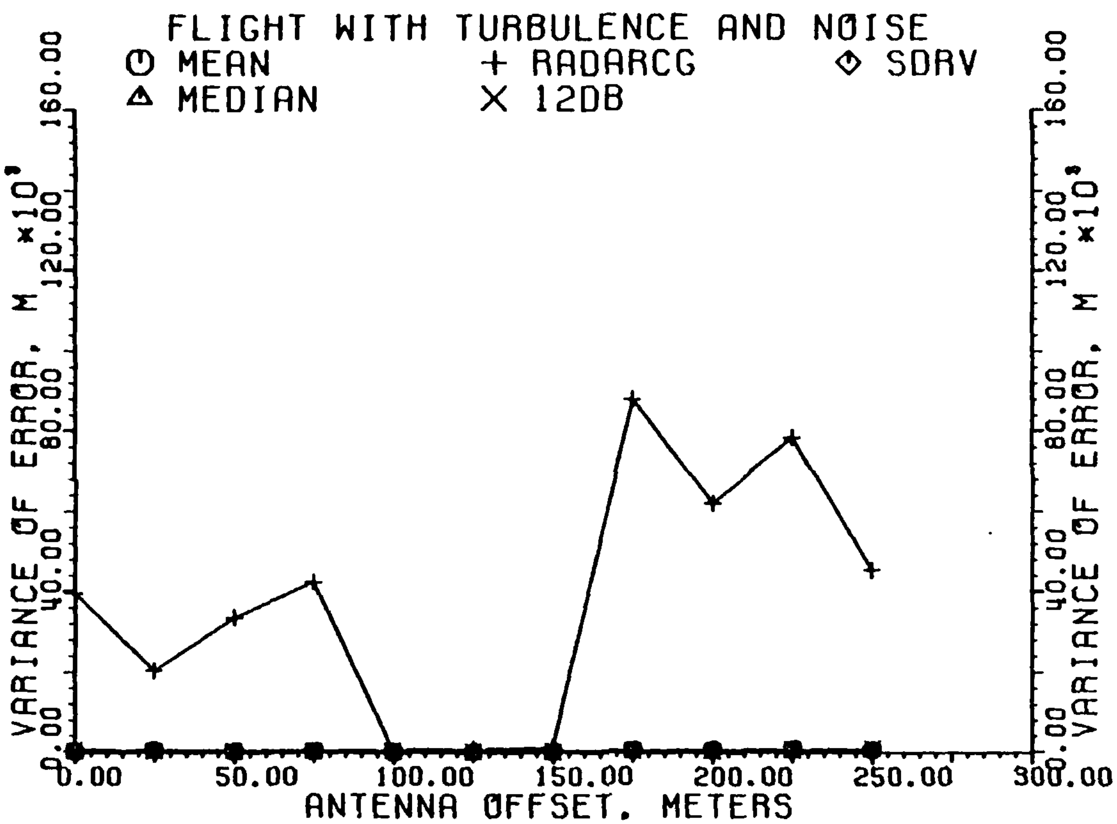

Figure 5-68. Variance of error of estimators in meters for a granularity of 9 beam pointing locations. Each data point is the result of one flight, all scans with a SNR at or below 10 dB used.

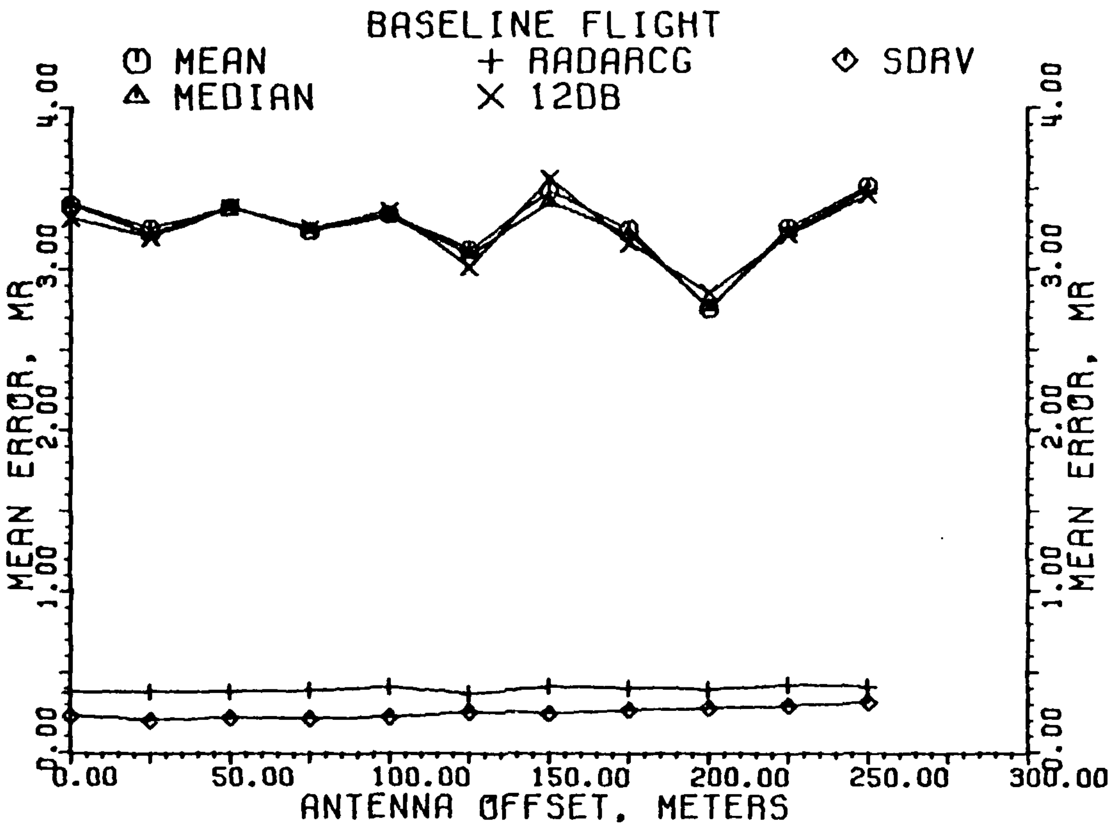

Figure 5-69. Mean error of estimators in milliradians for a granularity of 29 beam pointing locations. Each data point is the result of one flight, all scans used.

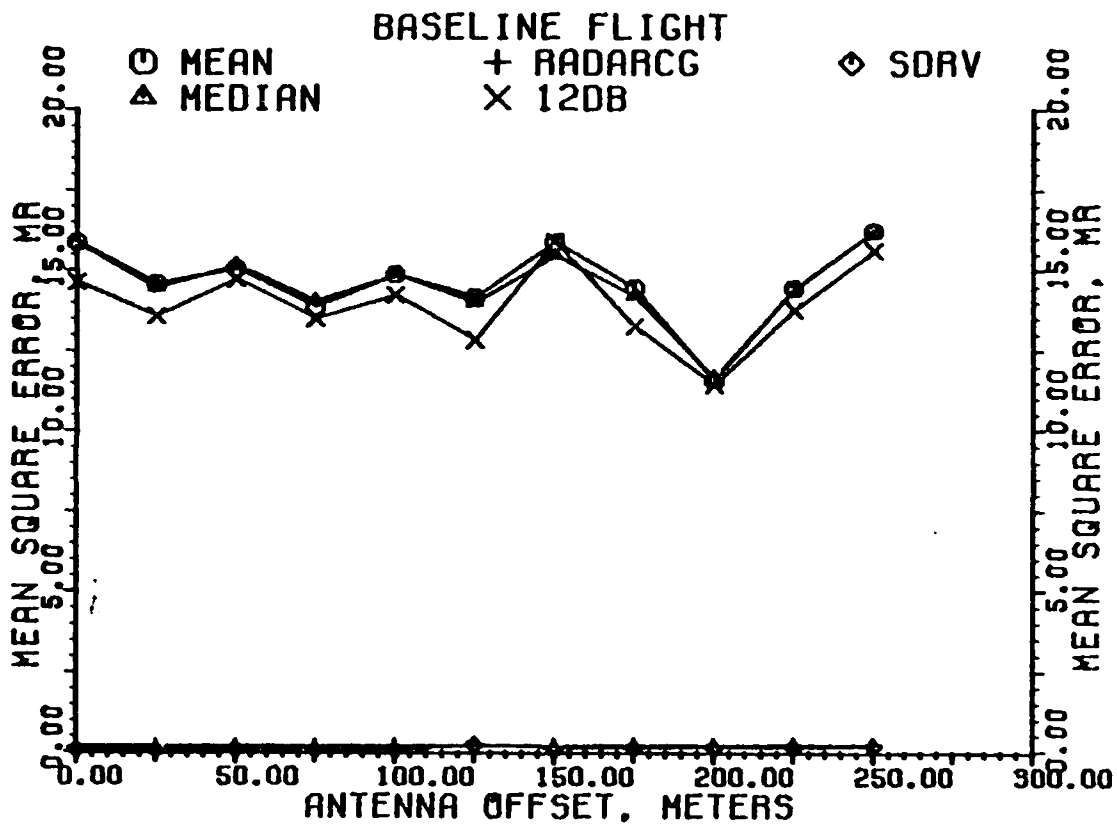

Figure 5-70. Mean square error of estimators in milliradians for a granularity of 29 beam pointing locations. Each data point is the result of one flight, all scans used.

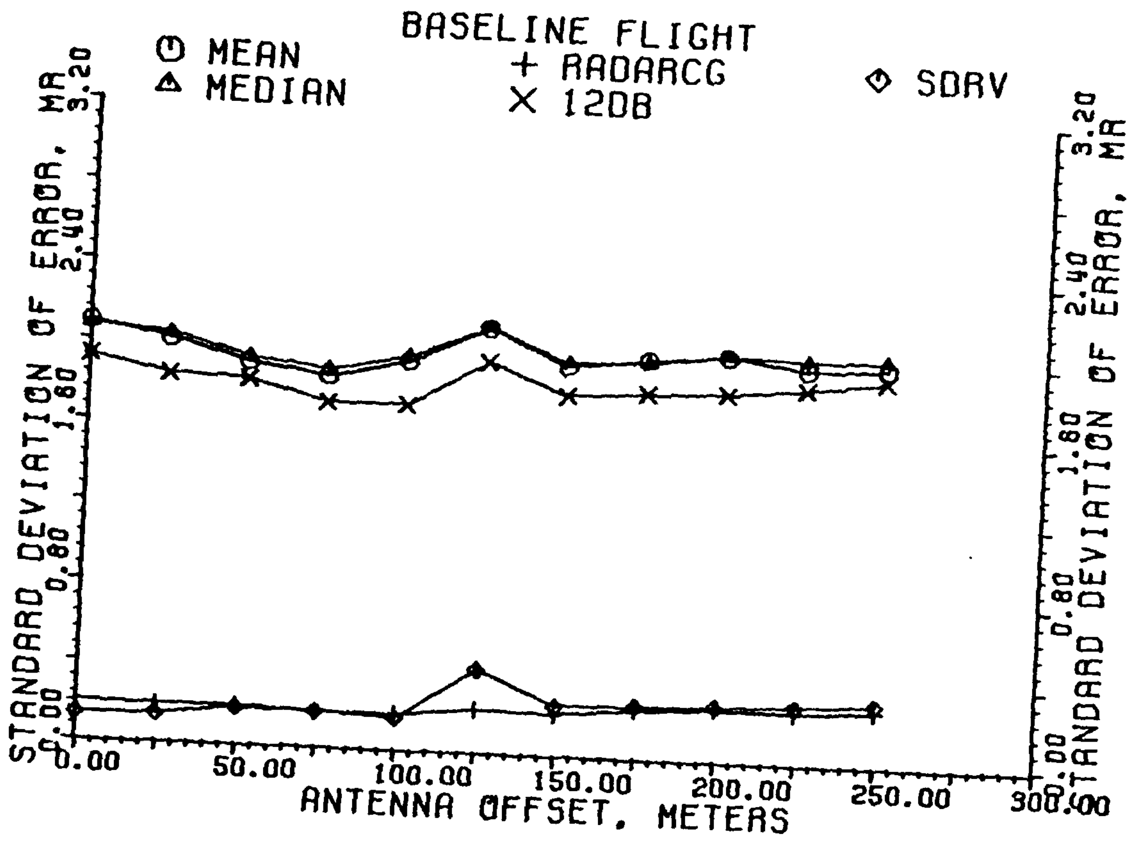

Figure 5-71. Standard deviation of error of estimators in milliradians for a granularity of 29 beam pointing locations. Each data point is the result of one flight, all scans used.

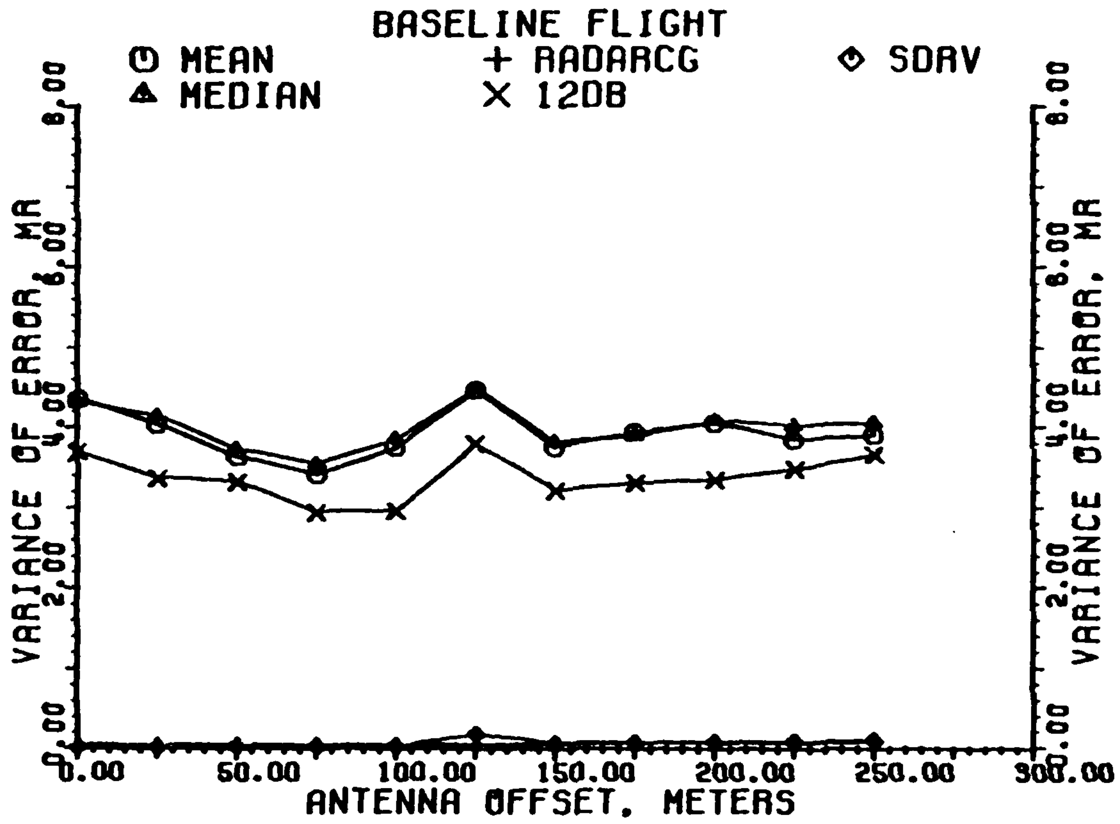

Figure 5-72. Variance of error of estimators in milliradians for a granularity of 29 beam pointing locations. Each data point is the result of one flight, all scans used.

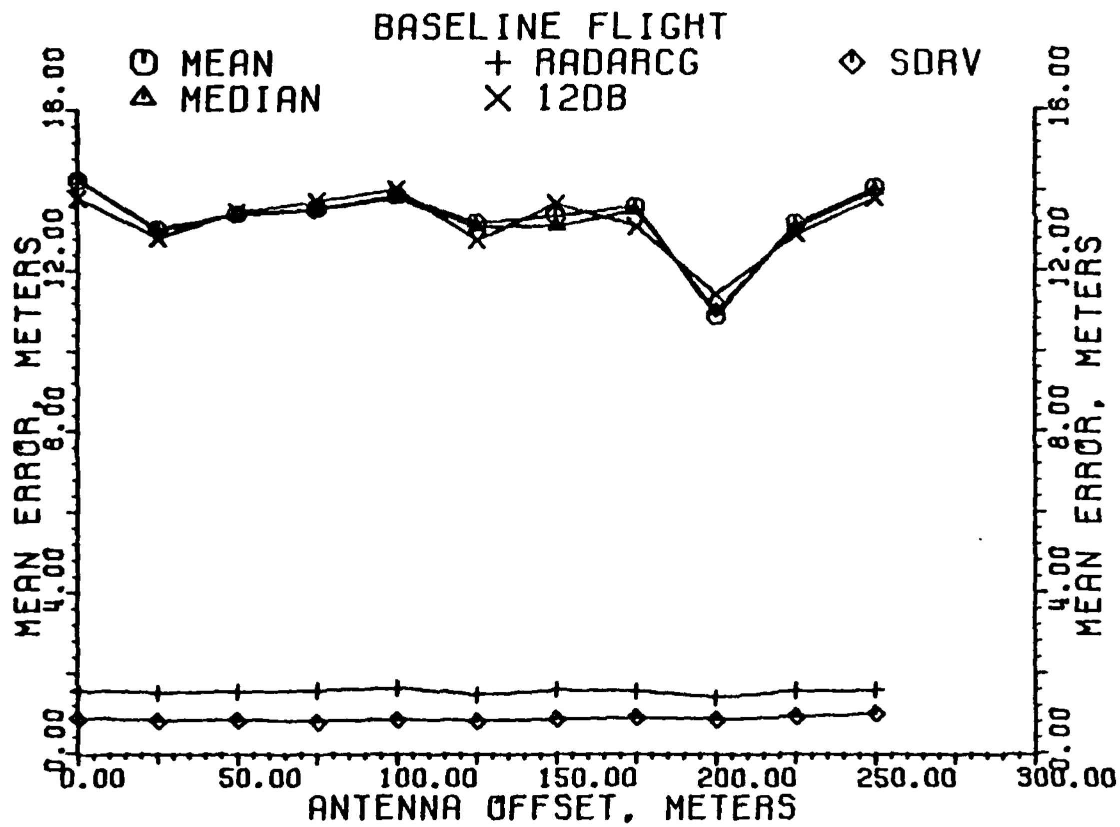

Figure 5-73. Mean error of estimators in meters for a granulatity of 29 beam pointing locations. Each data point is the result of one flight, all scans used.

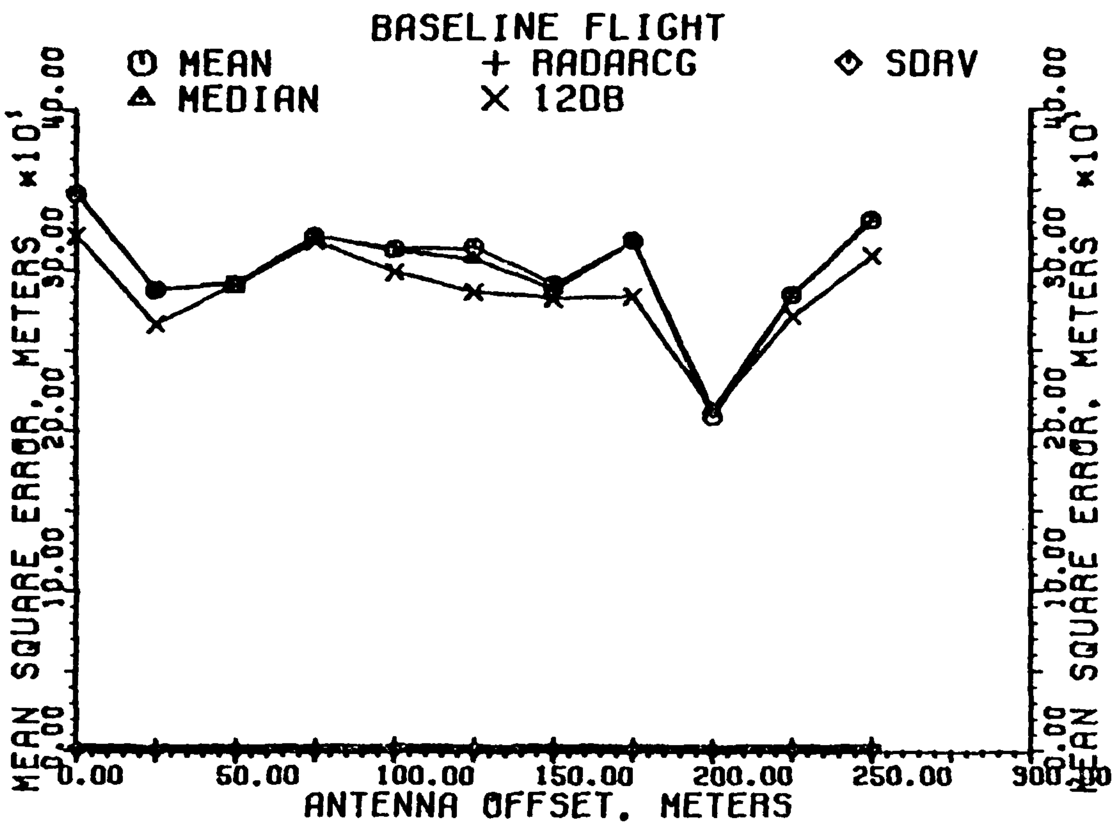

Figure 5-74. Mean square error of estimators in meters for a granularity of 29 beam pointing locations. Each data point is the result of one flight, all scans used.

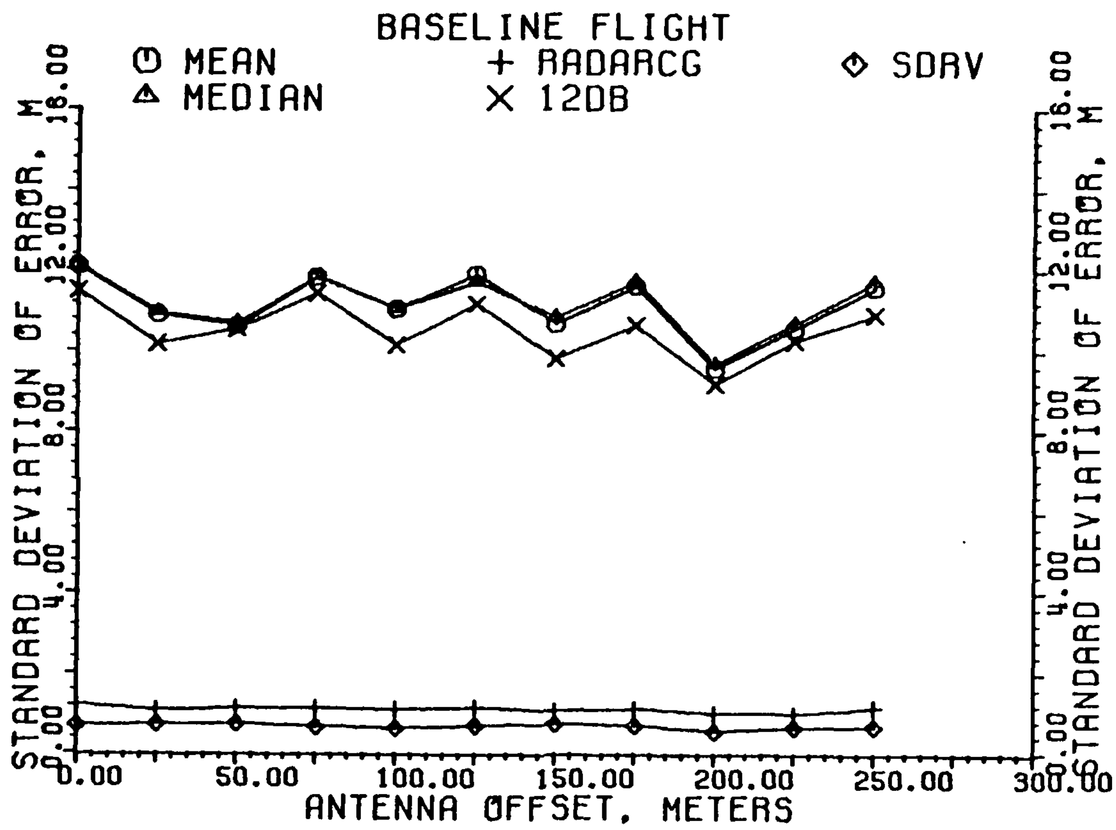

Figure 5-75. Standard deviation of error of estimators in meters for a granularity of 29 beam pointing locations. Each data point is the result of one flight, all scans used.

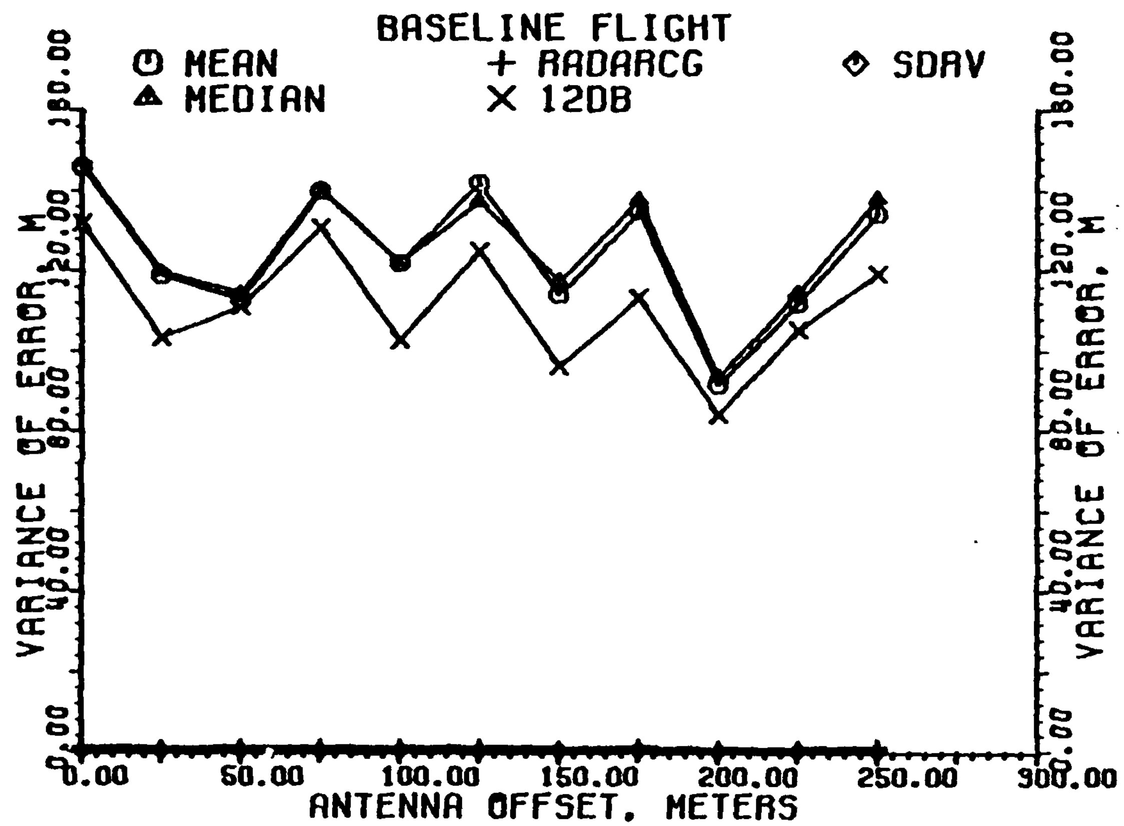

Figure 5-76. Variance of error of estimators in meters for a granularity of 29 beam pointing locations. Each data point is the resule of one flight, all scans used.

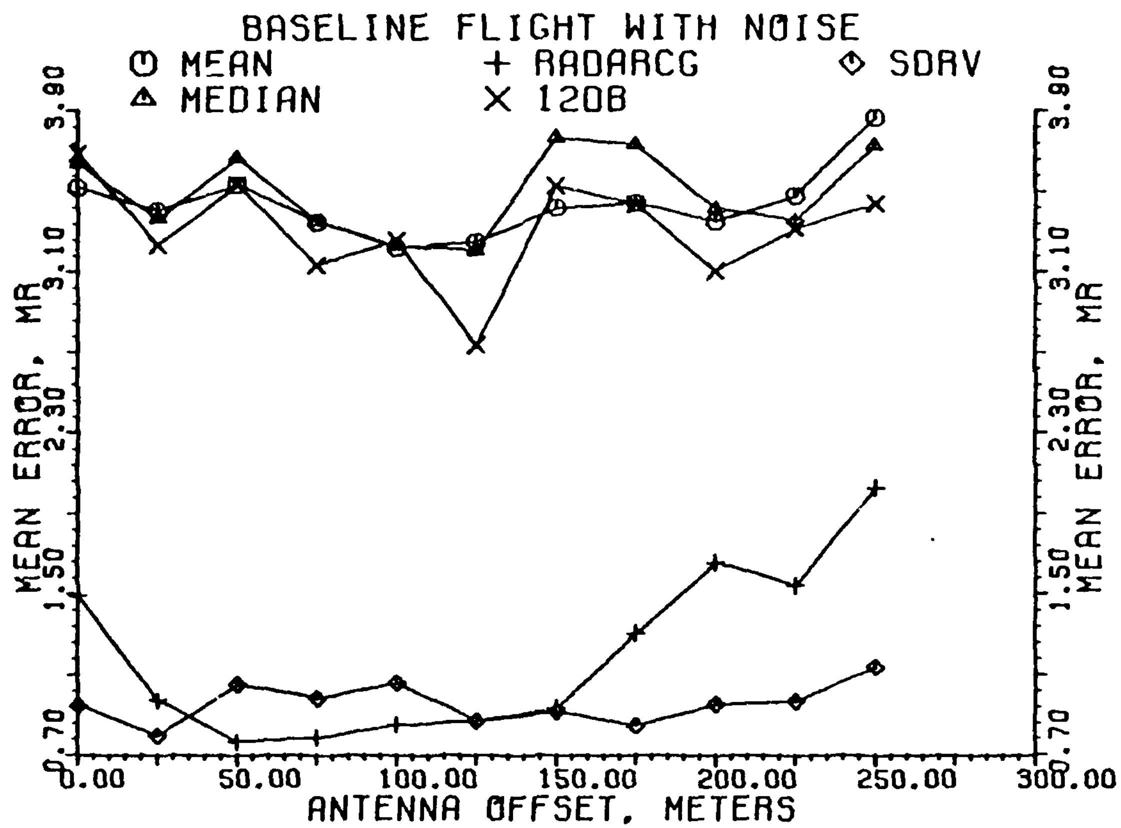

Figure 5-77. Mean error of estimators in milliradians for a granularity of 29 beam pointing locations. Each data point is the result of one flight, all scans used.

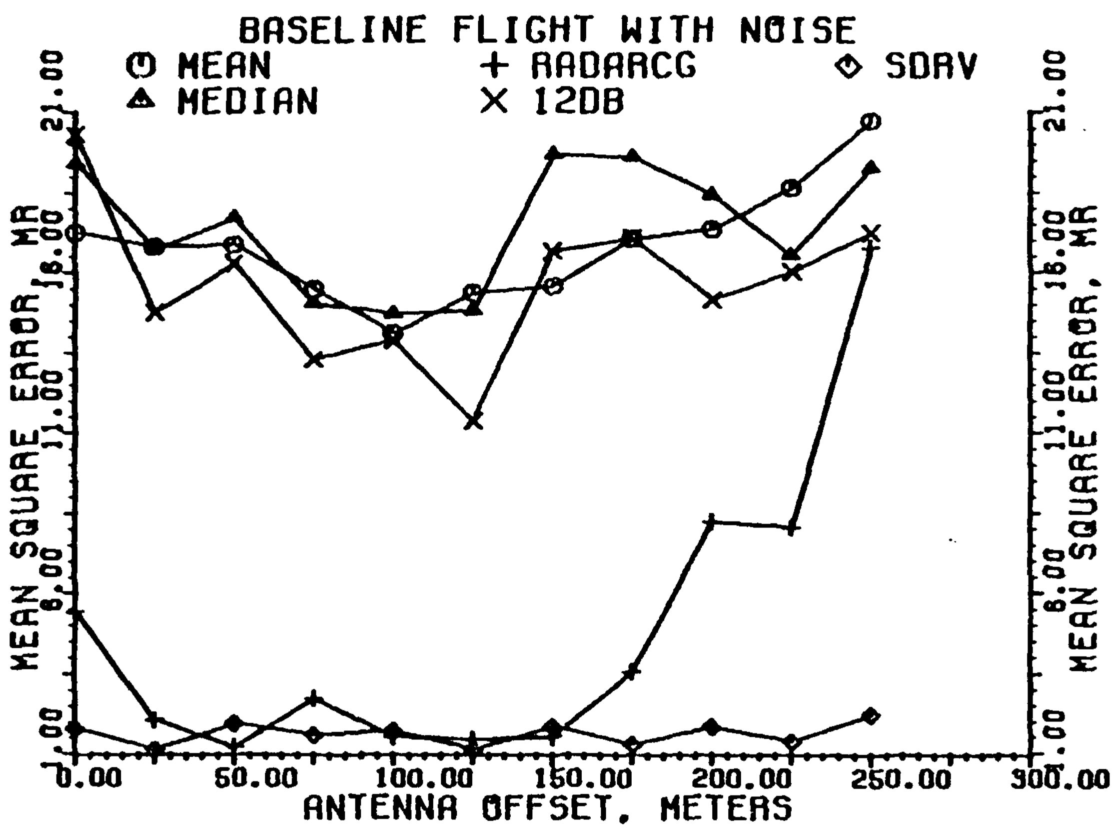

Figure 5-78. Mean square error of estimators in milliradians for a granularity of 29 beam pointing locations. Each data point is the result of one flight, all scans used.

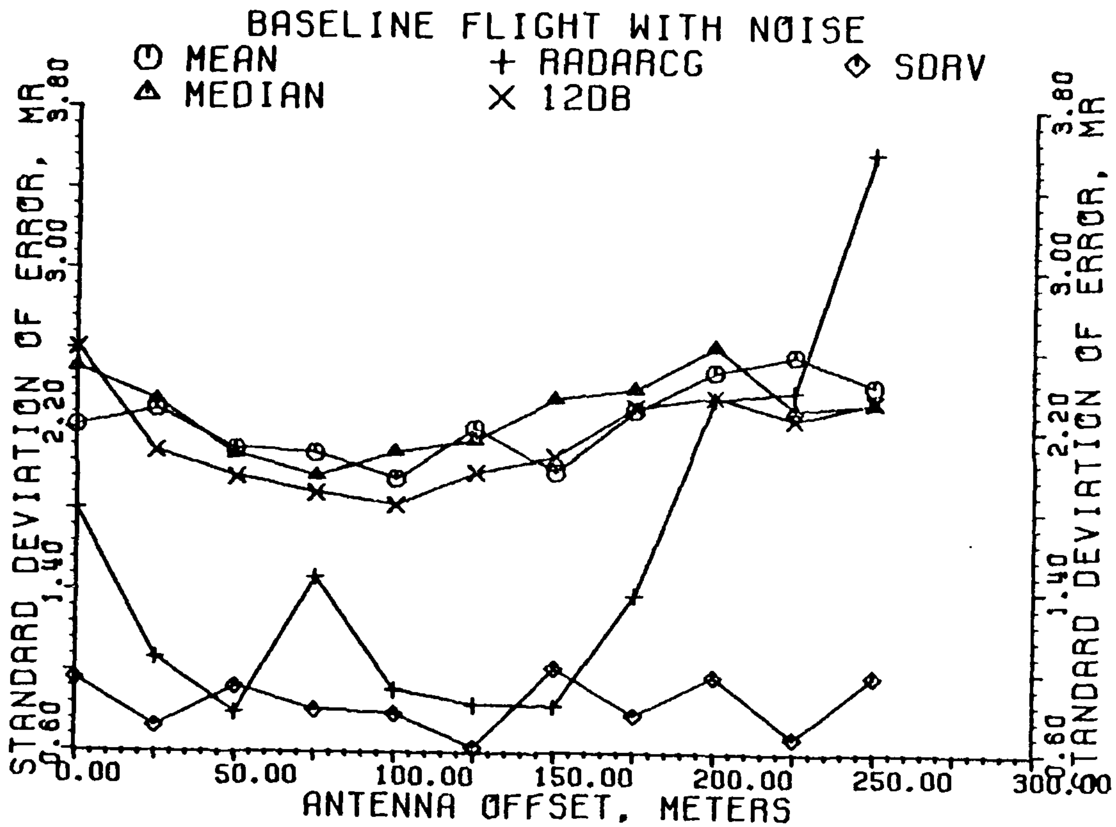

Figure 5-79. Standard deviation of error of estimators in milliradians for a granularity of 29 beam pointing locations. Each data point is the result of one flight, all scans used.

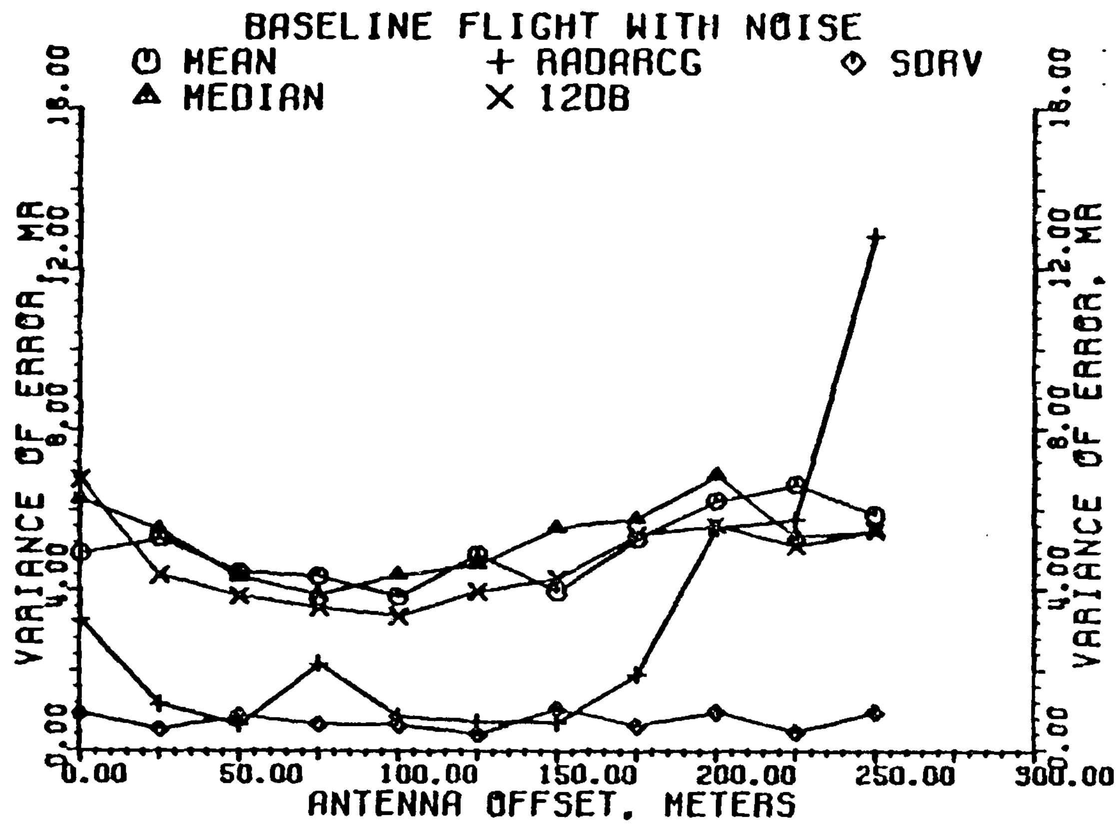

Figure 5-80. Variance of error of estimators in milliradians for a granularity of 29 beam pointing locations. Each data point is the result of one flight, all scans used.

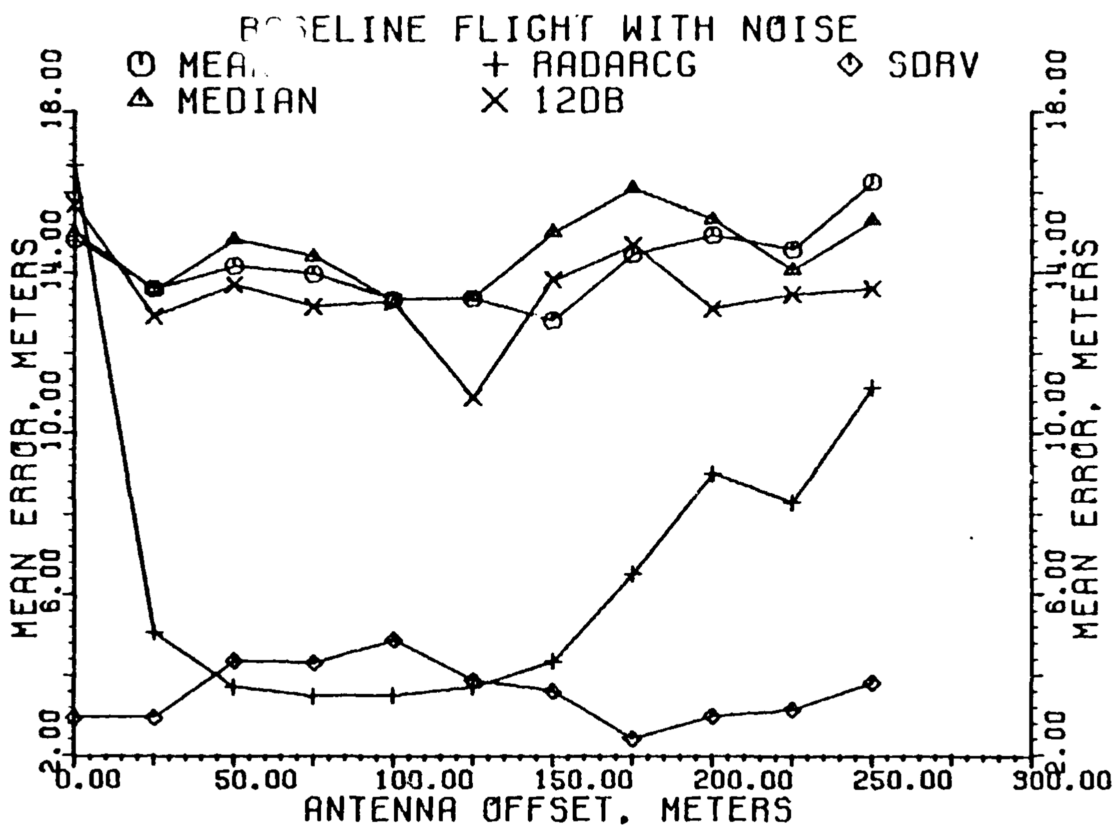

Figure 5-81. Mean error of estimators in meters for a granularity of 29 beam pointing locations. Each data point is the result of one flight, all scans used.

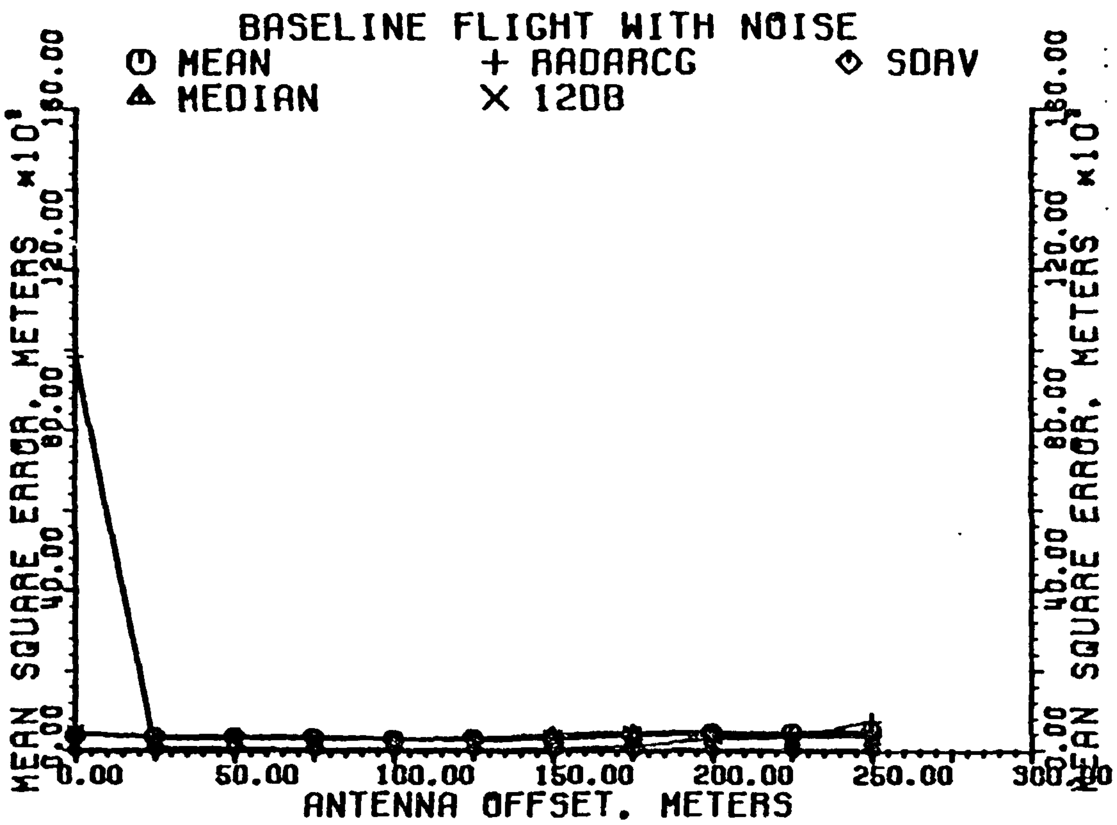

Figure 5-82. Mean square error of estimators in meters for a granularity of 29 beam pointing locations. Each data point is the result of one flight, all scans used.

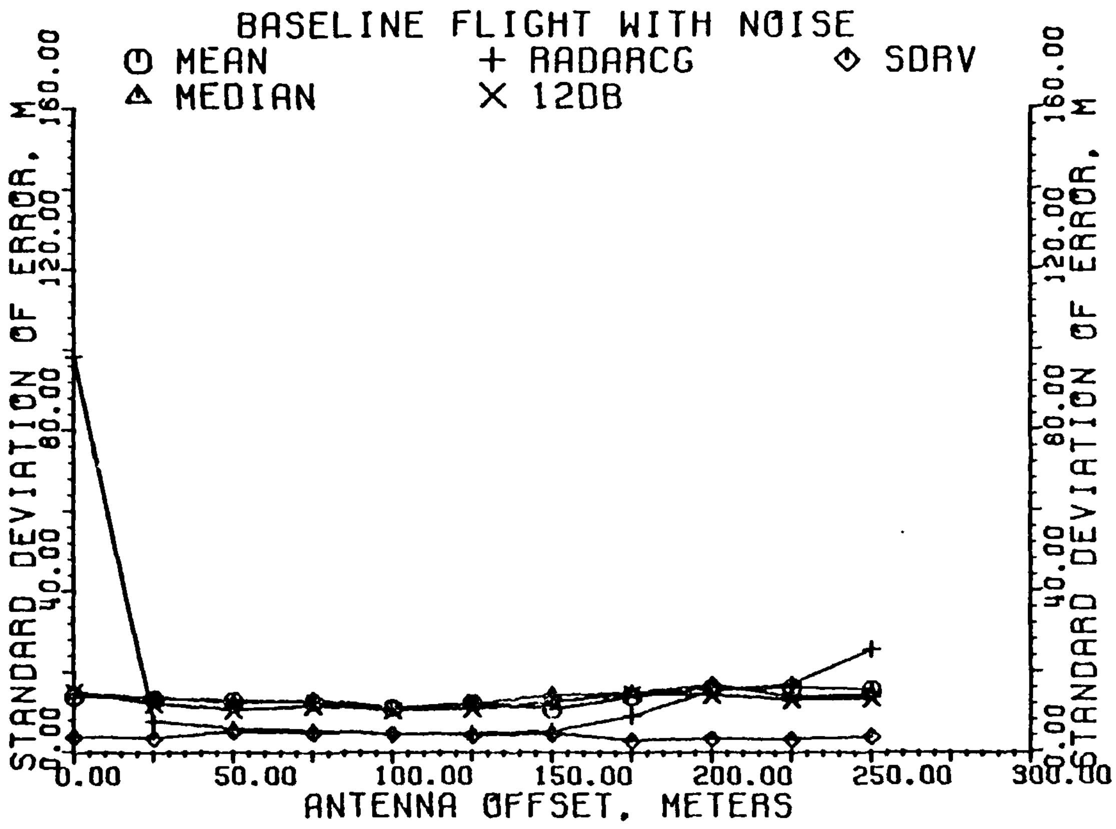

Figure 5-83. Standard deviation of error of estimators in meters for a granularity of 29 beam pointing locations. Each data point is the result of one flight, all scans used.

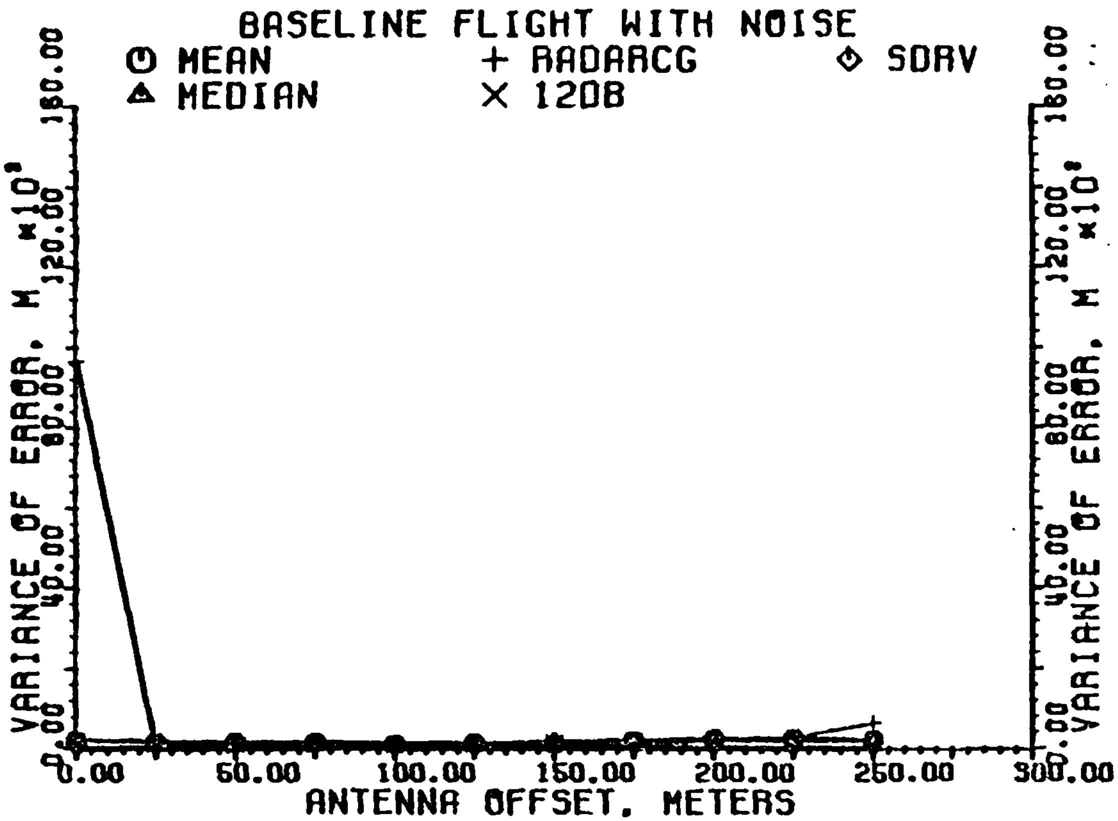

Figure 5-84. Variance of error of estimators in meters for a granularity of 29 beam pointing locations. Each data point is the result of one flight, all scans used.

The results of the flights with turbulence, Figures 5-85 through 5-92, show results similar to the baseline flights, just as the flights with turbulence were similar to the baseline flights with a scanning granularity of 9 beam locations. This is due to the lack of noise in the scan returns.

The flights with noise and turbulence for all scans, shown in Figures 5-93 through 5-100, indicates a slight degradation of estimating quality in the thresholding methods from the baseline flights. The second derivative method was degraded, but clearly remains the most accurate of the estimators. The mean error in milliradians of the radar centroid algorithm indicates that the mean error is less than that of the thresholding methods, but the mean square error in milliradians and meters, Figures 5-94 and 5-98, and the mean error in meters, Figure 5-97, are in excess of the thresholding methods.

Selecting only those scans which are equal to, or greater than 13 dB, the estimating ability of the methods was examined. Figures 5-101 through 5-108 are the results of the flights with noise, scans 13 dB and greater only. As was to be expected, RADARCG is the best estimator in periods of high SNR, and the thresholding estimators are of equal quality. With turbulence effects, Figures 5-109 through 5-116, all estimators are degraded moderately. As in the flights with noise, RADARCG is the most accurate estimator, followed by SDRV, with the thresholding techniques of lower quality.

The accuracy of the estimators using scans with SNRs of 10 dB or less in flights with noise are depicted in Figures 5-117 through 124. The second derivative appears to be the best of the estimators in noise,

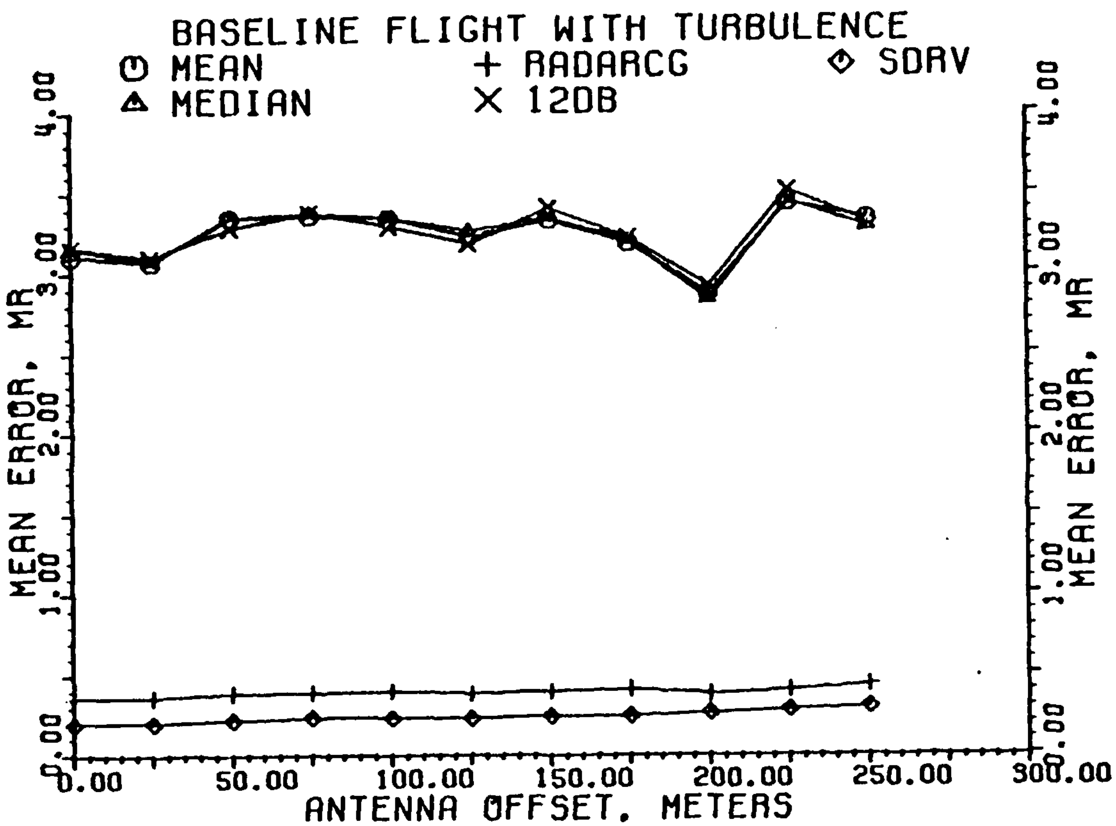

Figure 5-85. Mean error of estimators in milliradians for a granularity of 29 beam pointing locations. Each data point is the result of one flight, all scans used.

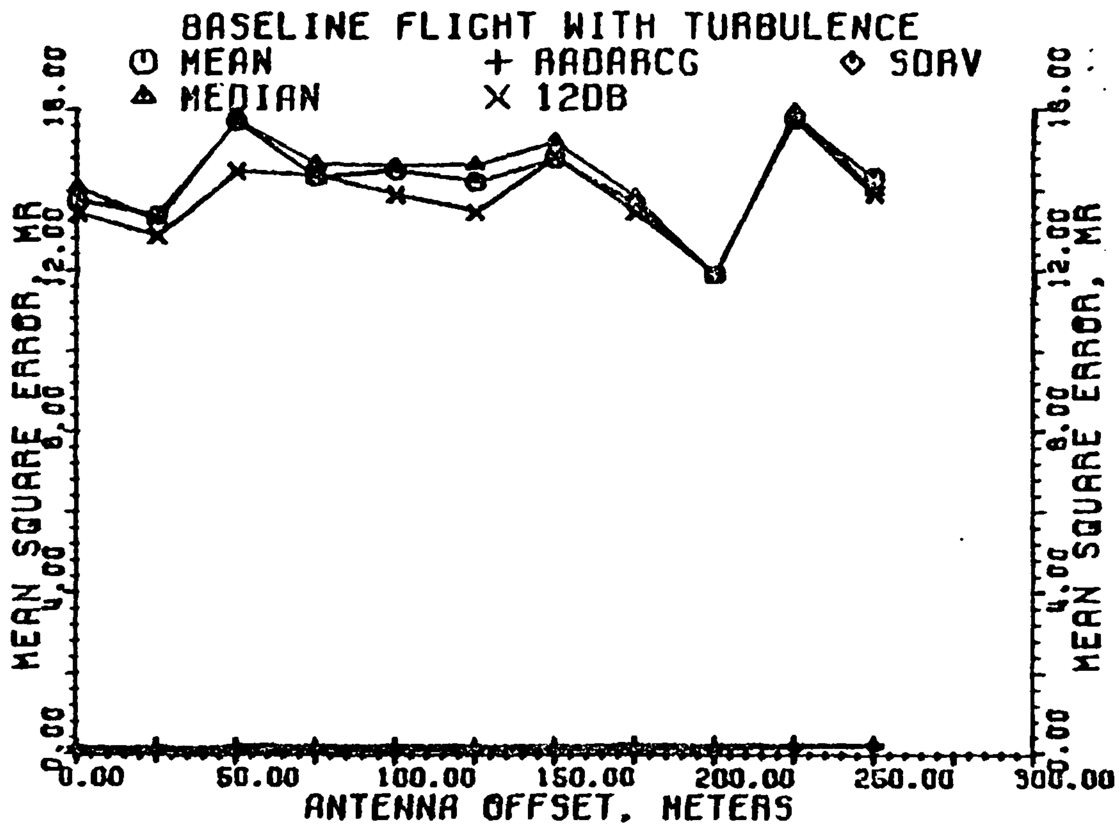

Figure 5-86. Mean square error of estimators in milliradians for a granularity of 29 beam pointing locations. Each data point is the result of one flight, all scans used.

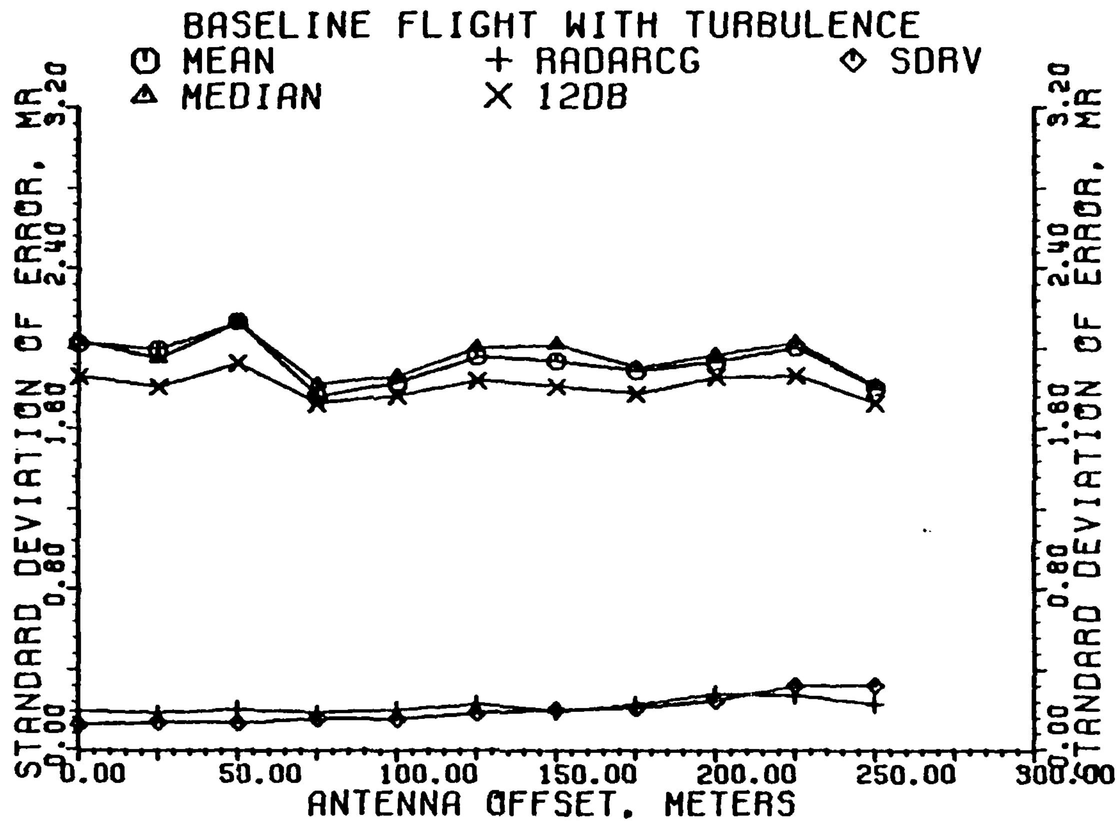

Figure 5-87. Standard deviation of error of estimators in milliradians for a granularity of 29 beam pointing locations. Each data point is the result of one flight, all scans used.

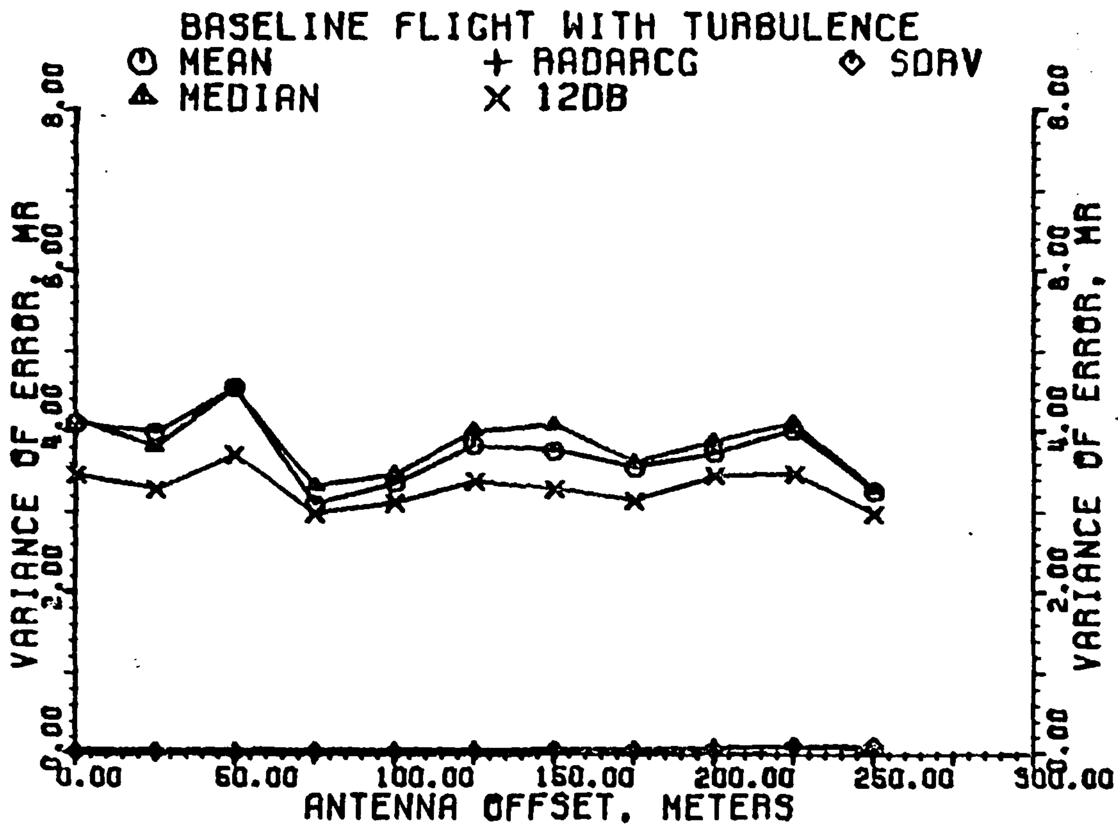

Figure 5-88. Variance of error of estimators in milliradians for a granularity of 29 beam pointing locations. Each data point is the result of one flight, all scans used.

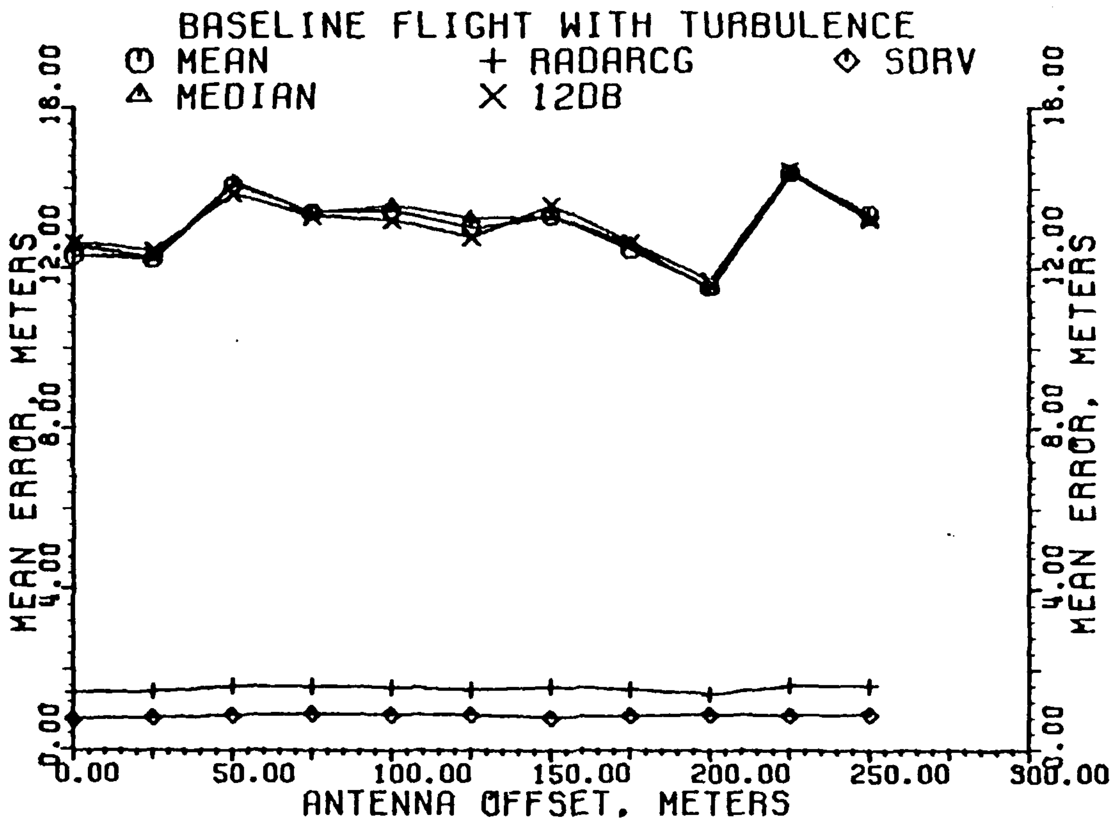

Figure 5-89. Mean error of estimators in meters for a granularity of 29 beam pointing locations. Each data point is the result of one flight, all scans used.

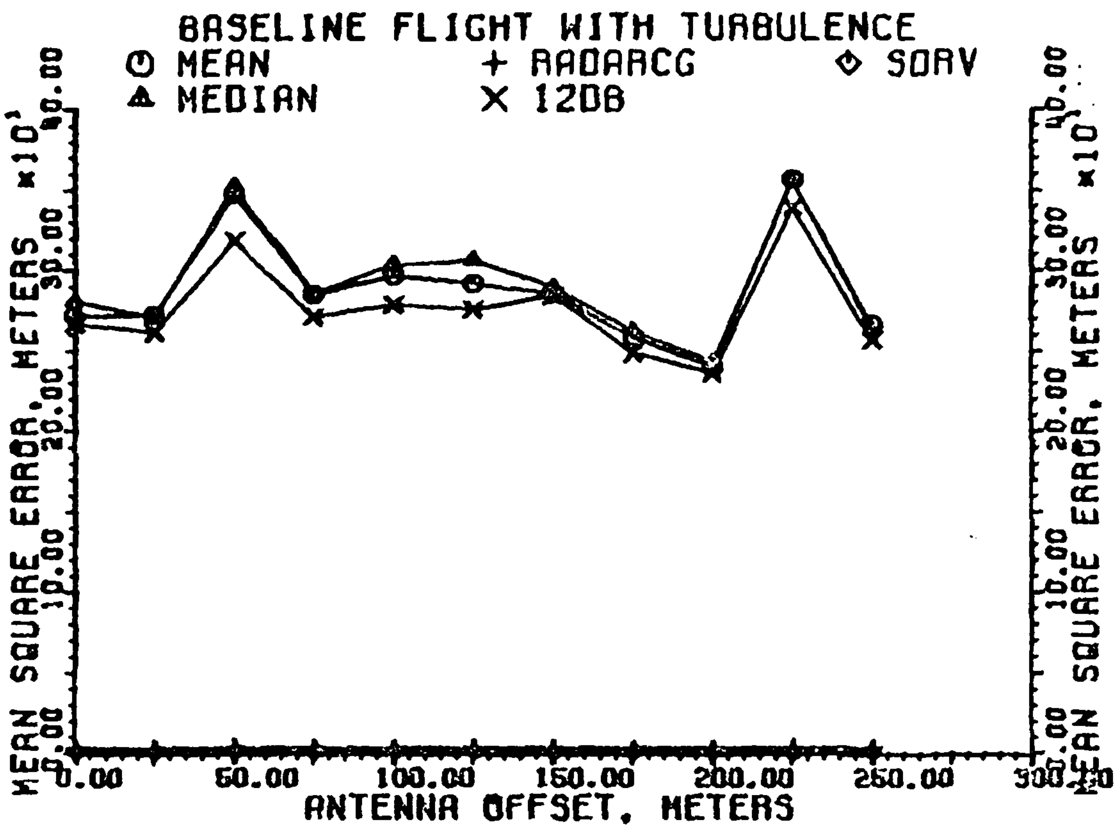

Figure 5-90. Mean square error of estimators in meters for a granularity of 29 beam pointing locations. Each data point is the result of one flight, all scans used.

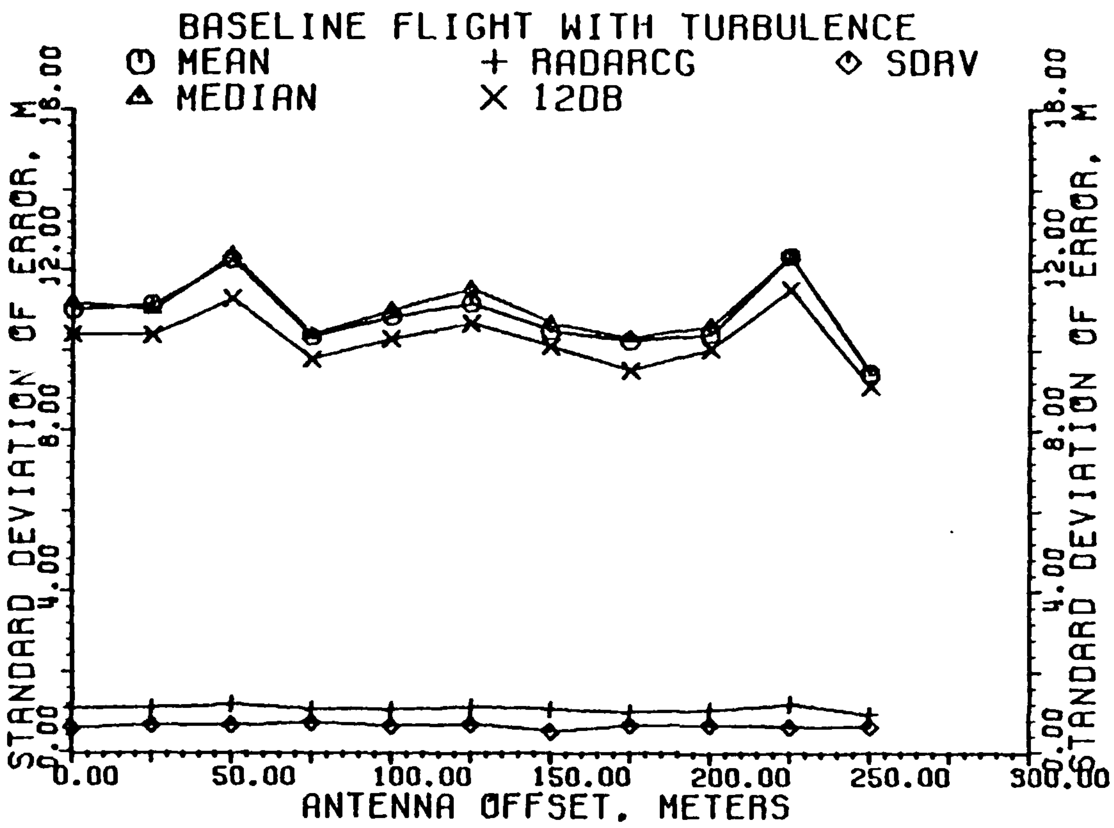

Figure 5-91. Standard deviation of error of estimators in meters for a granularity of 29 beam pointing locations. Each data point is the result of one flight, all scans used.

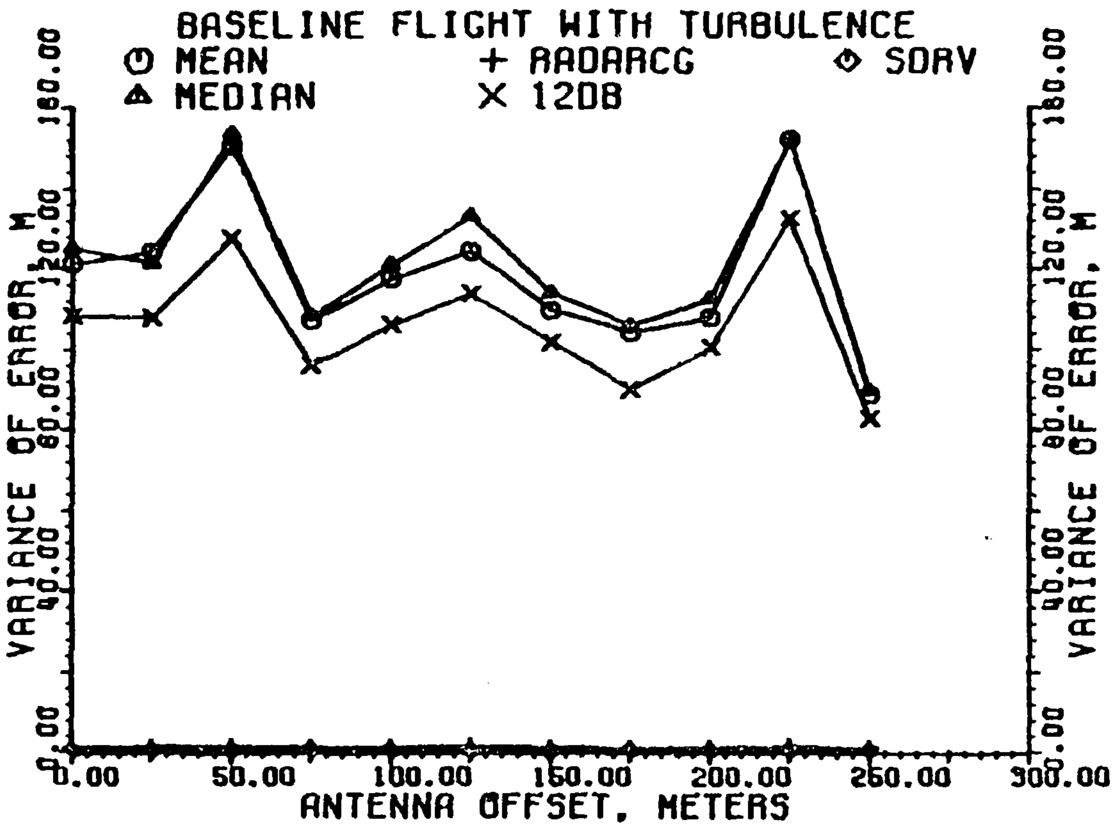

Figure 5-92. Variance of error of estimators in meters for a granularity of 29 beam pointing locations. Each data point is the result of one flight, all scans used.

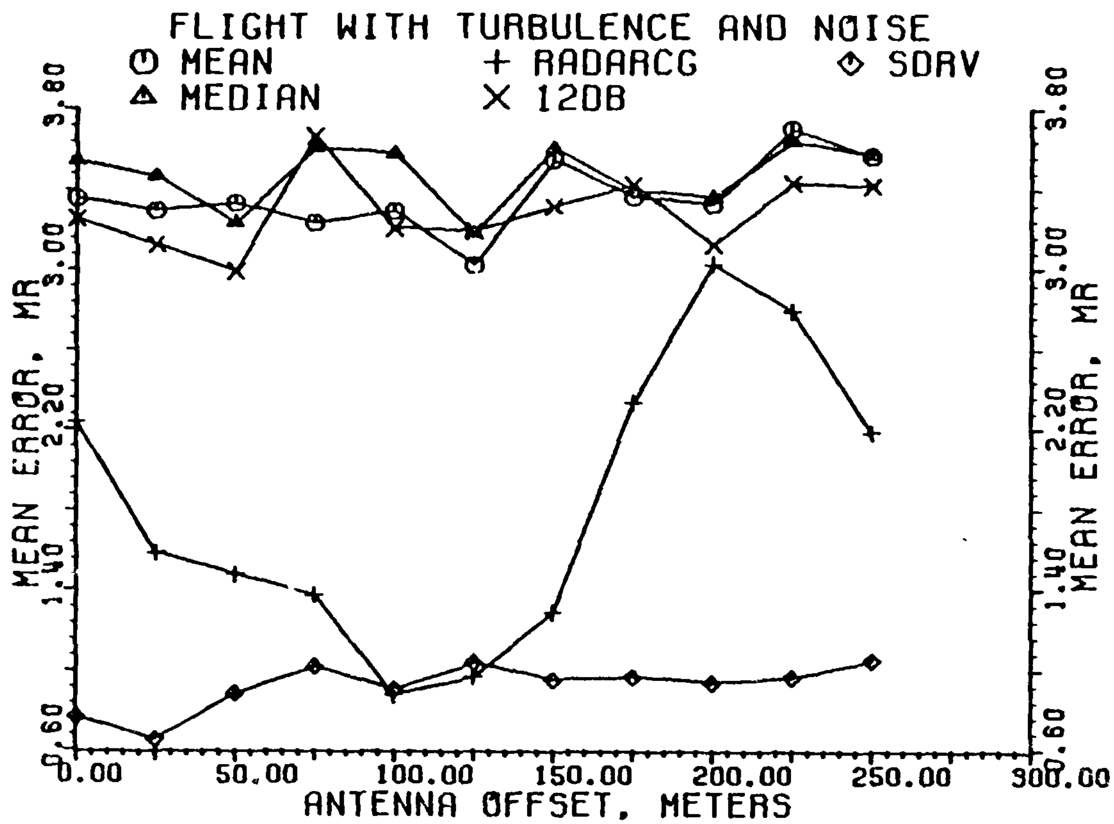

Figure 5-93. Mean error of estimators in milliradians for a granularity of 29 beam pointing locations. Each data point is the result of one flight, all scans used.

AD-A110 862 GEORGIA INST OF TECH ATLANTA ENGINEERING EXPERIMENT --ETC F/G 17/7
MARINE AIR TRAFFIC CONTROL AND LANDING SYSTEM (MATCALS INVESTIG--ETC(U)
SEP 81 E R GRAF, C L PHILLIPS, S A STARKS N00039-80-C-0032
UNCLASSIFIED GIT/EES-1-A-2550-VOL-1 NL

3 of 5
AD A110862

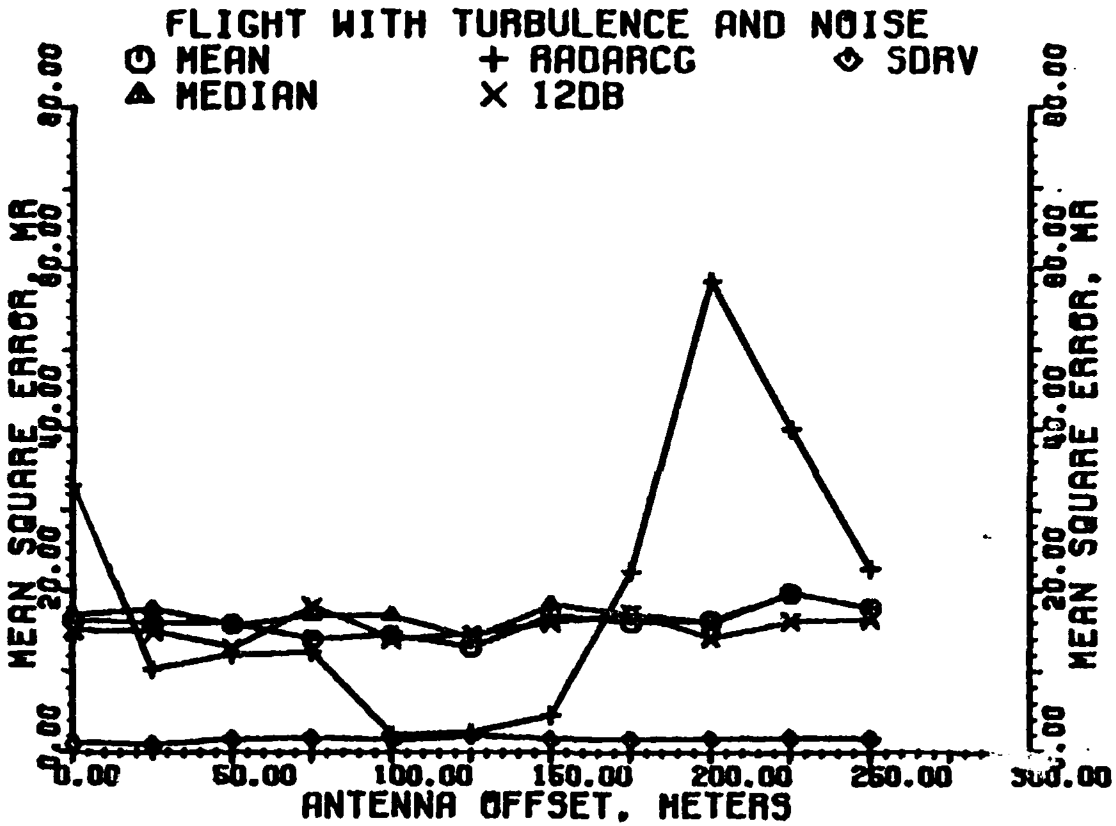

Figure 5-94. Mean square error of estimators in milliradians for a granularity of 29 beam pointing locations. Each data point is the result of one flight, all scans used.

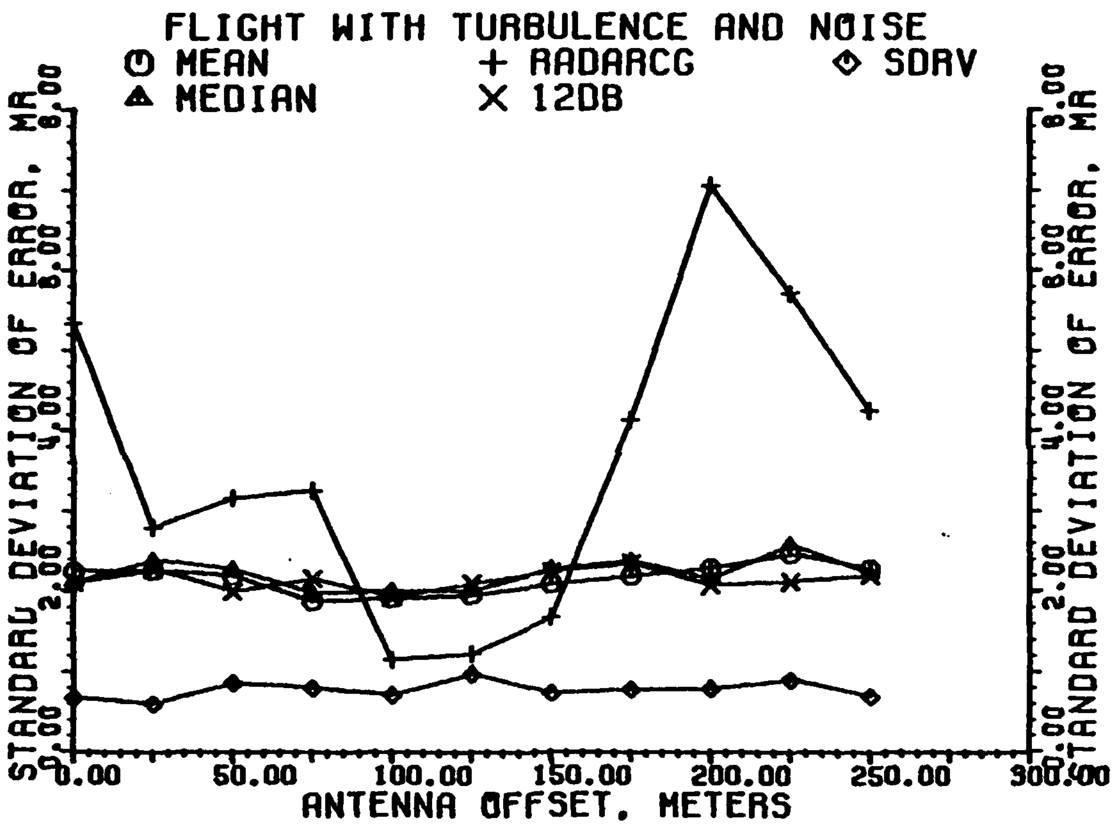

Figure 5-95. Standard deviation of error of estimators in milliradians for a granularity of 29 beam pointing locations. Each data point is the result of one flight, all scans used.

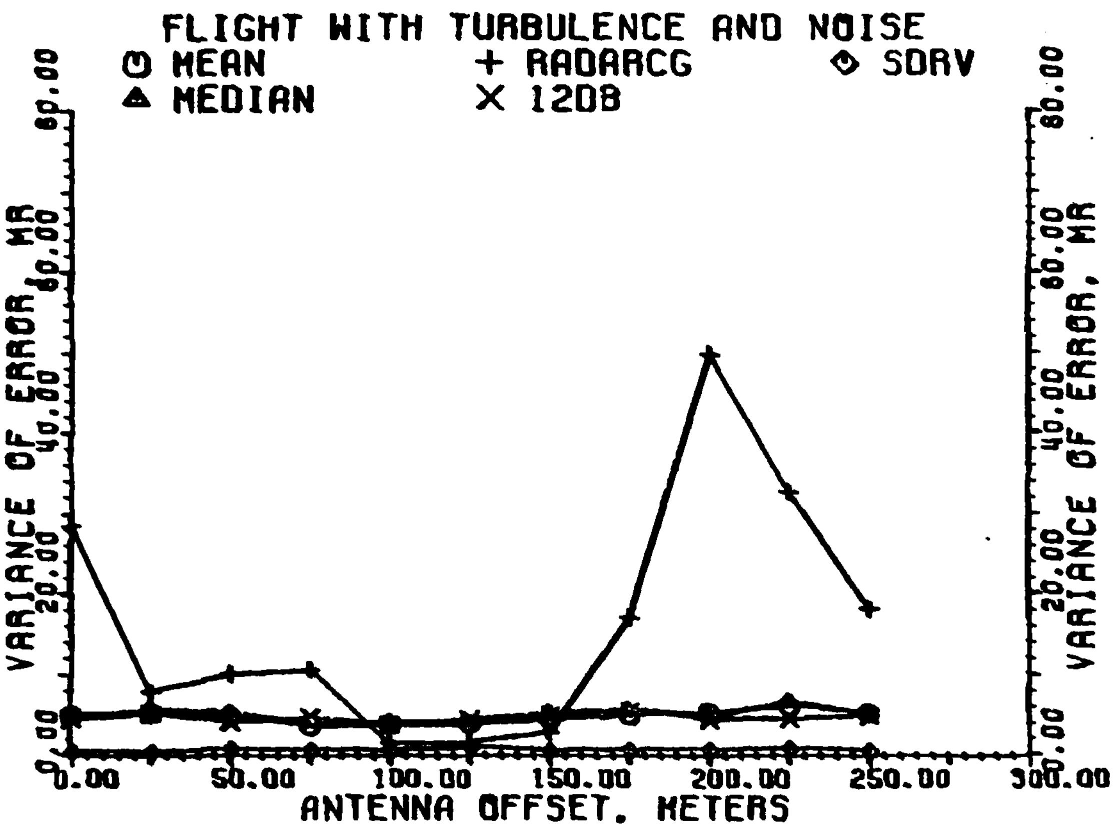

Figure 5-96. Variance of error of estimators in milliradians for a granularity of 29 beam pointing locations. Each data point is the result of one flight, all scans used.

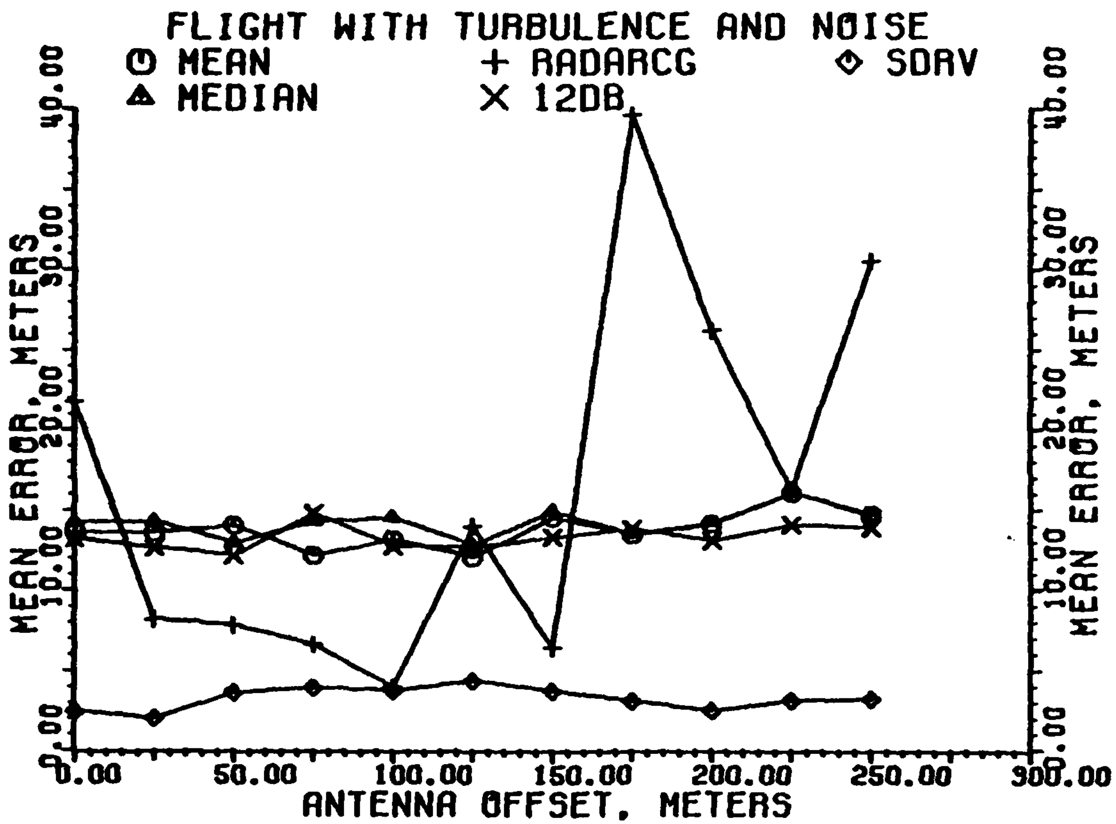

Figure 5-97. Mean error of estimators in meters for a granularity of 29 beam pointing locations. Each data point is the result of one flight, all scans used.

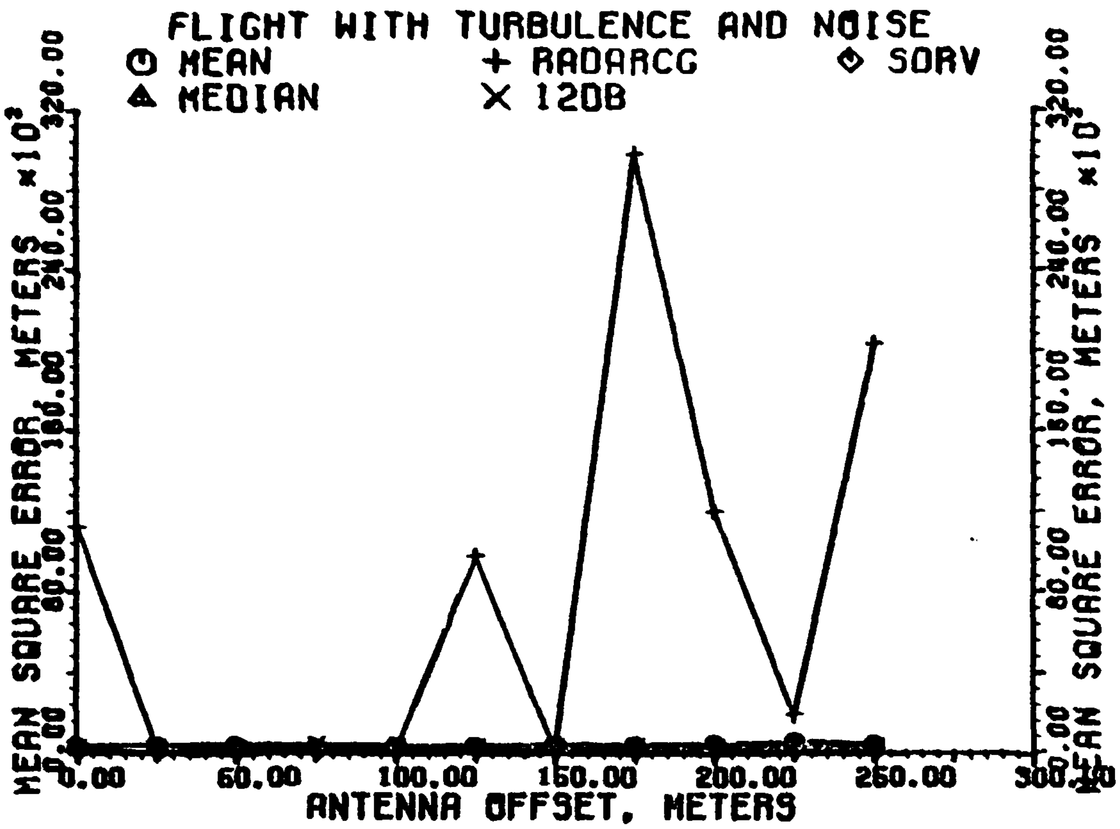

Figure 5-98. Mean square error of estimators in meters for a granularity of 29 beam pointing locations. Each data point is the result of one flight, all scans used.

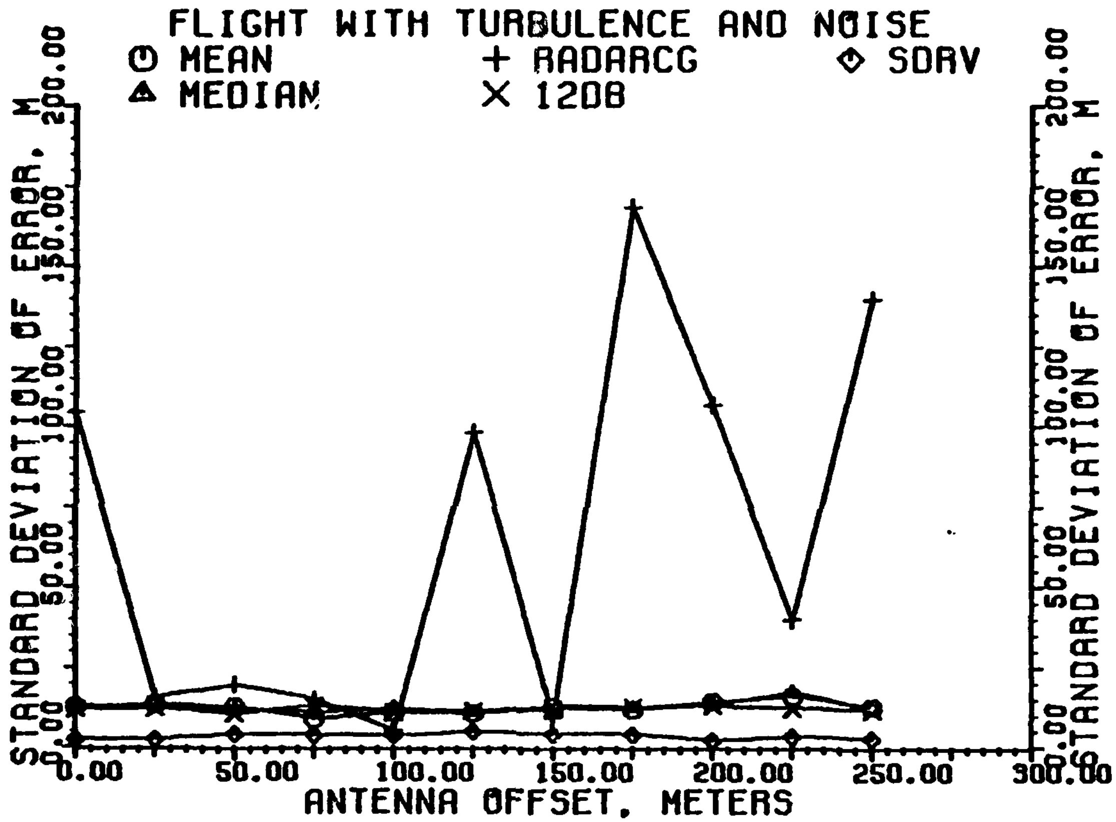

Figure 5-99. Standard deviation of error of estimators in meters for a granularity of 29 beam pointing locations. Each data point is the result of one flight, all scans used.

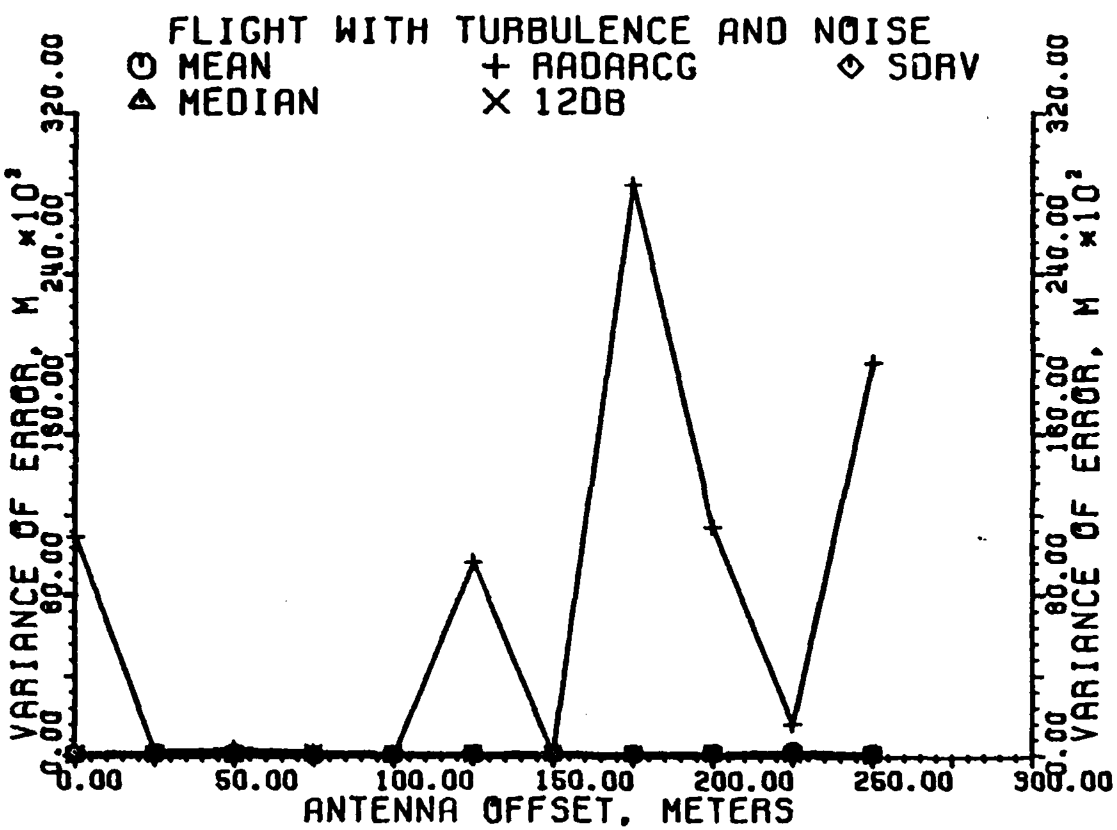

Figure 100. Variance of error of estimators in meters for a granularity of 29 beam pointing locations. Each data point is the result of one flight, all scans used.

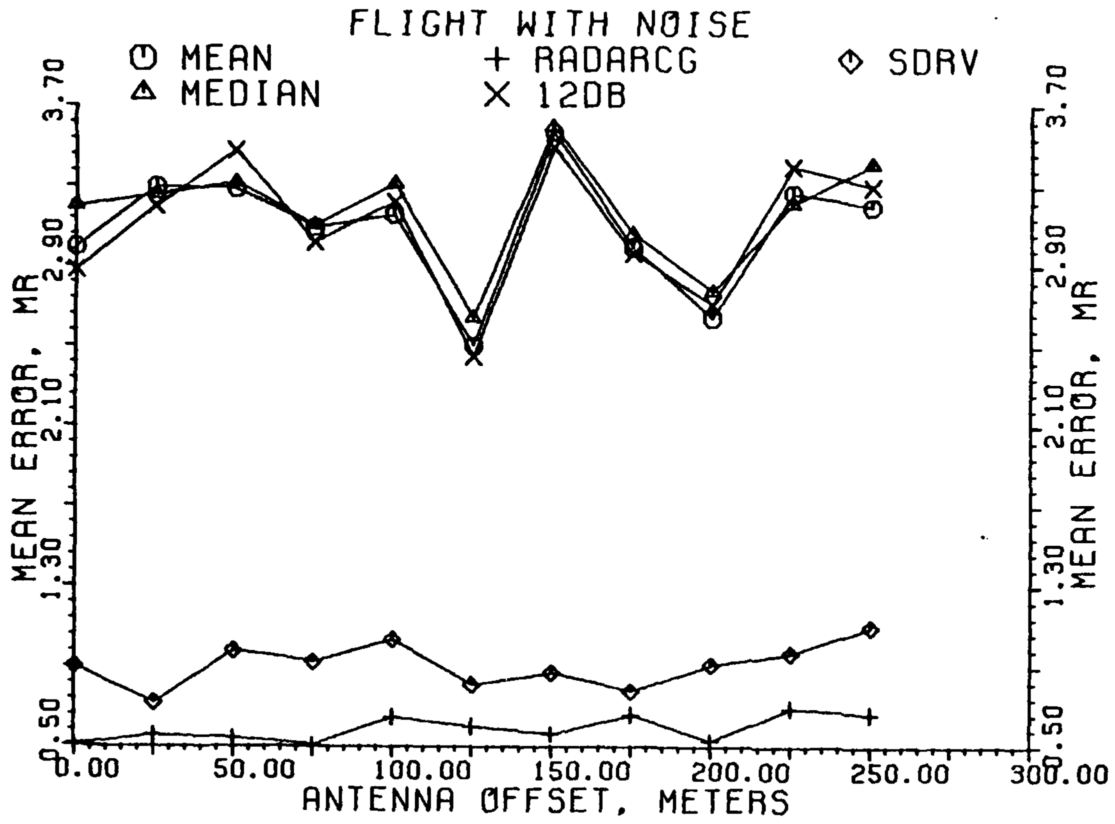

Figure 5-101. Mean error of estimators in milliradians for a granularity of 29 beam pointing locations. Each data point is the result of one flight, all scans with a SNR 13 dB or greater used.

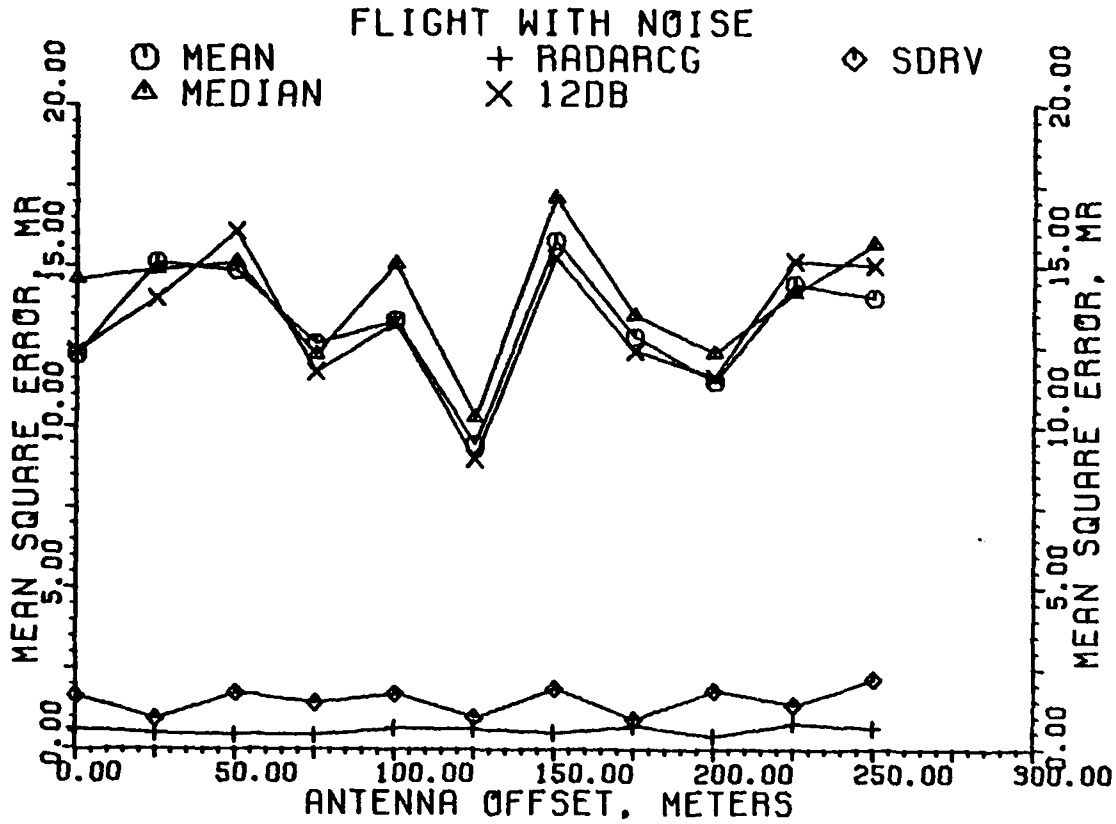

Figure 5-102. Mean square error of estimators in milliradians for a granularity of 29 beam pointing locations. Each data point is the result of one flight, all scans with a SNR 13 dB or greater used.

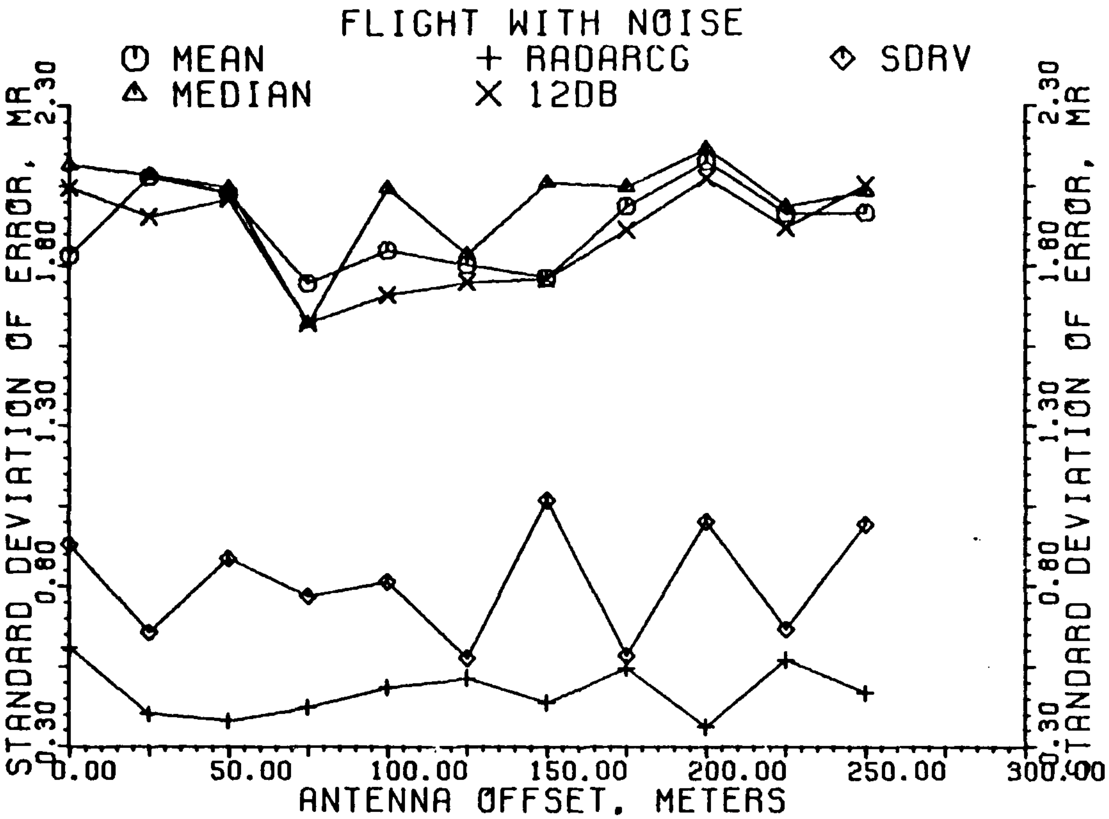

Figure 5-103. Standard deviation of error of estimators in milliradians for a granularity of 29 beam pointing locations. Each data point is the result of one flight, all scans with a SNR 13 dB or greater used.

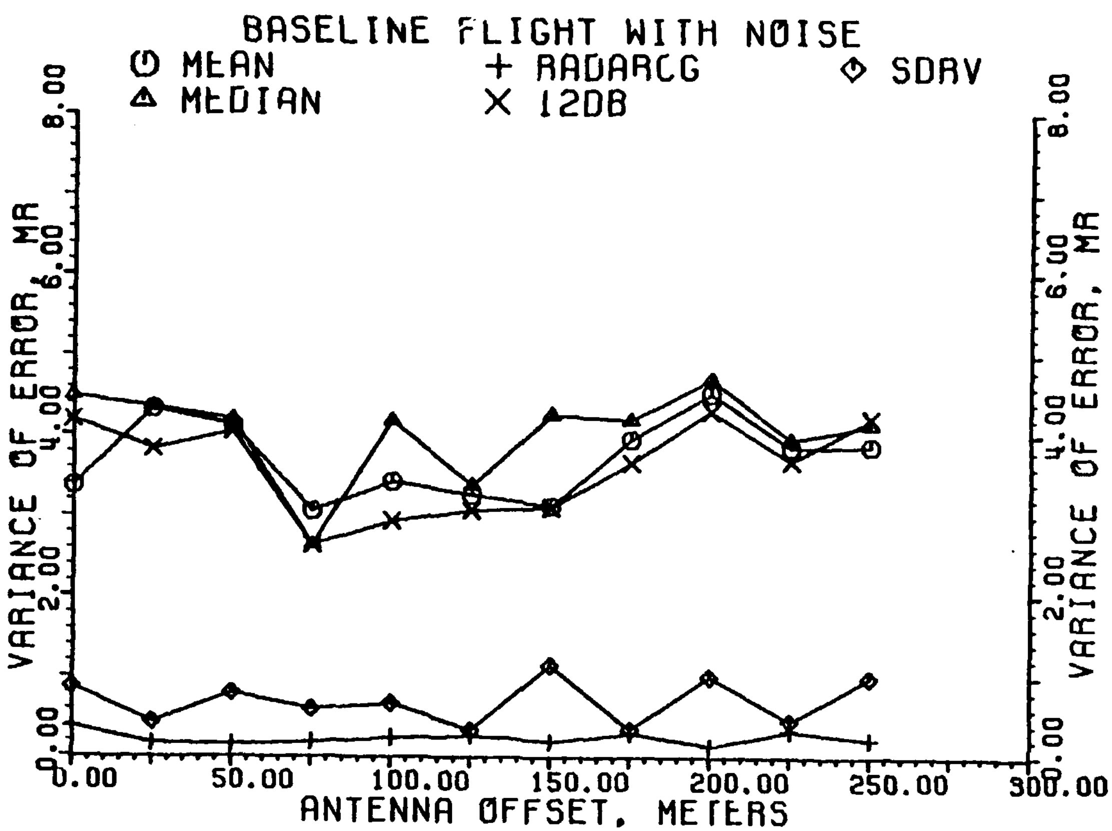

Figure 5-104. Variance of error of estimators in milliradians for a granularity of 29 beam pointing locations. Each data point is the result of one flight, all scans with a SNR 13 dB or greater used.

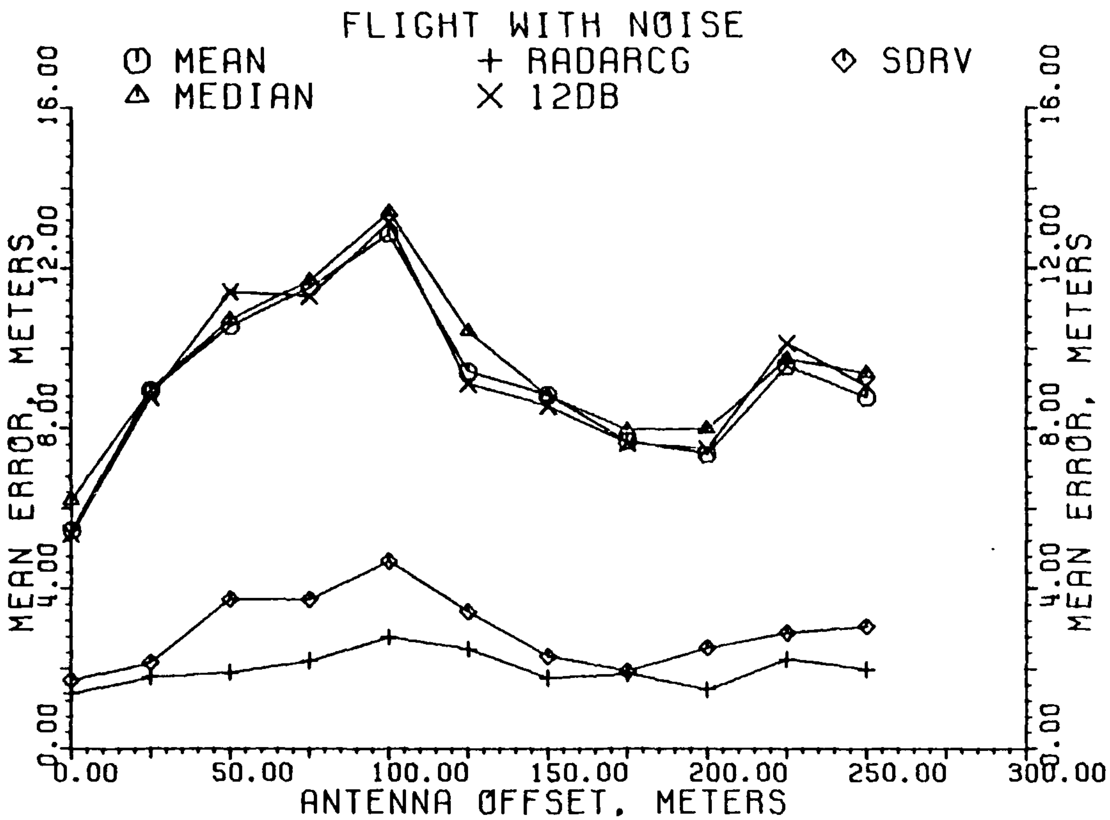

Figure 5-105. Mean error of estimators in meters for a granularity of 29 beam pointing locations. Each data point is the result of one flight, all scans with a SNR 13 dB or greater used.

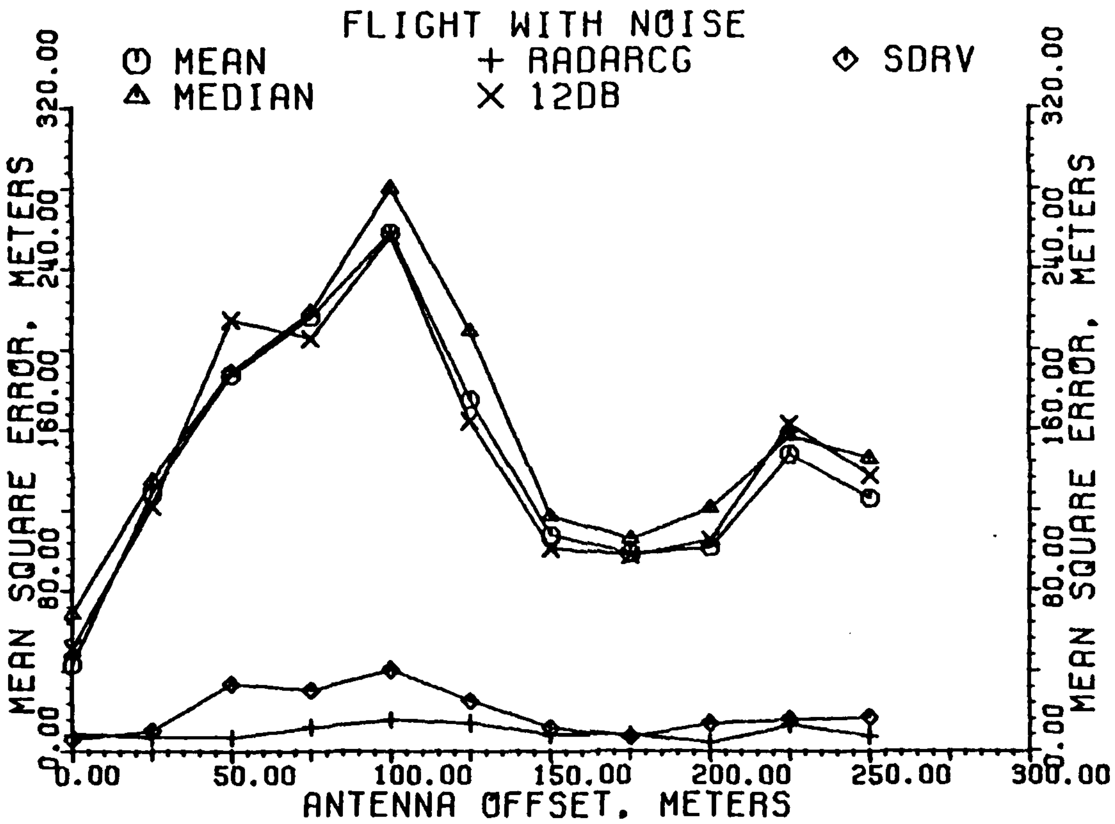

Figure 5-106. Mean square error of estimators in meters for a granularity of 29 beam pointing locations. Each data point is the result of one flight, all scans with a SNR 13 dB or greater used.

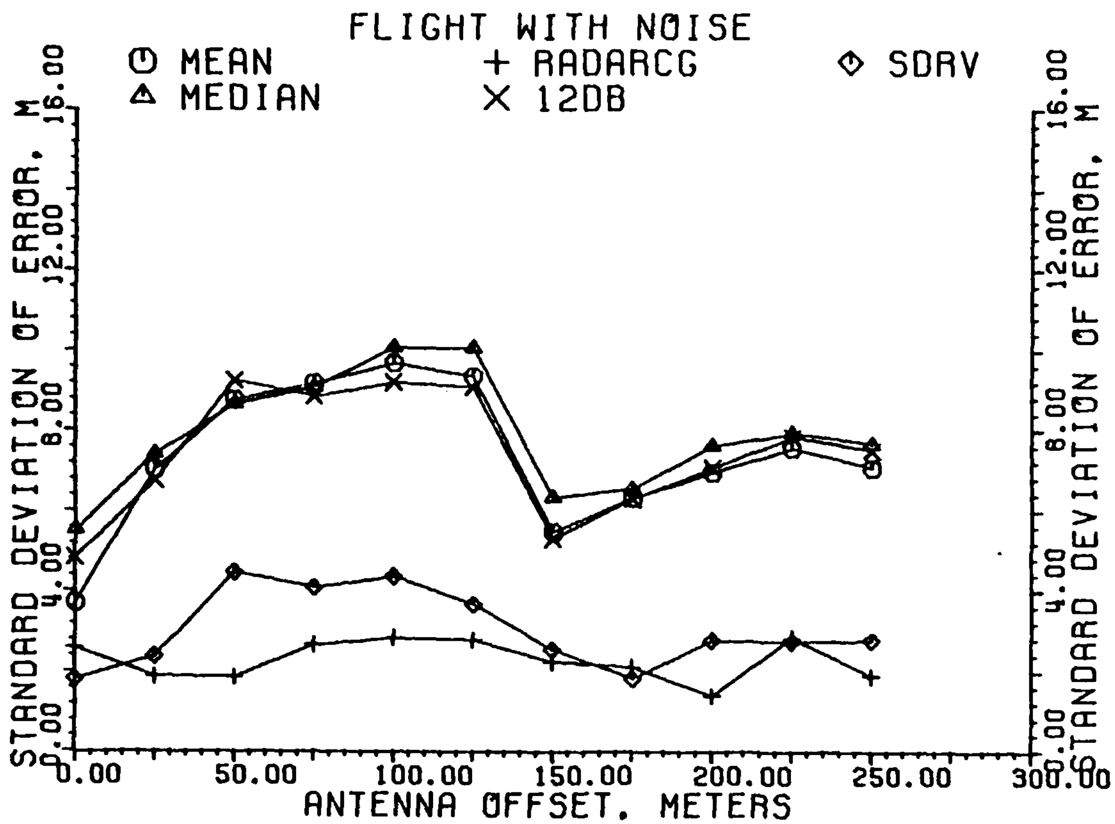

Figure 5-107. Standard deviation of error of estimators in meters for a granularity of 29 beam pointing locations. Each data point is the result of one flight, all scans with a SNR 13 dB or greater used.

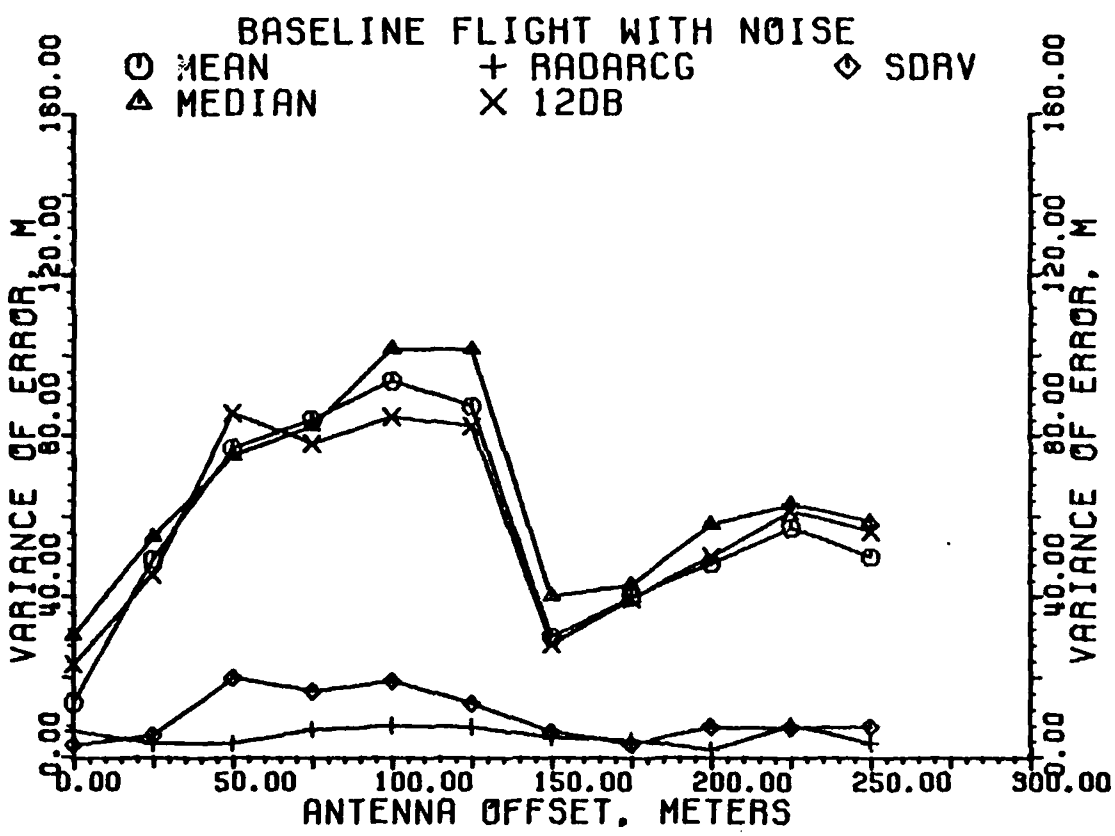

Figure 5-108. Variance of error of estimators in meters for a granularity of 29 beam pointing locations. Each data point is the result of one flight, all scans with a SNR of 13 dB or greater used.

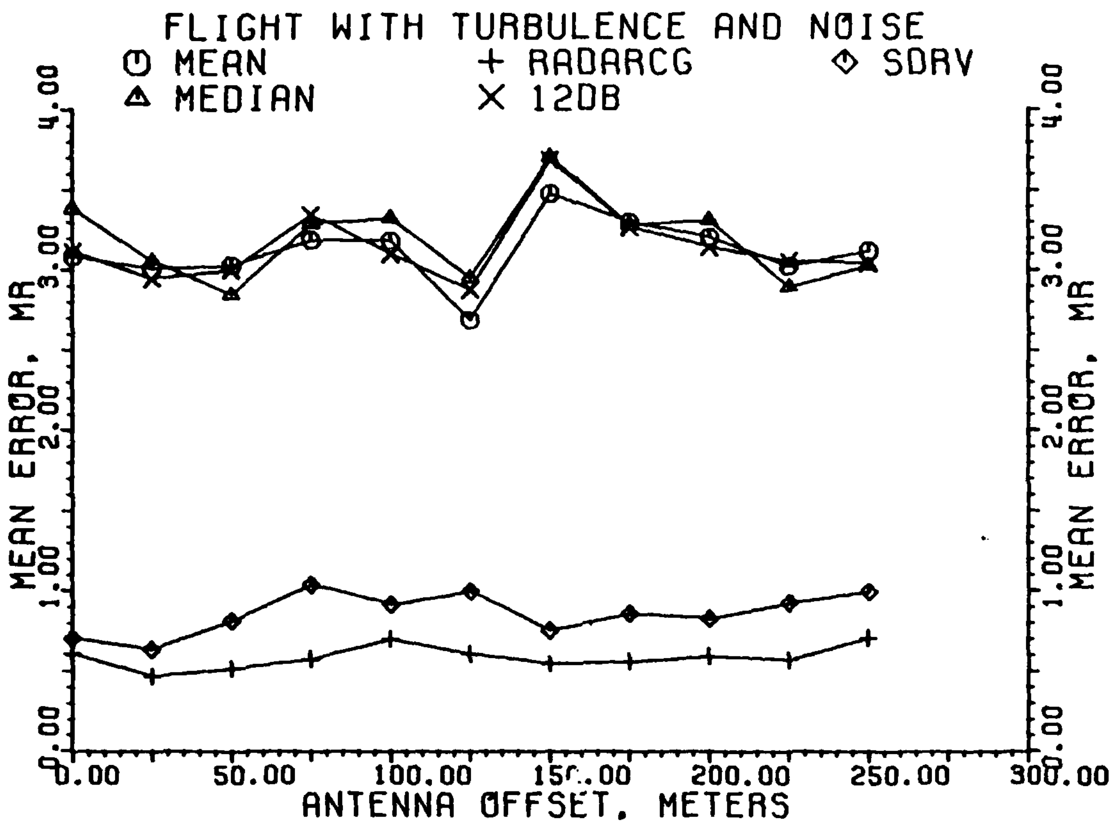

Figure 5-109. Mean error of estimators in milliradians for a granularity of 29 beam pointing locations. Each data point is the result of one flight, all scans with a SNR 13 dB or greater used.

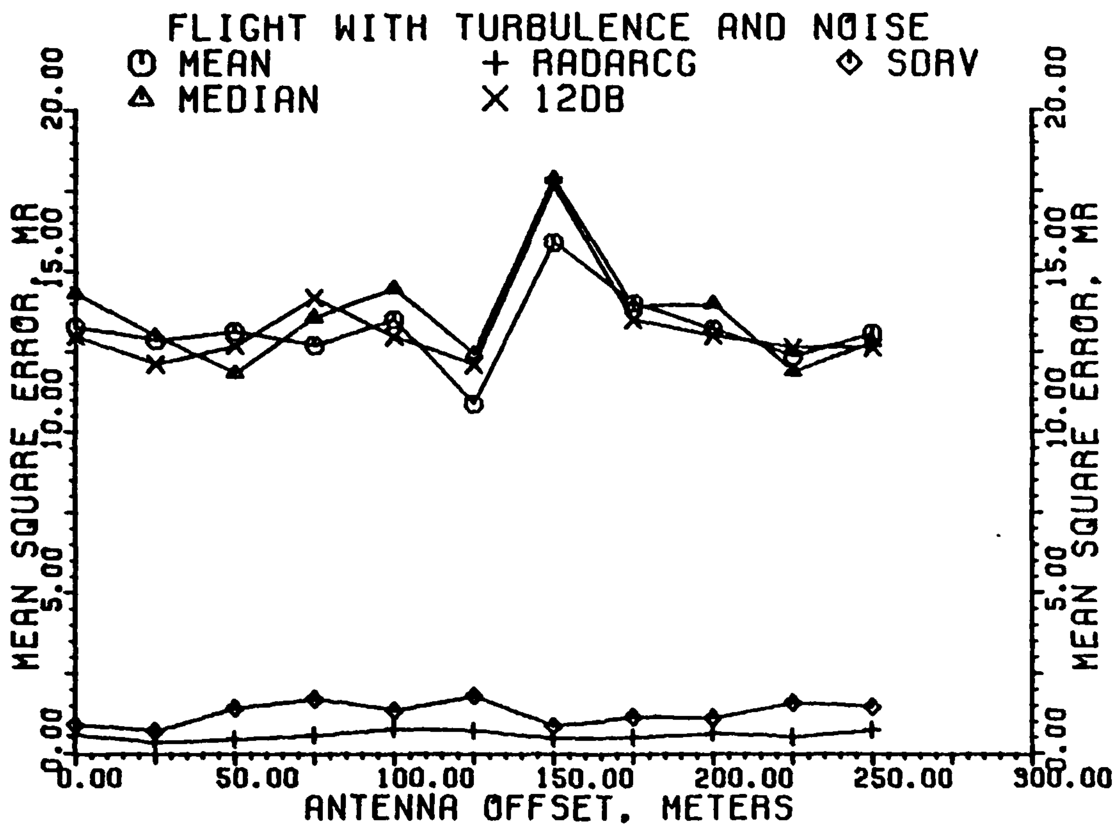

Figure 5-110. Mean square error of estimators in milliradians for a granularity of 29 beam pointing locations. Each data point is the result of one flight, all scans with a SNR 13 dB or greater used.

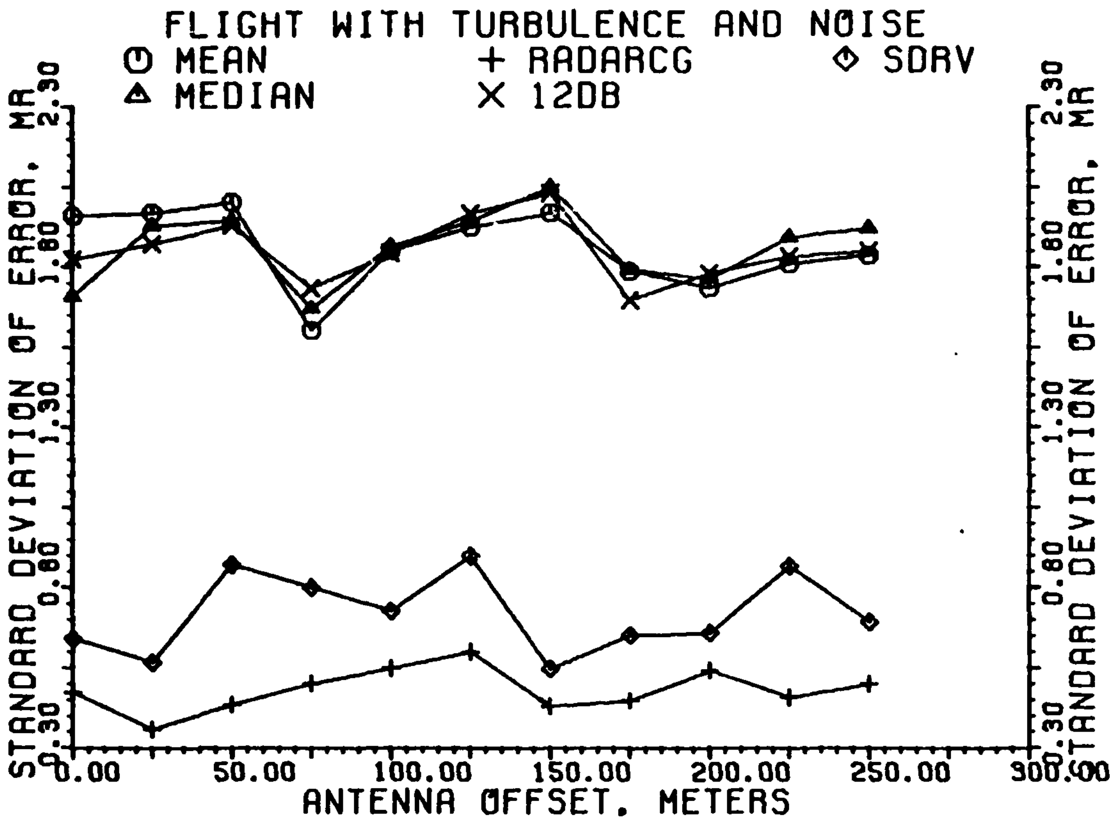

Figure 5-111. Standard deviation of error of estimators in milliradians for a granularity of 29 beam pointing locations. Each data point is the result of one flight, all scans with a SNR 13 dB or greater used.

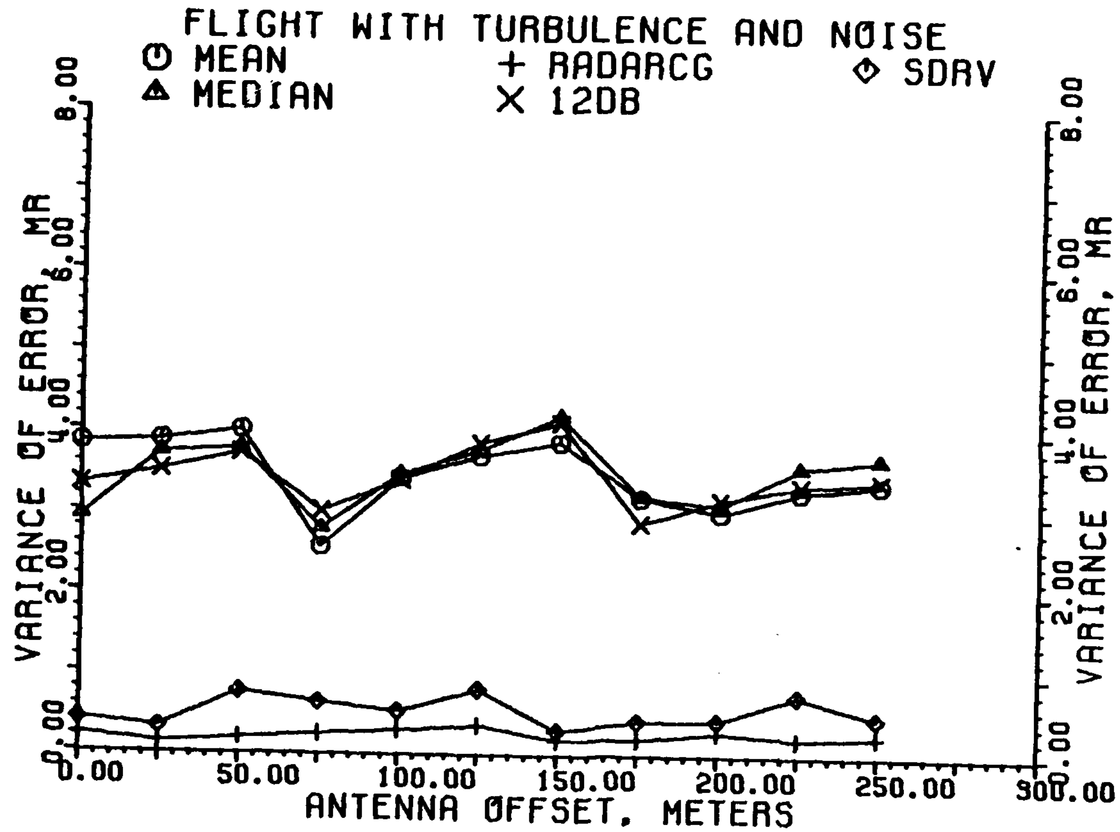

Figure 5-112. Variance of error of estimators in milliradians for a granularity of 29 beam pointing locations. Each data point is the result of one flight, all scans with a SNR 13 dB or greater used.

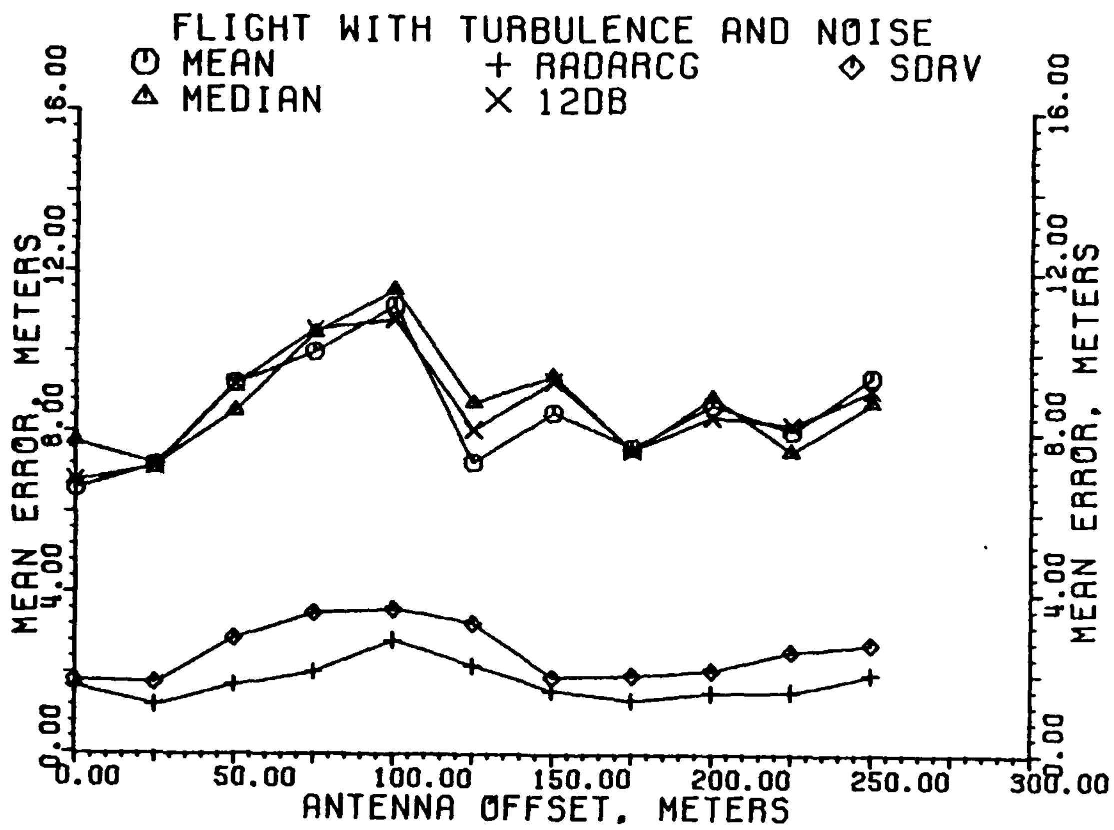

Figure 5-113. Mean error of estimators in meters for a granularity of 29 beam pointing locations. Each data point is the result of one flight, all scans with a SNR 13 dB or greater used.

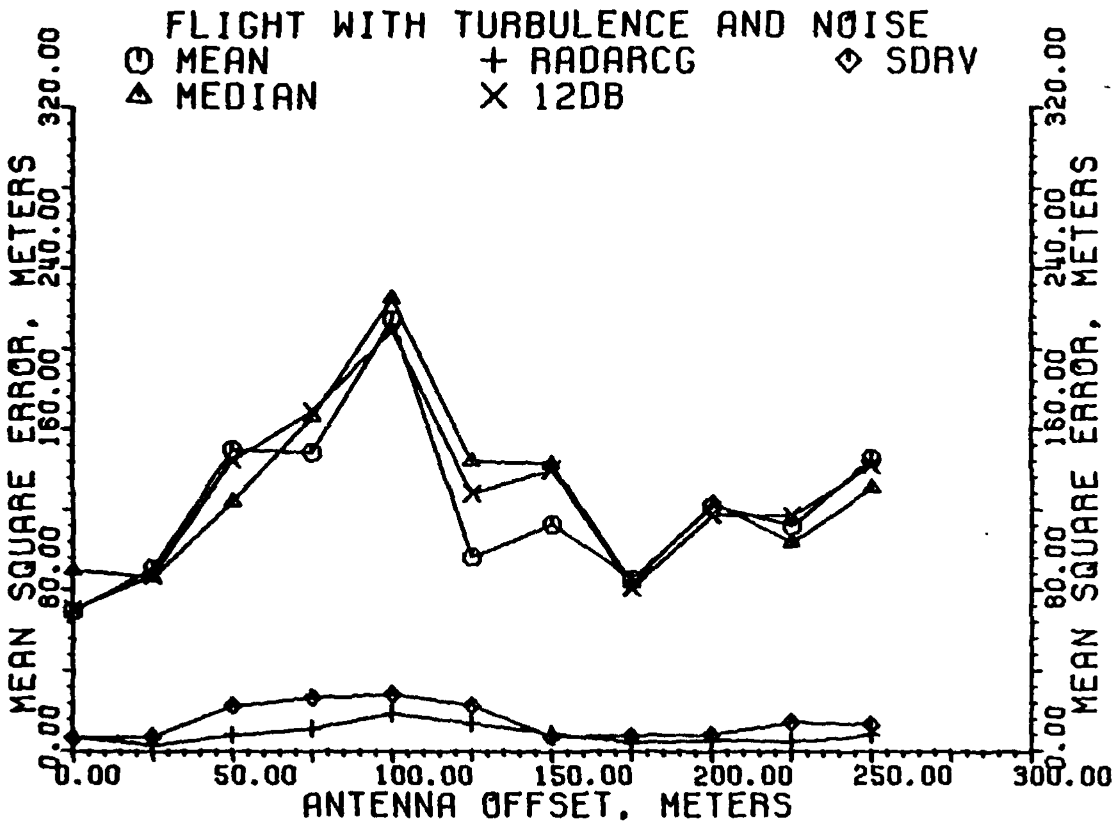

Figure 5-114. Mean square error of estimators in meters for a granularity of 29 beam pointing locations. Each data point is the result of one flight, all scans with a SNR dB or greater used.

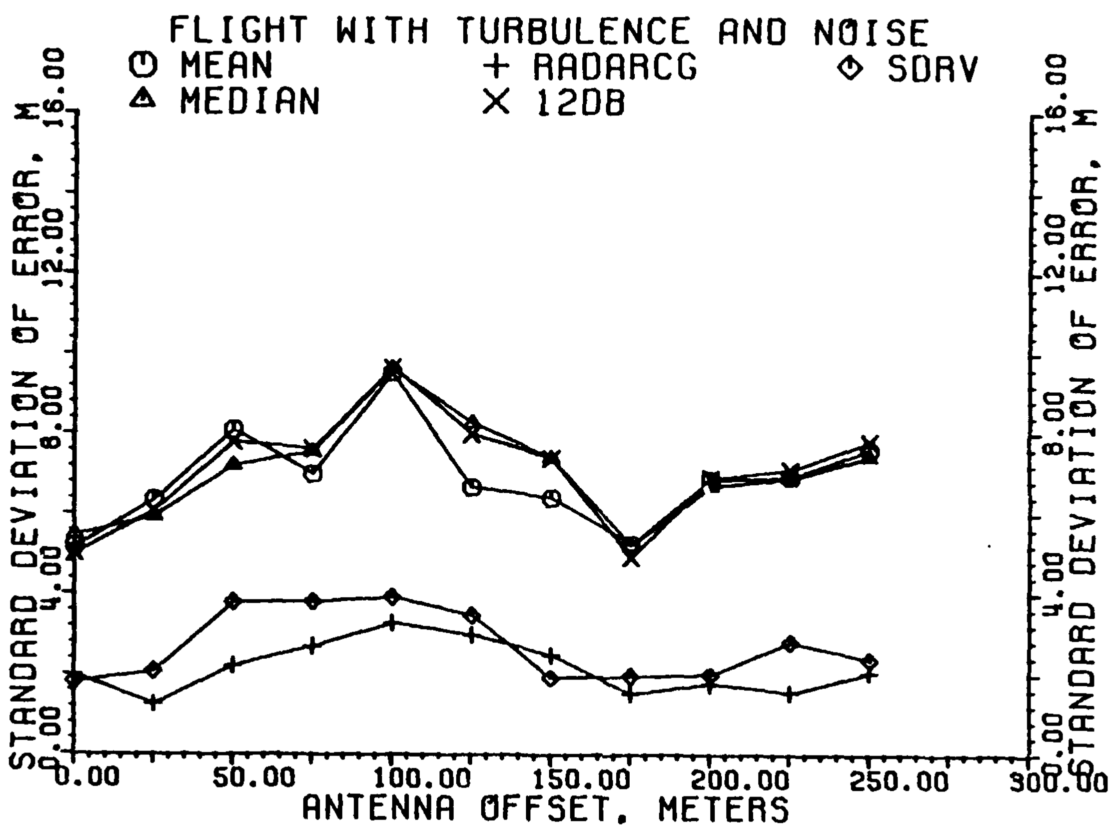

Figure 5-115. Standard deviation of error of estimators in meters for a granularity of 29 beam pointing locations. Each data point is the result of one flight, all scans with a SNR 13 dB or greater used.

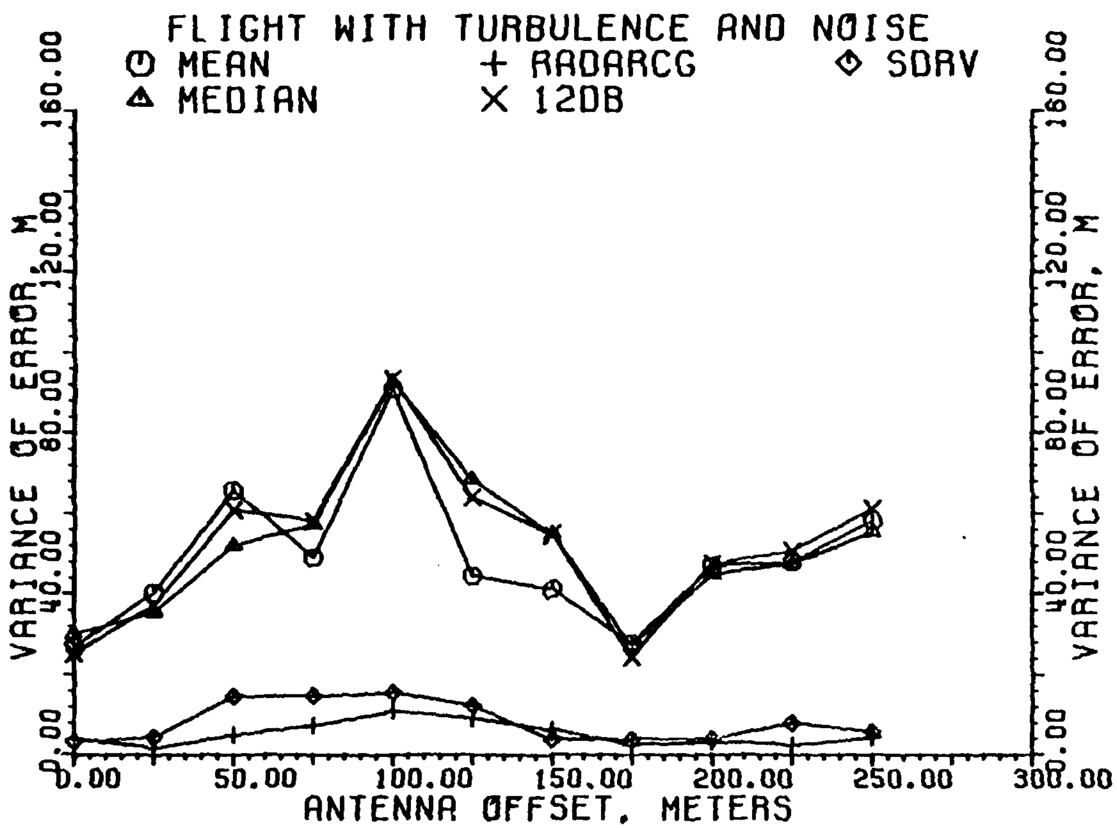

Figure 5-116. Variance of error of estimators in meters for a granularity of 29 beam pointing locations. Each data point is the result of one flight, all scans with a SNR 13 dB or greater used.

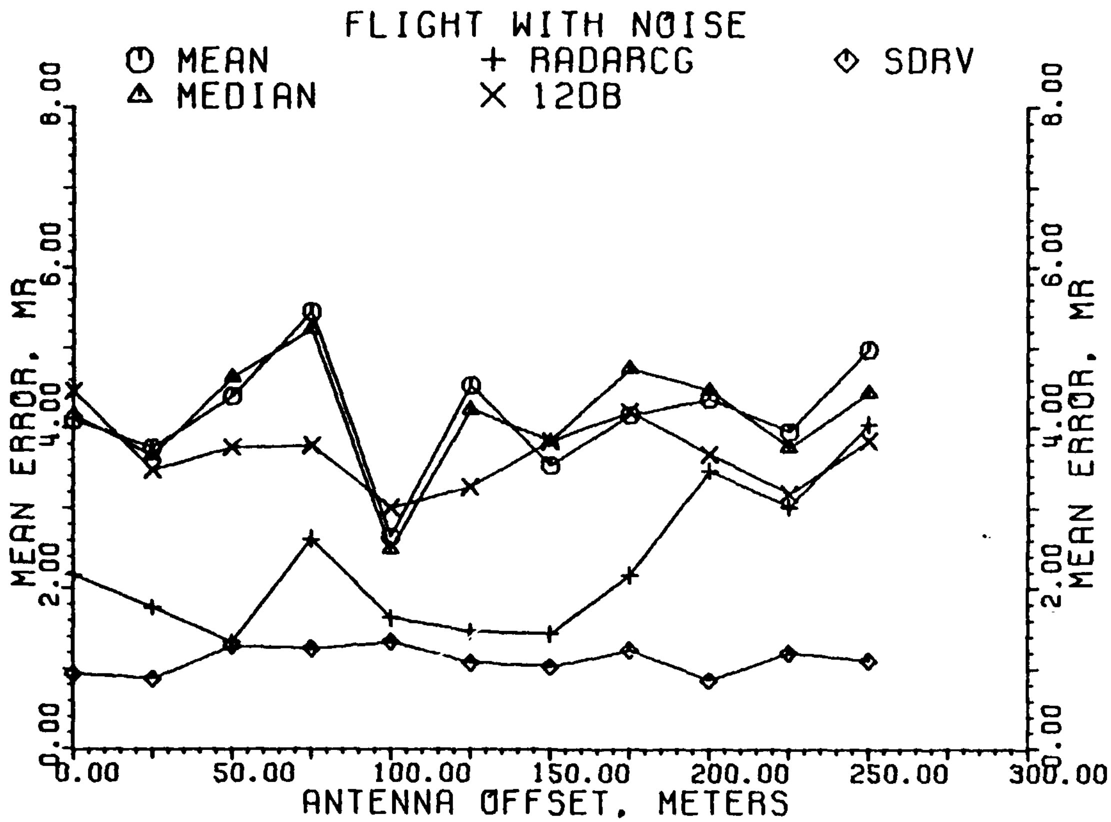

Figure 5-117. Mean error of estimators in milliradians for a granularity of 29 beam pointing locations. Each data point is the result of one flight, all scans with a SNR at or below 10 dB used.

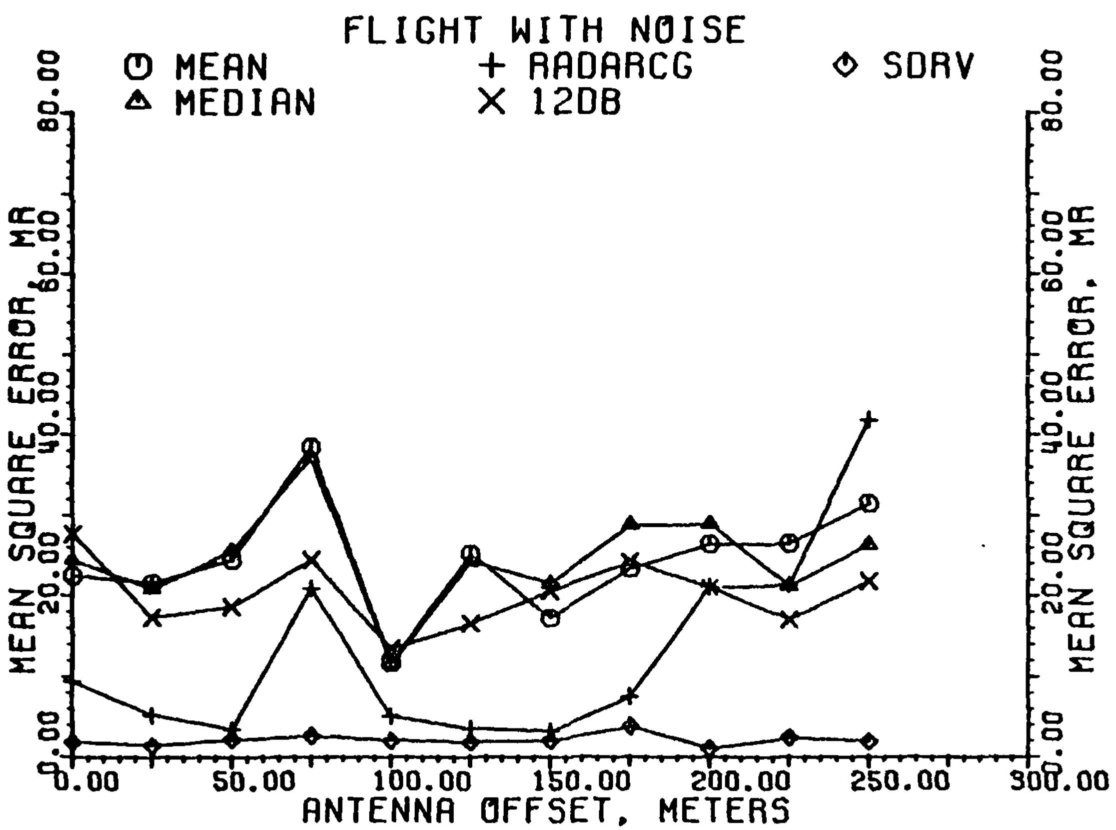

Figure 5-118. Mean square error of estimators in milliradians for a granularity of 29 beam pointing locations. Each data point is the result of one flight, all scans with a SNR at or below 10 dB used.

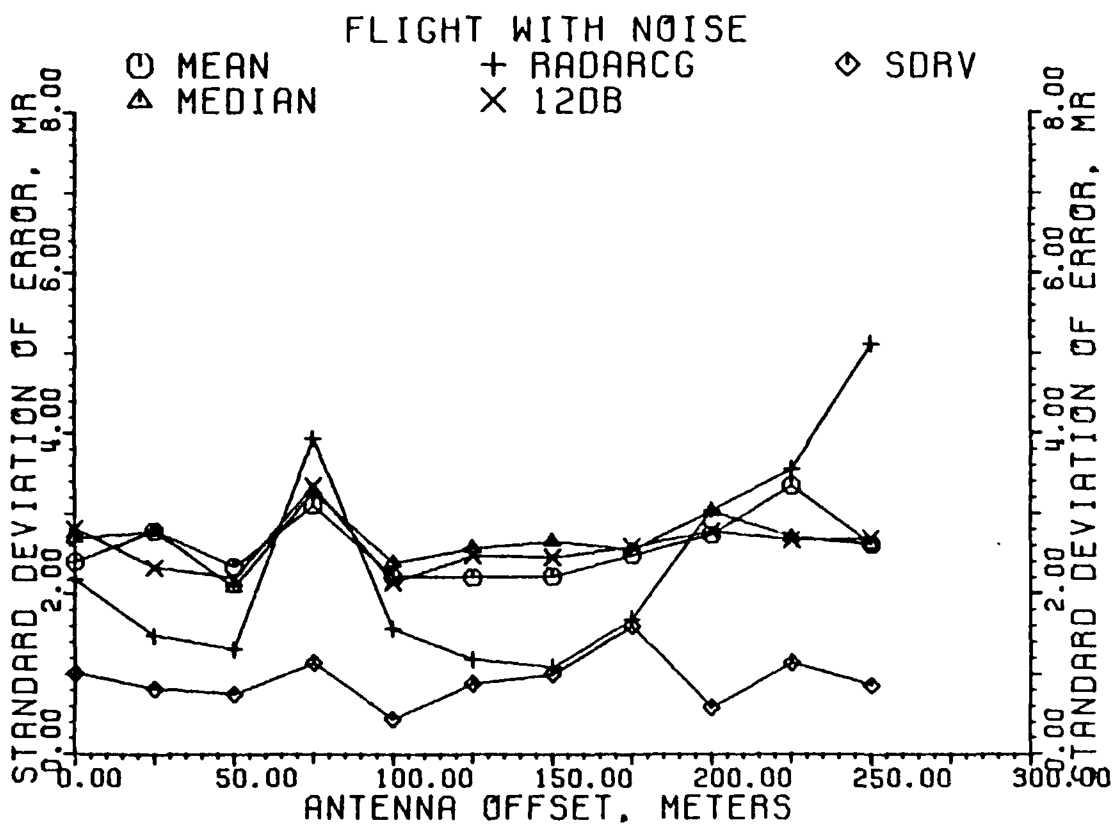

Figure 5-119. Standard deviation of error of estimators in milliradians for a granularity of 29 beam pointing locations. Each data point is the result of one flight, all scans with a SNR at or below 10 dB used.

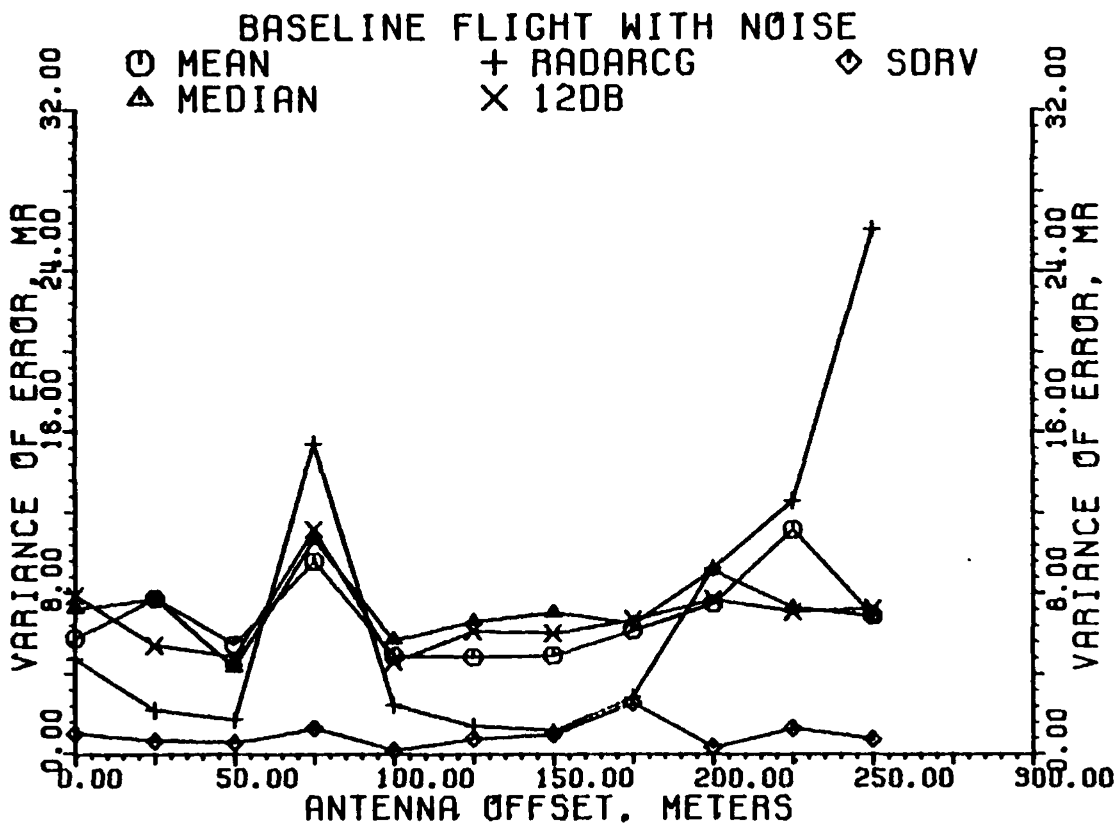

Figure 5-120. Variance of error of estimators in milliradians for a granularity of 29 beam pointing locations. Each data point is the result of one flight, all scans with a SNR at or below 10 dB used.

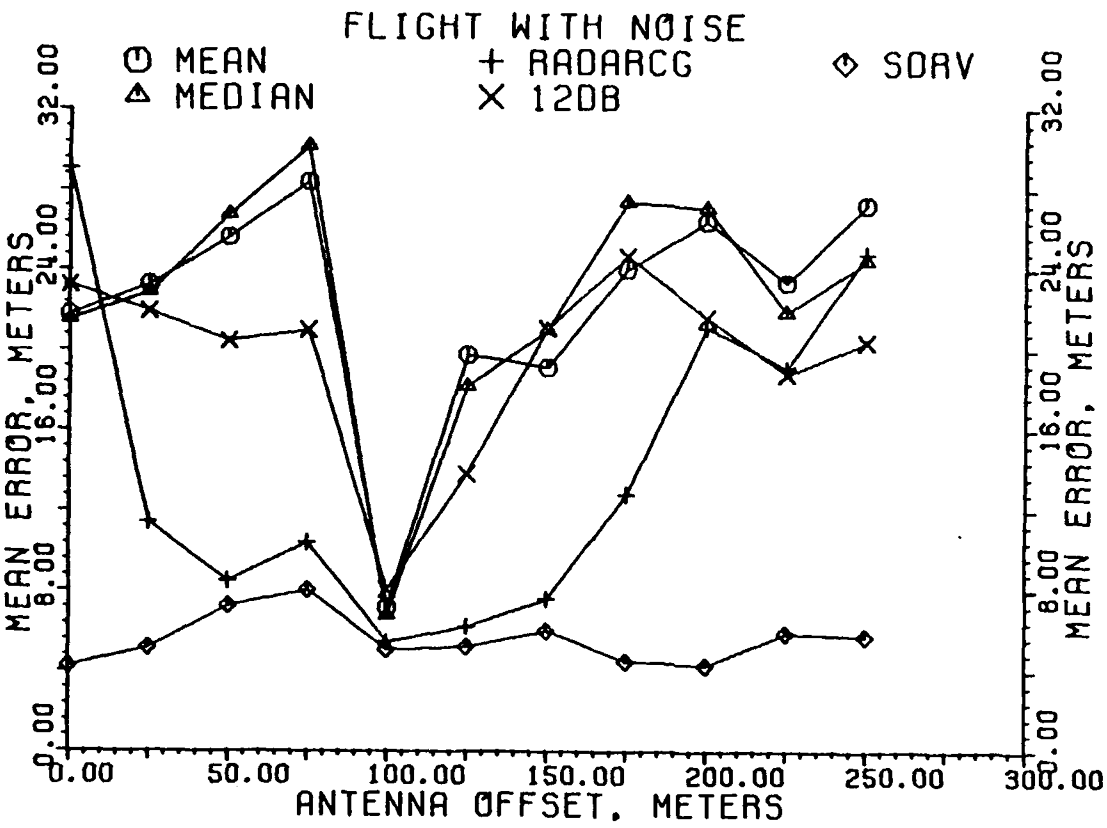

Figure 5-121. Mean error of estimators in meters for a granularity of 29 beam pointing locations. Each data point is the result of one flight, all scans with a SNR at or below 10 dB used.

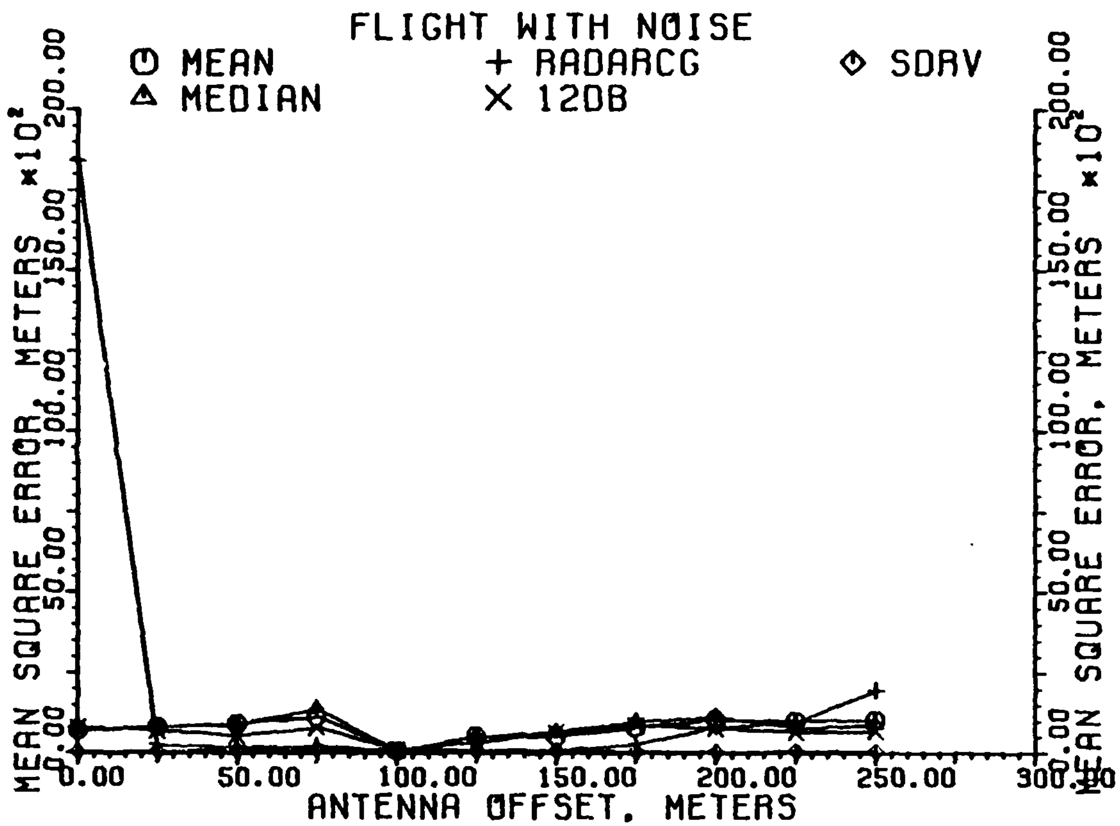

Figure 5-122. Mean square error of estimators in meters for a granularity of 29 beam pointing locations. Each data point is the result of one flight, all scans with a SNR at or below 10 dB used.

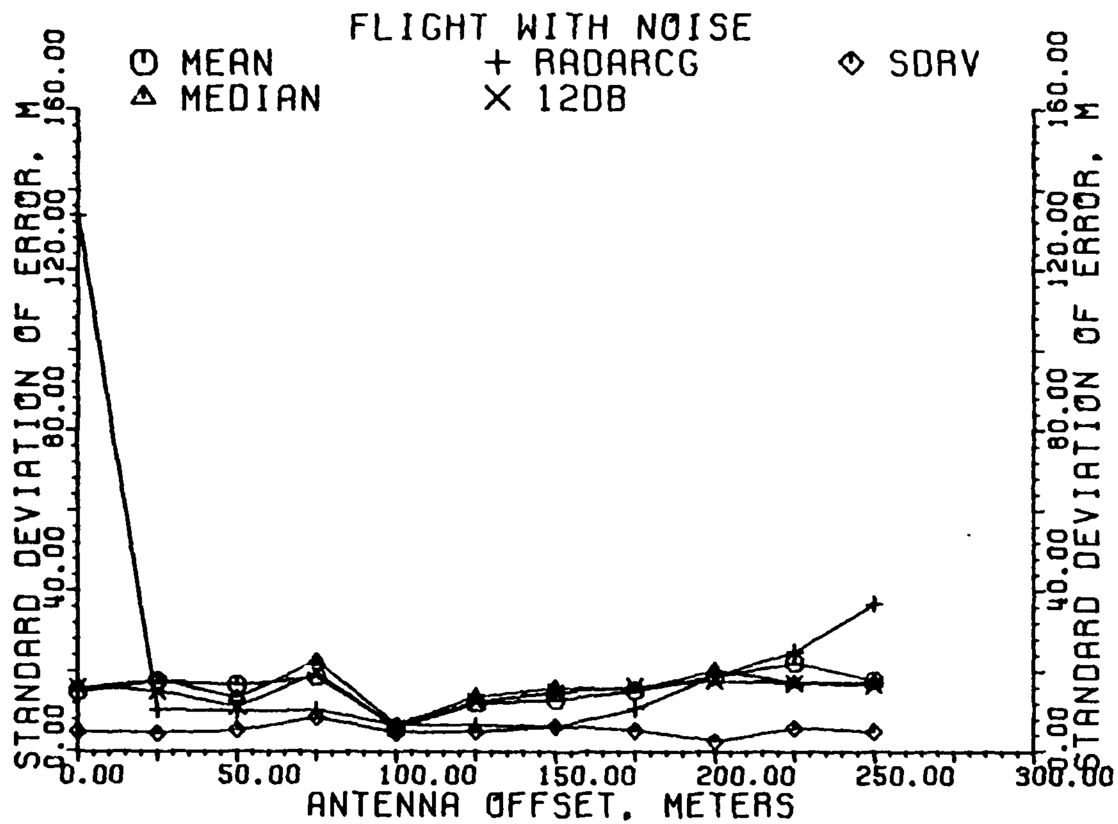

Figure 5-123. Standard deviation of error of estimators in meters for a granularity of 29 beam pointing locations. Each data point is the result of one flight, all scans with a SNR at or below 10 dB used.

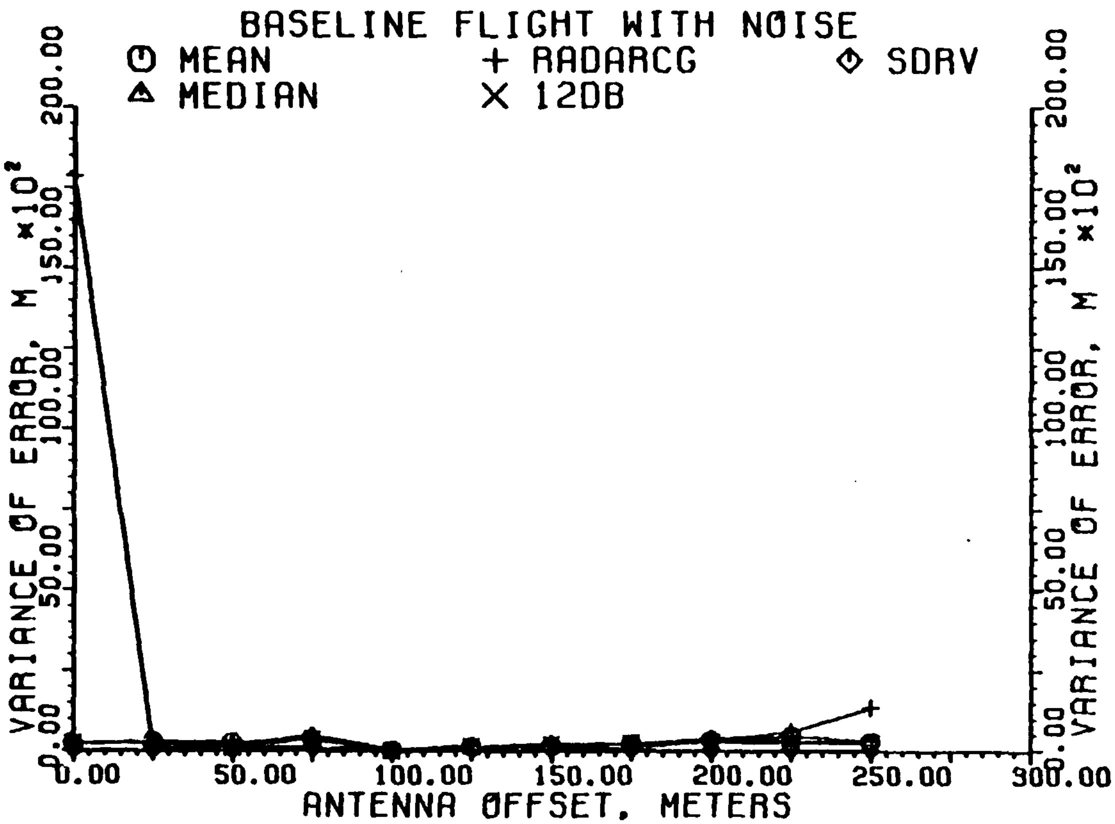

Figure 5-124. Variance of error of estimators in meters for a granularity of 29 beam pointing locations. Each data point is the result of one flight, all scans with a SNR at or below 10 dB used.

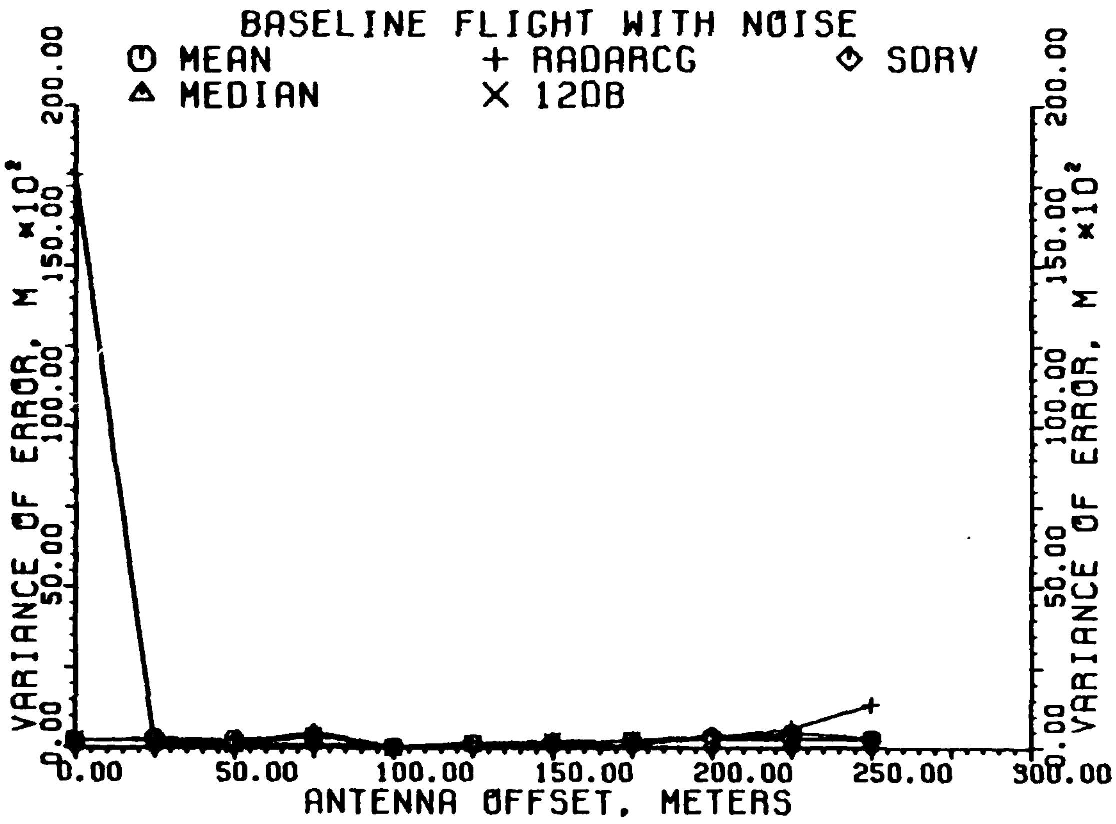

Figure 5-124. Variance of error of estimators in meters for a granularity of 29 beam pointing locations. Each data point is the result of one flight, all scans with a SNR at or below 10 dB used.

due to the method of rejecting scans which do not satisfy the criteria. RADARCG has a lower mean and mean square error than the thresholding methods, but it is not robust in noise. Comparison to Figures 5-53 through 5-60 discloses a general improvement in all estimators, due to the increased data provided by a scan of finer granularity.

The error due to scans with signal-to-noise ratios of 10 dB or lower in the flights with turbulence and noise, Figures 5-125 to 5-132, is on the order of the flights without turbulence. The thresholding estimators show no additional degradation due to turbulence. However, both RADARCG and SDRV experience an increase in error, particularly with the antenna at a large distance from the runway. SDRV is still the most accurate of the estimators, but RADARCG is greatly affected by the noise and produces estimates of the target location with greater error than the thresholding methods.

Having discussed the error produced by the estimators with scanning granularities which permit the averaging of 1 and 2 beam location returns in its windows, the discussion of a still finer scanning granularity is in order. With 49 beam locations in the scanning window, the returns from four beam pointing locations are averaged in each window of the second derivative algorithms.

The baseline flights, Figures 5-133 through 5-140, show little improvement in the mean or mean square error for the thresholding methods or RADARCG. The standard deviation and variance of the thresholding methods did improve, causing their plots to closely coincide. The second derivative method displays an improvement in estimating capability,

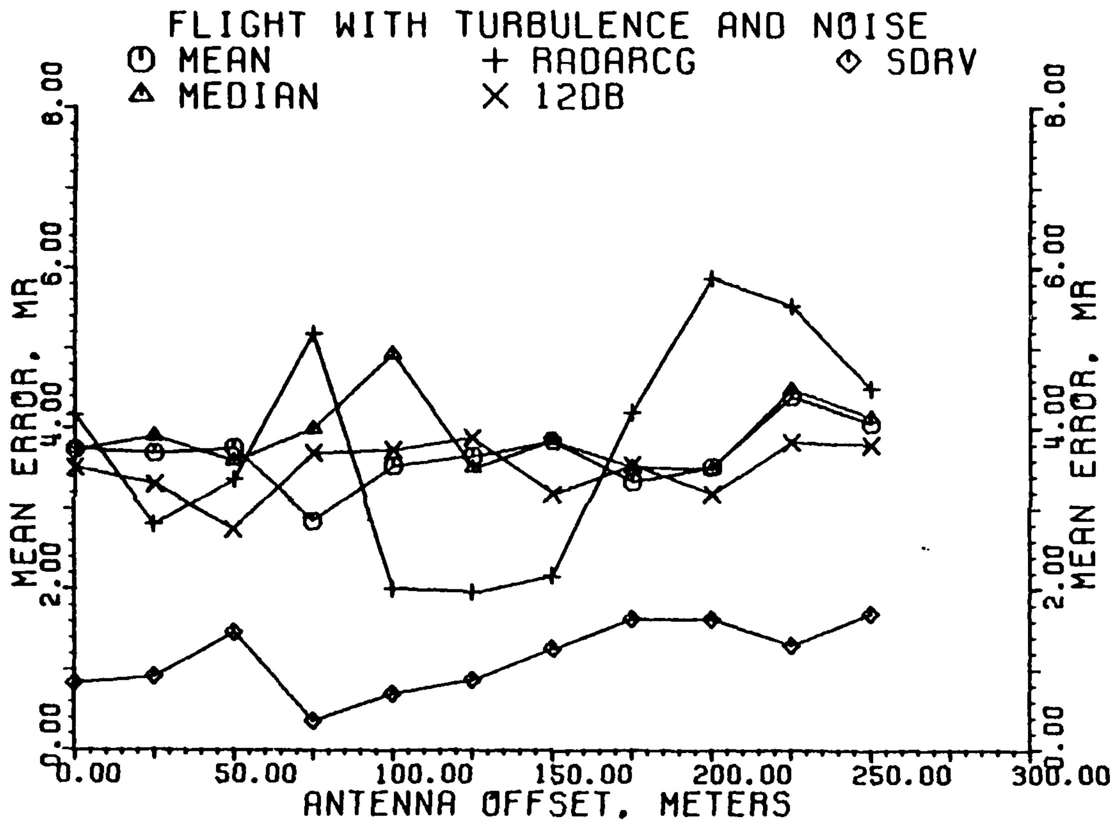

Figure 5-125. Mean error of estimators in milliradians for a granularity of 29 beam pointing locations. Each data point is the result of one flight, all scans with a SNR at or below 10 dB used.

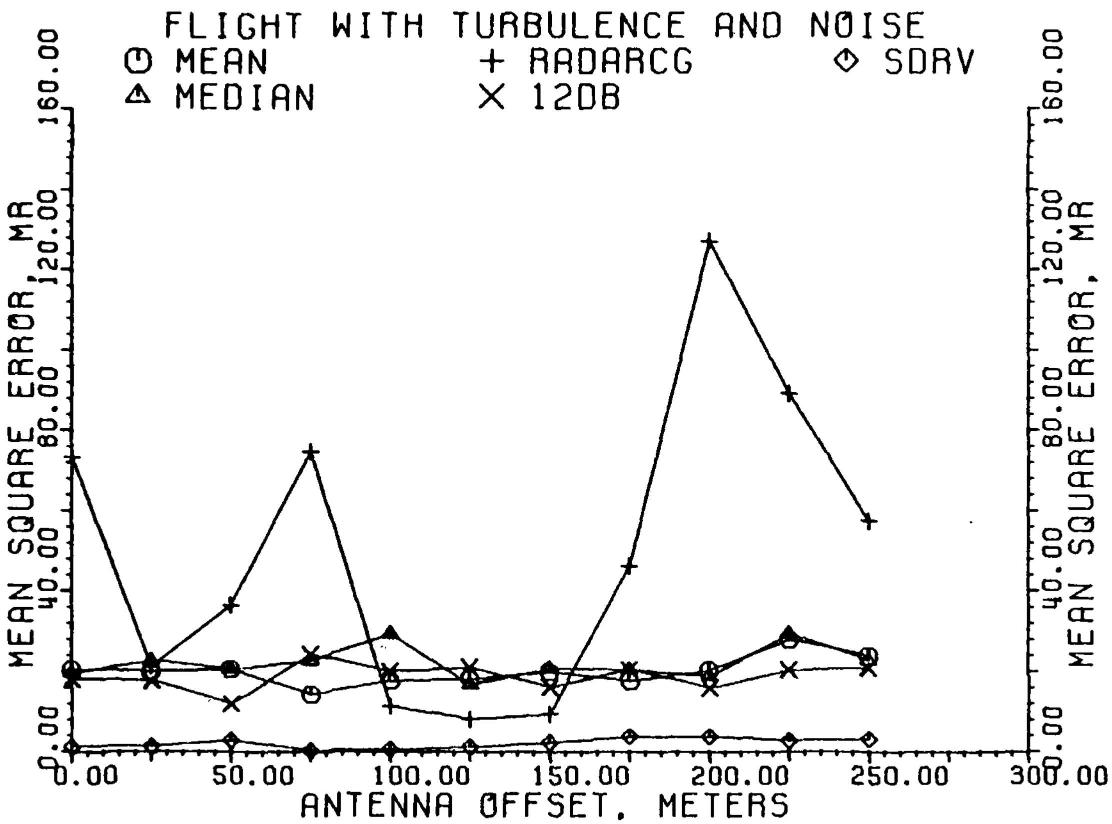

Figure 5-126. Mean square error of estimators in milliradians for a granularity of 29 beam pointing locations. Each data point is the result of one flight, all scans with a SNR at or below 10 dB used.

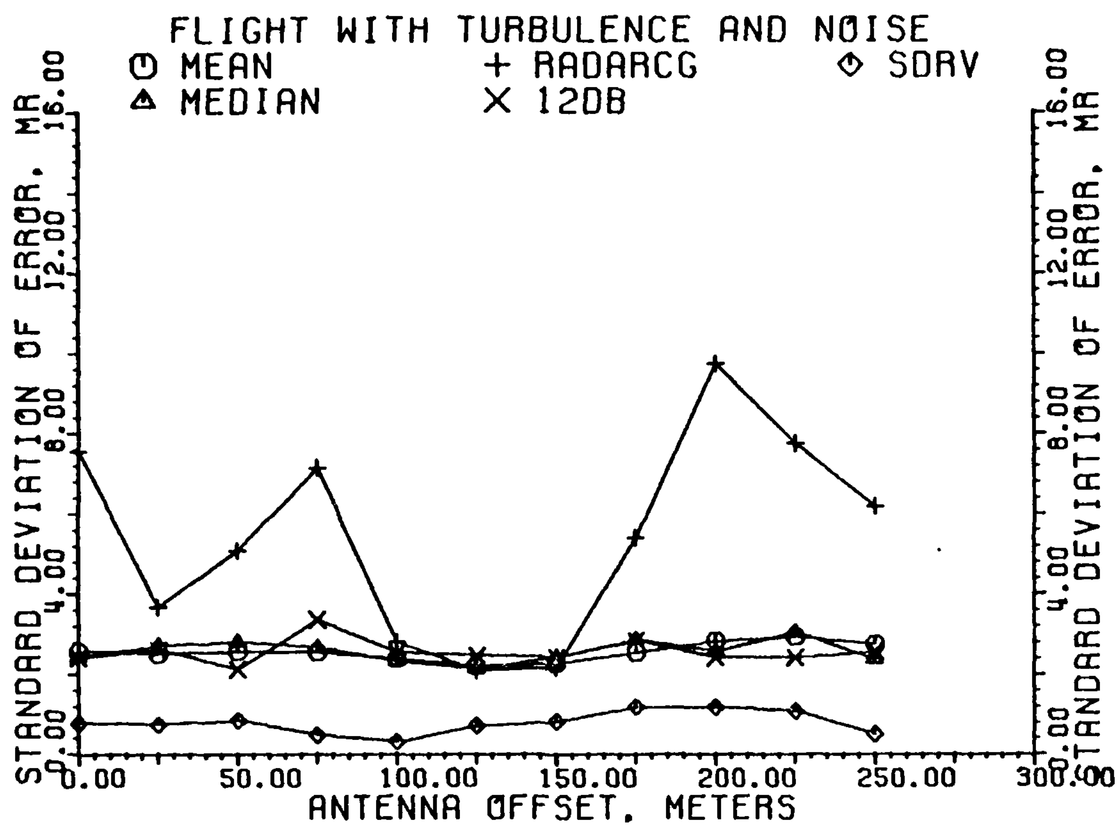

Figure 5-127. Standard deviation of error of estimators in milliradians for a granularity of 29 beam pointing locations. Each data point is the result of one flight, all scans with a SNR at or below 10 dB used.

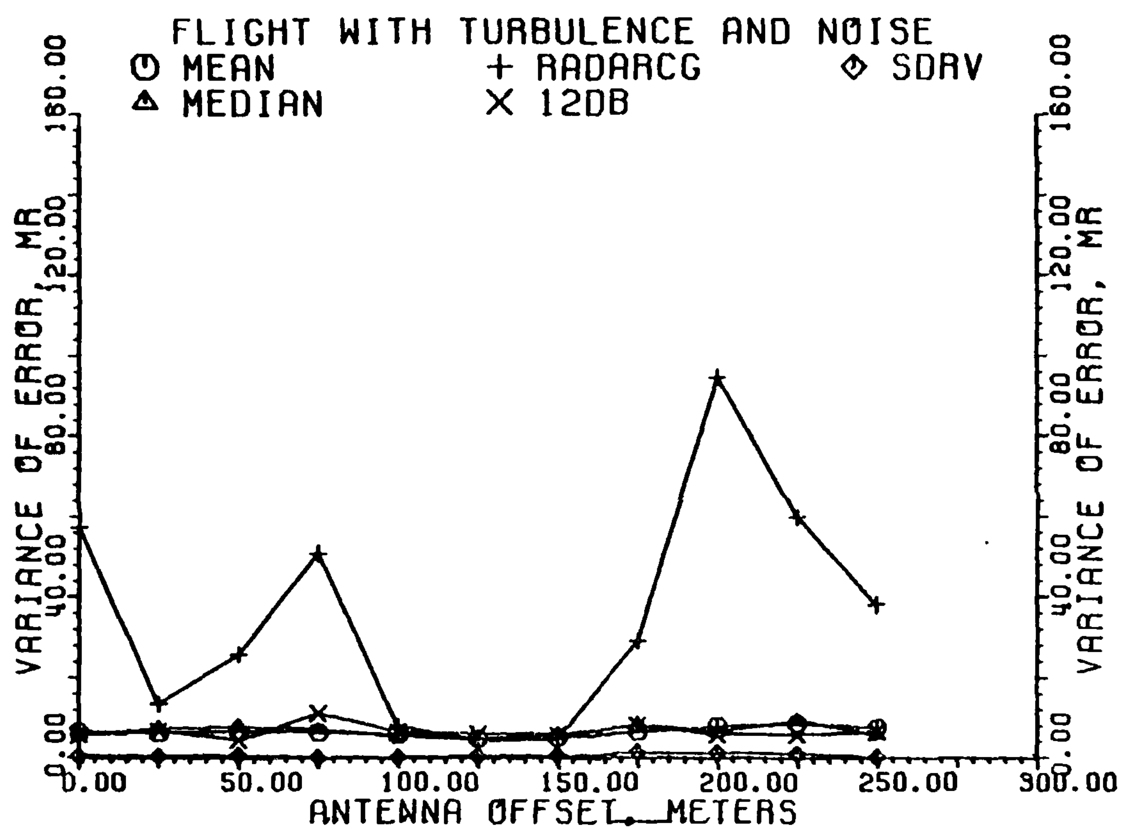

Figure 5-128. Variance of error of estimators in milliradians for a granularity of 29 beam pointing locations. Each data point is the result of one flight, all scans with a SNR at or below 10 dB used.

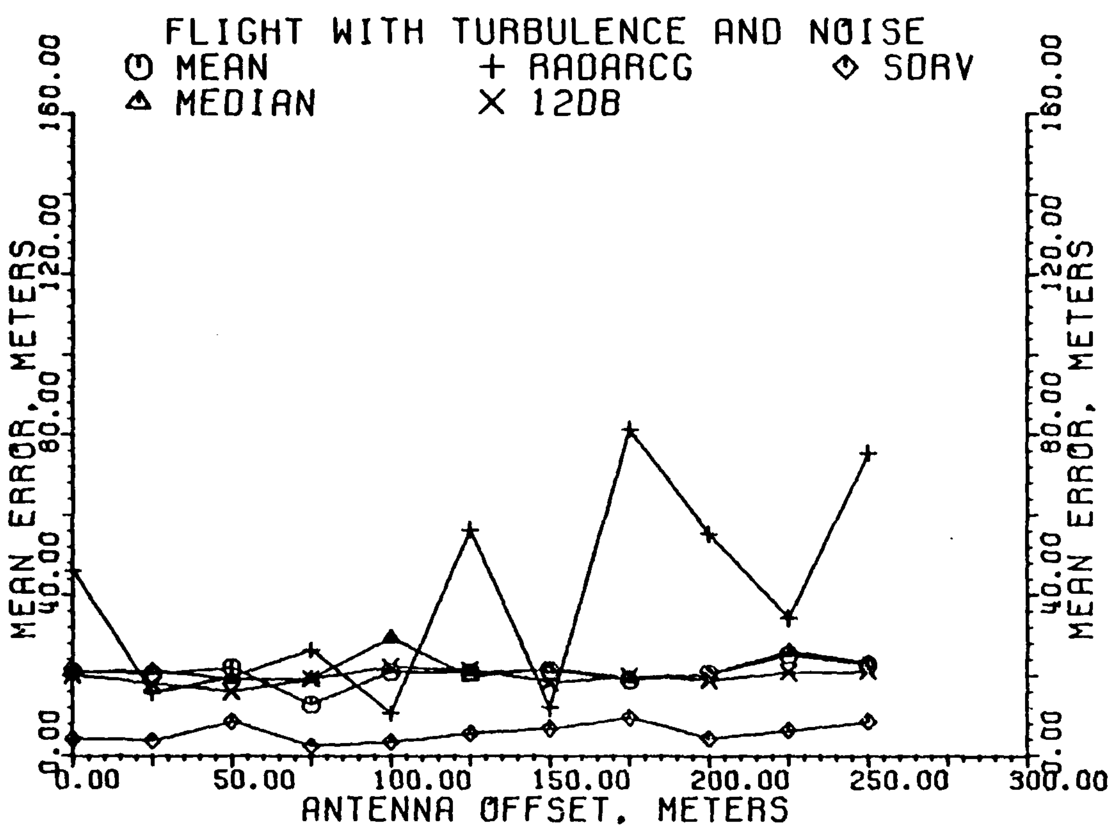

Figure 5-129. Mean error of estimators in meters for a granularity of 29 beam pointing locations. Each data point is the result of one flight, all scans with a SNR at or below 10 dB used.

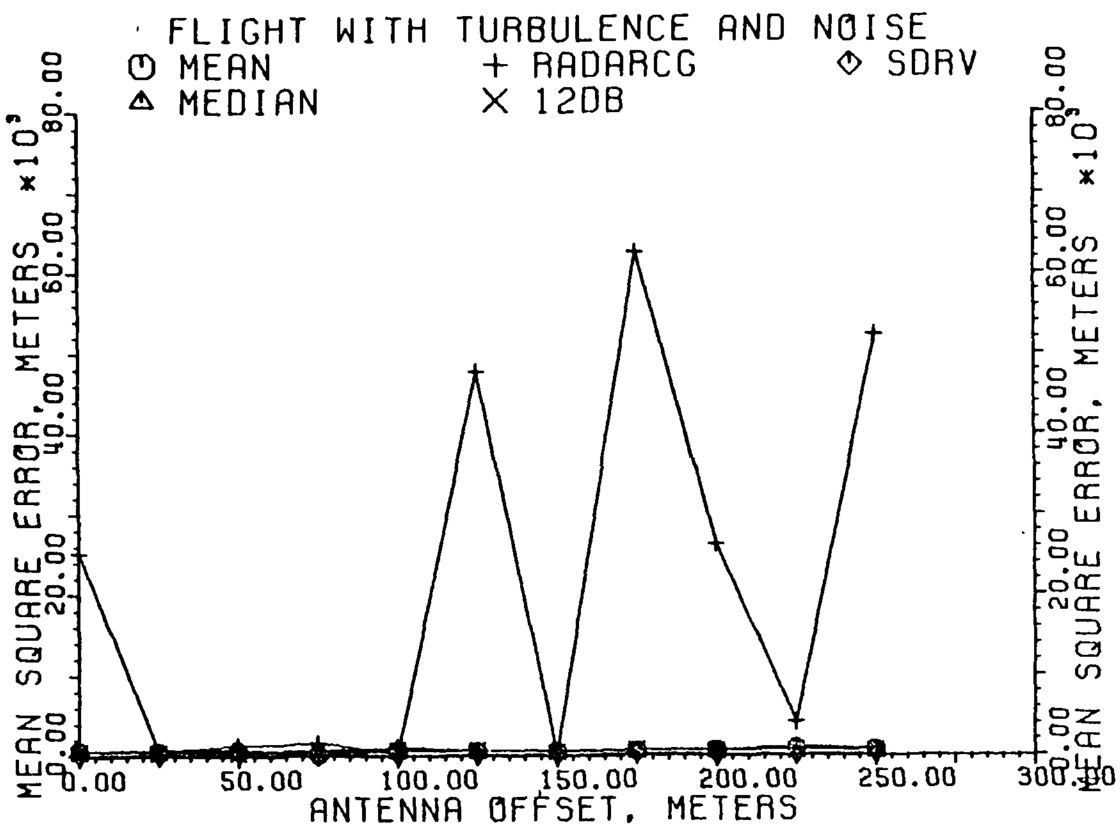

Figure 5-130. Mean square error of estimators in meters for a granularity of 29 beam pointing locations. Each data point is the result of one flight, all scans with a SNR at or below 10 dB used.

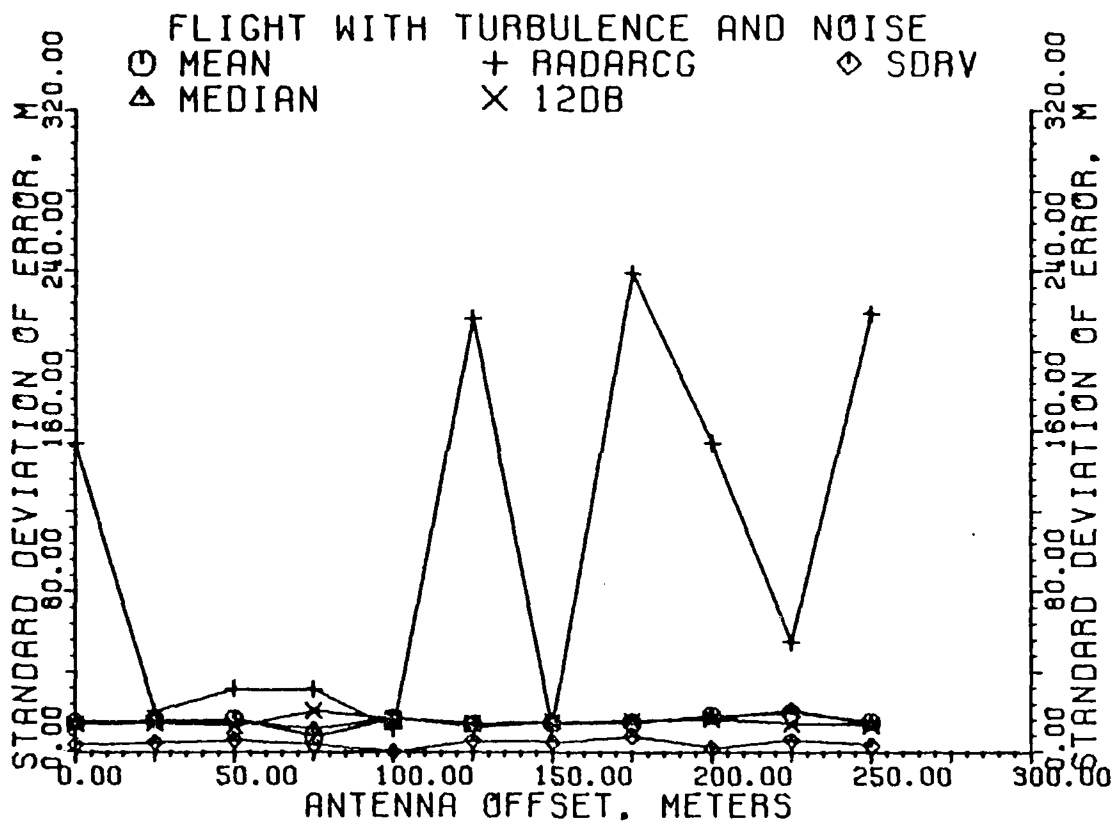

Figure 5-131. Standard deviation of error of estimators in meters for a granularity of 29 beam pointing locations. Each data point is the result of one flight, all scans with a SNR at or below 10 dB used.

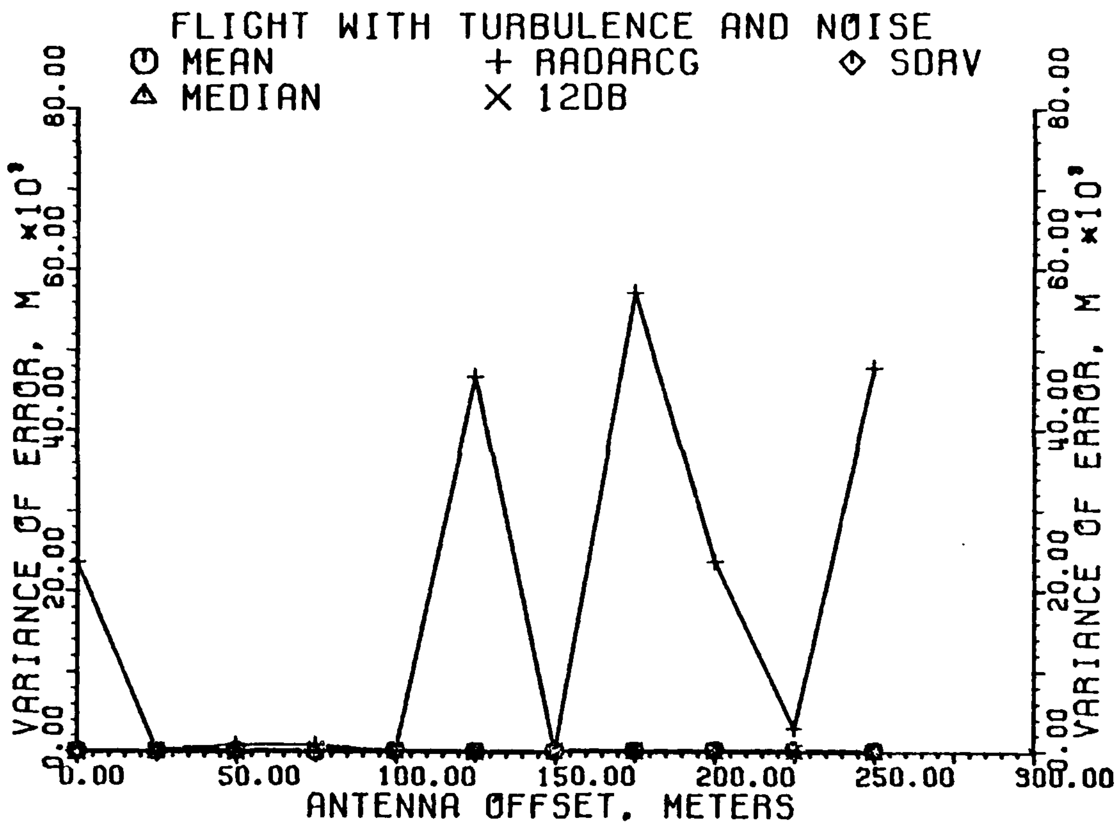

Figure 5-132. Variance of error of estimators in meters for a granularity of 29 beam pointing locations. Each data point is the result of one flight, all scans with a SNR at or below 10 dB used.

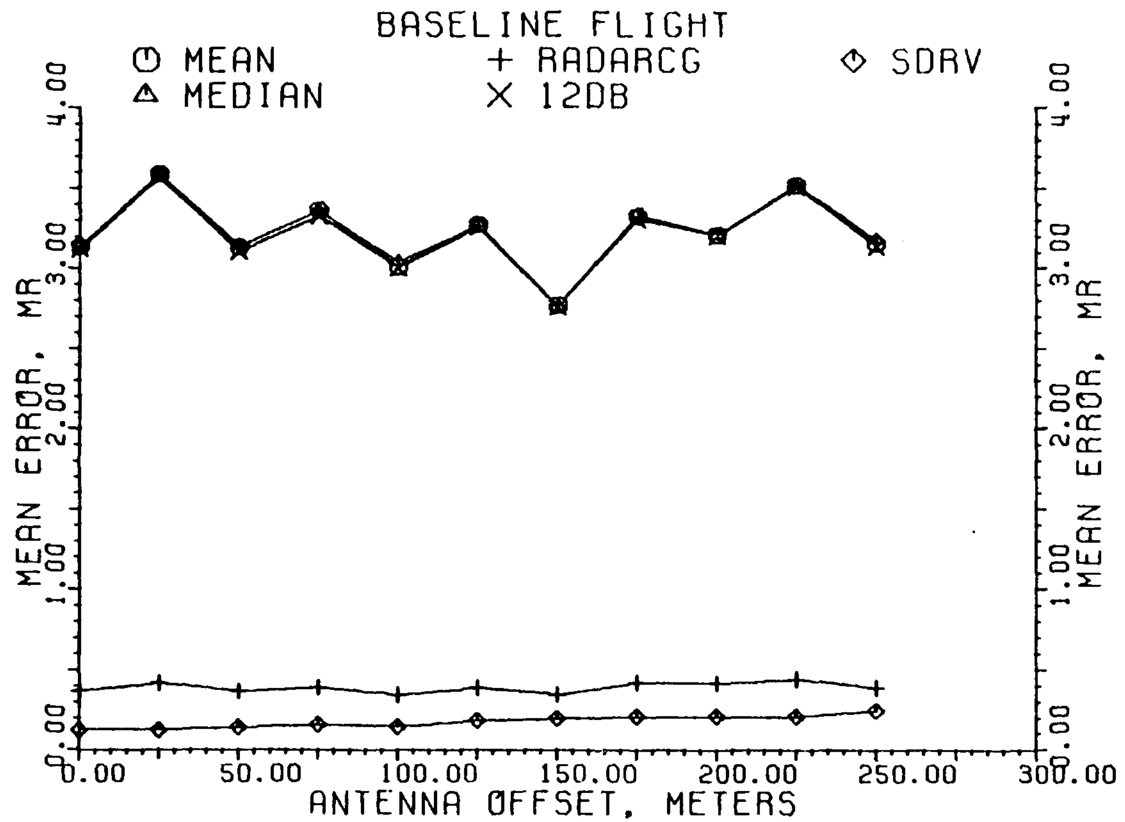

Figure 5-133. Mean error of estimators in milliradians for a granularity of 49 beam pointing locations. Each data point is the result of one flight, all scans used.

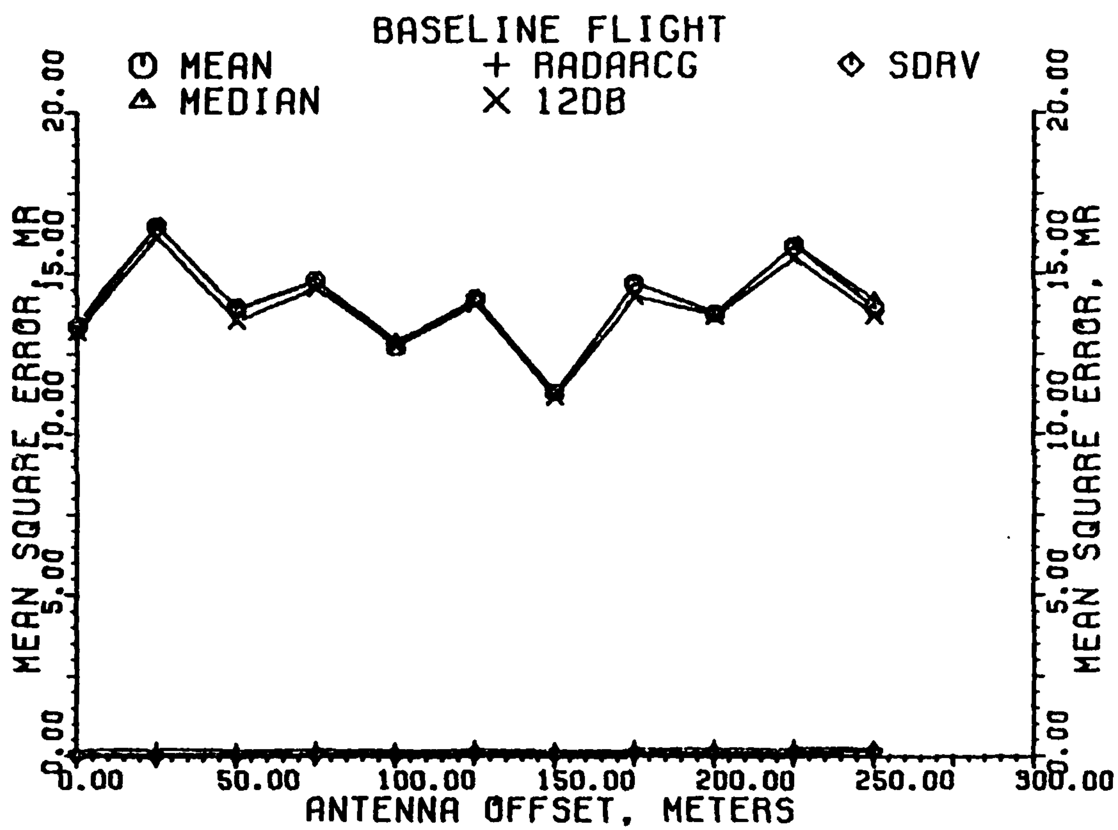

Figure 5-134. Mean square erroɪ of estimators in milliradians for a granularity of 49 beam pointing locations. Each data point is the result of one flight, all scans used.

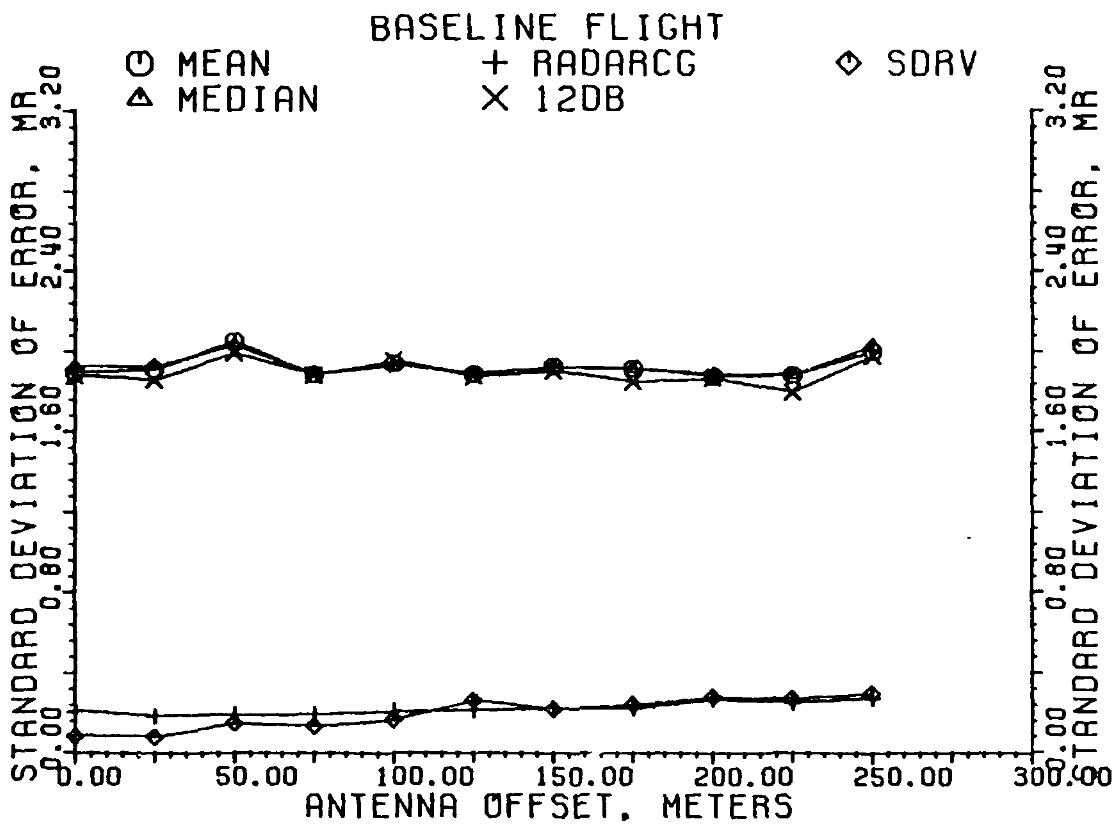

Figure 5-135. Standard deviation of error of estimators in milliradians for a granularity of 49 beam pointing locations. Each data point is the result of one flight, all scans used.

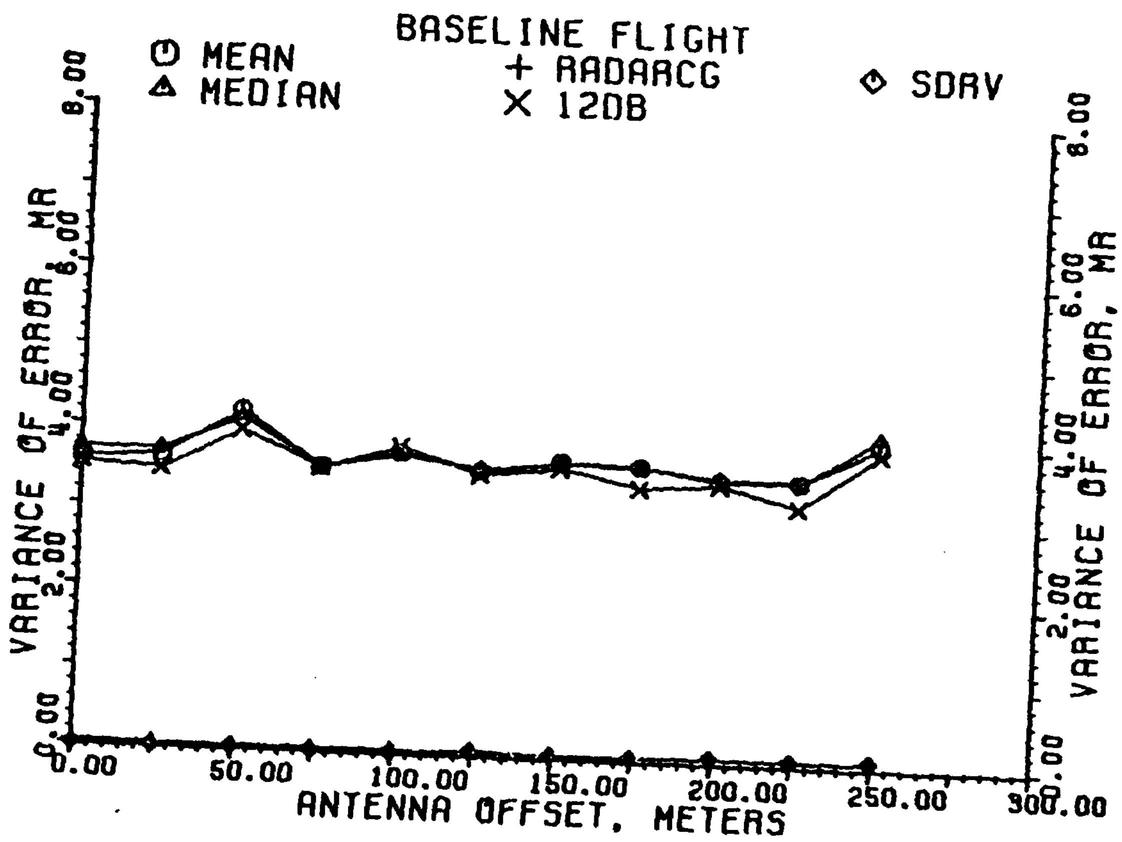

Figure 5-136. Variance of error of estimators in milliradians for a granularity of 49 b[illegible] pointing locations. Each data point is the result of o[illegible] flight, all scans used.

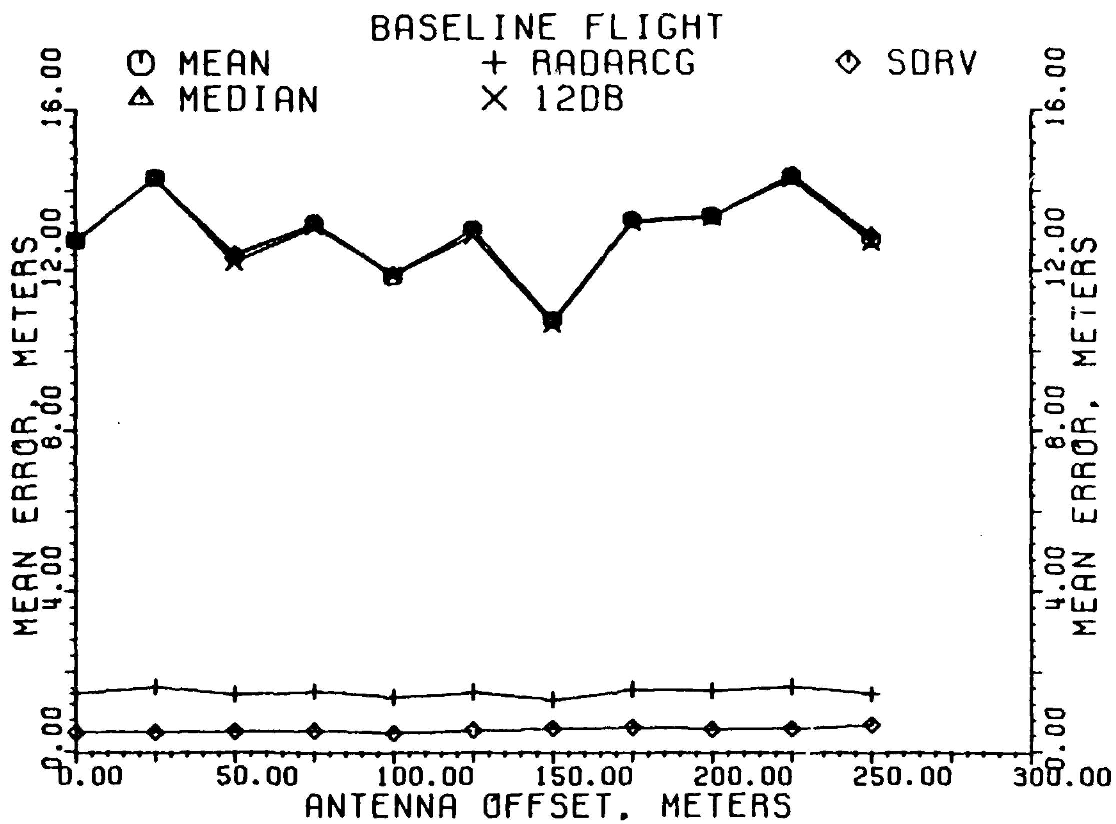

Figure 5-137. Mean error of estimators in meters for a granularity of 49 beam pointing locations. Each data point is the result of one flight, all scans used.

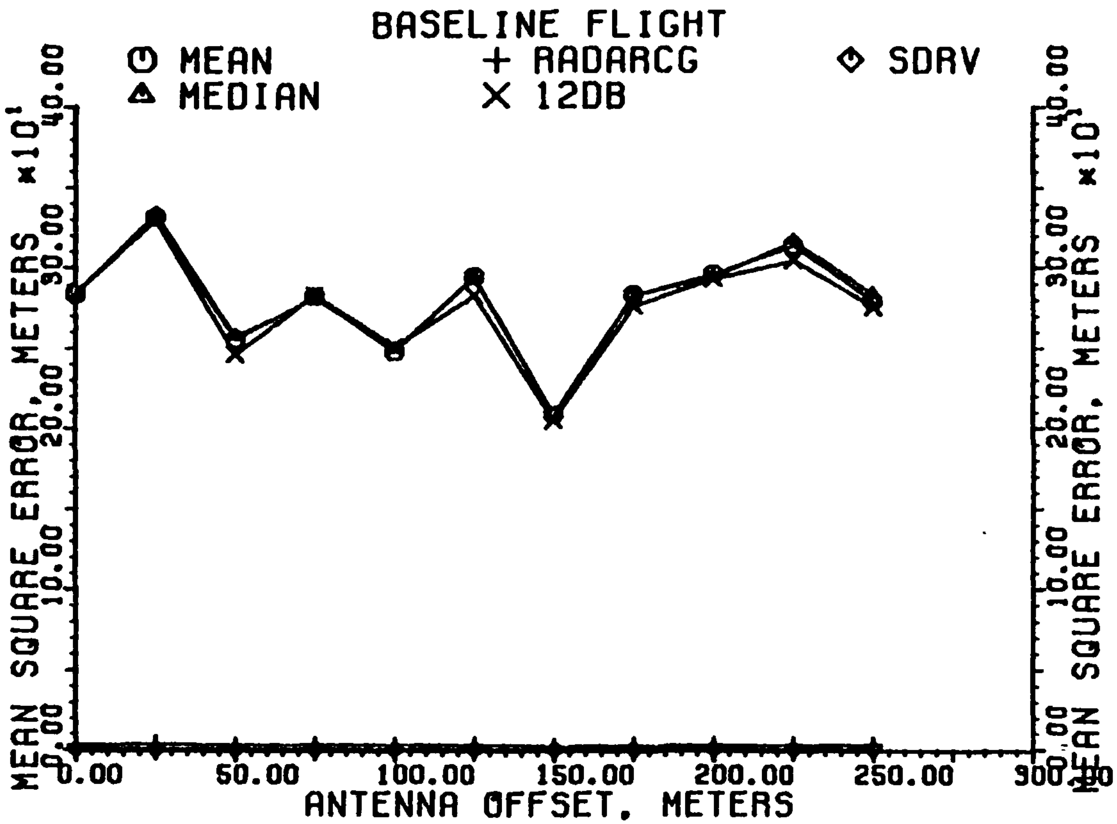

Figure 5-138. Mean square error of estimators in meters for a granularity of 49 beam pointing locations. Each data point is the result of one flight, all scans used.

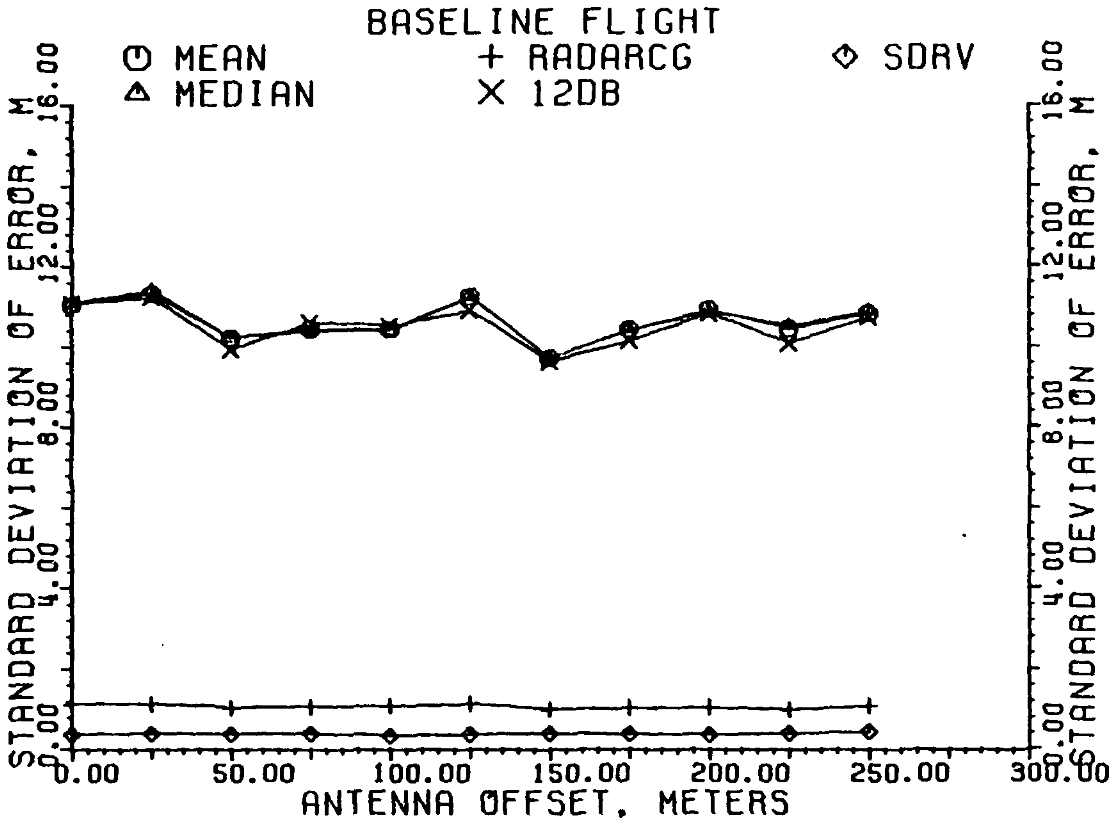

Figure 5-139. Standard deviation of error of estimators in meters for a granularity of 49 beam pointing locations. Each data point is the result of one flight, all scans used.

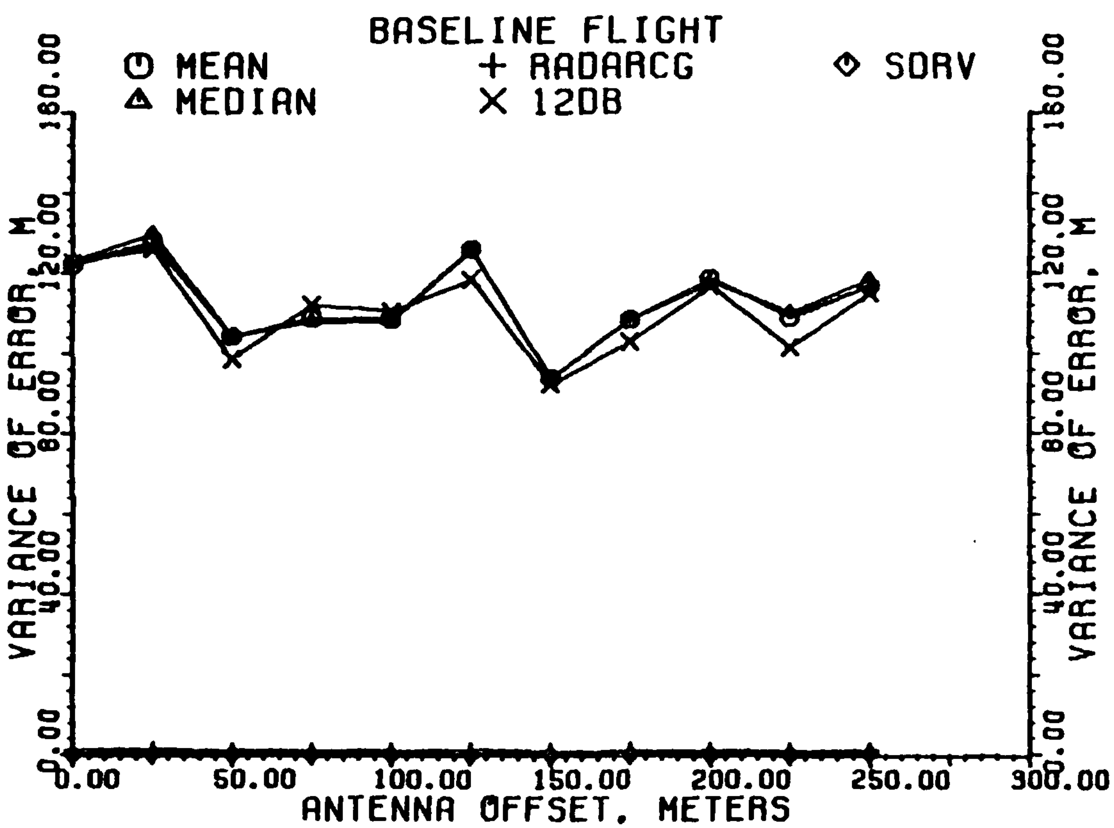

Figure 5-140. Variance of error of estimators in meters for a granularity of 49 beam pointing locations. Each data point is the result of one flight, all scans used.

and is the most robust of the estimators with regard to antenna offset location versus actual meter error.

The flights with noise, Figures 5-141 through 5-148, show an improvement in all estimators over the 29 beam location scans, RADARCG in particular. The standard deviation and variance of the errors are more stable than in the coarser granularities, due to the increase in data points upon which a location decision can be made.

The baseline flights with turbulence, Figures 5-149 through 5-156, show little change over those baseline flights without turbulence (Figures 5-133 to 5-140). There is a curious jump in the standard deviation and variance of the SDRV milliradian error at antenna locations of 225 and 250 meters from the runway, Figures 5-151 and 5-152, but there is only the slightest deviation from a straight line at those antenna locations in the plots of the standard deviation and variance of the error in meters, Figures 5-155 and 5-156. The error probably occurred at close range.

The flights with turbulence and noise, Figures 5-157 through 5-164, indicate that SDRV is again the estimator with the least error in turbulence and noise. There is an improvement in all estimators over the coarser granularities, particularly in the case of RADARCG. The estimator is much more stable in the higher data rates, but the standard deviation and variance are still in excess of those of the thresholding methods.

As before, it would be advantageous to examine the performance of the estimators at the increased data rate in both high and low scan SNR's.

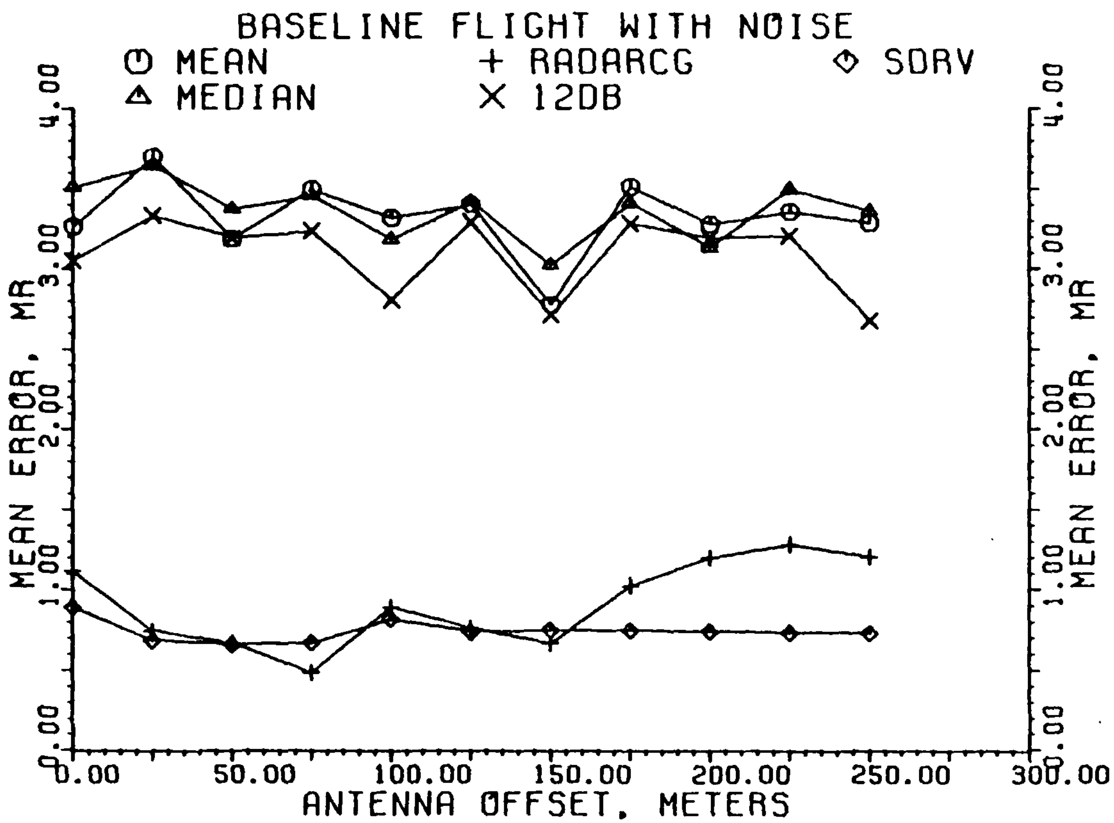

Figure 5-141. Mean error of estimators in milliradians for a granularity of 49 beam pointing locations. Each data point is the result of one flight, all scans used.

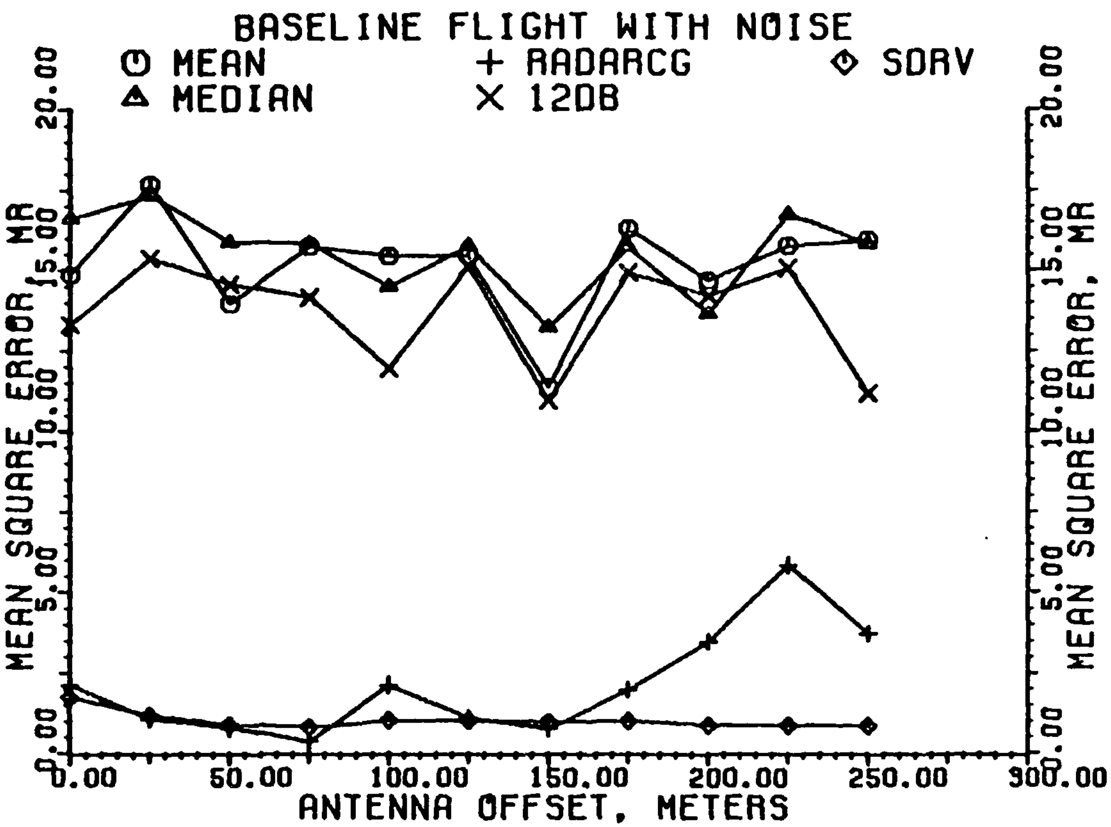

Figure 5-142. Mean square error of estimators in milliradians for a granularity of 49 beam pointing locations. Each data point is the result of one flight, all scans used.

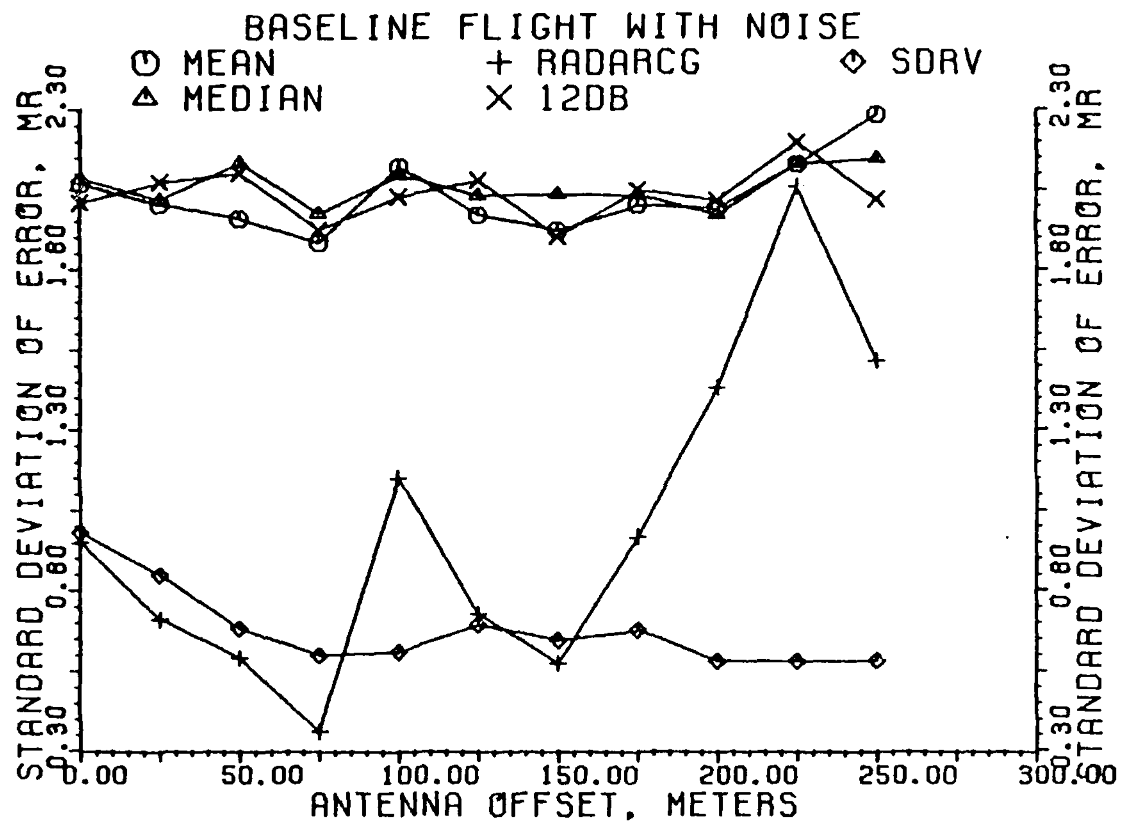

Figure 5-143. Standard deviation of error of estimators in milliradians for a granularity of 49 beam pointing locations. Each data point is the result of one flight, all scans used.

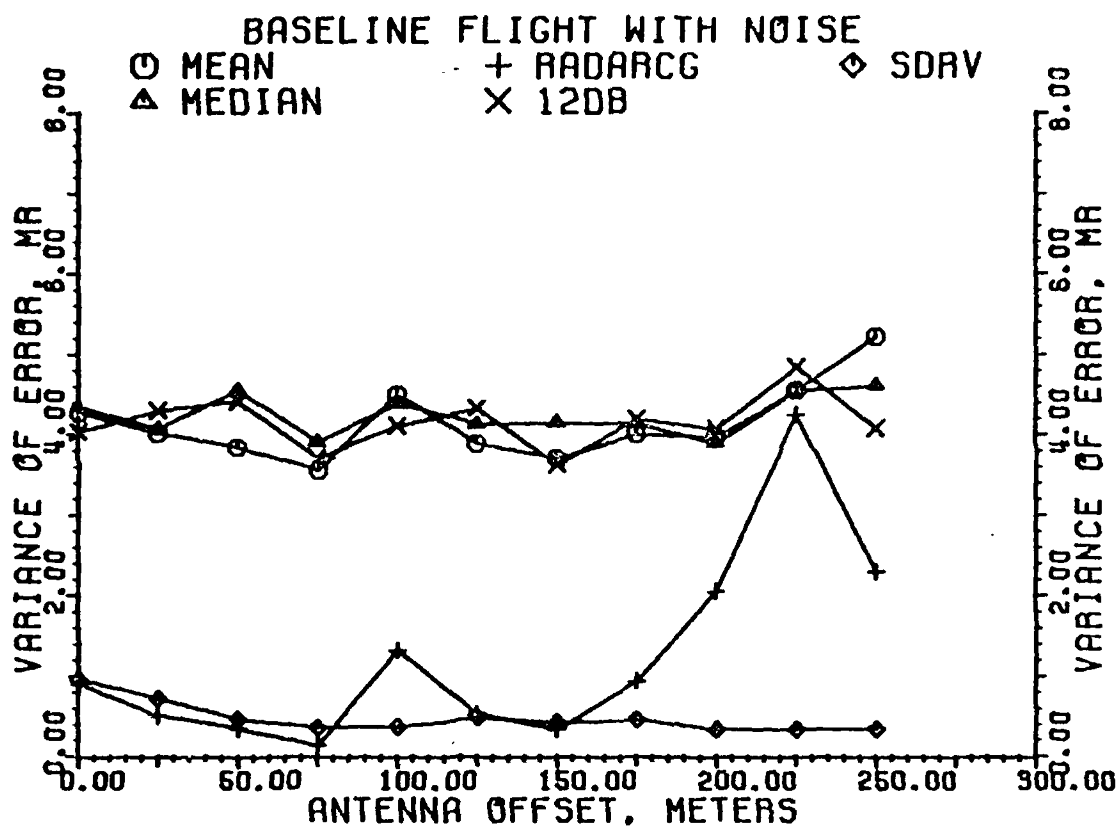

Figure 5-144. Variance of error of estimators in milliradians for a granularity of 49 beam pointing locations. Each data point is the result of one flight, all scans used.

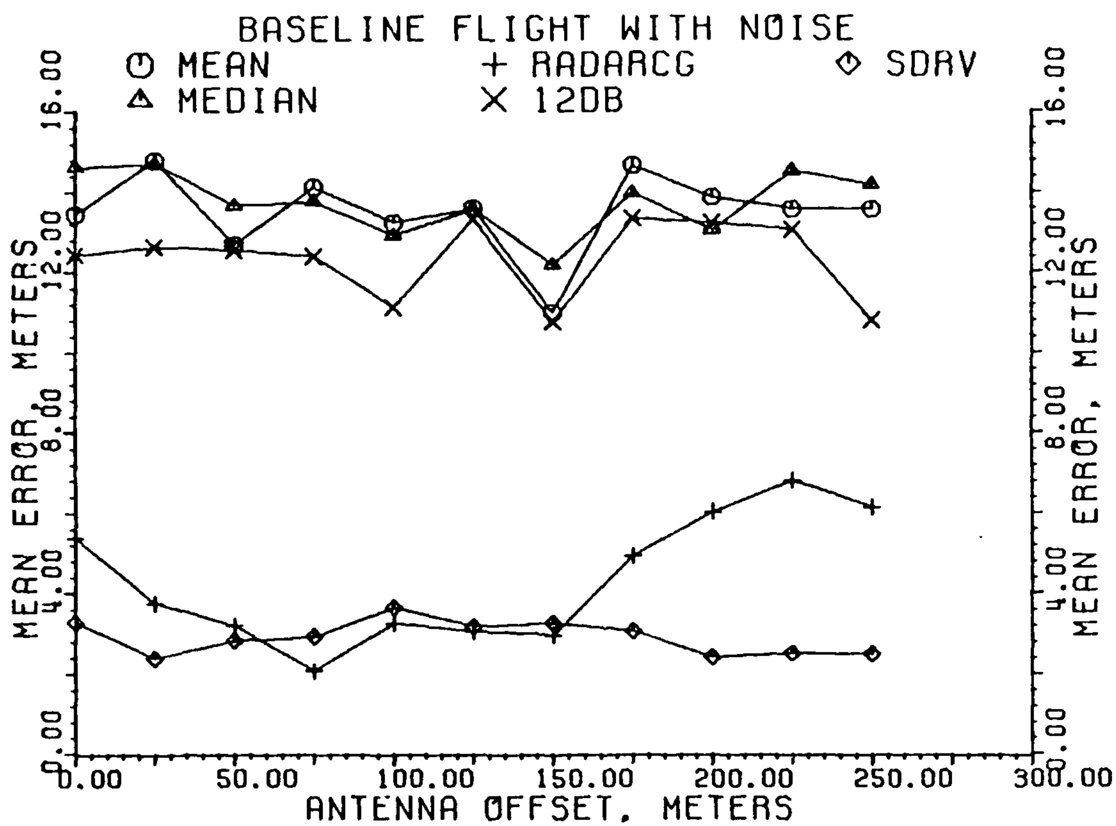

Figure 5-145. Mean error of estimators in meters for a granularity of 49 beam pointing locations. Each data point is the result of one flight, all scans used.

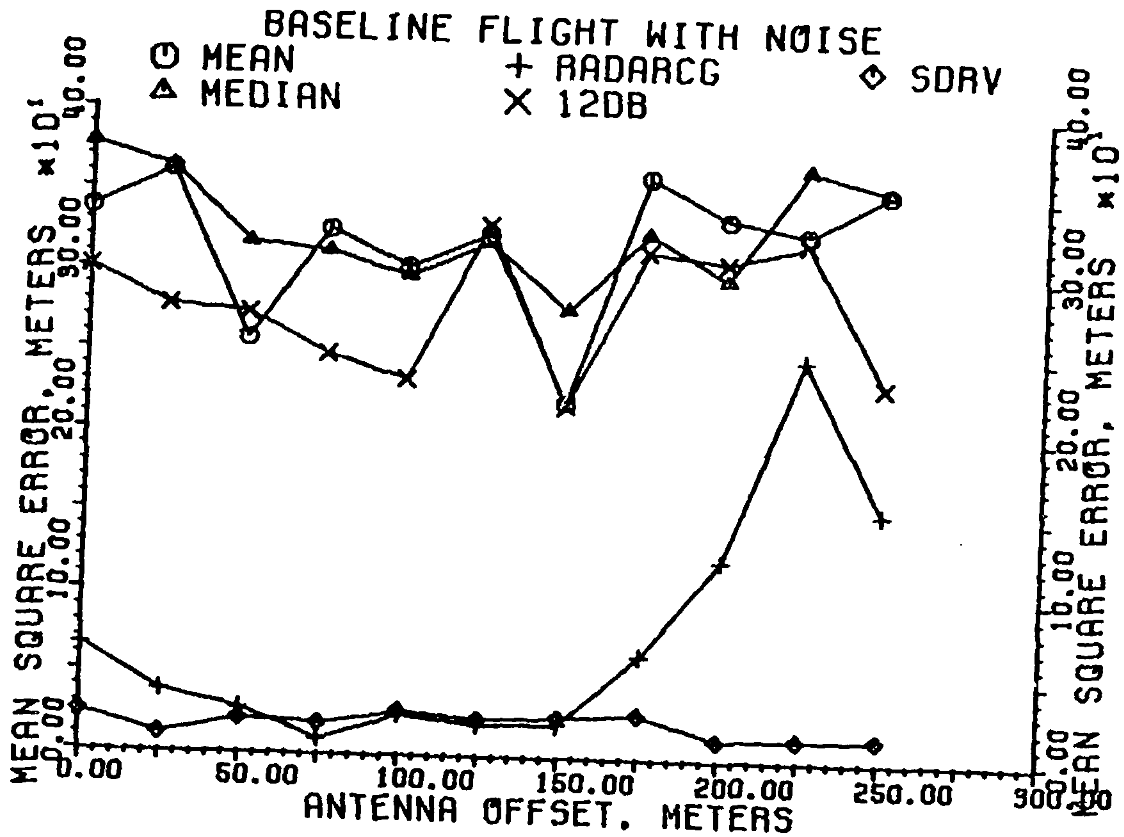

Figure 5-146. Mean square error of estimators in meters for a granularity of 49 beam pointing locations. Each data point is the result of one flight, all scans used.

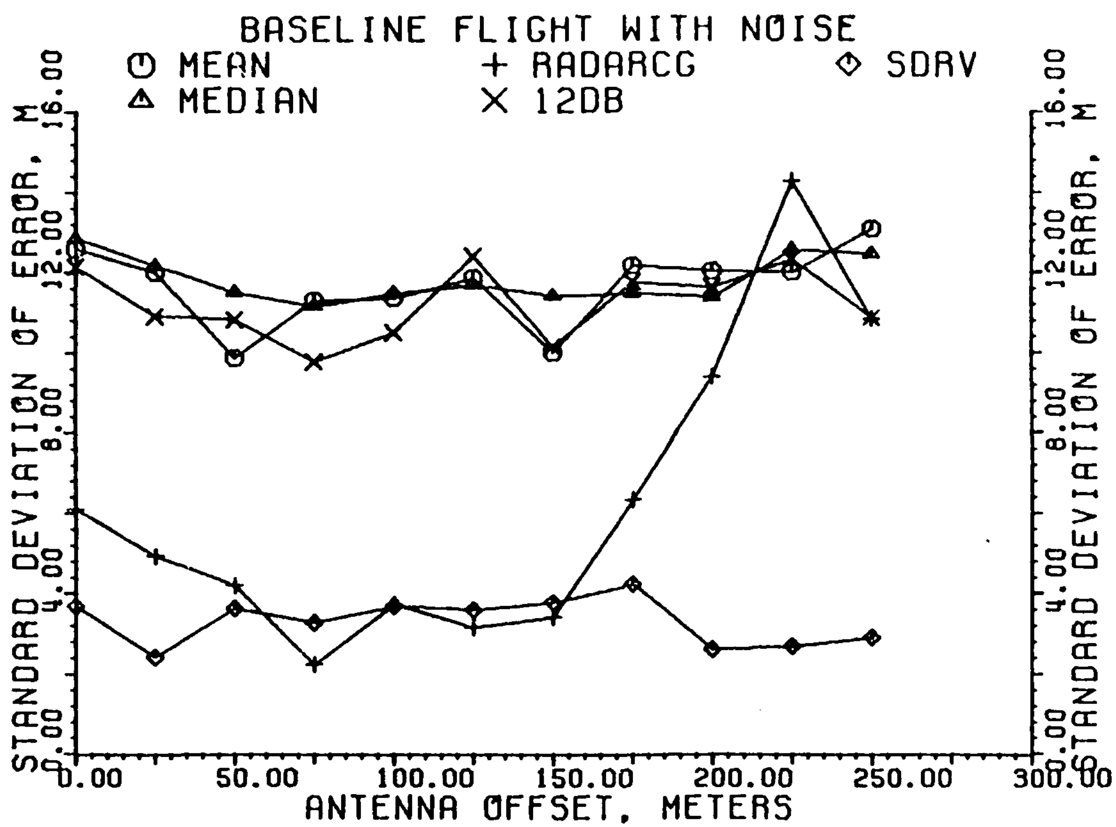

Figure 5-147. Standard deviation of error of estimators in meters for a granularity of 49 beam pointing locations. Each data point is the result of one flight, all scans used.

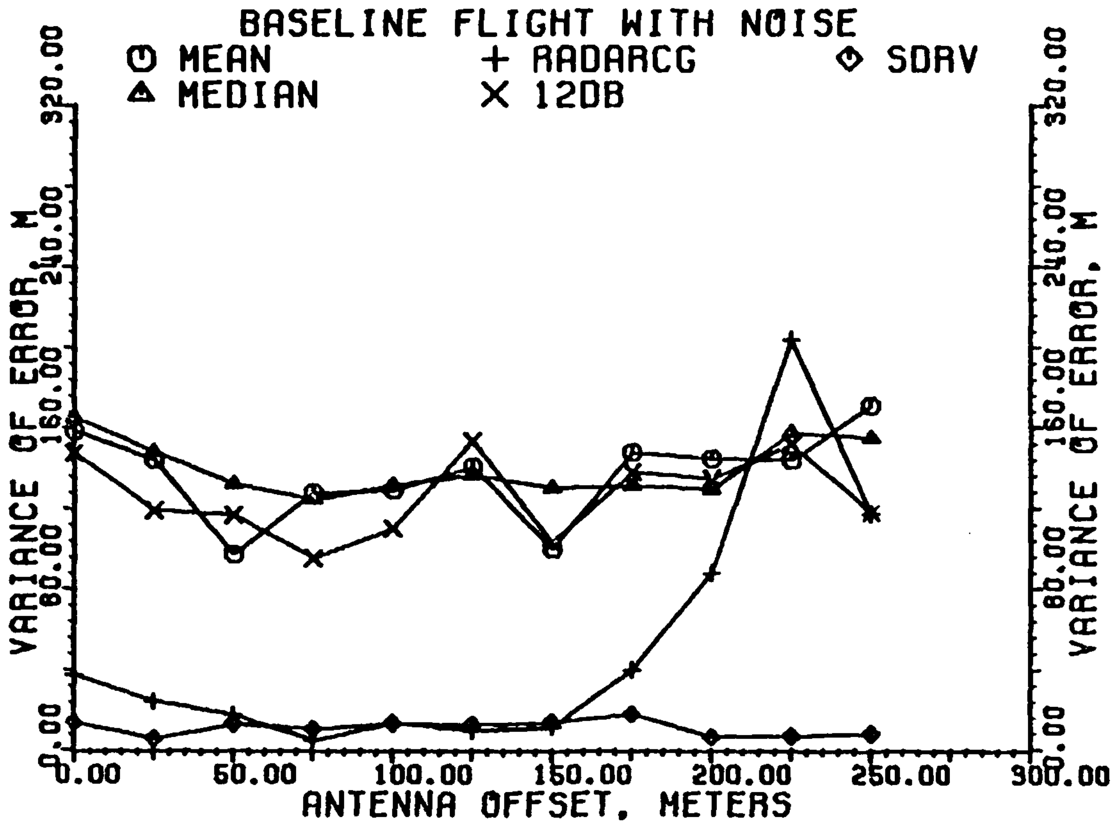

Figure 5-148. Variance of error of estimators in meters for a granularity of 49 beam pointing locations. Each data point is the result of one flight, all scans used.

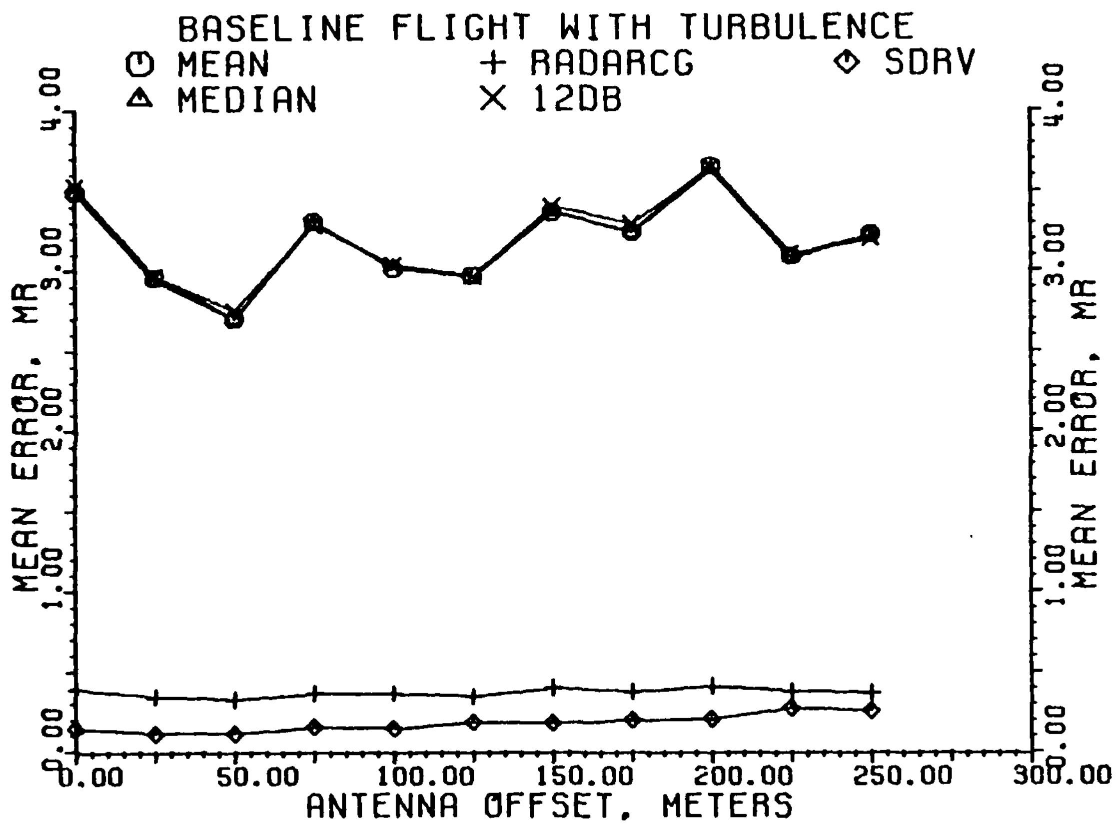

Figure 5-149. Mean error of estimators in milliradians for a granularity of 49 beam pointing locations. Each data point is the result of one flight, all scans used.

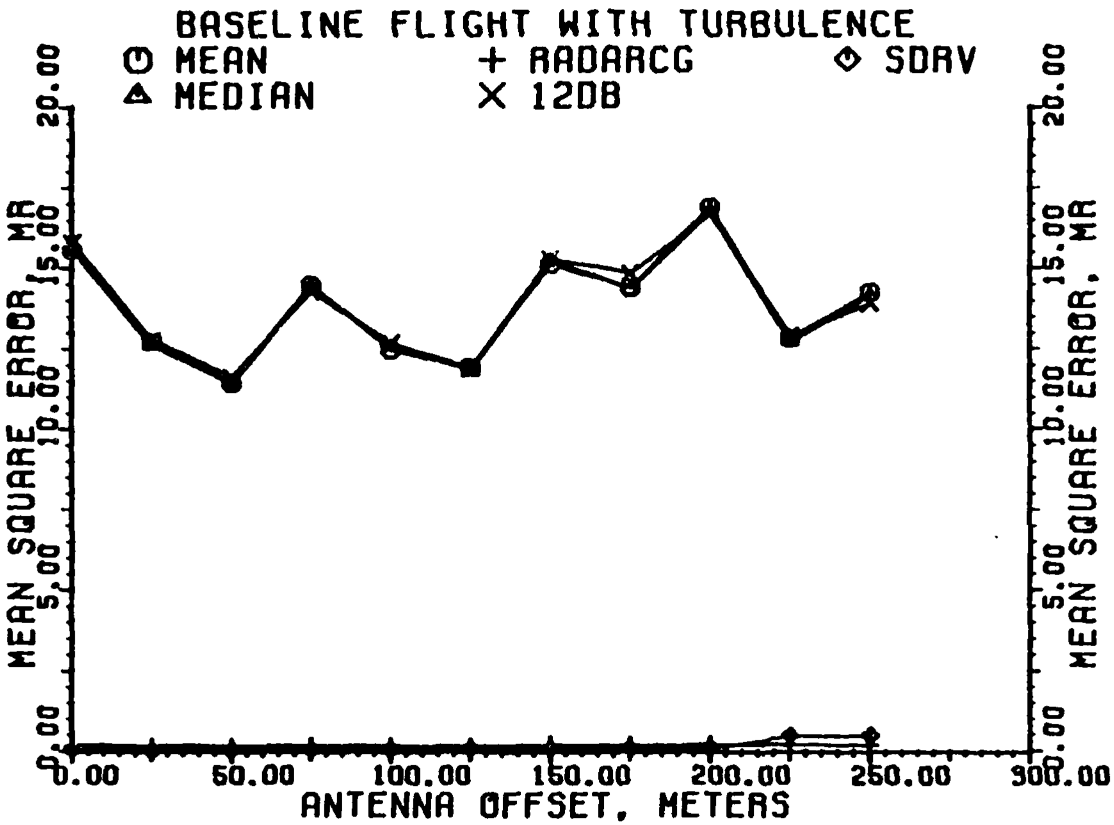

Figure 5-150. Mean square error of estimators in milliradians for a granularity of 49 beam pointing locations. Each data point is the result of one flight, all scans used.

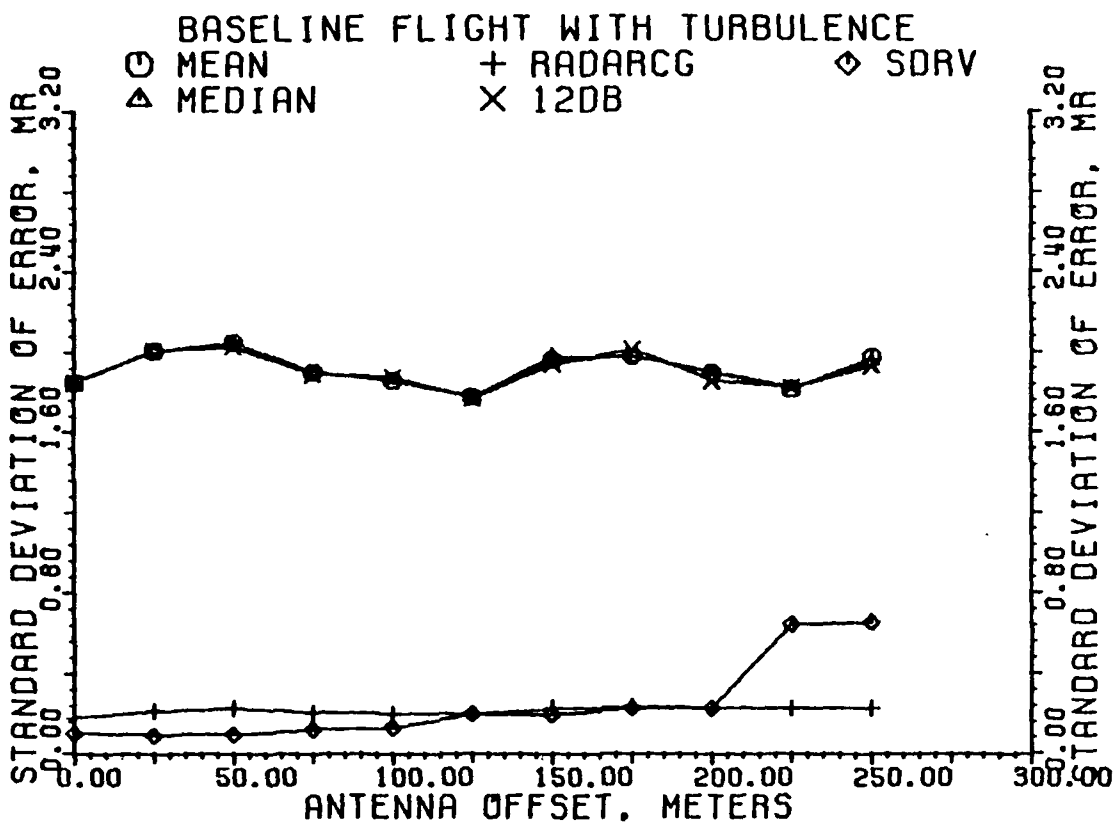

Figure 5-151. Standard deviation of error of estimators in milliradians for a granularity of 49 beam pointing locations. Each data point is the result of one flight, all scans used.

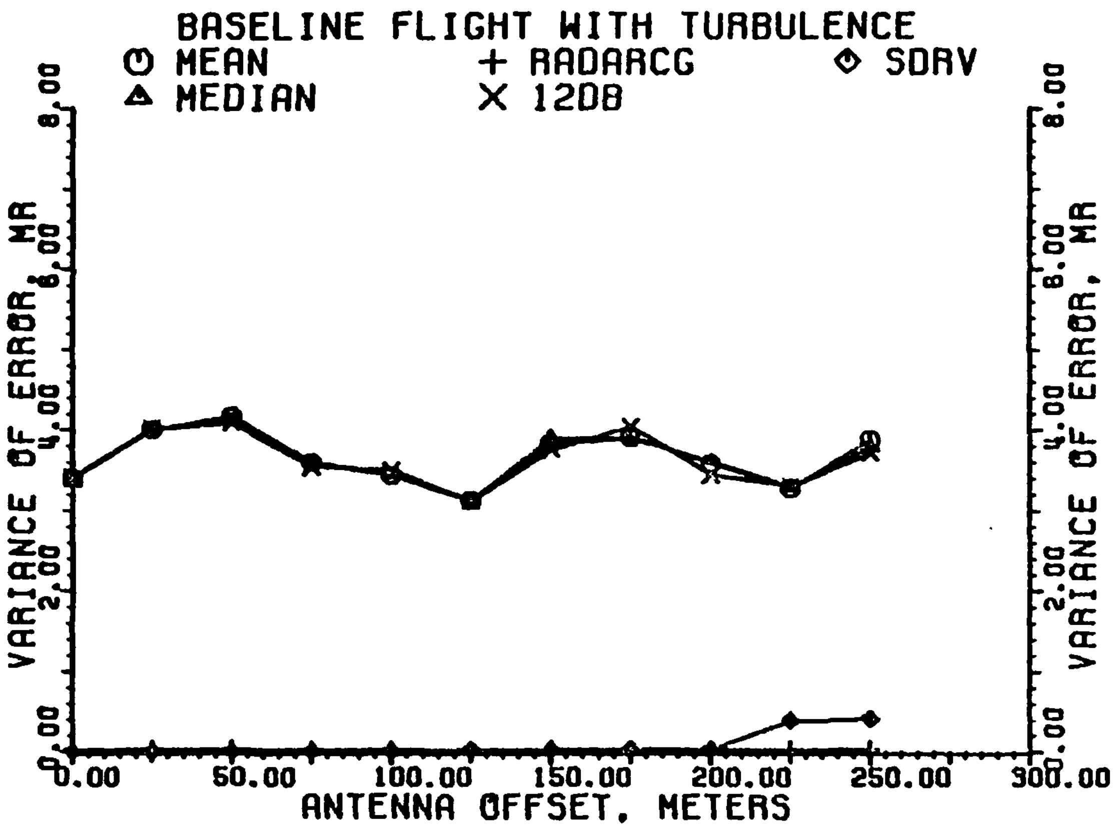

Figure 5-152. Variance of error of estimators in milliradians for a granularity of 49 beam pointing locations. Each data point is the result of one flight, all scans used.

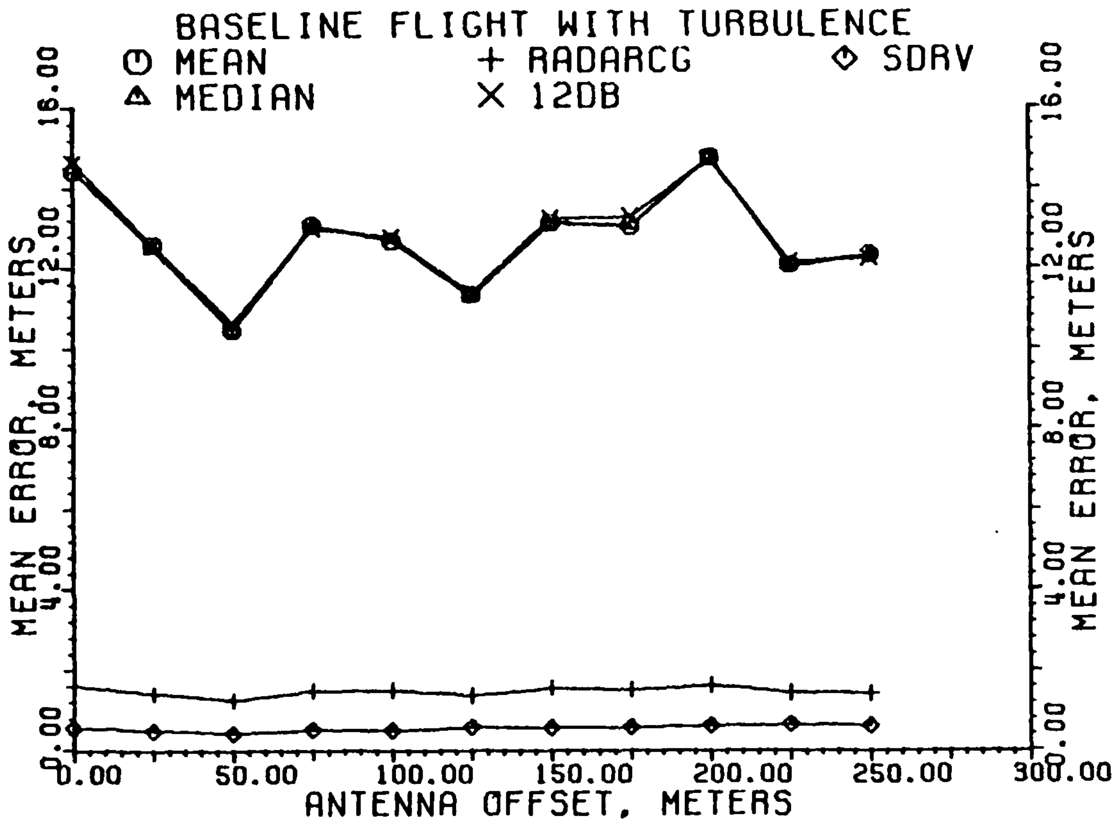

Figure 5-153. Mean error of estimators in meters for a granularity of 49 beam pointing locations. Each data point is the result of one flight, all scans used.

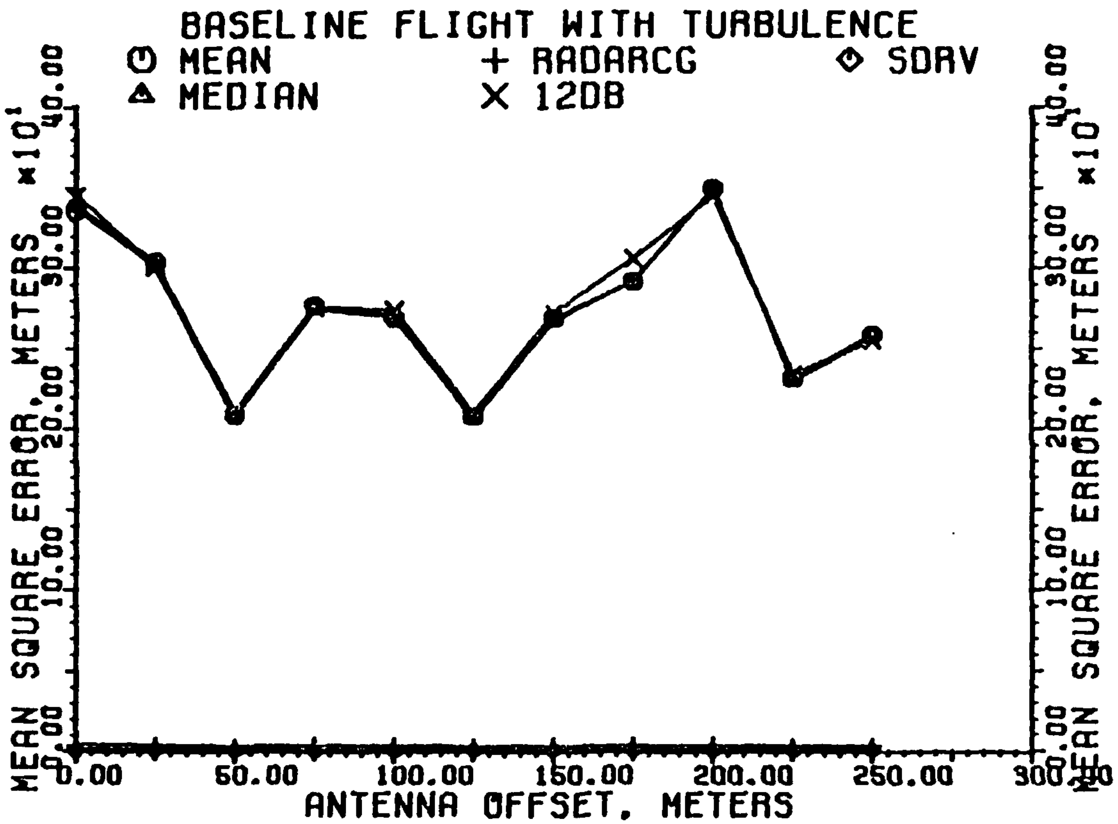

Figure 5-154. Mean square error of estimators in meters for a granularity of 49 beam pointing locations. Each data point is the result of one flight, all scans used.

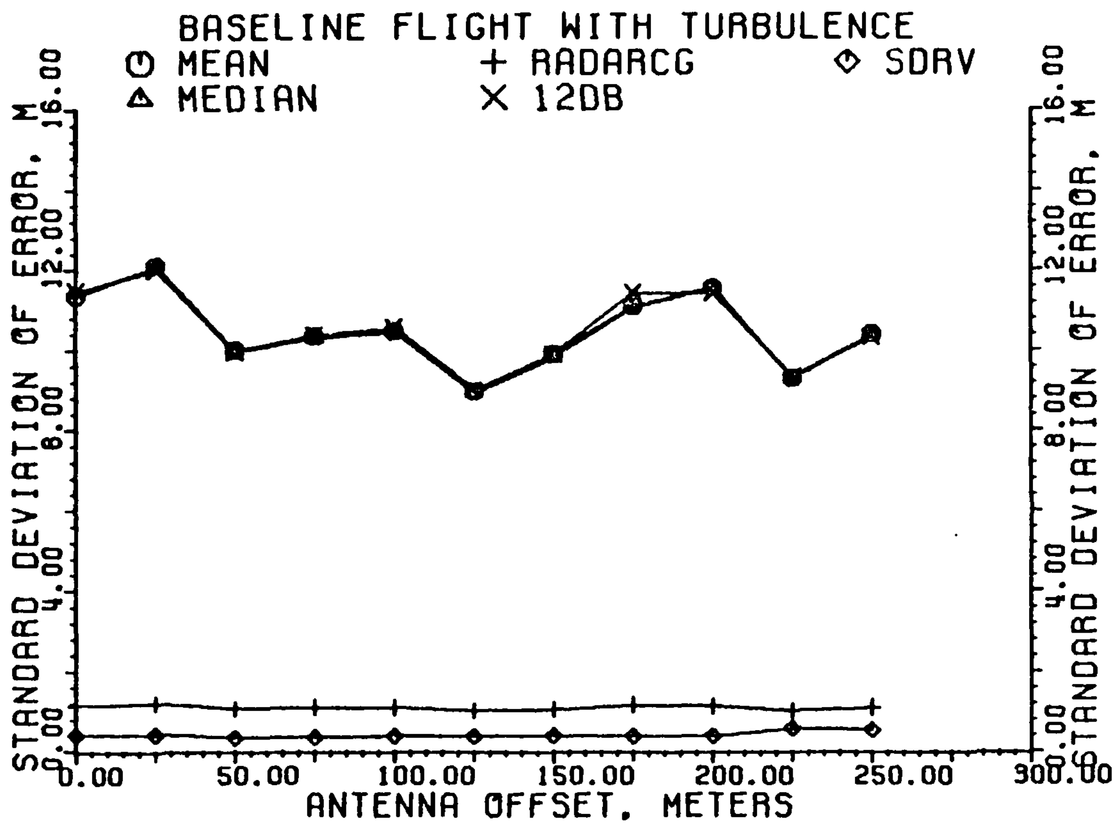

Figure 5-155. Standard deviation of error of estimators in meters for a granularity of 49 beam pointing locations. Each data point is the result of one flight, all scans used.

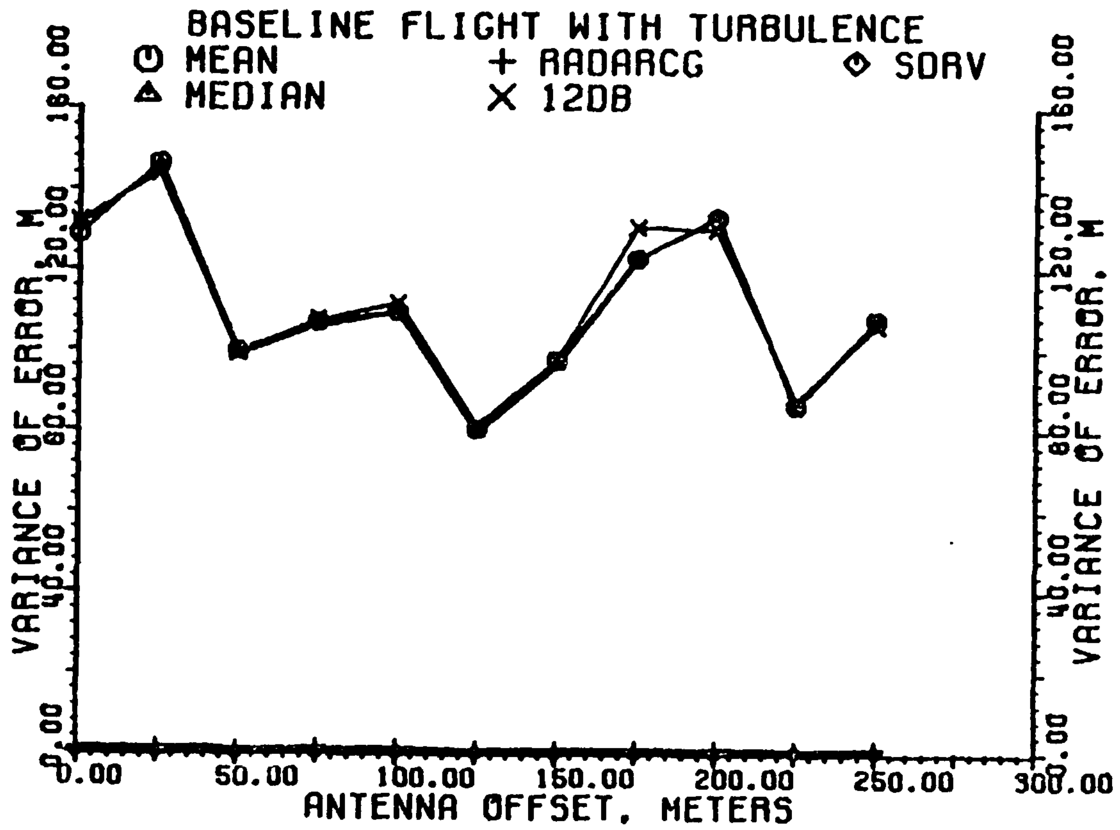

Figure 5-156. Variance of error of estimators in meters for a granularity of 49 beam pointing locations. Each data point is the result of one flight, all scans used.

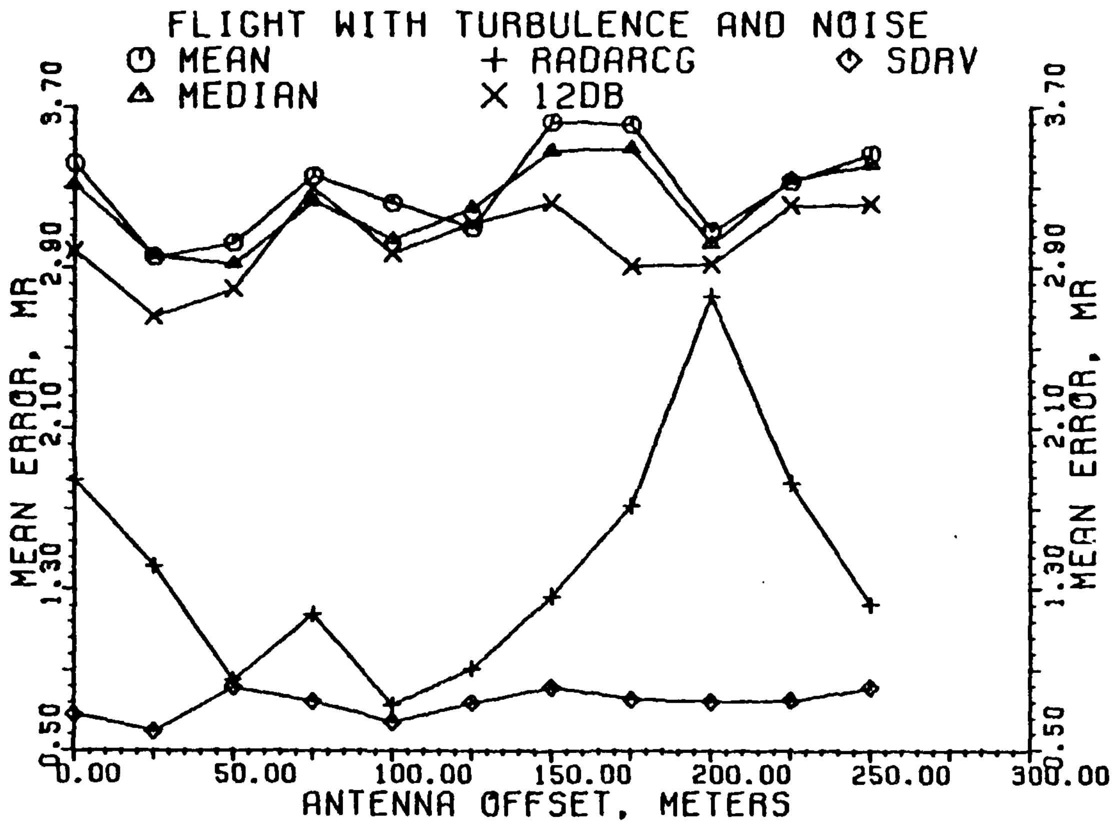

Figure 5-157. Mean error of estimators in milliradians for a granularity of 49 beam pointing locations. Each data point is the result of *one flight, all* scans used.

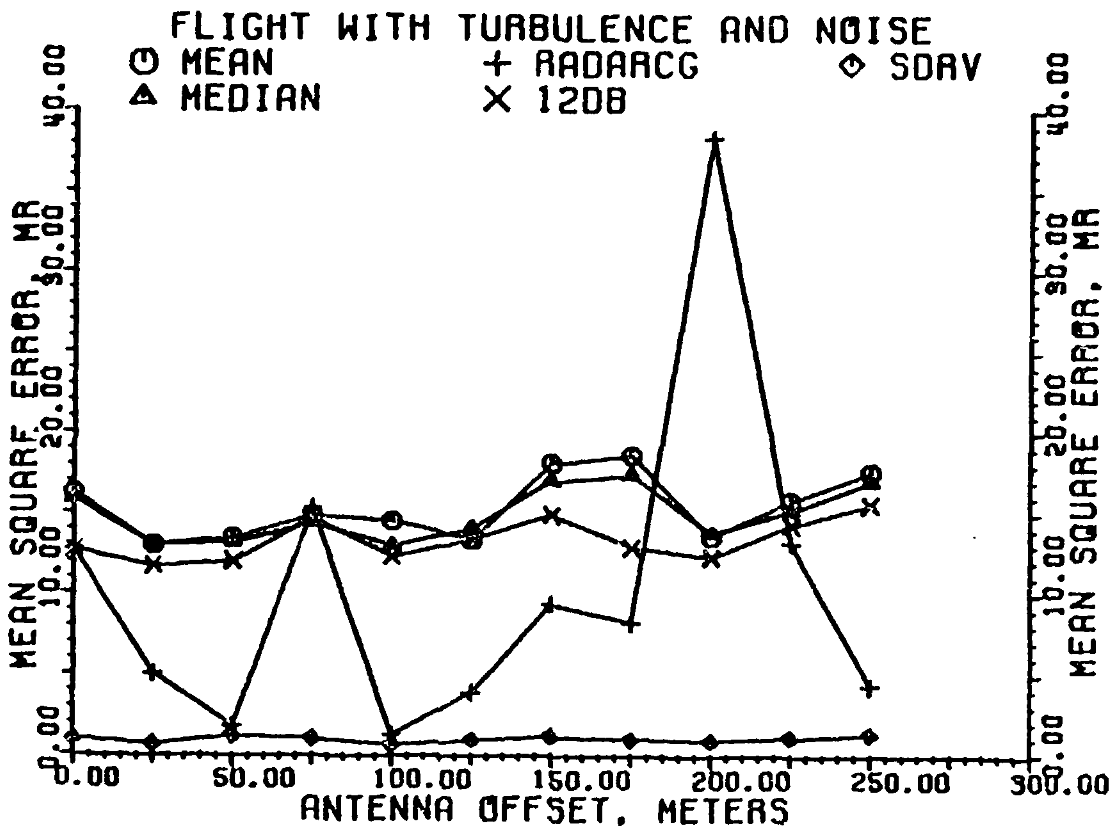

Figure 5-158. Mean square error of estimators in milliradians for a granularity of 49 beam pointing locations. Each data point is the result of one flight, all scans used.

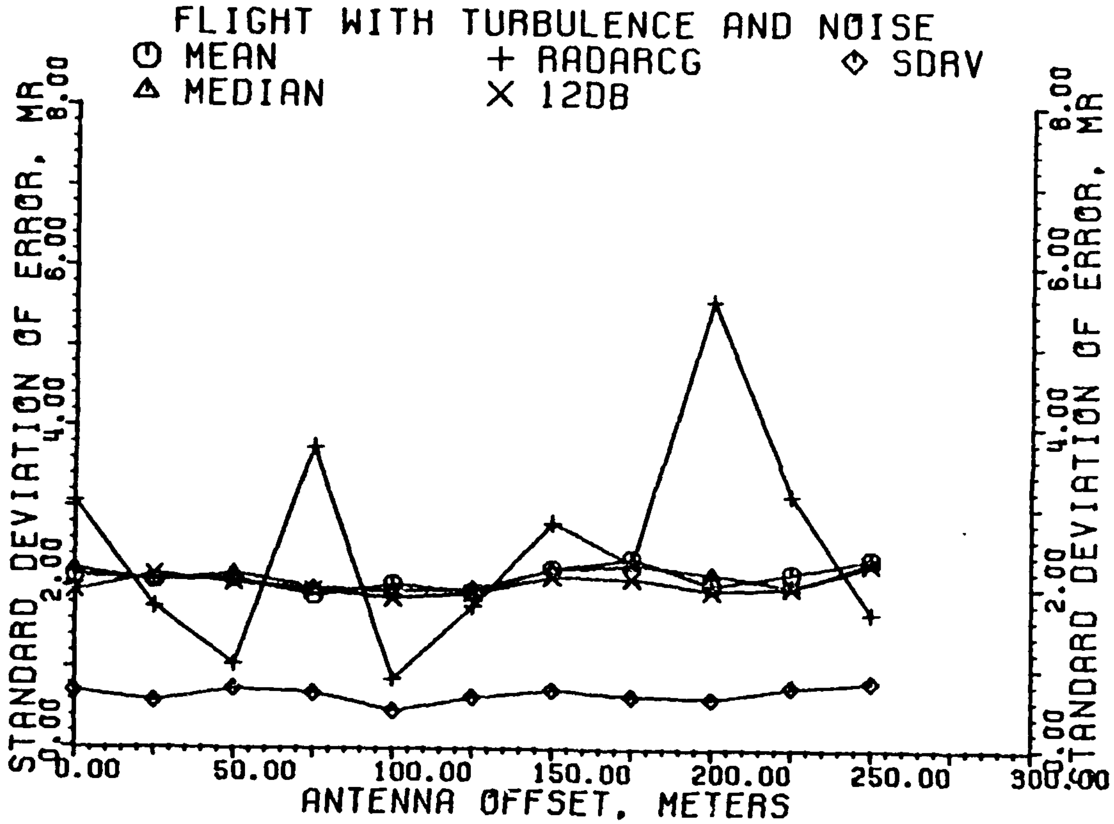

Figure 5-159. Standard deviation of error of estimators in milliradians for a granularity of 49 beam pointing locations. Each data point is the result of one flight, all scans used.

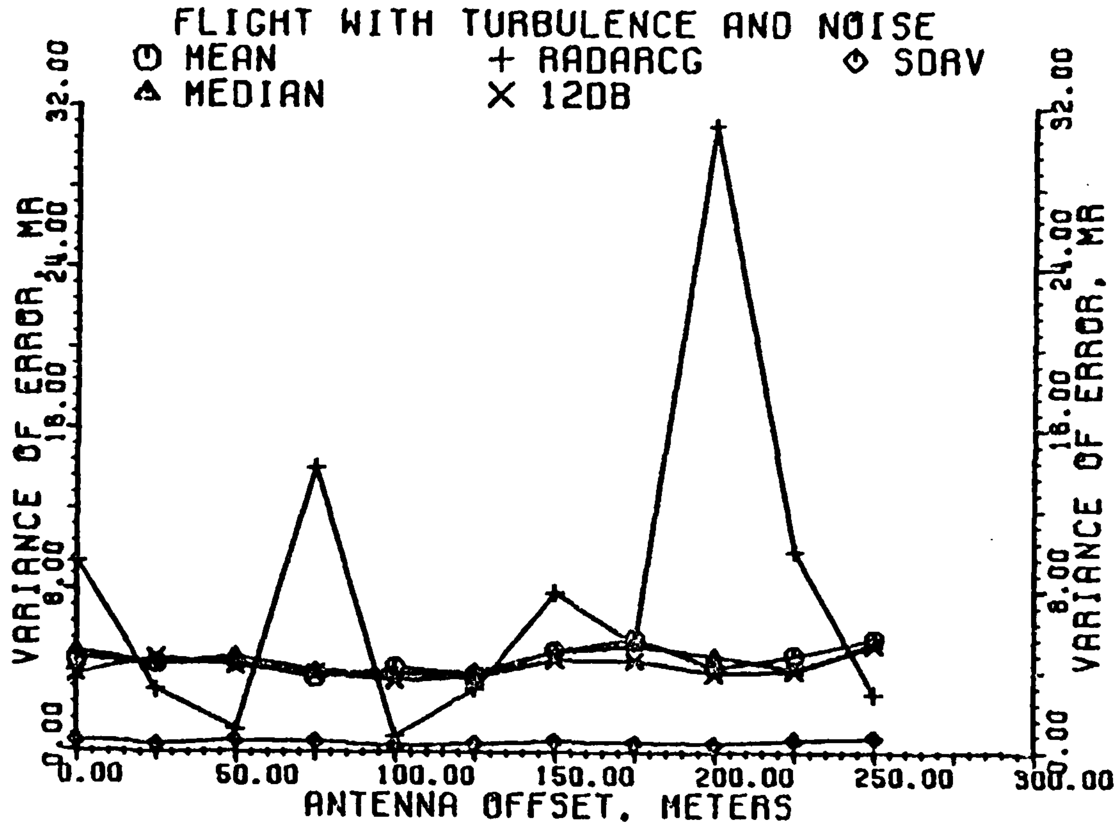

Figure 5-160. Variance of error of estimators in milliradians for a granularity of 49 *beam pointing locations. Each data point is* the result of one flight, all scans used.

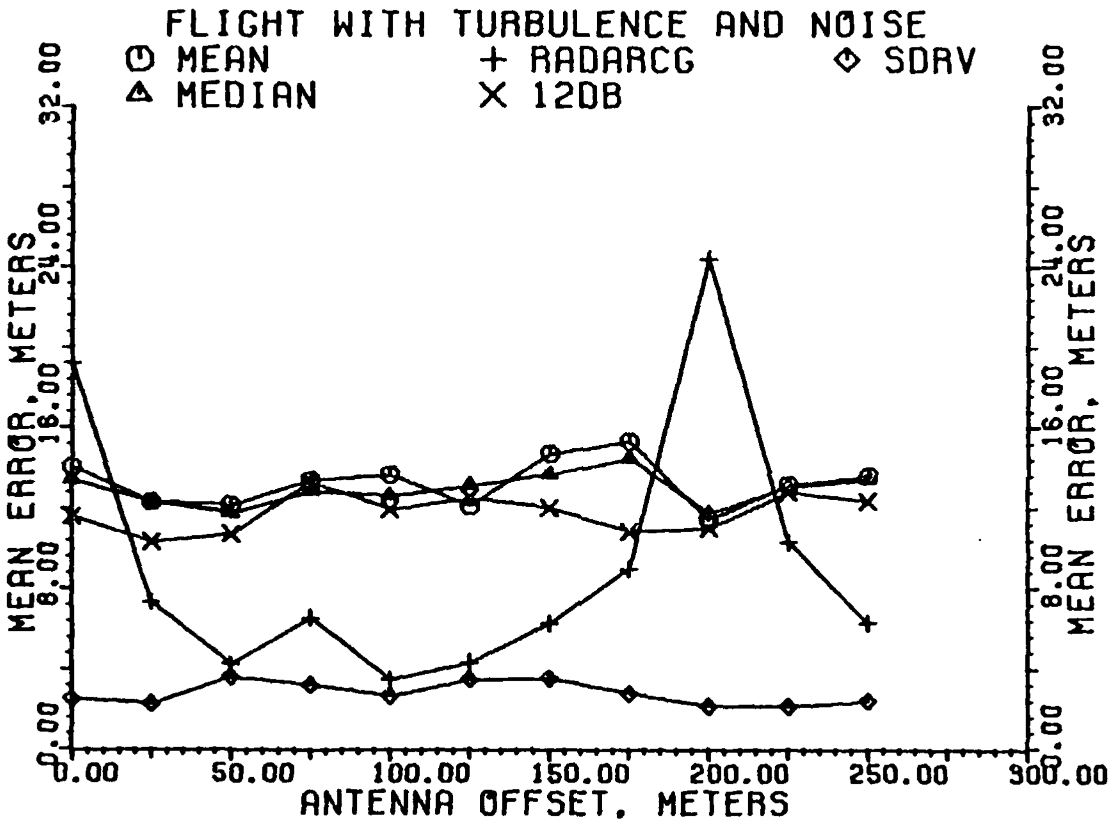

Figure 5-161. Mean error of estimators in meters for a granularity of 49 beam pointing locations. Each data point is the result of one flight, all scans used.

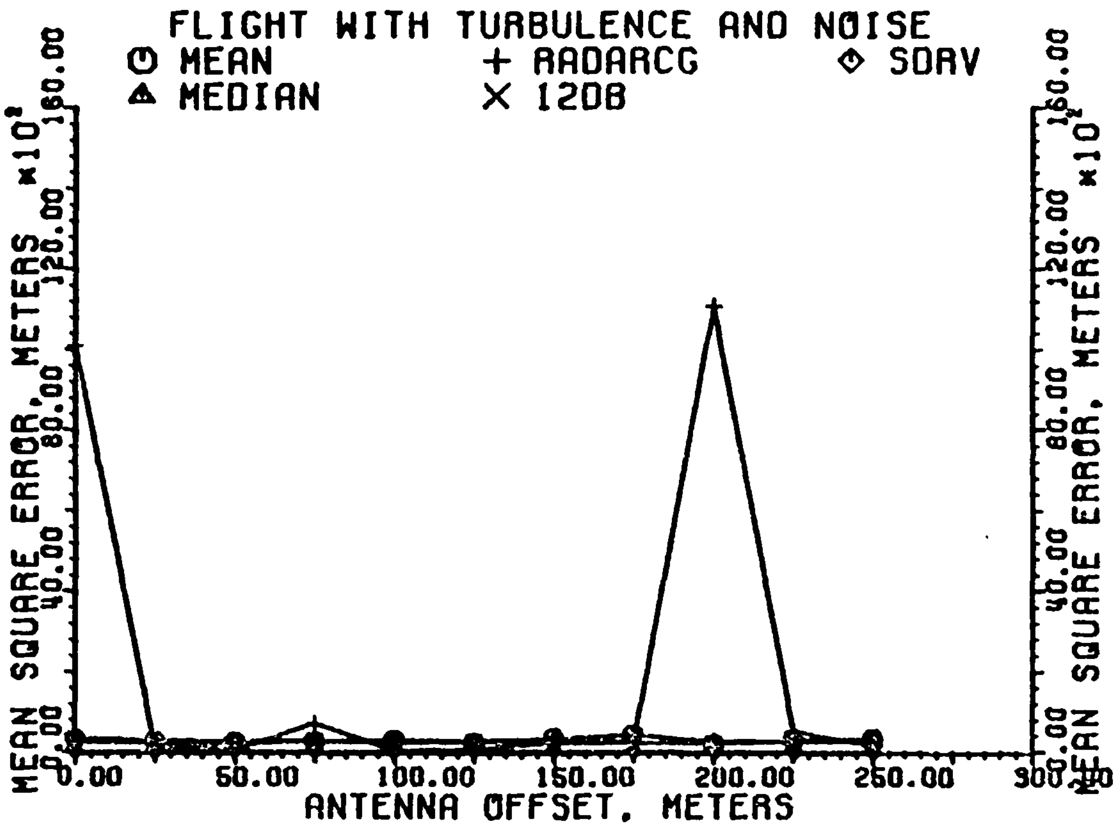

Figure 5-162. Mean square of estimators in meters for a granularity of 49 beam pointing locations. Each data point is the result of one flight, all scans used.

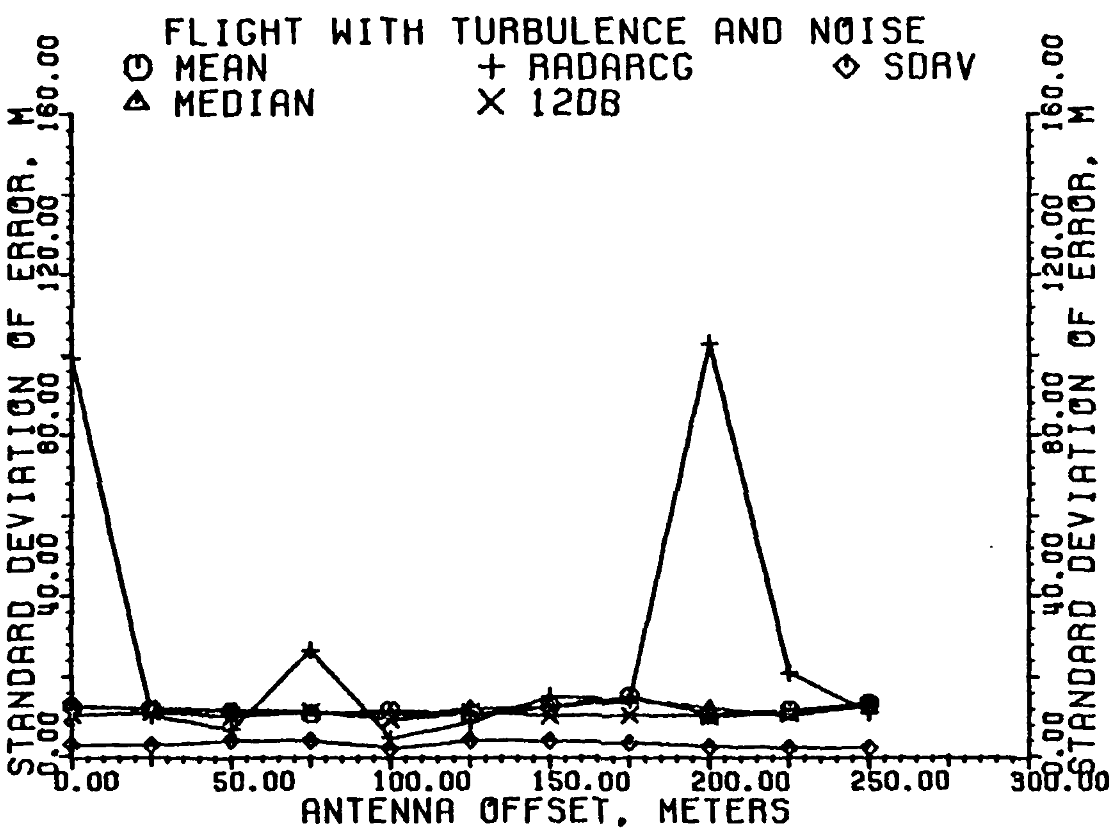

Figure 5-163. Standard deviation of error of estimators in meters for a granularity of 49 beam pointing locations. Each data point is the result of one flight, all scans used.

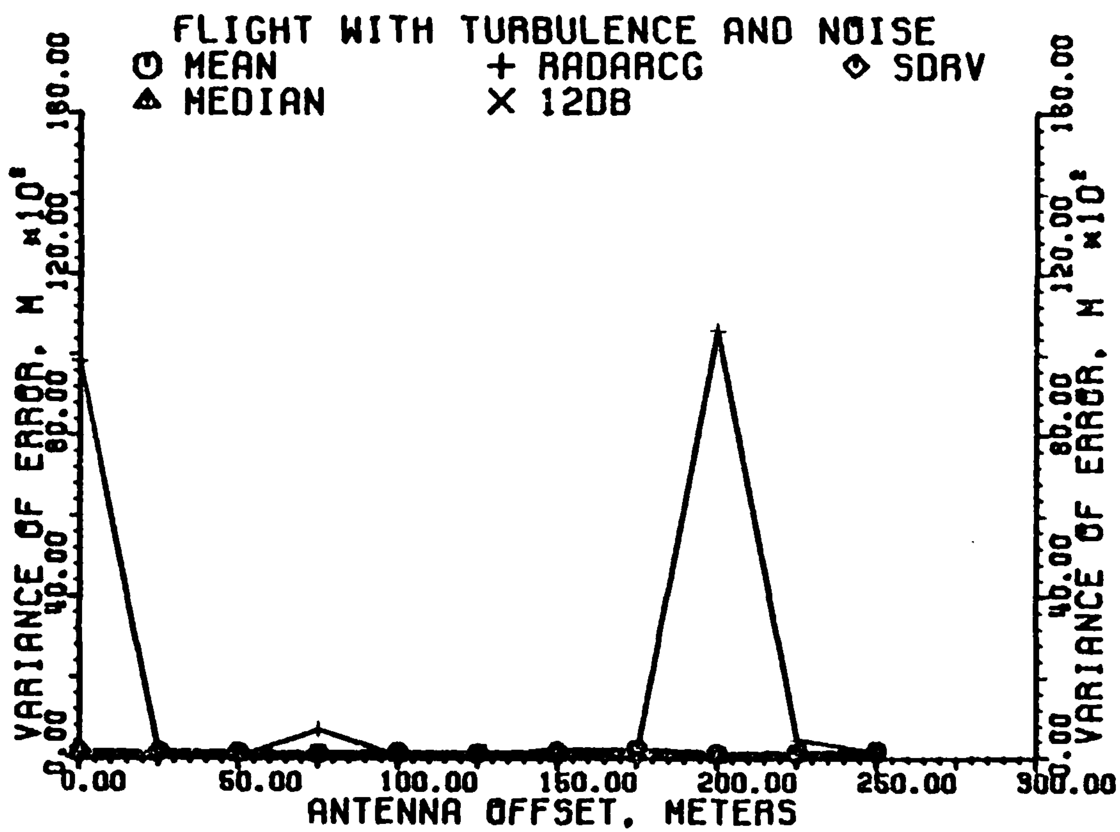

Figure 5-164. Variance of error of estimators in meters for a granularity of 49 beam pointing locations. Each data point is the result of one flight, all scans used.

Figures 5-165 through 5-172 are the results of the calculation of the mean error, mean square error, and the standard deviation and variance of the error in milliradians and meters using only the data from those scans of a flight with a SNR of at least 13 dB. The figures show the RADARCG estimator to be the most accurate, in contrast the SDRV was most accurate when the scan SNR was infinite (baseline flights). The three thresholding methods are all comparable, with a slight edge given to the mean estimator.

The addition of turbulence, Figures 5-173 through 5-180, shows little change from the flights without turbulence. This again indicates that little decorrelation occurs from pulse to pulse due to turbulence for this simulation.

The scans less than or equal to a SNR of 10 dB for a flight with noise were selected and the data plotted in Figures 5-181 through 5-188. Most noticeable is the improvement in RADARCG. The algorithm, now having more data points to assimilate, is working well in reducing the effects of noise. The most accurate and robust estimator is still SDRV, although the choise is not as obvious as it was in the coarser granularities. It is interesting to note, by comparing Figure 5-53 with Figure 5-181 for example, that the mean error in milliradians of SDRV for nine beam locations, scans less than 10 dB, is at least as accurate as are the thresholding estimators under those same conditions, but using 49 beam locations.

The flights with turbulence and noise, scans at or below 10 dB, are plotted in Figures 5-189 through 5-196. All estimators are improved over similar conditions with the coarser granularities. Note that the second

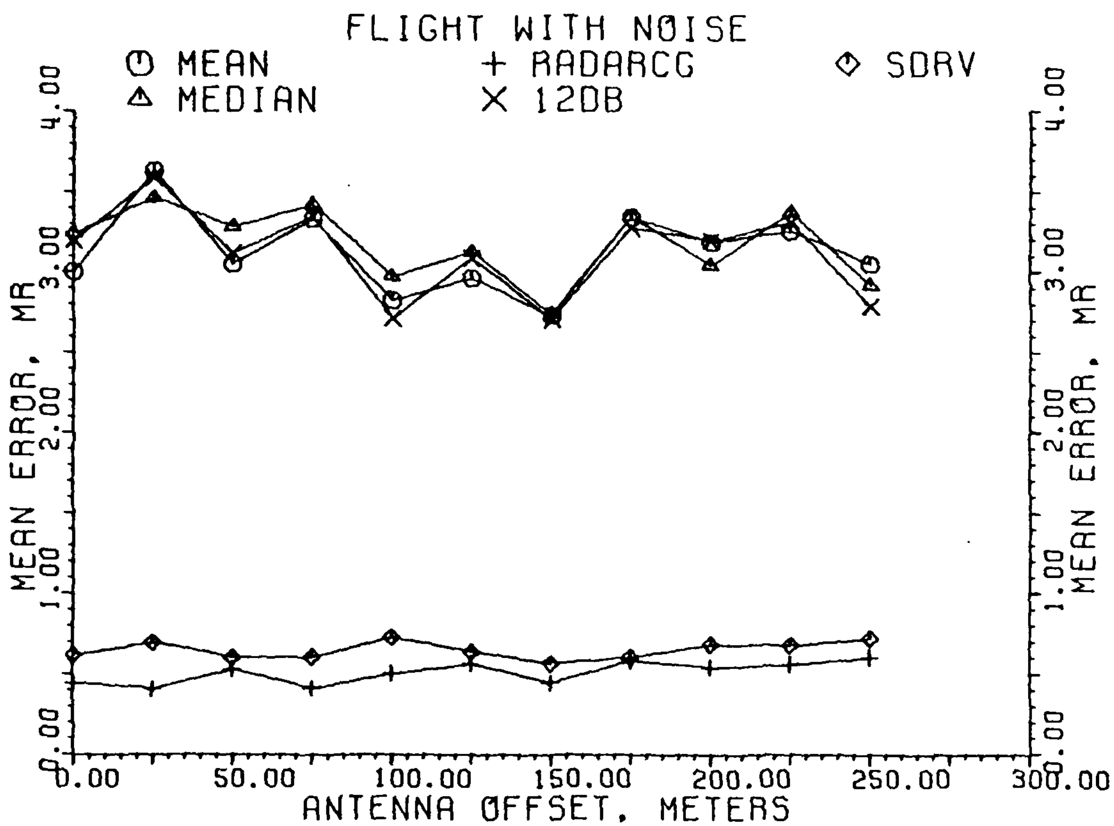

Figure 5-165. Mean error of estimators in milliradians for a granularity of 49 beam pointing locations. Each data point is the result of one flight, all scans with a SNR 13 dB or greater used.

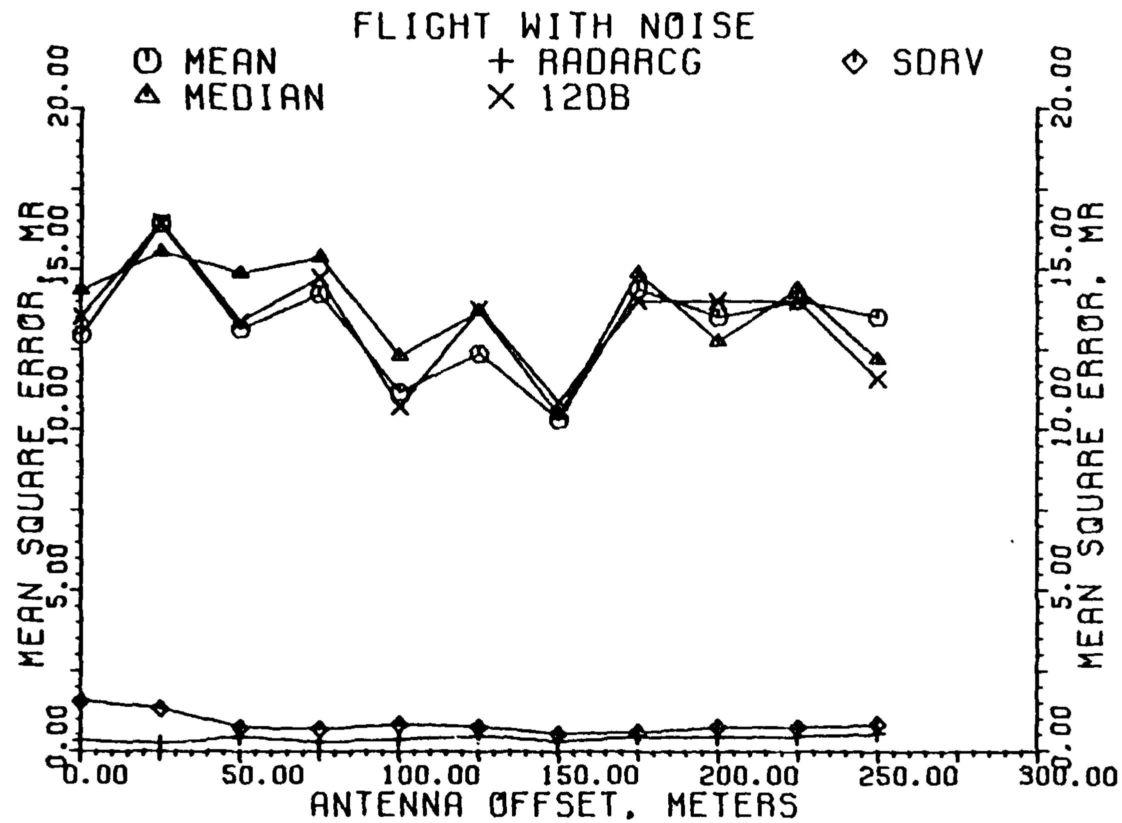

Figure 5-166. Mean square error of estimators in milliradians for a granularity of 49 beam pointing locations. Each data point is the result of one flight, all scans with a SNR 13 dB or greater used.

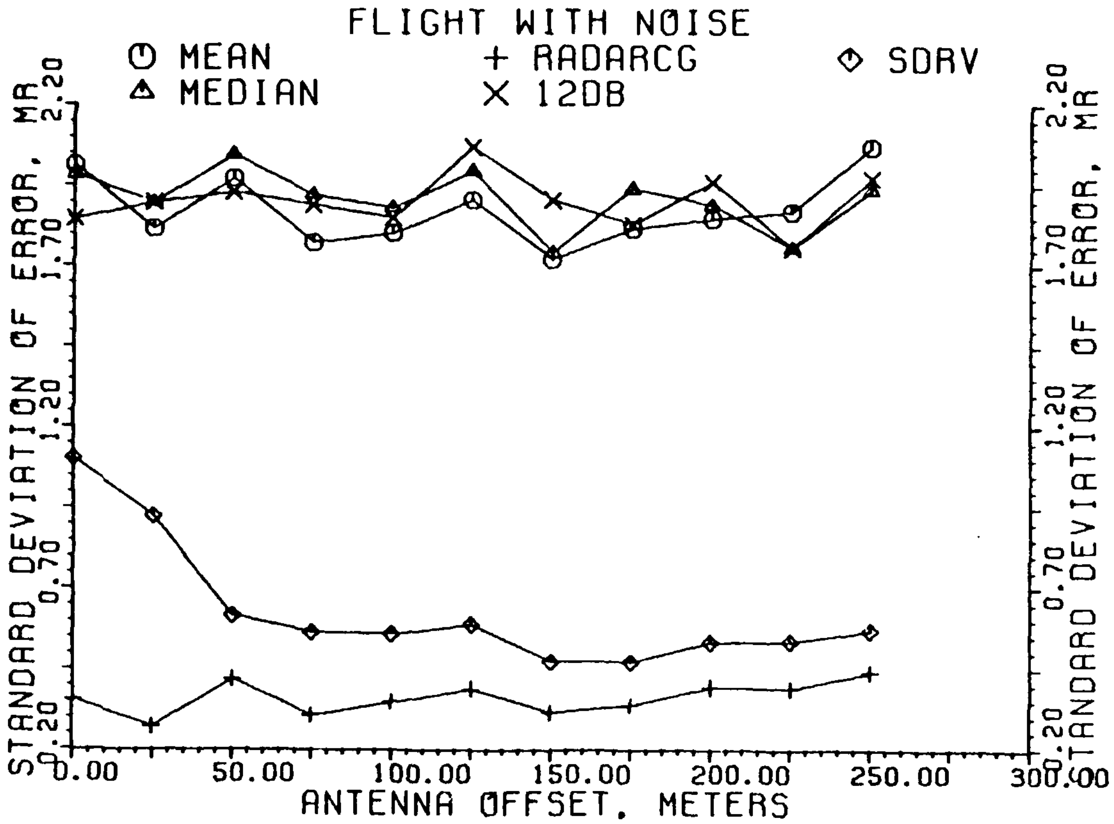

Figure 5-167. Standard deviation of error of estimators in milliradians for a granularity of 49 beam pointing locations. Each data point is the result of one flight, all scans with a SNR 13 dB or greater used.

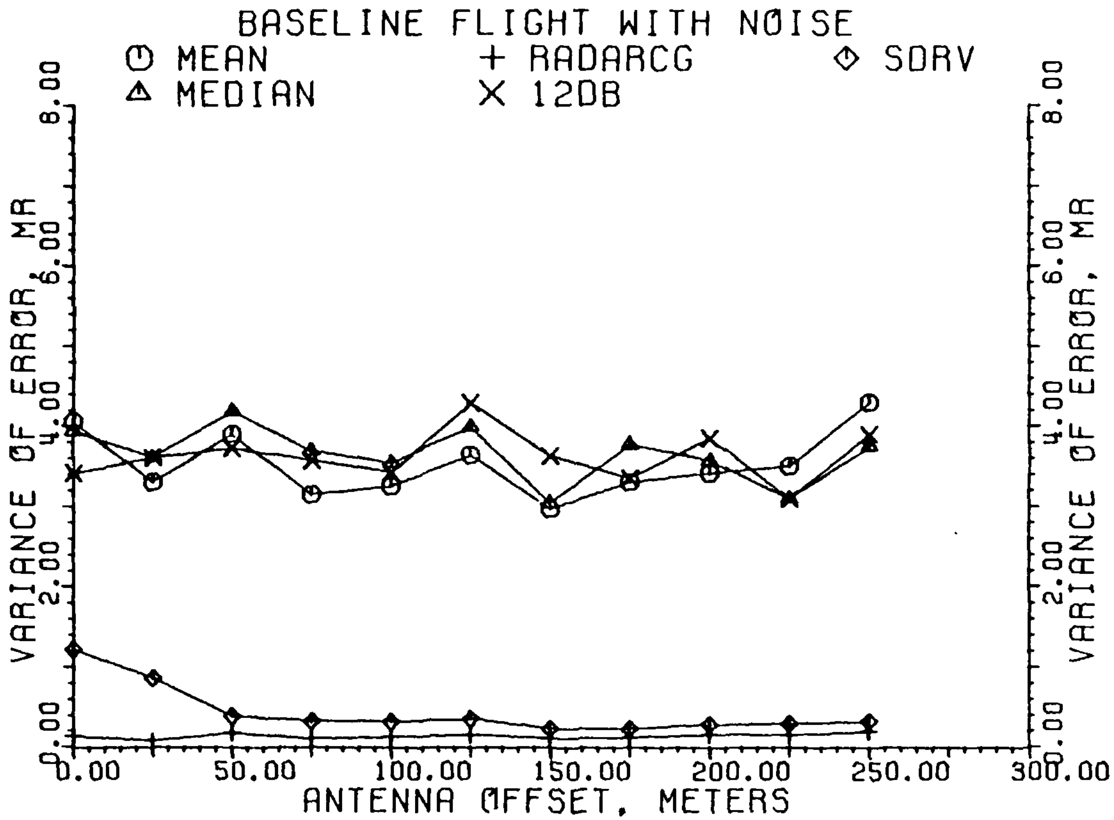

Figure 5-168. Variance of error of estimators in milliradians for a granularity of 49 beam pointing locations. Each data point is the result of one flight, all scans with a SNR 13 dB or greater used.

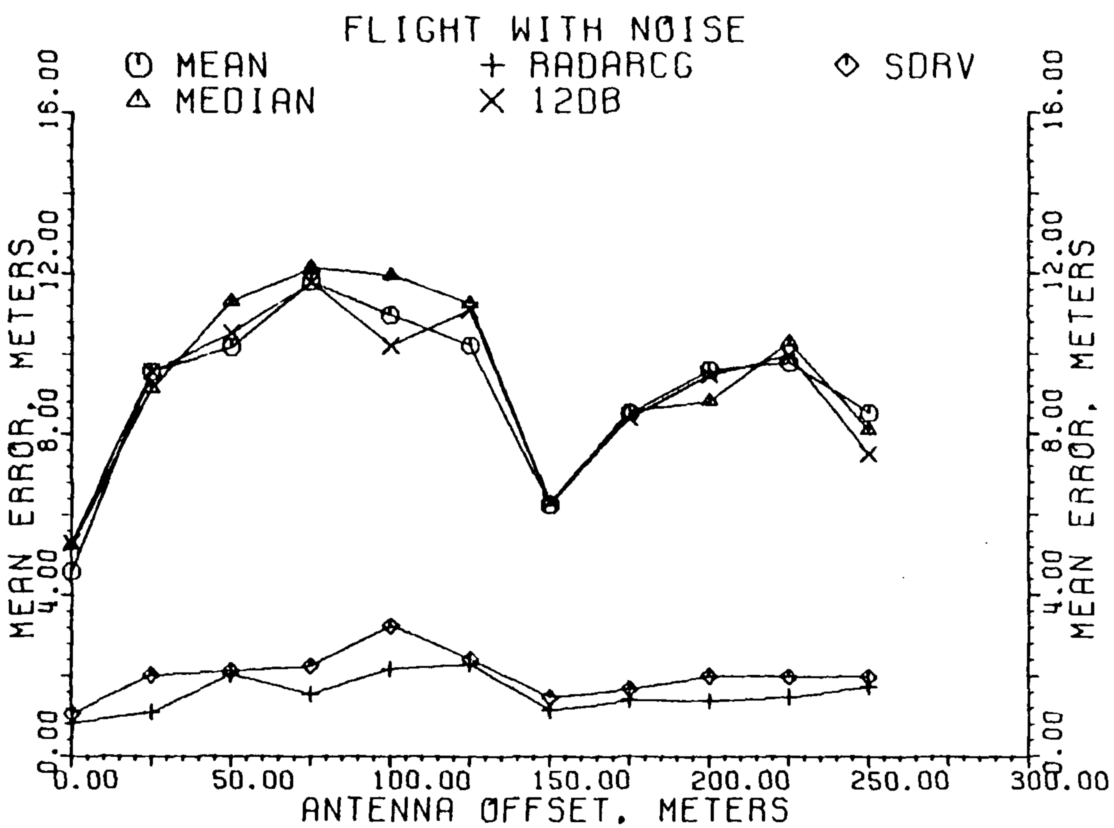

Figure 5-169. Mean error of estimators in meters for a granularity of 49 beam pointing locations. Each data point is the result of one flight, all scans with a SNR 13 dB or greater used.

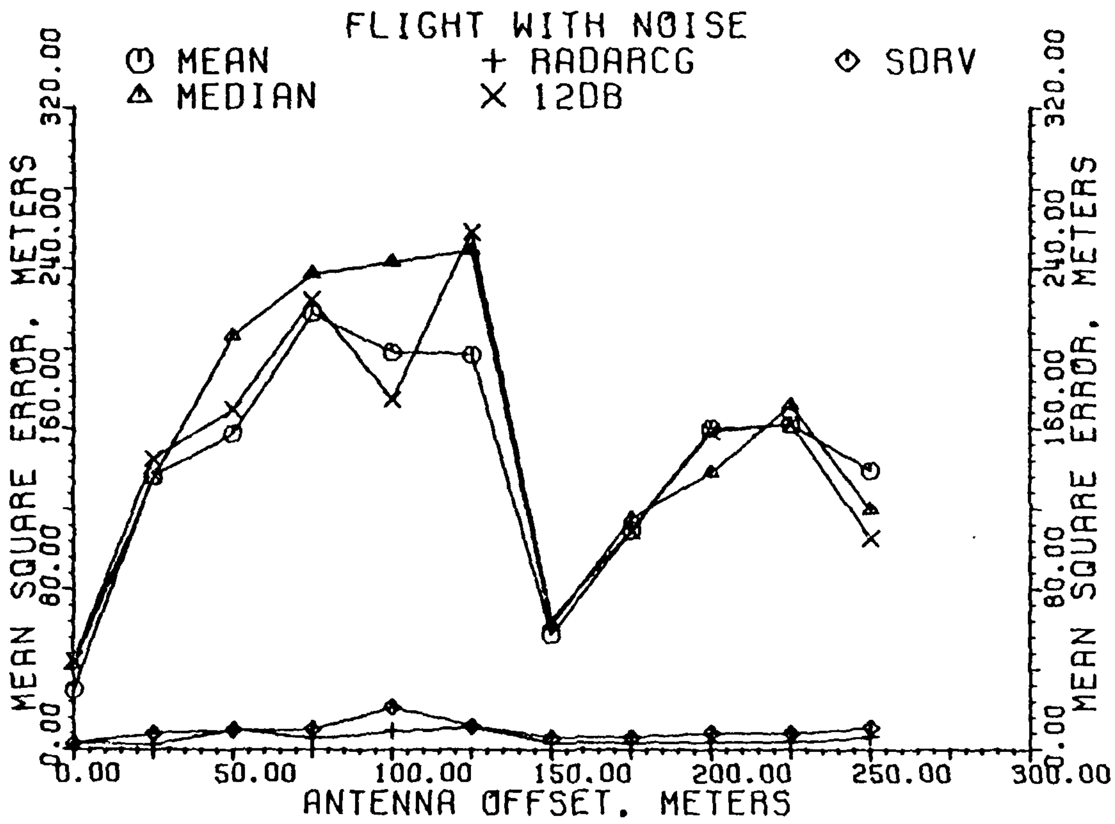

Figure 5-170. Mean square error of estimators in meters for a granularity of 49 beam pointing locations. Each data point is the result of one flight, all scans with a SNR 13 dB or greater used.

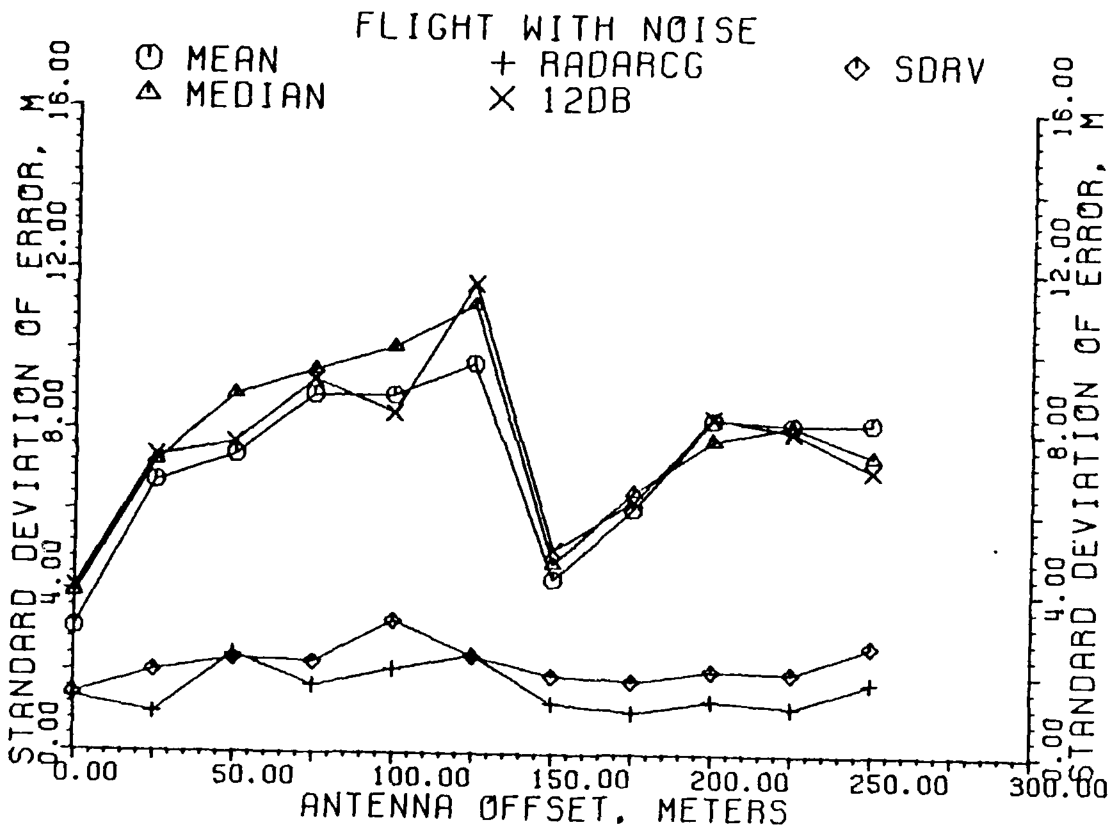

Figure 5-171. Standard deviation of error of estimators in meters for a granularity of 49 beam pointing locations. Each data point is the result of one flight, all scans with a SNR 13 dB or greater used.

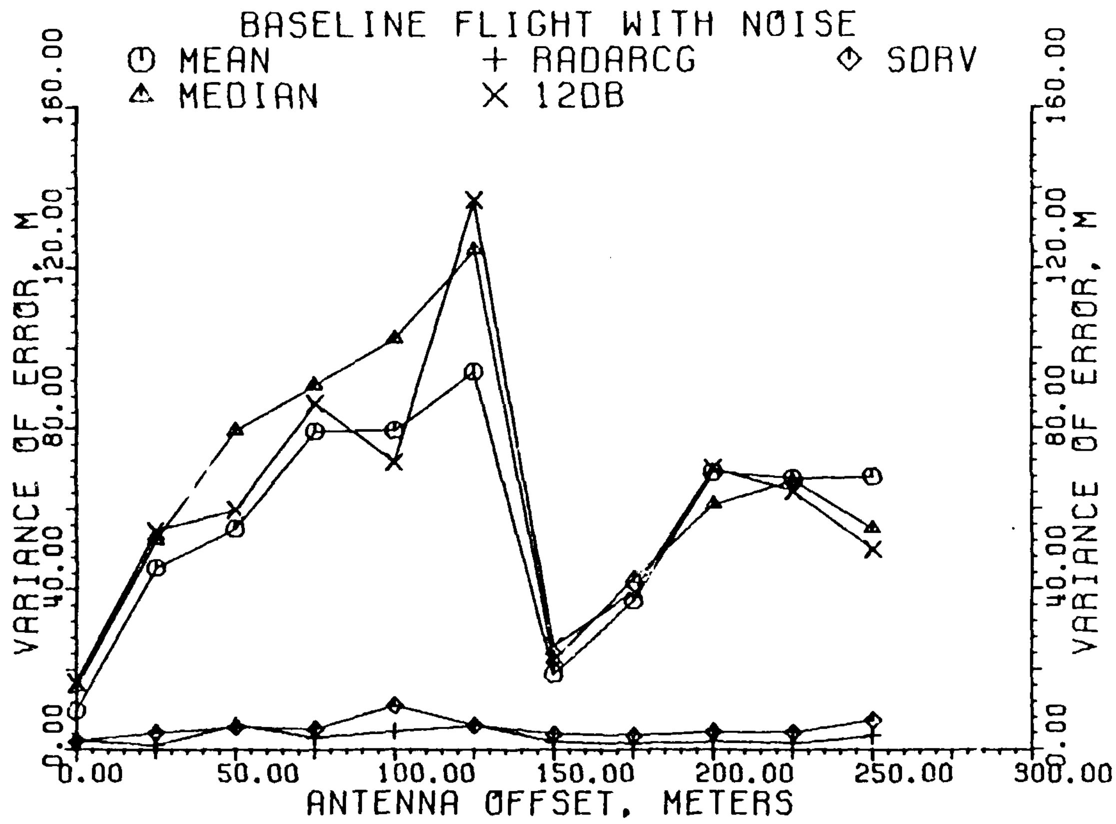

Figure 5-172. Variance of error of estimators in meters for a granularity of 49 beam pointing locations. Each data point is the result of one flight, all scans with a SNR 13 dB or greater used.

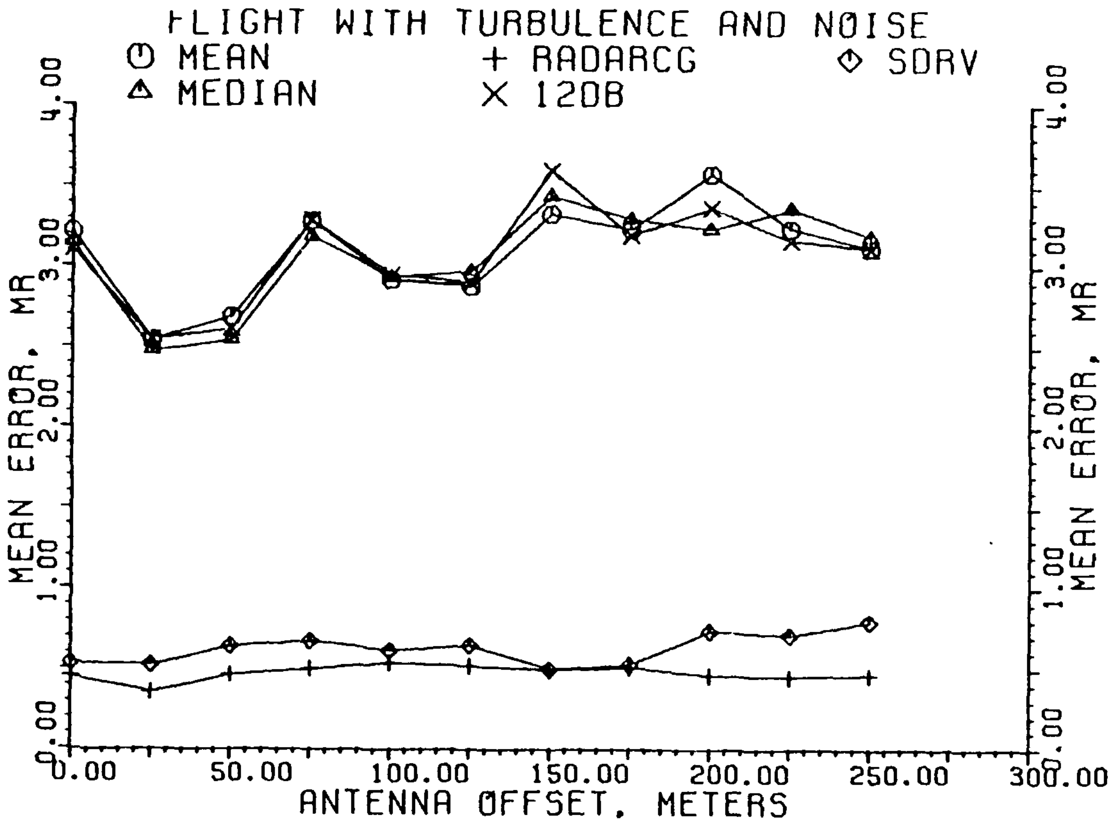

Figure 5-173. Mean error of estimators in milliradians for a granularity of 49 beam pointing locations. Each data point is the result of one flight, all scans with a SNR 13 dB or greater used.

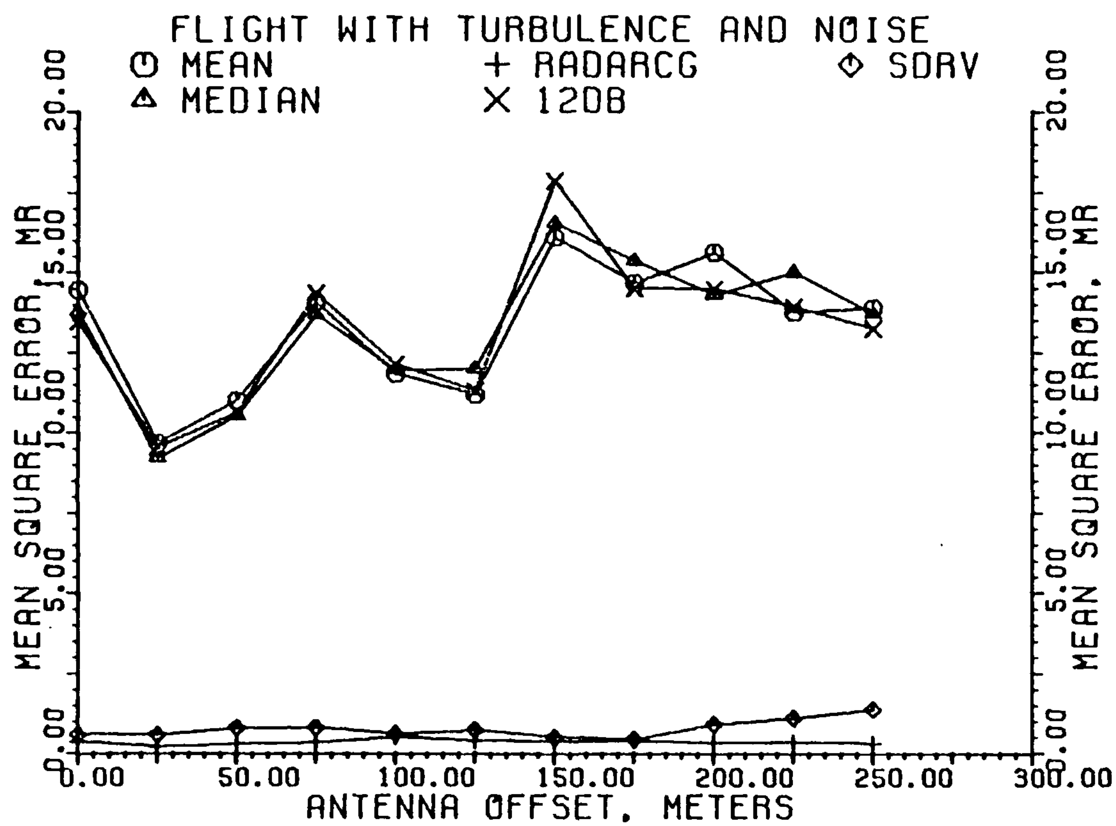

Figure 5-174. Mean square error of estimators in milliradians for a granularity of 49 beam pointing locations. Each data point is the result of one flight, all scans with a SNR 13 dB or greater used.

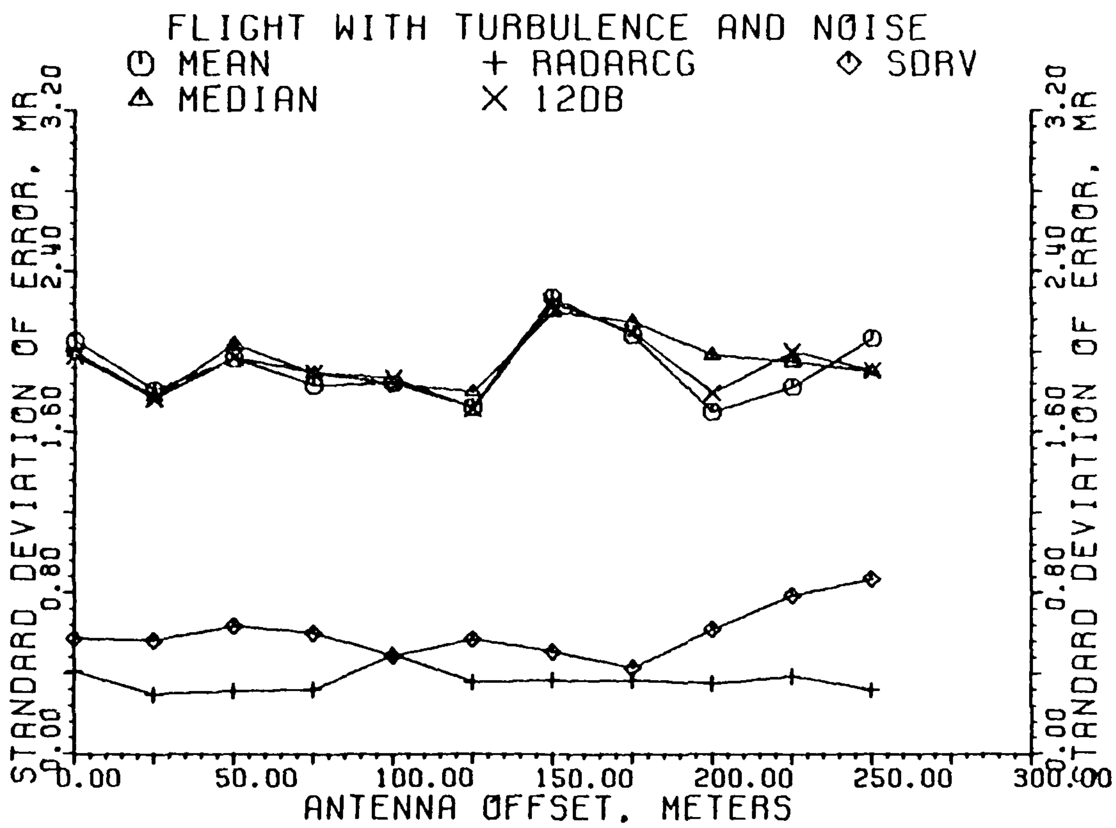

Figure 5-175. Standard deviation of error of estimators in milliradians for a granularity of 49 beam pointing locations. Each data point is the result of one flight, all scans with a SNR 13 dB or greater used.

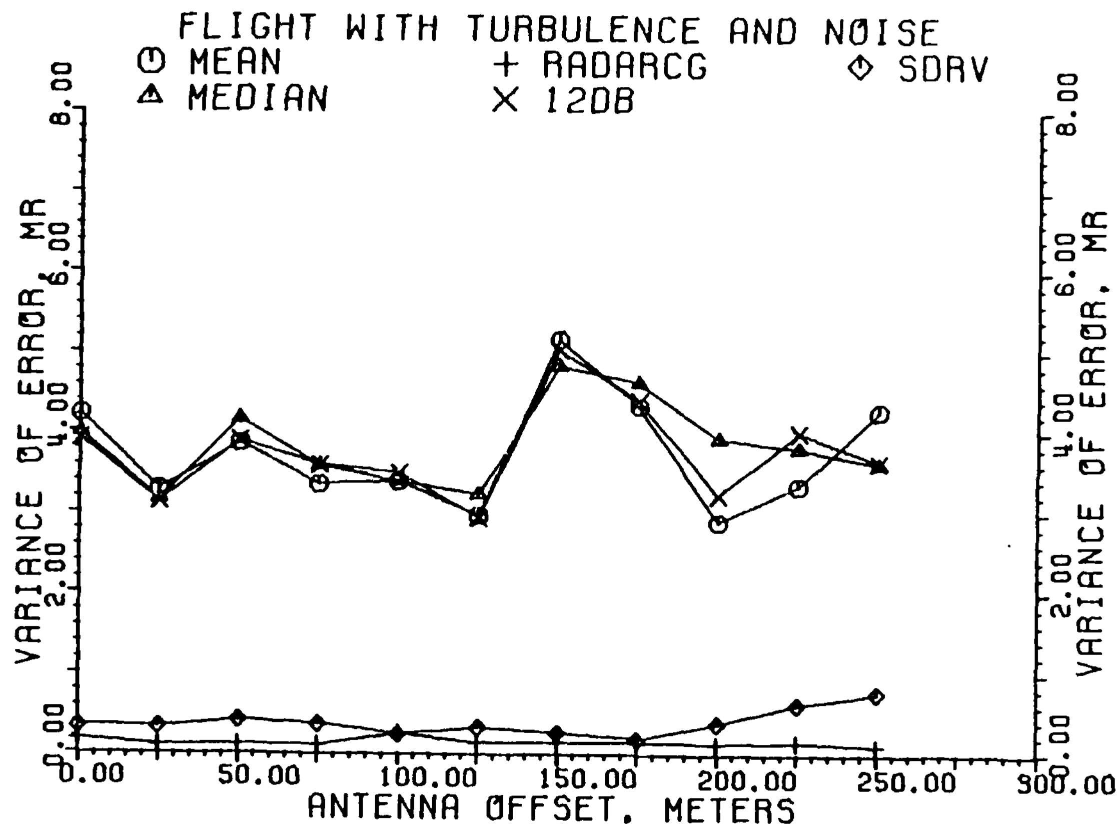

Figure 5-176. Variance of error of estimators in milliradians for a granularity of 49 beam pointing locations. Each data point is the result of one flight, all scans with a SNR 13 dB or greater used.

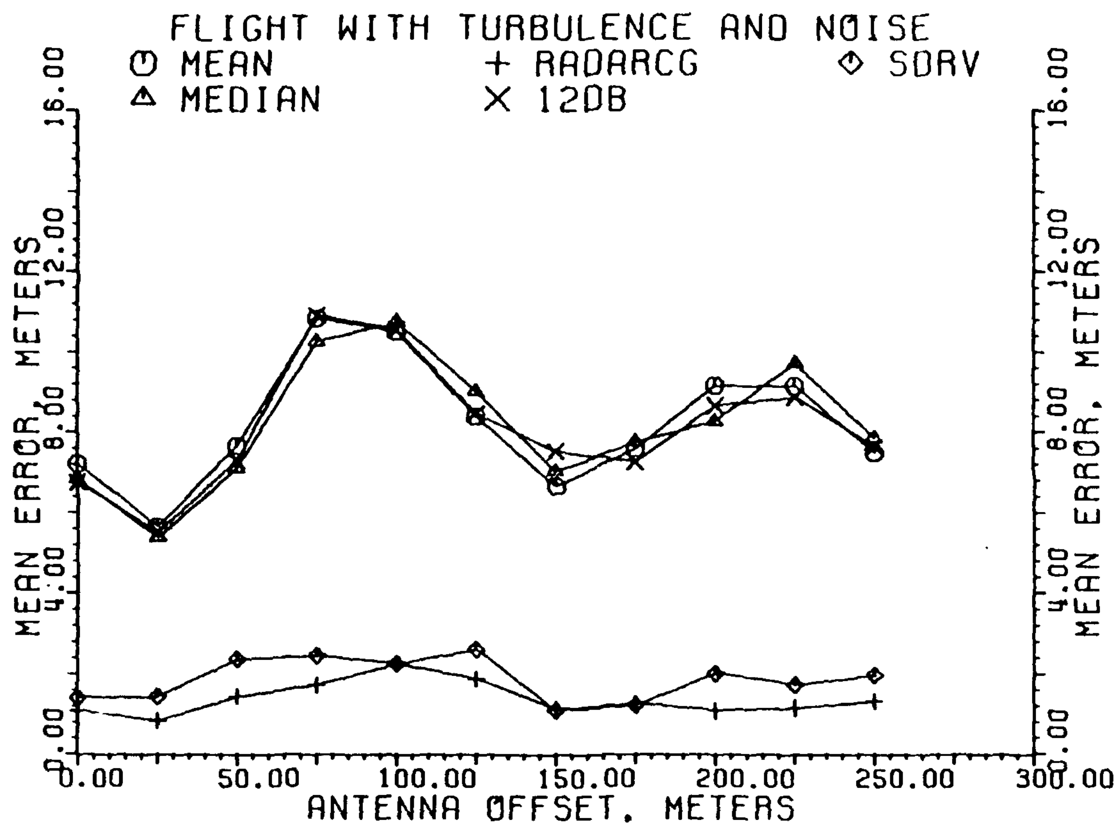

Figure 5-177. Mean error of estimators in meters for a granularity of 49 beam pointing locations. Each data point is the result of one flight, all scans with a SNR 13 dB or greater used.

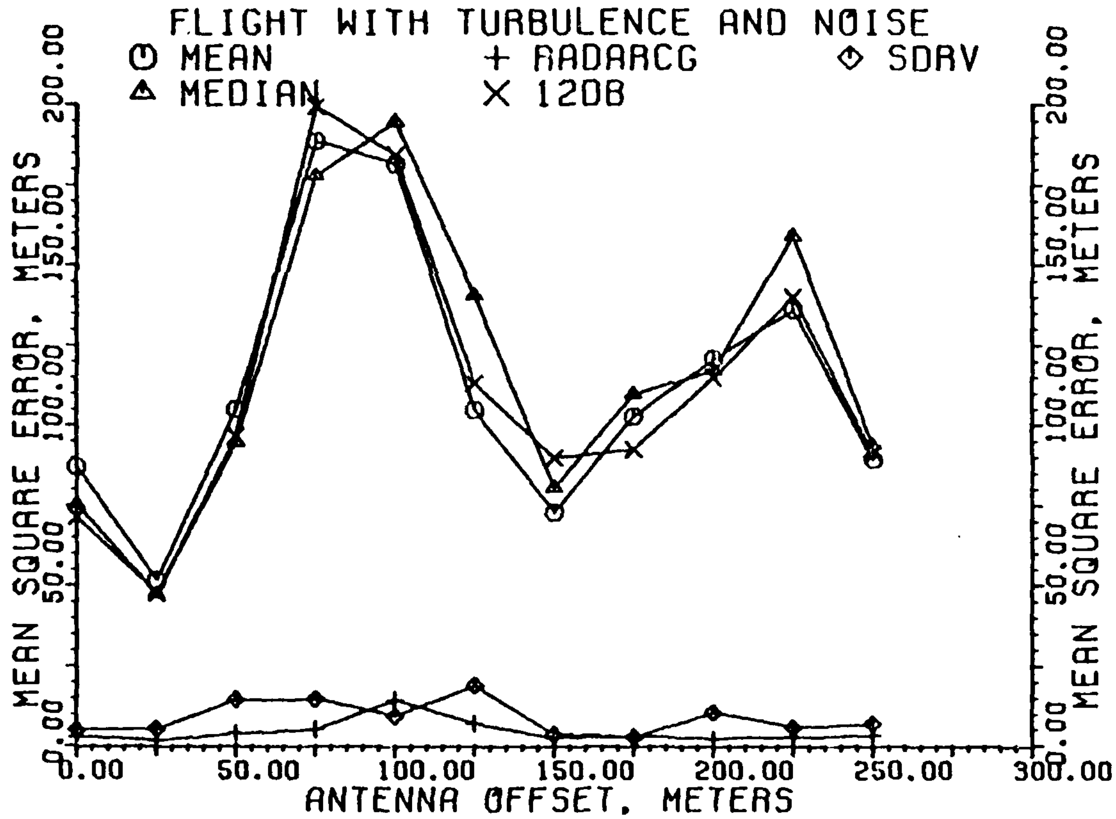

Figure 5-178. Mean square error of estimators in meters for a granularity of 49 beam pointing locations. Each data point is the result of one flight, all scans with a SNR 13 dB or greater used.

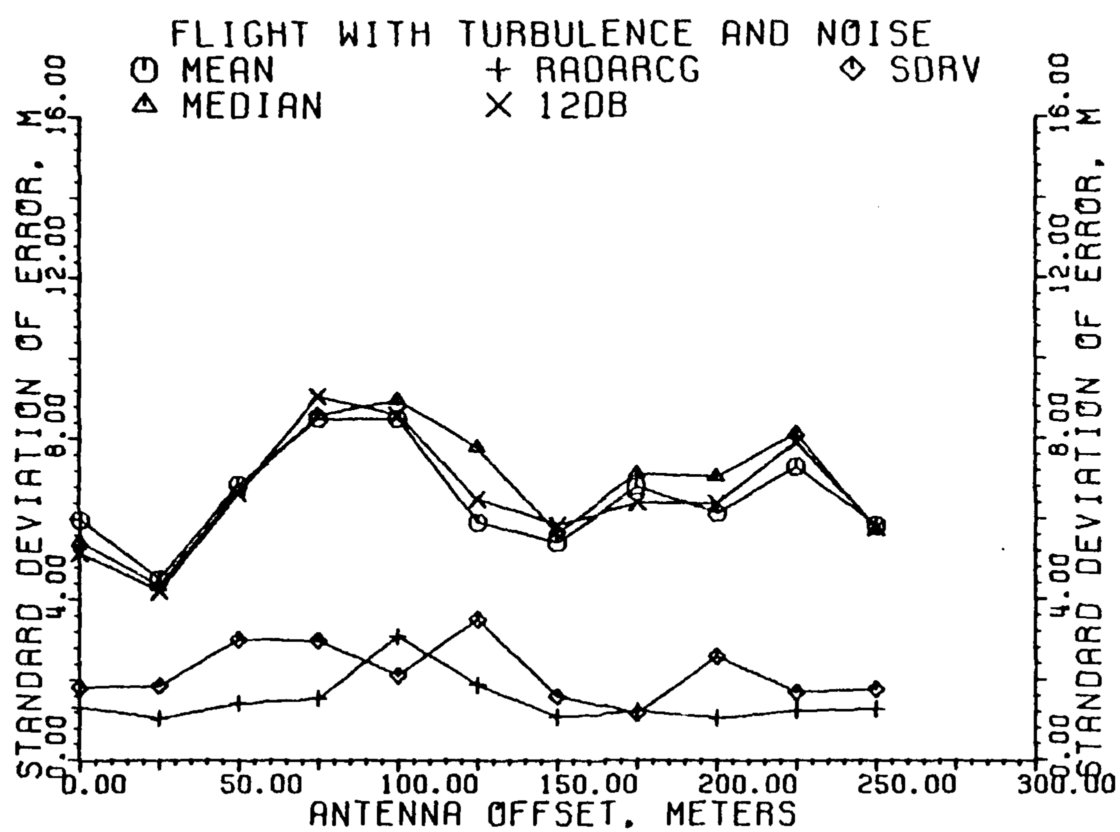

Figure 5-179. Standard deviation of error of estimators in meters for a granularity of 49 beam pointing locations. Each data point is the result of one flight, all scans with a SNR 13 dB or greater used.

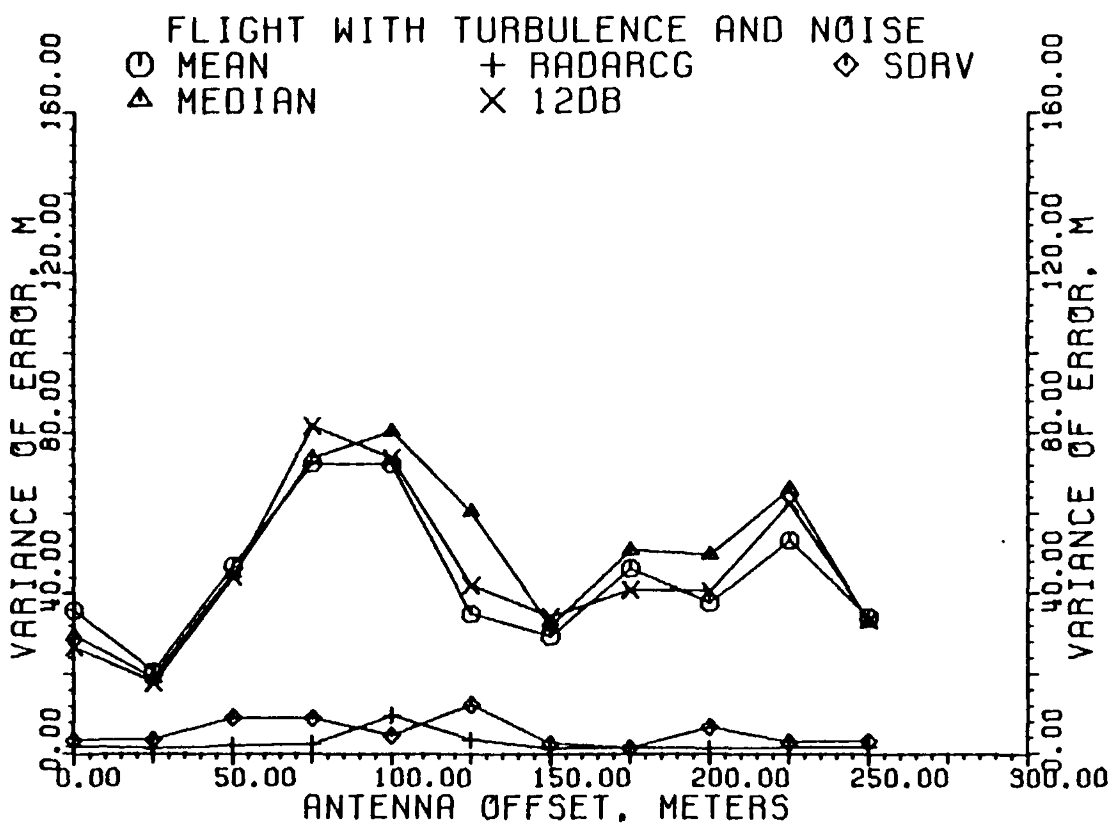

Figure 5-180. Variance of error of estimators in meters for a granularity of 49 beam pointing locations. Each data point is the result of one flight, all scans with a SNR 13 dB or greater used.

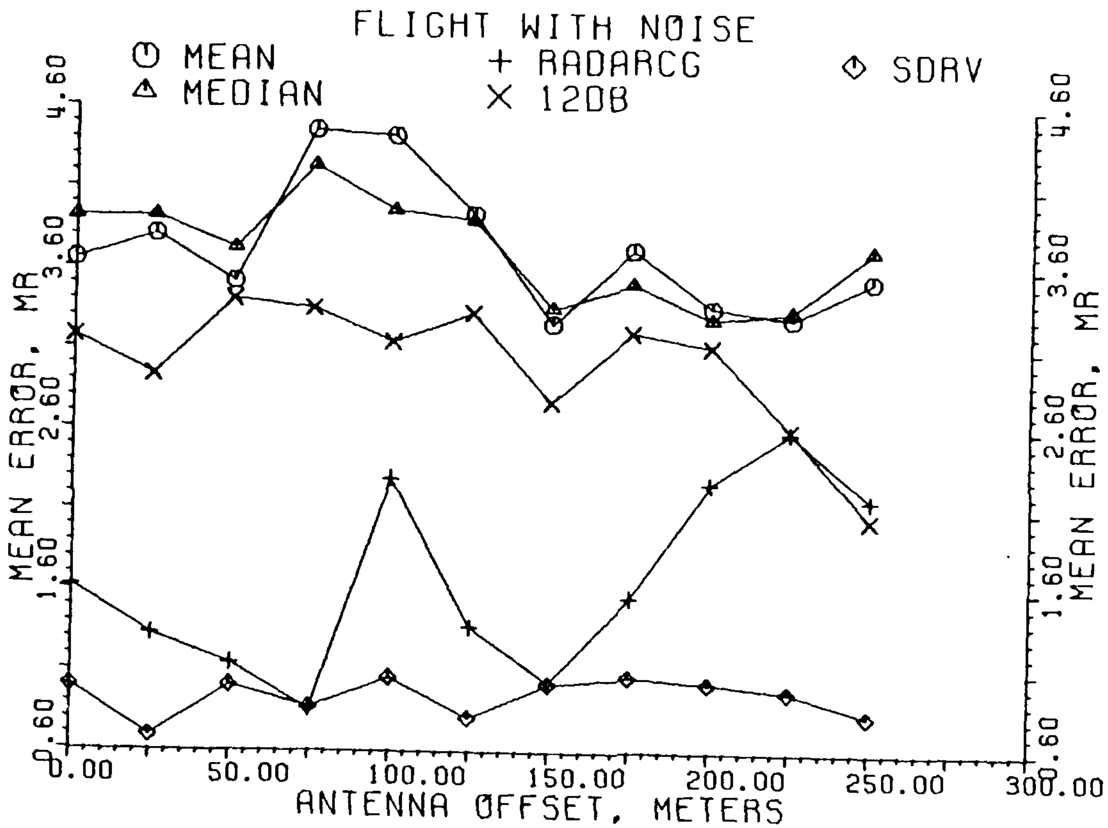

Figure 5-181. Mean error of estimators in milliradians for a granularity of 49 beam pointing locations. Each data point is the result of one flight, all scans with a SNR at or below 10 dB used.

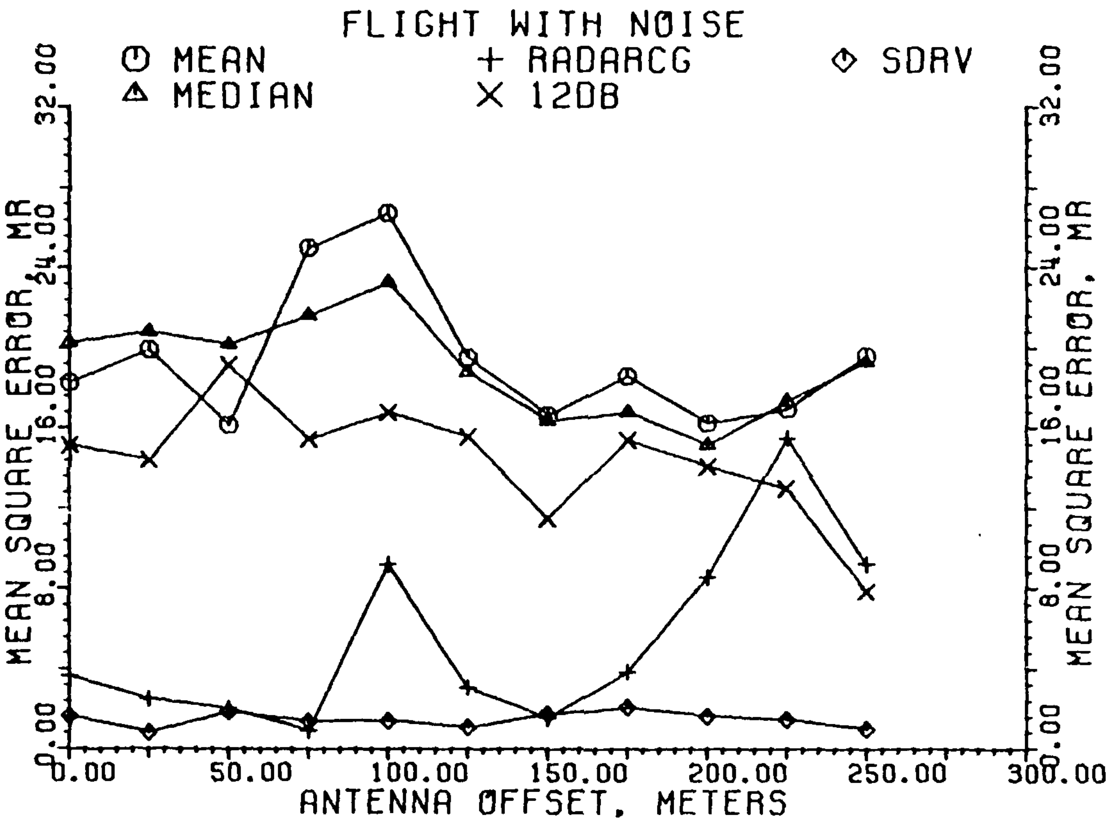

Figure 5-182. Mean square error of estimators in milliradians for a granularity of 49 beam pointing locations. Each data point is the result of one flight, all scans with a SNR at or below 10 dB used.

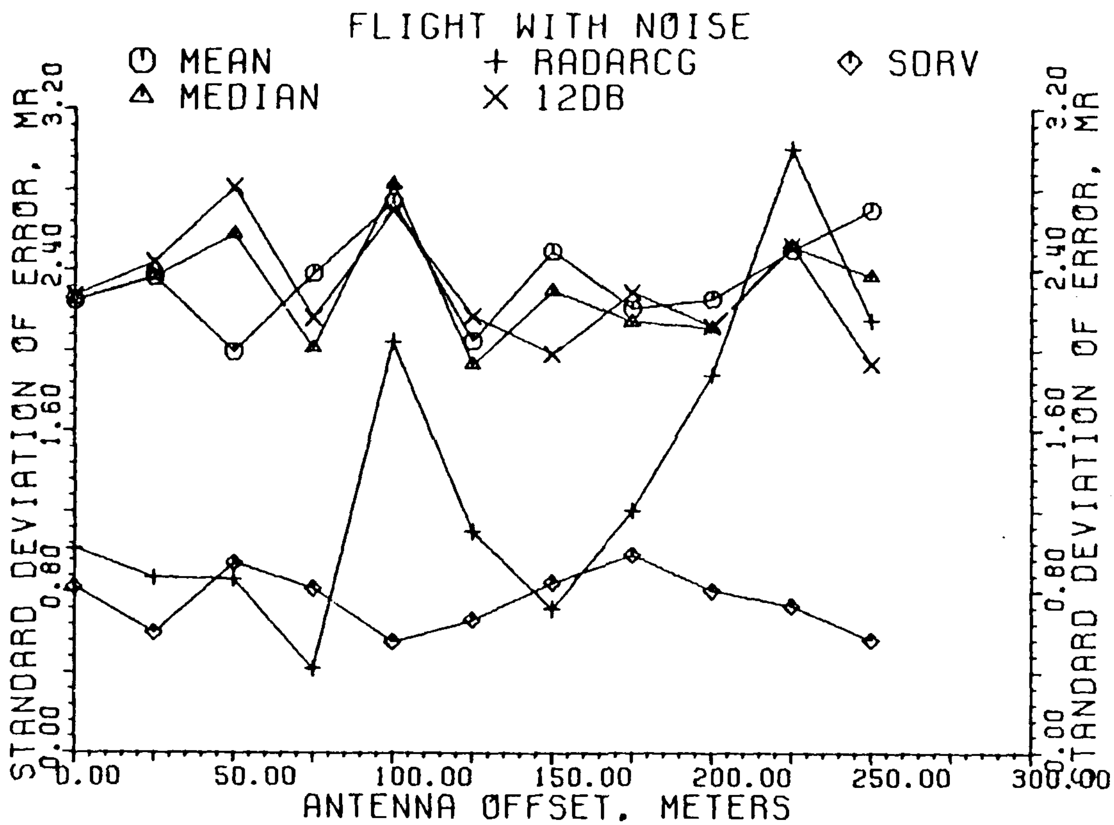

Figure 5-183. Standard deviation of error of estimators in milliradians for a granularity of 49 beam pointing locations. Each data point is the result of one flight, all scans with a SNR at or below 10 dB used.

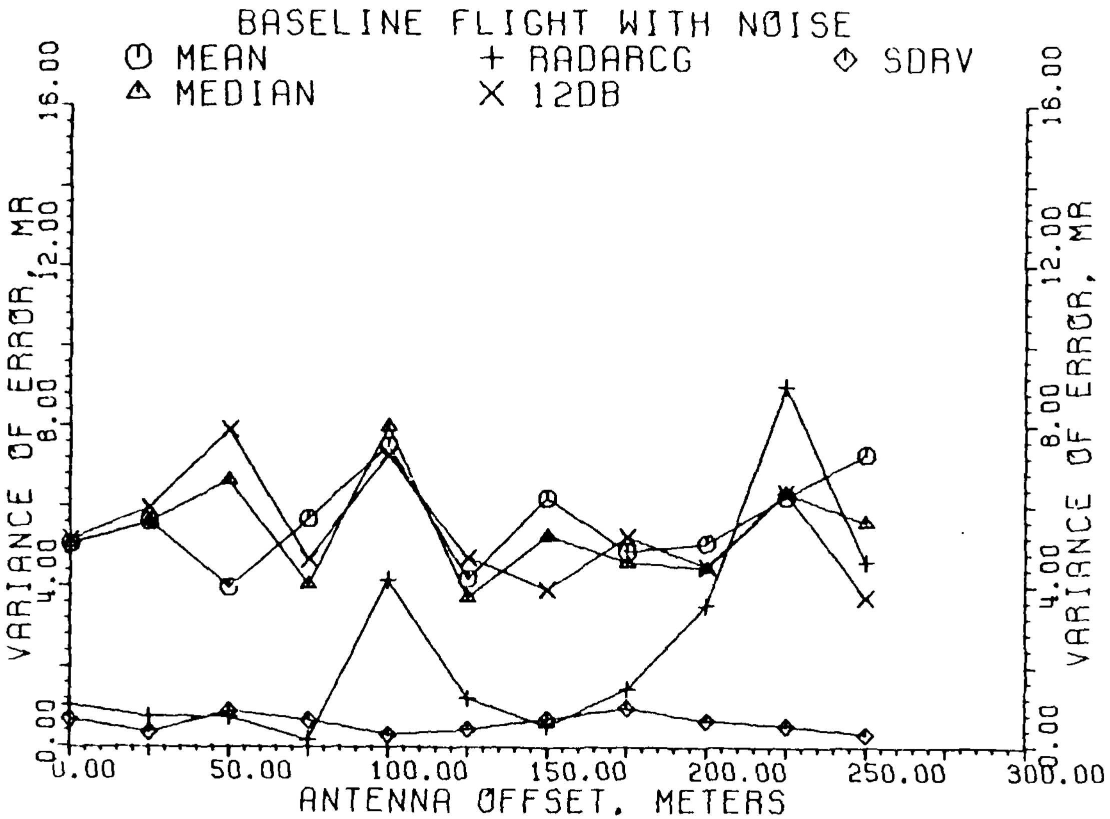

Figure 5-184. Variance of error of estimators in milliradians for a granularity of 49 beam pointing locations. Each data point is the result of one flight, all scans with a SNR at or below 10 dB used.

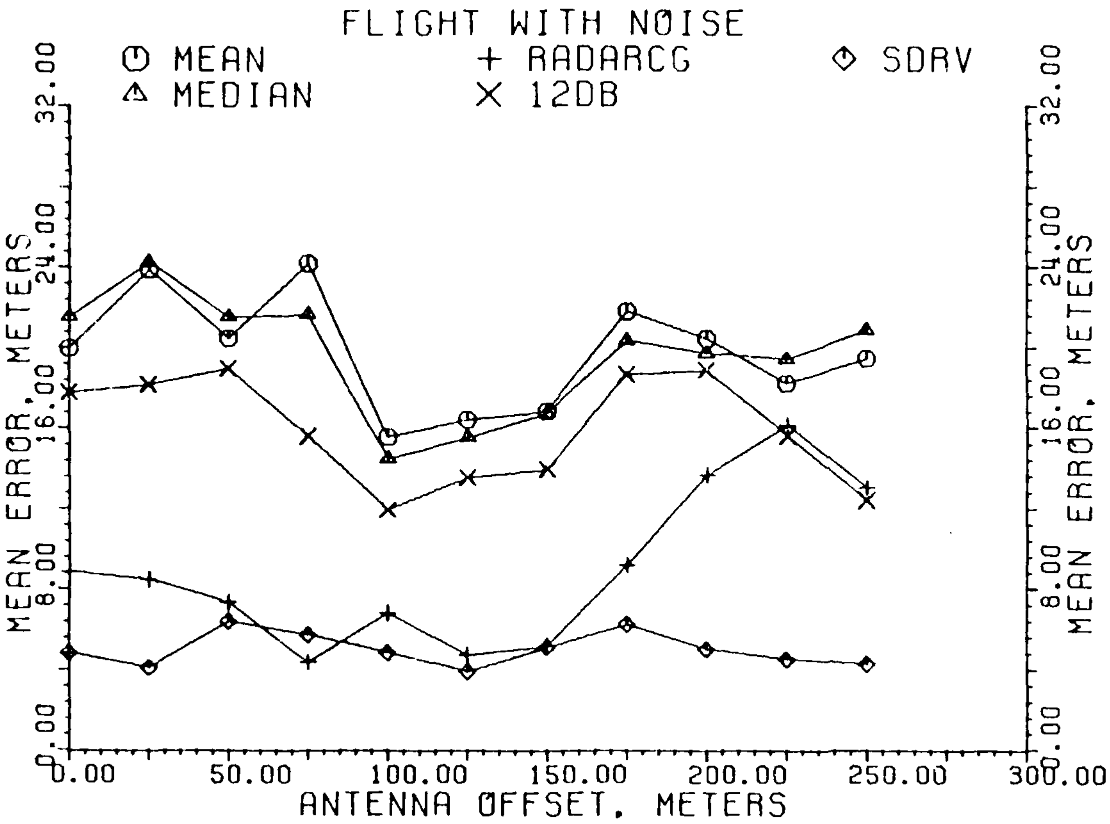

Figure 5-185. Mean error of estimators in meters for a granularity of 49 beam pointing locations. Each data point is the result of one flight, all scans with a SNR at or below 10 dB used.

AD-A110 862 GEORGIA INST OF TECH ATLANTA ENGINEERING EXPERIMENT --ETC F/G 17/7
MARINE AIR TRAFFIC CONTROL AND LANDING SYSTEM (MATCALS INVESTIG--ETC(U)
SEP 81 E R GRAF, C L PHILLIPS, S A STARKS N00039-80-C-0032
UNCLASSIFIED GIT/EES-1-A-2550-VOL-1 NL

4 OF 5
AD
A110862

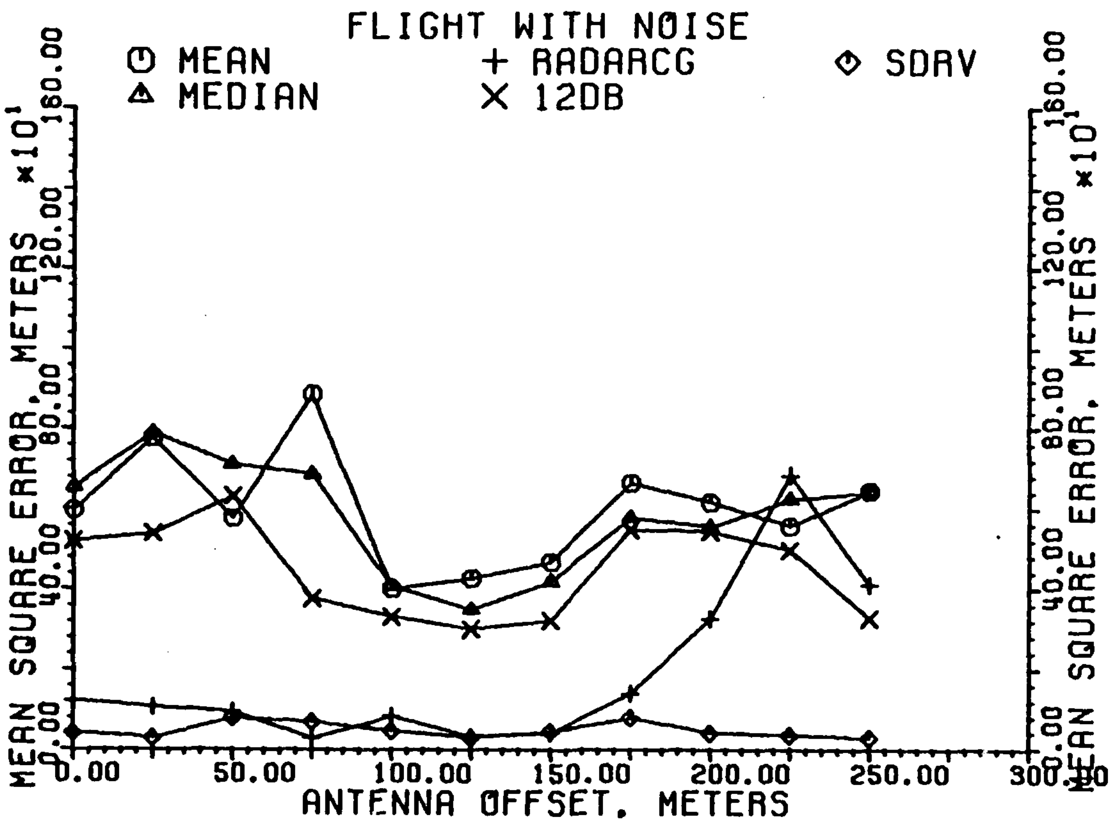

Figure 5-186. Mean square error of estimators in meters for a granularity of 49 beam pointing locations. Each data point is the result of one flight, all scans with a SNR at or below 10 dB used.

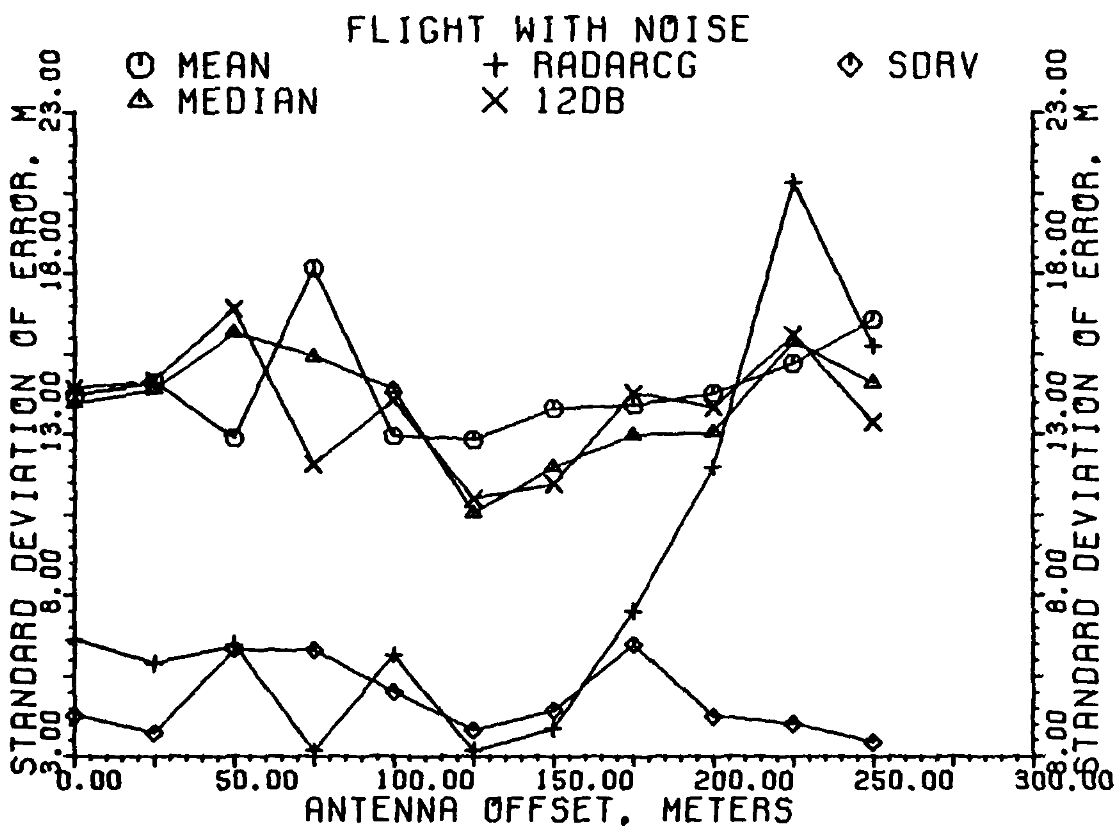

Figure 5-187. Standard deviation of error of estimators in meters for a granularity of 49 beam pointing locations. Each data point is the result of one flight, all scans with a SNR at or below 10 dB used.

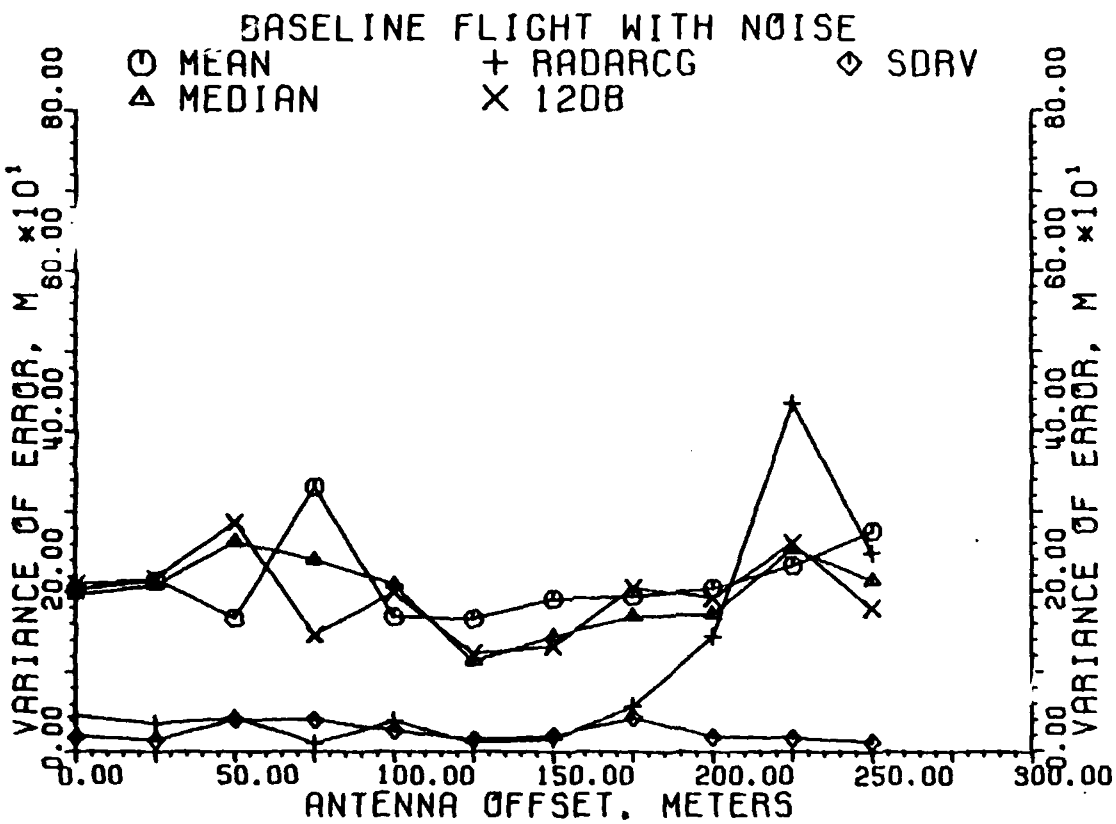

Figure 5-188. Variance of error of estimators in meters for a granularity of 49 beam pointing locations. Each data point is the result of one flight, all scans with a SNR at or below 10 dB used.

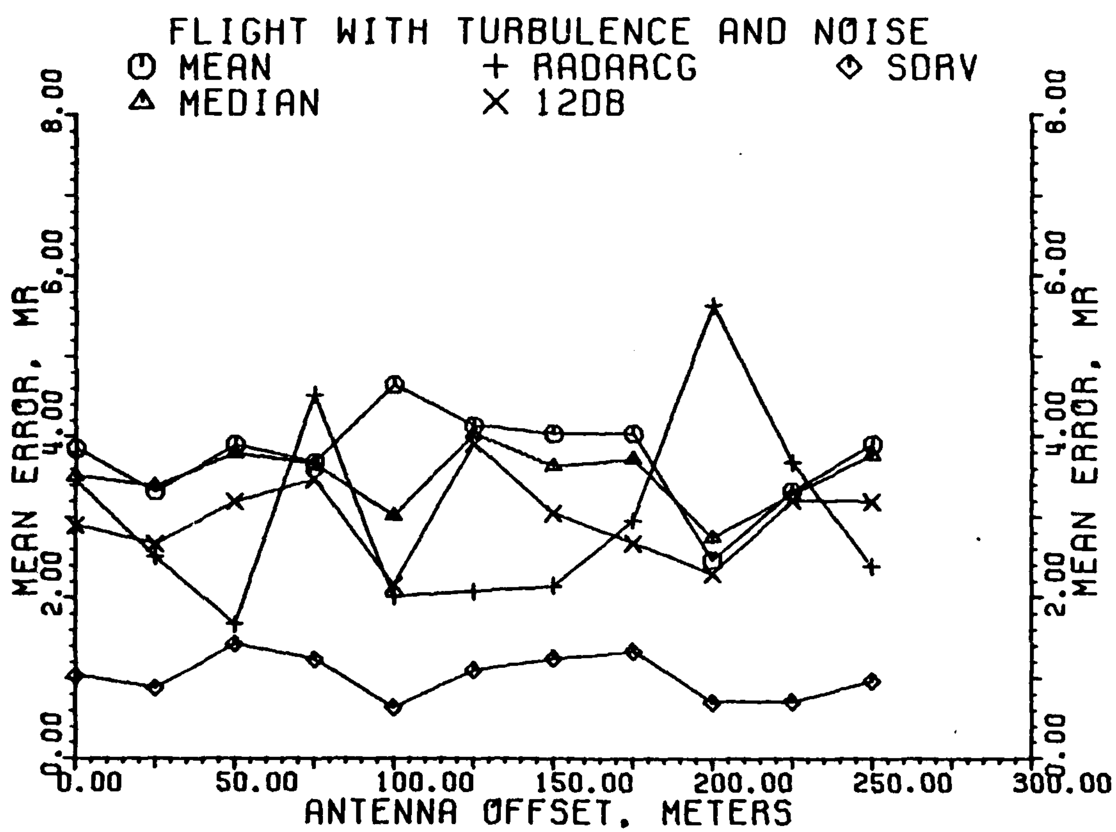

Figure 5-189. Mean error of estimators in milliradians for a granularity of 49 beam pointing locations. Each data point is the result of one flight, all scans with a SNR at or below 10 dB used.

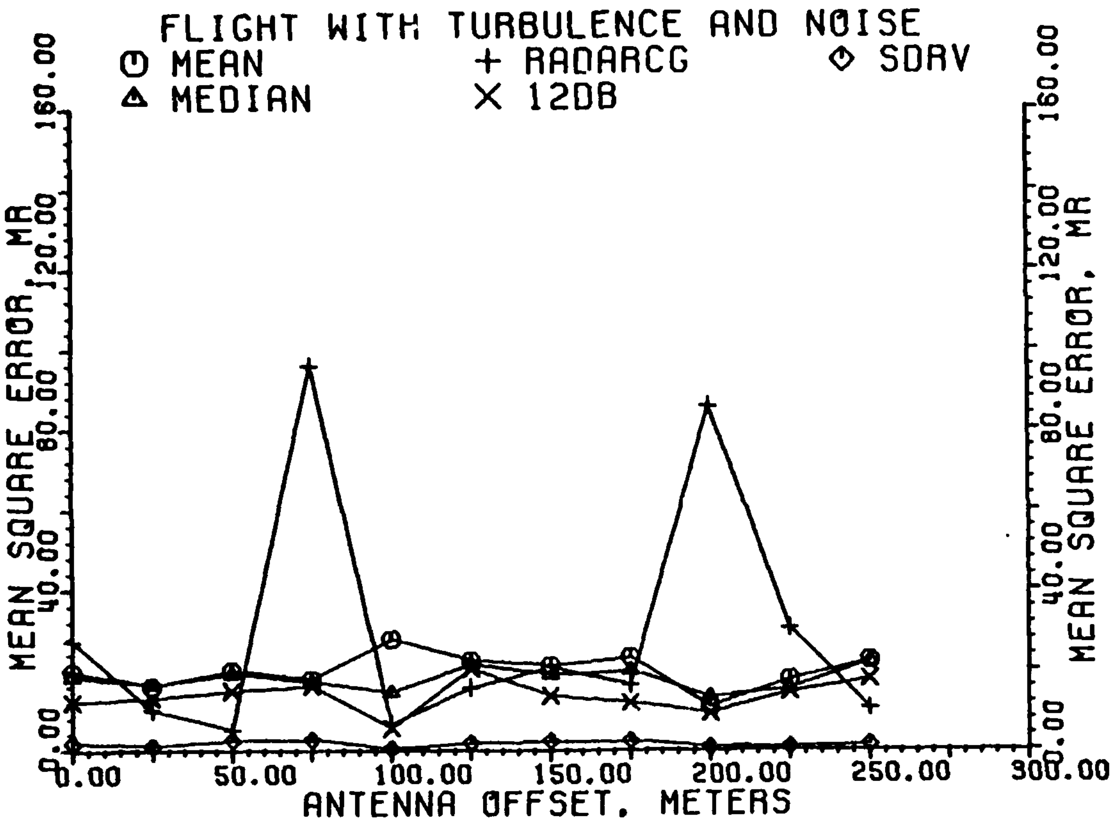

Figure 5-190. Mean square error of estimators in milliradians for a granularity of 49 beam pointing locations. Each data point is the result of one flight, all scans with a SNR at or below 10 dB used.

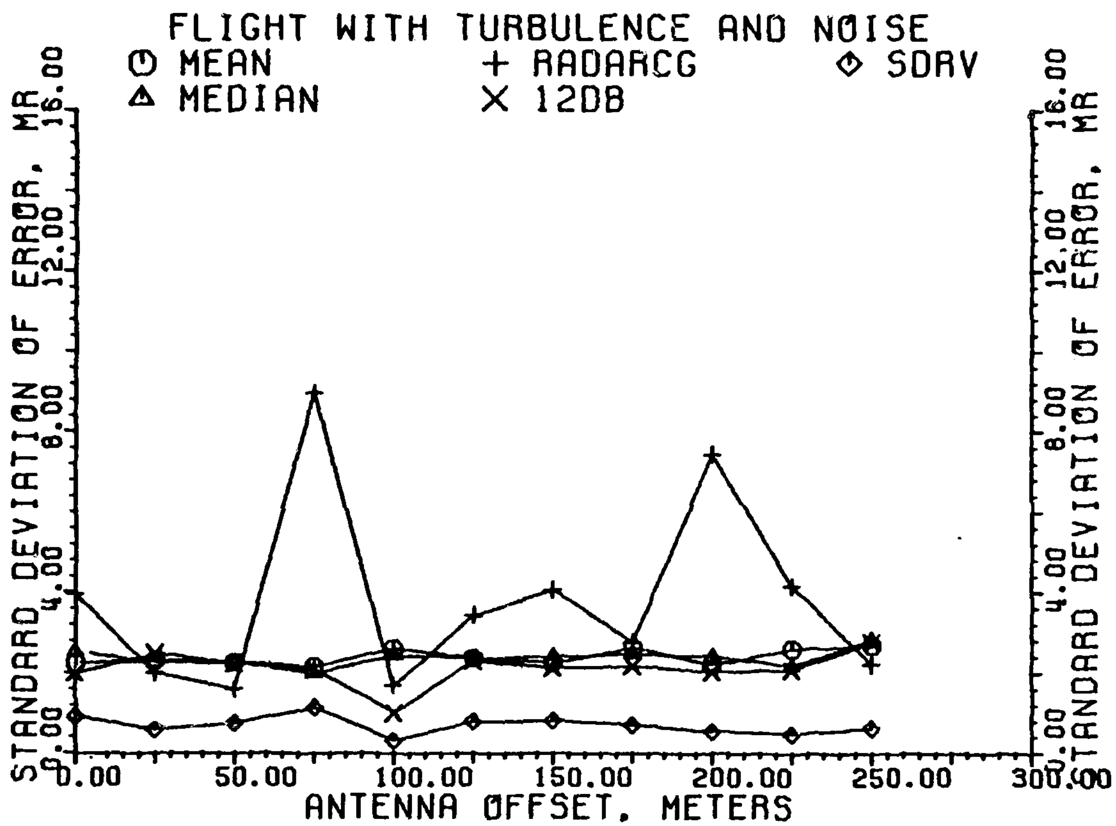

Figure 5-191. Standard deviation of error of estimators in milliradians for a granularity of 49 beam pointing locations. Each data point is the result of one flight, all scans with a SNR at or below 10 dB used.

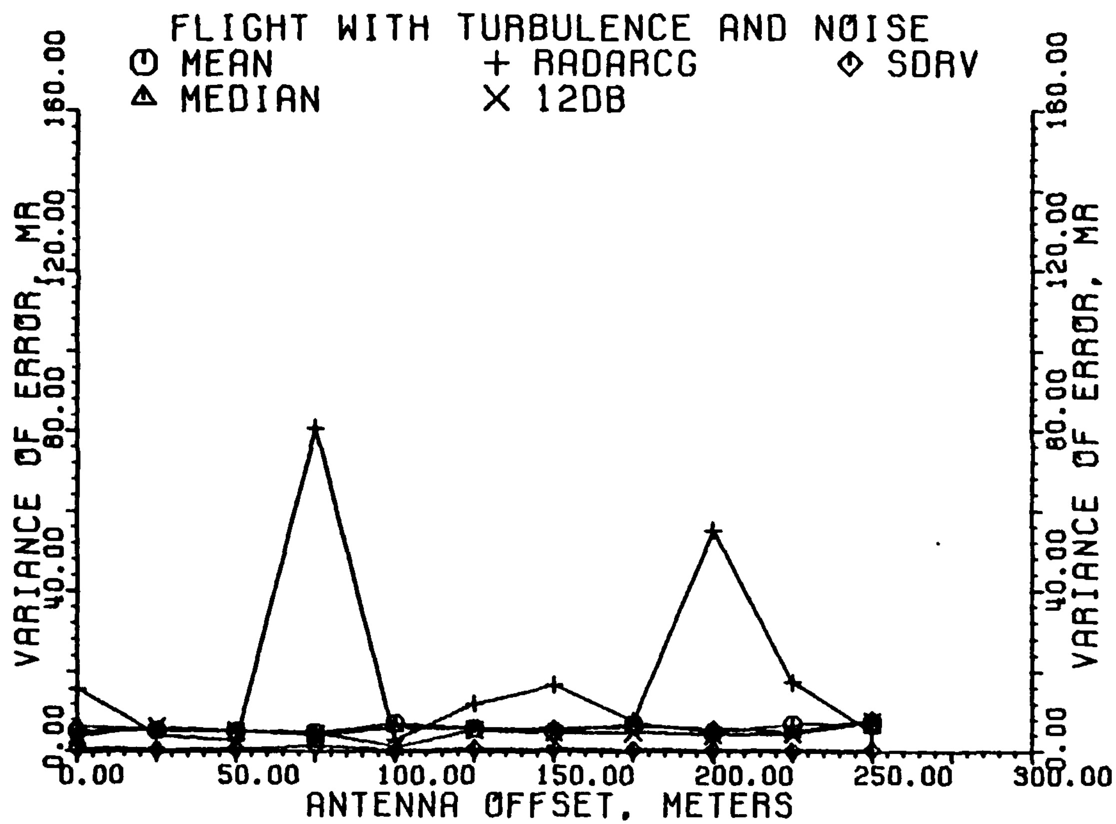

Figure 5-192. Variance of error of estimators in milliradians for a granularity of 49 beam pointing locations. Each data point is the result of one flight, all scans with a SNR at or below 10 dB used.

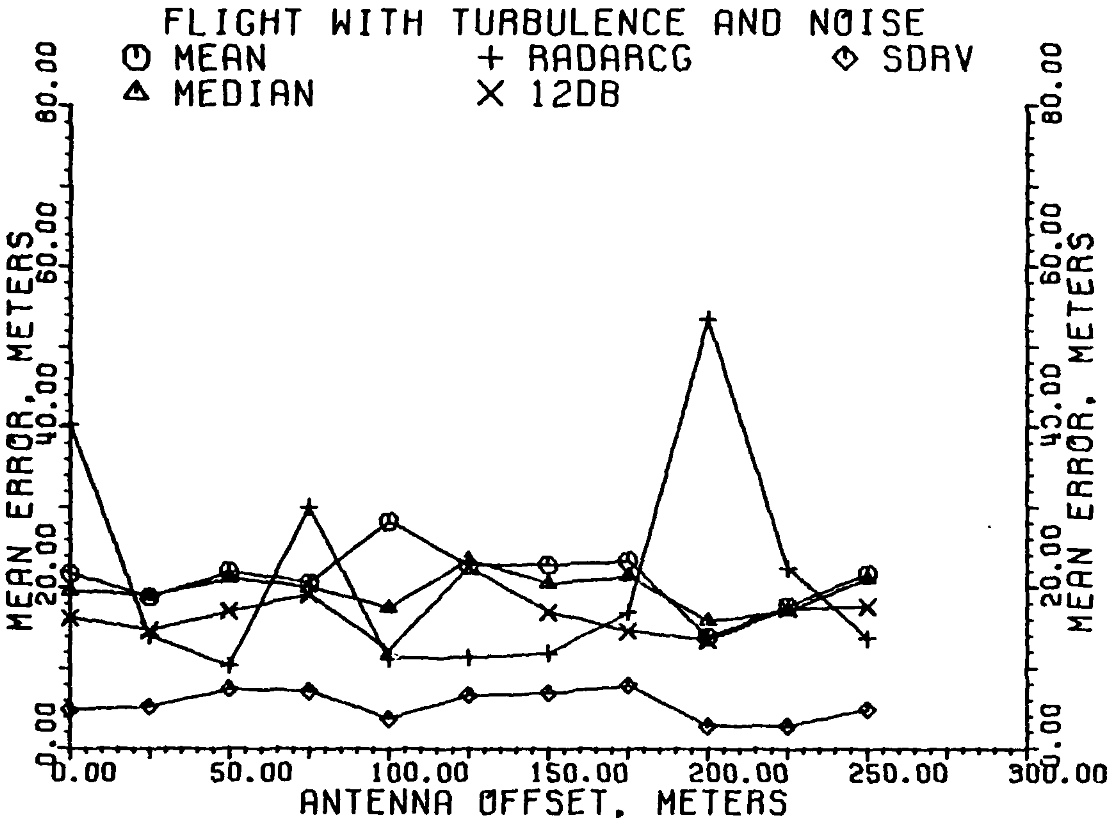

Figure 5-193. Mean error of estimators in meters for a granularity of 49 beam pointing locations. Each data point is the result of one flight, all scans with a SNR at or below 10 dB used.

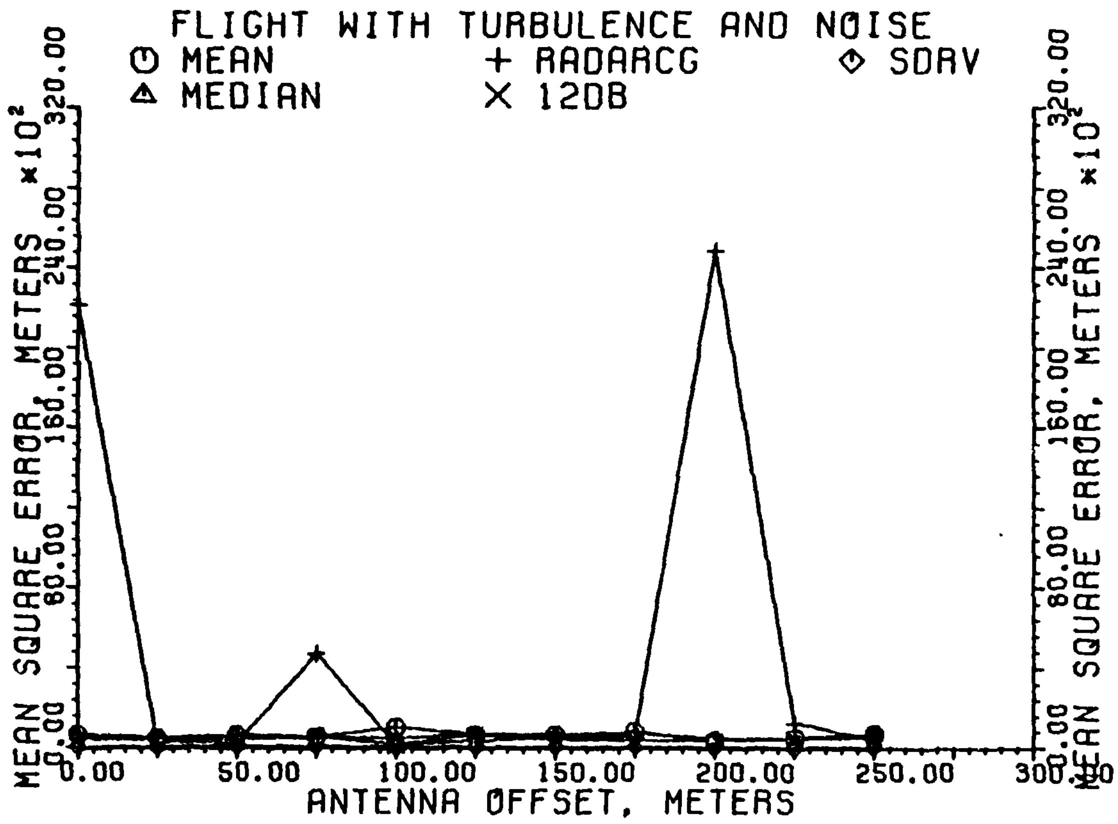

Figure 5-194. Mean square error of estimators in meters for a granularity of 49 beam pointing locations. Each data point is the result of one flight, all scans with a SNR at or below 10 dB used.

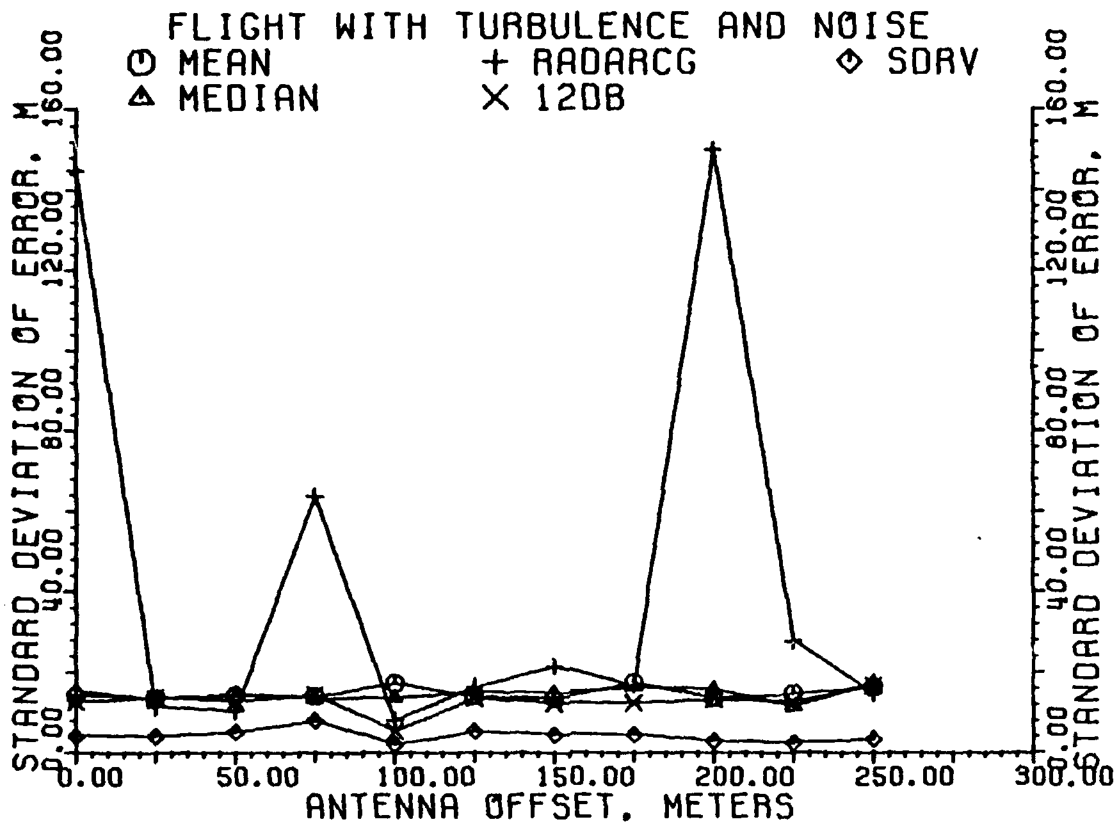

Figure 5-195. Standard deviation of error of estimators in meters for a granularity of 49 beam pointing locations. Each data point is the result of one flight, all scans with a SNR at or below 10 dB used.

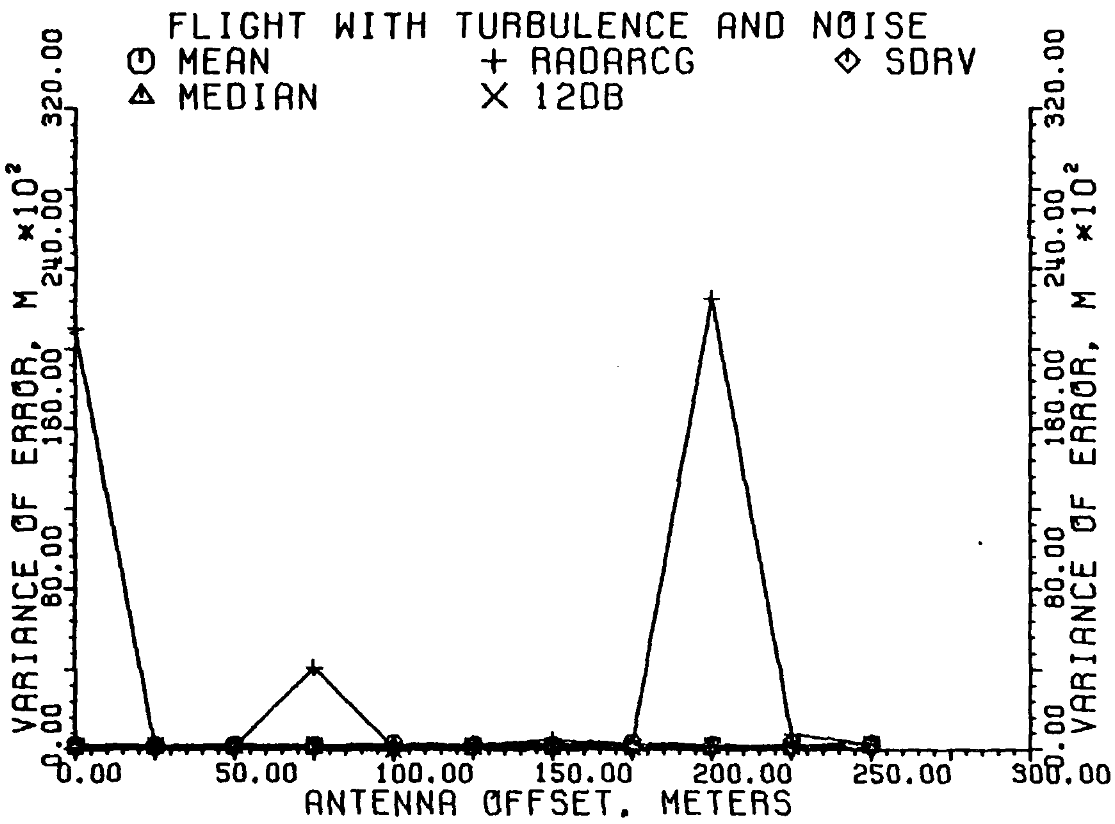

Figure 5-196. Variance of error of estimators in meters for a granularity of 49 beam pointing locations. Each data point is the result of one flight, all scans with a SNR at or below 10 dB used.

derivative estimator, using only those scans at or below 10 dB, is still more accurate than the thresholding methods in baseline flights, Figures 5-133 through 5-140.

Since there was little or no effect of antenna location on the error of the estimators, we shall consider the effect of scan granularity on error for only one antenna location which shall be 125 meters from the runway centerline. For the next 32 figures, all scans will be included in the analysis regardless of scan SNR.

The errors plotted as a function of granularity for baseline flights are shown in Figures 5-197 through 5-204. The most surprising aspect of these plots is that there is no decrease in error with the increase in scanning granularity, except for SDRV which generally improves with the finer granularities. It would then appear that, on the average, the limit of accuracy for the thresholding methods, RADARCG, and SDRV is 3 mr, 0.4 mrad, and 0 mrad, respectively, as shown by Figure 5-197. The standard deviation and variance also show little change with the exception of SDRV, which decreases.

Figures 5-205 through 5-212 are the results of the baseline flights with noise. The thresholding estimators do not increase in accuracy with an increase in granularity, but rather converge on a value of error. Both the second derivative and RADARCG improve with finer granularities. The second derivative has an increase in error between the granularities of 9 and 23, when there is only one beam location in each window. Two beam locations are in each window with granularities of 23 through 29, three beam locations are used from 31 to 45, and granularities of 47 and 49 use four beam locations in each window. Note that the error is a relative

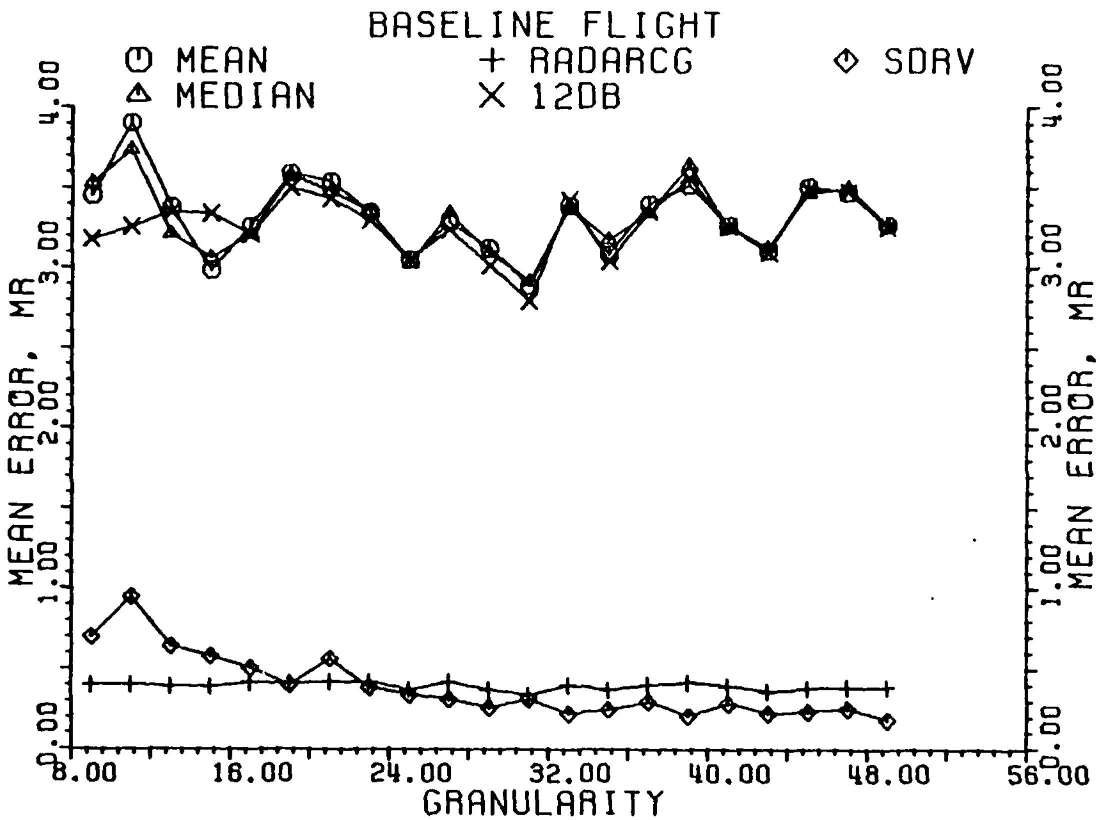

Figure 5-197. Mean error of estimators in milliradians with the antenna located 125 M from the runway centerline. Each data point is the result of one flight, all scans used.

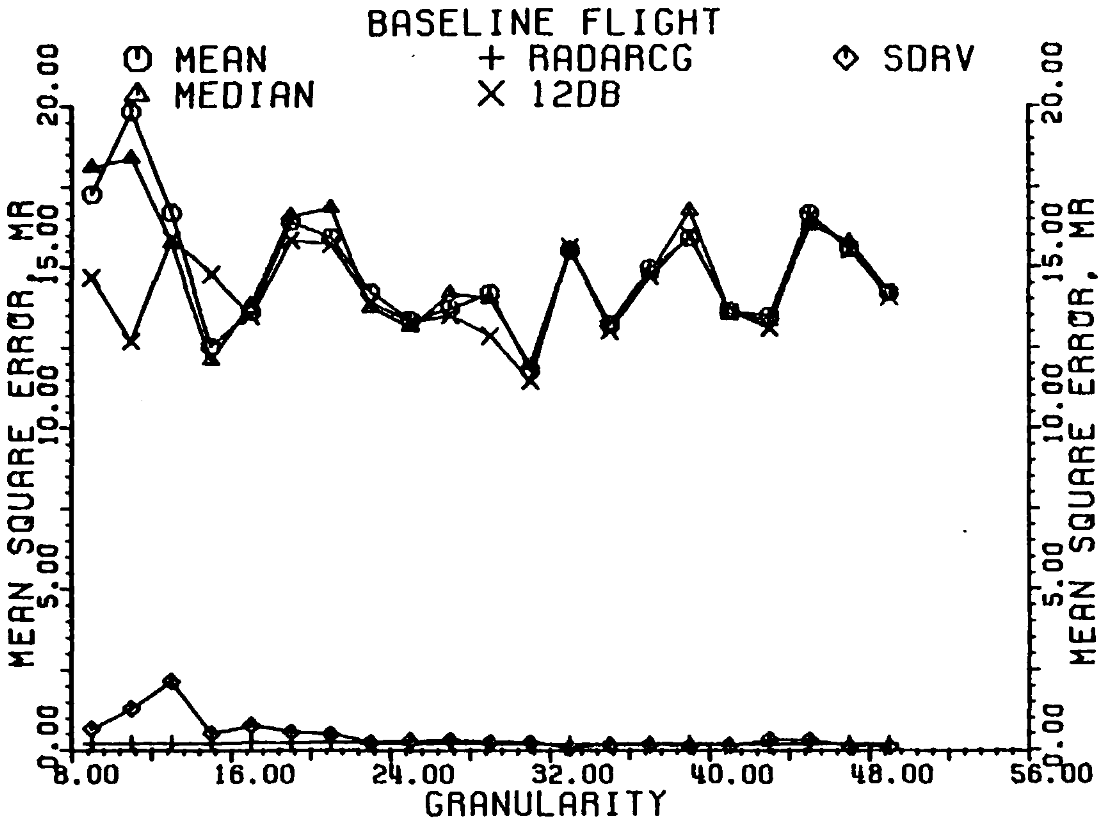

Figure 5-198. Mean square error of estimators in milliradians with the antenna located 125 M from the runway centerline. Each data point is the result of one flight, all scans used.

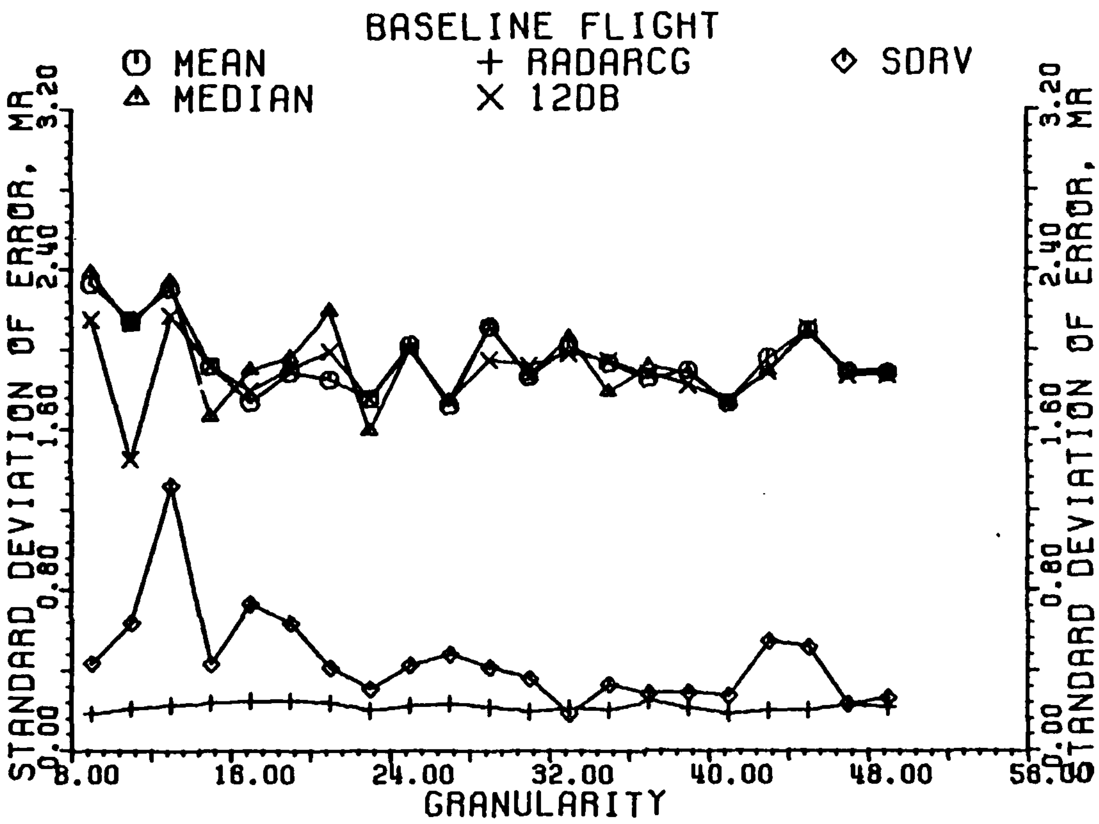

Figure 5-199. Standard deviation of error of estimators in milliradians with the antenna located 125 M from the runway centerline. Each data point is the result of one flight, all scans used.

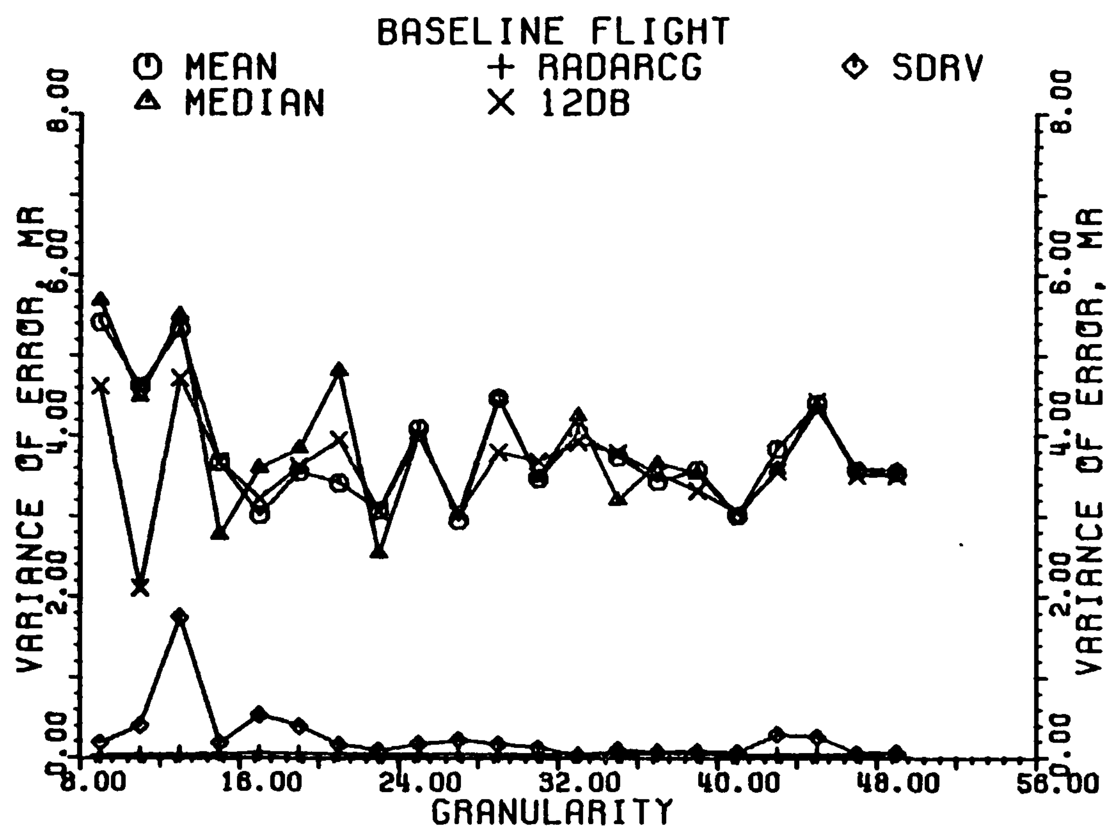

Figure 5-200. Variance of error of estimators in milliradians with the antenna located 125 M from the runway centerline. Each data point is the result of one flight, all scans used.

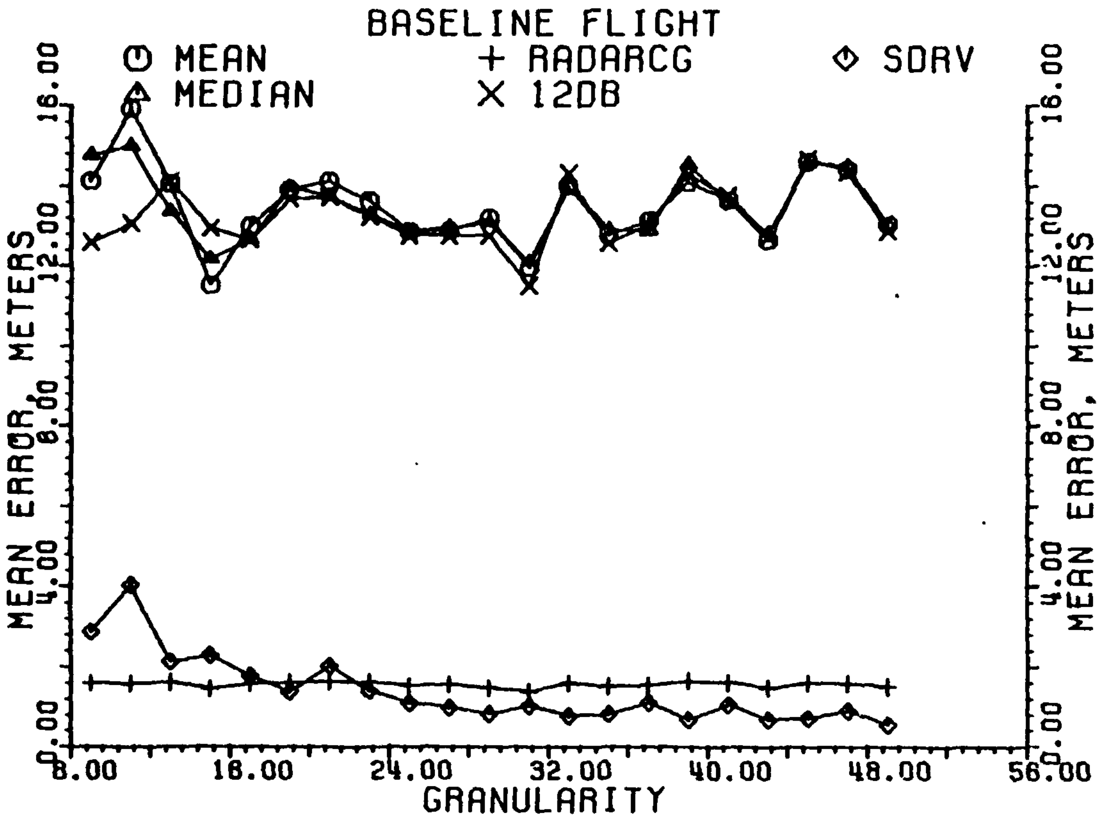

Figure 5-201. Mean error of estimators in meters with the antenna located 125 M from the runway centerline. Each data point is the result of one flight, all scans used.

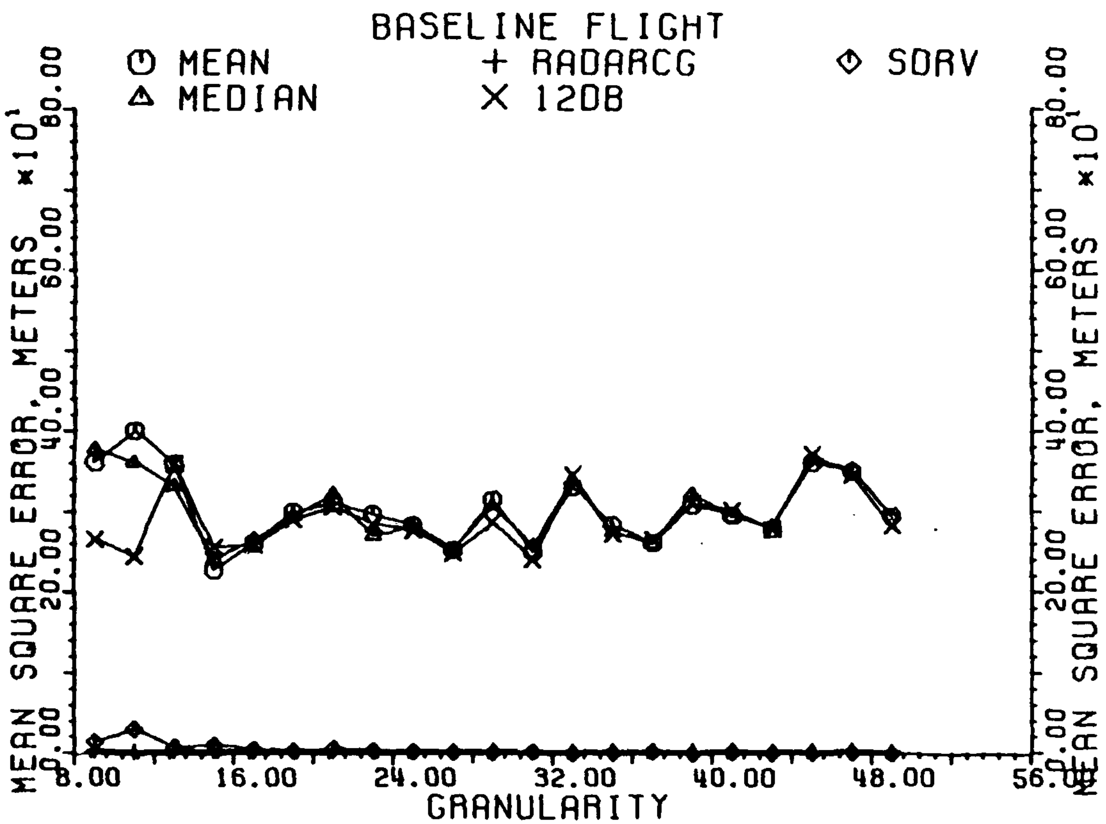

Figure 5-202. Mean square error of estimators in meters with the antenna located 125 M from the runway centerline. Each data point is the result of one flight, all scans used.

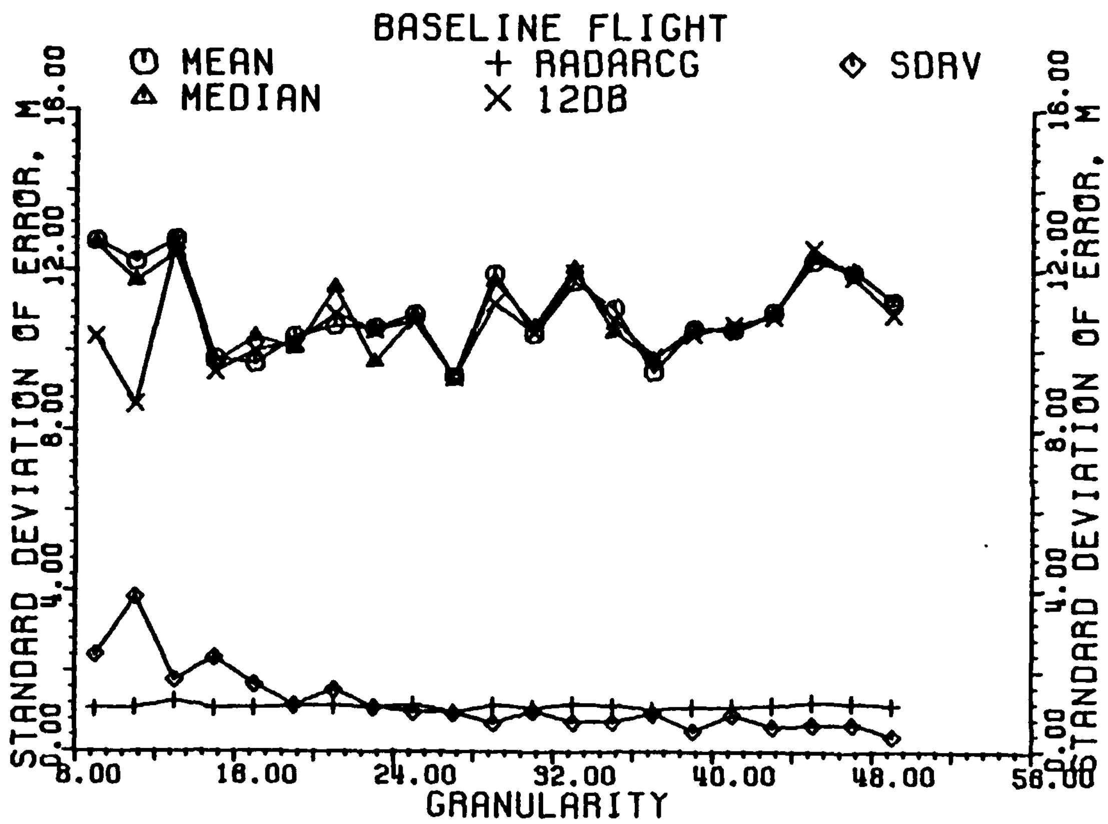

Figure 5-203. Standard deviation of error of estimators in meters with the antenna located 125 M from the runway centerline. Each data point is the result of one flight, all scans used.

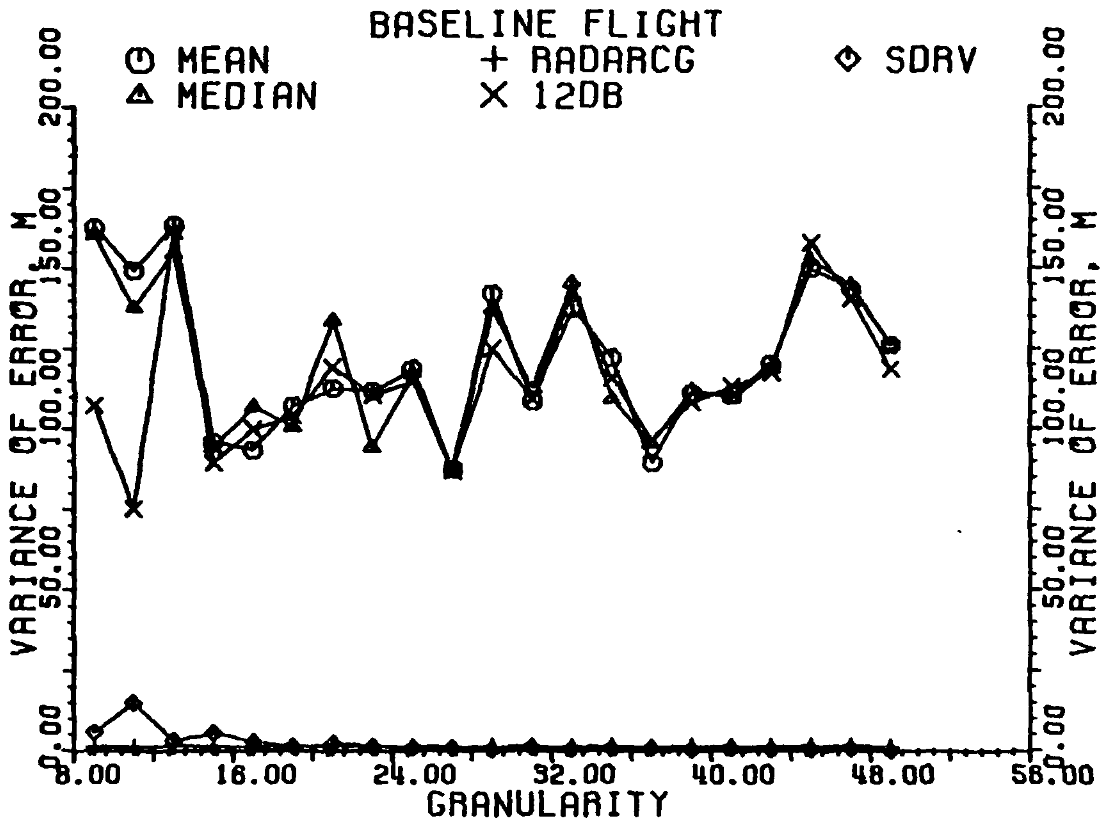

Figure 5-204. Variance of error of estimators in meters with the antenna located 125 M from the runway centerline. Each data point is the result of one flight, all scans used.

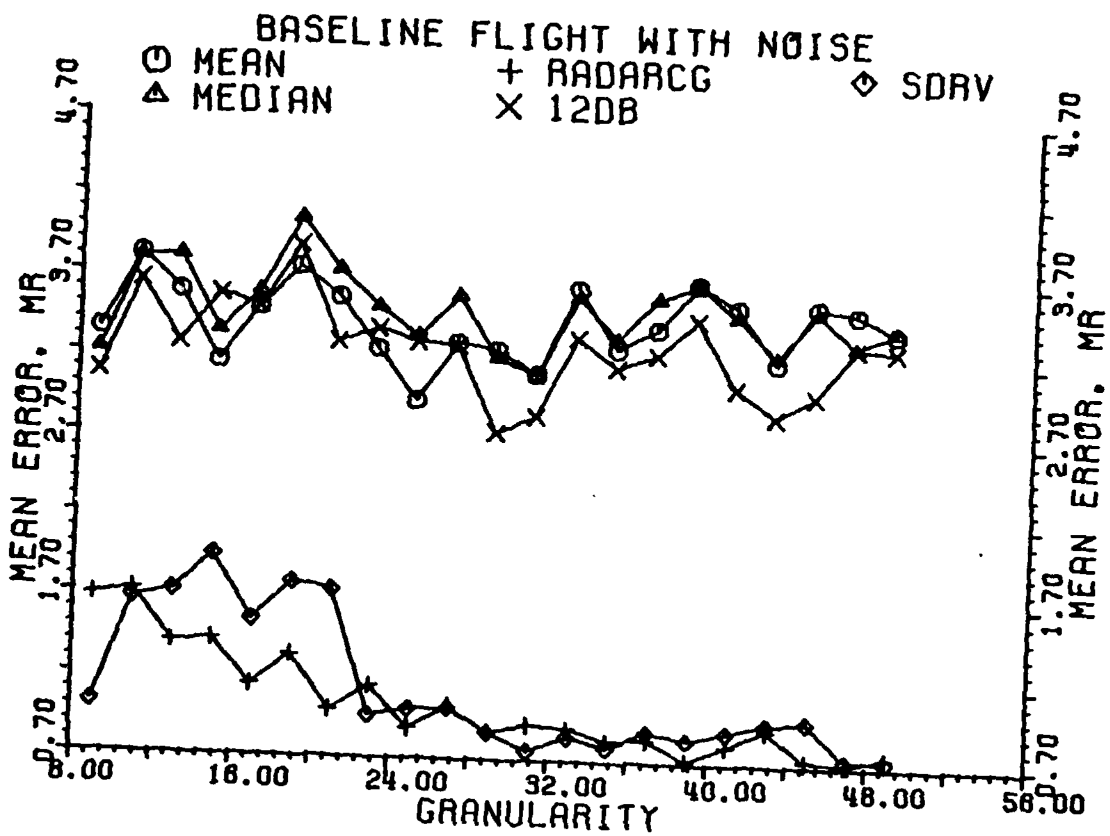

Figure 5-205. Mean error of estimators in milliradians with the antenna located 125 M from the runway centerline. Each data point is the result of one flight, all scans used.

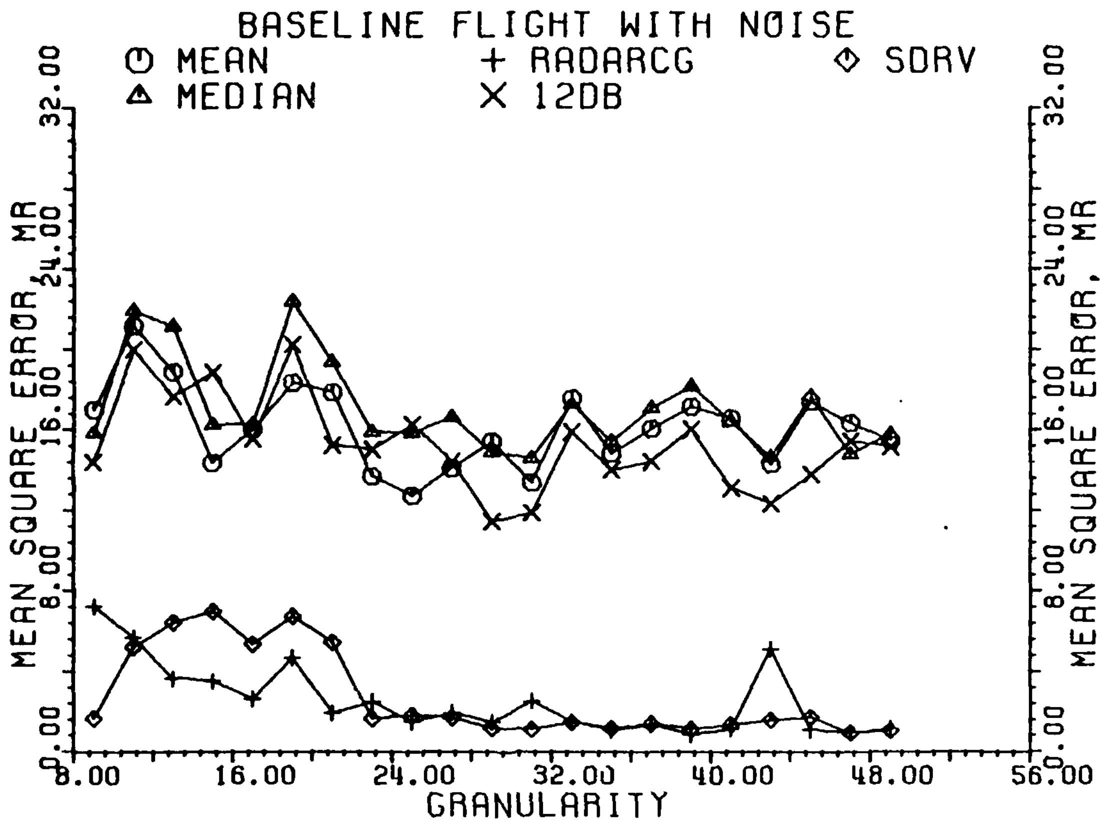

Figure 5-206. Mean square error of estimators in milliradians with the antenna located 125 M from the runway centerline. Each data point is the result of one flight, all scans used.

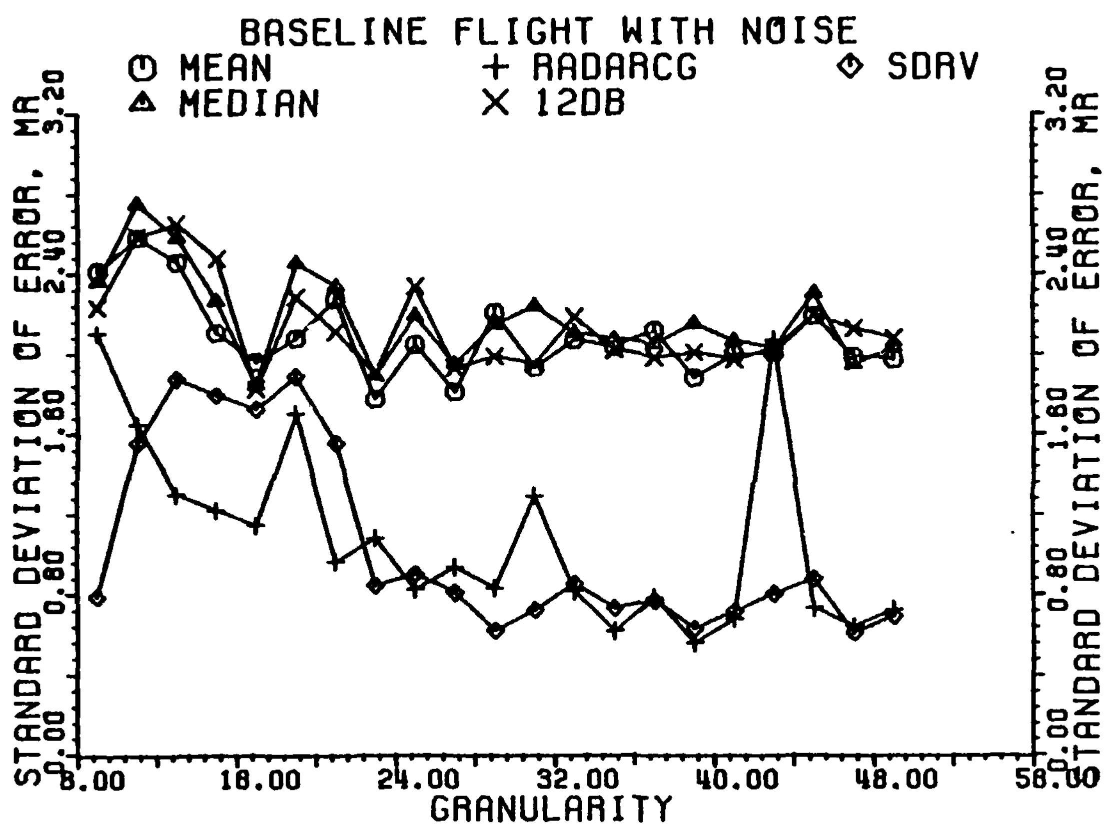

Figure 5-207. Standard deviation of error of estimators in milliradians with the antenna located 125 M from the runway centerline. Each data point is the result of one flight, all scans used.

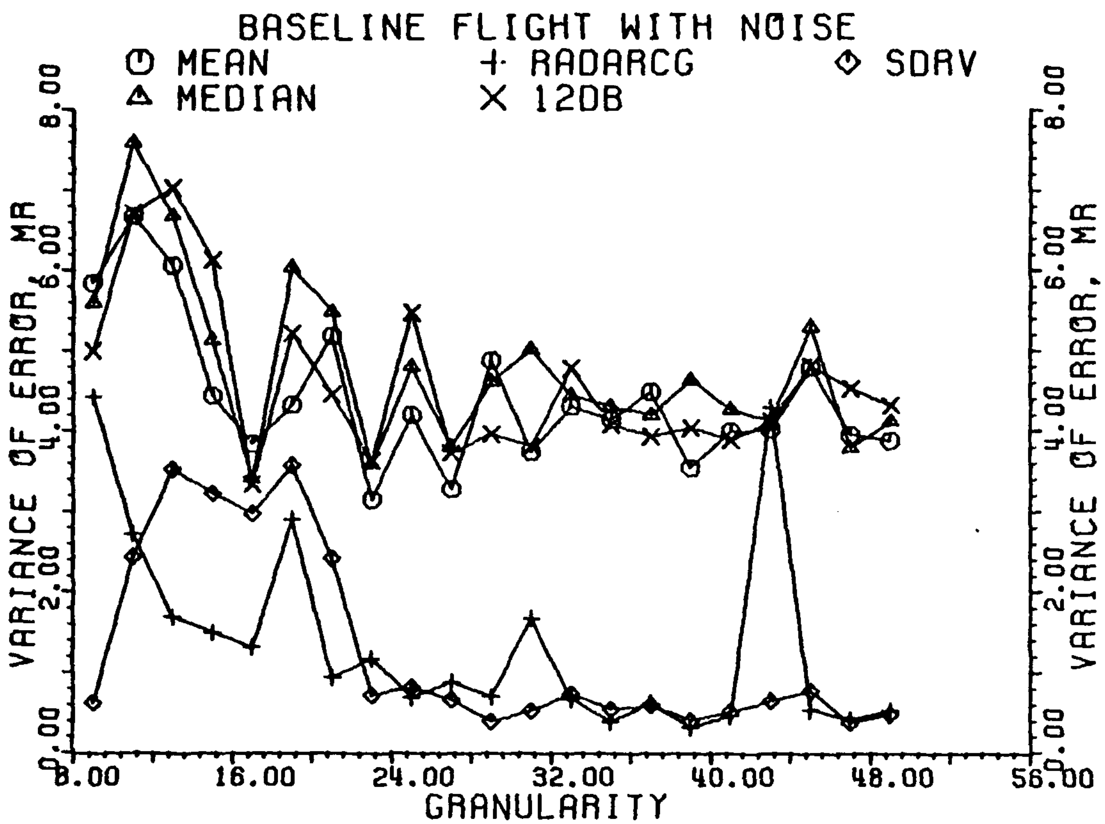

Figure 5-208. Variance of error of estimators in milliradians with the antenna located 125 M from the runway centerline. Each data point is the result of one flight, all scans used.

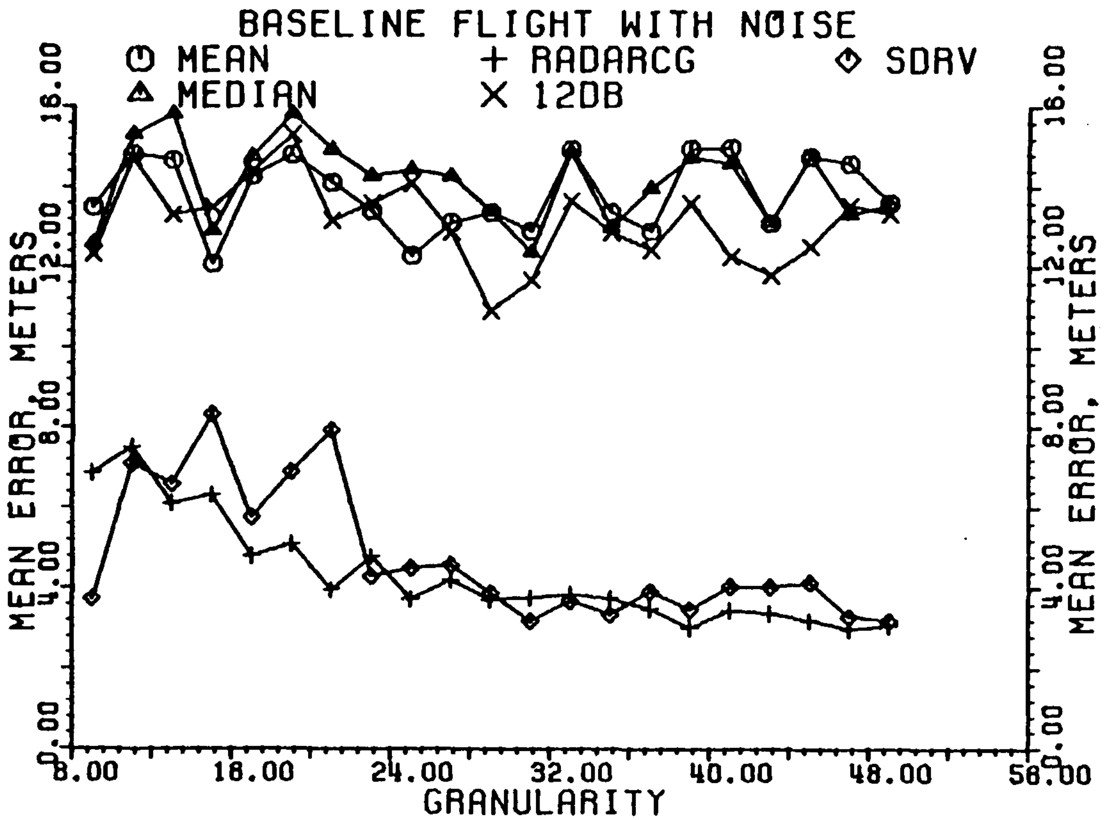

Figure 5-209. Mean error of estimators in meters with the antenna located 125 M from the runway centerline. Each data point is the result of one flight, all scans used.

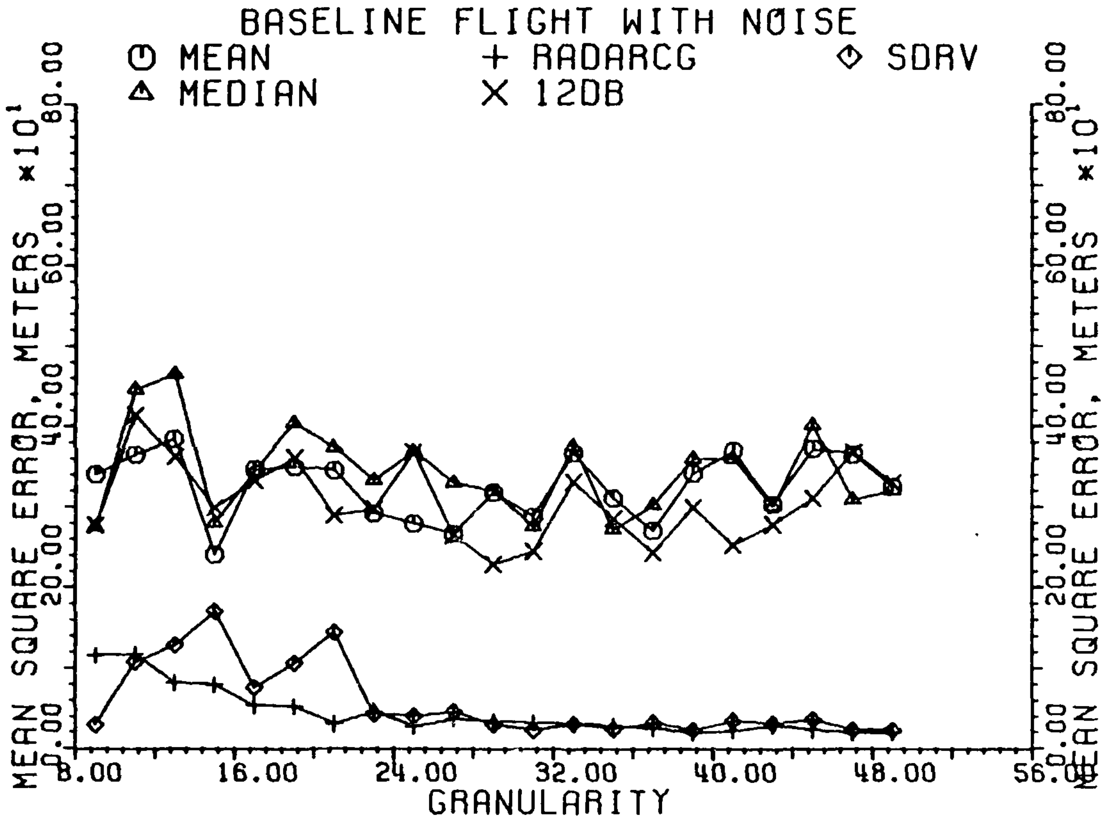

Figure 5-210. Mean square error of estimators in meters with the antenna located 125 M from the runway centerline. Each data point is the result of one flight, all scans used.

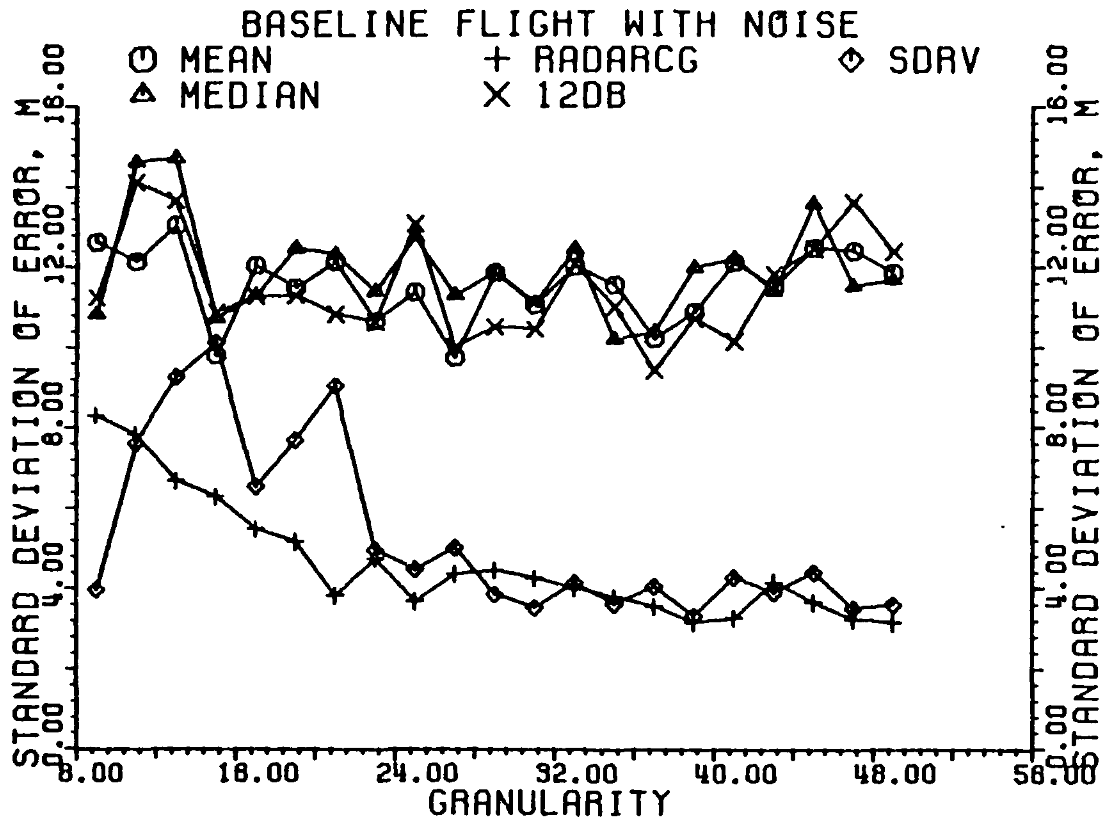

Figure 5-211. Standard deviation of error of estimators in meters with the antenna located 125 M from the runway centerline. Each data point is the result of one flight, all scans used.

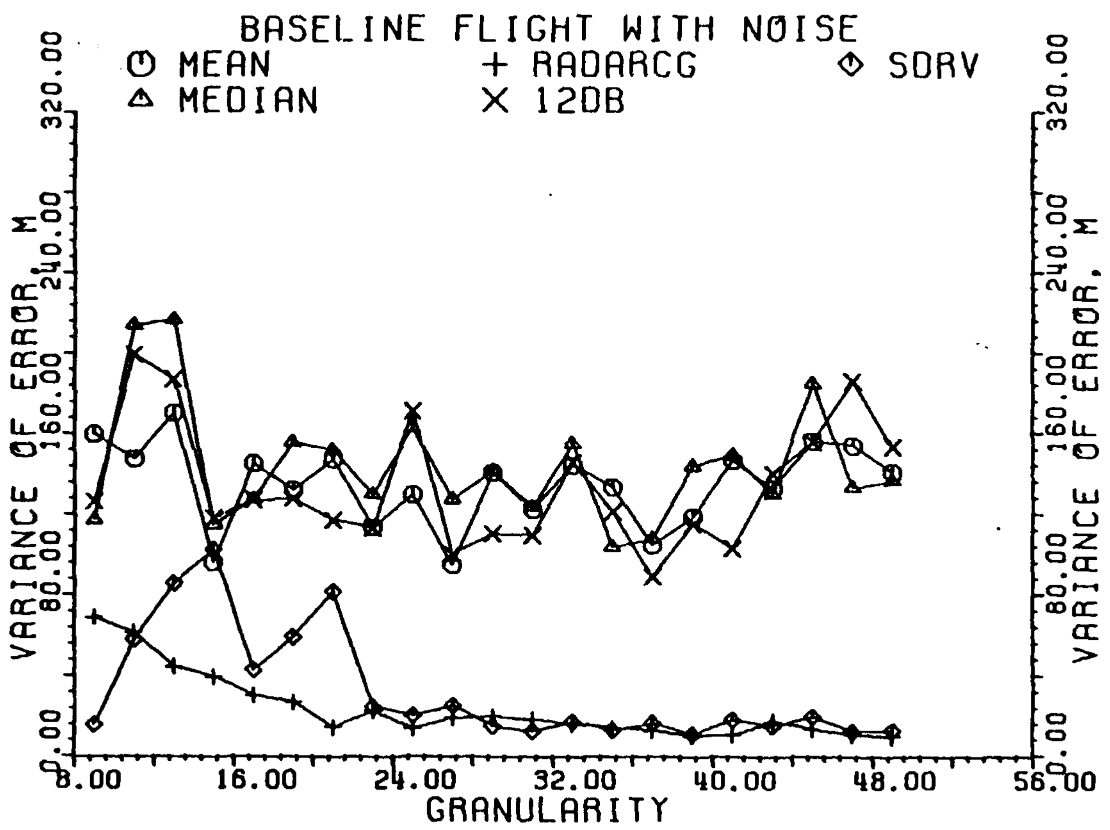

Figure 5-212. Variance of error of estimators in meters with the antenna located 125 M from the runway centerline. Each data point is the result of one flight, all scans used.

minimum at granularities of 9, 23, 3[illegible], and 47. This implies that the coarsest granularity for the windows to hold a desired number of beam locations should be used to minimize error. This result is to be expected. The second derivative method is scan shape oriented, and works best when the four windows just fit into half of the scan return. Shrinking the size of the windows in angle makes it more difficult for the algorithm to detect the maximum slope, and easier to trigger on noise. Spreading out the windows forces any major change in signal strength to the target related, not noise related. Therefore, the coarser the granularity the better the algorithm works for a given number of beam locations in each window. The most favorable granularity is the antenna null-to-null beamwidth divided by the number of beam pointing locations minus one.

The flights with turbulence, Figures 5-213 through 5-220, again show little change from the baseline flights.

The flights with turbulence and noise, Figures 5-221 through 5-228, again show the second derivative to be the best estimator, especially with the finer granularities. The thresholding methods are still close to each other, but the 12 dB method appears best, followed by the mean. RADARCG is a bit unusual, as the mean error in both milliradians and meters, Figures 5-221 and 5-225, show it to be quite good, yet the deviation and variance of the estimator is quite poor, especially in actual meter error, Figures 5-227 and 5-228. The difference between the mean error in meters, Figure 5-225, and the mean-square error, Figure 5-226, is quite large, indicating that when RADARCG missed the target, it missed by a sizeable amount.

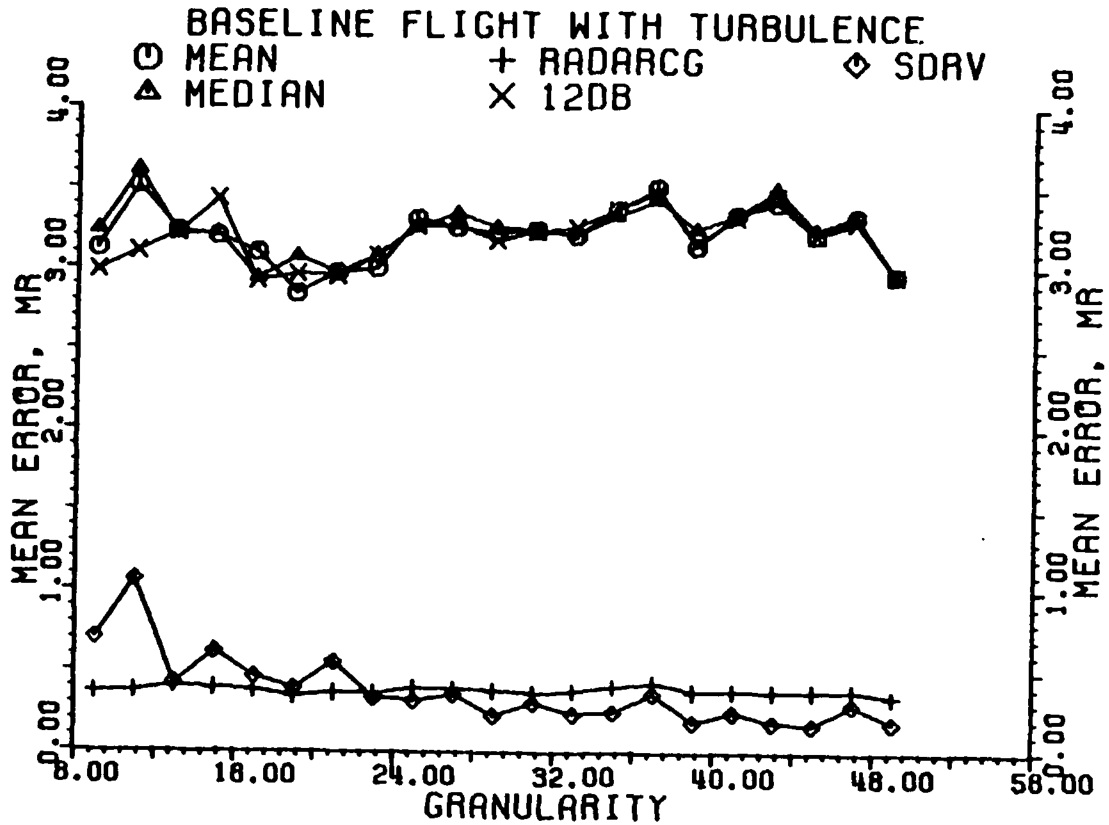

Figure 5-213. Mean error of estimators in milliradians with the antenna located 125 M from the runway centerline. Each data point is the result of one flight, all scans used.

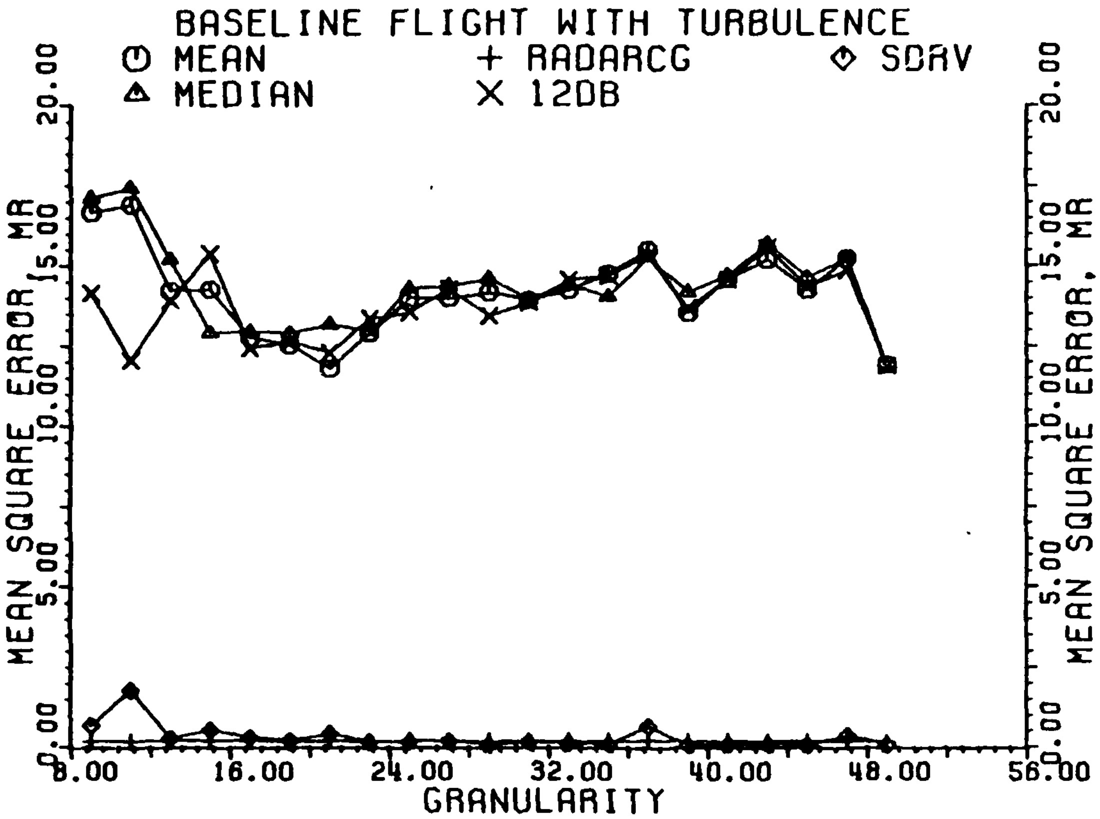

Figure 5-214. Mean square error of estimators in milliradians with the antenna located 125 M from the runway centerline. Each data point is the result of one flight, all scans used.

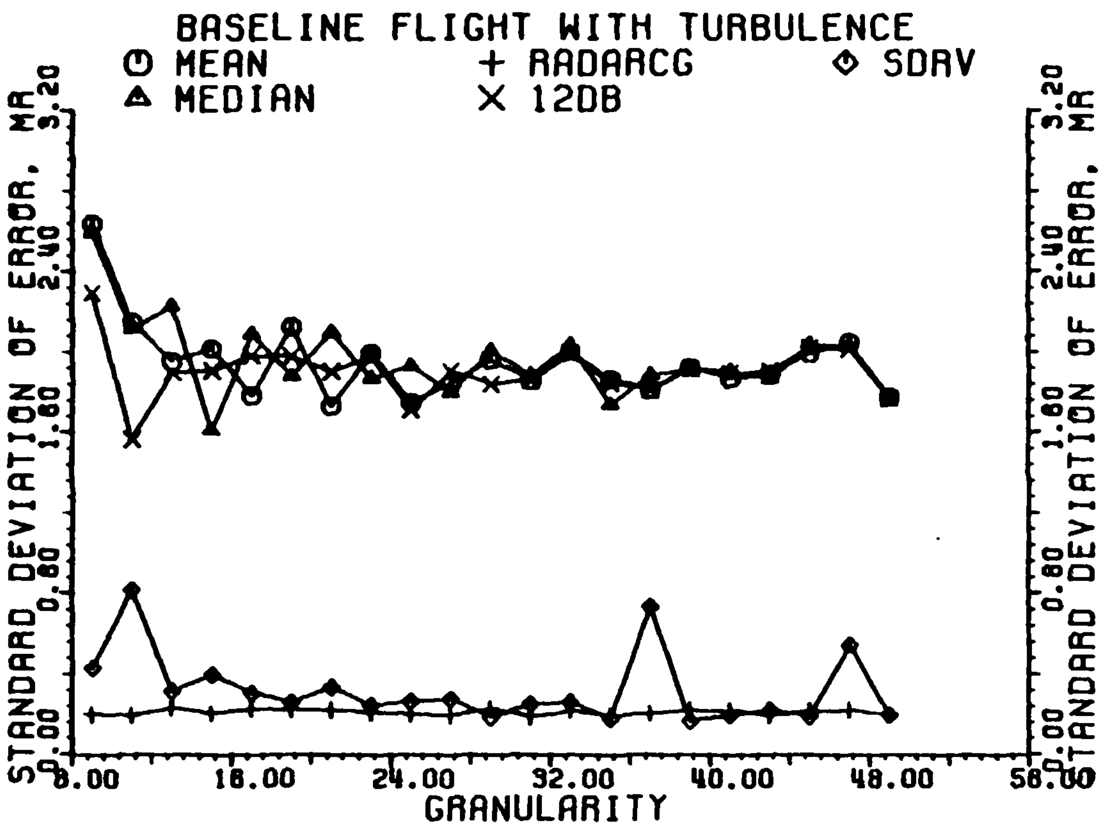

Figure 5-215. Standard deviation of error of estimators in milliradians with the antenna located 125 M from the runway centerline. Each data point is the result of one flight, all scans used.

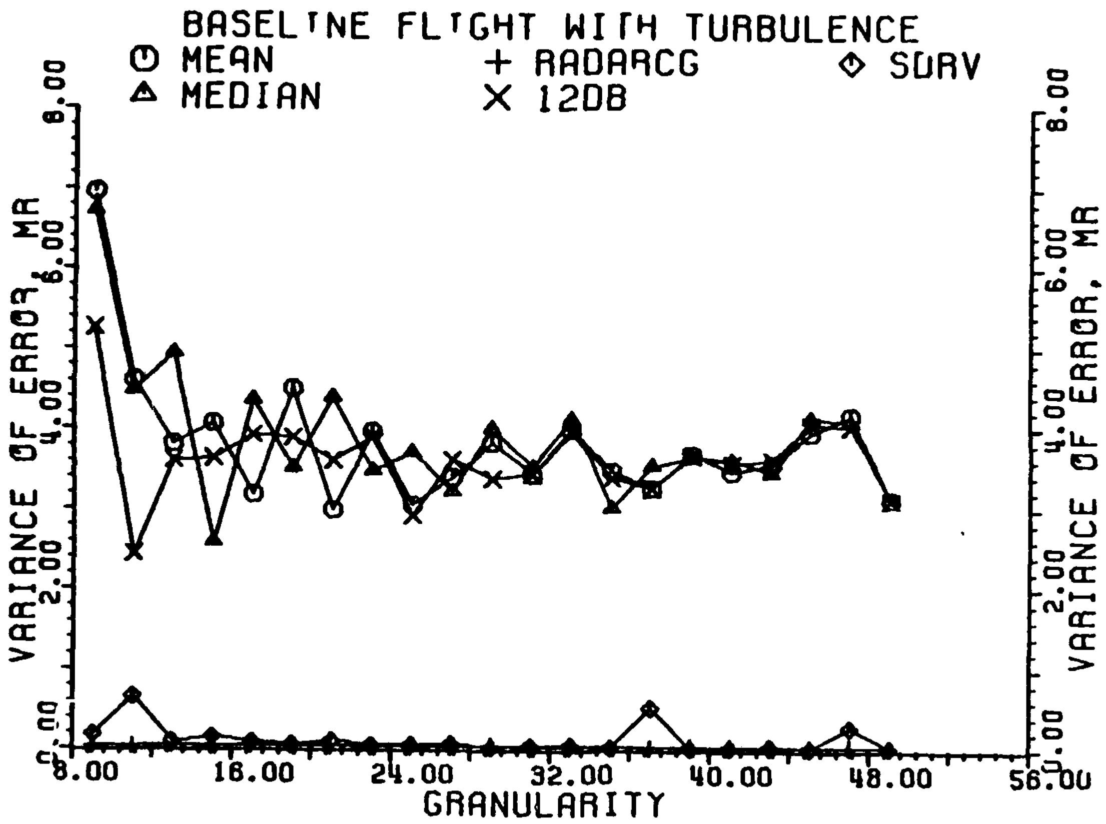

Figure 5-216. Variance of error of estimators in milliradians with the antenna located 125 M from the runway centerline. Each data point is the result of one flight, all scans used.

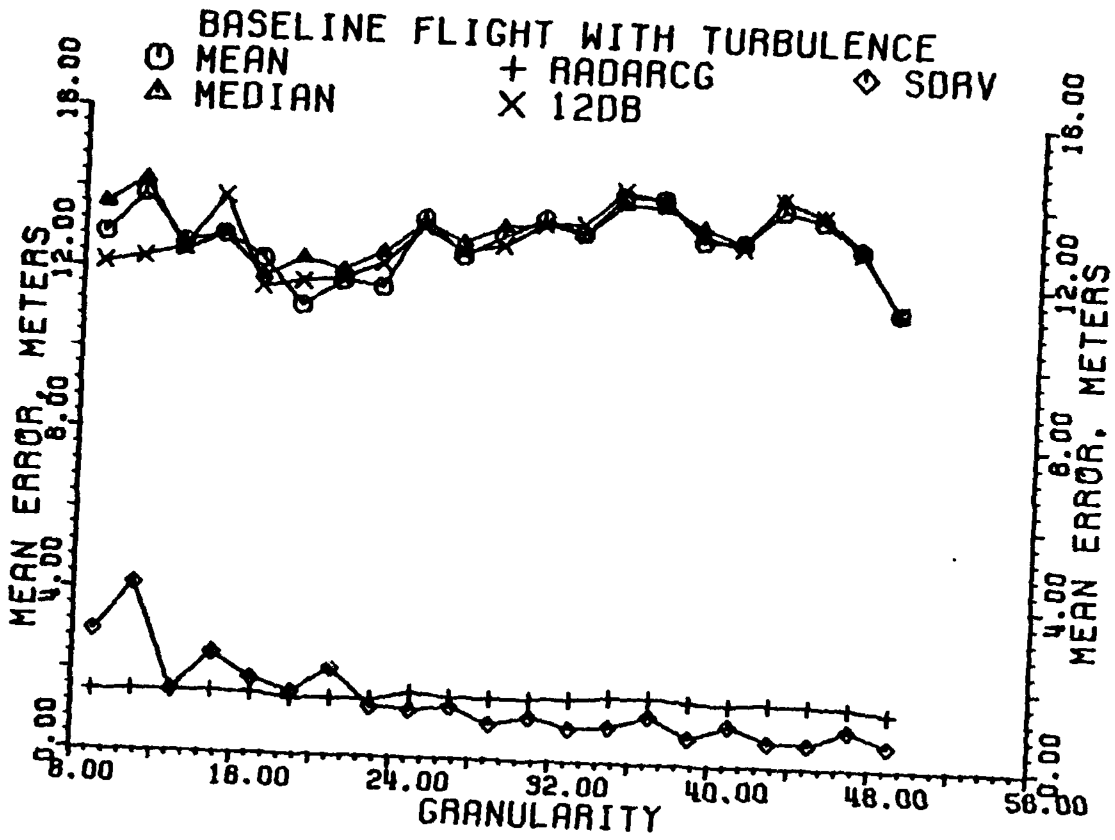

Figure 5-217. Mean error of estimators in meters with the antenna located 125 M from the runway centerline. Each data point is the result of one flight, all scans used.

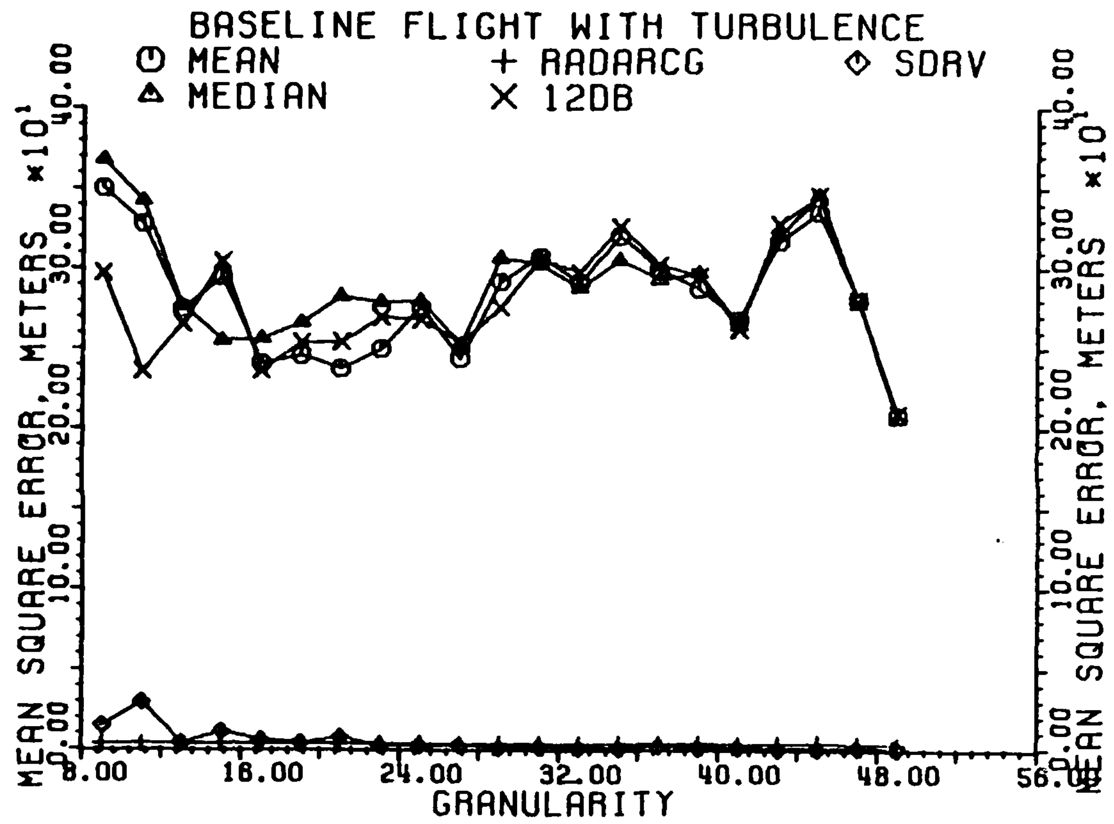

Figure 5-218. Mean square error of estimators in meters with the antenna located 125 M from the runway centerline. Each data point is the result of one flight, all scans used.

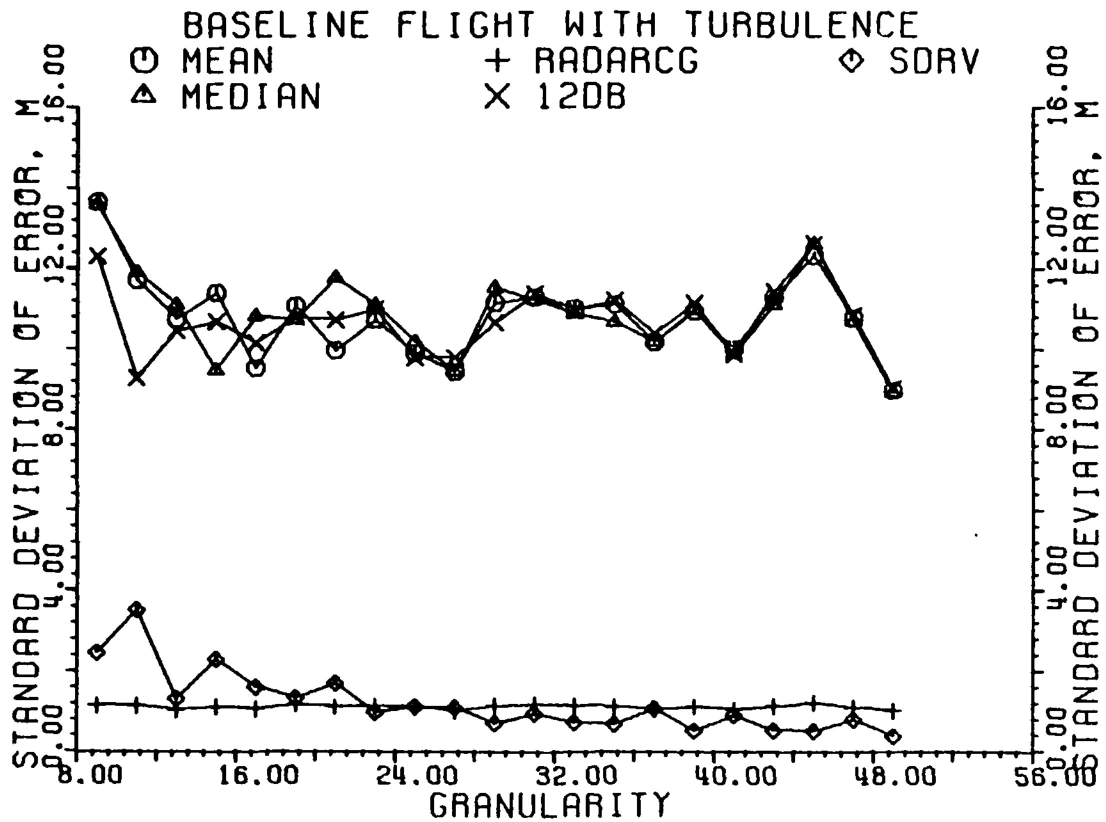

Figure 5-219. Standard deviation of error of estimators in meters with the antenna located 125 M from the runway centerline. Each data point is the result of one flight, all scans used.

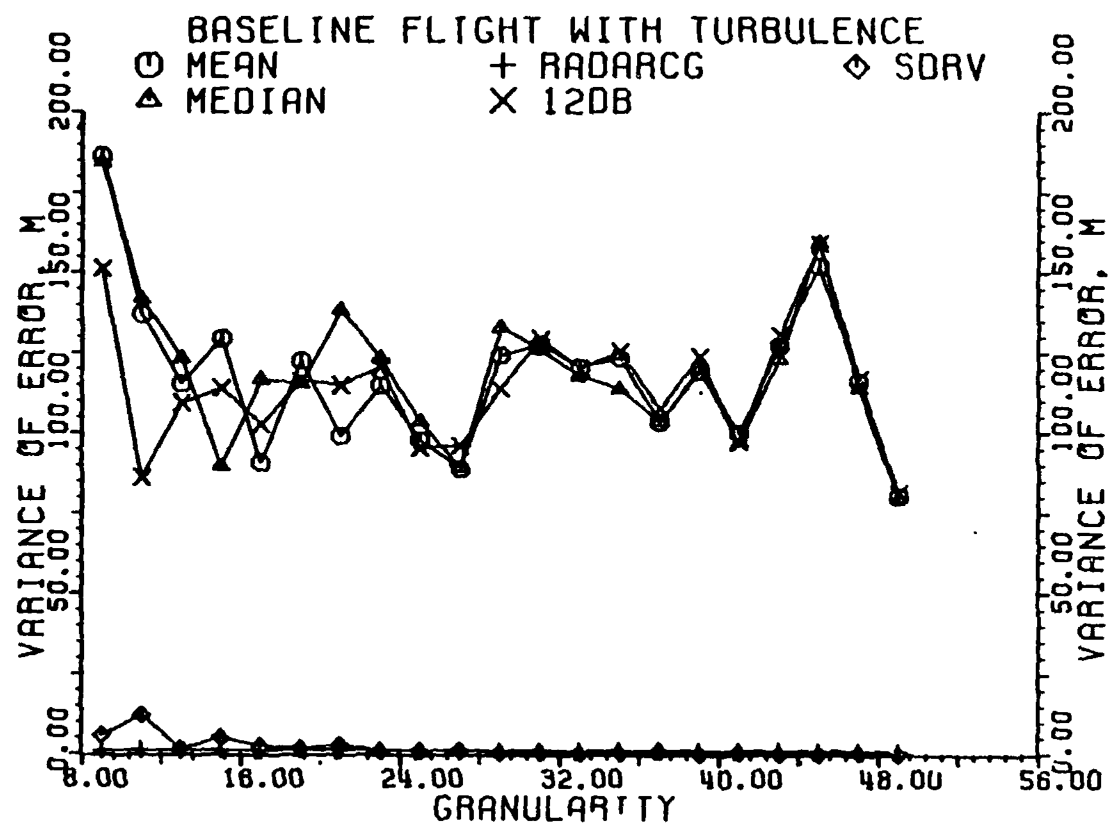

Figure 5-220. Variance of error of estimators in meters with the antenna located 125 *M from the runway* centerline. Each data point is the result of one flight, all scans used.

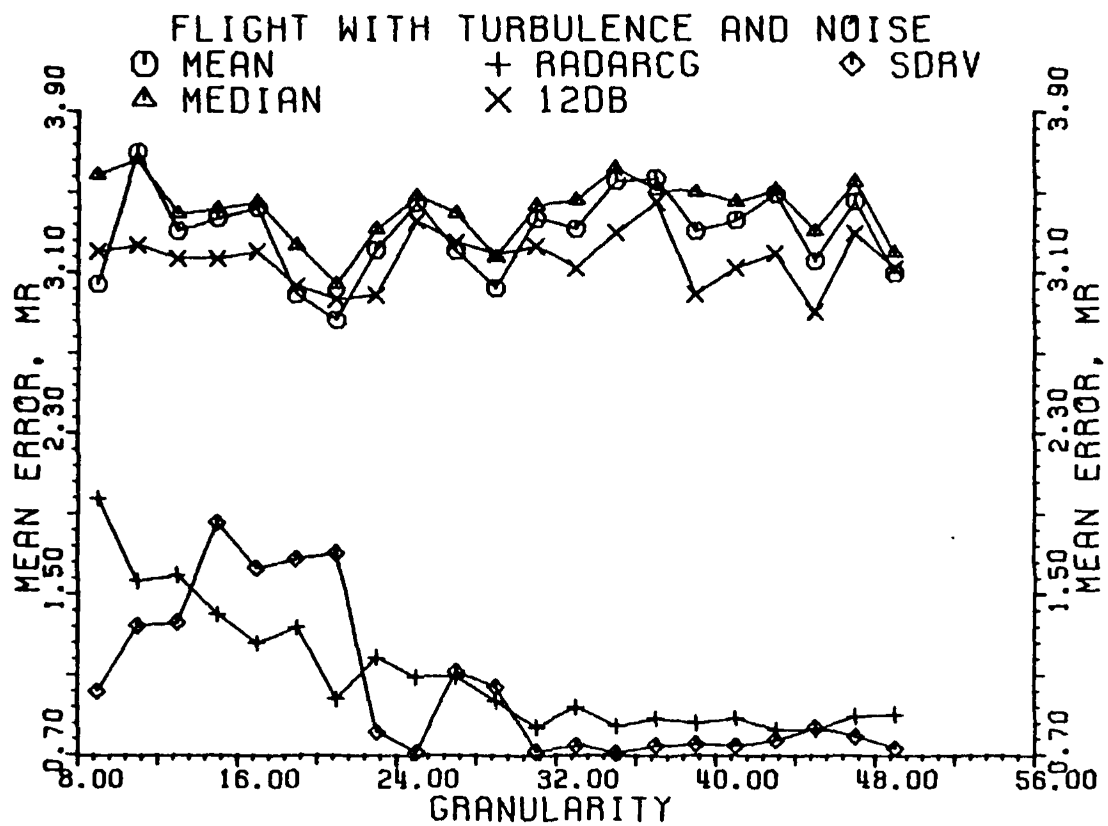

Figure 5-221. Mean error of estimators in milliradians with the antenna located 125 M from the runway centerline. Each data point is the result of one flight, all scans used.

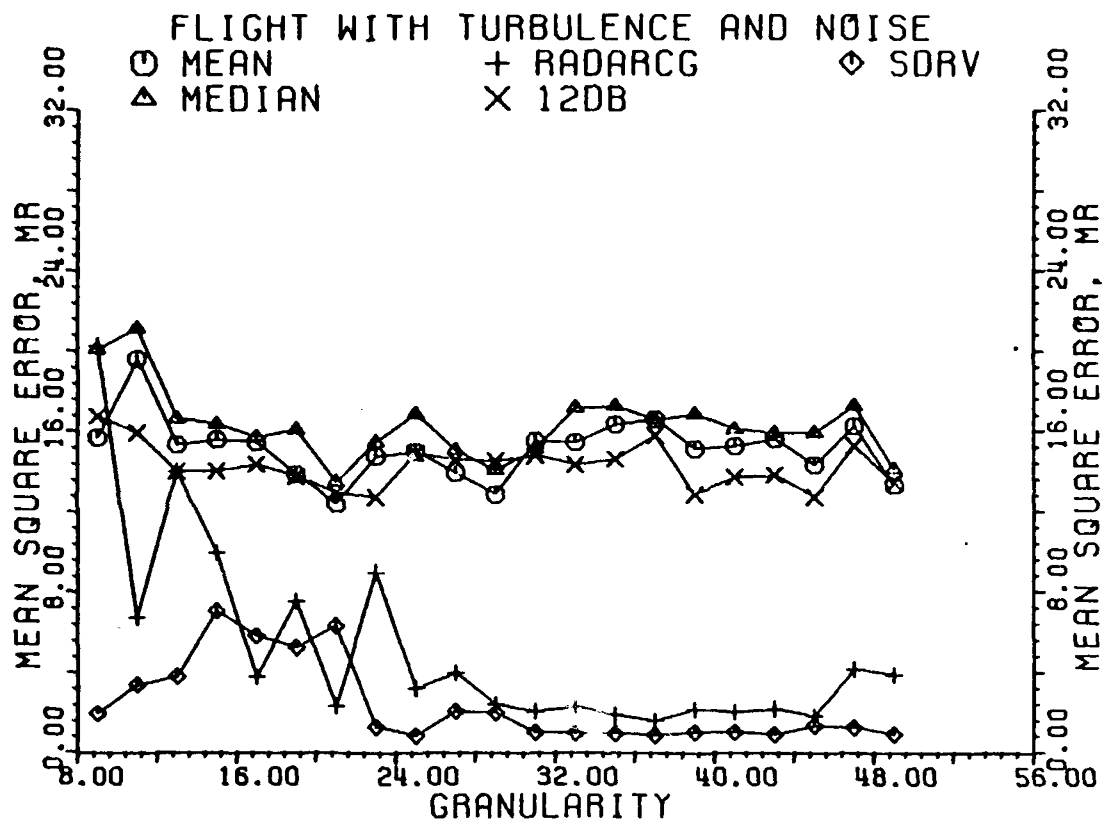

Figure 5-222. Mean square error of estimators in milliradians with the antenna located 125 M from the runway centerline. Each data point is the result of one flight, all scans used.

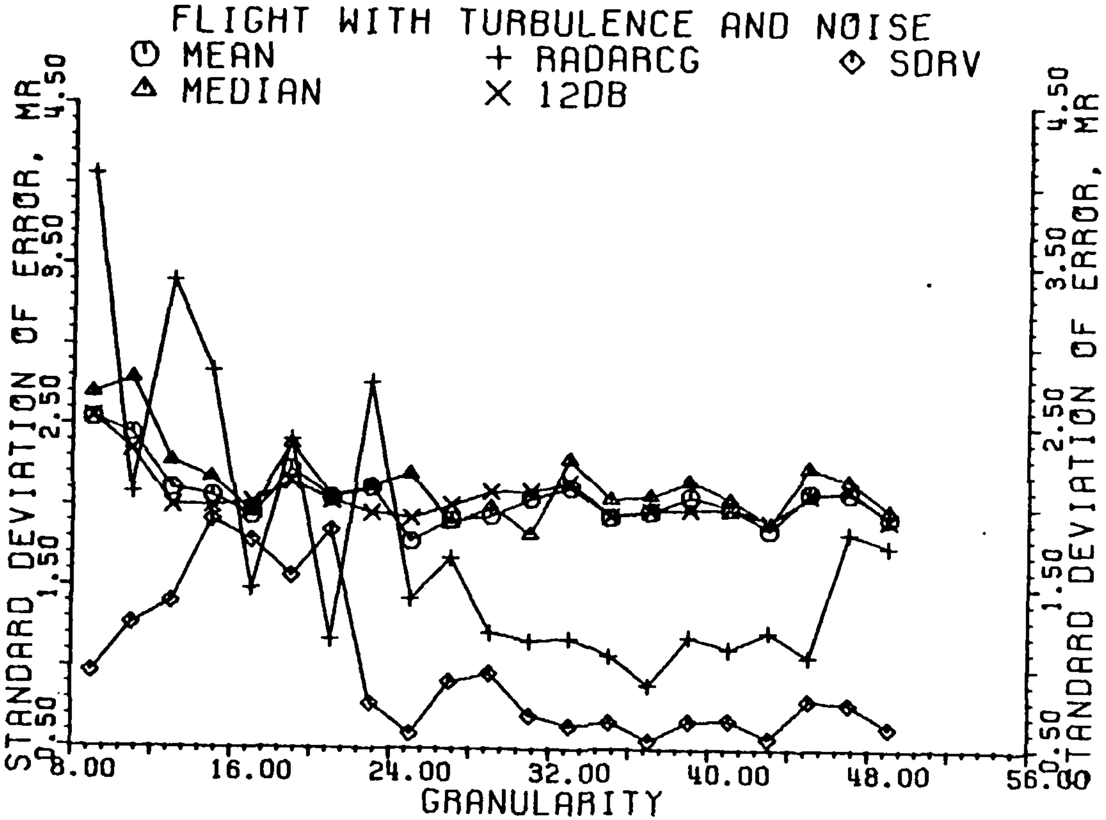

Figure 5-223. Standard deviation of error of estimators in milliradians with the antenna located 125 M from the runway centerline. Each data point is the result of one flight, all scans used.

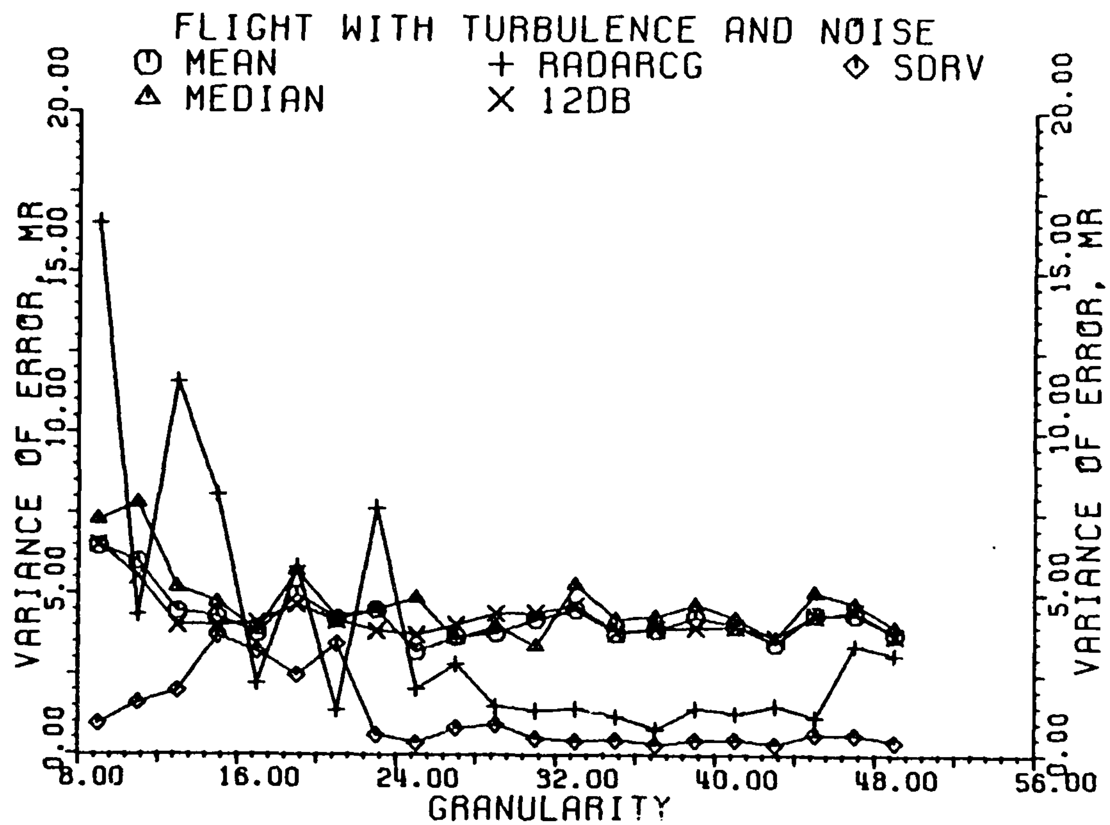

Figure 5-224. Variance of error of estimators in milliradians with the antenna located 125 M from the runway centerline. Each data point is the result of one flight, all scans used.

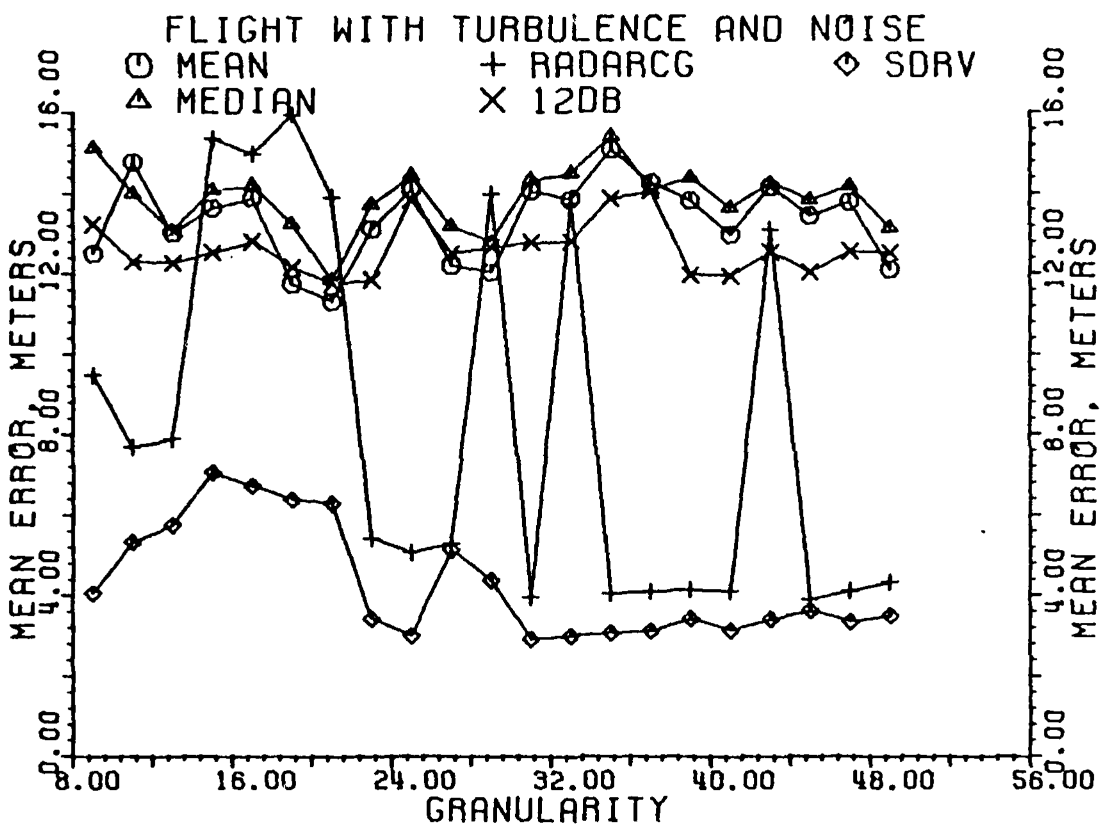

Figure 5-225. Mean error of estimators in meters with the antenna located 125 M from the runway centerline. Each data point is the result of one flight, all scans used.

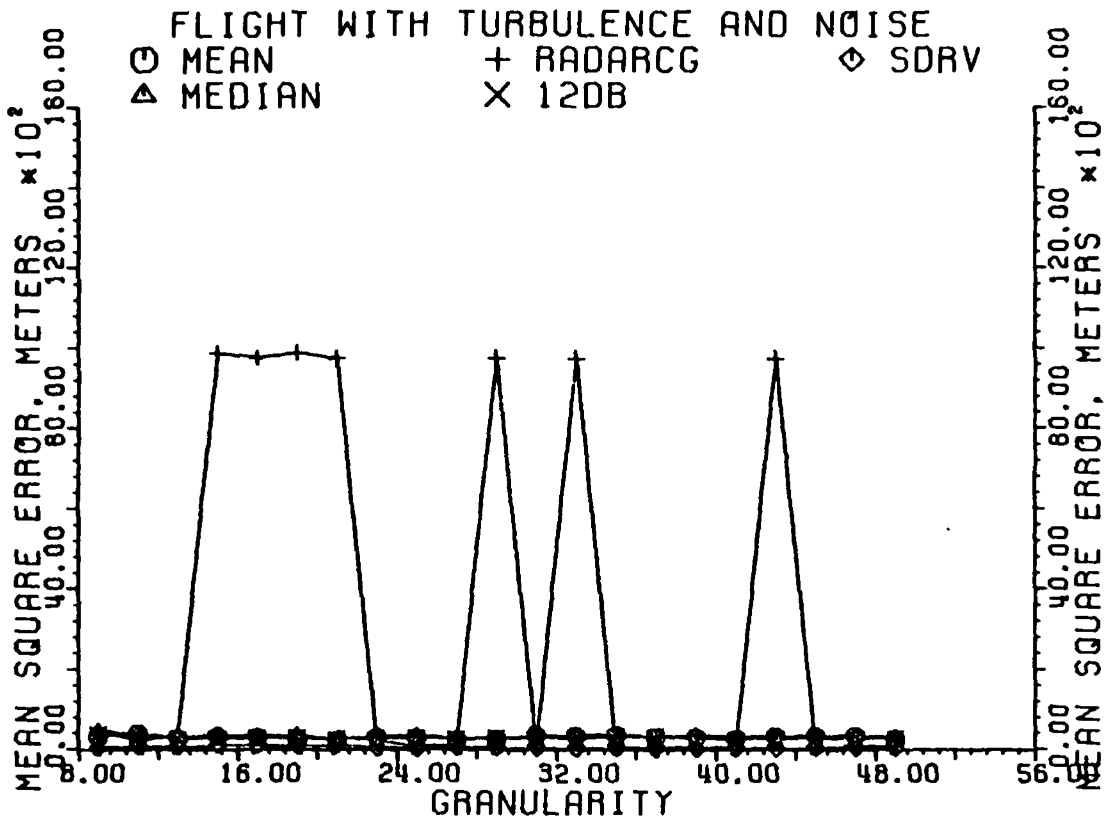

Figure 5-226. Mean square error of estimators in meters with the antenna located 125 M from the runway centerline. Each data point is the result of one flight, all scans used.

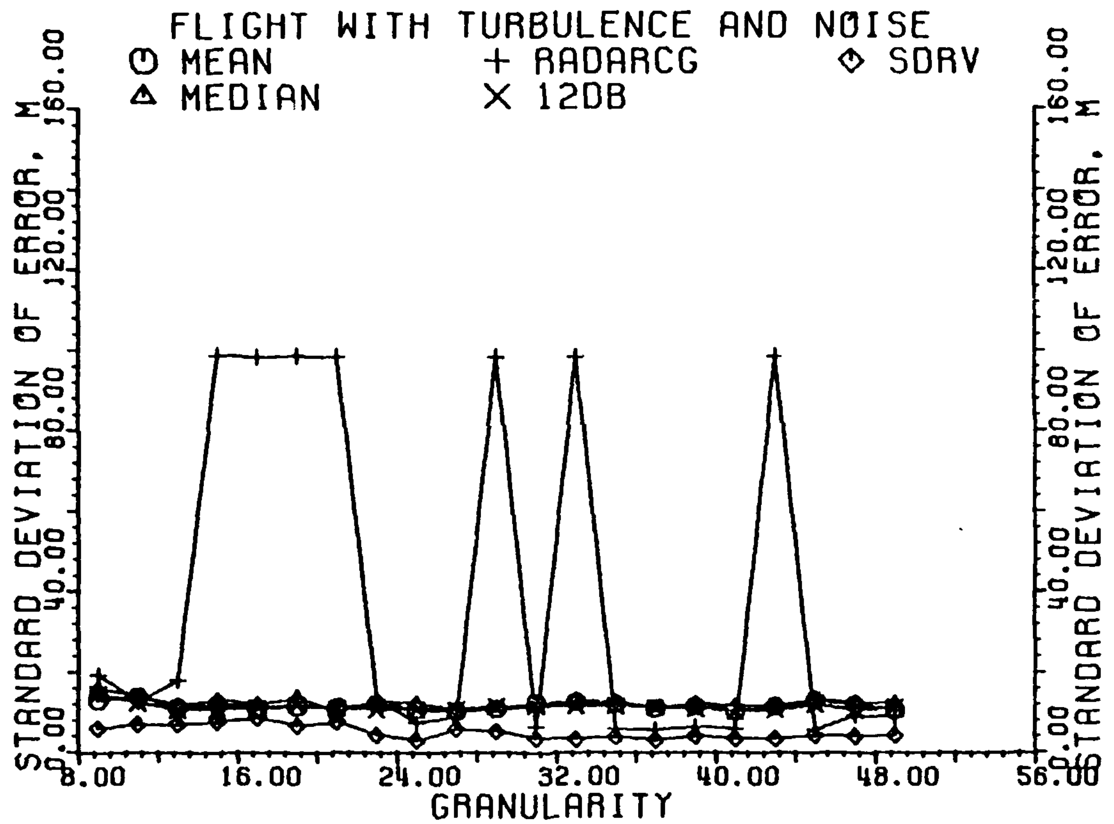

Figure 5-227. Standard deviation of error of estimators in meters with the antenna located 125 M from the runway centerline. Each data point is the result of one flight, all scans used.

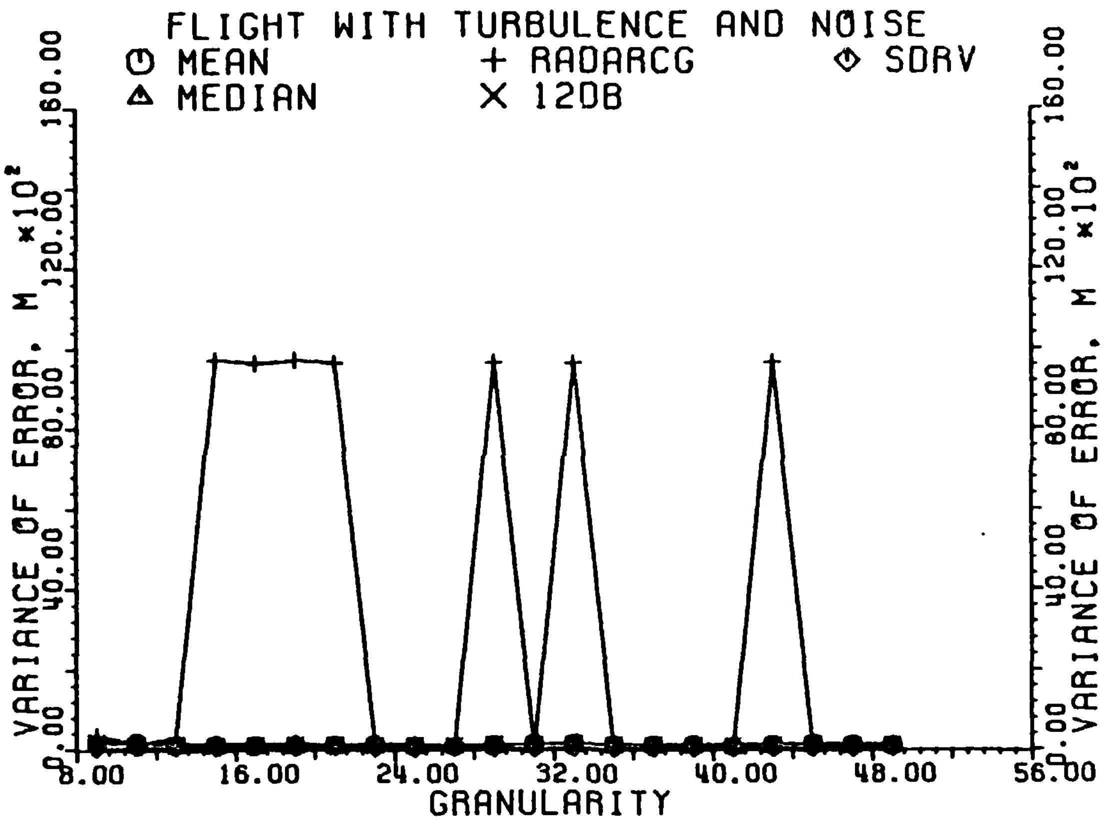

Figure 5-228. Variance of error of estimators in meters with the antenna located 125 M from the runway centerline. Each data point is the result of one flight, all scans used.

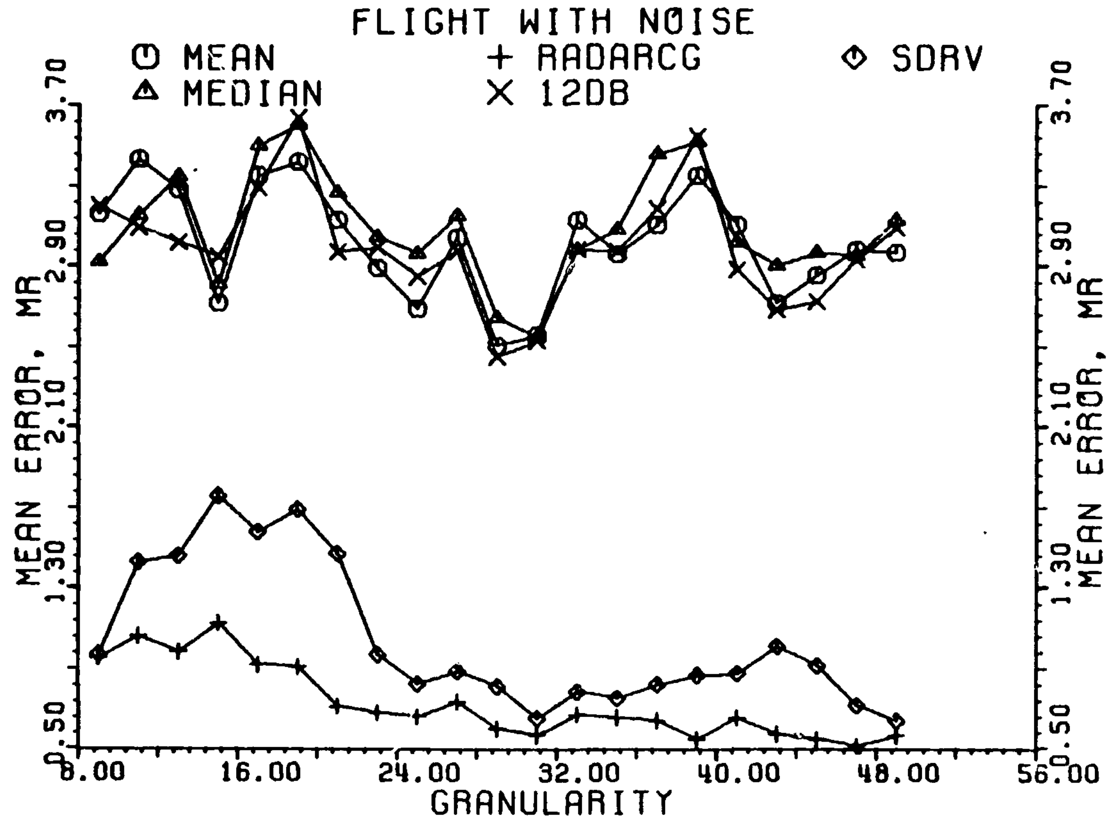

Figure 5-229. Mean error of estimators in milliradians with the antenna located 125 M from the runway centerline. Each data point is the result of one flight, all scans with a SNR 13 dB or greater used.

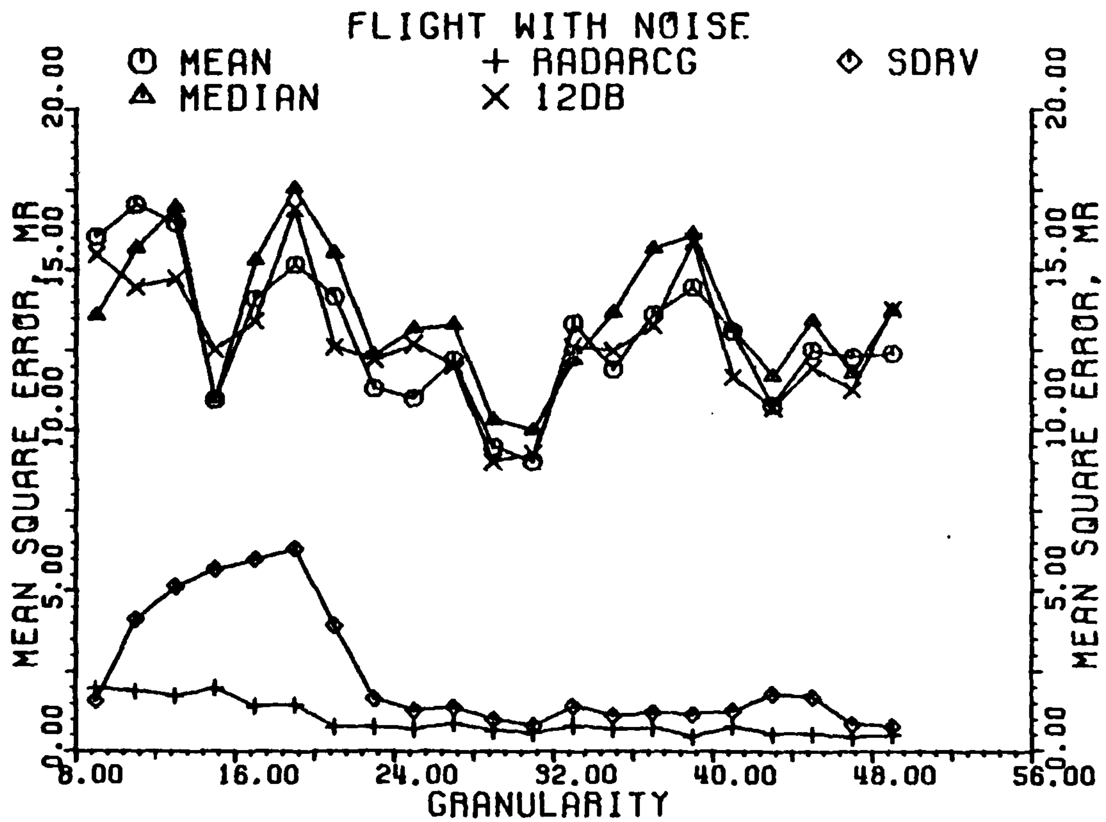

Figure 5-230. Mean square error of estimators in milliradians with the antenna located 125 M from the runway centerline. Each data point is the result of one flight, all scans with a SNR 13 dB or greater used.

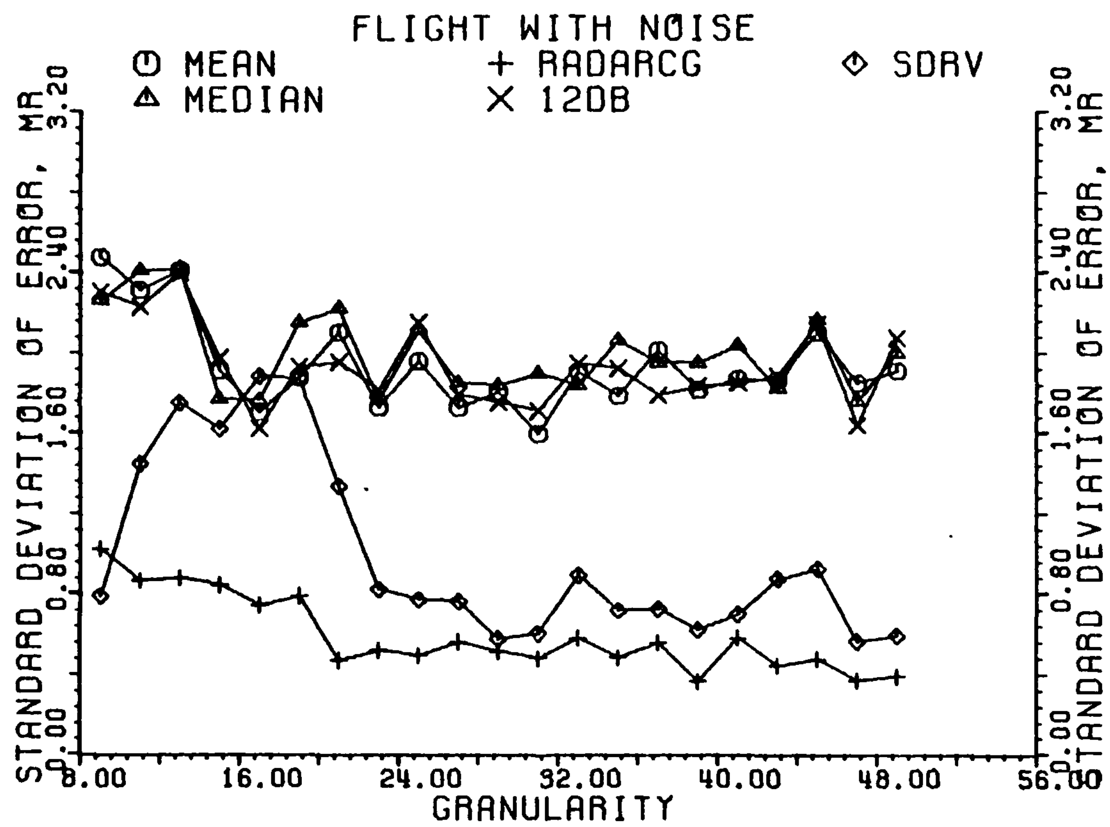

Figure 5-231. Standard deviation of error of estimators in milliradians with the antenna located 125 M from the runway centerline. Each data point is the result of one flight, all scans with a SNR 13 dB or greater used.

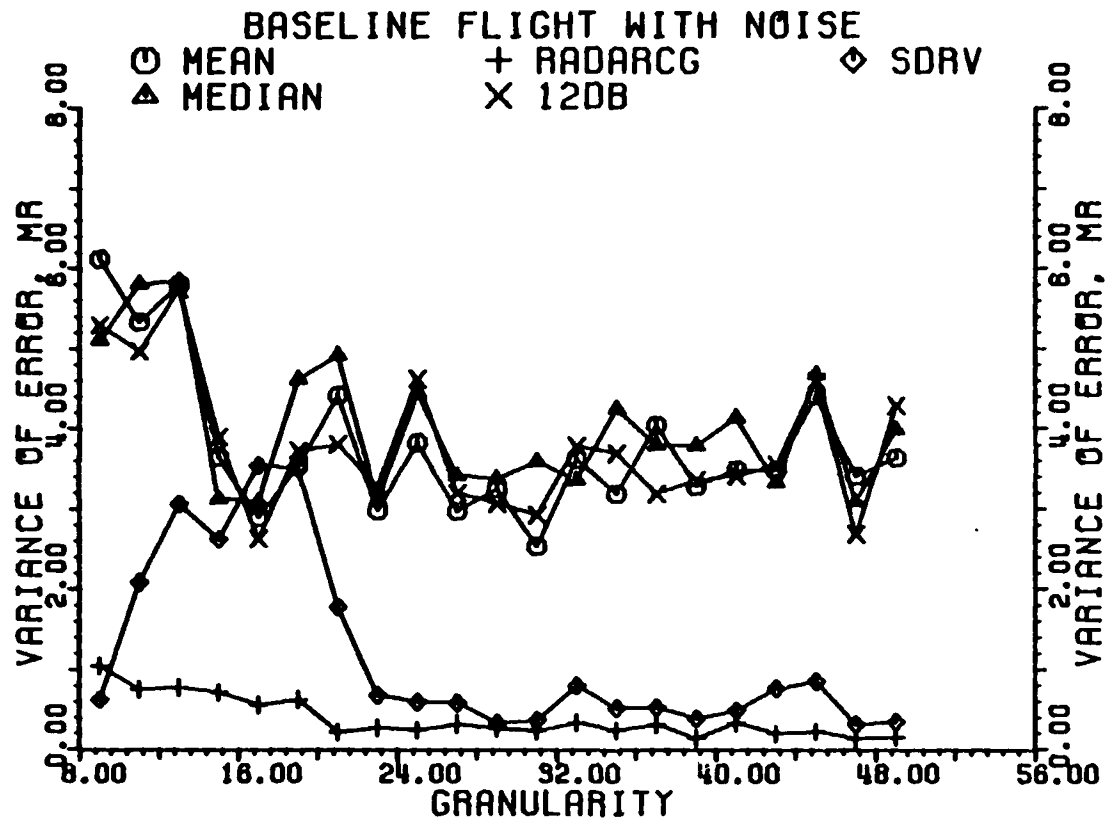

Figure 5-232. Variance of error of estimators in milliradians with the antenna located 125 M from the runway centerline. Each data point is the result of one flight, all scans with a SNR 13 dB or greater used.

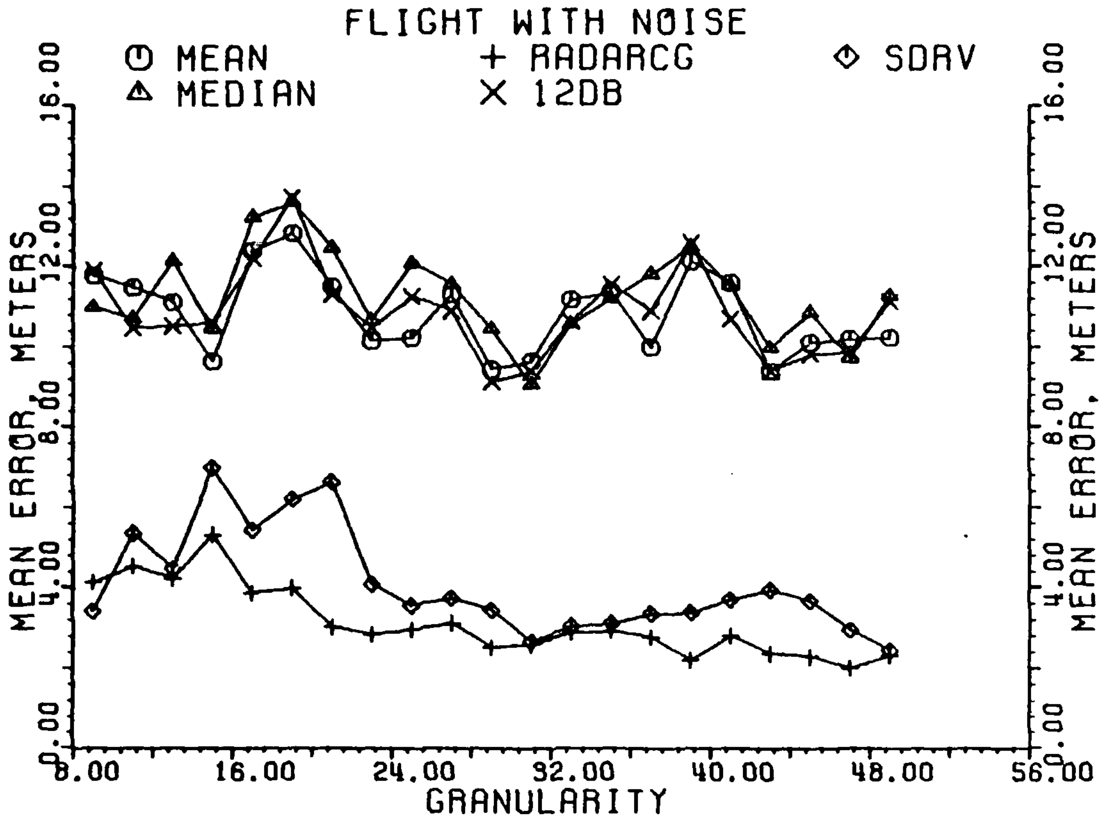

Figure 5-233. Mean error of estimators in meters with the antenna located 125 M from the runway centerline. Each data point is the result of one flight, all scans with a SNR 13 dB or greater used.

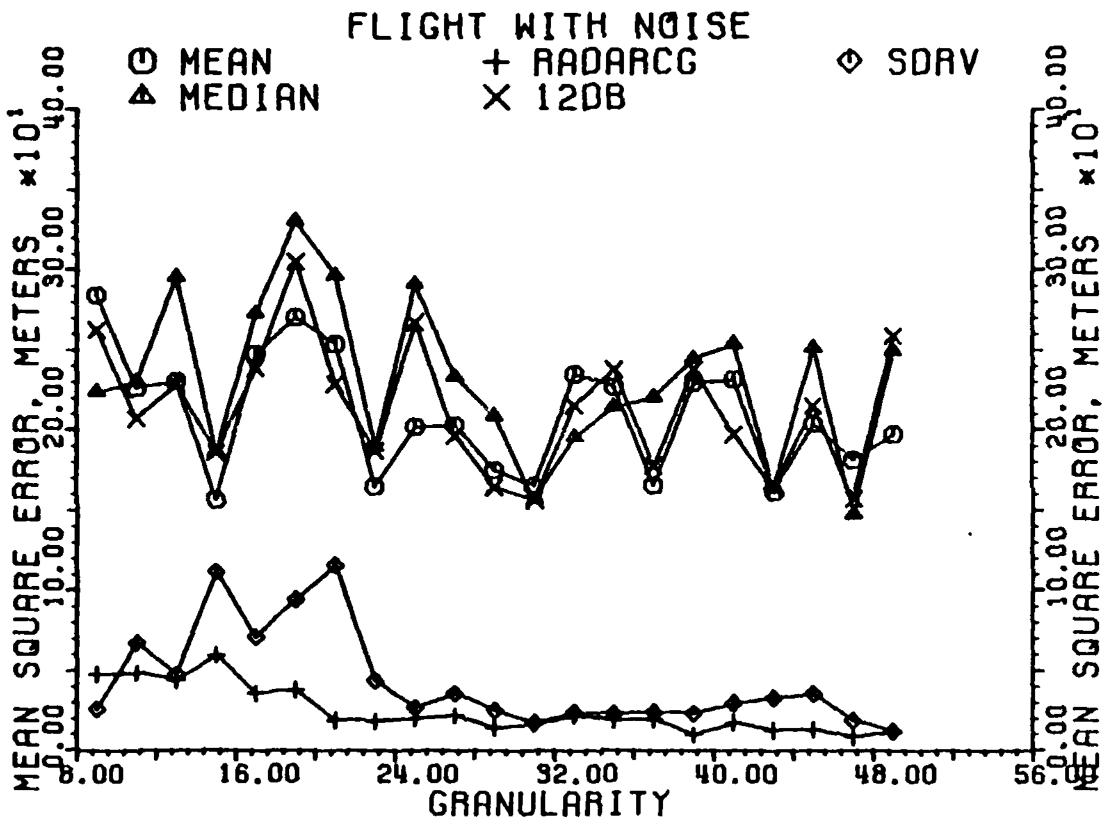

Figure 5-234. Mean square error of estimators in meters with the antenna located 125 M from the runway centerline. Each data point is the result of one flight, all scans with a SNR 13 dB or greater used.

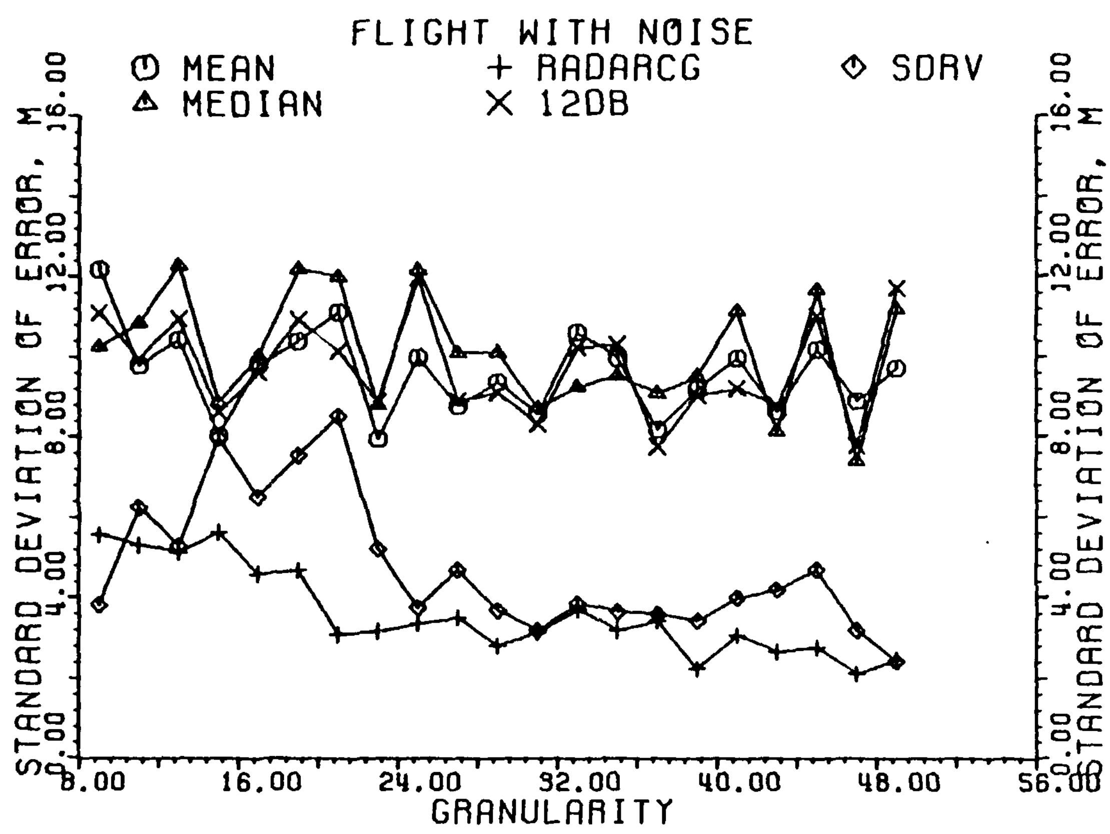

Figure 5-235. Standard deviation of error of estimators in meters with the antenna located 125 M from the runway centerline. Each data point is the result of one flight, all scans with a SNR 13 dB or greater used.

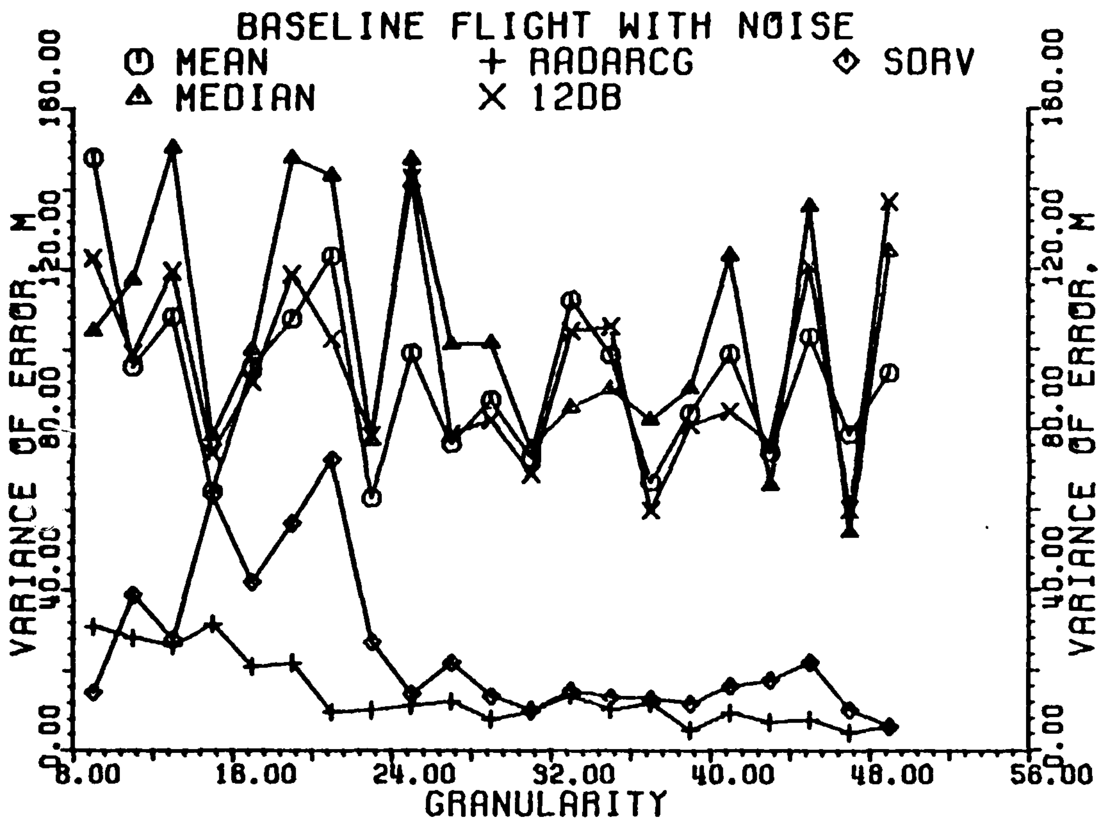

Figure 5-236. Variance of error of estimators in meters with the antenna located 125 M from the runway centerline. Each data point is the result of one flight, all scans with a SNR 13 dB or greater used.

Proceeding to the scans with a SNR of at least 13 dB, Figures 5-229 through 5-236, the flight with noise only shows the RADARCG estimator to be the most accurate and reliable with respect to granularity. The second derivative is generally better than the thresholding methods, decisively so in the finer granularities. The thresholding methods are of equal quality in high SNRs.

The flights with turbulence and noise, Figures 5-237 through 5-224, again show RADARCG to be the best estimator in periods of high signal strength. The second derivative is the next best method, degrading to the level of the thresholding estimators for the granularities between 15 and 21 beam locations in the scan. The mean estimator appears the best in accuracy of the thresholding methods, followed by 12 dB and the median estimators, in that order.

The scans with SNR's of 10 dB or less for the flights with noise are plotted in Figures 5-245 through 5-252. The degradation of all estimators is evident. RADARCG and SDRV are the two best estimators particularly in the higher granularities. The 12 dB thresholding method again distinguishes itself as the best of the thresholding methods in noise, although the mean and median methods are similar in ability.

The flights with turbulence and noise, Figures 5-253 through 5-260, now show SDRV to be the most accurate, and RADARCG to be the least accurate. The thresholding methods do not appear to be affected by the turbulence. It is shown that there is no general improvement in the accuracy of the thresholding estimators with an increasing number of beam pointing locations in the scan. If the target returns are below the noise floor, then no amount of data will display the target without some

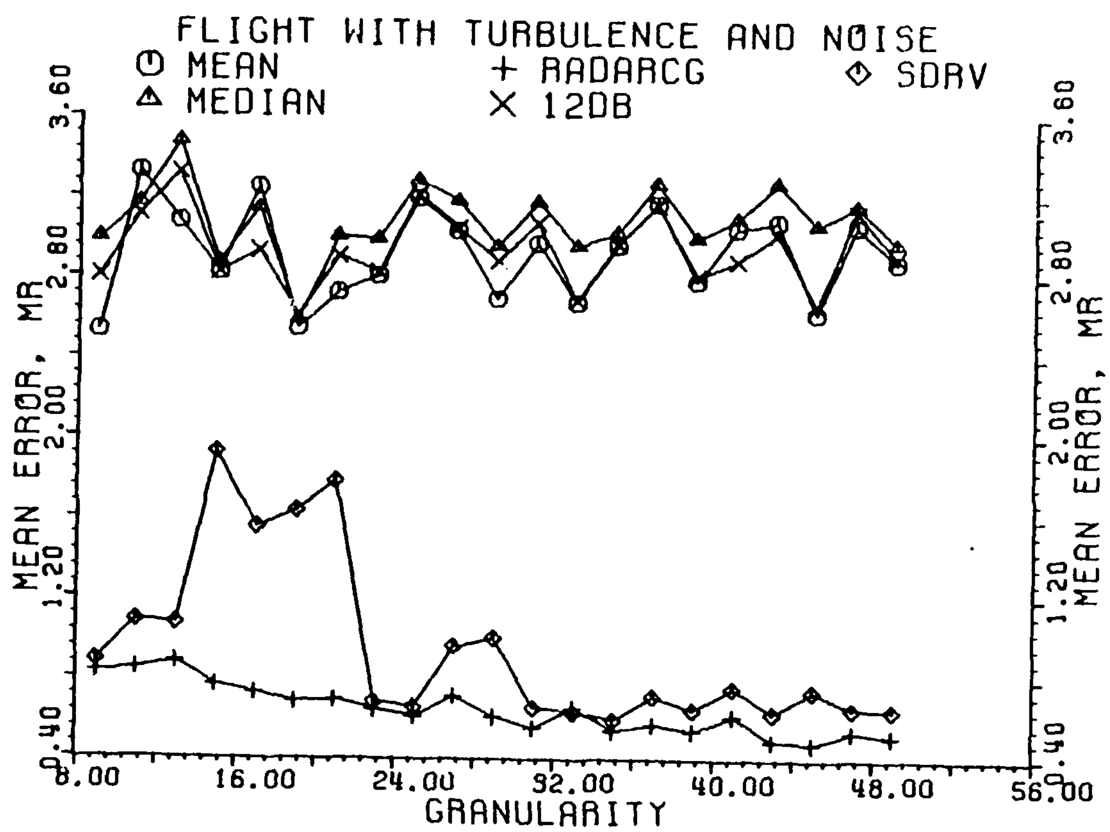

Figure 5-237. Mean error of estimators in milliradians with the antenna located 125 M from the runway centerline. Each data point is the result of one flight, all scans with a SNR 13 dB or greater used.

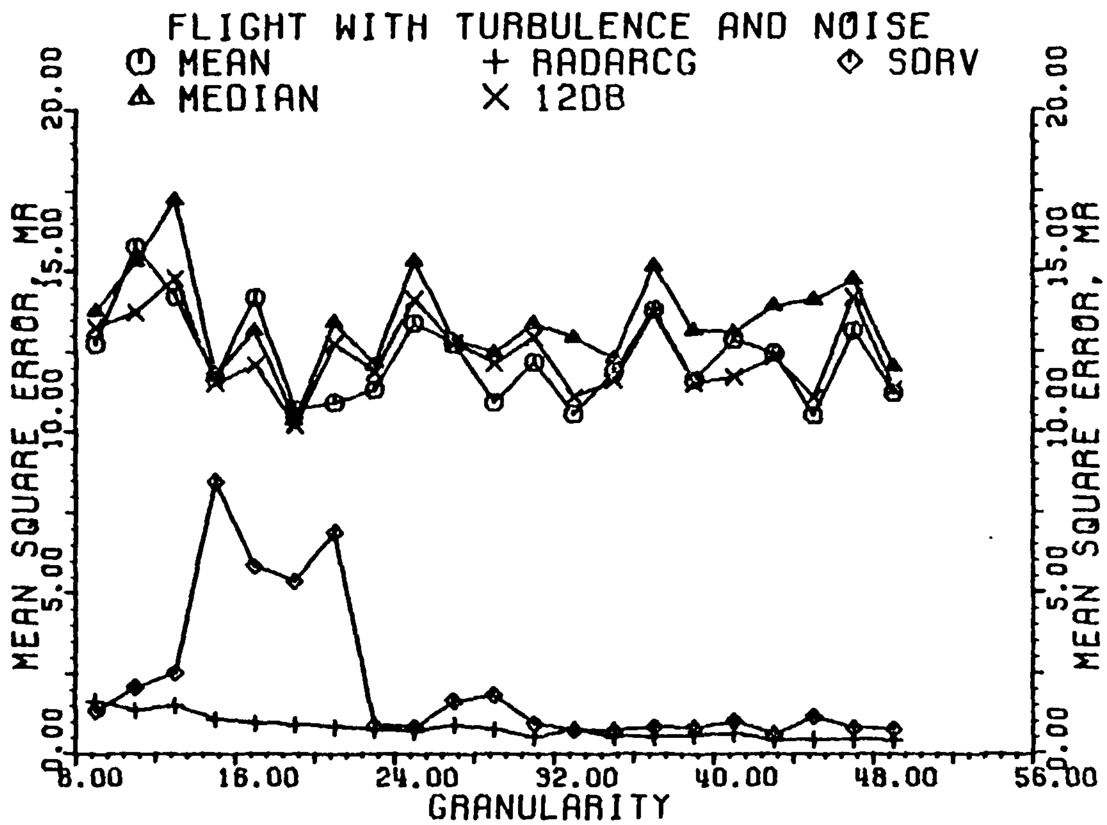

Figure 5-238. Mean square error of estimators in milliradians with the antenna located 125 M from the runway centerline. Each data point is the result of one flight, all scans with a SNR dB or greater used.

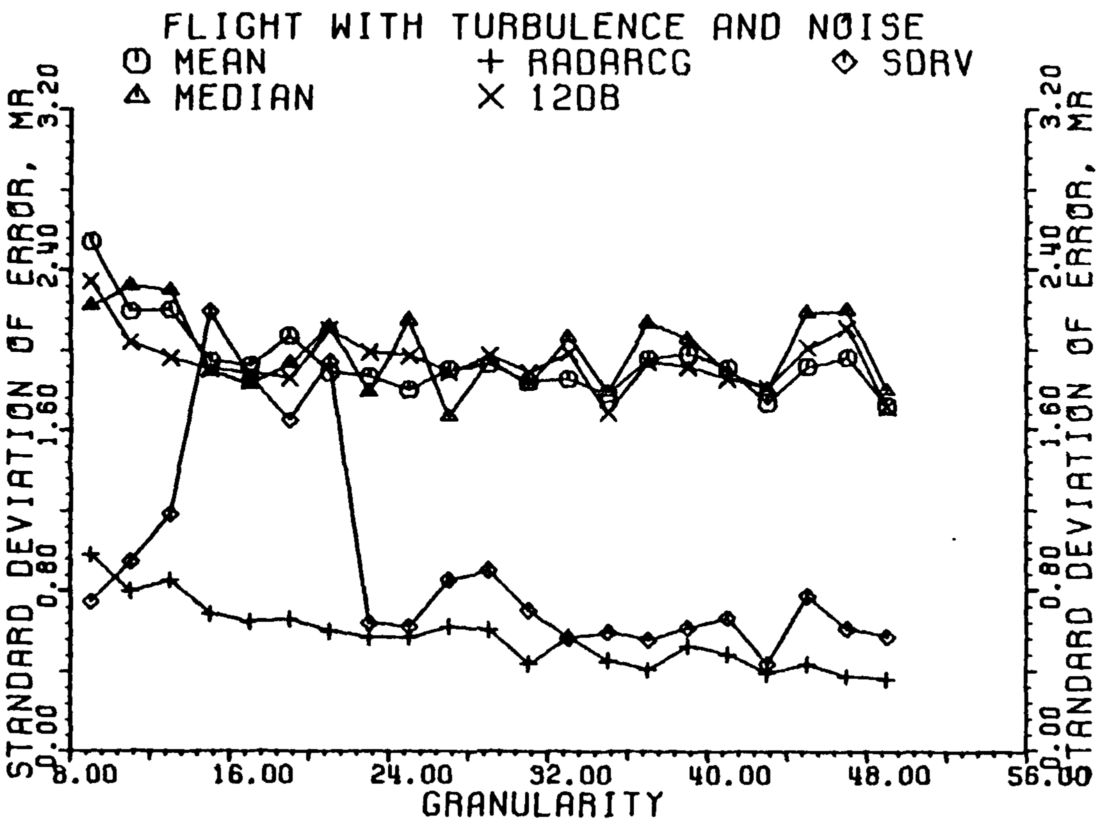

Figure 5-239. Standard deviation of error of estimators in milliradians with the antenna located 125 M from the runway centerline. Each data point is the result of one flight, all scans with a SNR 13 dB or greater used.

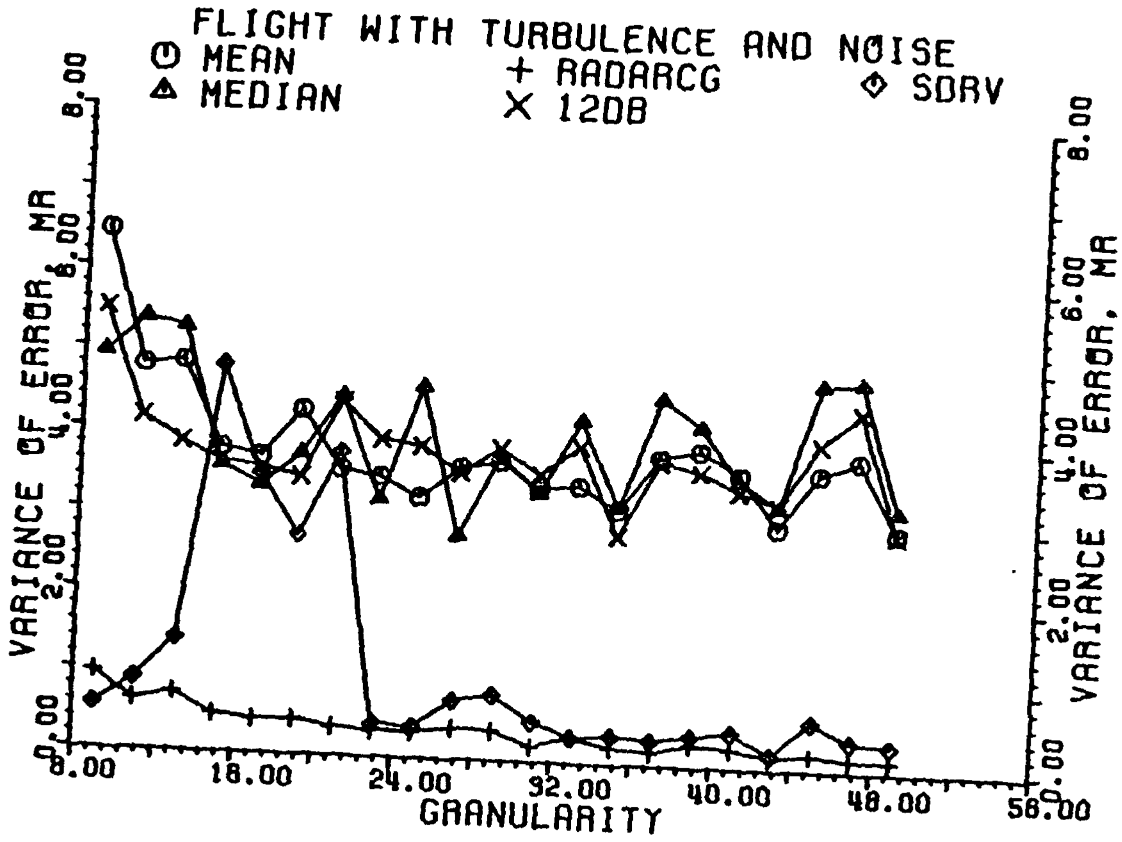

Figure 5-240. Variance of error of estimators in milliradians with the antenna located 125 M from the runway centerline. Each data point is the result of one flight, all scans with a SNR 13 dB or greater used.

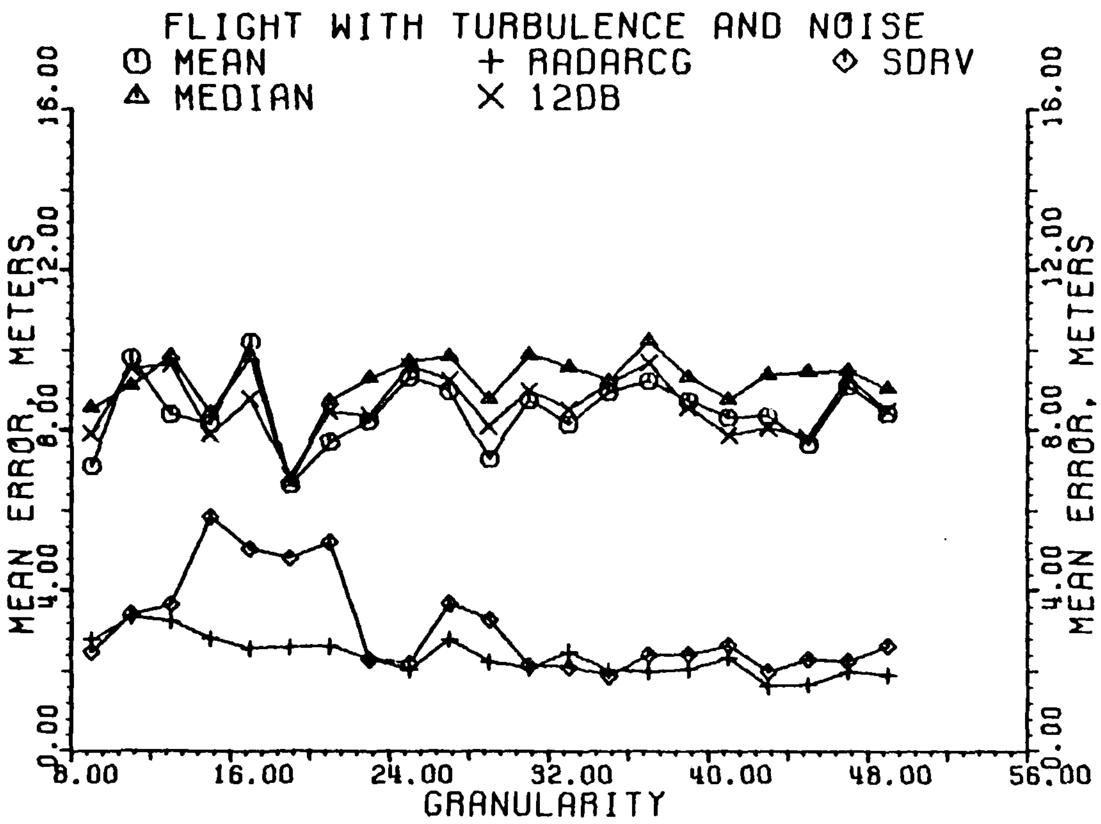

Figure 5-241. Mean error of estimators in meters with the antenna located 125 M from the runway centerline. Each data point is the result of one flight, all scans with a SNR 13 dB or greater used.

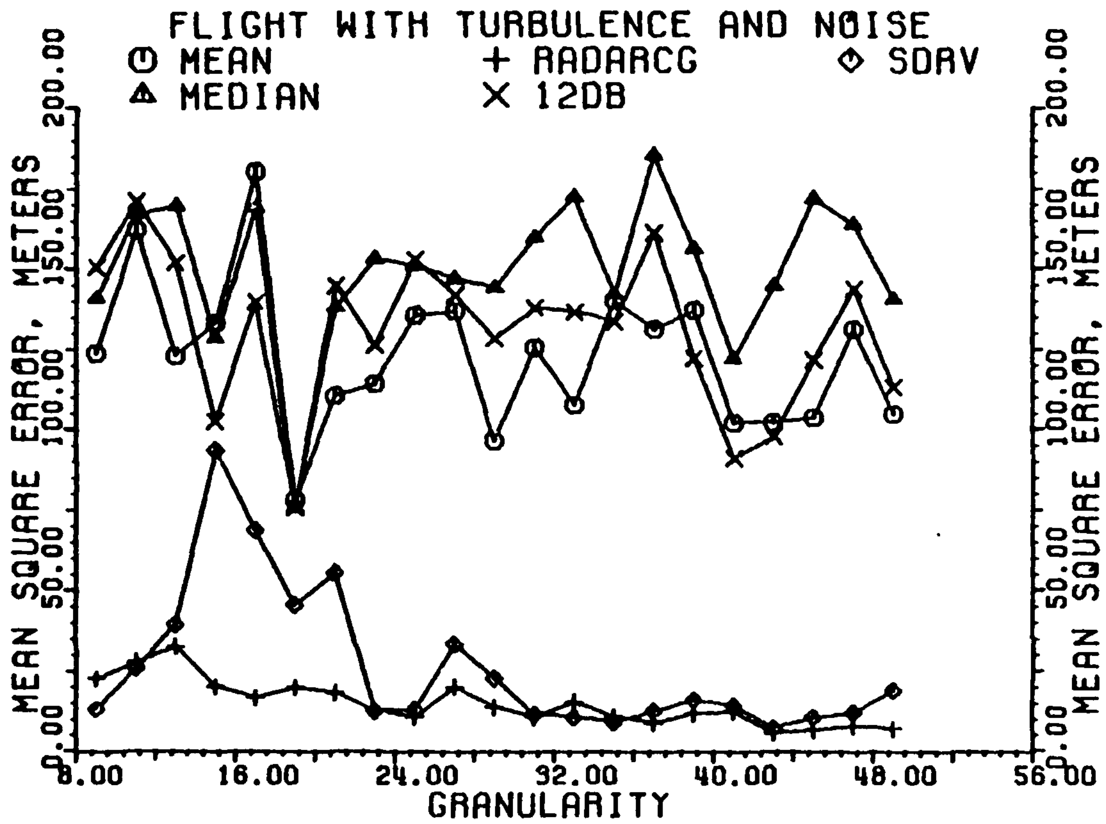

Figure 5-242. Mean square error of estimators in meters with the antenna located 125 M from the runway centerline. Each data point is the result of one flight, all scans with a SNR 13 dB or greater used.

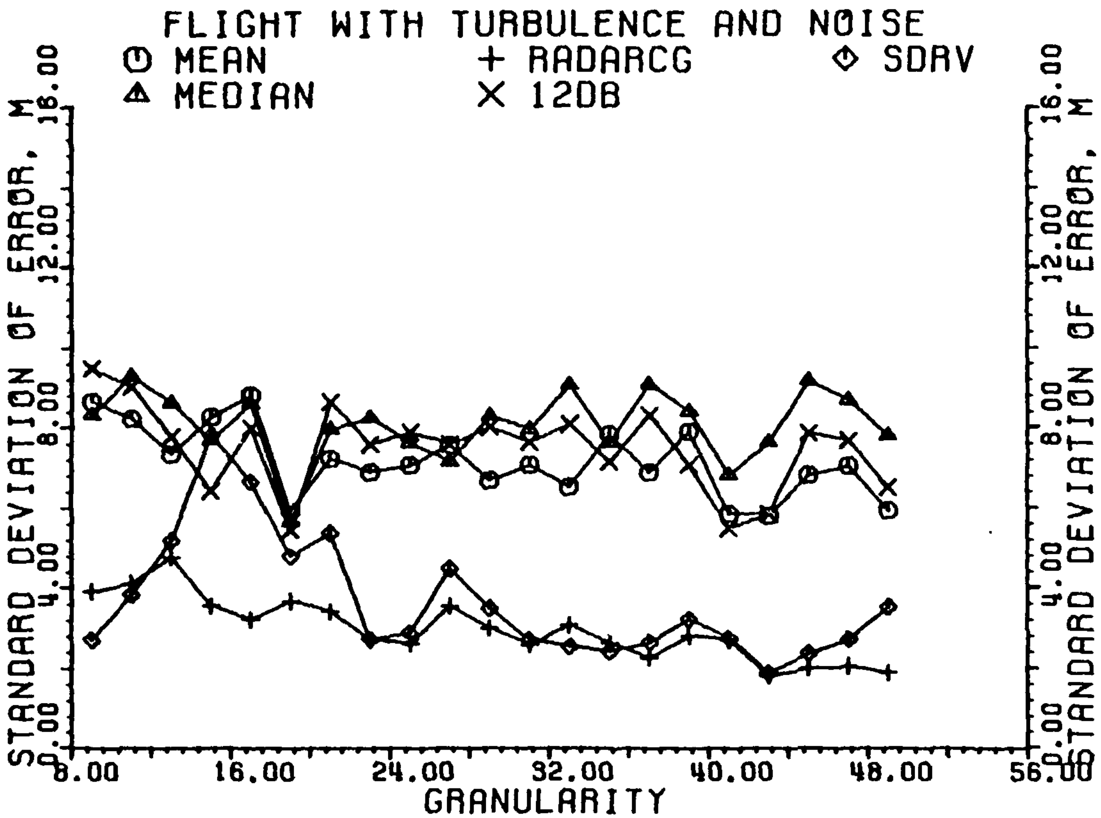

Figure 5-243. Standard deviation of error of estimators in meters with the antenna located 125 M from the runway centerline. Each data point is the result of one flight, all scans with a SNR 13 dB or greater used.

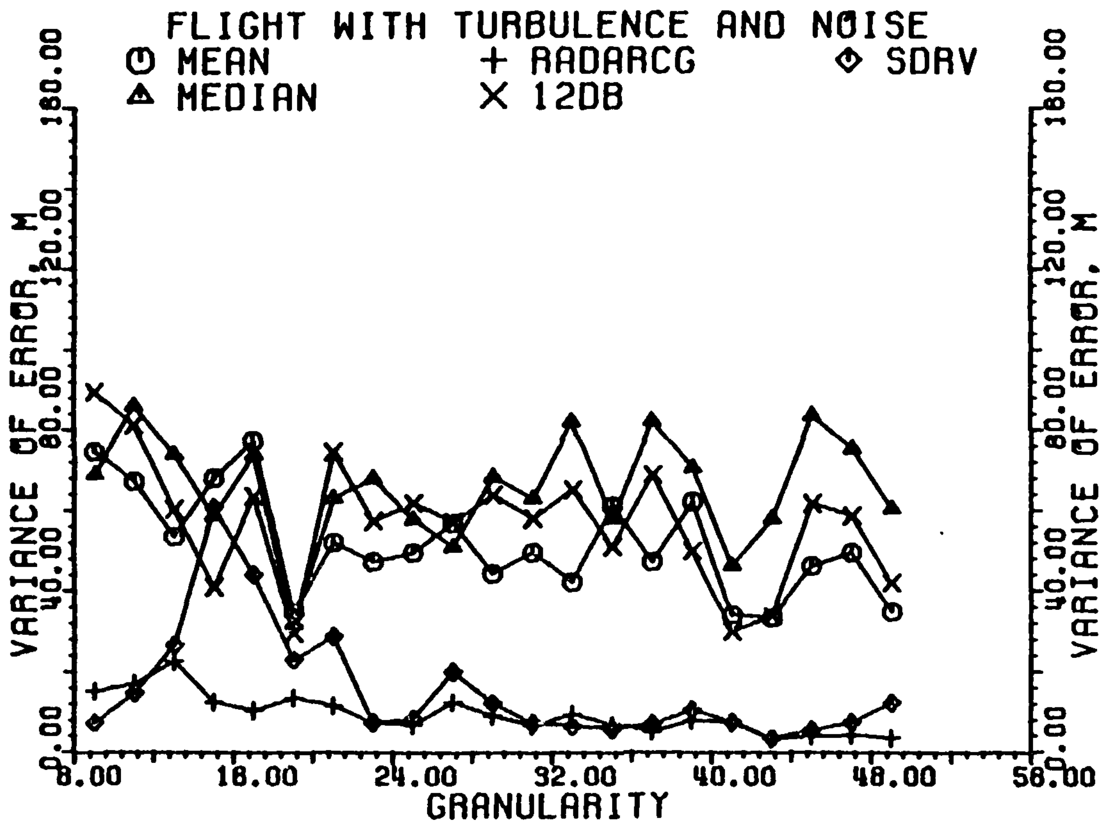

Figure 5-244. Variance of error of estimators in meters with the antenna located 125 M from the runway centerline. Each data point is the result of one flight, all scans with a SNR 13 dB or greater used.

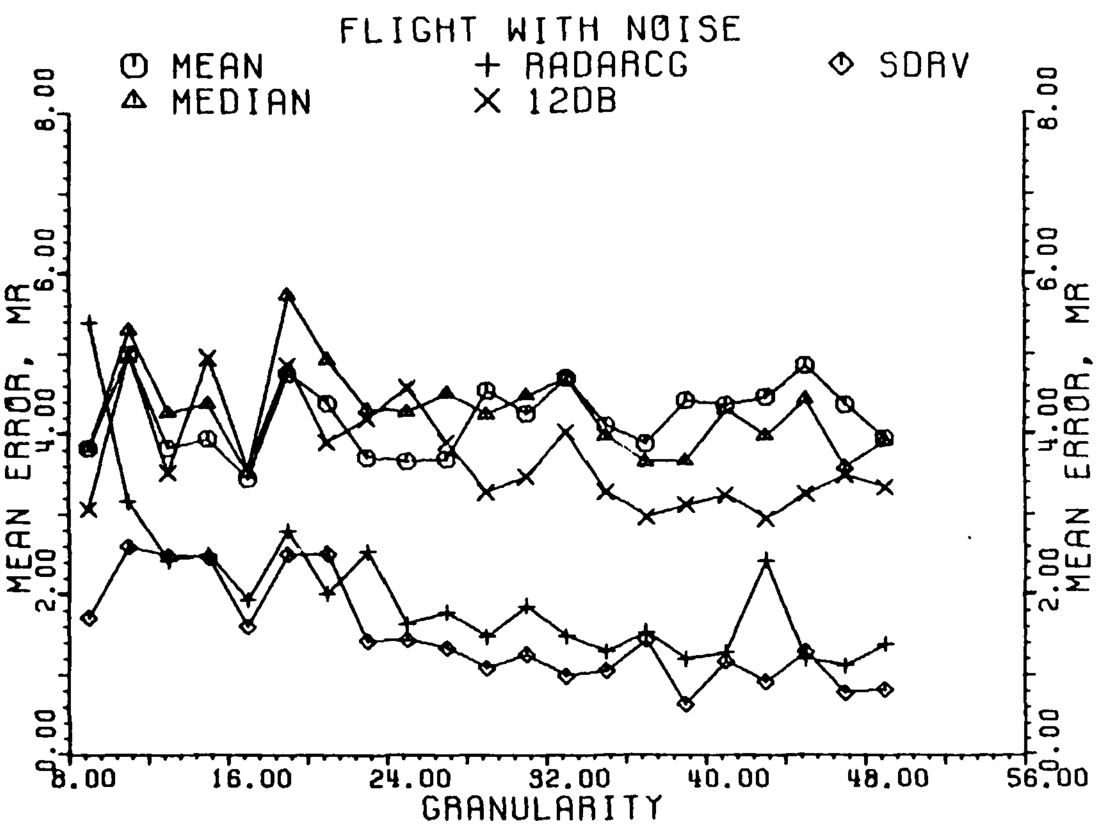

Figure 5-245. Mean error of estimators in milliradians with the antenna 125 M from the runway centerline. Each data point is the result of one flight, all scans with a SNR at or below 10 dB used.

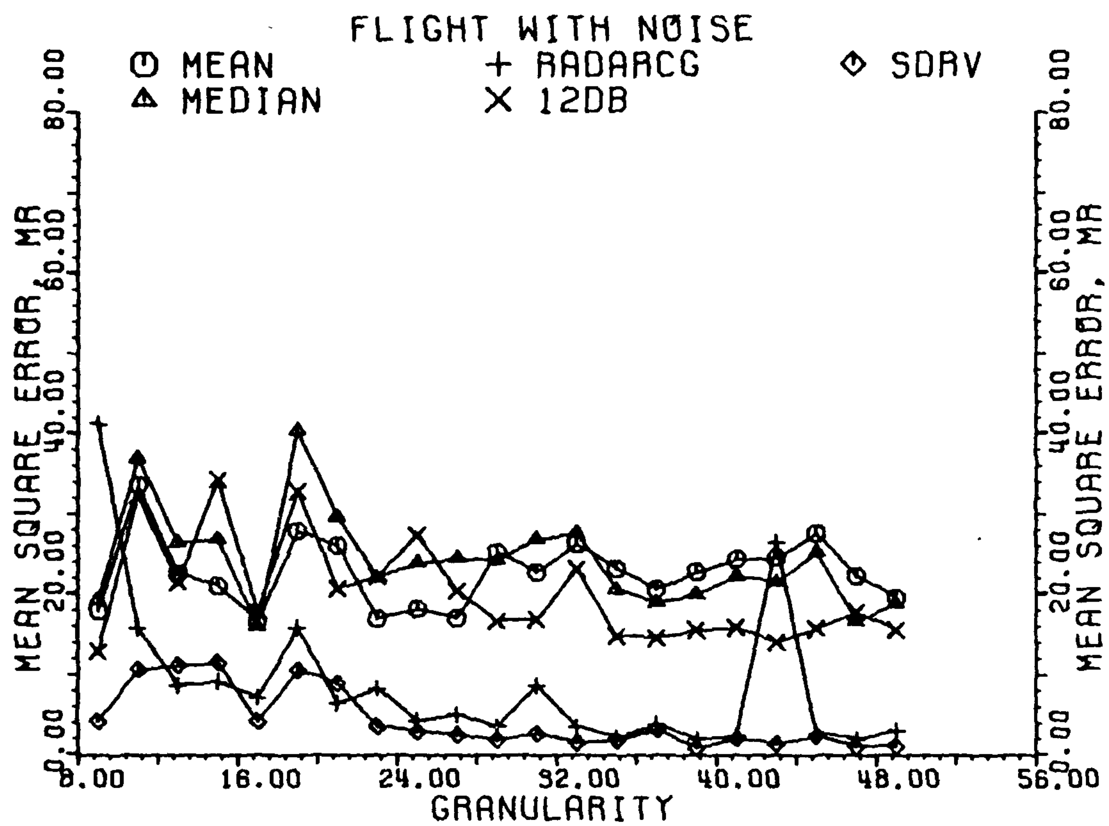

Figure 5-246. Mean square error of estimators in milliradians with the antenna 125 M from the runway centerline. Each data point is the result of one flight, all scans with a SNR at or below 10 dB used.

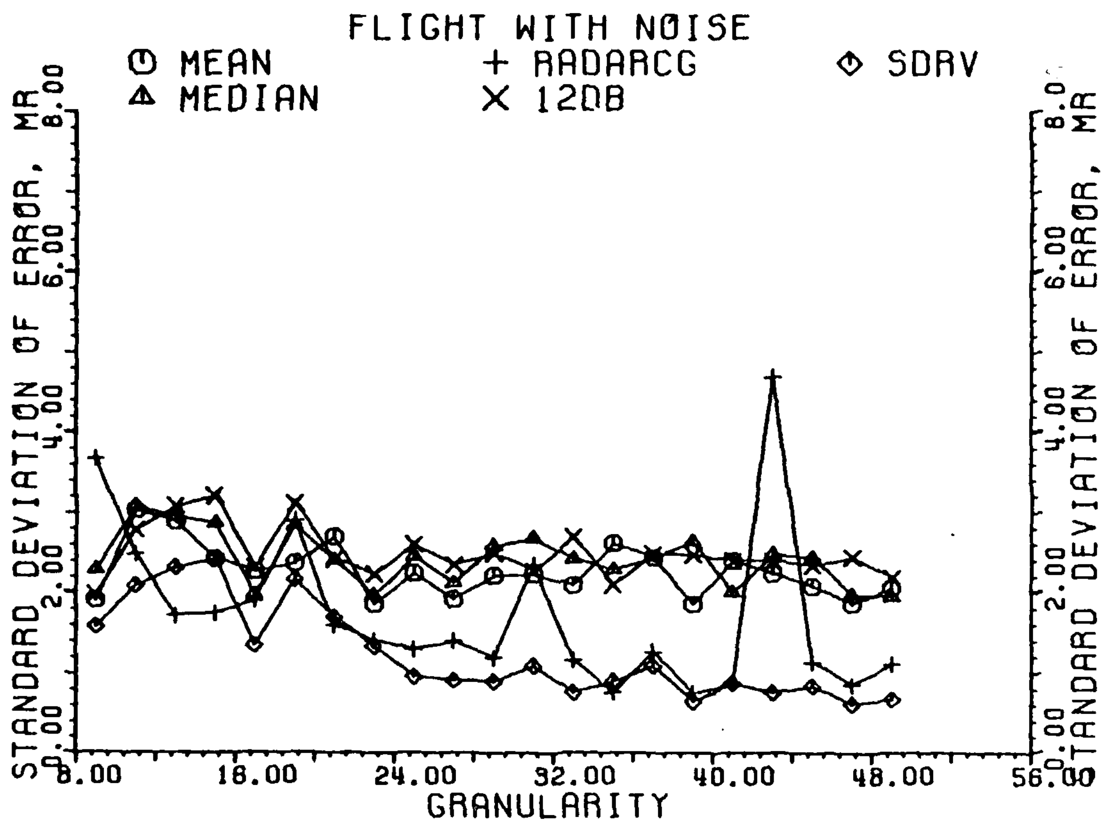

Figure 5-247. Standard deviation of error of estimators in milliradians with the antenna 125 M from the runway centerline. Each data point is the result of one flight, all scans with a SNR at or below 10 dB used.

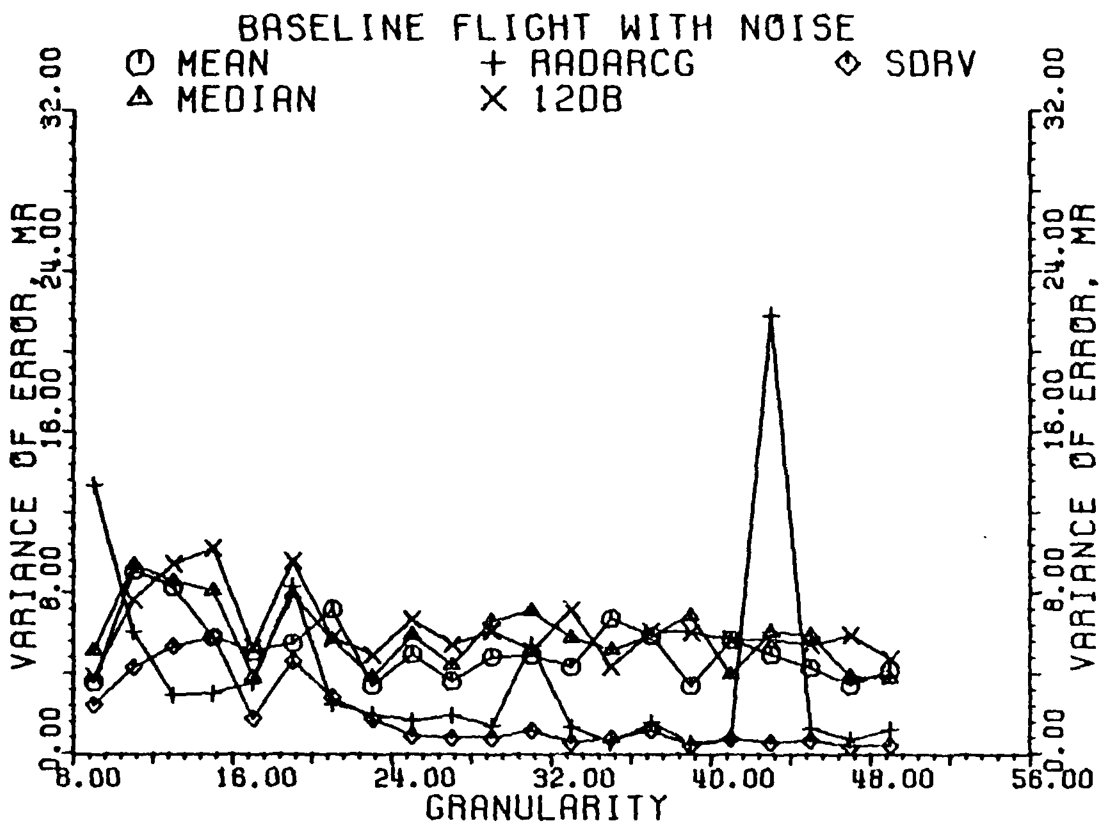

Figure 5-248. Variance of error of estimators in milliradians with the antenna 125 M from the runway centerline. Each data point is the result of one flight, all scans with a SNR at or below 10 dB used.

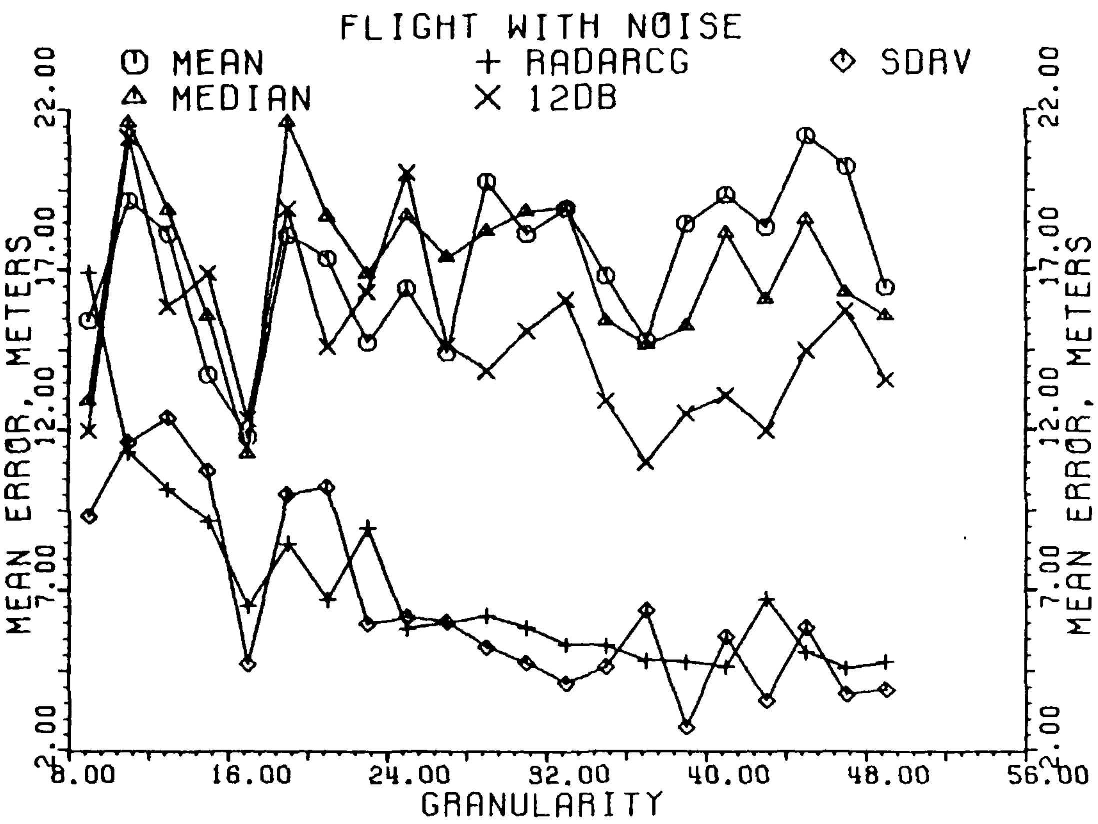

Figure 5-249. Mean error of estimators in meters with the antenna 125 M from the runway centerline. Each data point is the result of one flight, all scans with a SNR at or below 10 dB used.

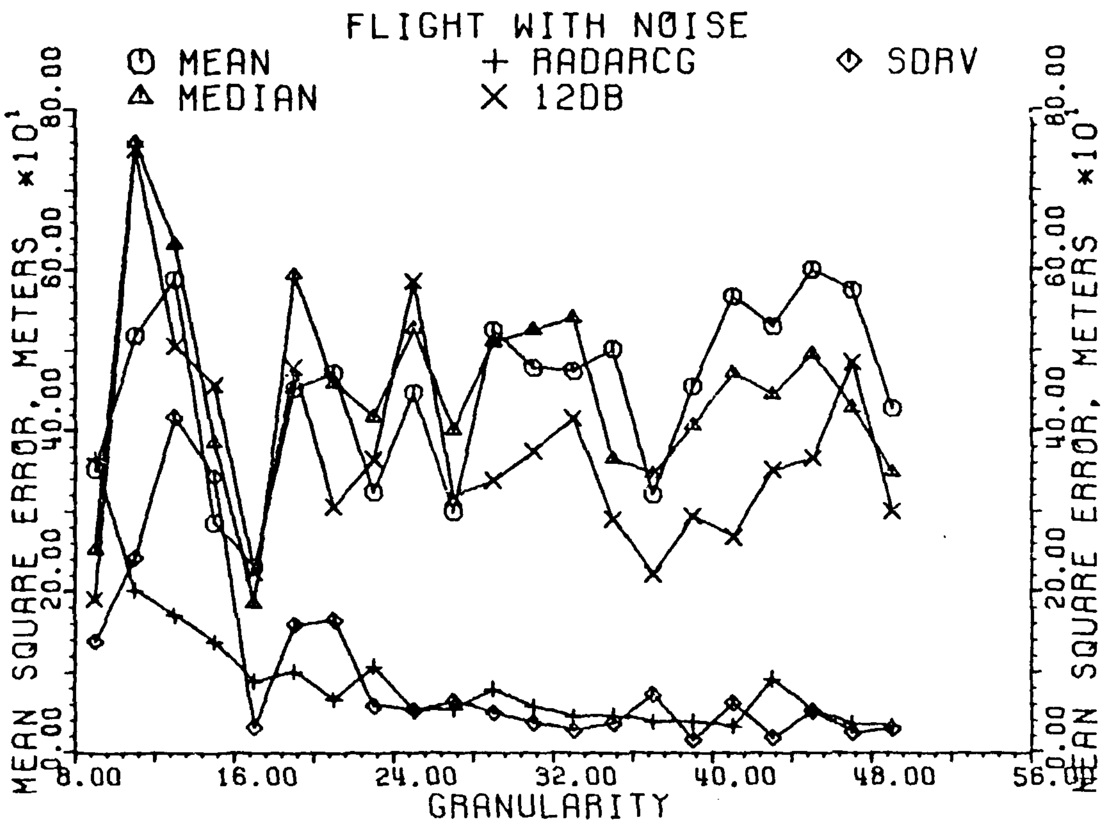

Figure 5-250. Mean square error of estimators in meters with the antenna 125 M from the runway centerline. Each data point is the result of one flight, all scans with a SNR at or below 10 dB used.

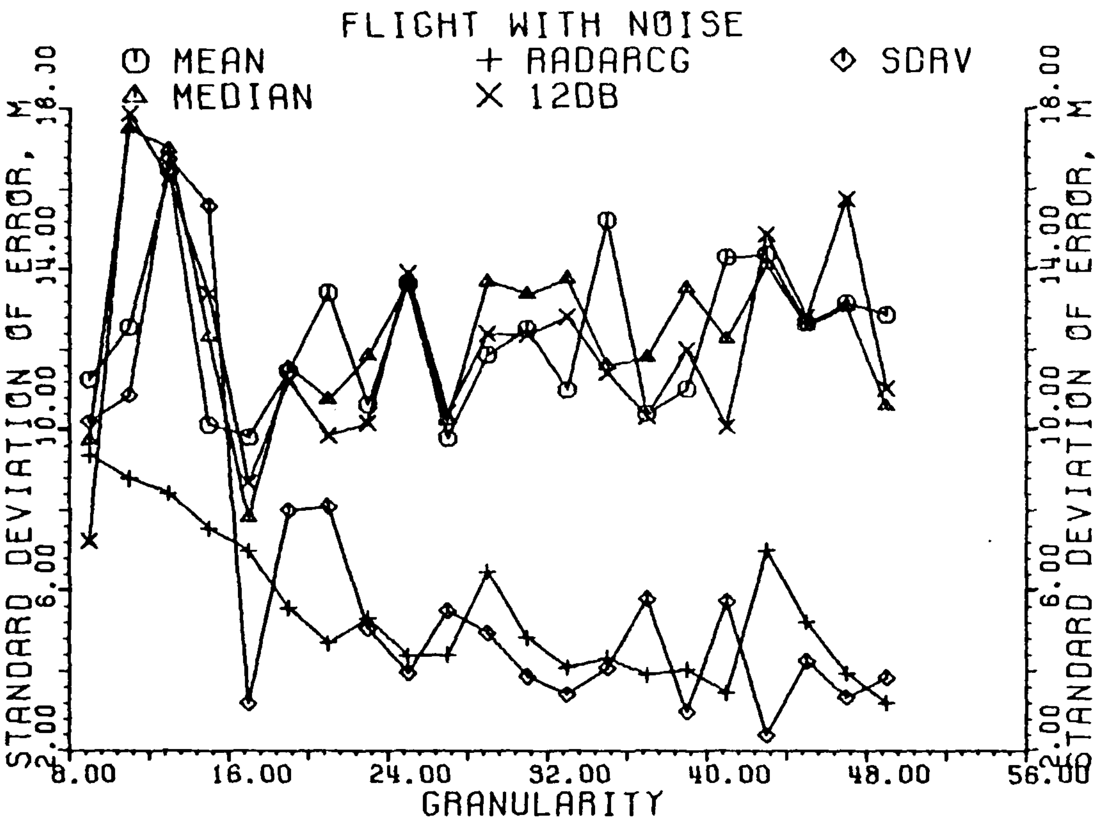

Figure 5-251. Standard deviation of error of estimators in meters with the antenna 125 M from the runway centerline. Each data point is the result of one flight, all scans with a SNR at or below 10 dB used.

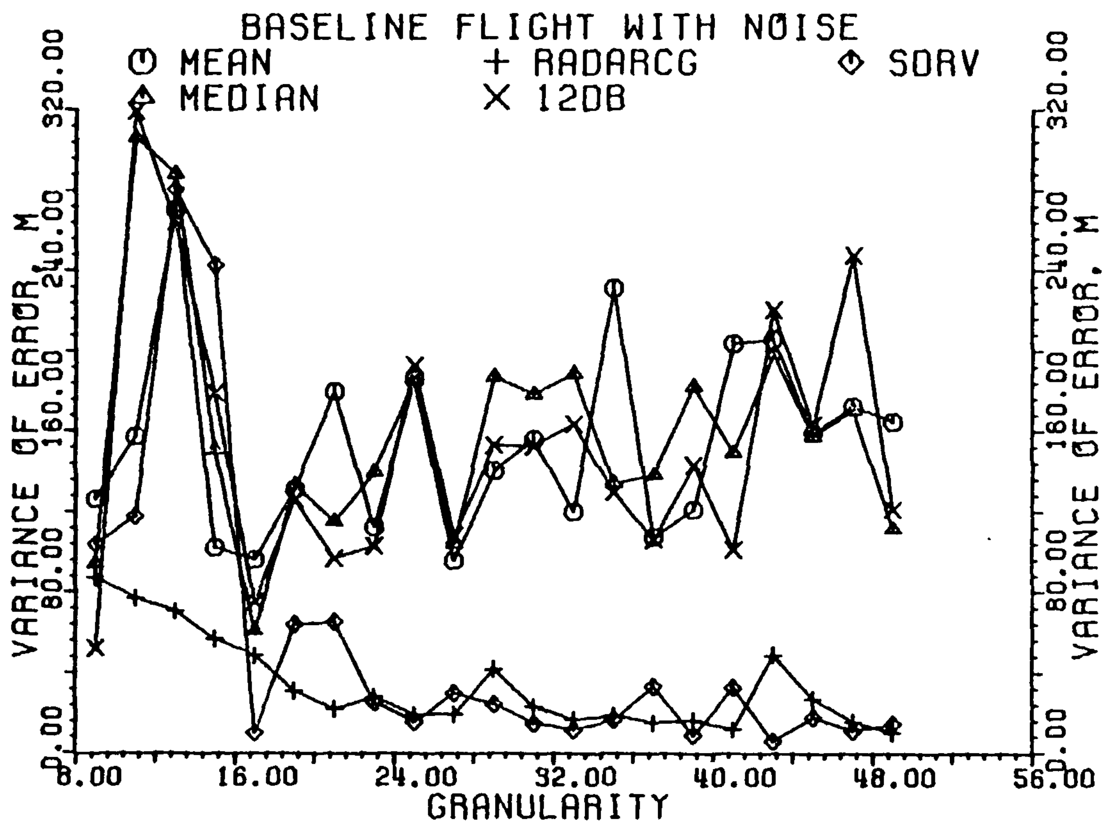

Figure 5-252. Variance of error of estimators in meters with the antenna 125 M from the runway centerline. Each data point is the result of one flight, all scans with a SNR at or below 10 dB used.

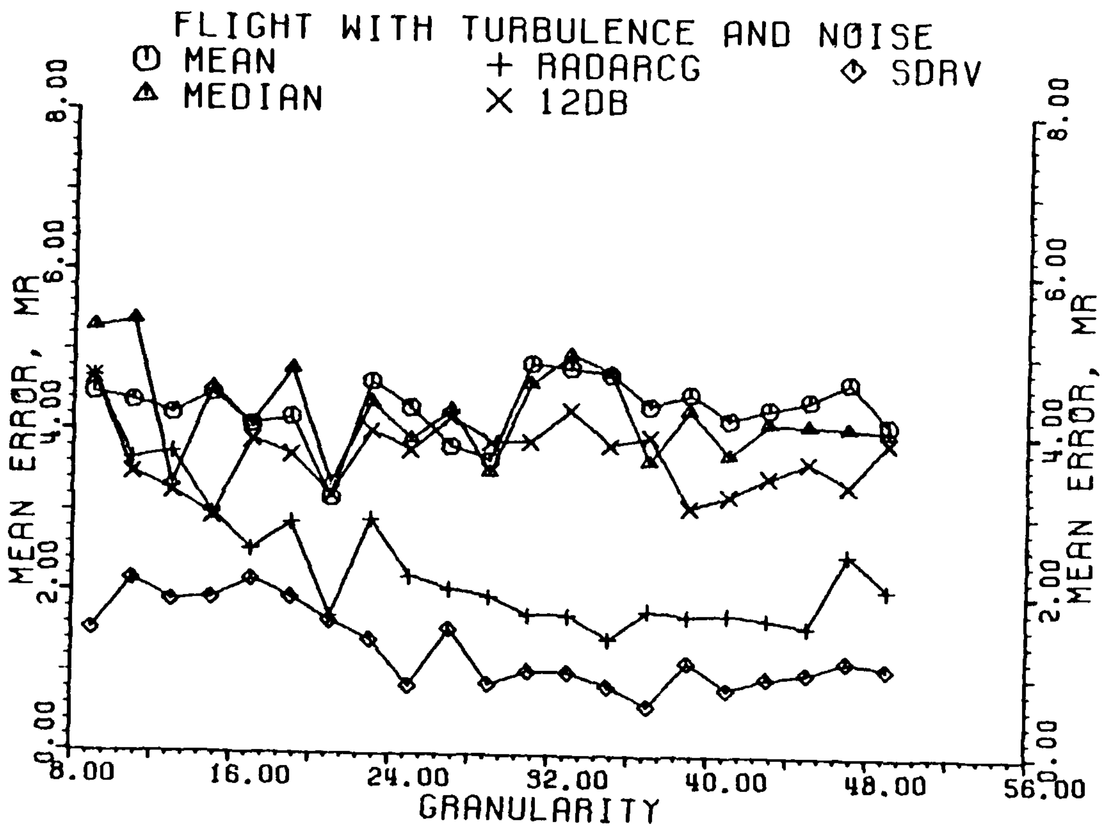

Figure 5-253. Mean error of estimators in milliradians with the antenna 125 M from the runway centerline. Each data point is the result of one flight, all scans with a SNR at or below 10 dB used.

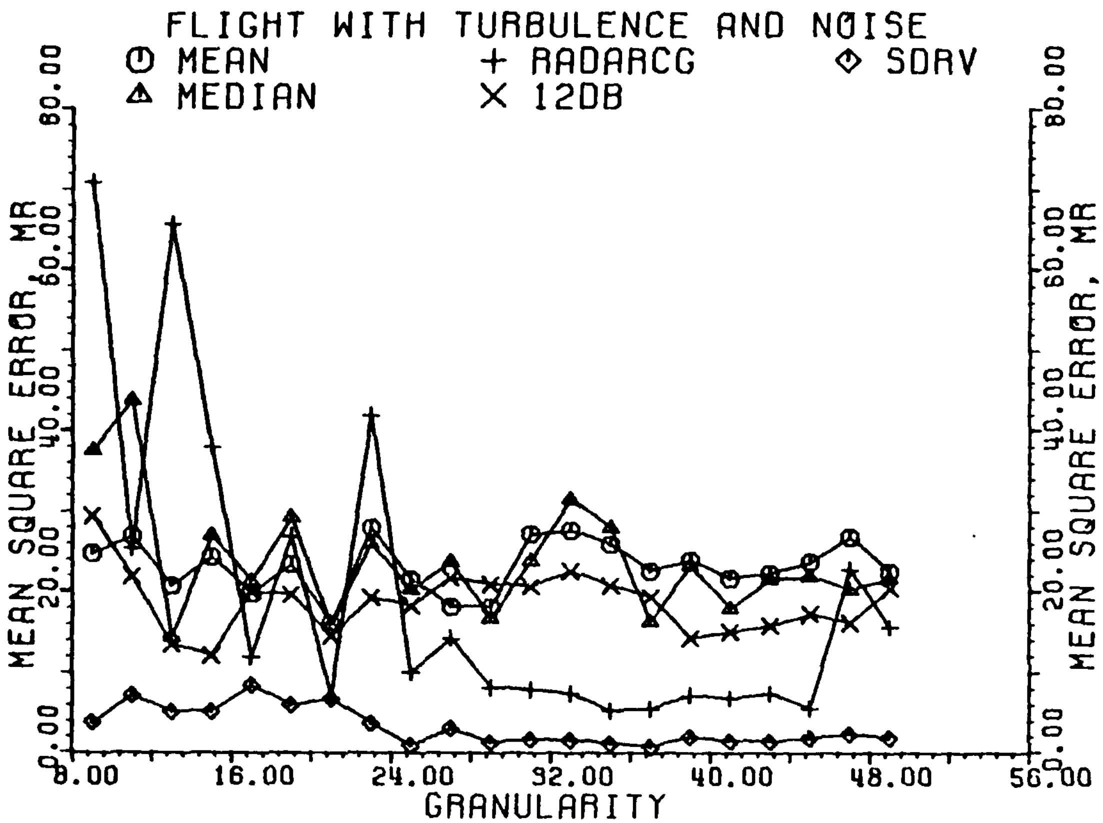

Figure 5-254. Mean square error of estimators in milliradians with the antenna 125 M from the runway centerline. Each data point is the result of one flight, all scans with a SNR at or below 10 dB used.

sort of filtering action. The thresholding methods have none, so their accuracy is limited by the amount of signal rising out of the noise floor. With enough beam locations in each window, SDRV can, in theory, be able to average out the noise in the target. When averaging is not done, as in the granularities at and below 21 beam locations, SDRV is only marginally better than the thresholding methods,as shown by the standard deviation and variance in milliradians, Figures 5-255 and 5-256. When averaging occurs in the higher granularities, the method stands by itself.

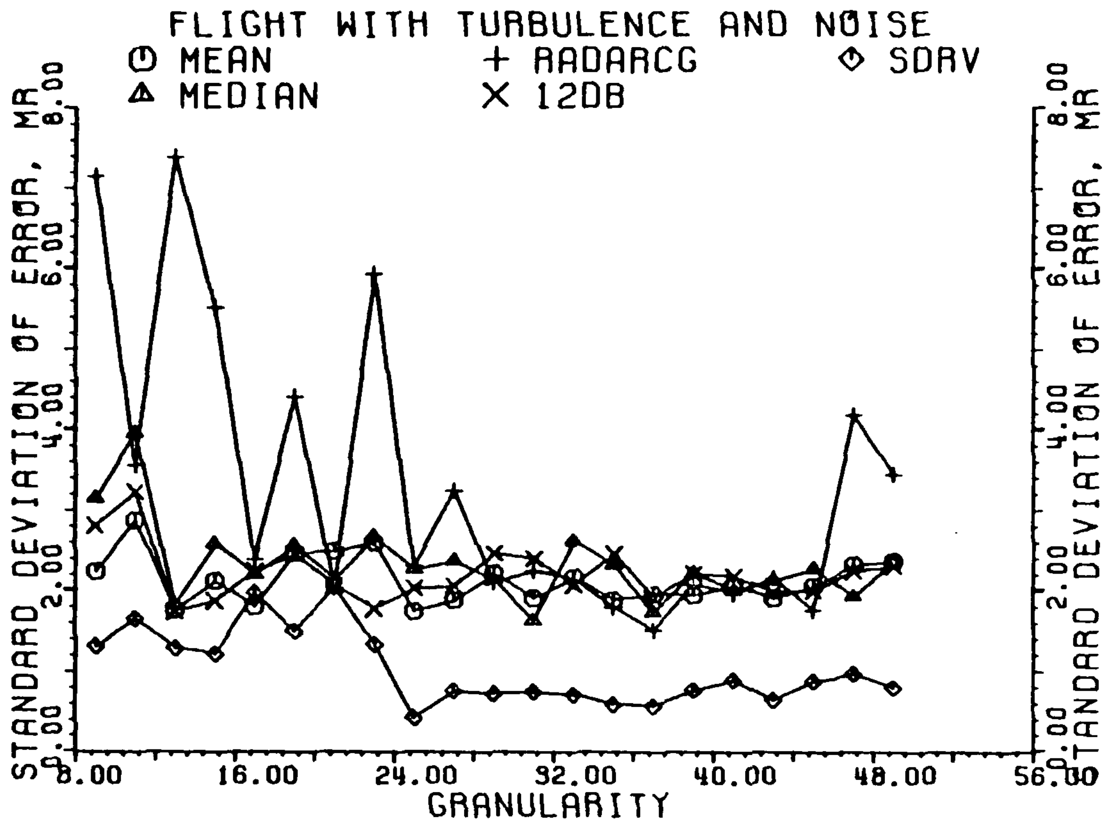

Figure 5-255. Standard deviation of error of estimators in milliradians with the antenna 125 M from the runway centerline. Each data point is the result of one flight, all scans with a SNR at or below 10 dB used.

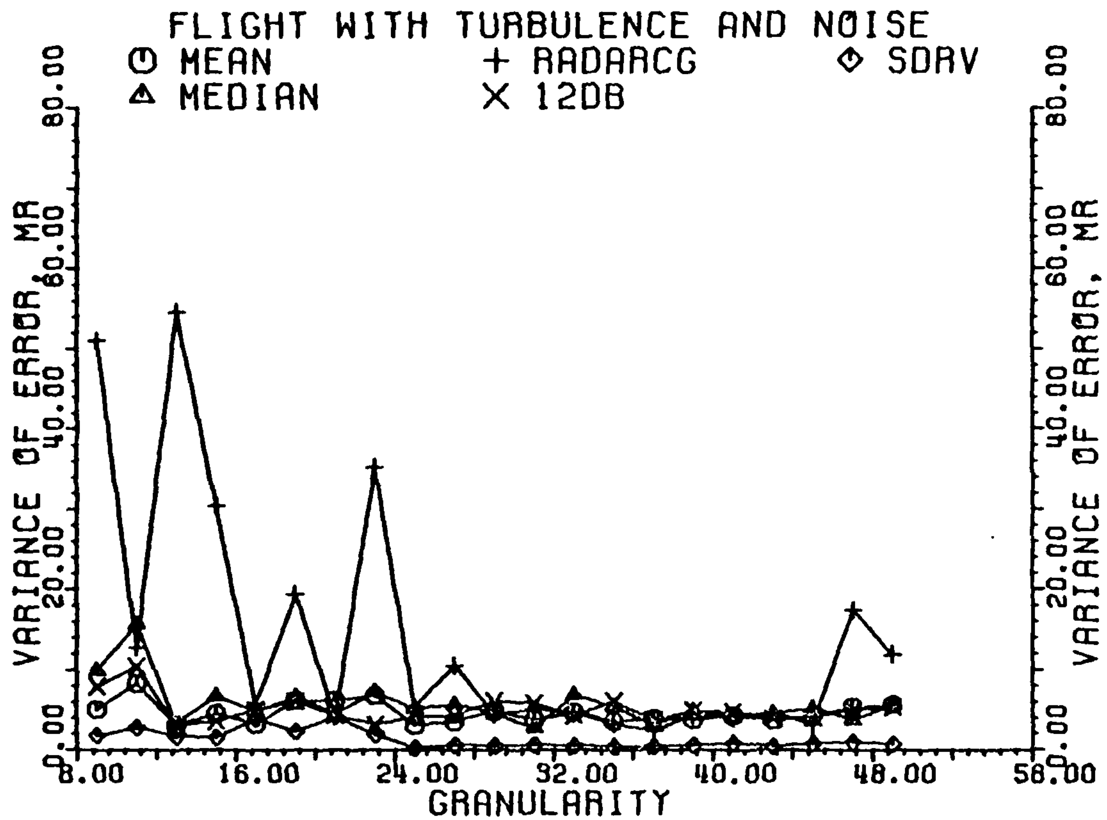

Figure 5-256. Variance of error of estimators in milliradians with the antenna 125 M from the runway centerline. Each data point is the result of one flight, all scans with a SNR at or below 10 dB used.

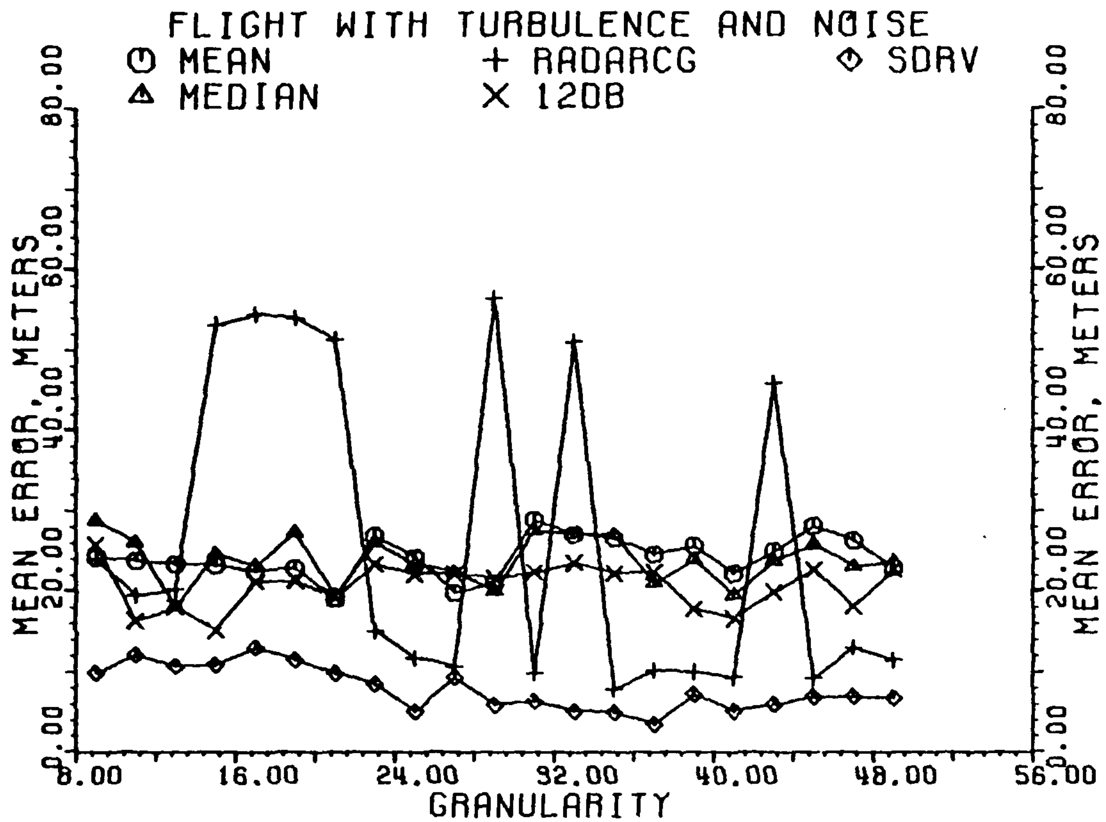

Figure 5-257. Mean square of estimators in meters with the antenna 125 M from the runway centerline. Each data point is the result of one flight, all scans with a SNR at or below 10 dB used.

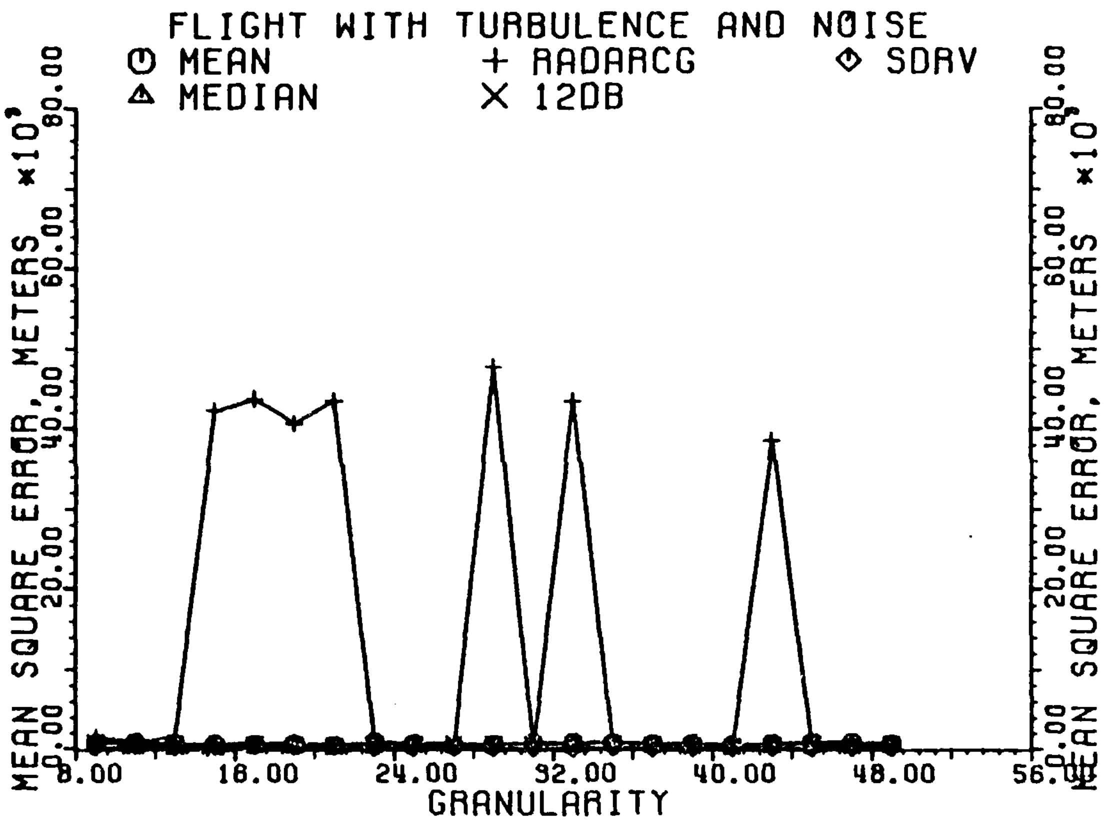

Figure 5-258. Mean square error of estimators in meters with the antenna 125 M from the runway centerline. Each data point is the result of one flight, all scans with a SNR at or below 10 dB used.

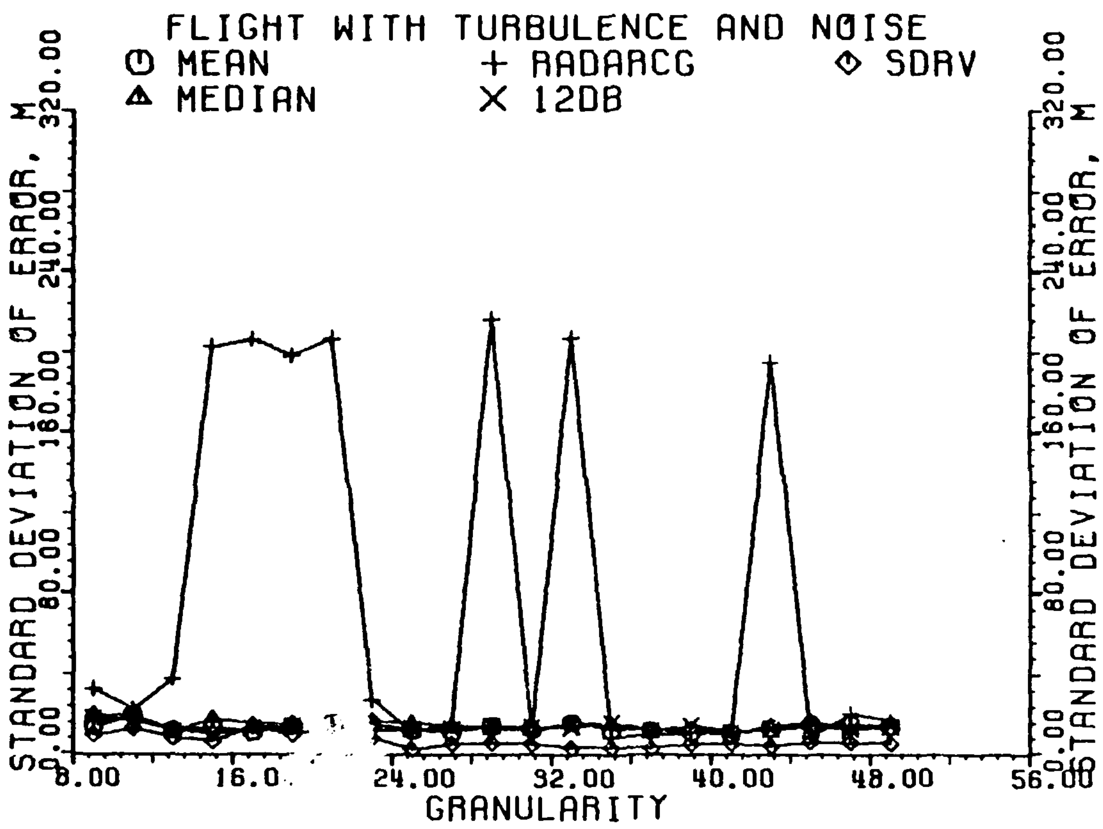

Figure 5-259. Standard deviation of error of estimators in meters with the antenna 125 M from the runway centerline. Each data point is the result of one flight, all scans with a SNR at or below 10 dB used.

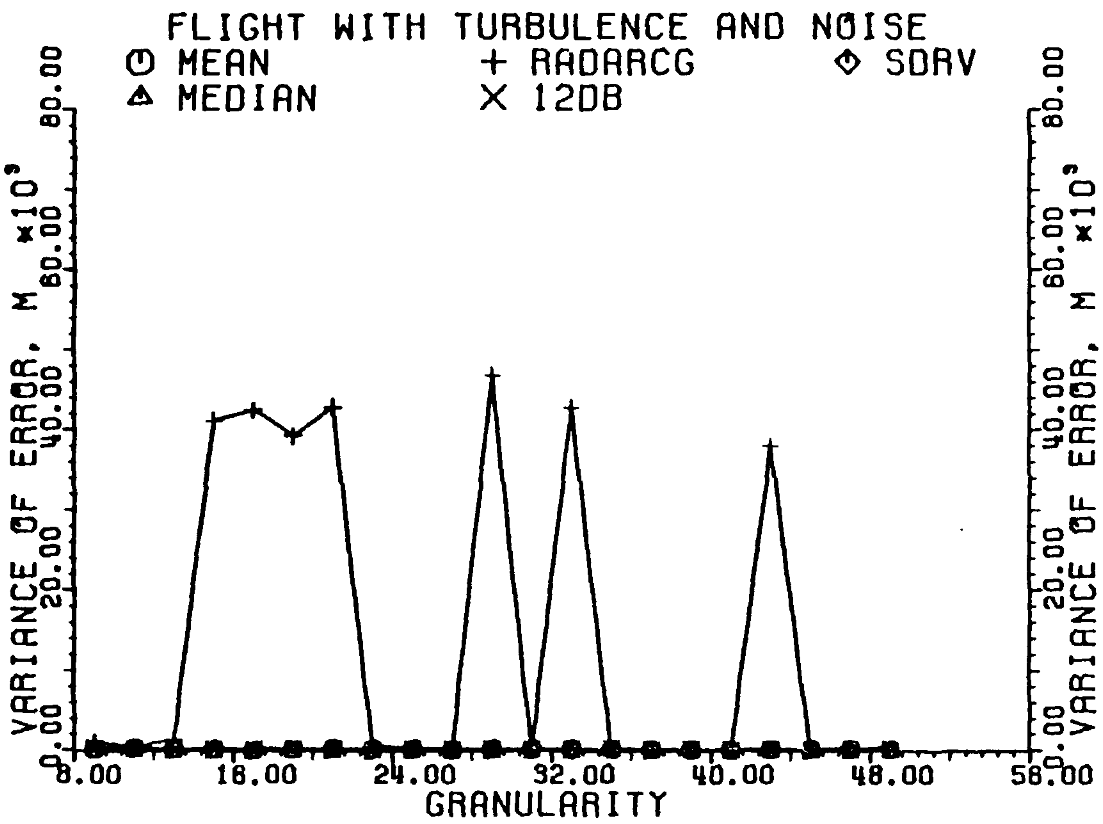

Figure 5-260. Variance of error of estimators in meters with the antenna 125 M from the runway centerline. Each data point is the result of one flight, all scans with a SNR at or below 10 dB used.

VI. SUMMARY

The subject of this work was to introduce a new non-thresholding algorithm, and to determine the estimating ability of it with a second non-thresholding algorithm (radar center of gravity) and three thresholding techniques, two post-determined (mean and median) and one predetermined (12 dB). It was observed that during periods of high signal-to-noise ratio the radar center of gravity was superior to the other methods, with the second derivative method a very close second. With the same signal-to-noise ratios, the thresholding methods were of equal estimating ability, with a slight favoring of the 12 dB threshold. The addition of turbulence alone into the simulation did not appreciably affect the error produced by the estimators since there was no noise floor present in the computer simulation. Therefore, the signal-to-noise ratio was infinite, regardless of the actual return amplitude of the scan, and the flights with only turbulence were really just baseline flights revisited.

When 15 dB of zero-mean random gaussian noise was added to the baseline flight or flight with turbulence scan returns, the second derivative method emerged as the most accurate estimator, especially in periods of low signal-to-noise ratio. The radar center of gravity is degraded because it always makes a location estimate, regardless of whether or not a target is present. With enough beam locations, the noise will average out, and the estimator will improve as shown by the plots of error versus granularity. The thresholding methods also make an estimate of target location regardless of the presence or absence of a target, except in the rare instance when no two consecutive returns are above the scan threshold. In this simulation, if there is no target, but only noise, the mean estimator will calculate a threshold close to zero. Since gaussian noise is randomly positive and negative, the probability that all returns in the scan be alternately positive and negative is low. Therefore, the probability that the there is at least one instance where two consecutive returns are positive is high, and a "target" is found, since two positive returns are above the threshold. Again in the noise only case, the median estimator will set the threshold at the median return amplitude, which will be approximately zero, and the above argument holds for this estimator also. In the case of the 12 dB estimator, 12 dB down from a noise voltage places the threshold in noise, and the above argument can be reapplied. Therefore, none of the above estimators are truely capable of target detection, since the estimators will do their best to find a "target" regardless of whether or not one is present. Only the second derivative method is able to make a decision as to the absence or presence of a target by operating on the shape of the scan return. If no target is present, the shape of the return is flat with zero slope and a constant second derivative. If a target is present, the slope will change and the second derivatives of each set of estimator windows will change sign, locating the point of maximum slope and therefore a target edge. The plots of scan SNR versus average number of scans, Figures 4-13, 14, 17, 18, 21, and 22, show the second derivative method to reject those scans of low SNR. The plots of error for low SNR, in particular Figures 5-253 through 5-260, show that when a scan is accepted and a decision of target location is made, that the decision is accurate, because even in noise the basic scan shape was suitable enough to detect and locate a target.

The figures of error versus antenna offset show no apparent increase in error due to antenna offset. This is primarily due to the high PRF which "stops" the target in the flight path during the scan. Even with a large granularity, the target will move only on the order of its own length during the scan. So the effect due to translation is small. Since the target movement is small, in translation as well as in rotation due to turbulence, the modulation of the radar cross section of the target is small, and that effect is also negligible. Therefore, the results of this computer simulation is accurate in those regards. Yet, in actual practice, error is expected when the antenna is delocated from the runway. This error is introduced by the ranging accuracy of the radar. If the antenna is a distance to the left of the runway, and the range estimate is short of the actual target location, then the estimate of position will place the target to the left of the runway independent of the error to the target centroid in milliradians.

The plots of error versus granularity display little decrease in error with an increase in granularity for the thresholding methods, but does show an increase in robustness with granularity. Both non-thresholding methods improve in both average error and robustness with granularity.

Overall, The second derivative algorithm is clearly the estimator least prone to error and most robust in estimating ability for virtually all granularities in the presence of noise. The radar center of gravity estimator is most accurate in periods of high SNR and with fine granularities. It suffers degradation in noise, and in large noise becomes unusable as an estimator due to noise outliers in the scan returns. The thresholding methods are rather robust but less accurate than the second derivative method and RADARCG with high SNRs.

Pulse economy is of great importance. That estimator which uses the fewest pulse transmissions without an increase in target location will in general be the estimator employed in practice. The 12 dB thresholding method is especially suited to pulse economy. When a target edge is found, scanning translates to the other side of the scanning window, saving pulse transmissions by removing the requirement to fully scan the target. The second derivative method does require that the target be scanned more fully than the 12 dB method, as shown in Figures 5-1 to 5-4. While this reduces the probability of false alarm, it requires the expenditure of additional ulse transmissions in the scanning window. However, virtually every data point on the 256 figures in the previous chapter have shown the mean error, mean square error, and standard deviation and variance of the error of SDRV to be less than the 12 dB estimator. How do these methods compare in terms of target location accuracy versus pulse budget?

A plot of average pulses used per scan versus granularity is shown in Figure 6-1. It should be pointed out that in this simulation, time was incremented as though 3 pulses were transmitted at each beam location, but only one pulse was used. Since there is a one to one correspondence

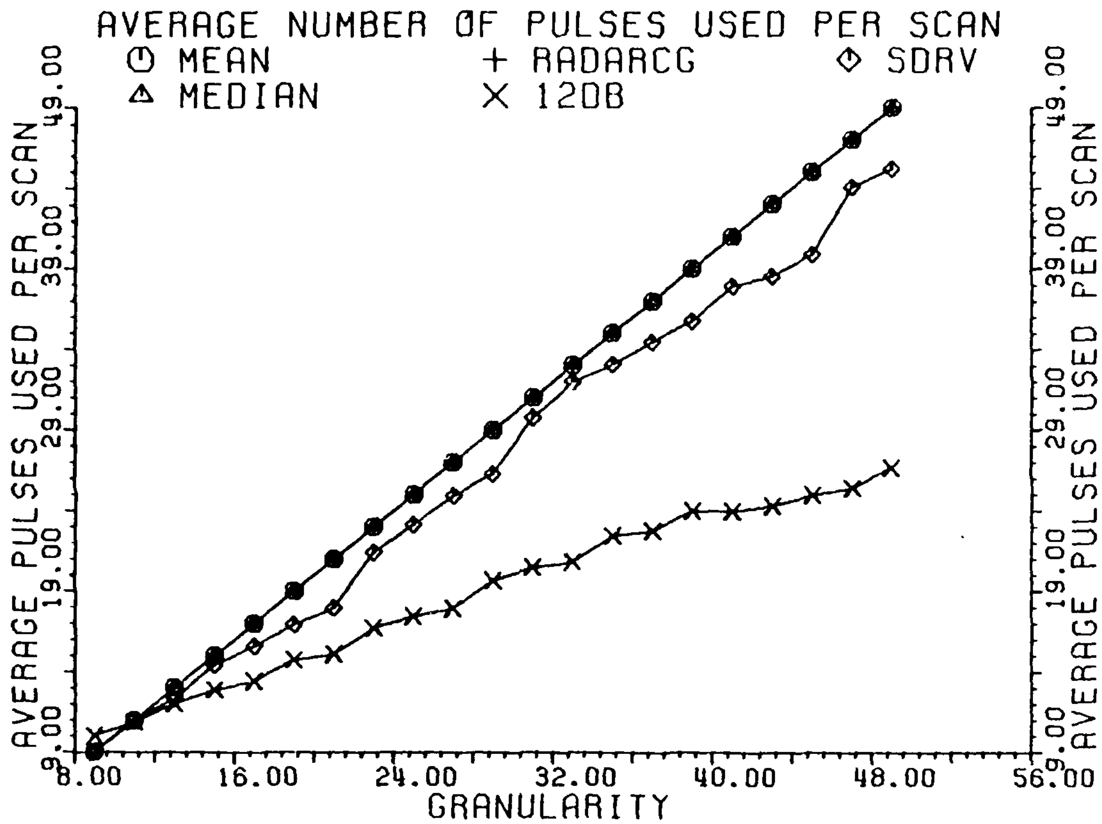

Figure 6-1. Average number of pulses used per scan. Each data point is the result of 103 scans on the target.

between pulses per scan and the number of beam pointing locations in the scan, the mean, median and RADARCG estimators use a number of pulses equal to the scanning granularity. The 12 dB method transmits one pulse in the direction of the target to set the threshold, and thus uses one pulse before the start of the scan. The second derivative estimator has the capability of rescanning part of the target twice due to the nature of the algorithm. As such, it can use more pulses than the magnitude of the scanning granularity. Referring to Figure 6-1, the 12 dB estimator is shown to use about half of the pulses budgeted for the scan. The second derivative stays very close to the pulse budget, sometimes re-scanning the target more frequently at certain granularities. Those are the granularities where the number of beam locations in each window of the estimator increases by one. The highest granularities that do not increase the number of beam locations in the windows, namely the granularities 21, 29, and 45, have the least pulse usage but the highest error.

In periods of high SNR, what should be expected with regards to pulse usage? Figure 6-2 is a plot of the average number of pulses used per scan, only those scans of at least 13 dB selected. There is almost no change in the number of pulses used by SDRV. The 12 dB method used more pulses, because it had set the threshold higher due to the increase in return amplitude.

In periods of low SNR, as shown by Figure 6-3, the 12 dB method used fewer pulses, because it was able to trigger on noise at the ends of the scanning window, rather than triggering on the target itself. Also as expected, there was a slight increase in the number of pulsed used by

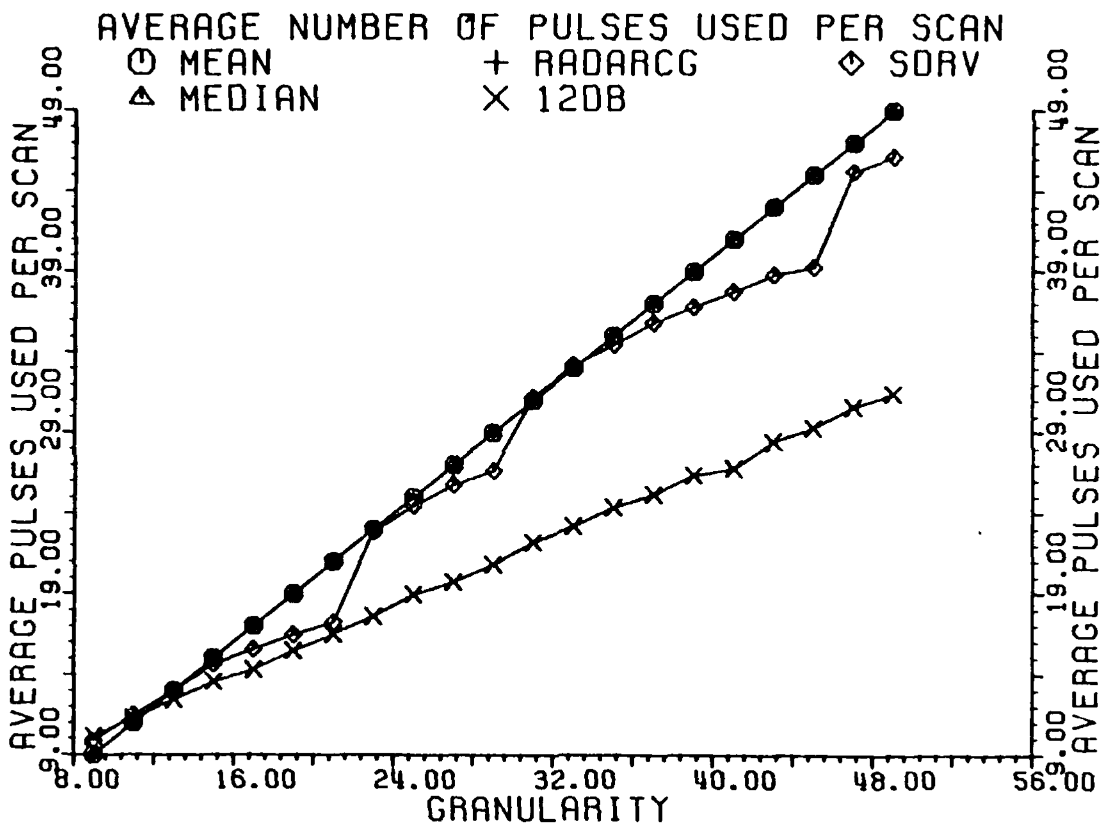

Figure 6-2. Average number of pulses used per scan. Each data point is the result of one flight, all scans with a SNR 13 dB or greater used.

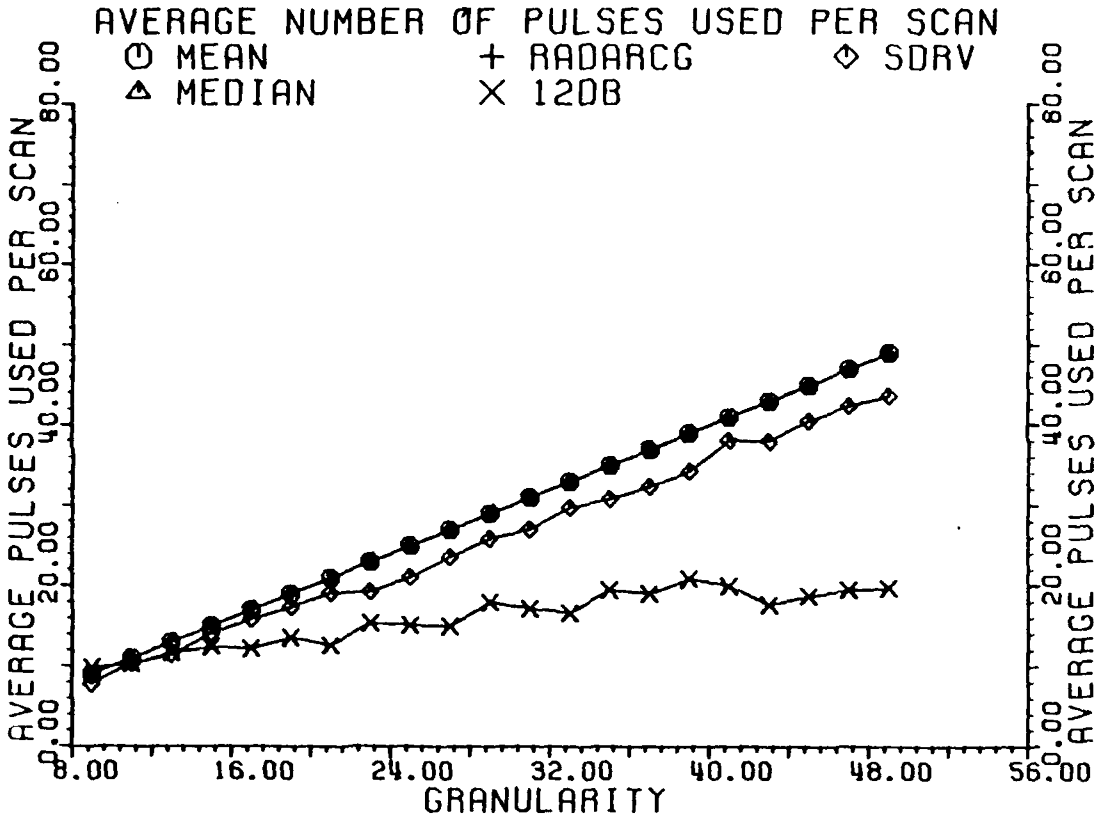

Figure 6-3. Average number of pulses used per scan. Each data point is the result of one flight, scan SNR at or below 10 dB used.

SDRV as it was forced to search further in the scan to locate a target, the noise alone being unable to satisfy the algorithm.

But we have not yet addressed the posed question - what is the relationship between pulses used and error induced? Returning to Figure 5-221, let us choose the granularity where the 12 dB estimator is the most accurate. This would be a granularity of 45 beam locations in the scanning window. From Figure 6-1, the 12 dB method used approximately 25 pulses per scan, on the average, at that granularity. Moving directly across the figure to the left, it is observed that the second derivative method used about 25 pulses per scan with a granularity of 27 beam locations in the scanning window. Returning to Figure 5-221, the mean error of the second derivative algorithm at a granularity of 27 beam locations is approximately 1 mrad. From the same figure, using 27 pulses per scan (granularity of 45), the 12 dB estimator had a mean error of about 2.7 mrad. Further, comparison of the results of SDRV at a granularity of 27, Figures 5-197 through 5-260, with the results of the 12 dB estimator at a granularity of 47, shows the second derivative algorithm to be clearly superior. Since the mean, median, and RADARCG estimators all use more pulses than the 12 dB threshold, SDRV is also more efficient per pulse than those methods.

It is instructive to examine the error of the estimators as a function of range. Since the 12 dB estimator is representative of the thresholding estimators, only the data for it was plotted against the output of the RADARCG and SDRV methods in the accompanying figures. The data was obtained by using the results of the eleven flights with noise and turbulence representing each antenna offset location at all 21 scanning granularities, regardless of scan SNR. The data is plotted in Figures 6-4 to 6-11, error as a function of scan number. The first scan occurred with the target 4.0 nmi from the antenna, and the 103rd scan occurred with the target over the release point. Clearly shown is the consistency of the 12 dB thresholding method and the SDRV method with about half the error. Also clearly shown is the marked lack of robustness of RADARCG. This is most pronounced at far range, and decreases to the level of SDRV at close range. Note that RADARCG appears to be more accurate but less robust than SDRV at close range from the plots in milliradians, Figures 6-4 to 6-7, but was actually approaching the quality of SDRV as seen in the plots with error in meters, Figures 6-8 to 6-11. Finally, the plots show the error to reduce as the target approaches, an expected result.

It is appropriate to conclude this work with a comparison of the estimators on a pulse-by-pulse basis. Since a typical radar system has a limited pulse budget, it is prudent to employ the centroid estimator which uses the pulses expended most efficiently. The following figures are plots of the average (mean) error of an estimator per pulse as a function of the average number of pulses used in the scan. Each data point is the result of 11 flights of which the total error was divided by the total number of pulses used to obtain a single data point. Figures 6-12 and 6-13, the error-pulse ratio in milliradians and meters, respectively, used all scans regardless of SNR. The second derivative estimator is clearly shown to use the available pulse budget most efficiently by having the least error per pulse for any amount of pulses budgetted in that scan. Note that the SDRV method is most efficient with pulse integration, and

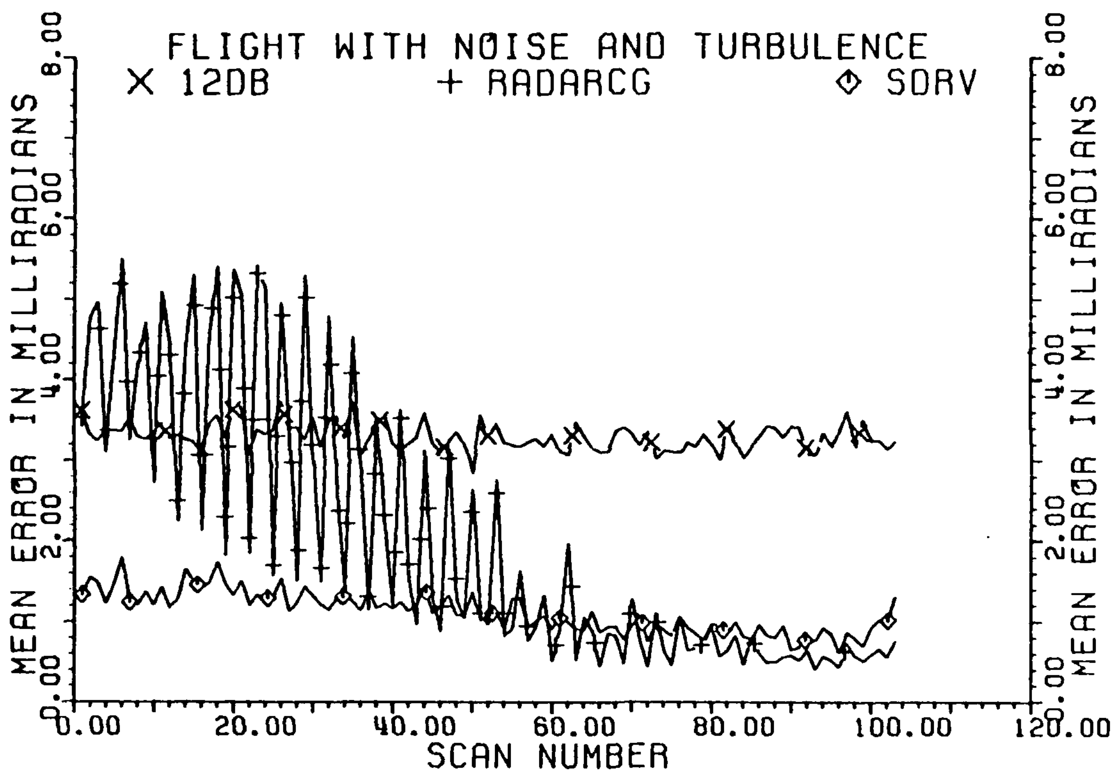

Figure 6-4. Mean error in milliradians as a function of scan number for flights with noise and turbulence, all scans used.

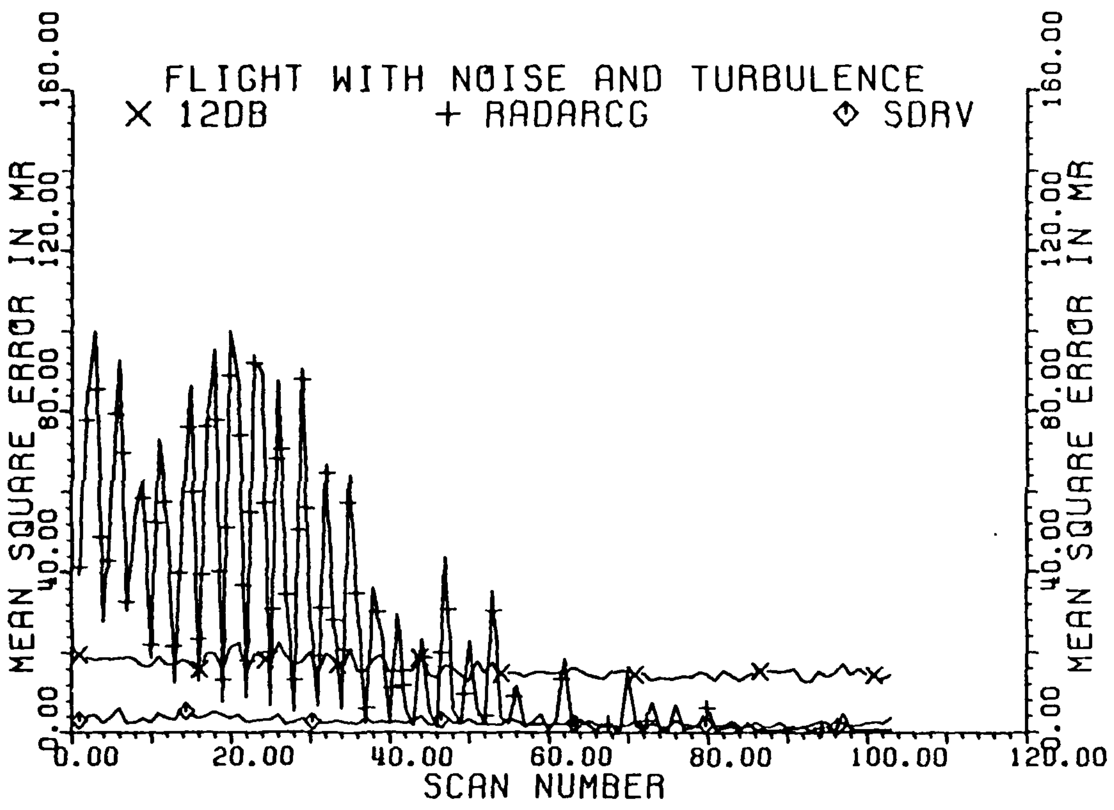

Figure 6-5. Mean square error in milliradians as a function of scan number for flights with noise and turbulence, all scans used.

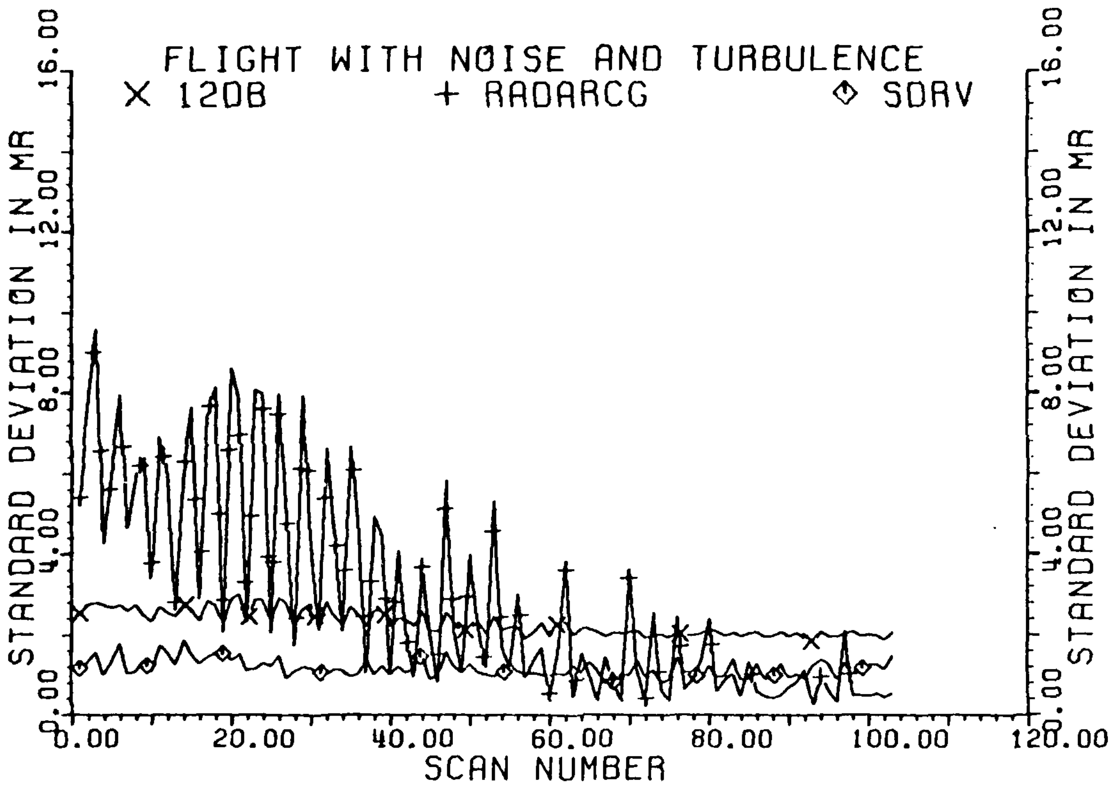

Figure 6-6. Standard deviation of error in milliradians as a function of scan number for flights with noise and turbulence, all scans used.

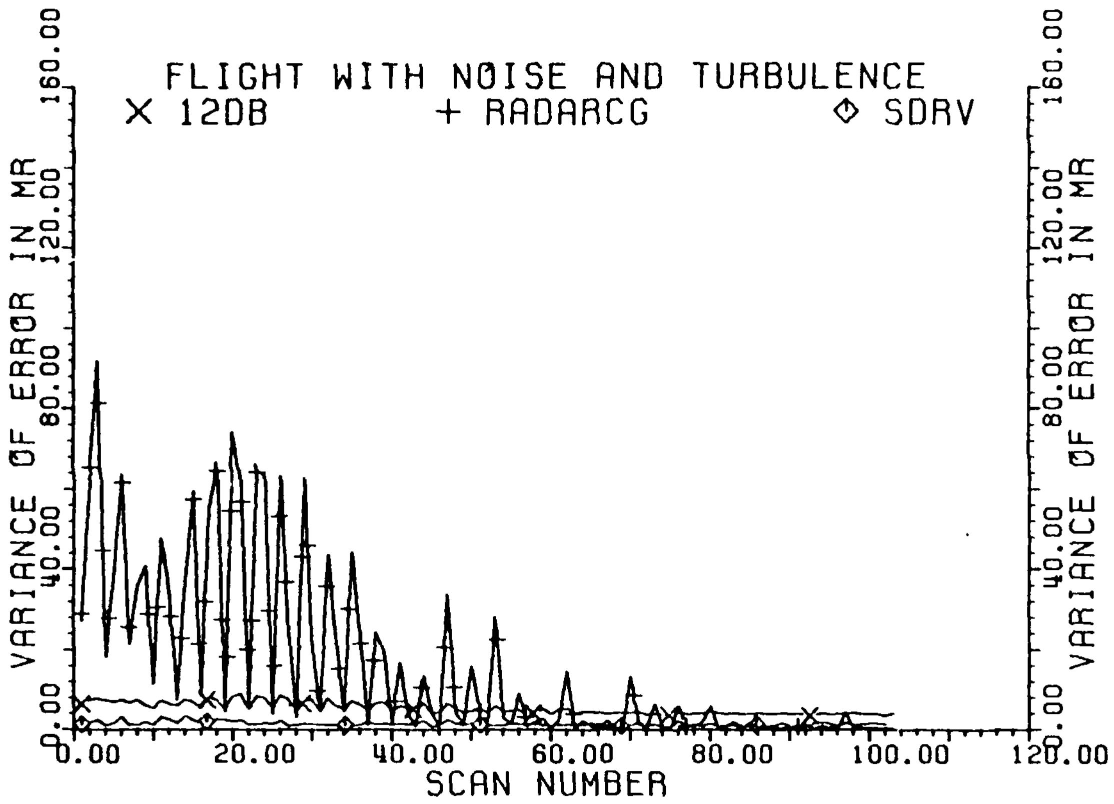

Figure 6-7. Variance of error in milliradians as a function of scan number for flights with noise and turbulence, all scans used.

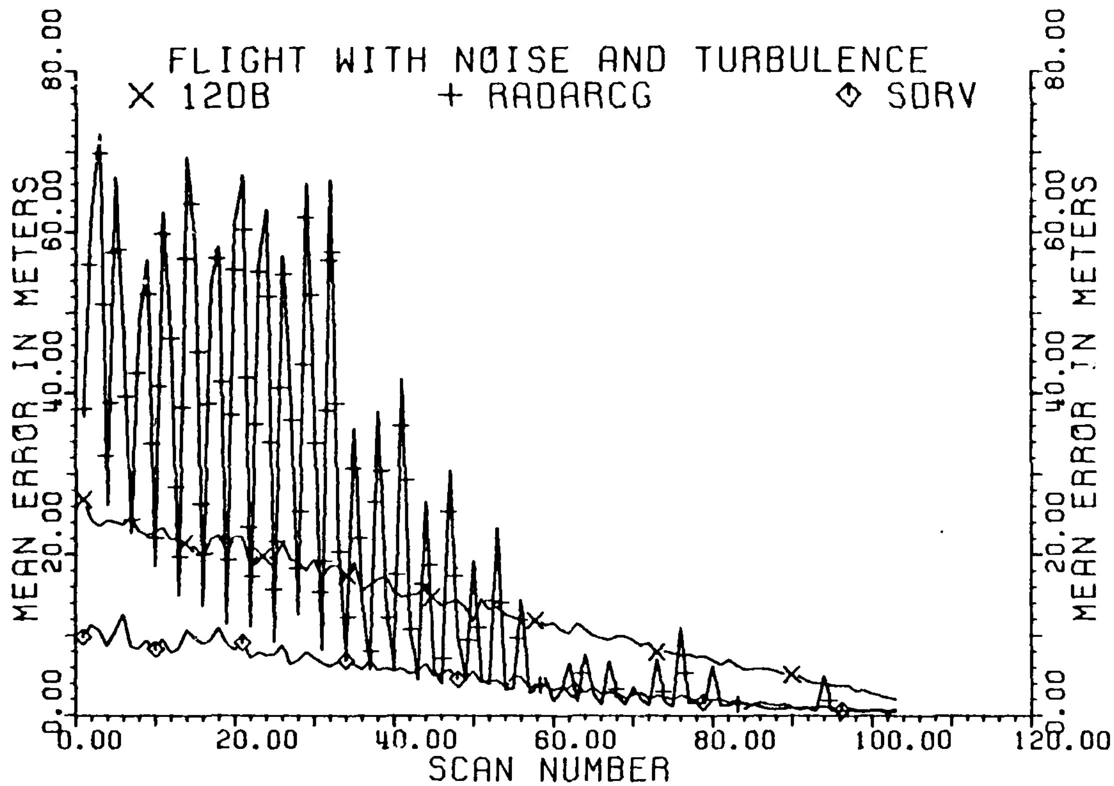

Figure 6-8. Mean error in meters as a function of scan number for flights with noise and turbulence, all scans used.

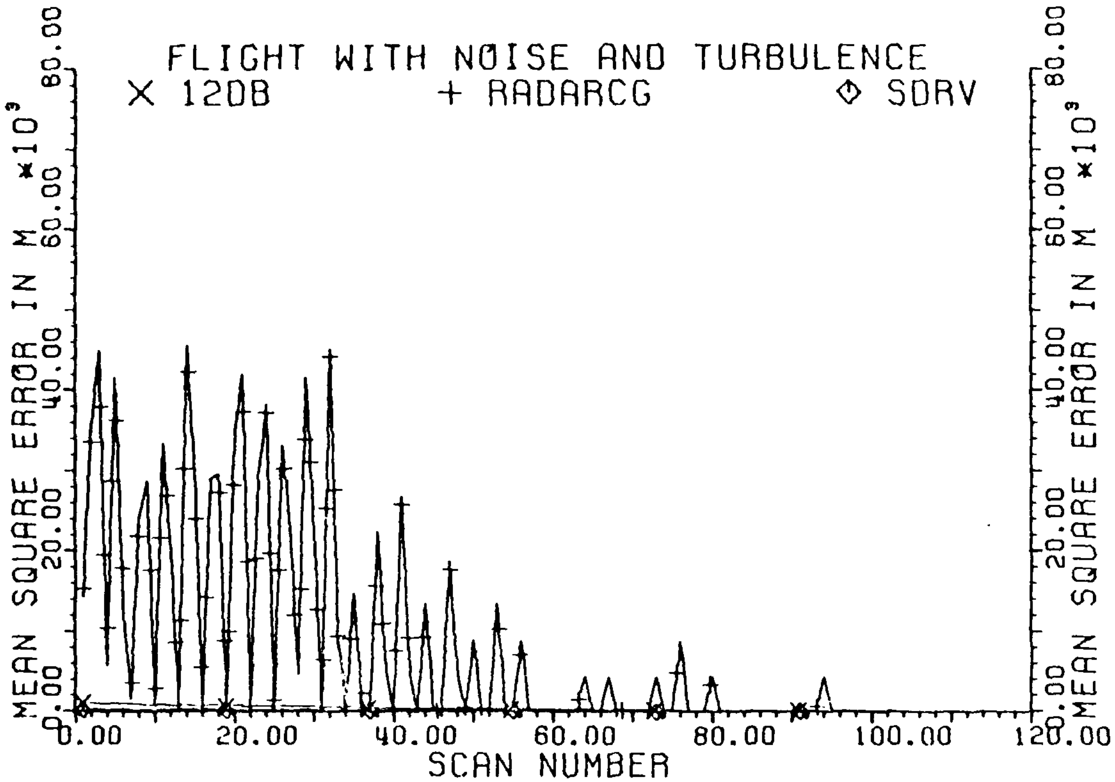

Figure 6-9. Mean square error in meters as a function of scan number for flights with noise and turbulence, all scans used.

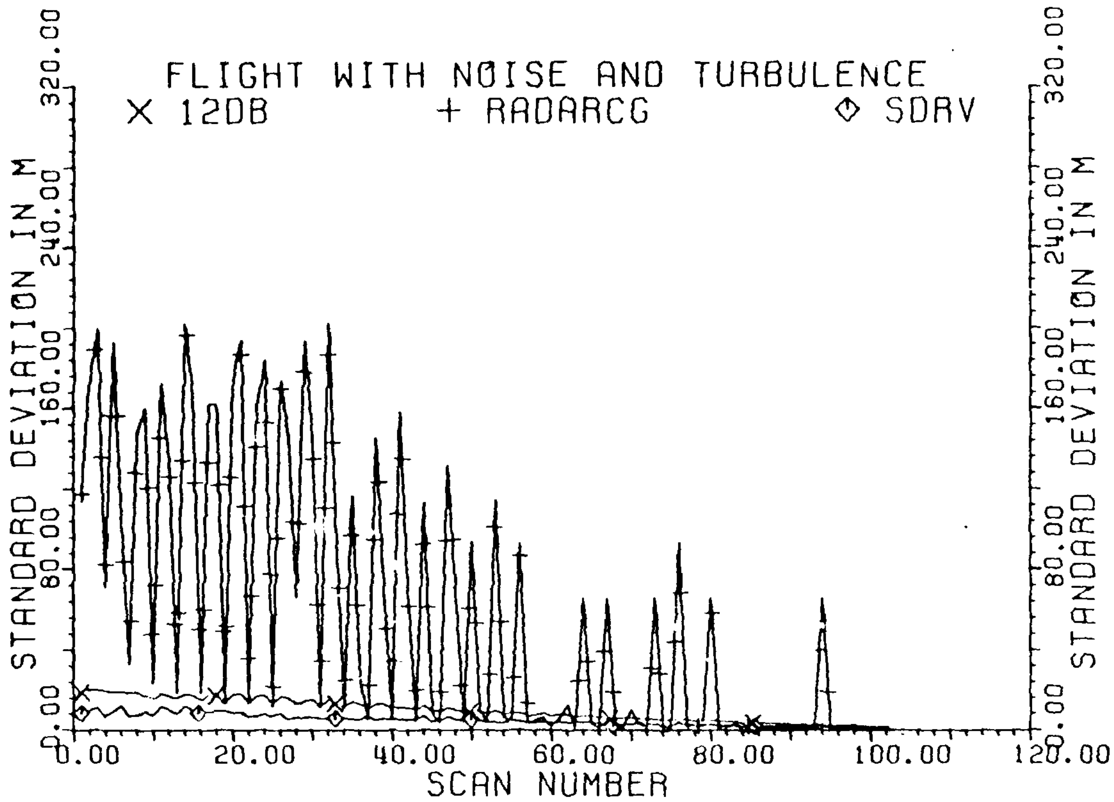

Figure 6-10. Standard deviation of error in meters as a function of scan number for flights with noise and turbulence, all scans used.

AD-A110 862 GEORGIA INST OF TECH ATLANTA ENGINEERING EXPERIMENT --ETC F/G 17/7
MARINE AIR TRAFFIC CONTROL AND LANDING SYSTEM (MATCALS INVESTIG--ETC(U)
SEP 81 E R GRAF, C L PHILLIPS, S A STARKS N00039-80-C-0032
UNCLASSIFIED GIT/EES-1-A-2550-VOL-1 NL

5 of 5
AD A110862

END
DATE FILMED
3 82
DTIC

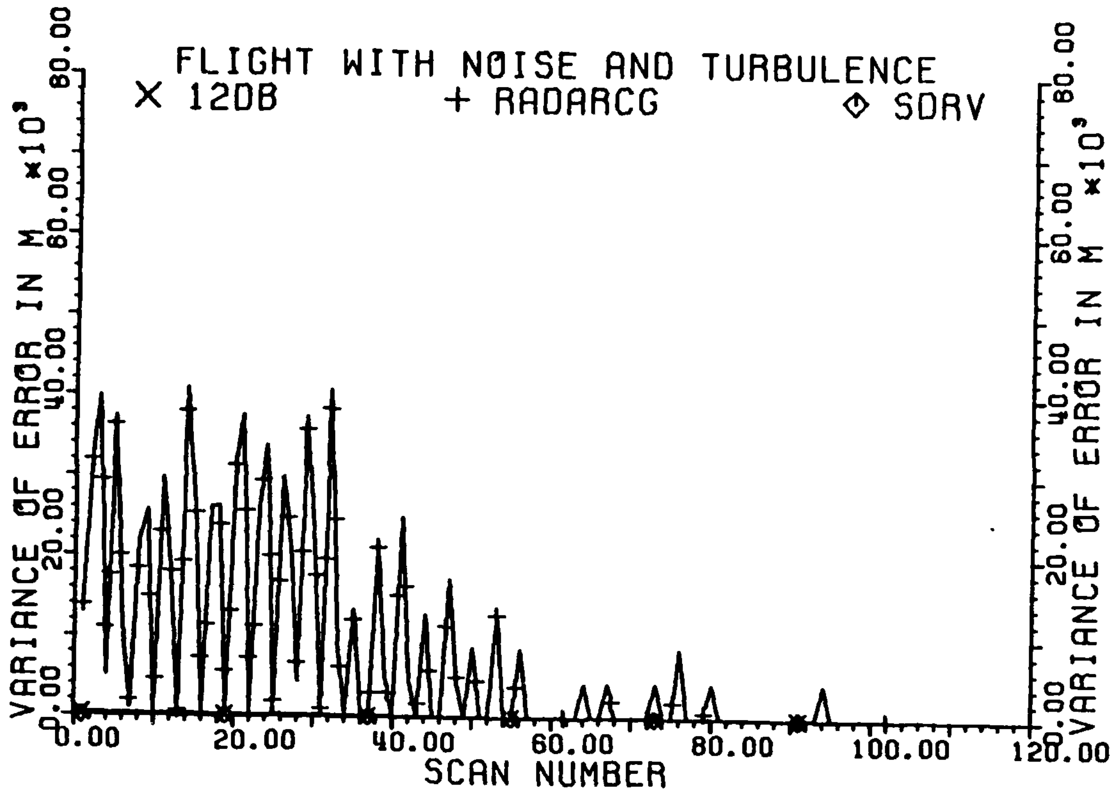

Figure 6-11. Variance of error in meters as a function of scan number for flights with noise and turbulence, all scans used.

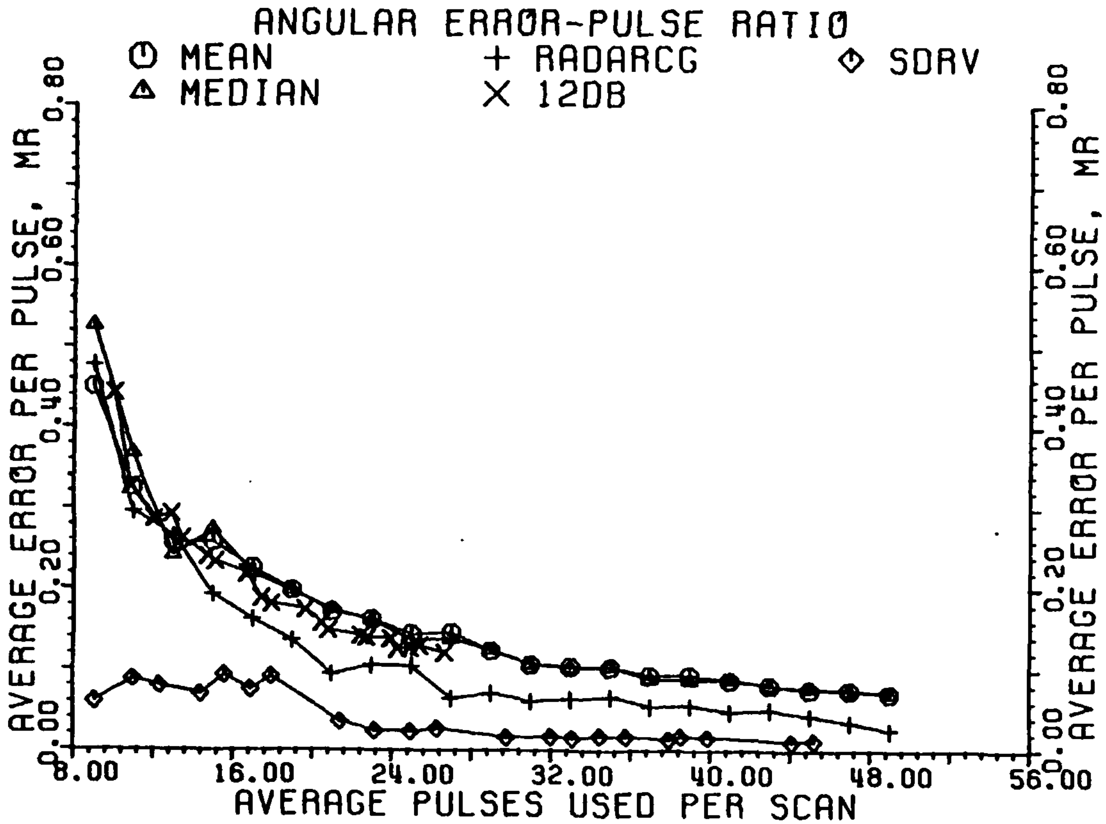

Figure 6-12. Angular error-pulse ratio for flights with noise and turbulence, all scans used.

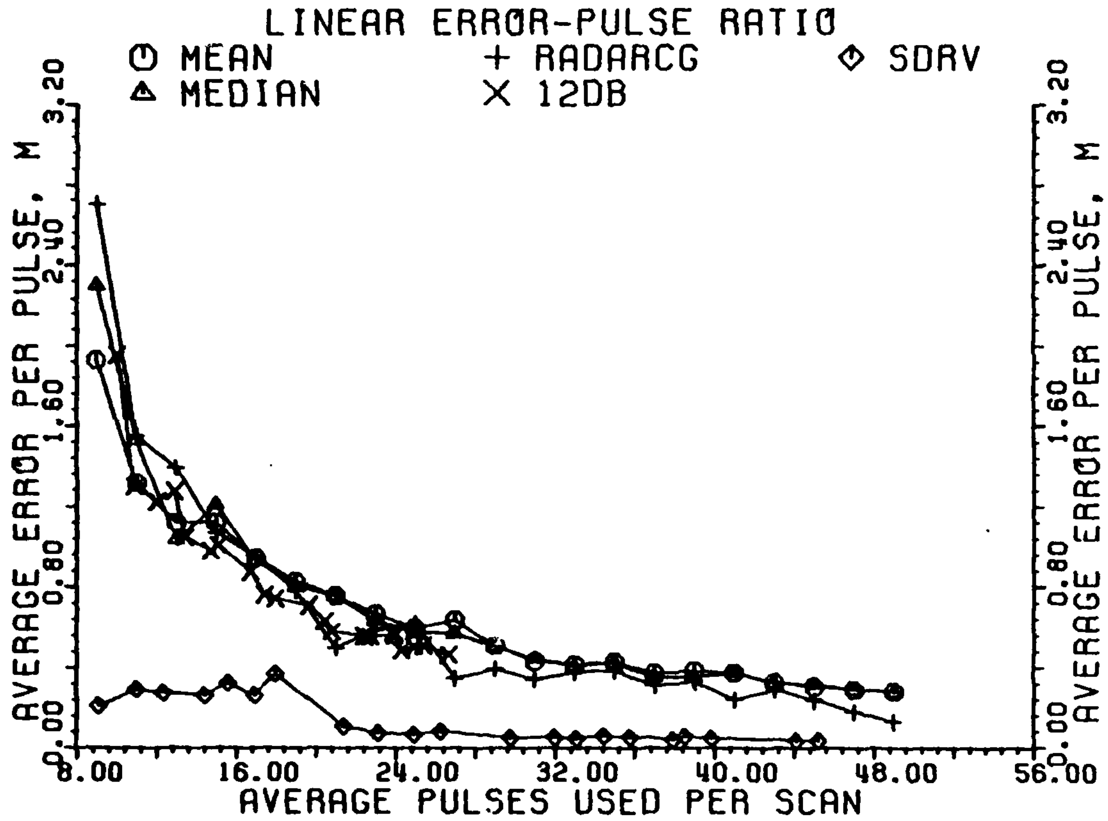

Figure 6-13. Linear error-pulse ratio for flights with noise and turbulence, all scans used.

that the other estimators approach the quality of SDRV at low pulse usage only with finer granularities.

For comparison, in periods of high SNR, RADARCG is of the same quality as SDRV with pulse integration, as shown in Figures 6-14 and 6-15. The thresholding methods are of equal quality. As is to be expected, SDRV is the most efficient estimator in low SNR, Figures 6-16 and 6-17, with RADARCG least efficient. Here the effect of pulse integration in the SDRV algorithm is most dramatic.

In conclusion, the second derivative algorithm is shown to have the least error per pulse used in comparison to the other estimators employed in this simulation. It is the most robust of those compared due to the unique scan rejection capability inherent in the architecture of the algorithm.

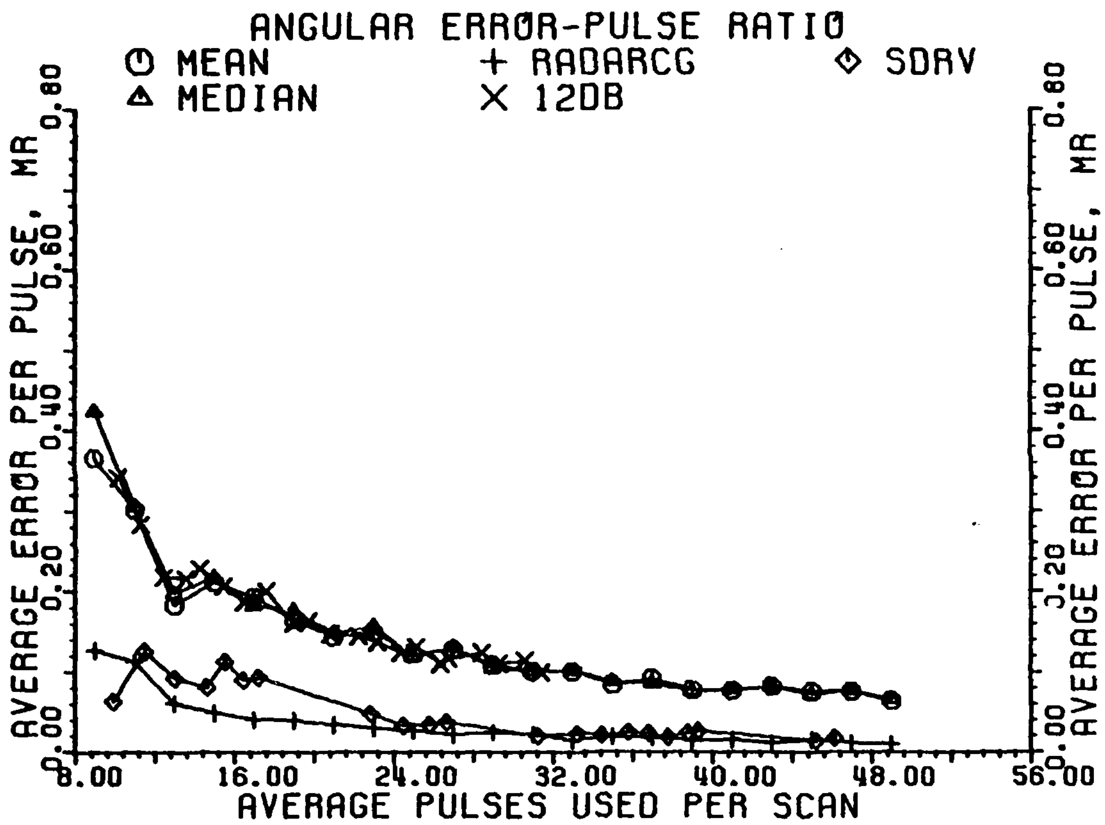

Figure 6-14. Angular error-pulse ratio for flights with noise and turbulence, all scans with a SNR 13 dB or greater used.

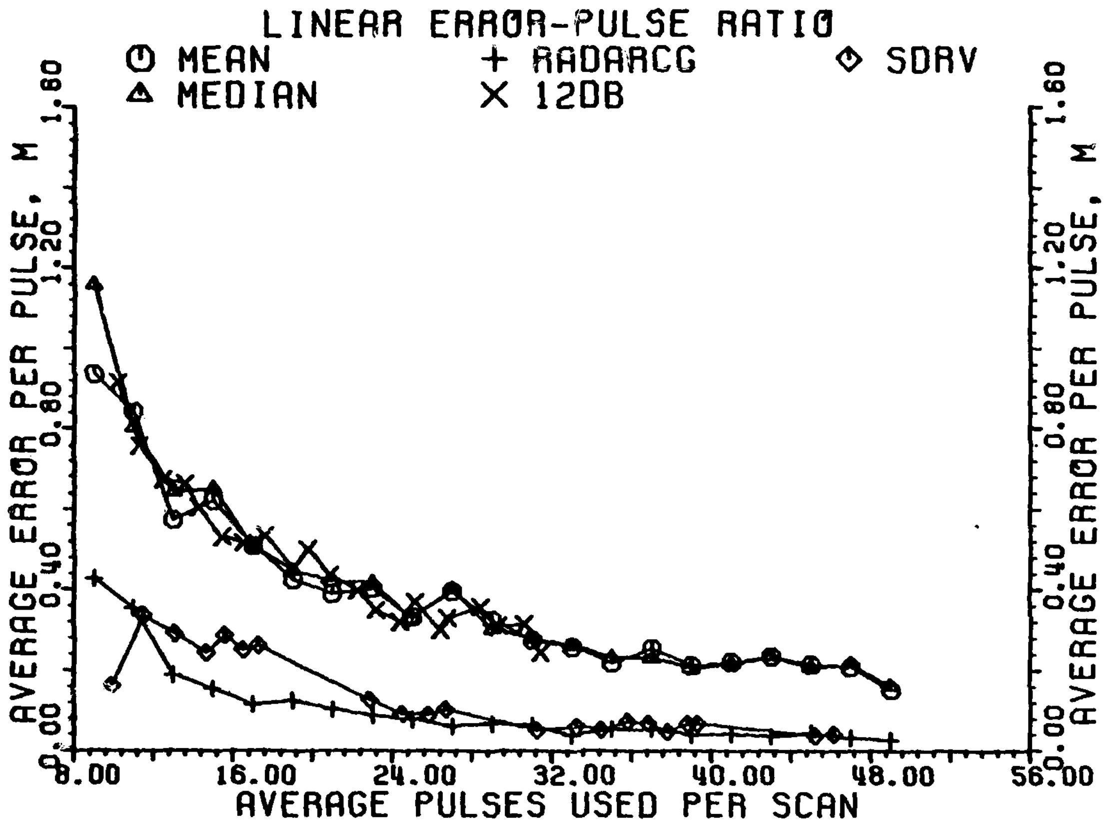

Figure 6-15. Linear error-pulse ratio for flights with noise and turbulence, all scans with a SNR 13 dB or greater used.

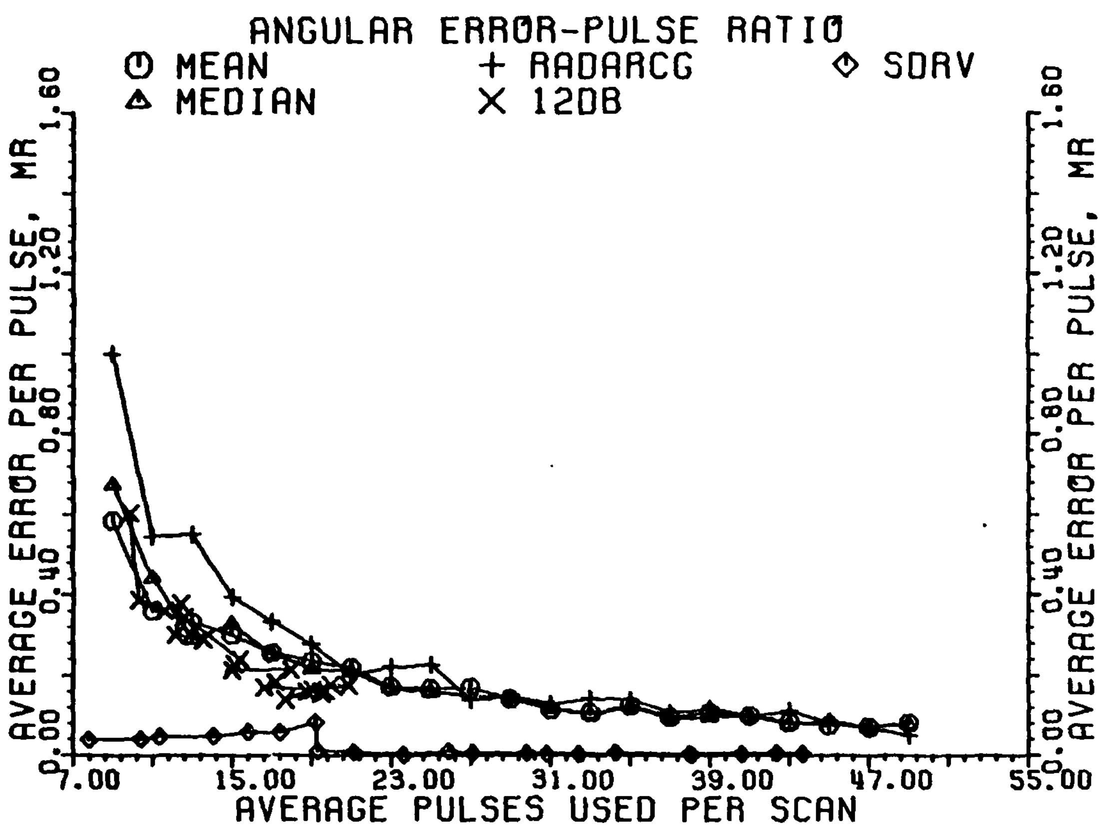

Figure 6-16. Angular error-pulse ratio for flights with noise and turbulence, all scans with a SNR at or below 10 dB used.

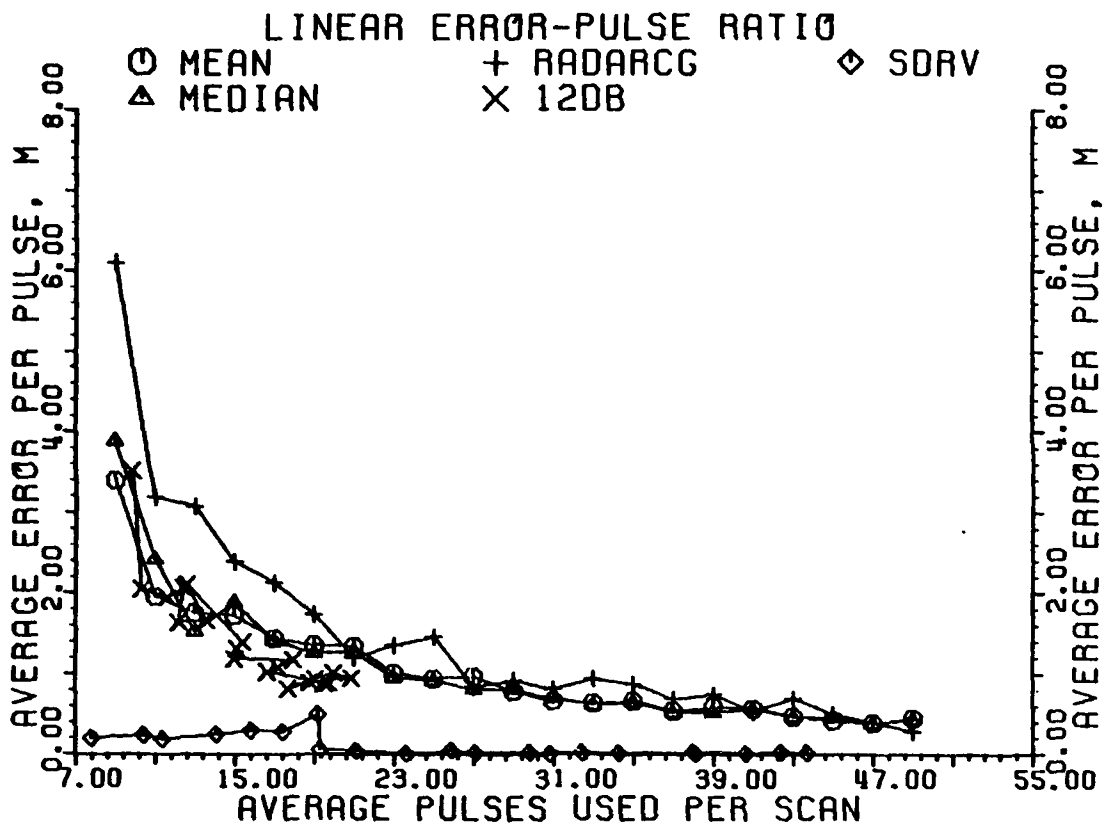

Figure 6-17. Linear error-pulse ratio for flights with noise and turbulence, all scans with a SNR at or below 10 dB used.

REFERENCES

[1] E. Giaccari and G. Nucci, "A Family of Air Traffic Control Radars," IEEE Transactions on Aerospace and Electronic Systems, Vol. AES-15, No. 3, pp. 378-396, May, 1979.

[2] W. W. Shrader, "Radar Technology Applied to Air Traffic Control," IEEE Transactions on Communications, Vol. COM-21, No. 5, pp. 591-605, May, 1973.

[3] C. E. Mueke, et. al., "New Techniques Applied to Air-Traffic Control Radars," Proceedings of the IEEE, Vol. 62, No. 6, pp. 716-723, June, 1974.

[4] G. A. Gilbert, "Historical Development of the Air Traffic Control System," IEEE Transactions on Communications, Vol. COM-21, No. 5, pp. 364-375, May, 1973.

[5] ITT Gilfillan, "AN/TPN-22 Mode I Final Report," Contract N00039-75-C-0021, pg. 3-2, August, 1979.

[6] J. M. Loomis and E. R. Graf, "Frequency-agility processing to reduce radar glint pointing error," IEEE Transactions on Aerospace and Electronic Systems, Vol. AES-11, No. I, January, 1975.

[7] M. I. Skolnik, Introduction to Radar Systems, 2nd Edition, New York: McGraw-Hill, 1980, Chapter 2.

[8] G. A. Gordon and P. Casowitz, "Raster scan track of a radar scatterer ensemble," IEEE Transactions on Aerospace and Electronic Systems, Vol. AES-8, No. 6, November, 1972.

[9] Harold R. Ward, "A method for setting a test signal level relative to noise," IEEE Transactions on Aerospace and Electronic Systems, Vol. AES-13, No. 6, pp. 707-709, November, 1977.

APPENDIX

This appendix contains a complete listing of the FORTRAN program used to compute the flight of the target and the output of the centroid estimators. The program is extensively documented and a reading of the comment cards reveals much about the computations that are performed.

The program requires 15 minutes to compile and execute one flight with a granularity of 29 beam pointing locations on an IBM 3031 computer.

The plots presented in the text are special purpose programs developed to be compatible with the plotting facilities at Auburn University.

```
C***********************************************************************
C   NOTE:  THIS IS THE MATCALS RADAR SIMULATION AS MODIFIED APR 1981
C
C***********************************************************************
C
C
C
C***********************************************************************
C
C
C                          PARAMETER LIST
C
C                                A
C   AR=DUMMY VARIABLE, CONTAINS THE SUM OF RANDOM FLOATING POINT NUMBERS
C   AZ=MAIN PROG: ANTENNA AZIMUTH TO EACH SCATTERER
C      SUBROUTINES: RAW RETURNS IN AZIMUTH
C   AZDIM= AZIMUTH DIMENSION ON THE SCANNING WINDOW.
C   AZO=AZIMUTH ANGLE TO TARGET AXIS
C   AZBW= HALF OF THE AZIMUTH BEAMWIDTH BETWEEN NULLS.
C   AZSPC= AZIMUTH SPACING OF BEAMS IN BEAMWIDTHS, USED TO INCREMENT
C          THE ANTENNA BEAM POINTING POSITION (IF YOU WANT THE BEAM TO
C          MOVE TWO POSITIONS AT A SHOT, SET AZSPC=2).
C   AZTHRS= AZIMUTH THRESHOLD DETERMINED FROM MEAN, MEDIAN, OR TWELVE
C           DB SUBROUTINES.
C
C                                B
C
C                                C
C   CBLOCA,CBLOCE= CENTER BEAM LOCATION IN AZIMUTH,ELEVATION IN RADAR
C                  COORDINATES. EQUAL TO PAZ,PEL WHEN LOCK=1.
C   CHI= YAW ANGLE.
C
C                                D
C   DGAIN= ANTENNA GAIN
C   DELTA= MAXIMUM ANTENNA POINTING ERROR.
C
C                                E
C   EBSCT= BACKSCATTERED E-FIELD.
C   EL=MAIN PROG: ANTENNA ELEVATION TO EACH SCATTERER
C      THRESHOLDING SUBROUTINES: RAW RETURNS IN ELEVATION
C   ELBW=HALF OF AN ELEVATION BWFN.
C   ELDIM= ELEVATION DIMENSION ON THE SCANNING WINDOW.
C   ELO=ELEVATION TO TARGET AXIS
C   ELSCAN=ON/OFF INPUT VARIABLE CONTROL FOR ELEVATION SCAN OPTION.
C   ELSPC= ELEVATION SPACING OF BEAMS IN BEAMWIDTHS.
C   ELTHRS= ELEVATION THRESHOLD DETERMINED BY MEAN, MEDIAN, OR TWELVE
C           DB SUBROUTINES.
C
C                                F
C   FHLH= FIRST HIT, LAST HIT THRESHOLDING PROCEDURES
C   FLTIME= SIMULATION TIME IN INTEGER SECONDS.
C   FREQ=FREQUENCY.
C   FXA=FINAL ANTENNA X COORDINATE LOCATION
C
C                                G
C   GAMMA= PITCH ANGLE.
C   GLSLP=GLIDESLOPE IN DEGREES.
```

```
C     GRANA= AZIMUTH NULL-TO-NULL SCAN GRANULARITY, DETERMINED BY ADDIM.
C     GRANE= AS IN GRANA, BUT IN ELEVATION.
C     GRNG=PROJECTION OF RNG ON X-Y PLANE.
C
C                                 H
C     HEIGHT=HEIGHT OF ANTENNA CENTER.
C
C                                 I
C     ICODE=CODE FOR CHOICE OF SCATTERING MODELS IN RCS.
C     INCXA=INTEGER BY WHICH ANTENNA X COORDINATE IS INCREMENTED.
C     IX=RANDOM NUMBER GENERATOR ENTRANCE NUMBER.
C     IXA=INTIAL ANTENNA X COORDINATE.
C     IY=INTEGER OUTPUT OF RANDOM NUMBER GENERATOR AND USED AS THE
C        NEW INPUT TO THE RANDU ROUTINE THE NEXT TIME IT IS CALLED.
C
C                                 J
C
C                                 K
C     K= WAVE NUMBER.
C
C                                 L
C     LABEL= A DUMMY VARIABLE USED TO KEEP TRACK OF THE FLOW OF
C            DATA IN THE CENTROID CALCULATIONS
C     LAMBDA=WAVELENGTH.
C
C                                 M
C     MEANA= MEAN AZIMUTH VOLTAGE
C     MEANE= MEAN ELEVATION VOLTAGE
C     MEDA,MEDE= MEDIAN VOLTAGE RETURN IN AZIMUTH AND ELEVATION
C                DETERMINED BY MEDIAN SUBROUTINE WHICH IS PASSED
C                TO PHLH AS THRESHOLD.
C     MTI=MOVING TARGET INDICATION.
C     MU= ROLL ANGLE.
C
C                                 N
C     NLOC=NUMBER OF TRANSMISSIONS IN EACH SCANNING WINDOW.
C     NUM= NUMBER OF SCATTERERS IN EACH TARGET COMPLEX.
C
C                                 O
C     OMEGA=RADIAN FREQUENCY OF THE TARGET MOTIONS, IN RAD/SECOND.
C
C                                 P
C     PANGLE= PRESENT ANGLE TO CROSS-TRACK CENTER AS SEEN FROM RUNWAY.
C     PCA= PHI TO TARGET CENTROID IN AZIMUTH. DETERMINED BY THRESHOLDING
C          PROCEDURES AND PASSED TO ERROR SUBROUTINE FOR COMPARISON
C          AGAINST ACTUAL TARGET LOCATION.
C     PERIOD=PERIOD OF THE SELECTED TARGET MOTION, IN SECONDS.
C     PHI=SPHERICAL COORDINATE.(TARGET)
C     PRATE=PITCH RATE OF THE TARGET MODEL, IN DEGREES/SECOND.
C     PWRT=PEAK TRANSMIT POWER.
C
C                                 Q
C
C                                 R
C     RCGAZ= RADAR CENTER OF GRAVITY IN AZIMUTH AS SEEN BY
C            RUNWAY AND DETERMINED BY RADARC.
```

```
C   PCGEL= RADAR CENTER OF GRAVITY IN ELEVATION AS SEEN BY
C          RUNWAY AND DETERMINED BY RADARC.
C   RETVOL=INPUT OPTION TO DISPLAY SCAN RETURN VOLTAGES.
C   RNG= RANGE TO EACH SCATTERER IN THE TARGET COMPLEX.
C   RNGTGT=RANGE TO THE TARGET, IN NAUTICAL MILES.
C   RRATE=ROIL RATE OF THE TARGET MODEL, IN DEGREES/SECOND.
C
C                            S
C   SCAT= AN ARRAY DIMENSIONED (#SCAT,4). CONTAINS COORDINATES OF
C        EACH SCATTERER IN TARGET COORDINATES AND THE RCS OF EACH.
C   SIGNLA,SIGNLE= THE SIGNAL AMPLITUDE WHEN THE BEAM IS CENTERED ON
C                  TARGET IN AZIMUTH AND ELEVATION, USED TO DETERMINE
C                  THE SNR FOR THAT SCAN.
C   SNRAZ,SNREL= THE SIGNAL TO NOISE (POWER) RATIO DETERMINED BY
C                (SIGNAL AMPLITUDE/RMS NOISE VOLTAGE)=SQRT(2*SNR)
C   SPEED= TARGET SPEED IN MPH.
C   SUMV= ARGUMENT USED TO SUM VOLTAGES TOGETHER IN RADARC.
C   SUMVTH= ARGUMENT USED TO SUM VOLTAGE RETURN TIMES THE ANGLE
C          TO THAT RETURN AS SEEN FROM THE ANTENNA.
C
C                            T
C   TCE= THETA TO TARGET CENTROID IN ELEVATION, DETERMINED BY
C        THRESHOLDING PROCEDURES AND PASSED TO ERROR SUBROUTINE
C        FOR COMPARISON AGAINST ACTUAL TARGET LOCATION AS SEEN
C        BY THE ANTENNA.
C   THETA=SPHERICAL COORDINATE.(TARGET)
C   THRESH= THRESHOLD USED IN FHLH (FIRST HIT LAST HIT) SUBROUTINE
C   TIME= TIME VARIABLE USED FOR DEAD TIME BETWEEN SCANS.
C   TIMEI= INITIAL TIME OF SCENARIO AND TIME VARIABLE.
C   TIMEP= PULSE TIME
C   TPHSFT= PHASE SHIFTER RESPONSE TIME.
C
C                            U
C   UCERTA,UCERTE= THE AMOUNT OF BEAM POINTING ERROR INTRODUCED INTO
C                  THE PLACEMENT OF THE ANTENNA BEAM, CONSTANT THROUGH-
C                  OUT A SCAN, BUT RANDOMLY CHANGING FROM SCAN TO SCAN.
C
C                            V
C   VDIRCT= DIRECT VOLTAGE RETURN.
C   VLT= VOLTAGE MATRIX DIMENSIONED (JSCAN,II). JSCAN=1 ARE AZIMUTH
C        VOLTAGES, JSCAN=2 ARE ELEVATION VOLTAGES, II=SCAN SIZE.
C   VNRMS= THE RMS NOISE VOLTAGE FOR THAT SCAN COMPUTED BY SQUARING
C         EACH NOISE VOLTAGE, SUMMING THEM, AND THEN TAKING THE SQUARE
C         ROOT OF THE AVERAGE NOISE VOLTAGE SQUARED.
C
C                            W
C
C                            X
C   XA,YA,HEIGHT= INITIAL COORDINATES OF THE RADAR ANTENNA.
C   XD,YD,ZD= DOUBLE PRECISION RADAR COORDINATES OF TARGET LOCATION.
C   XDIP,YDIP,ZDIP= RADAR COORDINATES OF THE SCATTERERS WITH RESPECT
C        TO THE LOCATION OF THE ANTENNA.
C   XO,YO,ZO= TARGET POSTION ALONG TRAJECTORY, IN RADAR COORDINATES.
C
C                            Y
C   YFL= REAL RANDOM NUMBER BETWEEN 0 AND 1 FROM OUTPUT OF THE
C        OUTPUT OF THE RANDU SUBROUTINE.
```

```
C   YRATE=YAW RATE OF THE TARGET MODEL, IN DEGREES/SECOND.
C
C                                 Z
C
C
C*********************************************************************
      DIMENSION VLT(2,49),SCAT(3,4),TODAY(8),AZRADR(49),VNOISE(2,49)
      DOUBLE PRECISION ELV(49),AZI(49)
      INTEGER OPTION(5),ELSCAN,FXA,RETVOL,COUNTA,COUNTE,PRF
      DOUBLE PRECISION XDIF,YDIF,ZDIF,XD,YD,ZD
      REAL MUR,LAMBDA,MU,LV,LS,VRMS(2,49),K
      INTEGER AZDIM,ELDIM,DIM,AGILE,EDIV,ADIV,FLTIME,PLS12,PLSFD,PLSSD
      COMMON/RPY/RRATE,PRATE,YRATE,OMEGA,SPEED,GLSLP,RNGTGT,
     *AZ,GRNG
      COMMON/RTA/MU,GAMMA,CHI,XO,YO,ZO
      COMMON/SCATM/SCAT,NUM
      COMMON/WAVE/K,MUR,EPSR
      COMMON /ALL/ELV,AZI,RANGE,OPTION,LABEL,ELDIM,AZDIM,ELSCAN,DELTA
      COMMON /RADR/PEL,PAZ,CBLOCE,CBLOCA,GRANE,GRANA,AZBW,ELBW,LOCK
      COMMON /FILEIT/XMEAN,XMED,XRADRC,X12DB,XSDRV,SNRAZ,PLS12,
     *PLSFD,PLSSD,DMEAN,DMED,DRADRC,D12DB,DSDRV
      COMMON/FOURIV/COUNTE,COUNTA,MODEE,MODEA,MSDRV,SNREL,MODE12,MODA12
C
      DATA PI,PI2,TPI,RADDEG,DEGRAD,SQP2,C/3.141592,1.570796,
     *6.283185,57.29578,.0174533,12.56637,3.0E+08/
      DATA ITABLE,JUST1/1,0/
C*********************************************************************
C
C     D A T A   I N P U T   F O R M A T
C
C          COL.       VARIABLE NAME  OPTIONS
C
C          1          ICODE          1 - JETMOD #1 AS TARGET MODEL
C                                    2 - ONE POINT ISOTROPIC SCATTERER
C
C          2          NOISE          0 - NO GAUSSIAN NOISE
C                                    1 - ADD GAUSSIAN NOISE TO RETURN
C
C          3          IRPY           0 - NO ROLL,PITCH, OR YAW
C                                    1 - ROLL, PITCH AND YAW ARE INCLUDED
C
C          4          LOCK           0 - ADD UNCERTAINTY OF TARGET LOCA-
C                                        TION INTO ANTENNA SCANNING.
C                                    1 - LOCK ANTENNA ON TARGET
C
C          5-7        IXA            INITIAL INTEGER STARTING LOCATION OF
C                                    ANTENNA X COORDINATE, METERS.
C
C          8-10       FXA            FINAL INTEGER ANTENNA LOCATION, METERS
C
C          11-13      INCXA          INTEGER BY WHICH XA IS INCREMENTED
C                                    FROM IXA TO FXA.  IF RUN USES ONLY
C                                    ONE ANTENNA LOCATION, SET IXA=FXA,
C                                    INCXA=ANY NON-ZERO POSITIVE INTEGER.
C
C          14         IFILES         0 - NO OUTPUT TO DATA FILES
C                                    1 - OUTPUT TO DATA FILES
```

```
C                                   ** NOTE: PROPER JCL MUST BE INSERTED **
C
C       15        IPRINT            0 -NO DETAILED OUTPUT OF SOLUTION
C                                   1 - DETAILED OUTPUT OF SOLUTION
C
C       16        ELSCAN            1 - ELEVATION SCAN NOT USED.
C                                   2 - ELEVATION SCAN USED.
C
C       17        RETVOL            0 - OFF
C                                   1 - DISPLAY SCAN VOLTAGES, ELEVATION
C                                       AND THEN AZIMUTH
C
C       18-19     AZDIM             ODD INTEGERS BETWEEN 6 AND 50
C       20-21     ELDIM             ODD INTEGERS BETWEEN 6 AND 50
C       22-24     FLTIME
C
C
C
C       ON THE NEXT LINE, ENTER 0 OR 1 FOR THRESHOLDING METHOD:
C
C       1         MEAN              0 - OFF
C                                   1 - CALCULATE MEAN
C
C       2         MEDIAN            0 - OFF
C                                   1 - CALCULATE MEDIAN
C
C       3         RADARCG           0 - OFF
C                                   1 - CALCULATE WEIGHTED ANGLES
C
C       4         TWELVE DB         0 - OFF
C                                   1 - ON
C
C       5         SECOND            0 - OFF
C                 DERIVATIVE        1 - ON
C
C ********************************************************************
C
      CALL DATE(TODAY)
      WRITE(6,1) (TODAY(I),I=1,8)
    1 FORMAT('1 ',8A4)
      READ (5,100) ICODE,NOISE,IRPY,LOCK,IXA,FXA,INCXA,IFILES,IPRINT,
     *ELSCAN,RETVOL,AZDIM,ELDIM,FLTIME
      READ(5,2) (OPTION(I),I=1,5)
    2 FORMAT(6I1)
      WRITE(6,4)
    4 FORMAT(' THE FOLLOWING INFORMATION WAS READ IN')
      WRITE(6,5)ICODE,NOISE,IRPY,LOCK
    5 FORMAT(' ICODE= ',I1,' NOISE=',I1,' IRPY=',I1,' LOCK=',I1)
      WRITE(6,6) IXA,FXA,INCXA,IFILES,IPRINT,ELSCAN,RETVOL
    6 FORMAT (' IXA=',I3,2X,'FXA=',I3,' INCXA=',I3,' IFILES=',I1,
     *' IPRINT=',I1,' ELSCAN=',I2,'  RETVOL=',I1)
      WRITE(6,7) AZDIM,ELDIM
    7 FORMAT (' AZDIM=',I2,2X,'ELDIM=',I2)
      WRITE (6,8) FLTIME
    8 FORMAT(2X,'FLTIME=',I4)
      WRITE(6,10) (OPTION(I),I=1,3)
   10 FORMAT(' MEAN= ',I1,' MEDIAN= ',I1,' RADARC= ',I1)
```

```
      WRITE(6,11) (OPTION(I),I=4,5)
   11 FORMAT(' TWELVE DB= ',I1,' SECOND DERIVATIVE=',I1)
      WRITE(6,103)
C        THE FOLLOWING LIST OF VARIABLES CAN BE CHANGED TO
C        OBSERVE THE INFLUENCE OF PARTICULAR FACTORS ON TRACKING
C        PERFORMANCE.
C
C   RANDOM GENERATOR SEED
C
      IX=65549
C
C   ANTENNA:
C
      NTI=3
      AZBW=.916
      ELBW=.996
      YA=-500.0
      HEIGHT=3.0
      C=3.0E+08
      FREQ=9.1E+09
      PWRT=10.0E+05
      LAMBDA=3.0E+08/FREQ
      K=2.0*PI/LAMBDA
      AZSPC=1.0
      ELSPC=1.0
C
C   ANTENNA UNCERTAINTY FACTOR - GIVES +/-4 M ERROR AT RANGE=620 M
C
      DELTA=ATAN2(4.,620.)
      IF(LOCK.EQ.1) DELTA=0.
      GRANA=(AZBW*DEGRAD+DELTA)*2.0/(FLOAT(AZDIM)-1.)
      GRANE=(ELBW*DEGRAD+DELTA)*2.0/(FLOAT(ELDIM)-1.)
C
C   TARGET
C
      SPEED=148.63636
      SPEED=SPEED*.4470399
      GLSLP=3.5
      RNGTGT=3.72
      PERIOD=3.0
      PRATE=5.0
      YRATE=5.0
      RRATE=10.0
C
C   SCANNING TIME:
C
      TIMEI=0.0
      PRF=6000
      TIMEP=(1.0/PRF)*FLOAT(NTI)
      TPHSFT=10E-06
      TIME=1.0-(TIMEP*(ELDIM+(ELDIM-1)/2)+(AZDIM+(AZDIM-1)/2)*TPHSFT)
C
C   CONVERSIONS.
C
      BASF =9.1E+09
      GLSLP=GLSLP*DEGRAD
      RNGTGT=RNGTGT*1853.2288
```

```
      OMEGA=2*PI/PERIOD
      PRATE=PRATE*DEGRAD
      RRATE=RRATE*DEGRAD
      YRATE=YRATE*DEGRAD
      SNREL=1E75
      SNRAZ=1E75
      INIT=0
C
C**********************************************************************
C
C   MAIN LOOP:  THIS LOOP CONSTRUCTION CAUSES THE AZIMUTH (A) AND THE
C        ELEVATION (E) TO CHANGE, SCANNING THE ANTENNA. NOTE THAT THE
C        SIMULATION SCANS FIRST IN AZIMUTH WITH E=0 (BEAM ON TARGET IN
C        ELEVATION), AND THEN SCANS IN ELEVATION WITH A=0 (BEAM ON
C        TARGET IN AZIMUTH).
C
C**********************************************************************
      DO 52 JXA=IXA,FXA,INCXA
      XA=-FLOAT(JXA-1)
      NSCANS=0
      SNREL=999.99
      SNRAZ=999.99
      NSCANS=0
      TIMEI=0.0
      JUST1=0
      DO 13 JK=1,AZDIM
      VLT(1,JK)=0.0
   13 VRMS(1,JK)=0.0
      DO 14 JK=1,ELDIM
      VLT(2,JK)=0.0
   14 VRMS(2,JK)=0.0
      WRITE(6,15)XA,YA,HEIGHT
   15 FORMAT('1',' ANTENNA POSITION WITH RESPECT TO END OF RUNWAY:',
     +' XA= ',F10.3,' YA= ',F10.3,' HEIGHT= ',F10.3)
      DO 50 NPLT=1,PLTIME
      IF (NPLT.EQ.1) GO TO 16
      TIMEI=TIMEI+TIME
   16 CONTINUE
C
C     INCREMENT TIME IF ELEVATION SCAN IS NOT CALCULATED.
C
      IF(ELSCAN.NE.2)ELSCAN=1
      IF((NPLT.GT.1).AND.ELSCAN.EQ.1)TIMEI=TIMEI+TIMEP*
     *(ELDIM+(ELDIM-1)/2)+TPHSFT*((AZDIM-1)/2)
      DO 31 JSCAN=1,ELSCAN
C
C     GET A RANDOM NUMBER FOR ANTENNA POINTING UNCERTAINTY. IF LOCKED
C     ON, CALLING RANDU NOW WILL MAINTAIN THE SAME SET OF SCAN NOISE.
C
      CALL RANDU(IX,IY,YFL)
      IX=IY
      IF(JSCAN.EQ.1)A=-(AZDIM-1)/2
      IF(JSCAN.EQ.2.OR.LOCK.EQ.1) GO TO 17
C
C     THE CENTER BEAM POINTING LOCATION IS GIVEN AN UNCERTAINTY OF +/-4
C     METERS AT THE RELEASE POINT BY MOVING THE STARTING LOCATION OF
C     THE NULL-TO-NULL SCAN RANDOMLY.
```

```
C
      UCERTA=2.*(YFL-0.5)*DELTA/GRANA
      A=A+UCERTA
   17 IF(JSCAN.EQ.1)E=0
      IF(JSCAN.EQ.1)UCERTE=0.
      IF(JSCAN.EQ.2)A=0
      IF(JSCAN.EQ.2)UCERTA=0.
      IF(JSCAN.EQ.2)E=-(ELDIM-1)/2
      IF(JSCAN.EQ.1.OR.LOCK.EQ.1)GO TO 18
      UCERTE=2.*(YFL-0.5)*DELTA/GRANE
      E=E+UCERTE
   18 IF(JSCAN.EQ.1)DIM=AZDIM
      IF(JSCAN.EQ.2)DIM=ELDIM
      DO 30 II=1,DIM
      IF(JSCAN.EQ.1.AND.II.GT.1)TIMEI=TIMEI+TPHSFT
      IF(JSCAN.EQ.2.AND.II.GT.1)TIMEI=TIMEI+TISEP
      IF(JSCAN.EQ.1)AZRADR(II)=GRANA*A
   19 CONTINUE
C**********************************************************************
C
C   SUBROUTINE TRAJ:  THIS SUBROUTINE GENERATES THE CURRENT LOCATION
C        OF THE TARGET ON A GIVEN TRAJECTORY.  ALSO GENERATED ARE
C        PERIODIC VALUES OF ROLL, PITCH, AND YAW, CORRESPONDING
C        TO LOCAL TURBULENCE AND WIND SHEAR.
C
C**********************************************************************
      CALL TRAJ(TIMEI,IRPY)
      IF(YO.LE.90.0) GO TO 20
      GO TO 21
   20 WRITE(6,130)  TIMEI,NSCANS
      GO TO 51
   21 CONTINUE
C**********************************************************************
C
C        FIND THE ANTENNA LOCATION IN THE TARGET COORDINATE SYSTEM.
C        THESE ARE NOT SPHERICAL PHI AND THETA, BUT RELATIVE ANGLES
C        FROM TARGET TO ANTENNA.  THE CENTER OF THE ENTIRE COORDINATE
C        SYSTEM IS THE RUNWAY TOUCHDOWN POINT, NOT THE ANTENNA LOCATION.
C
C**********************************************************************
      CALL ROTAT2(XA,YA,HEIGHT,X1,Y1,Z1)
      PHI=-ATAN2(X1,Y1)+PI/2.0
      THETA=ATAN2(SQRT(X1**2+Y1**2),Z1)
C**********************************************************************
C
C        THE BACKSCATTER CROSS SECTION OF EACH SCATTERER IN THE
C        TARGET COMPLEX IS NOW DETERMINED FOR A GIVEN ANTENNA
C        POSITION IN TARGET COORDINATES.
C
C**********************************************************************
      CALL RCS(THETA,PHI,ICODE)
      IF (IPRINT.EQ.0) GO TO 22
      WRITE(6,132)
      WRITE(6,121)  TIMEI
      WRITE(6,122)  A,E
      WRITE(6,104)
      WRITE(6,124)  XO,YO,ZO
```

```
      PMU=MU*RADDEG
      PGAMMA=GAMMA*RADDEG
      PCHI=CHI*RADDEG
      WRITE(6,125) PMU,PGAMMA,PCHI
      WRITE(6,104)
      PP=PHI*RADDEG
      TT=THETA*RADDEG
      WRITE(6,115)
      WRITE(6,116) PP,TT
      WRITE(6,104)
      SCATF=10.0*ALOG10(SCAT(1,4))
      SCATRW=10.0*ALOG10(SCAT(2,4))
      SCATLW=10.0*ALOG10(SCAT(3,4))
      WRITE(6,112)
      WRITE(6,113) SCATF,SCATRW,SCATLW
   22 CONTINUE
C***********************************************************************
C
C   FIND TARGET ORIGIN IN RADAR COORDINATES
C
C***********************************************************************
      XDIF=DBLE(X0)-DBLE(XA)
      YDIF=DBLE(Y0)-DBLE(YA)
      ZDIF=DBLE(Z0)-DBLE(HEIGHT)
      GRNG=SQRT(SNGL(XDIF)**2+SNGL(YDIF)**2)
      GNDRNG=GRNG
      RANGE=SQRT(SNGL(XDIF)**2+SNGL(YDIF)**2+SNGL(ZDIF)**2)
      HT=SNGL(ZDIF)
      AZ0=ATAN2(SNGL(XDIF),SNGL(YDIF))
      EL0=ATAN2(SNGL(ZDIF),GRNG)
      IF(II.NE.((DIM+1)/2))GO TO 90
      PAZ=AZ0
      PEL=EL0
      CBLOCA=AZ0+GRANA*UCERTA
      CBLOCE=EL0+GRANA*UCERTE
C***********************************************************************
C
C        COMPUTE ELEVATION AND AZIMUTH ANGLES TO THE BEAM POINTING
C        POSITION WITHIN THE SCANNING WINDOW.
C
C***********************************************************************
   90 AZ1=AZ0+GRANA*A
      EL1=EL0+GRANE*E
      IF (IPRINT.EQ.0) GO TO 23
      WRITE(6,117)
      PEL0=EL0*RADDEG
      PAZ0=AZ0*RADDEG
      WRITE(6,118) PEL0,PAZ0,RANGE
      WRITE(6,104)
   23 CONTINUE
      VDIRCT=0.0
C***********************************************************************
C
C   SUB-LOOP:  THIS LOOP SUMS THE BACKSCATTER FROM EACH OF THE
C        SCATTERERS IN THE TARGET COMPLEX.
C
C***********************************************************************
```

```
      DO 25 I=1,NUM
C*********************************************************************
C
C   FIND SCATTERER IN RADAR COORDINATES
C
C*********************************************************************
      CALL ROTAT(SCAT(I,1),SCAT(I,2),SCAT(I,3),XD,YD,ZD)
      XDIF=XD-XA
      YDIF=YD-YA
      ZDIF=ZD-HEIGHT
      RNG =SQRT(SNGL(XDIF)**2+SNGL(YDIF)**2+SNGL(ZDIF)**2)
      GRNG=SQRT(SNGL(XDIF)**2+SNGL(YDIF)**2)
C*********************************************************************
C
C        COMPUTE AZIMUTH AND ELEVATION ANGLES TO SCATTERER IN RADAR
C        COORDINATES.
C
C*********************************************************************
      AZ=ATAN2(SNGL(XDIF),SNGL(YDIF))
      EL=ATAN2(SNGL(ZDIF),GRNG)
      IF (IPRINT.EQ.0) GO TO 24
      WRITE(6,119)
      PEL=EL*RADDEG
      PAZ=AZ*RADDEG
      WRITE(6,120) I,PEL,PAZ,RNG
      WRITE(6,104)
   24 CONTINUE
      AZD=AZ1-AZ
      ELD=EL1-EL
      CALL ANTENA(AZD,ELD,DGAIN)
C*********************************************************************
C
C        EBSCT IS THE COMPLEX E-FIELD FOR THE SCATTERER OF INTEREST
C        IN THIS PARTICULAR SCAN.  NOTE THAT THIS FIELD IS RIGHT
C        OR LEFT CIRCULARLY POLARIZED BACKSCATTER, AND BECAUSE OF
C        ANTENNA POLARIZATION SENSITIVITY, APPROXIMATELY HALF THE
C        BACKSCATTER POWER IS AVAILABLE FOR PROCESSING.
C
C*********************************************************************
      RGT=RNG**2*4.0*PI
      EBSCT=LAMBDA*SQRT((SCAT(I,4)*PWRT*377.)/RGT)
      VDIRCT=VDIRCT+DGAIN*(EBSCT**2)
   25 CONTINUE
C*********************************************************************
C
C        VRMS IS THE SUM OF THE COMPLEX BACKSCATTER VOLTAGES
C        INDUCED BY EACH OF THE TARGET COMPLEX SCATTERERS.
C
C*********************************************************************
      IF (IPRINT.EQ.0) GO TO 26
      PD=(ABS(VDIRCT)**2)*10E+05
      PGN=10.0*ALOG10(DGAIN)
      WRITE(6,127) VDIRCT,PD
      PEL1=EL1*RADDEG
      PAZ1=AZ1*RADDEG
      WRITE(6,126) PGN,PEL1,PAZ1
      WRITE(6,104)
```

```
   26 CONTINUE
      VLT(JSCAN,II)=VDIRCT
      IF(JSCAN.EQ.1.AND.II.EQ.((AZDIM+1)/2))SIGNLA=VDIRCT
      IF(JSCAN.EQ.2.AND.II.EQ.((ELDIM+1)/2))SIGNLE=VDIRCT
      IF(NOISE.EQ.0)GO TO 28
C*********************************************************************
C
C     ADD GAUSSIAN NOISE USING "RANDU" AND "GAUSS"
C
C     15 DB OF NOISE IS ADDED AS FOLLOWS:
C       IF (SIGNAL AMPLITUDE/RMS NOISE VOLTAGE)=SQRT(2*SNR), THEN WITH
C       SIGNAL AMPLITUDE=3.1 (AT A RELATIVE MAXIMUM AT RANGE),
C       RMS NOISE VOLTAGE=S=0.3899
C
C*********************************************************************
      S=0.3898
      AM=0.0
C*********************************************************************
C
C    GAUSS
C       COMPUTES A NORMALLY DISTRIBUTED RANDOM NUMBER WITH A GIVEN
C       MEAN AND STANDARD DEVIATION.
C
C    DESCRIPTION OF PARAMETERS
C        IX -IX MUST CONTAIN AN ODD INTEGER NUMBER WITH NINE OR
C            LESS DIGITS ON THE FIRST ENTRY TO GAUSS. THEREAFTER
C            IT WILL CONTAIN A UNIFORMLY DISTRIBUTED INTEGER RANDOM
C            NUMBER GENERATED BY THE SUBROUTINE FOR USE ON THE NEXT
C            ENTRY TO THE SUBROUTINE.
C        S  -THE DESIRED STANDARD DEVIATION OF THE NORMAL
C            DISTRIBUTION.
C        AM -THE DESIRED MEAN OF THE NORMAL DISTRIBUTION.
C        V  -THE VALUE OF THE COMPUTED NORMAL RANDOM VARIABLE.
C
C    REMARKS
C        THIS ROUTINE USES RANDU WHICH IS SYSTEM/360 SPECIFIC.
C
C    SUBROUTINES REQUIRED
C        RANDU
C
C    METHOD
C        USES 12 UNIFORM RANDOM NUMBERS TO COMPUTE NORMAL RANDOM
C        NUMBERS BY CENTRAL LIMIT THEOREM. THE RESULT IS THEN
C        ADJUSTED TO MATCH THE GIVEN MEAN AND STANDARD DEVIATION.
C        THE UNIFORM RANDOM NUMBERS COMPUTED WITHIN THE SUBROUTINE
C        ARE FOUND BY THE POWER RESIDUE METHOD.
C
C*********************************************************************
      AR=0.0
      DO 27 IN=1,12
      CALL RANDU(IX,IY,YFL)
      IX=IY
   27 AR=AR+YFL
      V=(AR-6.0)*S+AM
      VNOISE(JSCAN,II)=V
C
C     NOW ADD NOISE TO VOLTAGE RETURN
```

```
C
      VLT(JSCAN,II)=VLT(JSCAN,II)+V
      IF(IPRINT.EQ.1)WRITE(6,101)VLT(JSCAN,II)
      IF(NOISE.EQ.1)GO TO 29
C
C     CYCLE RANDU IF NOISE IS OFF TO MAINTAIN SAME ANTENNA UNCERTAINTY
C     FOR ALL FLIGHTS.
C
      DO 28 IN=1,12
      CALL RANDU(IX,IY,YFL)
   28 IX=IY
   29 IF(JSCAN.EQ.1)A=A+AZSPC
      IF(JSCAN.EQ.2)E=E+ELSPC
C
C     IF ELEVATION SCAN IS USED, ADVANCE TIME TO MOVE BEAM.
C
      IF(JSCAN.EQ.1.AND.ELSCAN.EQ.2.AND.DIM.EQ.AZDIM)TIMEI=TIMEI+
     *TIMEP*((ELDIM-1)/2)+TPHSFT*((AZDIM-1)/2)
   30 CONTINUE
   31 CONTINUE
      NSCANS=NSCANS+1
      IF(NOISE.EQ.0)GO TO 35
C*********************************************************************
C
C                    CALCULATE SIGNAL TO NOISE RATIO
C
C                              AZIMUTH
C
C*********************************************************************
      VNSQ=0.0
      DO 33 JJJ=1,AZDIM
      VNOISE(1,JJJ)=VNOISE(1,JJJ)**2
   33 VNSQ=VNSQ+VNOISE(1,JJJ)
      VNRMS=SQRT(VNSQ/AZDIM)
      SNRAZ=0.5*(SIGNLA/VNRMS)**2
      SNRAZ=10.0*ALOG10(SNRAZ)
      IF(ELSCAN.EQ.1)GO TO 35
C
C                              ELEVATION
C
      VNSQ=0.0
      DO 34 JJJ=1,ELDIM
      VNOISE(2,JJJ)=VNOISE(2,JJJ)**2
   34 VNSQ=VNSQ+VNOISE(2,JJJ)
      VNRMS=SQRT(VNSQ/ELDIM)
      SNREL=0.5*(SIGNLE/VNRMS)**2
      SNREL=10.0*ALOG10(SNREL)
   35 IF((OPTION(1).EQ.1.OR.OPTION(2).EQ.1.OR.OPTION(3).EQ.1.OR.
     *OPTION(4).EQ.1.OR.OPTION(5).EQ.1.)
     *.AND.JUST1.EQ.1.AND.IPRINT.EQ.0)WRITE(6,105)
      DO 36 I=1,AZDIM
   36 AZI(I)=DBLE(VLT(1,I))
      DO 37 I=1,ELDIM
   37 ELV(I)=DBLE(VLT(2,I))
      IF(RETVOL.EQ.1)WRITE(6,133)(ELV(III),III=1,ELDIM)
      IF(RETVOL.EQ.1)WRITE(6,104)
      IF(RETVOL.EQ.1)WRITE(6,133)(AZI(III),III=1,AZDIM)
```

```
      IF(OPTION(1).EQ.0.AND.OPTION(2).EQ.0.AND.OPTION(3).EQ.0.AND.
     *OPTION(4).EQ.0.AND.OPTION(5).EQ.0)GO TO 45
      IF(JUST1.EQ.1.AND.IPRINT.EQ.1)GO TO 39
      IF(JUST1.EQ.1) GO TO 44
      JUST1=1
      WRITE(6,38)
   38 FORMAT(//,54X,' CENTROID MEASUREMENTS',//,
     *' NOTE: A MINUS SIGN ON AZIMUTH ERROR MEANS THE ',
     *'CALCULATED TARGET POSITION IS TO THE LEFT OF THE ACTUAL',
     *' LOCATION.',/,
     *'       A MINUS SIGN ON ELEVATION ERROR MEANS THE ',
     *'CALCULATED TARGET POSITION IS BELOW THE ACTUAL LOCATION.',
     */,' THE FOLLOWING APPLIES TO 12DB AND SDRV:',/,
     *6X,'THE TWO NUMBERS PRECEDING THE METHOD NAME ARE THE MODE ',
     *'FLAGS IN ELEVATION AND AZIMUTH, RESPECTIVELY.',/,6X,
     *'FOR 12DB, MODE=0 MEANS ALL RETURNS IN THAT SCAN WERE ABOVE THE ',
     *'12DB THRESHOLD. MODE=1 MEANS AT LEAST ONE RETURN WAS ABOVE THE',
     */,6X,'THRESHOLD.  FOR SDRV, MODE=0 MEANS THE SCAN WAS REJECTED ',
     *'DUE TO NOISE OR SHAPE CRITERION.  MODE=2 MEANS THE',/,6X,
     *'CENTROID WAS CALCULATED BY FINDING THE MAXIMUM SLOPES ON ',
     *'THE RETURN.',/,
     *6X,'THE TWO TWO-DIGIT NUMBERS FOLLOWING THE METHOD NAME ARE THE',
     *' NUMBER OF PULSES USED IN THE ELEVATION AND AZIMUTH SCANS,',/,
     *6X,'RESPECTIVELY.')
    9 WRITE(6,40)
    4 FORMAT(/,131('_'),/,48X,'|',33X,'|',/)
      WRITE(6,41)
   41 FORMAT('+',21X,'ACTUAL',20X,'|',12X,'CALCULATED',
     *11X,'|',22X,'ERROR',/,48X,'|',33X,'|')
      WRITE(6,42)
   42 FORMAT('+',130('_'),/,1X,'RANGE IN METERS    SNR IN DB ELEVATION',
     *1X,'AZIMUTH |',4X,'METHOD     ELEVATION  AZIMUTH |',3X,'ELEVATION',
     *7X,'|',9X,'AZIMUTH',/,1X,'ANTENNA  RUNWAY',5X,'EL',4X,
     *'AZ  DEGREES   DEGREES |',15X,'DEGREES   DEGREES | MILLIRADIANS ',
     *' METERS   | MILLIRADIANS  METERS')
      WRITE(6,43)
   43 FORMAT('+',130('_'))
   44 IF (OPTION(1).EQ.1) CALL MEAN
      IF (OPTION(2).EQ.1) CALL MEDIAN
      IF (OPTION(3).EQ.1) CALL RADARC
      IF (OPTION(4).EQ.1) CALL T12DB
      IF (OPTION(5).EQ.1) CALL SDRV(INIT,NOISE)
      INIT=1
      IF(IPRINT.EQ.1)WRITE(6,102)
C
C     WRITE TO DATASETS
C
   45 IF(IFILES.EQ.0) GO TO 50
      WRITE(10,106)XA,RANGE,XMEAN,XMED,XRADRC,X12DB,XSDRV,SNRAZ,
     *PLS12,PLSPD,PLSSD
      WRITE(11,106)XA,RANGE,DMEAN,DMED,DRADRC,D12DB,DSDRV,SNRAZ,
     *PLS12,PLSPD,PLSSD
   50 CONTINUE
   51 CONTINUE
   52 CONTINUE
      STOP
  100 FORMAT (4I1,3I3,4I1,2I2,1I3,F5.2,F3.1)
```

```
101 FORMAT(5X,' RETURN VOLTAGE WITH NOISE= ',E15.8)
102 FORMAT('1')
103 FORMAT('-')
104 FORMAT('0')
105 FORMAT(48X,'|',33X,'|',24X,'|',/,48X,'|',33X,'|',24X,'|')
106 FORMAT(9E16.8,3I2)
112 FORMAT('0',10X,'RCS OF FUSELAGE,RIGHT WING,AND LEFT WING (DBSM)')
113 FORMAT('0',' FUSELAGE=',F10.4,' RHWING=',F10.4,' LHWING=',F10.4)
115 FORMAT('0',10X,'ANTENNA ASPECT ANGLES,WITH RESPECT TO THE ',
   *'TARGET')
116 FORMAT(' ',15X,'PHI=',F12.9,1X,'THETA=',F12.9)
117 FORMAT('0',10X,'TARGET CENTER LOCATION IN RADAR COORDINATES')
118 FORMAT(' ',15X,'ELEVATION=',F10.6,1X,'AZIMUTH=',F10.6,1X,
   *'RANGE=',F10.4)
119 FORMAT('0',10X,'SCATTERER LOCATION IN RADAR COORDINATES')
120 FORMAT(' ',10X,'SCAT#',I2,1X,'ELEVATION=',F10.6,1X,
   *'AZIMUTH=',F10.6,1X,'RANGE=',F10.4)
121 FORMAT('0',10X,'SCANNING TIME=',F12.6,' MILLISECONDS')
122 FORMAT('0',10X,'AZ & EL BEAM CORRECTION NUMBERS FROM BORESIGHT: ',
   *'A=',F5.2,' E=',F5.2)
124 FORMAT('0',5X,'CURRENT LOCATION OF TARGET CENTE : X=',F12.7,1X,
   *'Y=',F12.7,1X,'Z=',F12.7)
125 FORMAT('0',5X,'CURRENT VALUES FOR TARGET ANGULAR MOTION(DEGREES):'
   *' ROLL=',F6.3,1X, 'PITCH=',F6.3,1X,'YAW=',F6.3)
126 FORMAT('0',5X,'GAIN=',F12.8,'DB AT EL=',F10.6,' & AZ=',F10.6,
   *2X,'(DEGREES)')
127 FORMAT('0',5X,'RETURN VOLTAGE=',F16.13,2X,'DIRECT POWER=',
   *E16.8,1X,'MICROWATTS')
130 FORMAT('0','FREEZE COMMAND POINT; SIMULATION ENDS.  ELAPSED TIME',
   *'= ',F12.8,1X,'SECONDS, #SCANS=',I10)
132 FORMAT('0',100('*'))
133 FORMAT(7F16.8)
    END
```

```
BLOCK DATA
COMMON /ALL/ELV,AZI,RANGE,OPTION,LABEL,ELDIM,AZDIM,ELSCAN,DELTA
REAL*8 ELV(49)/49*0.0D0/,AZI(49)/49*0.0D0/
INTEGER OPTION(5),ELDIM,AZDIM,ELSCAN
END
```

```
      SUBROUTINE RANDU(IX,IY,YFL)
C*********************************************************************
C
C     PURPOSE
C        COMPUTES UNIFORMLY DISTRIBUTED RANDOM REAL NUMBERS BETWEEN 0
C        AND 1.0 AND RANDOM INTEGERS BETWEEN ZERO AND 2**31. EACH ENTRY
C        USES AS INPUT AN INTEGER RANDOM NUMBER AND PRODUCES A NEW
C        INTEGER AND REAL RANDOM NUMBER.
C
C     DESCRIPTION OF PARAMETERS
C        IX -FOR THE FIRST ENTRY THIS MUST CONTAIN ANY ODD INTEGER
C            NUMBER WITH NINE OR LESS DIGITS.  AFTER THE FIRST ENTRY,
C            IX SHOULD BE THE PREVIOUS VALUE OF IX COMPUTED BY THIS
C            SUBROUTINE.
C        IY -A RESULTANT INTEGER RANDOM NUMBER REQUIRED FOR THE NEXT
C            ENTRY TO THE ROUTINE.  THE RANGE OF THIS NUMBER IS BETWEEN
C            ZERO AND 2**31.
C        YFL-THE RESULTANT UNIFORMLY DISTRIBUTED, FLOATING POINT,
C            RANDOM NUMBER IN THE RANGE 0 TO 1.0.
C
C     REMARKS
C        THIS ROUTINE IS SPECIFIC TO SYSTEM/360 AND WILL PRODUCE
C        2**29 TERMS BEFORE REPEATING.  THE REFERENCE BELOW DISCUSSES
C        SEEDS (65539 HERE), RUN PROBLEMS, AND PROBLEMS CONCERNING
C        RANDOM DIGITS USING THIS GENERATION SCHEME.  MACLAREN AND
C        MARSAGLIA, JACM 12, PP.83-89, DISCUSS CONGRUENTED GENERATION
C        METHODS AND TESTS.  THE USE OF TWO GENERATORS OF THE RANDU
C        TYPE, ONE FILLING A TABLE AND ONE PICKING FROM THE TABLE,
C        IS OF BENEFIT IN SOME CASES.  65549 HAS BEEN SUGGESTED AS A
C        SEED WHICH HAS BETTER STATISTICAL PROPERTIES FOR HIGH ORDER
C        BITS OF GENERATED DEVIATE.  SEEDS SHOULD BE CHOSEN IN ACCOR-
C        DANCE WITH THE DISCUSSION GIVEN IN THE REFERENCE BELOW.
C        ALSO, IT SHOULD BE NOTED THAT IF FLOATING POINT RANDOM NUMBERS
C        ARE DESIRED, AS ARE AVAILABLE FROM RANDU, THE RANDOM CHARAC-
C        TERISTICS OF THE FLOATING POINT DEVIATES HAVE HIGH PROBABILITY
C        OF HAVING A TRAILING LOW ORDER ZERO BIT IN THEIR FRACTIONAL
C        PART.
C
C     METHOD
C        POWER RESIDUE METHOD DISCUSSED IN IBM MANUAL C20-8011,
C        RANDOM NUMBER GENERATION AND TESTING.
C
C*********************************************************************
      IY=IX*65539
      IF(IY)5,6,6
    5 IY=IY+2147483647+1
    6 YFL=IY
      YFL=YFL*.4656613E-9
      RETURN
      END
```

```
      SUBROUTINE ROTAT(XSCAT,YSCAT,ZSCAT,XD,YD,ZD)
C***********************************************************************
C
C     THIS SUBROUTINE COMPUTES THE RADAR COORDINATES OF THE
C     POINT (XSCAT,YSCAT,ZSCAT) GIVEN IN TARGET COORDINATES
C
C
C  XD,YD,ZD ARE RADAR COORDINATES OF POINT.
C  XSCAT,YSCAT,ZSCAT ARE TARGET COORDINATES OF POINT.
C  X0,Y0,Z0 ARE TRANSLATION COORDINATES.
C  CHI IS YAW ANGLE - POSITIVE ROTATION ABOUT THE Z-AXIS.
C  GAMMA IS PITCH ANGLE - POSITIVE ROTATION ABOUT THE Y-AXIS.
C  MU IS ROLL ANGLE - POSITIVE ROTATION ABOUT THE X-AXIS.
C  THE ROTATIONS ARE ALWAYS PERFORMED IN THE ORDER - YAW-PITCH-ROLL.
C
C***********************************************************************
      REAL MU
      DOUBLE PRECISION XD,YD,ZD,DBLE
      COMMON/RTA/MU,GAMMA,CHI,X0,Y0,Z0
    1 CG=COS(GAMMA)
      CC=COS(CHI)
      CM=COS(MU)
      SG=SIN(GAMMA)
      SC=SIN(CHI)
      SM=SIN(MU)
      SMSG=SM*SG
      CMSG=CM*SG
      XD=DBLE(CG*CC*XSCAT+(SMSG*CC-CM*SC)*YSCAT+
     +(CMSG*CC+SM*SC)*ZSCAT)+DBLE(X0)
      YD=DBLE(CG*SC*XSCAT+(SMSG*SC+CM*CC)*YSCAT+
     +(CMSG*SC-SM*CC)*ZSCAT)+DBLE(Y0)
      ZD=DBLE(-SG*XSCAT+SM*CG*YSCAT+CM*CG*ZSCAT)+DBLE(Z0)
      RETURN
      END
```

```
      SUBROUTINE ROTAT2(XA,YA,HEIGHT,X1,Y1,Z1)
C*********************************************************************
C
C     THIS SUBROUTINE COMPUTES THE TARGET COORDINATES OF THE
C     POINT (XA,YA,HEIGHT) DESCRIBED IN RADAR COORDINATES
C
C
C  X1,Y1,Z1 ARE TARGET COORDINATES OF POINT.
C  XA,YA,HEIGHT ARE RADAR COORDINATES OF POINT.
C  X0,Y0,Z0 ARE TRANSLATION COORDINATES.
C  CHI IS YAW ANGLE - POSITIVE ROTATION ABOUT THE Z-AXIS.
C  GAMMA IS PITCH ANGLE - POSITIVE ROTATION ABOUT THE Y-AXIS.
C  MU IS ROLL ANGLE - POSITIVE ROTATION ABOUT THE X-AXIS.
C  THE ROTATIONS ARE ALWAYS PERFORMED IN THE ORDER - YAW-PITCH-ROLL.
C
C*********************************************************************
      REAL MU
      COMMON/RTA/MU,GAMMA,CHI,X0,Y0,Z0
      X2=XA-X0
      Y2=YA-Y0
      Z2=HEIGHT-Z0
      CG=COS(GAMMA)
      CC=COS(CHI)
      CM=COS(MU)
      SG=SIN(GAMMA)
      SC=SIN(CHI)
      SM=SIN(MU)
      SGCC=SG*CC
      SGSC=SG*SC
      CGZ2=CG*Z2
      X1=CG*CC*X2+CG*SC*Y2-SG*Z2
      Y1=(SM*SGCC-CM*SC)*X2+(SM*SGSC+CM*CC)*Y2+SM*CGZ2
      Z1=(CM*SGCC+SM*SC)*X2+(CM*SGSC-SM*CC)*Y2+CM*CGZ2
      RETURN
      END
```

```
      SUBROUTINE TRAJ(TIME,IRPY)
      REAL MU
      COMMON/RPY/RRATE,PRATE,YRATE,OMEGA,SPEED,GLSLP,R,
     *AZ,GRNG
      COMMON/RTA/MU,GAMMA,CHI,X0,Y0,Z0
    1 PI=3.141593
      X0=0.0
      Y0=COS(GLSLP)*(R-SPEED*TIME)
      Z0= Y0*TAN(GLSLP)
      IF (IRPY.EQ.0) GO TO 20
      TERM=SIN(OMEGA*TIME)
      MU=(RRATE/OMEGA)*TERM
      GAMMA=(PRATE/OMEGA)*TERM
      CHI=(YRATE/OMEGA)*TERM
      RETURN
   20 MU=0.0
      CHI=0.0
      GAMMA=0.0
      RETURN
      END
```

```
      SUBROUTINE RCS(THETA,PHI,ICODE)
      DIMENSION SCAT(3,4)
      COMMON/WAVE/K,MUR,EPSR
      COMMON/SCATN/SCAT,NUM
      REAL K
      DATA PI,PI2S,PI2/3.141593,2.467401,1.570796/
C***********************************************************************
C
C          RCS COMPLEX CODE
C     1:  JETMOD#1
C
C     2:  1 POINT SCATTERER MODEL
C
C***********************************************************************
      DO 2 I=1,3
    2 SCAT(I,4)=1E-10
      GO TO (100,200),ICODE
C***********************************************************************
C
C     JETMOD#1 RCS TARGET MODEL
C
C***********************************************************************
  100 NUM=3
      ALPHA=ARCOS(SIN(THETA)*COS(PHI))
      DELTA=ARCOS(SIN(THETA)*SIN(PHI))
      SCAT(1,1)=0.0
      SCAT(1,2)=-3.0
      SCAT(1,3)=0.0
      SCAT(2,1)=-8.0
      SCAT(2,2)=0.0
      SCAT(2,3)=0.0
      SCAT(3,1)=+8.0
      SCAT(3,2)=0.0
      SCAT(3,3)=0.0
      DXFUS=2.0
      DYFUS=10.0
      DZFUS=3.0
      DXLWNG=4.0
      DYLWNG=6.0
      DZLWNG=2.0
      DXRWNG=4.0
      DYRWNG=6.0
      DZRWNG=2.0
      FUSX=COS((K*DXFUS/2.0)*COS(ALPHA))
      FUSY=COS((K*DYFUS/2.0)*COS(DELTA))
      FUSZ=COS((K*DZFUS/2.0)*COS(THETA))
      WNGRX=COS((K*DXRWNG/2.0)*COS(ALPHA))
      WNGRY=COS((K*DYRWNG/2.0)*COS(DELTA))
      WNGRZ=COS((K*DZRWNG/2.0)*COS(THETA))
      WNGLX=COS((K*DXLWNG/2.0)*COS(ALPHA))
      WNGLY=COS((K*DYLWNG/2.0)*COS(DELTA))
      WNGLZ=COS((K*DZLWNG/2.0)*COS(THETA))
      AFUSEL=10.0*(THETA-PI/2.0)**2+1.0
      AWNGEL=100.0*(THETA-PI/2.0)**2+1.0
      IF(ABS(PHI).LE.PI/2.0) GO TO 10
      AFUSAZ=(75.0/PI2S)*(ABS(PHI)-PI)**2+8.0
      GO TO 15
```

```
   10 AFUSAZ=(75.0/PI2S)*PHI**2+8.0
   15 CONTINUE
      ARWGAZ=1.0-SIN(PHI)
      ALWGAZ=1.0+SIN(PHI)
C
C   COMPUTE FUSELAGE RCS
C
      SCAT(1,4)=AFUSEL*AFUSAZ*ABS(FUSX+FUSY+FUSZ)
C
C   COMPUTE RH WING RCS
C
      SCAT(2,4)=AWNGEL*ARWGAZ*ABS(WNGRX+WNGRY+WNGRZ)
C
C   COMPUTE LH WING RCS
C
      SCAT(3,4)=AWNGEL*ALWGAZ*ABS(WNGLX+WNGLY+WNGLZ)
      RETURN
C*********************************************************************
C
C         COMPUTATION OF 1 POINT SCATTERER RCS
C
C*********************************************************************
 200  NUM=1
      SCAT(1,1)=0.0
      SCAT(1,2)=0.0
      SCAT(1,3)=0.0
      SCAT(1,4)=1.0
      RETURN
      END
```

```
      SUBROUTINE ANTENA(AZ,EL,GAIN)
      REAL K
      INTEGER ELA,ELA2,ELB,ELB2
      COMMON/WAVE/K,MUR,EPSR  .
      DATA PI/3.141593/
      DATA ELA,ELB/35,35/
      DATA D1,D2,SCALE/0.03,0.029,10.0E+05/
      PHI=PI/2.-AZ
      THETA=PI/2.0-EL
      B1=COS(THETA)*D1*K
      B2=SIN(THETA)*COS(PHI)*D2*K
      R1=0.
      DO 100 I=1,ELA
  100 R1=R1+COS(B1*FLOAT(I))
      R1=2.*R1+1.0
      R2=0.
      DO 200 I=1,ELB
  200 R2=R2+COS(B2*FLOAT(I))
      R2=2.*R2+1.0
      R1R2=R1*R2
      GAIN=R1R2*R1R2/SCALE
      RETURN
      END
```

```
      SUBROUTINE MEAN
C*********************************************************************
C
C     THIS SUBROUTINE CALCULATES THE MEAN RETURN VOLTAGE IN
C     AZIMUTH AND ELEVATION (SEPARATELY) WHICH IS THEN USED
C     AS THE THRESHOLD IN FHLH TO LOCATE THE TARGET CENTROID.
C
C*********************************************************************
      REAL*8 EL(49),AZ(49),SUM,MEANE,MEANA
      COMMON /ALL/ EL,AZ,RANGE,OPTION,LABEL,ELDIM,AZDIM,ELSCAN,DELTA
      INTEGER OPTION(5),ELDIM,AZDIM,ELSCAN
      IF(ELSCAN.EQ.1)GO TO 4
      SUM=0.0
      MEANE=0.0
      DO 2 I=1,ELDIM
    2 SUM=SUM+EL(I)
      MEANE=SUM/FLOAT(ELDIM)
    4 SUM=0.0
      DO 5 I=1,AZDIM
    5 SUM=SUM+AZ(I)
      MEANA=SUM/FLOAT(AZDIM)
      LABEL=1
      CALL FHLH(MEANE,MEANA)
      RETURN
      END
```

```
      SUBROUTINE MEDIAN
C**********************************************************************
C
C      THIS SUBROUTINE DETERMINES THE MEDIAN VALUE OF RETURN
C      VOLTAGE, AND PASSES THIS VALUE AS THRESHOLD TO PHLH.
C
C**********************************************************************
      COMMON /ALL/ EL,AZ,RANGE,OPTION,LABEL,ELDIM,AZDIM,ELSCAN,DELTA
      COMMON /RADR/ PEL,PAZ,CBLOCE,CBLOCA,GRANE,GRANA,AZBW,ELBW,LOCK
      REAL*8 EL(49),AZ(49),MEDE,MEDA,VOLT(2,49)/98*0.0D0/
      INTEGER OPTION(5),ELDIM,AZDIM,CHANGE,LIMIT(2),ELSCAN
      L=2
      IF(ELSCAN.EQ.1)L=1
      DO 4 K=1,AZDIM
    4 VOLT(1,K)=AZ(K)
      DO 5 K=1,ELDIM
    5 VOLT(2,K)=EL(K)
      LIMIT(1)=AZDIM-1
      LIMIT(2)=ELDIM-1
    1 CHANGE=0
      DO 2 I=1,L
      LL=LIMIT(I)
      DO 3 J=1,LL
      IF(VOLT(I,J).LT.VOLT(I,J+1)) GO TO 3
      VHOLD=VOLT(I,J)
      VOLT(I,J)=VOLT(I,J+1)
      VOLT(I,J+1)=VHOLD
      CHANGE=CHANGE+1
    3 CONTINUE
    2 CONTINUE
      IF(CHANGE.NE.0)GO TO 1
      MIDAZ=(AZDIM+1)/2
      MIDEL=(ELDIM+1)/2
      MEDA=VOLT(1,MIDAZ)
      MEDE=VOLT(2,MIDEL)
      LABEL=2
      CALL PHLH(MEDE,MEDA)
      RETURN
      END
```

```
      SUBROUTINE T12DB
C*************************************************************************
C
C     THIS SUBROUTINE COMPUTES A THRESHOLD T2DB DOWN FROM THE COMPUTED
C     RETURN VOLTAGE WHEN THE ANTENNA BEAM IS ON THE TARGET.  NOTE THAT
C     IF -12=20*LOG(VTHRES/VCENTER), THEN VTHRES=0.25118864*VCENTER.
C
C*************************************************************************
      COMMON/ALL/EL,AZ,RANGE,OPTION,LABEL,ELDIM,AZDIM,ELSCAN,DELTA
      COMMON /RADR/ REL,RAZ,CBLOCE,CBLOCA,GRANE,GRANA,AZBW,ELBW,LOCK
      COMMON/FOURIV/COUNTE,COUNTA,MODEE,MODEA,MSDBV,SNREL,MODE12,MODA12
      INTEGER OPTION(5),ELDIM,AZDIM,PHA,LHA,PHE,LHE,AZS,ELS,COUNTE,
     *COUNTA,ELSCAN
      DOUBLE PRECISION EL(49),AZ(49),VCENTR,ELTHRS,AZTHRS
      MODE12=1
      MODA12=1
      MIDDLE=(AZDIM+1)/2
      VCENTR=AZ(MIDDLE)
      AZTHRS=0.25118864*VCENTR
      DO 1 I=1,AZDIM
      IF(AZTHRS.GE.AZ(I)) GO TO 2
    1 CONTINUE
      MODA12=0
    2 MIDDLE=(ELDIM+1)/2
      VCENTR=EL(MIDDLE)
      ELTHRS=0.25118864*VCENTR
      IF(ELSCAN.EQ.1)ELTHRS=0.0
      DO 3 I=1,ELDIM
      IF(ELTHRS.GE.EL(I)) GO TO 4
    3 CONTINUE
      MODE12=0
    4 LABEL=4
      CALL PYLH(ELTHRS,AZTHRS)
      RETURN
      END
```

```
      SUBROUTINE FHLR(ELTHRS,AZTHRS)
C*********************************************************************
C
C     THIS SUBROUTINE USES THE THRESHOLDS CALCULATED BY MEAN
C     AND/OR MEDIAN TO DETERMINE THE TARGET CENTROID.  AN EDGE
C     OF THE TARGET IS DEFINED WHEN TWO CONSECUTIVE VOLTAGE
C     RETURNS EXCEED THE CALCULATED THRESHOLD.  THE CENTROID IS
C     THEN MIDWAY BETWEEN THE EDGES.  A HIT IS A VOLTAGE EXCEEDING
C     THE THRESHOLD.
C
C*********************************************************************
      DOUBLE PRECISION VOLT(49),EL(49),AZ(49),ELTHRS,AZTHRS,THRESH
      COMMON /ALL/ EL,AZ,RANGE,OPTION,LABEL,ELDIM,AZDIM,ELSCAN,DELTA
      COMMON /RADB/ PEL,PAZ,CBLOCE,CBLOCA,GRANE,GRANA,AZBW,ELBW,LOCK
      COMMON/FOURIT/COUNTE,COUNTA,MODEE,MODEA,MSDEV,SNREL,MODE12,MODA12
      INTEGER OPTION(5),ELDIM,AZDIM,FHA,LHA,FHE,LHE,AZS,ELS,COUNTE,
     *COUNTA,ELSCAN
      COUNTA=1
      COUNTE=1
      MODEA=3
      MODEE=3
      TCE=0.0
C
C     CALCULATE FIRST HIT IN AZIMUTH
C
      DO 1 AZS=1,AZDIM
      IF((AZ(AZS).GE.AZTHRS).AND.(AZ(AZS+1).GE.AZTHRS))GO TO 2
    1 CONTINUE
      PCA=8E5
      MODEA=0
      GO TO 5
    2 FHA=AZS
      COUNTA=COUNTA+AZS+1
C
C     CALCULATE LAST HIT IN AZIMUTH
C
      DO 3 AZS=1,AZDIM
      IF((AZ(AZDIM-AZS+1).GE.AZTHRS).AND.(AZ(AZDIM-AZS).GE.AZTHRS))
     *GO TO 4
    3 CONTINUE
      WRITE(6,12)
    4 LHA=AZDIM-AZS+1
      PCA=(FLOAT(LHA+FHA)/2.-FLOAT((AZDIM+1)/2))*GRANA+CBLOCA
      COUNTA=COUNTA+AZS+1
C
C     CALCULATE FIRST HIT IN ELEVATION
C
    5 IF(ELSCAN.EQ.1)GO TO 10
      DO 6 ELS=1,ELDIM
      IF((EL(ELS).GE.ELTHRS).AND.(EL(ELS+1).GE.ELTHRS))GO TO 7
    6 CONTINUE
      TCE=8E5
      MODEE=0
      GO TO 10
    7 FHE=ELS
      COUNTE=COUNTE+ELS+1
C
```

```
C     CALCULATE LAST HIT IN ELEVATION
C
      DO 8 ELS=1,ELDIM
      IF((EL(ELDIM-ELS+1).GE.ELTHRS).AND.(EL(ELDIM-ELS).GE.ELTHRS))
     *GO TO 9
    8 CONTINUE
      WRITE(6,14)
    9 LHE=ELDIM-ELS+1
      COUNTE=COUNTE+ELS+1
C
C     CALCULATE AZ AND EL CENTROID ESTIMATIONS
C
      TCE=(FLOAT(LHE+FHE)/2.-FLOAT((ELDIM+1)/2))*GRANE+CBLOCE
   10 CALL ERROR(TCE,PCA)
   12 FORMAT(' ERROR OCCURRED IN LOOP 3, FHLH')
   14 FORMAT(' ERROR OCCURRED IN LOOP 8, FHLH')
      RETURN
      END
```

```
      SUBROUTINE RADARC
C*****************************************************************
C
C     THIS SUBROUTINE CALCULATES THE AMPLITUDE-WEIGHTED RADAR
C     RETURN TO DETERMINE THE RADAR CENTER OF GRAVITY (RADARC).
C     FORMULA USED IS (SUM OF VOLTAGES TIMES ANGLE AT THAT
C     VOLTAGE) DIVIDED BY (SUM OF THE VOLTAGES).
C
C*****************************************************************
      COMMON /ALL/ EL,AZ,RANGE,OPTION,LABEL,ELDIM,AZDIM,ELSCAN,DELTA
      COMMON /RADR/ REL,RAZ,CBLOCE,CBLOCA,GRANE,GRANA,AZBW,ELBW,LOCK
      DOUBLE PRECISION EL(49),AZ(49),VOLT(49)
      INTEGER ELDIM,AZDIM,OPTION(5),DIM,ELSCAN
      RCGEL=0.0
      IF(ELSCAN.EQ.1)GO TO 3
      SUMWTH=0.0
      SUMW=0.0
      J=1
      DIM=ELDIM
      CENTER=(DIM+1)/2.
      GRAN=GRANE
      PANGLE=CBLOCE
      DO 2 I=1,DIM
    2 VOLT(I)=EL(I)
    1 DO 10 I=1,DIM
      SUMWTH=SUMWTH+VOLT(I)*((I-CENTER)*GRAN+PANGLE)
   10 SUMW=SUMW+SNGL(VOLT(I))
      IF(J.EQ.2)GO TO 20
      RCGEL=SUMWTH/SUMW
    3 SUMWTH=0.0
      SUMW=0.0
      J=2
      DIM=AZDIM
      CENTER=(DIM+1)/2.
      GRAN=GRANA
      PANGLE=CBLOCA
      DO 11 I=1,DIM
   11 VOLT(I)=AZ(I)
      GO TO 1
   20 RCGAZ=SUMWTH/SUMW
      LABEL=3
      CALL ERROR(RCGEL,RCGAZ)
      RETURN
      END
```

```
      SUBROUTINE ERROR(TCE,PCA)
C*******************************************************************
C
C     THIS SUBROUTINE CALCULATES THE ERROR BETWEEN THE LOCATION
C     OF THE TARGET CENTROID DETERMINED BY THE ESTIMATOR SUBROUTINES
C     TO THE ACTUAL LOCATION OF THE TARGET AS SEEN BY THE RADAR.
C
C*******************************************************************
      COMMON /ALL/ EL,AZ,RANGE,OPTION,LABEL,ELDIM,AZDIM,ELSCAN,DELTA
      COMMON /RADR/ PEL,PAZ,CBLOCE,CBLOCA,GRANE,GPANA,AZBW,ELBW,LOCK
      COMMON /FILEIT/ XMEAN,XMED,XRADRC,X12DB,XSDRV,SNRAZ,PLS12,
     *PLSFD,PLSSD,DMEAN,DMED,DRADRC,D12DB,DSDRV
      COMMON/FOURIV/COUNTE,COUNTA,MODEE,MODEA,MSDRV,SNREL,MODE12,MODA12
      COMMON /RTA/ MU,GAMMA,CHI,X0,Y0,Z0
      DOUBLE PRECISION EL(49),AZ(49)
      INTEGER OPTION(5),ELDIM,AZDIM,COUNTA,COUNTE,ELSCAN,PLS12,PLSFD,
     *PLSSD
      RADDEG=57.29578
C
C     ERROR CALCULATION
C
      ERREL=TCE-PEL
      ERRAZ=PCA-PAZ
      ELM=RANGE*SIN(ERREL)
      AZM=RANGE*SIN(ERRAZ)
      TCED=TCE*RADDEG
      PCAD=PCA*RADDEG
      PELD=PEL*RADDEG
      PAZD=PAZ*RADDEG
      IF(MODEA.EQ.0) ERRAZ=1E71
C
C     CONVERTING TO MILLIRADIANS
C
      ERREL=ERREL*1E3
      ERRAZ=ERRAZ*1E3
C
      IF(LABEL.EQ.1)XMEAN=ERRAZ
      IF(LABEL.EQ.2)XMED=ERRAZ
      IF(LABEL.EQ.3)XRADRC=ERRAZ
      IF(LABEL.EQ.4)X12DB=ERRAZ
      IF(LABEL.EQ.5)XSDRV=ERRAZ
      IF(LABEL.EQ.4)PLS12=COUNTA
      IF(LABEL.EQ.5)PLSSD=COUNTA
      IF(LABEL.EQ.1)DMEAN=AZM
      IF(LABEL.EQ.2)DMED=AZM
      IF(LABEL.EQ.3)DRADRC=AZM
      IF(LABEL.EQ.4)D12DB=AZM
      IF(LABEL.EQ.5)DSDRV=AZM
C
C     OUTPUT ERROR DATA
C
      IF(LABEL.EQ.3)MODEE=8
      IF(LABEL.EQ.3)MODEA=8
      WRITE(6,1)RANGE,Y0,SNREL,SNRAZ,PELD,PAZD
      IF(LABEL.EQ.1)WRITE(6,2)
      IF(LABEL.EQ.2)WRITE(6,3)
      IF(LABEL.EQ.3)WRITE(6,4)
```

```
      IF(LABEL.EQ.4) WRITE(6,6) MODE12,MODA12,COUNTE,COUNTA
      IF(LABEL.EQ.5) WRITE(6,5) MODEE,MODEA,COUNTE,COUNTA
      IF(ELSCAN.EQ.1) GO TO 11
      IF(MODEE.NE.0) WRITE(6,7) TCED,ERREL,ELM
      IF(MODEE.EQ.0) WRITE(6,9)
   11 IF(MODEA.NE.0) WRITE(6,8) PCAD,ERRAZ,AZM
      IF(MODEA.EQ.0) WRITE(6,10)
    1 FORMAT(2F8.2,2X,F5.1,1X,F5.1,1X,F6.2,3X,F5.2,3X,'|')
    2 FORMAT('+',49X,'     MEAN',24X,'|',24X,'|')
    3 FORMAT('+',49X,'   MEDIAN',23X,'|',24X,'|')
    4 FORMAT('+',49X,'   RADARCG',22X,'|',24X,'|')
    5 FORMAT('+',49X,2I1,1X,'SDRV',1X,2I2,20X,'|',24X,'|')
    6 FORMAT('+',49X,2I1,1X,'12DB',1X,2I2,20X,'|',24X,'|')
    7 FORMAT('+',63X,F6.2,15X,G10.3,1X,F7.2)
    8 FORMAT('+',73X,F6.2,29X,G10.3,2X,F7.2)
    9 FORMAT('+',85X,'*REJECTED*',2X,'*REJECT*')
   10 FORMAT('+',108X,'*REJECTED*',3X,'*REJECT*')
      RETURN
      END
```

```
      SUBROUTINE SDRV(INIT,NOISE)
      COMMON /ALL/EL,AZ,RANGE,OPTION,LABEL,ELDIM,AZDIM,ELSCAN,DELTA
      COMMON/RADB/PEL,PAZ,CBLOCE,CBLOCA,GRANE,GRANA,AZBW,ELBW,LOCK
      COMMON/POUBI7/COUNTE,CCUNTA,MODEE,MODEA,MSDRV,SNREL,MODE12,MODA12
      REAL*8 EL(49),AZ(49),VREF,VLT(4)/4*0.0D0/,VOLT(2,49)/98*0.0D0/,
     *VEND,SUM
      INTEGER ELDIM,AZDIM,OPTION(5),A,B,C,D,DIM,ELSCAN,PULSES,Q,
     *COUNTE,COUNTA,COUNT,MODEE,MODEA
      REAL NOSLIM,N
C*************************************************************************
C
C     THIS SUBROUTINE CALCULATES AN ESTIMATE OF THE TARGET CENTROID
C     POSITION BASED ON THE SHAPE OF THE RETURN.
C       THE CENTROID IS CALCULATED AS FOLLOWS:
C     HALF THE SCAN IS BROKEN INTO FOUR 'WINDOWS'. THE RETURNS FROM THE
C     BEAM POINTING LOCATIONS INSIDE THE WINDOWS ARE AVERAGED TOGETHER
C     TO OBTAIN FOUR MEAN VALUES. THESE FOUR MEAN VALUES ARE EXPECTED TO
C     TAKE ON ONE HALF OF A BELL SHAPE. AN EDGE IS PLACED AT THE POINT
C     OF MAXIMUM SLOPE, OR WHERE THE SECOND DERIVATIVE CHANGES SIGN. IF
C     NO CHANGE IN SIGN OCCURRED, OR IF THE MAX SLOPE WAS BELOW THE
C     NOISE CRITERION, THE WINDOWS ARE SHIFTED AND THE PROCESS REPEATED.
C     THE WINDOWS ARE ALLOWED TO SHIFT TWO WINDOW WIDTHS FROM THE END OF
C     THE SCAN, OR TO THE FEDGE.  A SCAN REJECTED DUE TO SHAPE OR NOISE
C     IS TAGGED MODE=0. IF A CENTROID IS CALCULATED, THE SCAN IS TAGGED
C     MODE=2.
C
C*************************************************************************
      NOSLIM=0.3898*1.5
      IF (INIT.EQ.1) GO TO 30
      VREF=0.
      SUM=0.
      N=0.
   30 VEND=0.
      MODEE=0
      MODEA=0
      COUNTE=0
      COUNTA=0
      TCE=0.0
      PCA=0.0
      DO 1 I=1,AZDIM
    1 VOLT(2,I)=AZ(I)
      IF(ELSCAN.EQ.1)GO TO 12
      DO 2 I=1,ELDIM
    2 VOLT(1,I)=EL(I)
      DIM=ELDIM
      GRAN=GRANE
      BW=ELBW
      J=1
    3 I=1
      INC=1
      FEDGE=0.0
      SEDGE=0.0
C*************************************************************************
C
C                            BEGIN MAIN LOOP
C
C          FIND SIZE OF WINDOW AND DETERMINE NECESSARY PARAMETERS
```

```
C
C*********************************************************************
C
C         TO DETERMINE THE PROPER SIZE WINDOW, WE FIRST NEED TO CALCULATE
C       THE OPTIMUM WINDOW SIZE WITH A "LOCKED ON" ANTENNA BEAM, THE
C       CENTER BEAM POINTING LOCATION BEING NORMAL ON THE TARGET.
C         IF AN UNLOCKED ANTENNA BEAM IS USED, THE OPTIMUM WINDOW SIZE IS
C       THE SAME AS IN THE LOCKED ON CASE.  WE THEN DETERMINE THE MAXIMUM
C       NUMBER OF BEAM LOCATIONS WITH THE WIDER GRANULARITY TO MAINTAIN
C       THE OPTIMUM WINDOW SIZE.
C
C*********************************************************************
      MIDPT=(DIM+1)/2
      A4TH=FLOAT(MIDPT)/4.0
      A4THMI=AINT(A4TH)
      REMAIN=(A4TH-A4THMI)*4.0
      PULSES=INT(A4THMI)
      LIMIT=DIM-6*PULSES
      COUNT=4*PULSES-1
      Q=0
      IF (LOCK.EQ.1) GO TO 4
      GRANOP=2.*BW*0.0174533/(FLOAT(DIM)-1.)
      WIDTHO=PULSES*GRANOP
      FACTOR=WIDTHO/GRAN-AINT(WIDTHO/GRAN)
      IF(FACTOR.GT.0.75)PULSES=INT(WIDTHO/GRAN)+1
      IF(FACTOR.LE.0.75)PULSES=INT(WIDTHO/GRAN)
      IF(PULSES.EQ.0)PULSES=1
      LIMIT=DIM-6*PULSES
      COUNT=4*PULSES-1
C*********************************************************************
C
C                           BEGIN INNER LOOP
C
C*********************************************************************
C
C                       CALCULATE VOLTAGE WINDOWS
C
C*********************************************************************
    4 IF(Q.EQ.LIMIT.OR.(INC.EQ.-1.AND.I.LE.INT(FEDGE)))GO TO 11
      COUNT=COUNT+1
      Q=Q+1
      DO 5 JJ=1,4
    5 VLT(JJ)=0.0D0
      DO 7 JJJ=1,4
      K=I+(PULSES*(JJJ-1))
      IF(JJJ.EQ.1.AND.INC.EQ.1)VEND=VOLT(J,K)
      L=I+PULSES*JJJ-1
      IF(JJJ.EQ.4.AND.INC.EQ.-1)VEND=VOLT(J,K)
      IF(JJJ.EQ.2)HIT=FLOAT(L)+0.5
      DO 6 II=K,L
    6 VLT(JJJ)=VLT(JJJ)+VOLT(J,II)
    7 VLT(JJJ)=VLT(JJJ)/FLOAT(PULSES)
      IF(INC.EQ.-1) GO TO 8
      A=1
      B=2
      C=3
      D=4
```

```
      GO TO 9
    9 A=4
      B=3
      C=2
      D=1
C*****************************************************************
C
C                         FIND DERIVATIVES
C
C*****************************************************************
C
C        THE FIRST DERIVATIVE OR SLOPE BETWEEN TWO ADJACENT WINDOW
C     VOLTAGES IS THE INNER MINUS THE OUTER VOLTAGE, DIVIDED BY A UNIT
C     ANGLE.  THE SECOND DERIVATIVE OR RATE OF CHANGE OF SLOPE IS THE
C     INNER MINUS THE OUTER FIRST DERIVATIVE.  SINCE THE MAXIMUM SLOPE
C     OCCURS WHEN THE SECOND DERIVATIVE IS ZERO, WE LOOK FOR THE CHANGE
C     IN SIGN OF THE SECOND DERIVATIVE.
C
C        IF THE CHANGE IN SIGN IS NOT FOUND, OR IF THE MAXIMUM SLOPE IS
C     LESS THAN THE NOISE CRITERION, THE WINDOWS ARE ADVANCED OR THE
C     SCAN REJECTED ACCORDINGLY.
C
C*****************************************************************
C
C     REJECT SCAN IF MEAN VOLTAGE B IS BELOW THE VOLTAGE REFERENCE.
C
C*****************************************************************
    9 IF(VLT(B).LT.VREF) GO TO 10
      FDAB=SNGL(VLT(B)-VLT(A))
      FDBC=SNGL(VLT(C)-VLT(B))
      SDB=FDBC-FDAB
      IF(SDB.LT.0.0)GO TO 10
      FDCD=SNGL(VLT(D)-VLT(C))
      SDC=FDCD-FDBC
      IF(SDC.GT.0)GO TO 10
      IF(NOISE.EQ.1.AND.FDBC.LT.NOSLIM)GO TO 10
      IF(PULSES.NE.1.AND.FDCD.LT.0.0)GO TO 10
      IF(INC.EQ.-1)GO TO 14
      FEDGE=HIT
C*****************************************************************
C
C     SETUP FOR SECOND EDGE
C
C*****************************************************************
      I=DIM-4*PULSES+1
      Q=0
      INC=-1
      COUNT=COUNT+4*PULSES-1
      GO TO 4
C
C     ADVANCE WINDOWS
C
   10 I=I+INC
      SUM=SUM+VEND
      N=N+1.
      VREF=SUM/N
      GO TO 4
```

```
C*****************************************************************************
C
C     IF THE PROGRAM REACHED THIS POINT, THEN NO SET OF
C     RETURNS PASSED THE CRITERION FOR THIS SCAN.
C
C*****************************************************************************
   11 IF(J.EQ.2)GO TO 13
      COUNTE=COUNT
      MODEE=0
C*****************************************************************************
C
C     SETUP FOR AZIMUTH
C
C*****************************************************************************
   12 DIM=AZDIM
      GRAN=GRANA
      BW=AZBW
      J=2
      GO TO 3
   13 MODEA=0
      COUNTA=COUNT
      GO TO 16
C*****************************************************************************
C
C                          FIND TARGET CENTER
C
C*****************************************************************************
   14 SEDGE=HIT
      IF(J.EQ.2) GO TO 15
      TCE=((SEDGE+FEDGE)/2.-FLOAT(MIDPT))*GRANE+CBLOCE
      MODEE=2
      COUNTE=COUNT
      GO TO 12
   15 PCA=((SEDGE+FEDGE)/2.-FLOAT(MIDPT))*GRANA+CBLOCA
      MODEA=2
      COUNTA=COUNT
   16 LABEL=5
      CALL ERROR(TCE,PCA)
      RETURN
      END
```

END

DATE
FILMED
3-82

DTIC